



Investigation and Therapeutic Targeting of
Metabolic Dependencies in Malignant Brain
Tumours

Magretta Dovi Adiamah

Thesis submitted in partial fulfilment of the requirements for the degree of

Doctor of Philosophy

Translational and Clinical Research Institute

Newcastle University

March 2020

Declaration

I certify that no part of the material documented in this thesis has previously been submitted for a degree or other qualification in this or any other university. I declare that this thesis represents my own unaided work, carried out by myself, except where it is acknowledged otherwise in the thesis text.

Magretta Dovi Adiamah

March 2020

Abstract

Malignant brain tumours are highly lethal cancers that affect the adult and paediatric populations. Glioblastoma (GBM), the common high-grade CNS tumour in adulthood is highly lethal with median patient survival of only 14.6 months despite aggressive treatment. Fatty acid oxidation (FAO) was previously established as a metabolic dependency in GBM-stem like cells which can contribute to tumour progression. Targeting this pathway in combination with standard therapy, may offer more effective treatment strategy for GBM. In childhood, medulloblastoma (MB) is the common primary malignant brain tumour and despite advances in its molecular sub-classification and risk-stratification a subset remain difficult to treat. MB_{GRP3} patients represent around 25% of all medulloblastoma cases. Amplification and elevated expression of *MYC* is a notable abnormality in this group and also correlates with poorer clinical outcomes. Since direct targeting of *MYC* remains elusive, understanding and exploiting metabolic dependencies in *MYC*-amplified MB_{GRP3} may reveal novel therapeutic opportunities.

For this project, *in vivo* and *in vitro* metabolic profiling using magnetic resonance imaging and spectroscopy was utilised to evaluate metabolic alterations and associated with the pathobiology of GBM and MB. Metabolic profiling in GBM focused on tumour progression and treatment-induced changes following combination therapy using the FAO inhibitor, etomoxir alongside temozolomide chemotherapy in a clinically relevant model of GBM. To better understand the role of *MYC* in MB metabolism, we engineered three independent *MYC*-amplified MB_{GRP3} cell lines (D425, D283, HDMB03), to each harbour doxycycline-inducible anti-*MYC* shRNAs (two independent species) or a non-silencing shRNA control. We utilised ¹H high resolution magic angle spectroscopy (HRMAS) and stable isotope resolved metabolomics to assess changes in intracellular metabolites and pathway dynamics when *MYC* expression was modulated.

Findings from the GBM study supported previous observations suggesting FAO inhibition was a viable strategy for targeting GBM. For MB, MYC knockdown (KD) resulted in a marked reduction in proliferation and cell cycle progression analogous to MYC-dependent cancer phenotypes. Metabolic profiling revealed consistent MYC-dependent changes in metabolites across the three *MYC*-amplified cell lines. Notably, glycine was consistently found to be accumulated following MYC KD cells. ¹³C-glucose labelling showed a reduction in serine and glycine synthesis following MYC knockdown. In human primary tumours, expression of PHGDH, the rate limiting enzyme in *de novo* serine synthesis, was associated with *MYC* amplification and poorer survival outcomes. Furthermore, *MYC* expressing cells showed greater sensitivity to pharmacological inhibition of PHGDH compared to *MYC* KD (Group 3) and SHH subgroup cell lines.

Together, these findings provide insights into the metabolic vulnerabilities of the most common malignant brain tumours arising in children and adults, and suggest novel therapeutic opportunities. Combination therapy using etomoxir and temozolomide could provide more effective therapy for GBM. Furthermore, metabolic profiling uncovered *MYC*-dependent metabolic alterations and revealed the *de novo* serine/glycine synthesis pathway as a novel and clinically relevant therapeutic target in Group 3 *MYC*-amplified MB.

Acknowledgments

Firstly, a thank you to my supervisors, past and present. I would like to thank Dr Elizabeth Stoll who gave me the opportunity of coming to Newcastle for this PhD. I have so many fond memories of the Stoll lab and the super-woman team we had. I am forever grateful for all that you have taught me and for instilling a passion for neuro-oncology research. I would like to thank Dr Ross Maxwell, for being the last man standing and a continual force behind my PhD. There were some sketchy bits in the middle but you saw me through this, providing much needed support and guidance. I would also extend my gratitude towards Professor Ian Hickson and Professor Steve Clifford who stepped up and offered me a new research home. I have really appreciated your inputs and mentorship along the years. I would also like to thank my panel members, Professor Andrew Blamire and Dr Lisa Russell for their advice and contributions to my work.

My sincerest gratitude to the paediatric brain tumour group, particularly the members of the MYC biology team (infamously known as the MYC sisters) Thanks you to Dr Janet Lindsey (MYC Queen) for imparting on me her extensive knowledge of all things MYC. To Dr Florence Burté, I would not have come this far without you. Thank you for all the help, for the constructive criticisms and allowing my ramblings on metabolism.

To my colleagues at the Herschel, thank you for fostering a positive environment that helped to keep a smile on my face. I have had the pleasure of working alongside and learning from you. I have made some wonderful friends who have made this a lasting experience. I appreciate you all for the support and the laughter that kept me going. Thank you for being there through the difficult times and for supplying me with much needed sugar-based snacks.

To the Thompson-Adiamah clan, thank you for pushing me over the years and for instilling in me the drive and resilience, which ultimately enabled to complete my PhD. You have always been my loudest supporters and I appreciate your encouragement over the years. Finally, to Phil, for gifting me a Bob Ross T-shirt, which reads “Ever make mistakes in life? Let’s make them birds. Yeah, they’re birds now” which I wore on the challenging days to help lighten things up. Thank you for your thoughtfulness, being so dependable and readiness to jump in and help.

Table of Contents

Declaration	i
Abstract	ii
Acknowledgments	iv
Table of Contents	v
List of abbreviations	x
List of Figures	xvii
List of Tables	xxiii
Chapter 1 Introduction	1
1.1 Overview of altered metabolism in cancer	2
1.1.1 Glycolysis	3
1.1.2 The tricarboxylic acid cycle.....	8
1.1.3 Electron transport chain.....	10
1.1.4 Fatty acid β -oxidation.....	9
1.1.5 Regulation of metabolic reprogramming.....	12
1.2 Exploiting metabolic dependencies for cancer biomarkers and therapy ..	15
1.2.1 Targeting altered metabolism	15
1.2.2 Imaging altered metabolism.....	21
1.3 Epidemiology of central nervous system tumours.....	25
1.3.1 Overview of malignant brain in adults and children	25
1.3.2 Spectrum of brain tumours	26
1.4 Malignant glioma.....	30
1.4.1 Aetiology and epidemiology.....	30
1.4.2 Clinical presentation.....	31
1.4.3 Treatment strategies in glioblastoma.....	31
1.4.4 Molecular classification and heterogeneity of glioblastoma	32
1.4.5 Altered metabolism in glioma.....	35
1.5 Medulloblastoma	38
1.5.1 Treatment of medulloblastoma	39
1.5.2 Histopathological features of medulloblastoma.....	40
1.5.3 Risk stratification of medulloblastoma.....	42

1.5.4	Genetic abnormalities and subgroup classification of medulloblastoma	44
1.5.5	The role of <i>MYC</i> in cancer	50
1.5.6	Role of <i>MYC</i> in medulloblastoma	59
1.5.7	Challenges in treating <i>MYC</i> -amplified Group 3 MB	61
1.6	Research background.....	63
1.7	Aims of project	64
Chapter 2 Materials and Methods.....		65
2.1	Methods used for Chapter 3.....	66
2.1.1	Mouse neural stem cell culture	66
2.1.2	Syngeneic mouse model of glioma	67
2.1.3	<i>In vitro</i> ¹ H NMR spectroscopy	68
2.1.4	<i>In vivo</i> magnetic resonance imaging and spectroscopy.....	68
2.2	Methods used for Chapter 4.....	70
2.2.1	Medulloblastoma cell culture.....	70
2.2.2	Protein extraction and quantification	73
2.2.3	Simple western immunoassays (WES).....	74
2.2.4	Antibodies.....	74
2.2.5	Cell growth curves	75
2.2.6	Cell cycle analysis.....	75
2.2.7	Cellular bioenergetics using XF analyser	76
2.3	Methods used for Chapter 5.....	77
2.3.1	¹ H High resolution magic angle spectroscopy (HRMAS).....	77
2.3.2	¹³ C- Glucose labelling	79
2.4	Methods used for Chapter 6.....	80
2.4.1	Gene expression analysis.....	80
2.4.2	Immunohistochemistry	80
2.4.3	Cell viability assays.....	82
2.4.4	Pharmacological inhibition of PHGDH.....	83
2.4.5	Molecular cloning	84
2.4.6	Lentiviral preparation	85
2.4.7	Titration of lentivirus.....	85
2.4.8	Generation of PHGDH knockout cell lines	86
2.4.9	Clonogenic assays	86
2.4.10	Incucyte™ growth assay.....	87
Chapter 3 Investigating fatty acid oxidation in a syngeneic mouse model of Glioblastoma		88

3.1	Introduction.....	89
3.2	Aims	94
3.3	Results.....	95
3.3.1	Monitoring tumour development in an <i>in vivo</i> mouse model of GBM.....	95
3.3.2	Evaluating the feasibility of monitoring neurochemical changes during tumour development.....	101
3.3.3	Metabolic characteristics of oncogenically transformed mouse neural progenitor cells using one dimensional ¹ H NMR	104
3.4	Discussion	110
3.4.1	The syngeneic mouse model of GBM provides a tool for studying tumourigenesis and pharmacological testing.....	110
3.4.2	Considerations for <i>in vivo</i> spectroscopy for the detection of brain metabolites	112
3.4.3	<i>In vitro</i> NMR spectroscopy reveals age-associated metabolic changes.....	113
Chapter 4 Characterising the bioenergetics of <i>MYC</i>-amplified group 3 medulloblastoma		
		116
4.1	Introduction.....	117
4.2	Aims	121
4.3	Results.....	122
4.3.1	Phenotypic assessment of <i>MYC</i> modulation in MB _{GRP3} cell lines	122
4.3.2	Alterations in metabolic enzymes in response to suppression of <i>MYC</i>	131
4.3.3	Characterising changes in bioenergetics in response to <i>MYC</i> expression.....	140
4.4	Discussion	145
4.4.1	<i>MYC</i> knockdown causes slowed proliferation and G1 arrest	145
4.4.2	Expression of metabolic enzymes is impacted upon <i>MYC</i> knockdown.....	147
4.4.3	Functional changes in mitochondria function and cellular energetics upon <i>MYC</i> knockdown.....	150
Chapter 5 Metabolic profiling of <i>MYC</i>-inducible MB_{GRP3} cell lines using high resolution magic angle spectroscopy		
		153
5.1	Introduction.....	154
5.2	Aims	157
5.3	Results.....	158
5.3.1	Experimental design and analysis pipeline	158
5.3.2	Analysis of ¹ H NMR spectra of MB _{GRP3} <i>MYC</i> -regulable cell lines using spectral binning	161

5.3.3	Analysis of metabolite concentrations derived from ¹ H NMR spectra.....	179
5.3.4	Utilising ¹³ C -glucose tracing to understand pathway dynamics of <i>MYC</i> -amplified medulloblastoma cells	192
5.4	Discussion	200
5.4.1	HRMAS based metabolomics for the identification of novel <i>MYC</i> -driven changes	200
5.4.2	<i>MYC</i> expression influences usage of the <i>de novo</i> serine and glycine pathway	203
5.4.3	Study limitations	206
Chapter 6. Exploiting upregulation of the <i>de novo</i> serine and glycine synthesis pathway as a novel therapeutic strategy for <i>MYC</i>-amplified medulloblastoma		
		207
6.1	Introduction.....	208
6.2	Aims	213
6.3	Results.....	214
6.3.1	Establishing clinical relevance of the serine and glycine pathway in medulloblastoma patient cohorts	214
6.3.2	<i>MYC</i> -dependent alterations in the <i>de novo</i> serine and glycine pathway	231
6.3.3	Response of MB parental cell lines with varying <i>MYC</i> expression to PHGDH inhibition.....	238
6.3.4	Phenotypic assessment of MB _{GRP3} cells following PHGDH inhibition using NCT503 and CBR5884	243
6.3.5	CRISPR-mediated loss of PHGDH in parental MB _{GRP3} cell lines.....	258
6.4	Discussion	268
6.4.1	Primary MB _{GRP3} display upregulated expression of SGP enzymes	268
6.4.2	Response of MB _{GRP3} cell lines to modulation of PHGDH function using NCT503	268
6.4.3	Nutrient sensing pathway response to post NCT503 treatment.....	269
6.4.4	Loss of PHGDH is detrimental to MB _{GRP3} cells under serine limiting conditions	271
Chapter 7 Discussion.....		
		273
7.1	Overview	274
7.2	Summary	275
7.2.1	Inhibition of fatty acid oxidation in malignant gliomas: Exploring combination therapy and metabolic profiling	275
7.2.2	Exploring metabolic dependencies of <i>MYC</i> -amplified MB _{GRP3}	278
7.3	Future directions	283

7.3.1	Etomoxir in combination with temozolomide: a promising treatment strategy for Glioblastoma?	283
7.3.2	Imaging and monitoring therapy response using advanced imaging techniques	284
7.3.3	Exploring metabolic features of Glioblastoma	284
7.3.4	Cellular response of fatty acid oxidation inhibition in oncogenic mouse NSCs and human NSCs: Metabolic plasticity of GBM cells	285
7.3.5	Inhibition of PHGDH as a novel therapeutic strategy to counteract <i>MYC</i> -driven tumourigenesis in MB	287
7.3.6	The role one carbon metabolism in <i>MYC</i> -amplified Group 3 MB	289
7.3.7	Comprehensive analysis of Group 3 MB altered bioenergetics. Integration of ‘omics’ data and generation of genome scale models to characterise MB-specific metabolic alterations.....	290
7.4	Concluding remarks.....	291
	Appendices	292
	References	348

List of abbreviations

+	Positive
AA	Amino Acid
ADI-PEG20	Arginine Depleting Enzyme PEGylated Arginine Deiminase
ALL	Acute Lymphoblastic Leukaemia
AM	Antimycin
AML	Acute Myeloid Leukaemia
AMPK	5' AMP-activated Protein Kinase
ANOVA	Analysis of Variance
AP	Antero-posterior
APC	Adenomatous polyposis coli
ATP	Adenosine Triphosphate
AU	Arbitrary Unit
BAK	Bcl-2 Homologous Antagonist/Killer
BBB	Blood Brain Barrier
BCA	Bicinchoninic acid
BCL-2	B-cell Lymphoma Two
BET	Bromodomain and Extra-Terminal motif
BHLH	Basic Helix Leucine Helix
BPGM	Bisphosphoglycerate Mutase
BPTES	Bis-2-(5-phenylacetamido-1,3,4-thiadiazol-2-yl)ethyl Sulfide
CACT	Carnitine-acylcarnitine translocase
CBP	CREB-binding protein
CBS	Cystathionine Beta-synthase
CBTRUS	Central Brain Tumor Registry of the United States
CDK	Cyclin D Kinase
CDKI	Cyclin D Kinase Inhibitor
CNBP	CCHC-Type Zinc Finger Nucleic Acid Binding Protein
CNS	Central Nervous System
COX	Cytochrome C oxidase
CRISPR	Clustered regularly Interspaced Palindromic Repeats
CRLB	Cramer-Rao LowerBound

CRUK	Cancer Research UK
CSC	Cancer Stem-like cell
CSF	Craniospinal Fluid
CT	Computed Tomography
DLBCL	Diffuse Large B-cell Lymphoma
DMEM	Dulbecco's Minimal Essential Medium
DMSO	Dimethyl Sulfoxide
DNA	Deoxyribonucleic Acid
DV	Dorso-ventral
ECAR	Extracellular Acidification Rate
EDTA	Ethylenediaminetetraacetic Acid
EGF	Epidermal Growth Factor
EGFR	Epidermal Growth Factor Receptor
ERK	Extracellular Regulated Kinase
ETC	Electron Transport Chain
ETX	Etomoxir
FA	Fatty Acid
FAD	Flavin Adenosine Dinucleotide (Oxidised form)
FADH₂	Flavin Adenosine Dinucleotide (Reduced form)
FAO	Fatty Acid Oxidation
FAS	Fatty Acid Synthesis
FASN	Fatty Acid Synthase
FASTMAP	Fast Automatic Shimming Technique by Mapping Along Projections
FBS	Foetal Bovine Serum
FCCP	Carbonyl Cyanide-4-(trifluoromethoxy)phenylhydrazone
FDG	Fluoro-Deoxy-Glucose
FDR	False Discovery Rate
FFPE	Formalin Fixed Paraffin Embedded
FGF	Fibroblast Growth Factor
FH	Fumarate Hydratase
FID	Free Induction Decay
FLT	¹⁸ F-Fluoro-tyrosine

GABA	Gamma Aminobutyric Acid
GAC	Glutaminase C
GAP	Glyceraldehyde 3-phosphate
GBM	Glioblastoma
GEMM	Genetically Engineered Mouse
GFAP	Glial Fibrillary Acidic Protein
GLDC	Glycine Decarboxylase
GLS	Glutaminase
GLUD	Glutamate Dehydrogenase
GLUT	Glucose Transporter
GLY	Glycine
GPC	Glycerophosphocholine
GSC	Glioblastoma Stem-like cells
GSEA	Gene Set Enrichment Analysis
GSH	Glutathione
GTML	Glt1-tTA (glutamate transporter 1-tetracycline transactivator) and tetracycline response element (TRE)-MYCN/luciferase (Luc)
HAT	Histone Acetyltransferase
HCC	Hepatocellular Carcinoma
HCL	Hydrochloric acid
HDAC	Histone Deacetylase
HIF	Hypoxia Inducible Factor
HK	Hexokinase
HRMAS	High Resolution Magic Angle Spectroscopy
HRP	Horeseradish Reactive Protein
IDH	Isocitrate Dehydrogenase
KD	Knockdown
KG	Ketoglutarate
KGA	Kidney Glutaminase
LC-MS	Liquid chromatography- Mass spectrometry
LCA	Large Cell/Anaplasia
LDH	Lactate Dehydrogenase

LDHA	Lactate Dehydrogenase A
LEF	Lymphoid Enhancer Factor
LOF	Loss of Function
MAOA	Monoamine oxidase A
MAS	Magic Angle Spectroscopy
MB	Medulloblastoma
MBEN	Medulloblastoma with Extensive Nodularity
MB_{GRP3}	Group 3 Medulloblastoma
MB_{GRP4}	Group 4 Medulloblastoma
MB_{SHH}	Sonic Hedgehog Medulloblastoma
MB_{WNT}	Wingless Medulloblastoma
MCT	Monocarboxylate Transporter
MGMT	O6-Methylguanine-DNA Methyltransferase
ML	Medial-lateral
MR	Magnetic Resonance
MRI	Magnetic Resonance Imaging
MRS	Magnetic Resonance Spectroscopy
MS	Mass Spectrometry
MYC	C-MYC homologue
MYC 2	MYC targeting shRNA construct 2
MYC 3	MYC targeting shRNA construct 3
MYC_{AMP}	MYC-Amplified
MYC_{KD}	MYC-Knockdown
MYCL	L-MYC homologue
MYCN	N-MYC homologue
NAA	N-Acetylaspartate
NAD⁺	Nicotinamide adenine dinucleotide (oxidised form)
NADH	Nicotinamide adenine dinucleotide (reduced form)
NADPH	Nicotinamide adenine dinucleotide phosphate
NCBI	National Center for Biotechnology Information
NCI	National Cancer Institute
NEAA	Non-essential Amino Acid
NGS	Next Generation Sequencing

NICE	National Institute for Health and Care Excellence
NMDA	N-methyl-D-aspartate Receptor
NMR	Nuclear Magnetic Resonance
NOESY	Nuclear Overhauser Spectroscopy
NOS	Nitrogen oxide Synthase
NPC	Neural Progenitor Cell
NS	Non-Silencing shRNA
NSC	Neural Stem Cell
NSCLC	Non-small Cell Lung Cancer
NTC	Non-Targeting Construct
OCR	Oxygen Consumption Rate
OG	Oligomycin
OXPHOS	Oxidative Phosphorylation
PBS	Phosphate-Buffered Saline
PC	Principal Component
PCA	Principal Component Analysis
PCR	Polymerase Chain Reaction
PDAC	Pancreatic Ductal Adenocarcinoma
PDGFR	Platelet-derived Growth Factor
PDH	Pyruvate Dehydrogenase
PDK	Pyruvate Dehydrogenase Kinase
PDX	Patient-Derived Xenograft
PEP	Phosphoenolpyruvate
PET	Positron Emission Tomography
PFK	Phosphofructose Kinase
PHGDH	Phosphoglycerate Dehydrogenase
PIPOX	Pipecolic Acid and Sarcosine Oxidase
PK	Pyruvate Kinase
PKM	Pyruvate Kinase M
PLS-DA	Partial Least Square-Discriminant Analysis
PPP	Pentose Phosphate Pathway
PRESS	Point Resolved Spectroscopy
PSAT	Phosphoserine Aminotransferase

PSPH	Phosphoserine Phosphatase
PTEN	Phosphatase And Tensin Homolog
PTM	Post-translational Modification
RAS	RAS GTPase
RB	Retinoblastoma gene
RCC	Renal Cell Carcinoma
RLU	Relative Luminescence Unit
RNA	Ribonucleic acid
ROI	Region of Interest
ROS	Reactive Oxygen Species
RT-qPCR	Real Time- Quantitative Polymerase Chain Reaction
RTK	Receptor Tyrosine Kinase
SAM	S-adenosylmethionine
SDH	Succinate Dehydrogenase
SEMS	Spin Echo Multi-slice Sequence
SER	Serine
SGP	Serine and Glycine Synthesis Pathway
SHH	Sonic Hedgehog
SHMT	Serine Hydroxymethyltransferase
SIRM	Stable Isotope Resolved Metabolomics
SMAC	Second Mitochondria-Derived Activator Of Caspase
SNR	Signal to Noise Ratio
SRB	Sulforhodamine B
SVZ	Subventricular Zone
SWI/SNF	Switch/Sucrose Non-Fermentable
TAD	Transactivation Domain
TARQUIN	Totally Automatic Robust Quantitation in NMR
TCGA	The Cancer Genome Atlas
TERT	Telomerase Reverse Transcriptase
TET	Tetracycline
TFRC	Transferrin Receptor
THF	Tetrahydrofolate
THR	Threonine

TIC	Tumour Initiating Cell
TIGAR	TP53-Inducible Glycolysis and Apoptosis Regulator
TMA	Tissue Microarray
TMSP	Trimethylsilylpropanoic acid
TMZ	Temozolomide
TNBC	Triple Negative Breast Cancer
TRRAP	Transactivation Transcriptional Associated Protein
TXNIP	Thioredoxin Interacting Protein
TYMS	Thymidylate Synthase
UK	United Kingdom
VAPOR	Variable Power RF pulses and Optimised Relaxation Delays
VHL	Von Hippel-Lindau
VIP	Variable Important Projections
WES	Simple Western
WHO	World Health Organisation
WNT	Wingless

List of Figures

FIGURE 1.1 THE EXPANDED HALLMARKS OF CANCER.....	3
FIGURE 1.2 OVERVIEW OF GLYCOLYSIS..	5
FIGURE 1.3 THE TRICARBOXYLIC ACID CYCLE.....	10
FIGURE 1.4 OVERVIEW OF THE ELECTRON TRANSPORT CHAIN.....	12
FIGURE 1.5 SCHEMATIC OF MITOCHONDRIAL FATTY ACID B-OXIDATION.....	11
FIGURE 1.6 OVERVIEW OF SIGNALLING PATHWAYS THAT CONTRIBUTE TO THE METABOLIC REWIRING OF CANCER CELLS.	13
FIGURE 1.7 MAGNETIC RESONANCE IMAGING AND SPECTROSCOPY.	22
FIGURE 1.8 DISTRIBUTION OF FDG-PET UPTAKE IN NORMAL BRAIN.....	24
FIGURE 1.9 INCIDENCE OF CHILDHOOD CANCERS IN THE UK.....	26
FIGURE 1.10 DISTRIBUTION OF CNS AND INTRACRANIAL TUMOURS.	27
FIGURE 1.11 AGE-ASSOCIATED MALIGNANCY OF BRAIN TUMOURS.....	28
FIGURE 1.12 MOLECULAR CLASSIFICATION OF GLIOBLASTOMA.....	34
FIGURE 1.13 MEDULLOBLASTOMA TUMOUR.	38
FIGURE 1.14 HISTOLOGICAL VARIANTS OF MEDULLOBLASTOMA.....	41
FIGURE 1.15 OVERVIEW OF WINGLESS (WNT) AND SONIC HEDGEHOG (SHH) SIGNALLING CASCADES IN MEDULLOBLASTOMA.	45
FIGURE 1.16 SUMMARY OF DEMOGRAPHICS, CLINICOPATHOLOGICAL AND MOLECULAR FEATURES OF MB SUBGROUPS.....	47
FIGURE 1.17 OVERALL SURVIVAL OF MEDULLOBLASTOMA SUBGROUPS	48
FIGURE 1.18 PROTEIN STRUCTURE OF MYC.....	51
FIGURE 1.19 OVERVIEW OF MYC PATHWAY.....	54
FIGURE 1.20 MYC-DRIVEN TRANSCRIPTIONAL REGULATION OF METABOLISM.	58
FIGURE 1.22 PLEIOTROPIC EFFECTS OF MYC. MOLECULAR AND CELLULAR FEATURES CONTRIBUTING TO MYC-DRIVEN TRANSFORMATION.	61
FIGURE 2.1 SCHEMATIC OF PLKO-TET-ON INDUCIBLE SYSTEM.....	71
FIGURE 2.2 SCHEMATIC DEPICTING THE PRINCIPLES OF SIMPLE WESTERN (WES).	74
FIGURE 3.1 ILLUSTRATION OF IN VIVO STUDY TIMELINE.	96
FIGURE 3.2 MRI IMAGES OF CORONAL SLICE SECTIONS OF MOUSE BRAIN ACQUIRED USING FOUR SEMS SEQUENCES.....	97
FIGURE 3.3 COMPARISON OF TUMOUR DEVELOPMENT ACROSS DRUG TREATMENT GROUPS.	99

FIGURE 3.4 HISTOLOGICAL CONFIRMATION OF GLIOBLASTOMA BEARING MICE IDENTIFIED BY MRI.....	100
FIGURE 3.5 COMPARISON OF SURVIVAL ACROSS DRUG TREATMENT GROUPS.	101
FIGURE 3.6 SCHEME OF ROI SELECTION FROM SEMS SEQUENCE 1 MRI IMAGES.....	102
FIGURE 3.7 CONCENTRATIONS OF BRAIN METABOLITES QUANTIFIED BY TARQUIN FROM NMR SPECTRA FOR M079 (CONTROL).....	103
FIGURE 3.8 MULTIVARIATE ANALYSIS OF ¹ H NMR METABOLITE PROFILES OF DRUG TREATED ONCOGENIC NPCs.....	105
FIGURE 3.9 UNSUPERVISED PCA ANALYSIS REVEALS VARIATION IN METABOLIC PROFILES OF 3 AND 12 MONTH DERIVED MOUSE NPCs.	107
FIGURE 3.10 METABOLIC PROFILES OF DIFFERENTIALLY AGED ONCOGENIC NPCs.....	109
FIGURE 4.1 MYC-DRIVEN REPROGRAMMING OF CELLULAR METABOLISM TO FUEL RAPID CANCER CELL GROWTH.	118
FIGURE 4.2 ANALYSIS OF MYC EXPRESSION LEVELS IN RESPONSE TO DOXYCYCLINE TREATMENT IN THE D425 NS, MYC 2 AND MYC 3 CELL LINES.....	123
FIGURE 4.3 ANALYSIS OF MYC EXPRESSION LEVELS IN RESPONSE TO DOXYCYCLINE TREATMENT IN THE D283 NS, MYC 2 AND MYC 3 CELL LINES.....	124
FIGURE 4.4 ANALYSIS OF MYC EXPRESSION LEVELS IN RESPONSE TO DOXYCYCLINE TREATMENT IN THE HDMB03 NS, MYC 2 AND MYC 3 CELL LINES.....	125
FIGURE 4.5 EFFECT OF MYC KNOCKDOWN ON PROLIFERATION OF D425 MYC-INDUCIBLE CELL LINES.	126
FIGURE 4.6 EFFECT OF MYC KNOCKDOWN ON PROLIFERATION OF D283 MYC-INDUCIBLE CELL LINES.	127
FIGURE 4.7 EFFECT OF MYC KNOCKDOWN ON PROLIFERATION OF HDMB03 MYC-INDUCIBLE CELL LINES.	128
FIGURE 4.8 IMPACT OF MYC KNOCKDOWN ON CELL CYCLE DISTRIBUTION IN MB _{GRP3} MYC REGULABLE CELL LINES.	130
FIGURE 4.9 EFFECT OF MYC KNOCKDOWN ON THE GLYCOLYTIC PATHWAY IN D425 MYC INDUCIBLE CELL LINES.	132
FIGURE 4.10 EFFECT OF MYC KNOCKDOWN ON THE GLYCOLYTIC PATHWAY IN D283 MYC INDUCIBLE CELL LINES.	133
FIGURE 4.11 EFFECT OF MYC KNOCKDOWN ON THE GLYCOLYTIC PATHWAY IN HDMB03 MYC INDUCIBLE CELL LINES.....	134
FIGURE 4.12 THE RATIOS OF PHOSPHORYLATED PDH AND TOTAL PDH IN MB _{GRP3} DOXYCYCLINE INDUCIBLE CELL LINES..	137

FIGURE 4.13 EFFECT OF MYC KNOCKDOWN ON THE GLUTAMINASE EXPRESSION IN THE MB _{GRP3} CELL LINES.	139
FIGURE 4.14 IMPACT OF MYC KNOCKDOWN ON ATP PRODUCTION.....	142
FIGURE 4.15 THE EFFECT OF MYC KNOCKDOWN ON SPARE RESPIRATORY CAPACITY IN MB _{GRP3} CELLS.....	144
FIGURE 5.1 FLOWCHART OF THE ANALYSIS PIPELINE USED FOR METABOLITE PROFILES OF MYC-REGULABLE MB _{GRP3} CELL LINES	159
FIGURE 5.2 PRINCIPAL COMPONENT ANALYSIS OF METABOLIC PROFILES FROM D425 CELL LINES INDICATING VARIANCES IN SPECTRA.....	163
FIGURE 5.3 CLUSTERED HEATMAP OF SPECTRAL BINS OF D425 CELL LINES.	164
FIGURE 5.4 PRINCIPAL COMPONENT ANALYSIS OF METABOLIC PROFILES FROM D283 CELL LINES INDICATING VARIANCES IN SPECTRA.....	165
FIGURE 5.5 CLUSTERED HEATMAP OF SPECTRAL BINS OF D283 CELL LINES.	167
FIGURE 5.6 PRINCIPAL COMPONENT ANALYSIS OF METABOLIC PROFILES FROM HDMB03 CELL LINES INDICATING VARIANCES IN SPECTRA..	168
FIGURE 5.7 CLUSTERED HEATMAP OF SPECTRAL BINS OF HDMB03 CELL LINES.....	169
FIGURE 5.8 POOLED MULTIVARIATE ANALYSIS OF MB _{GRP3} NS CELL LINES METABOLITE PROFILES.	172
FIGURE 5.9 POOLED MULTIVARIATE ANALYSIS OF MB _{GRP3} MYC 2 CELL LINES METABOLITE PROFILES.	173
FIGURE 5.10 POOLED MULTIVARIATE ANALYSIS OF MB _{GRP3} MYC 3 CELL LINES METABOLITE PROFILES.	174
FIGURE 5.11 CLUSTERED HEATMAP OF SPECTRAL BINS OF MB _{GRP3} MYC INDUCIBLE CELL LINES.....	177
FIGURE 5.12 SIGNIFICANTLY ALTERED SPECTRAL FEATURES IN MB _{GRP3} CELL LINES.....	178
FIGURE 5.13 METABOLITE PROFILES OF D425 CELL LINES FOLLOWING MYC KNOCKDOWN.	180
FIGURE 5.14 METABOLITE PROFILES OF D283 CELL LINES FOLLOWING MYC KNOCKDOWN.	181
FIGURE 5.15 METABOLITE PROFILES OF HDMB03 CELL LINES FOLLOWING MYC KNOCKDOWN.....	182
FIGURE 5.16 DISCRIMINANT METABOLITES IN THE POOLED MB _{GRP3} MYC 2 (ON) COMPARED TO MYC 2 (OFF) CELLS.	184
FIGURE 5.17 TOP 3 DISCRIMINANT METABOLITES IN THE POOLED MB _{GRP3} MYC 2 CELL LINES.....	185

FIGURE 5.18 DISCRIMINANT METABOLITES IN THE POOLED MB _{GRP3} MYC 3 (ON) COMPARED TO MYC 3 (OFF) CELLS.	186
FIGURE 5.19 TOP 3 DISCRIMINANT METABOLITES IN THE POOLED MB _{GRP3} MYC 3 CELL LINES.....	187
FIGURE 5.20 DISCRIMINANT METABOLITES IN THE POOLED MB _{GRP3} NS (ON) COMPARED TO NS DOX CTRL (ON) CELLS.....	188
FIGURE 5.21 TOP 3 DISCRIMINANT METABOLITES IN THE POOLED MB _{GRP3} NS CELL LINES.. ..	189
FIGURE 5.22 VENN DIAGRAM OF COMMON DISCRIMINANT METABOLITES BETWEEN THE MYC 2 HARBOURING CELL LINES FOLLOWING MYC KNOCKDOWN.....	191
FIGURE 5.23 VENN DIAGRAM OF COMMON DISCRIMINANT METABOLITES BETWEEN THE MYC 3 HARBOURING CELL LINES FOLLOWING MYC KNOCKDOWN.....	191
FIGURE 5.24 SCHEMATIC OF ISOTOPOLOGUES FOLLOWING ¹³ C -GLUCOSE LABELLING IN GLYCOLYSIS AND DE NOVO SERINE AND GLYCINE SYNTHESIS PATHWAY. ...	194
FIGURE 5.25 EFFECT OF MYC KNOCKDOWN ON THE ¹³ C -GLUCOSE LABELLING PATTERNS OF THE DE NOVO SERINE AND GLYCINE SYNTHESIS PATHWAYS.....	195
FIGURE 5.26 TIME COURSE ON FULLY LABELLED SERINE RELATED METABOLITES IN D425 MYC 2 CELL LINES.	199
FIGURE 5.27 SCHEMATIC OF SIMPLIFIED ONE CARBON METABOLISM.	201
FIGURE 6.1 GENE EXPRESSION PROFILING OF THE SERINE AND GLYCINE METABOLISM IN THE CAVALLI ET AL., MB _{GRP3} DATASET.	216
FIGURE 6.2 GENE EXPRESSION PROFILING OF SERINE AND GLYCINE METABOLISM-ASSOCIATED GENES IN MYC-AMPLIFIED AND NON-AMPLIFIED MB _{GRP3} PATIENTS IN THE NEWCASTLE DATASET.....	217
FIGURE 6.4 COMPARISON OF PHGDH EXPRESSION IN CEREBELLUM AND MEDULLOBLASTOMA TUMOUR SAMPLES.	220
FIGURE 6.5 IMMUNOHISTOCHEMICAL STAINING OF PHGDH ACROSS PRIMARY MEDULLOBLASTOMA PATIENT SAMPLES.....	221
FIGURE 6.6 EXPRESSION OF PHGDH ACROSS MEDULLOBLASTOMA SUBGROUPS.....	222
FIGURE 6.7 DISTRIBUTION OF PHGDH INTENSITY SCORES ACROSS MEDULLOBLASTOMA SUBGROUPS.	223
FIGURE 6.8 EXPRESSION OF PHGDH OF MYC-AMPLIFIED VERSUS NON-AMPLIFIED MB _{GRP3} . SIGNIFICANCE WAS DETERMINED USING T TEST.	224
FIGURE 6.9 EXPRESSION OF PHGDH OF MYCN-AMPLIFIED VERSUS NON-AMPLIFIED MB _{SHH} TUMOUR SAMPLES.....	226

FIGURE 6.10 EXPRESSION OF PHGDH OF MYCN-AMPLIFIED VERSUS NON-AMPLIFIED MBGRP4 TUMOUR SAMPLES.	227
FIGURE 6.11 KAPLAN MEIER SURVIVAL ANALYSIS OF PHGDH EXPRESSION IN THE TMA MEDULLOBLASTOMA WIDE COHORT.....	228
FIGURE 6.12 FOREST PLOTS OF COX PROPORTIONAL HAZARD MODELS FOR THE TMA COHORT ASSESSING PHGDH EXPRESSION AND OTHER CLINICOPATHOLOGICAL PARAMETERS.....	229
FIGURE 6.13 KAPLAN MEIER SURVIVAL ANALYSIS OF PHGDH EXPRESSION IN MB _{GRP3} TUMOURS.	230
FIGURE 6.14 EXAMINING PROTEIN EXPRESSION OF THE DE NOVO SERINE AND GLYCINE PATHWAY IN D425 MYC-REGULABLE CELL LINES.	232
FIGURE 6.15 EXAMINING PROTEIN EXPRESSION OF THE DE NOVO SERINE AND GLYCINE PATHWAY IN D425 MYC-REGULABLE CELL LINES.	233
FIGURE 6.16 EXAMINING PROTEIN EXPRESSION OF THE DE NOVO SERINE AND GLYCINE PATHWAY IN D425 MYC-REGULABLE CELL LINES.	234
FIGURE 6.17 RESPONSE OF MYC-REGULABLE MB _{GRP3} ISOGENIC CELLS TO NCT503 TREATMENT.....	237
FIGURE 6.18 PROTEIN EXPRESSION OF MYC ACROSS PARENTAL MB CELL LINES.	238
FIGURE 6.19 PROTEIN EXPRESSION OF THE DE NOVO SERINE AND GLYCINE ENZYMES IN PARENTAL MB CELL LINES.	239
FIGURE 6.20 RELATIONSHIP BETWEEN MYC EXPRESSION AND DE NOVO SERINE AND GLYCINE PATHWAY IN MEDULLOBLASTOMA CELL LINES.....	240
FIGURE 6.21 PHARMACOLOGICAL INHIBITION OF PHGDH IN MEDULLOBLASTOMA CELL LINES.	242
FIGURE 6.22 EFFECT OF NCT503 ON CLONOGENIC SURVIVAL IN MYC-AMPLIFIED MB _{GRP3} PARENTAL CELLS.	244
FIGURE 6.23 EFFECT OF CBR5884 ON CLONOGENIC SURVIVAL IN MYC-AMPLIFIED MB _{GRP3} PARENTAL CELLS.	245
FIGURE 6.24 EFFECT OF NCT503 ON CLONOGENIC SURVIVAL IN D425 MYC 2 CELLS.	247
FIGURE 6.25 EFFECT OF NCT503 ON CELL CYCLE PROGRESSION IN MYC-AMPLIFIED MB _{GRP3} PARENTAL CELLS.	249
FIGURE 6.26 EFFECT OF NCT503 ON MITOCHONDRIAL FUNCTION IN MYC-AMPLIFIED MB _{GRP3} PARENTAL CELL LINES.....	251
FIGURE 6.27 EFFECT OF NCT503 ON GLYCOLYTIC AND OXPHOS DEPENDENT ATP PRODUCTION IN MYC-AMPLIFIED MB _{GRP3} PARENTAL CELL LINES.	252

FIGURE 6.28 IMPACT OF NCT503 TREATMENT ON mTOR SIGNALLING IN MYC-AMPLIFIED MB _{GRP3} PARENTAL CELL LINES.....	255
FIGURE 6.29 QUANTITATIVE ANALYSIS OF THE mTOR PATHWAY IN MYC-AMPLIFIED MB _{GRP3} PARENTAL CELL LINES.....	256
FIGURE 6.30 IMPACT OF NCT503 ON mTOR SIGNALLING PATHWAY IN D425 MYC 2 ISOGENIC CELLS.....	257
FIGURE 6.31 PHGDH EXPRESSION IN MB _{GRP3} CELLS FOLLOWING CRISPR MEDIATED KNOCKDOWN OF PHGDH.....	259
FIGURE 6.32 CONSEQUENCE OF PHGDH LOSS ON PROLIFERATION OF MB _{GRP3} MYC-AMPLIFIED CELLS.....	261
FIGURE 6.33 RESPONSE OF D425 CELLS TO SERINE AND GLYCINE DEPLETED CONDITIONS. INCUCYTE LIVE CELL IMAGING ANALYSIS.....	263
FIGURE 6.34 RESPONSE OF D458 CELLS TO SERINE AND GLYCINE DEPLETED CONDITIONS. INCUCYTE LIVE CELL IMAGING ANALYSIS.....	264
FIGURE 6.35 RESPONSE OF HDMB03 CELLS TO SERINE AND GLYCINE DEPLETED CONDITIONS.....	265
FIGURE 6.36 EFFECT ON SERINE AND GLYCINE DEPRIVATION ON CLONOGENIC SURVIVAL OF MB _{GRP3} MYC-AMPLIFIED CELLS FOLLOWING PHGDH KNOCKDOWN.....	267
FIGURE 7.1 NOVEL TREATMENT STRATEGY FOR TARGETING GLIOBLASTOMA.....	277
FIGURE 7.2 SUMMARY OF DRUG STRATEGY FOR MYC-AMPLIFIED MB _{GRP3}	281

List of Tables

TABLE 1.1 LIST OF METABOLIC INHIBITORS UNDER CLINICAL INVESTIGATION.	16
TABLE 1.2 LIST OF GLYCOLYTIC TARGETS AND INHIBITORS.	17
TABLE 1.3 THE WHO CLASSIFICATION OF GLIOBLASTOMA AND CLINICOPATHOLOGICAL CHARACTERISTICS	35
TABLE 1.4 STAGING OF METASTATIC DISEASE BY CHANG ET AL., 1969	39
TABLE 1.5 PROGNOSTIC BIOMARKERS AND CLINICOPATHOLOGICAL FEATURES OF MB..	42
TABLE 1.6 THE WHO CLASSIFICATION OF MEDULLOBLASTOMA.	43
TABLE 2.1 ONCOGENIC NPCs AND GBM INITIATING CELLS USED IN THIS THESIS.....	66
TABLE 2.2 TARGET SEQUENCES FOR SHRNA CONSTRUCTS	71
TABLE 2.3 MYC-INDUCIBLE CELL LINES USED IN THIS THESIS	72
TABLE 2.4 LIST OF ANTIBODIES USED IN THIS THESIS	75
TABLE 2.5 PREPARATION OF CELL CYCLE ANALYSIS REAGENTS	76
TABLE 2.6 LIST OF PARENTAL MEDULLOBLASTOMA USED IN THIS STUDY.	84
TABLE 2.7 COMPOSITION OF SOLUTION A FOR TRANSFECTION	85
TABLE 2.8 MEDIA COMPOSITION FOR SERINE AND GLYCINE DEPRIVATION EXPERIMENTS	87
TABLE 4.1 LOG ₂ (FOLD CHANGE) OF METABOLIC ENZYME FOLLOWING MYC KNOCKDOWN IN MBGRP3 CELLS.....	135
TABLE 4.2 SUMMARY OF MYC-DEPENDENT PHENOTYPIC ALTERATIONS IN MB _{GRP3} MYC ISOGENIC CELL LINES.. ..	146
TABLE 5.1 MEAN DIFFERENCES IN UNLABELLED AND ¹³ C LABELLED METABOLITES IN THE D425 MYC 2 (ON) AND MYC 2 (OFF) CELLS.	196
TABLE 6.1 CLINICOPATHOLOGICAL FEATURES OF TMA COHORT.....	219
TABLE 6.2 TABLE OF IC ₅₀ VALUES FOR NCT503 AND CBR5884 FOLLOWING 72 H EXPOSURE IN MEDULLOBLASTOMA CELL LINES.. ..	243
TABLE 6.3 CELL CYCLE ANALYSIS IN MBGRP3 CELLS TREATED WITH NCT503	249

Chapter 1 Introduction

1.1 Overview of altered metabolism in cancer

Cancer is a disease driven by the acquisition of specific traits that enable tumour formation and these are commonly referred to as hallmarks of cancer. Hanahan and Weinberg described these in their seminal paper, highlighting features of cancer which distinguished them from normal untransformed cells (Figure 1.1). Specifically they described traits which include sustaining proliferative signalling, acquiring replicative immortality, evading growth suppressors, activation of angiogenesis, invasion and metastasis as the defining characteristics of cancer cells (Hanahan and Weinberg, 2000). Although altered metabolism had been previously described by Otto Warburg, even prior to the description of oncogenes, the recognition of metabolic rewiring of cancer cells was established much later (Hanahan and Weinberg, 2011). The principles of cancer metabolism are grounded on the altered metabolic requirements of cancer cells compared to normal cells which act to support the malignant phenotype associated with uncontrolled division and maintenance of a hyper-proliferative state even under limiting conditions. Much like the reporting of frequently deregulated oncogenes and tumour suppressors in cancer, certain metabolic alterations are frequently observed in cancer. The best described metabolic phenotype, the Warburg effect is determined by increased glycolytic flux and excessive lactate production under normoxia and is frequently observed in many cancer cells (Heiden et al., 2009).

The altered metabolic activities of cancer enables growth and proliferation during nutrient abundance, but more importantly it ensures survival during stress inducing conditions and periods of nutrient insufficiency (DeBerardinis et al., 2008). These adaptations enable plasticity and ensures selective advantage in a harsh tumour microenvironment (DeBerardinis et al., 2008). Furthermore, metabolic reprogramming can facilitate the dissemination of tumour cells to distant sites from primary tumours and support invasion and metastasis (Lee et al., 2019, Lehuédé et al., 2016). Cancer cells must also ensure redox homeostasis and avoid oxidative stress which could be detrimental. From these various altered metabolic pathways and states, several opportunities arise for cancer biomarker discovery, non-invasive imaging and therapeutic targeting. Cancers are highly heterogeneous owing to a diverse range of genetic abnormalities in oncogenes and tumour suppressors, although the metabolic pathways that drive bioenergetic, redox reactions and support macromolecular synthesis are finite. Interestingly this leads to commonalities in metabolic adaptations reported.

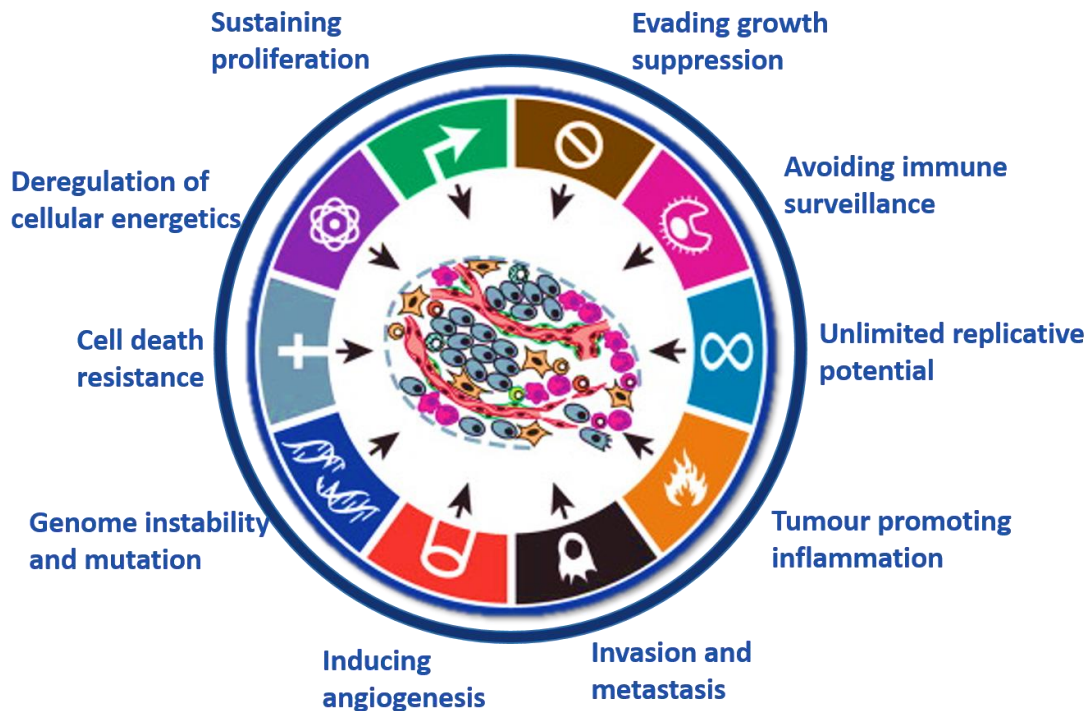


Figure 1.1 The expanded hallmarks of cancer. Adapted from (Hanahan and Weinberg, 2011).

1.1.1 Glycolysis

Glycolysis is a multistep process which involves the breakdown of glucose into two molecules of pyruvate for usage in downstream pathways (Figure 1.2). Glucose uptake from the extracellular milieu is facilitated by plasma membrane proteins known as glucose transporters (GLUT/SLC2A family) of which there are several isoforms with tissue specific localisation. GLUT1 (brain-specific) and GLUT4 (skeletal muscle) remain the best characterised. The first initial step of glucose catabolism is catalysed by hexokinase (HK) which phosphorylates glucose resulting in the formation of glucose 6-phosphate (G6P). The addition of the phosphoryl moiety is an ATP consuming process however, it crucially reduces glucose permeability and traps it within the cell (Bar-Even et al., 2012). Isomerisation of G6P leads to the formation of fructose 6-phosphate (F6P) facilitated by phospho-glucose isomerase (PGI). The activity of phospho-fructose kinase 1 (PFK1), forms the second phosphorylation and ATP consuming reaction of glycolysis where F6P is converted to fructose 1, 6-bisphosphate (F 1, 6 BP). The activity of PFK1 regulates the glycolytic rate and is allosterically activated by the product of its isozyme PFK2 which produces fructose 2, 6 bisphosphate (F 2, 6BP) balancing glycolysis and

gluconeogenesis (Ros and Schulze, 2013). Aldol cleavage of F1, 6 BP by aldolase generates glyceraldehyde 3-phosphate (GAP) and dihydroxyacetone phosphate (DHAP). The early events of glycolysis are commonly described as the preparatory phase and summarise the reactions involving six carbon units. DHAP can undergo isomerisation catalysed by triosephosphate isomerase (TPI) forming a second molecule of GAP which is subsequently utilised in a series of reactions termed the “pay off” phase (Bar-Even et al., 2012, Tanner et al., 2018).

The oxidation of GAP is catalysed by GAP dehydrogenase (GAPDH) coupled to reduction of nicotinamide adenine dinucleotide (NAD⁺) generating glycerate 1, 3 biphosphate (1,3GBP). Substrate-level phosphorylation generated from 1,3GBP to form 3-phosphoglycerate (3PG) initiates the first ATP generating step of glycolysis by phosphoglycerate kinase (PGK). 3PG is subsequently converted to 2-phosphoglycerate (2PG) by phosphoglycerate mutase (PGM). The activity of enolase generates phosphoenolpyruvate (PEP) from 2PG which can then be phosphorylated by pyruvate kinase (PK) producing another molecule of ATP and ultimately forming pyruvate. The net ATP gain from glycolysis is 2 ATP molecules since 2 ATP molecules are consumed in the preparatory phase and a total of 4 ATP molecules are generated from the two molecules of GAP produced (Bar-Even et al., 2012). The fate of pyruvate is numerous and is dependent on physiological conditions that are highly regulated by energetic demand and oxygen availability (Gray et al., 2014). Under normal physiological conditions, undifferentiated cells will convert pyruvate to acetyl-CoA which is tightly regulated by pyruvate dehydrogenase (PDH) for complete oxidation in the tricarboxylic cycle (TCA). In periods of reduced oxygen concentrations, pyruvate can be reduced to lactate by lactate dehydrogenase (LDH). Cancer cells function outside these physiological fate determinations by continually undergoing glycolysis even when oxygen is abundant (Warburg, 1956).

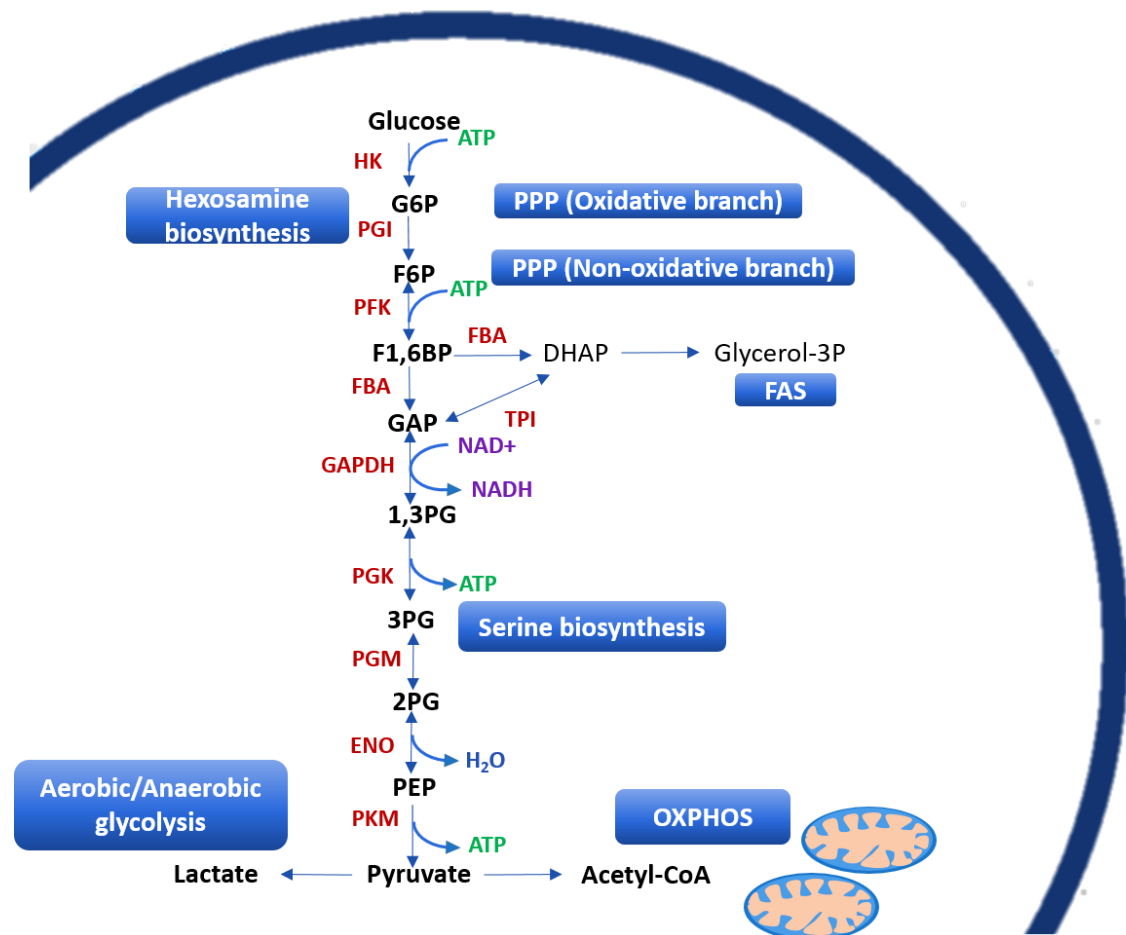


Figure 1.2 Overview of glycolysis. Depending on oxygen availability, cells will catabolise glucose to pyruvate and then pyruvate to acetyl-CoA which subsequently enters the TCA cycle and generating substrates required to drive oxidative phosphorylation (OXPHOS). In periods of oxygen scarcity, glucose is metabolised to lactate (fermentation). Cancer cells can undergo 'aerobic glycolysis' producing lactate when oxygen is abundant.

1.1.1.1 Warburg effect

The Warburg effect describes a phenomenon where cancer cells under sufficient oxygen concentrations preferentially undergo glycolysis instead of glucose oxidation in the mitochondria (Heiden et al., 2009). Initial hypotheses suggested that cancer cells had deficient mitochondria and thus utilised the less energy efficient pathway of aerobic glycolysis to fulfil ATP demands. This theory has since been proven incorrect as several studies have highlighted the retention of mitochondrial function and structural integrity in several tumours. In fact, some tumours are more oxidative and do not exhibit this glycolytic phenotype (Ashton et al., 2018, Viale et al., 2014). Nonetheless, this upregulation of glucose uptake and catabolism led to the advent of FDG-PET usage to monitor tumour progression, staging and treatment response in clinical settings (Almuhaideb et al., 2011, Som et al., 1980)

Constitutive uptake of glucose is not observed in untransformed cells due to a reliance on growth factor stimulation and matrix attachment which bind them to these extracellular cues (Palm and Thompson, 2017). Cancer cells can undergo anchorage independent growth and are not regulated by typical growth factor signalling. Instead, oncogenic alterations drive proliferation and eliminate dependence on extracellular stimuli (Yuan and Cantley, 2008). Deregulation of the P13K/AKT/mTOR signalling axis is implicated in the increased uptake and consumption of glucose in tumours (Menon and Manning, 2008, Wieman et al., 2007). Additionally, loss of inhibition resulting from loss of function (LOF) mutations occurring in negative regulators such as PTEN further potentiate aberrant glucose metabolism (Blouin et al., 2010, Morani et al., 2014). PI3K and its downstream effector Akt promote expression of GLUT1 and increase activity of HK. Furthermore, expression of PFK which catalyses the irreversible and committing step of glycolysis is also upregulated (Menon and Manning, 2008). RAS-driven tumours have reportedly high consumption of glucose owing to oncogenic activity of RAS which promotes expression of glucose transporters (White, 2013, Ying et al., 2012).

The alterations in metabolic pathways are thought to provide a selective advantage for growing cancer cells. Tumourigenic cells must meet the increased energetic demands required to sustain rapid proliferation (Heiden et al., 2009). The phenotypic adaptation of increased aerobic glycolysis at glance seems counterproductive and energy inefficient. Comparatively, OXPHOS generates 36 molecules of ATP from the complete oxidation of glucose however aerobic glycolysis provides a net gain of 2 ATP molecules. The OXPHOS genes are highly conserved in eukaryotes and subject to tight regulation (Rolfe and Brown, 1997). Glycolysis, however, is a much simpler pathway and has faster turnover for ATP compared to OXPHOS. It is now increasingly recognised that ATP is not a limiting factor for proliferating cancer cells but really it is the requirement for biosynthetic precursor assimilation into biomass that is critical in sustaining the aberrant growth observed (DeBerardinis and Chandel, 2016). The glycolytic pathway and its several branches which shuttle glycolytic intermediates for generating nucleotides, NADPH and other macromolecules, are what seemingly provides a growth advantage and fuel tumourigenesis.

1.1.1.2 Fulfilling biosynthetic requirements

The metabolic requirements of proliferating cancer cells differ tremendously to quiescent cells although it is noteworthy that the tumour bulk is defined by diverse populations, such as slow cycling stem-like cells and actively proliferating cells which have varied

metabolic requirements. Proliferating cells convert metabolic fuels such as glucose and glutamine, utilising carbon units from these sources to generate biomass to support continued cell cycle progression and ultimately producing daughter cells (Lee and Finkel, 2013). Biosynthetic reactions not only require carbon backbones, but are also reductive thus requiring large quantities of reducing species in the form of NADPH. The glycolytic pathway shunts intermediates into various biosynthetic pathways and provides a remarkable source of precursors for these reactions.

The intermediate G6P can be shunted into the oxidative branch of the PPP to generate ribose 5-phosphate which forms the sugar backbone of nucleic acids. DHAP can be utilised for the synthesis of glycerol 3-phosphate which contributes to phospholipid biosynthesis which in turn can aid membrane turnover which is important for growing tumour cells (Lin et al., 2015, Patra and Hay, 2014).

Remarkably, studies have shown that as much as 50% of glucose carbons enter the *de novo* serine and glycine pathway through the activity of phosphoglycerate dehydrogenase (PHGDH) which sequesters 3PG into this branch (Locasale et al., 2011). Focal amplification and overexpression of PHGDH is reported in melanoma and ER-negative breast cancers, leading to excessive production of non-essential AAs (NEAA) serine and glycine (Locasale et al., 2011, Possemato et al., 2011). Serine is a major contributor to one carbon metabolism and folate pools. The activity of two differentially localised serine hydroxymethyltransferases (SHMT) generate 5, 10 methylene-tetrahydrofolate, which undergoes a series of cyclical oxidation-reduction reactions, generating one-carbon THF species (Garrow et al., 1993, Tedeschi et al., 2013). These in turn are utilised in purine and thymidine biosynthesis in addition to S-adenosyl- methionine (SAM) which is the major substrate of methylation reactions (Ducker and Rabinowitz, 2017, Appling, 1991). Furthermore, the activity of the folate cycle generates a significant proportion of cellular NADPH, supporting biosynthesis (Fan et al., 2014). The enzyme methylene tetrahydrofolate dehydrogenase 2 (MTHFD2), involved in the mitochondrial branch of folate cycle, is frequently overexpressed in cancer, underscoring the importance of this pathway in tumourigenesis (Nilsson et al., 2014).

Additionally, glycolytic intermediates can also be utilised for post-translational modifications (PTM) of proteins. For instance, F6P coupled with glutamine may be utilised for hexosamine synthesis. The production of N-acetylglucosamine (GlcNac) supports glycosylation of proteins like *MYC* and increases protein stability (Makwana et al., 2019).

1.1.2 The tricarboxylic acid cycle

The TCA cycle is commonly referred to as the Krebs cycle, after the pioneering work of Hans Krebs in discovering the cyclical oxidation-reduction reactions responsible for oxidising acetyl groups (supplied by acetyl-CoA) to carbon dioxide in mitochondria (Krebs, 1940). The TCA is a hub of cellular metabolism integrating and transforming carbons supplied by metabolic fuels into ATP. It is also an important generator of biosynthetic intermediates which form the building blocks for amino acids, nucleotides and fatty acid synthesis (Berg *et al.*, 2002).

Acetyl-CoA enters the TCA and is condensed with oxaloacetate generating citrate. Citrate undergoes isomerisation to isocitrate which subsequently undergoes oxidative decarboxylation yielding α -ketoglutarate. Further oxidative decarboxylation reactions give rise to succinate which fuels the regeneration of oxaloacetate ensuring constant cycling and functioning of TCA cycle (illustrated in Figure 1.3). The TCA itself does not generate ATP but it accepts electrons from acetyl units and the hydrides (H^-) generated from these reactions are transferred and form two molecules of reduced NAD (NADH) and one molecule of reduced flavin adenine dinucleotide ($FADH_2$) which are utilised by the respiratory chain complexes to drive oxidative phosphorylation which generates a significant proportion of ATP.

Amino acids contribute to a wide range of cellular processes and are huge sources of carbon and nitrogen. The standard 20 amino acids (AA) provide building blocks for the synthesis of proteins, nucleotides, lipids, glutathione (GSH), and importantly also support TCA anaplerosis. The reliance on individual AAs is highly tissue-dependent and is driven by micro-environmental cues and as such is highly flexible. For example, glutamine is the most abundant AA in serum and plays a critical role in supporting TCA function. The TCA cycle can supply intermediates for macromolecule synthesis. For instance, citrate is shuttled into the cytoplasm where it can be utilised for FA synthesis (Rohrig and Schulze, 2016).

In order to prevent the TCA cycle functioning as a 'carbon sink', carbons removed must be replenished to ensure continual cycling. Pyruvate carboxylation to oxaloacetate in the mitochondria is the archetypical anaplerotic source. Glutamine also replenishes the TCA cycle through its conversion to glutamate and subsequently to α -ketoglutarate by glutaminase (GLS) and glutamate dehydrogenase (GLUD) respectively (Yang et al., 2017). Excessive glutamine consumption from exogenous sources is associated with rapidly proliferating cancer cells. Glutamine does not only support TCA anaplerosis, it also supports protein synthesis by providing carbon backbones. Importantly, amide nitrogen from glutamine can be utilised for purine and pyrimidine synthesis (Cory and Cory, 2006). Glutamine also supports the generation of glutathione (GSH), a tripeptide composed of glutamate, cysteine and glycine. The generation of glutamate from glutamine supports AA synthesis. For instance, PSAT1 converts phosphohydroxypyruvate to phosphoserine and generates α -ketoglutarate (α -KG) from glutamate as a by-product which can be supplied to the TCA cycle. The branched chain amino acids (BCAAs) are essential AAs which can also be utilised in energy metabolism. Particularly the catabolism of BCAAs into their equivalent ketoacids can undergo oxidative decarboxylation generating acyl-CoA by-products which can also enter the TCA cycle (Monirujjaman and Ferdouse 2014). Generally, AAs play an important physiological role in providing proteinogenic and ketogenic substrates and supporting TCA functions in a tissue-specific manner. In cancer cells, their importance is underscored by increased expression of AA transporters and their consumption.

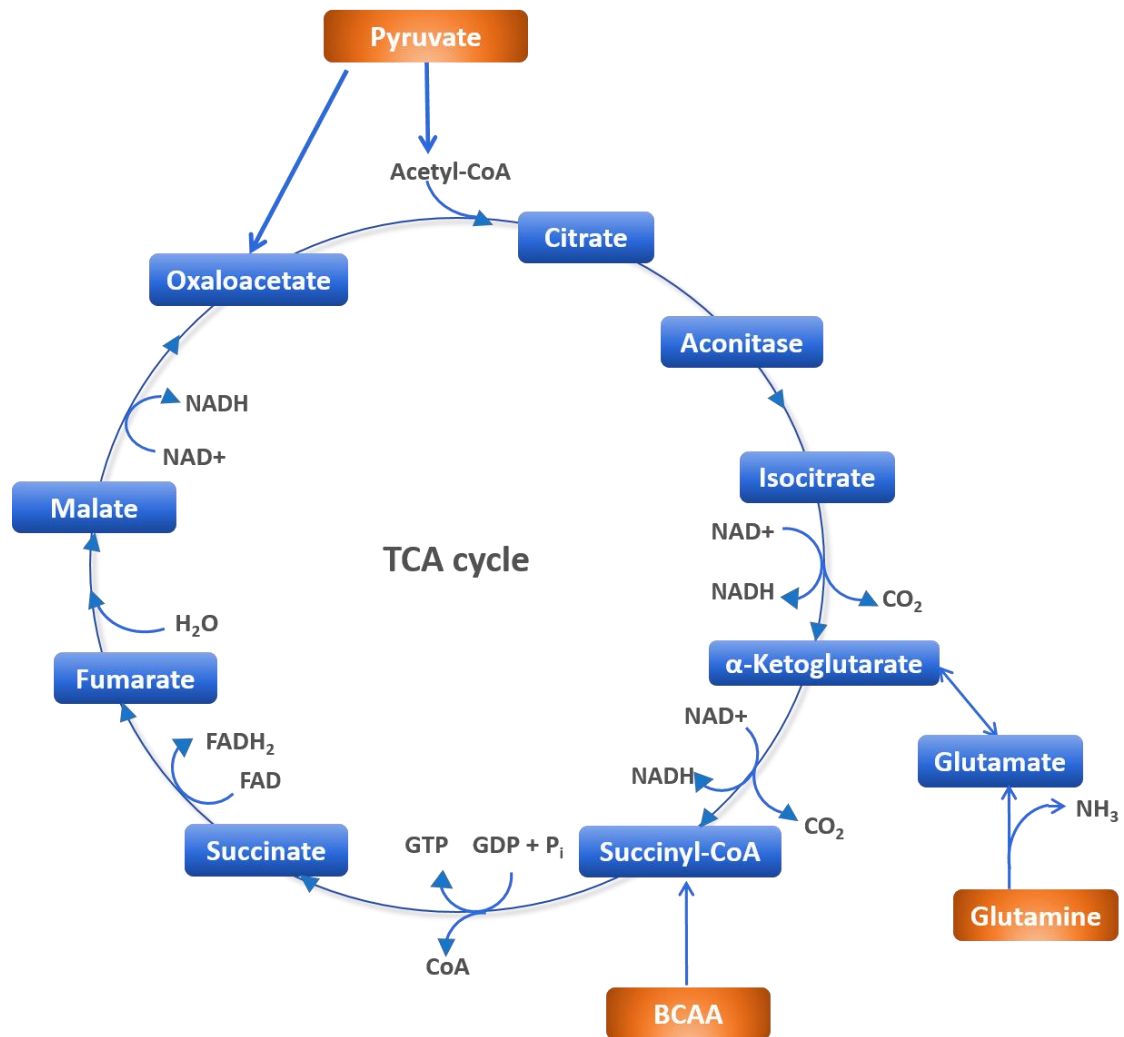


Figure 1.3 The tricarboxylic acid cycle. Overview of cyclical reactions of TCA cycle generating reducing agents NADH and FADH₂ which are subsequently utilised by the respiratory chain complexes. Metabolites highlighted in orange fulfill TCA anaplerosis.

1.1.3 Electron transport chain

The mammalian respiratory chain involves protein complexes situated on the inner mitochondrial membrane which act as electron carriers. The movement of electrons from one complex to the next generates proton motive force that drives F₁F₀ ATPase (Figure 1.4). The transport of electrons has two entry ports. Firstly, via Complex I (NADH-ubiquinone oxidoreductase) which is the entry point for electrons donated by NADH. Coenzyme Q, also termed ubiquinone, carries electrons from complex I to complex III. Complex II (succinate quinone oxidoreductase) can additionally receive electrons derived from TCA intermediate, succinate, which acts as an electron donor to FAD. The transfer of electron to coenzyme Q in this system does not amount to significant increases in free energy so is not coupled to ATP synthesis at this stage. FADH₂ derived electrons only

yield free energy at complex III and IV. Complex III and complex IV (cytochrome c oxidase) use cytochrome c to reduce oxygen which is the final electron acceptor in oxidative phosphorylation (OXPHOS) (Lodish H, 2000). In contrast to glycolysis, mitochondrial OXPHOS is an immense energetic source generating 36 ATP per mole of glucose that is catabolised.

Whilst OXPHOS has an immense capacity for generating ATP, it also generates by-products which could be detrimental to the expansion of rapidly proliferating cancer cells. Cancer cells must have sufficient antioxidant capacity to avoid oxidative stress caused by toxic by-products of metabolism. The main reactive oxygen species (ROS) by-products are hydrogen peroxide (H_2O_2), superoxide (O_2^-) and the hydroxyl radical (OH^\cdot). Superoxide accounts for the majority of ROS produced in the mitochondria through activity of ETC complexes (Murphy, 2009). To ensure survival, cancer cells must carefully balance generation of ROS, which in small quantities can induce positive cellular alterations supporting growth, with ROS elimination which avoids catastrophic build-up potentially leading to cell death (Martindale and Holbrook, 2002, Ranjan et al., 2006). In fact, low level ROS promotes modification of PKM2, inhibiting its activity which in turn causes a build-up of glycolytic intermediates upstream, which is shunted into the PPP producing NADPH (Anastasiou et al., 2011). NADPH is utilised for the reduction of GSH ensuring adequate antioxidant capacity (Moreno-Sánchez et al., 2018).

Overexpression of pathways generating GSH and other ROS scavengers such as peroxiredoxins is observed in cancer. Additionally the increase of ROS scavengers promotes resistance to DNA damage-inducing ionising radiation (Gorrini et al., 2013, Diehn et al., 2009). Increasing antioxidant capacity circumvents ROS-induced damage and maintains genomic integrity. It seems that ROS possess a significant risk to cellular health even in cancers; effectively targeting reliance on ROS scavenging pathways could provide opportunities for therapeutic targeting.

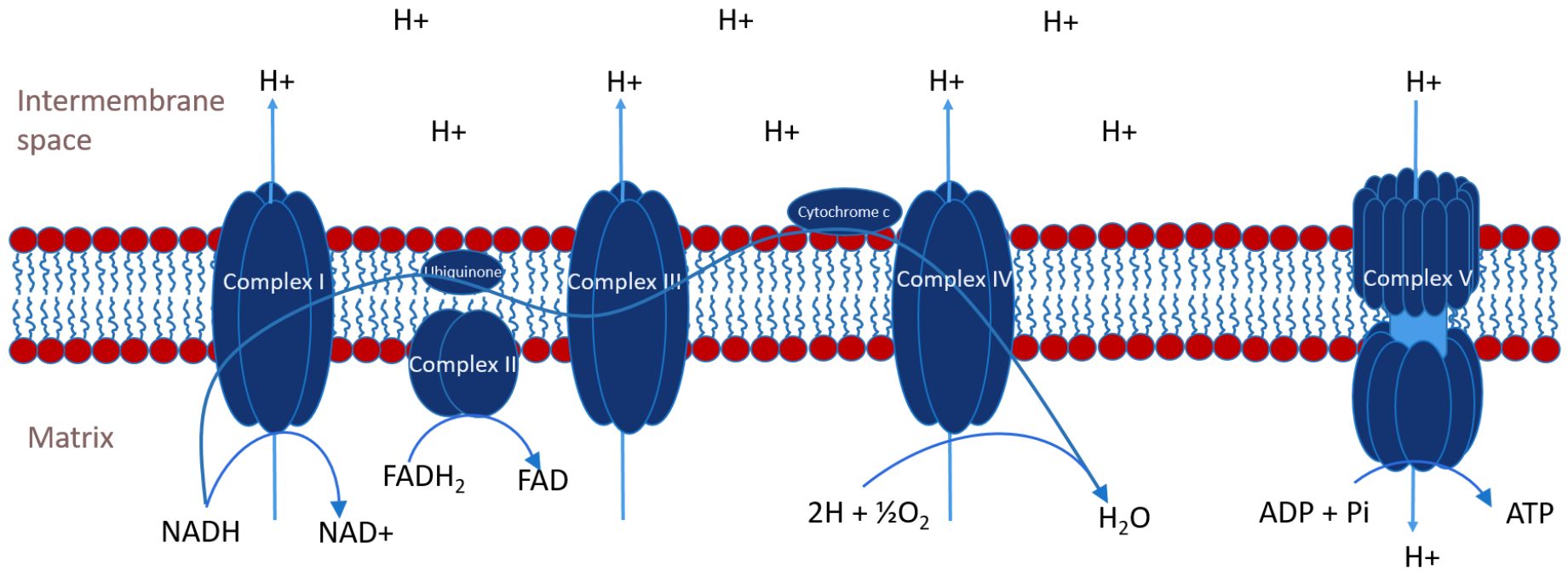


Figure 1.4 Overview of the electron transport chain. The ETC involves large protein complexes embedded in the inner mitochondrial membrane serving as electron transport transporters shuttling electrons from TCA generated NADH and FADH₂ to oxygen. Protons are pumped from the mitondrial matrix to the intermmembrane space. The generation of proton motive force is used to generate ATP.

1.1.4 Fatty acid β -oxidation

Fatty acids (FA) encompass a diverse range of metabolites with different chain lengths and number/positioning of carbon double bonds. They have a diverse role contributing to substrates required for membrane structure and dynamics and also playing a vital role in signal transduction (Menendez and Lupu, 2007). They can be sequestered into cytoplasmic organelles called lipid droplets which act as a reservoir of lipids which may be utilised to fulfil cellular requirements for FAs (Cabodevilla et al., 2013, Rambold et al., 2015, Welte, 2015). Furthermore, FAs can act as metabolic fuel substrates where their degradation through the fatty acid β -oxidation (FAO) pathway provides a significant supply of ATP and cofactors (Houten and Wanders, 2010).

Carnitine palmitoyl transferase shuttle

Acyl-CoAs within the cytoplasm are impermeable to the outer mitochondrial membrane. Entry of acyl-CoAs commits them to lysis, hence entry into mitochondria is a critical regulatory checkpoint and a major determinant of FAO. Carnitine palmitoyl transferase 1 (CPT1) sits on the outer mitochondrial membrane facing the cytoplasm where it catalyses the reaction converting acyl-CoAs into acylcarnitines. Inside the mitochondria, carnitine-acylcarnitine translocase (CACT) exchanges acylcarnitines for carnitines, ensuring relatively stable levels of carnitine in the cytosol to mitochondria. Carnitine palmitoyl transferase 2 (CPT2) sits on the inner mitochondrial membrane and is responsible for the reconversion of acylcarnitine to acyl-CoA which can then be catabolised (Figure 1.5).

There exist three isoforms of the CPT1 enzyme, CPT1A, CPT1B and CPT1C, which show tissue-specific expression. CPT1A is the more widely expressed isoform whereas CPT1C expression is limited to the brain. The product of FA synthesis, malonyl-CoA, binds to CPT1 and acts a physiological inhibitor of FAO ensuring FA homeostasis (McGarry et al., 1978). CPT1A has the highest binding affinity to malonyl-CoA making it the most prevalent isoform and the target for inhibition of FAO. Although CPT1C has sequence homology to the CPT1A and CPT1B isoforms; binds malonyl-CoA, it however does not possess acyl-transferase activity (Wolfgang et al., 2006). A metabolomics study found that there were only subtle changes in FAO metabolites in CPT1C knockouts, however increased levels of glutathione were observed (Lee and Wolfgang, 2012).

CPT1C is thought to contribute to the metabolic transformation of cancer cells. Its upregulation results in strong activation of the mTOR pathway in primary murine lung tumour models and contributes to rapamycin resistance (Zaugg et al., 2011). Additionally, its upregulation results in increased FAO, ATP generation in response to glucose deprivation and hypoxia. CPT1C knockdowns become more susceptible to metabolic stress as a result of decreased ATP production (Reilly and Mak, 2012). The contribution of CPT1C to FAO is still unclear but it may play a role in regulating response to metabolic stress.

Once inside the mitochondrial matrix, acyl-CoAs can be freely oxidised. FAO is a repeated process where acyl-CoA chains are shortened. Each round results in the production of acetyl-CoA released from the two carboxy-terminal carbons. FAO occurs in four principle steps- *Dehydration*- The acyl-CoA-ester undergoes dehydration catalysed the by acyl-CoA-dehydrogenases to trans-2-enoyl-coA. *Hydration*- Then hydration of the double bond to L-3-hydroxy-acyl-coA. *Dehydrogenation*- followed by dehydrogenated to 3-Keto-acyl-coA. *Thiolytic cleavage*- The final step involves a thiolytic cleavage producing acetyl-CoA and an acyl-CoA chain that is two carbons shorter. The resulting shorter acyl-CoA undergoes the process again until all carbons are liberated (Houten and Wanders, 2010). The production of ATP from FAO is through cofactor production and acetyl-CoA. Acetyl-CoA and reducing agents, NADH and FADH₂ generated by β -oxidation are destined for the TCA cycle and electron transport chain respectively. The complete oxidation of palmitate (16 carbons) generates 129 molecules of ATP.

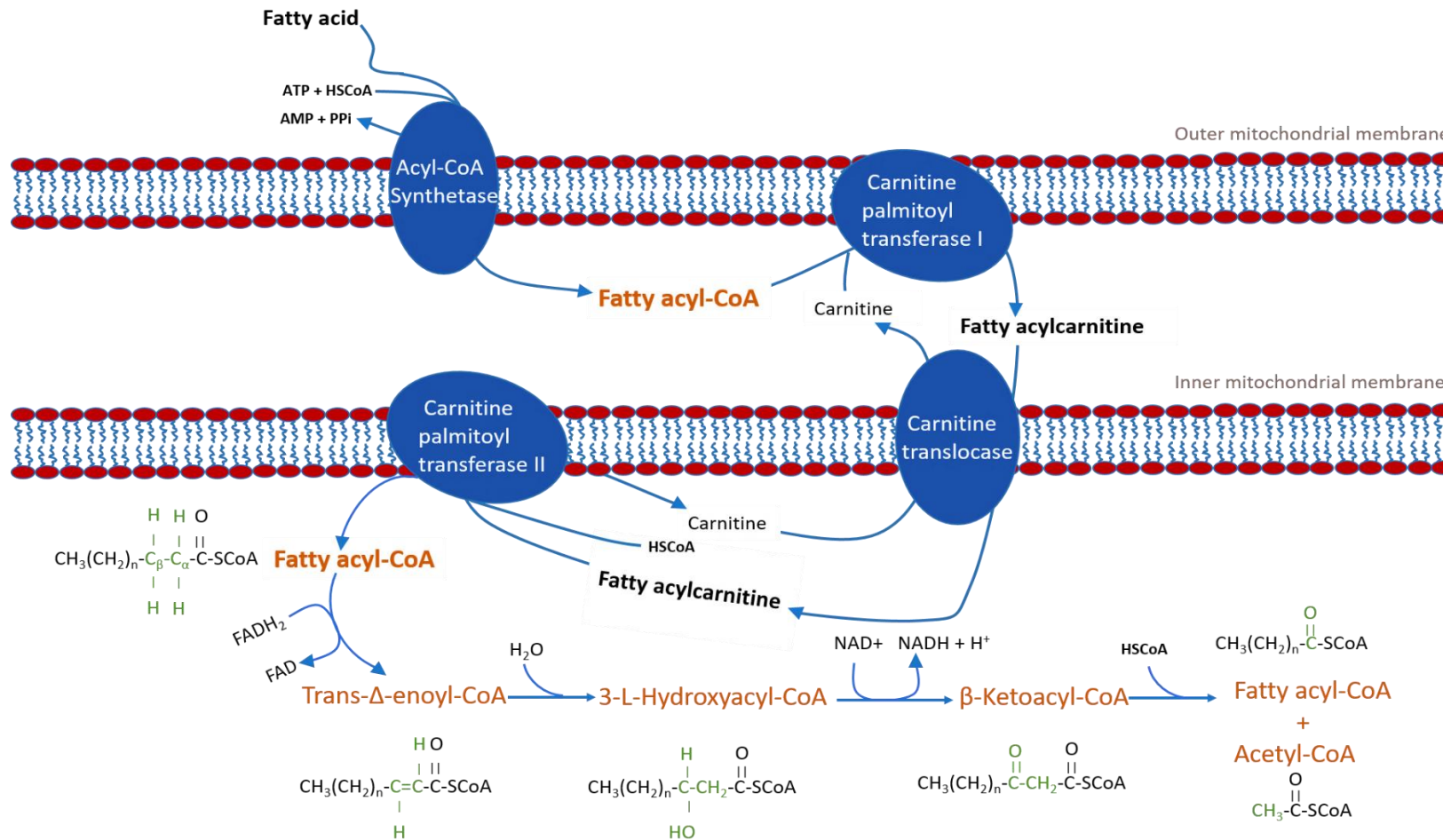


Figure 1.5 Schematic of mitochondrial fatty acid β -oxidation. Entry of fatty acids from cytosol into the mitochondria occurs through the Carnitine palmitoyl transferase shuttle. β -oxidation occurs via a spiral where each turn shortens the acyl-CoA by two carbon units. β -oxidation is catalysed by specific chain length enzymes in the mitochondrial matrix (King, 2020).

1.1.5 Regulation of metabolic reprogramming

It is well established that altered metabolism supports nutrient acquisition and synthesis of biomolecules enabling tumourigenesis, growth and survival (Figure 1.6). Metabolic pathways themselves actively facilitate modifications in gene regulatory networks particularly through the alteration of the epigenetic landscape (Li et al., 2019). Excessive generation of acetyl-CoA from glycolysis and uncoupling from mitochondrial respiration can impact chromatin structure through acetylation of histones and other proteins. Histone acetylation is associated with open chromatin and enables increased accessibility of transcriptional complexes. These reactions are intricately responsive to nutritional status and signalling events. Remarkably, Akt activation is correlated with global histone acetylation in glioblastoma (Lee et al., 2014). The catabolism of serine also fuels the generation of SAM. Disruption of serine catabolism leads to reduction of SAM and consequently affects histone and DNA methylation (Maddocks et al., 2016).

P53

Although the aberrant activity of metabolic enzymes is tethered to oncogenesis, mutations in oncogenes and loss of tumour suppressors can further alter the metabolic landscape of cancer. Oncogenes and tumour suppressors can exert transcriptional regulation on genes in a myriad of cellular processes; aberrant function of these regulators impacts metabolic gene expression. Loss of function mutations in *P53* are amongst the most frequently observed genetic abnormalities in human cancers (Olivier et al., 2010). Normal activity of P53 balances both glycolysis and mitochondrial respiration through the genes it activates. For instance, P53 mediates the expression of GLUT1/4, facilitating glucose uptake. Loss of P53 leads to upregulated glycolysis through loss of TIGAR (TP53-induced glycolysis and apoptosis regulator) which normally depletes levels of F2, 6BP and diverts glycolytic intermediates into the PPP, leading to reduction in glycolytic flux (Zhang et al., 2013). In the absence of P53, glycolysis can proceed unchecked due to unregulated PGAM function which rapidly increases flux in some cancers (Kondoh et al., 2005). Additionally, P53 supports OXPHOS through the induction of cytochrome oxidase c (SCO2) which modulates function of cytochrome C oxidase (COX). Mutant P53 cells have a noticeable decrease in aerobic respiration and reduced dependence on oxygen due to reduced activity of COX (Matoba et al., 2006).

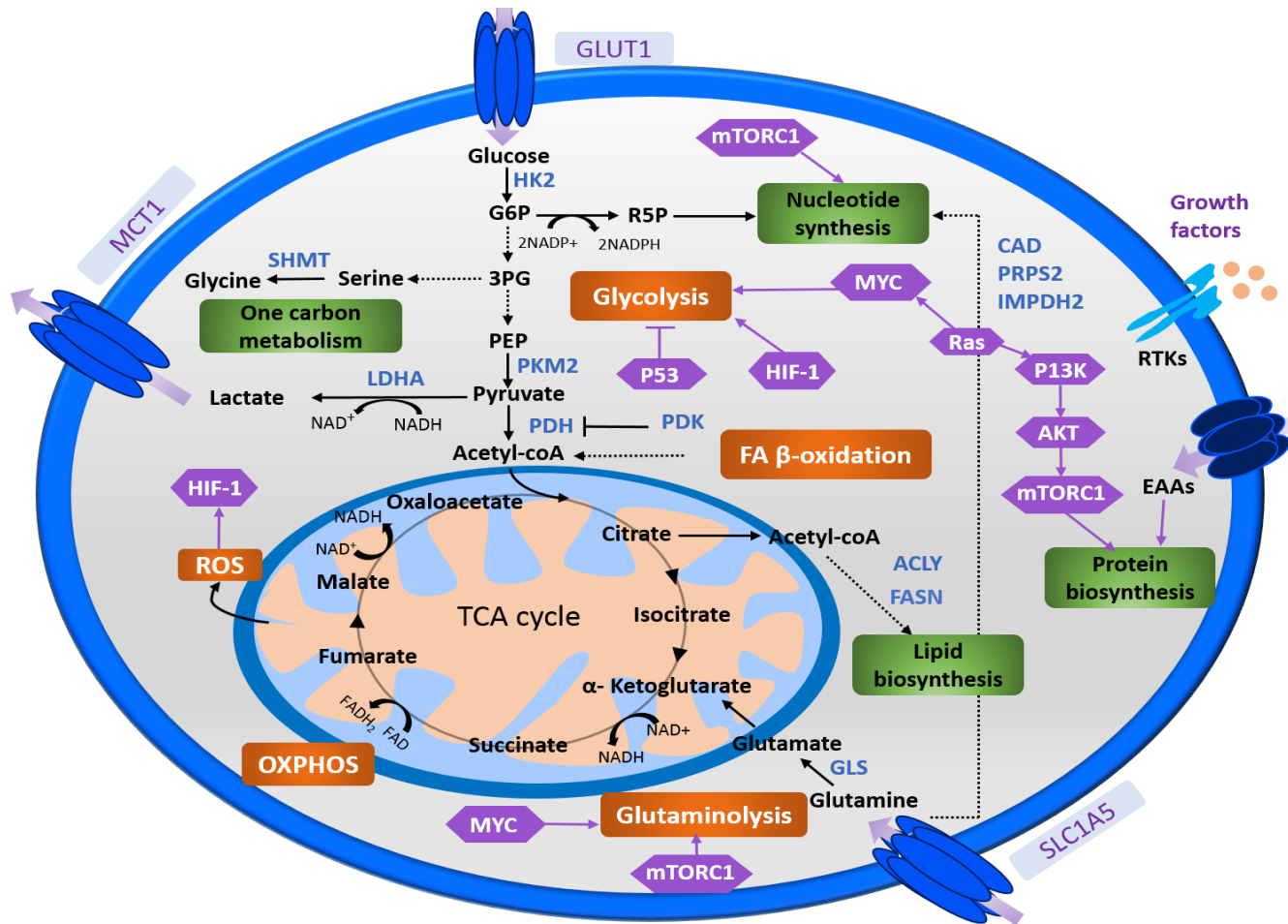


Figure 1.6 Overview of signalling pathways that contribute to the metabolic rewiring of cancer cells. Cancer cells induce anabolic growth pathways through aberrant mTORC1 signalling to induce nucleotide and protein synthesis. Oncogenic MYC activity and loss of function of P53 facilitate cancer metabolism gene expression programmes.

HIF1

The transcriptional regulator hypoxia inducible factor 1-alpha (HIF1), coordinates cellular response to hypoxia by shifting metabolism from oxygen-dependent respiration to glycolysis (Dengler et al., 2014). Decreased oxygen tension strongly induces HIF1 and stabilises the protein by preventing inhibition exerted by prolyl-hydroxylases (PHD). Interestingly, mutations in TCA cycle enzymes fumarate hydratase (FH) and succinate dehydrogenase (SDH), which leads to build-up of fumarate and succinate respectively, have been shown to inhibit the activity of prolyl-hydroxylation resulting in aberrant HIF signalling. These consequences further highlight how metabolites themselves influence metabolic pathways and cause alterations in regulatory networks. Aberrant signalling of PI3K/Akt/mTOR have been shown to stabilise HIF1 even in the absence of hypoxia (Zundel et al., 2000). The resultant effect is continual induction of glycolytic genes such as *HK2*, *LDHA*, and monocarboxylate transporters (MCT) which leads to enhanced glycolysis and expression of transporters which eliminate lactate and prevent build-up. Furthermore in kidney cancer, loss of the von Hippel-Lindau (VHL) tumour suppressor functions prevents ubiquitin-mediated proteosomal degradation of HIF1 (Maxwell et al., 1999).

MYC

Focal amplification and overexpression of *MYC* is a frequently observed genetic aberration in cancer (Meyer and Penn, 2008, Beroukhim et al., 2010). *MYC* is a pleiotropic transcription factor which orchestrates transcriptional programmes which support cellular processes such as proliferation, differentiation and cellular metabolism. Alteration in metabolic pathways are frequently associated with *MYC*-driven tumourigenesis which sustains rapid proliferation-associated malignant features by inducing rewiring of cellular metabolism which contributes to aberrant growth (Dang, 2013b, Dang et al., 2006). The metabolic reprogramming governed by deregulated *MYC* is covered in more detail in 1.5.5.3.

1.2 Exploiting metabolic dependencies for cancer biomarkers and therapy

1.2.1 Targeting altered metabolism

The alteration of metabolic networks in cancer offers opportunities for therapeutic targeting (Table 1.1). The effort to develop effective metabolic therapies must consider the effect of systemic administration of such drugs on the normal healthy cell population since these enzymes are often ubiquitously expressed. Consideration is needed for cell populations, that also exhibit similarities in metabolic phenotype i.e. stem cells or immune cells. Furthermore, are there cancer specific isoforms that could be uniquely targeted? Or is there a therapeutic window for the administration of metabolic therapies? The concept of therapies targeting metabolic reprogramming of cancer is not novel. There have been several successful antimetabolite therapies that are currently used in clinic. For example methotrexate, an antagonist of folate metabolism remains a part of chemotherapeutic regimens for certain cancers. In acute lymphoblastic leukaemia (ALL), the administration of asparaginase, the enzyme catalysing the conversion of asparagine to aspartate and ammonia is used to deplete plasma asparagine. Owing to the increased rates of protein synthesis, *de novo* synthesis of asparagine is limited and inadequately supplies leukaemic cells with this AA. This reliance on exogenous sources make them uniquely sensitive to asparaginase treatment (Avramis and Tiwari, 2006).

Further deliberations should focus on models used. *In vitro* testing of therapies is an important initial step identifying potential candidates. However nutrient availability in growth culture medium differs from that of the tumour microenvironment. *In vitro* conditions do not effectively mimic the spatiotemporal fluctuations in nutrients/oxygen experienced by the bulk tumours (Vande Voorde et al., 2019). Thus, *in vitro* findings must be confirmed in the preclinical setting using appropriate disease models. The use of syngeneic models, orthotopic patient-derived xenografts (PDX) and genetically engineered mouse models (GEMM) play an important role in deciphering metabolic phenotypes of cancers but also for preclinical evaluation. Utilising models that are immunocompetent, preserve blood brain barrier (BBB) and mimic tumour microenvironment more closely will likely aid the development and/or identification of more effective metabolic therapies.

Table 1.1 List of metabolic inhibitors under clinical investigation.

Metabolic Pathway	Target	Agent(s)	Phase of clinical investigations	Trial identifier (reference)
β -oxidation	CPT1	Etomoxir	Phase I/II for type 2 diabetes and heart failure	(Ratheiser et al., 1991) (Holubarsch et al., 2007)
Glutamine metabolism	GLS1	CB839	Phase I/II for NSCLC	NCT03831932
Glycolysis	MCT1	AZD3965	Phase I for Advanced solid tumours, DLBCL, Burkitt's lymphoma	NCT01791595
Lipid/Cholesterol biosynthesis	CK α	TCD717	Phase I Advanced solid tumours	NCT01215864
	HMGCR	Statins (FDA approved)	Phase III for breast cancer	NCT03971019
Mitochondrial metabolism	IDH	AG120	Phase I-II AML	NCT03013998 NCT03173248
	Complex I	Metformin (FDA approved)	Phase I-III (multiple ongoing trials)	NCT03109847 NCT01750567 NCT03829020
		Phenformin	Phase I for BRAF-mutated melanoma	NCT03026517

1.2.1.1 Targeting upregulated glycolysis in cancer

Enhanced glycolysis is associated with numerous cancers and has been the focus of therapeutic targeting with several tool compounds against various glycolytic components (Table 1.2). Overexpression of HK2 is frequently observed in cancer and has been shown to be required for the initiation and maintenance of tumour growth in breast and pancreatic cancers (Jae et al., 2009, Patra et al., 2013). Furthermore, in *KRAS*-driven PDAC (pancreatic ductal adenocarcinoma), genetic ablation and pharmacological inhibition of HK2 is associated with reduced metastatic potential and induces tumour regression (Anderson et al., 2017). Several compounds targeting various components of glycolysis have been introduced. For example, the glucose analogue 2-deoxyglucose (2DG), which has undergone phase I/II clinical trials with limited success owing to systemic toxicity (Raez et al., 2013, Stein et al., 2010). Although systemic toxicities of targeting glycolytic enzymes impedes use of certain agents, targeting LDHA which is the final catalytic step in aerobic glycolysis has been shown to be effective in non-small cell lung cancers (NSCLC) without systemic toxicity in mouse models. Furthermore inhibition of LDHA, impacted tumour initiating cells (TIC) of NSCLC (Xie et al., 2014). Another mode of targeting glycolysis, would be to directly target transporters that are overexpressed in cancer. For instance VHL-deficient renal cell carcinomas (RCC) upregulate GLUT1 and pharmacological inhibition has been shown to slow tumour progression (Chan et al., 2011). There is currently intense interest in the compound

AZD3965, which is a selective inhibitor of MCT1. Inhibition of MCT1 in diffuse large cell B cell lymphoma (DLBCL) has been shown to slow progression of these tumours (Noble et al., 2017). AZD3965 is now under clinical investigation for several lymphomas (CRUKD/12/004). Dual inhibition of both MCT1 and MCT4 has been shown to be synthetically lethal when combined with metformin treatment in cancer cells (Benjamin et al., 2018).

Table 1.2 List of glycolytic targets and inhibitors.

Targets	Inhibitors	Mechanism of action
GLUT1	WZB117	Inhibits glucose transport
HK	2-Deoxyglucose	Inhibits glucose phosphorylation
HK2	Lonidamide	Inhibits glycolysis and dissociates HK from mitochondria
HK	3-bromopyruvate	Inhibits glycolysis by acting as an alkylating agent
G6PD	6-AN	Inhibits NADP+ dependent G6PD
PKM2	TLN-232	Inhibits the dimeric isoform of PK
PDK	Dichloroacetic acid	Inhibits PDKs and promotes pyruvate oxidation
LDHA	FX11	Selective inhibitor
LDHA	GSK 2837808A	Selective inhibitor
MCT1	AZD3965	Inhibits lactate efflux

1.2.1.2 Targeting amino acid metabolism

Cancer cells consume a large range of AAs and are particularly reliant on biosynthetic precursors to enact the growth and hyper-proliferative programmes that enable continual growth (Lukey et al., 2017). Glutamine is the most abundant AA in plasma and is rapidly consumed in certain cancer contexts. For instance oncogenic K-Ras and MYC have been shown to drive glutamine addiction in NSCLC and gliomas respectively (Gaglio et al., 2011, Wise et al., 2008). Glutaminolysis supports TCA anaplerosis and maintains redox homeostasis through the overexpression of transaminases and reactions that generate NADPH. These characteristics make certain cancers uniquely sensitive to genetic ablation and pharmacological inhibition of enzymes involved in glutamine catabolism (Son et al., 2013, Xiang et al., 2015). There are numerous small molecule inhibitors and antimetabolites against glutaminase (GLS), the enzyme responsible for the conversion of glutamine to glutamate. BPTES and CB839 are selective allosteric inhibitors of GLS1

and have been shown to be effective against numerous glutamine-dependent cancers. CB839 displays better pharmacokinetics/potency and has entered several phase 1/ 2 clinical trials as a single agent or in combination with other chemotherapeutic agents in RCC and triple negative breast cancer (TNBC) (DeMichele et al., 2016, Meric-Bernstam et al., 2019). Glutamine addiction is enabled by excessive uptake from exogenous sources. Inhibition of SLC1A5 by the compound GNPA has been shown to decrease growth of NSCLC xenografts (Hassanein et al., 2015).

Asparaginase has been successfully used against adult and paediatric ALL. This therapeutic intervention relies on asparagine auxotrophy (inability to *de novo* synthesise) to impede tumour growth. A similar strategy is currently being investigated in ASS1-deficient tumours which are reliant on the availability of exogenous arginine (Riess et al., 2018). The combination of ADI-PEG20 and recombinant human arginase 1 to deplete plasma concentrations of arginine is being investigated in hepatocellular carcinoma (HCC) (Yau et al., 2013).

Serine and glycine represent a large proportion of the amino acids consumed by cancer cells. In fact a recent study identified that AA represent a large proportion of cancer cell biomass (Hosios et al., 2016). Furthermore, glycine consumption is associated with rapid proliferation and genetic disruption of SHMT2 in glycine dependent cancers have reduced growth and proliferation (Jain et al., 2012). The identification of small molecule inhibitors against PHGDH, has demonstrated the effectiveness of targeting this pathway in PHGDH-dependent tumours and those exhibiting increased rates of *de novo* serine synthesis (Mullarky et al., 2016, Pacold et al., 2016, Wang et al., 2017).

1.2.1.3 Mitochondrial metabolism

Targeting mitochondrial metabolism has emerged as a potential therapeutic intervention for cancer. Cancer cells exhibit plasticity in metabolic networks so it be could speculated that effective targeting of mitochondrial respiration could occur in conjunction with other metabolic agents. Metformin is a clinically approved diabetic drug which has been shown to be an effective anticancer agent (Kasznicki et al., 2014). It exerts its anticancer properties by reversibly inhibiting Complex I of the ETC (Birsoy et al., 2014). Currently there is an ongoing phase 3 clinical trial examining its efficacy as a single agent against early stage breast cancer (NCT01101438). There is also exploration of whether metformin could be used to mitigate the side effects of aggressive treatments, like in the case of administration of radioactive iodine in thyroid cancers (NCT03109847).

Furthermore, other studies have identified its potential use in cancer prevention. For instance, retrospective analysis of metformin treatment in diabetic patients revealed decreased cancer associated mortality (Bowker et al., 2010). Others have shown that metformin reduced risk of pancreatic cancer in diabetic patients (Zhou et al., 2017). An active phase 3 trial in this field is evaluating whether metformin can prevent the development of breast cancer in patients with atypical hyperplasia (NCT01905046).

1.2.1.4 Fatty acid oxidation and opportunities for therapeutic targeting

CPT1 and ATP generation

Fatty acid oxidation (FAO) as a bioenergetic pathway has an immense capacity to produce large quantities of ATP to fulfil energy requirements of tumour cell growth. The inhibition of CPT1 by etomoxir decreased ATP production in *MYC*-driven triple negative breast cancer (TNBC) *in vitro* and additionally slowed tumour progression in PDX models of TNBC (Camarda et al., 2016). FAO derived ATP may also support oncogenic signalling pathways. The use of transmitochondrial cybrids of TNBC revealed the phosphorylation and activation of Src was dependent on ATP generated from mitochondrial oxidative phosphorylation (Park et al., 2016). Genetic knockdown of CPT1 and CPT2, abolished Src autophosphorylation and inhibited metastasis. In some cancers (prostate, B cell lymphoma and high grade-gliomas etc.), FAO is the critical energy pathway and its impairment leads to a reduction in proliferation and survival due to ATP depletion (Liu et al., 2010, Lin et al., 2016, Caro et al., 2012). In ovarian cancer which has a high propensity of metastasising to the omentum, it has been shown that adipocytes provide lipids which can be utilised by ovarian cancer cells through β -oxidation supporting tumour growth (Nieman et al., 2011).

The production of the reducing species NADH and FADH₂ is important in the production of ATP. However, FAO also generates NADPH through the generation of acetyl-CoA. Citrate which is a product of the TCA cycle is exported into the cytosol where it is involved in NADPH producing reactions. GBM SF188 cells which are oxidative are susceptible to etomoxir treatment. Inhibition of FAO in these cells causes ATP depletion along with oxidative stress due to a reduction in NADPH and GSH content. Additionally, the LKB1-AMPK axis is required to maintain redox balance. Cells with inactivated AMPK exhibit NADPH depletion, oxidative stress which triggers apoptosis (Pike et al., 2011).

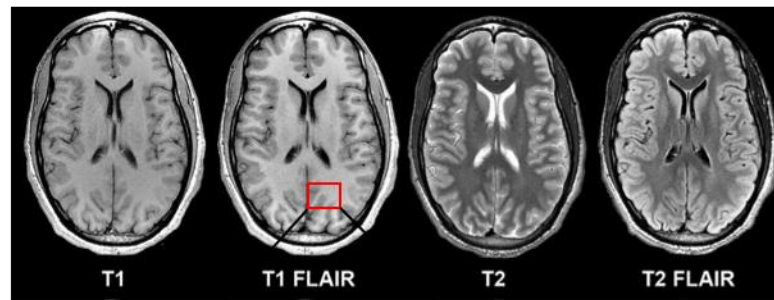
Prostate cancer, which is a slow growing tumour has been shown to be less reliant on aerobic glycolysis and uses lipids as its primary fuel source. The combination of etomoxir and orlistat (FAS inhibitor) produces a synergistic effect resulting in decreased expression of the androgen receptor, mTOR signalling and caspase 3 activation (Schlaepfer et al., 2014). The compound ST1326 which inhibits CPT1 results in growth arrest, mitochondrial damage and induces apoptosis and accumulation of lipids in leukaemic cells (Ricciardi et al., 2015). Inhibition of FAO by etomoxir also sensitises human leukaemic cells to apoptosis induction by ABT-737, a molecule that causes the release of pro-apoptotic BCL-2 proteins like BAK (Samudio et al., 2010). Furthermore, FAO regulates the apoptotic response by directly impacting BAK-dependent mitochondrial permeability transition.

1.2.2 Imaging altered metabolism

1.2.2.1 Utilising MRI and MRS to probe altered metabolism of tumours

Magnetic resonance imaging (MRI) and spectroscopy (MRS) are powerful and non-invasive tools used to obtain detailed anatomical information and biochemical signatures in tissue. The combination of imaging and spectroscopy allows the investigation of physiological processes and abnormalities associated with disease (Figure 1.7). ^1H MRS is the most commonly used nuclei for *in vivo* investigations due to the natural abundance of protons in tissue. MRS provides a steady state of tissue metabolite concentrations and ratios which are informative. In particular, when focused on regions of interest like the region of a tumour, it can inform on tumour metabolism and localised changes. *In vivo* brain spectroscopy provides information about the three predominant tissue components; water, metabolites and macromolecules. Metabolic profiles of normal tissue are relatively steady, but alterations in metabolism may be characteristic of disease. The metabolites frequently observed in brain spectra include N-acetyl aspartate (NAA), creatine (Cr), choline (Cho), lactate and lipids (Figure 1.7 B). NAA is a neuronal marker and decreased levels are often associated with disease state (Zhu and Barker, 2011). Cho is a marker associated with increased membrane synthesis which is associated with neoplasms with increased proliferation and expansion. Alterations in lipids have been detected using ^1H MRS. It has previously been reported that ^1H MRS visible lipids are prevalent in apoptotic and necrotic tumour regions (Hakumaki and Kauppinen, 2000, Liimatainen et al., 2006). High levels of lipid and lactate has been reported as correlative with poor survival in patients with GBM. High lactate is capable of inducing treatment resistance and also correlates with advanced disease and worse survival (Saraswathy et al., 2009, Sattler et al., 2010).

A



B

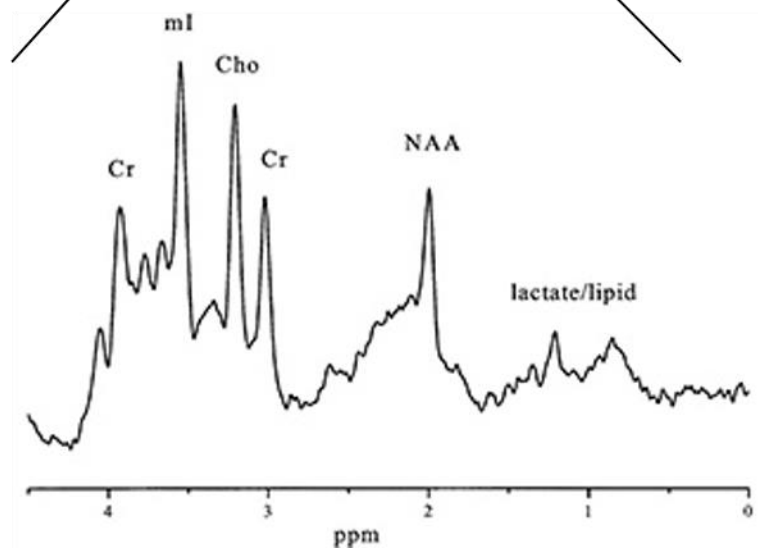


Figure 1.7 Magnetic resonance imaging and spectroscopy. A) Axial MR imaging of normal brain with varying contrast-weighted images B) Typical MR spectroscopy of brain metabolites. Fluid attenuated inversion recovery (FLAIR). Adapted from (Saraswathy et al., 2009)

Altered metabolism is a well-established feature of cancer (DeBerardinis and Chandel, 2016). Another feature not previously discussed are oncogenic metabolites (Oncometabolites). Oncometabolites are defined as an abnormal accumulation of a metabolite associated with genetic mutations in the corresponding enzyme. Importantly accumulation of oncometabolites drive pathophysiology, promote changes in the epigenome and can drive aggressiveness in cancers. The accumulation of oncometabolites offers opportunities for cancer biomarker discovery, tumour detection, monitoring progression and assessing effectiveness of treatment (Sciacovelli and Frezza, 2016). Mutations in TCA cycle enzymes are intricately linked with oncometabolites.

Accumulation of fumarate and succinate resulting from mutations in FH and SDH respectively are well characterised (Pollard et al., 2005). These mutations can occur from spontaneous somatic mutations but are also associated with hereditary paragangliomas and pheochromocytomas (Astuti et al., 2001, Baysal et al., 2000). Single allelic mutations in isocitrate dehydrogenase 1 and 2 (IDH1/IDH2) are observed in some glioma subtypes where they are associated with better prognosis. In acute myelogenous leukaemia (AML) however, IDH1 mutations are associated with worse prognosis. Nonetheless, mutations in IDH1 and IDH2 lead to the production of oncometabolite 2-hydroxyglutarate (2HG) instead of α KG.

The altered activity of IDH results in α KG depletion and inhibits reactions dependent of α KG which include activity of prolyl hydroxylase (PHD) which regulate HIF protein stability and also α KG-dependent DNA and histone methylation (Selak et al., 2005). The accumulation of 2HG is readily detected from serum sampling in IDH-mutant AML and indeed a reduction in 2HG levels is observed following cytotoxic treatment. Conversely, an increase in serum 2HG is observed in relapsing cases. In IDH-mutant gliomas however, MRI and MRS provide an opportunity for monitoring this type of tumour. Likewise, a reduction in tumour 2HG is observed following anticancer therapies (Andronesi et al., 2016). Using 3D MRS imaging, a recent phase 1 trial assessed the pharmacodynamics of recently developed IDH1 specific inhibitors in gliomas (Andronesi et al., 2018). Furthermore, others have utilised MRS to evaluate differences in metabolite profiles of IDH1 and IDH2 mutant gliomas (Shen et al., 2019).

1.2.2.2 Use of positron emission tomography for assessing changes in metabolism of cancer

The coupling of positron emission tomography (PET) with radiotracers results in an imaging modality capable of monitoring molecular and metabolic pathways and interactions occurring *in situ*. ^{18}F Fluoro-deoxyglucose-PET (FDG-PET) has been utilised in clinic to monitor alterations in glucose metabolism of normal brain and tumours (Figure 1.8) (Almuhaideb et al., 2011). The Warburg effect is associated with a concomitant rise in glucose uptake. FDG which is a glucose analogue is taken up via similar mechanisms and used to detect presence of tumours and monitor treatment response. The use of FDG-PET is limited for some cancers owing to high background in highly glycolytic tissues such as the brain (Chen et al., 2005). Other radiotracers have been developed to combat false positives arising from FDG use. Radiotracers such as ^{18}F -Fluoro-tyrosine (FLT) rely on increased proliferation of tumour cells. Phosphorylation of

FLT by thymidine kinase (upregulated in S phase of cell cycle) leads to accumulation of imaging signal. These tracers have shown improved performance compared to FDG in recurrent high grade gliomas (Chen et al., 2005). Since abnormal glutamine catabolism is also observed in cancer, glutamine based PET have been developed. ^{18}F -Fluoroglutamine (FGln) PET trials have been used to identify tumours displaying abnormal glutamine metabolism, particularly those with genetic abnormalities linked to glutamine addiction (Dunphy et al., 2018). Furthermore, FGln delineates tumours with low avidity for FDG in gliomas and has improved resolution from lower background (Venneti et al., 2015). Other tracers including ^{11}C and ^{18}F choline derivatives have shown limited success in distinguishing prostate cancers from other pathologies occurring in that anatomical location (Schwarzenbock et al., 2012). However, there is a lot of use of choline-based PET in prostate cancer, where the main advantage of more specific tracers such as ^{68}Ga -PSMA based agents, is in distinguishing tumour metastases from normal bone (which also shows choline uptake) (Han et al., 2018). Continual development of novel radiotracers will enable the detection and monitoring of a wide range on tumours based on their characteristic metabolic alterations.

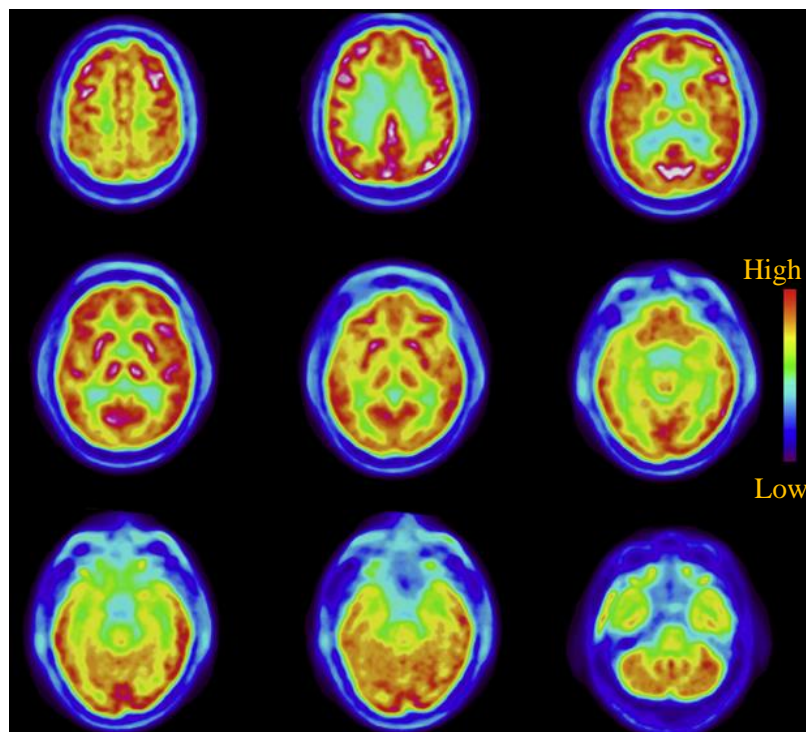


Figure 1.8 Distribution of FDG-PET uptake in normal brain. Axial slices of PET images of brain (Taken from (Scholl et al., 2014)). Key indicates uptake of FDG tracer.

1.3 Epidemiology of central nervous system tumours

1.3.1 Overview of malignant brain in adults and children

Almost 12,000 people are diagnosed with brain and intracranial tumours in the UK every year and paediatric brain tumours make up around 5% of these cases (Cancer Research UK 2019). Whilst central nervous system (CNS) tumours account for 3% of overall cancer incidence in the UK, paediatric brain tumours account for a quarter of childhood cancers and are the most commonly occurring solid tumour in children (Figure 1.9). There is a striking clinical difference between brain tumours in adults and children. In adults the most common non-malignant tumours meningiomas make up a majority of cases. The most common malignant tumours in adults are gliomas which are typically high-grade tumours with dismal outcomes (Ostrom et al., 2018). Although gliomas frequently occur in children, they are predominantly low-grade pilocytic tumours with differing biology (Pollack et al., 2002).

Embryonal tumours, of which medulloblastoma accounts for the majority of cases are the most common childhood brain malignancies (Ostrom et al., 2018). Five-year survival rates for childhood brain tumours is more favourable at around 65% (Packer, 2008). However, children are susceptible to late treatment effects resulting from therapeutic interventions which includes formation of secondary tumours from radiation therapy, developmental and hormonal abnormalities, and cognitive impairment. The challenges that arise when treating brain tumours include anatomical location; surgical intervention may not always achieve total removal of tumour mass due to infiltration into normal surrounding tissue. The brain is also enclosed by the BBB which tightly regulates exposure to factors/nutrients in general circulation, creating its own unique microenvironment and niche. This creates an obstacle for treatment with conventional and targeted therapies which may have limited exposure to tumour site from systemic drug administration (Aldape et al., 2019).

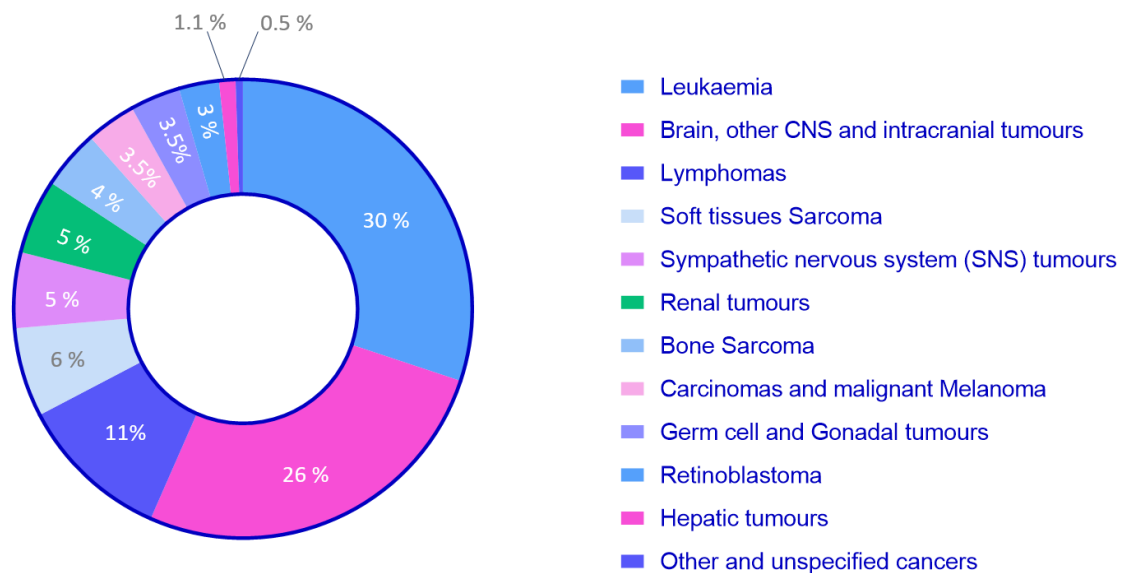


Figure 1.9 Incidence of childhood cancers in the UK. Figure generated from Childhood Cancer Great Britain & UK (CRUK 2019).

1.3.2 Spectrum of brain tumours

For brain tumours, age-associated tumour distribution and tumour location is frequently observed (Figure 1.10). Additionally the relative proportions of malignant and non-malignant brain tumours decrease with age (Figure 1.11 A). For instance, the incidence of tumours arising in the posterior fossa of the cerebellum decreases with age with the proportion of tumours involving this region being 17% in children/adolescents (0-19 years) compared to 6% (20-34 years) and 3% (35- 74 years) in adults (Merchant et al., 2010). More in depth focus on malignant paediatric brain tumours reveals decreased proportions of cases with increasing age particularly for medulloblastoma and pilocytic astrocytomas (Figure 1.11 B). Malignant brain tumours occurring in adults tend to be high-grade tumours, with GBM accounting for 47.7% (Ostrom et al., 2018). There is also a higher proportion of metastatic disease observed in adult brain tumours whereas this feature is less common in the paediatric population.

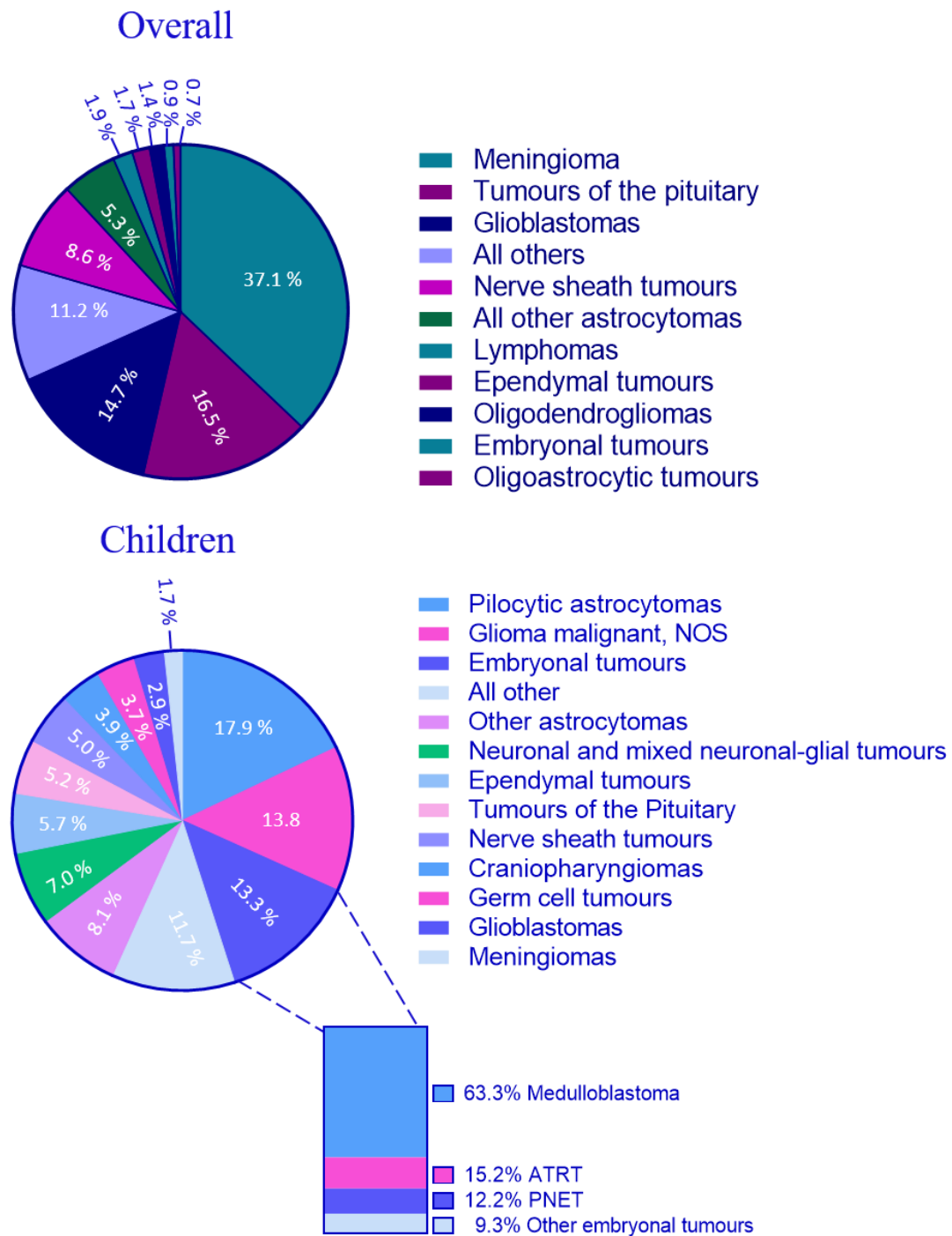


Figure 1.10 Distribution of CNS and intracranial tumours. A) Distribution of overall population B) Distribution of paediatric cases. Not otherwise specified (NOS); Atypical teratoid rhabdoid tumour (ATRT); Primitive neuroectodermal tumours (PNET). Data from CBTRUS Louis et al., 2018.

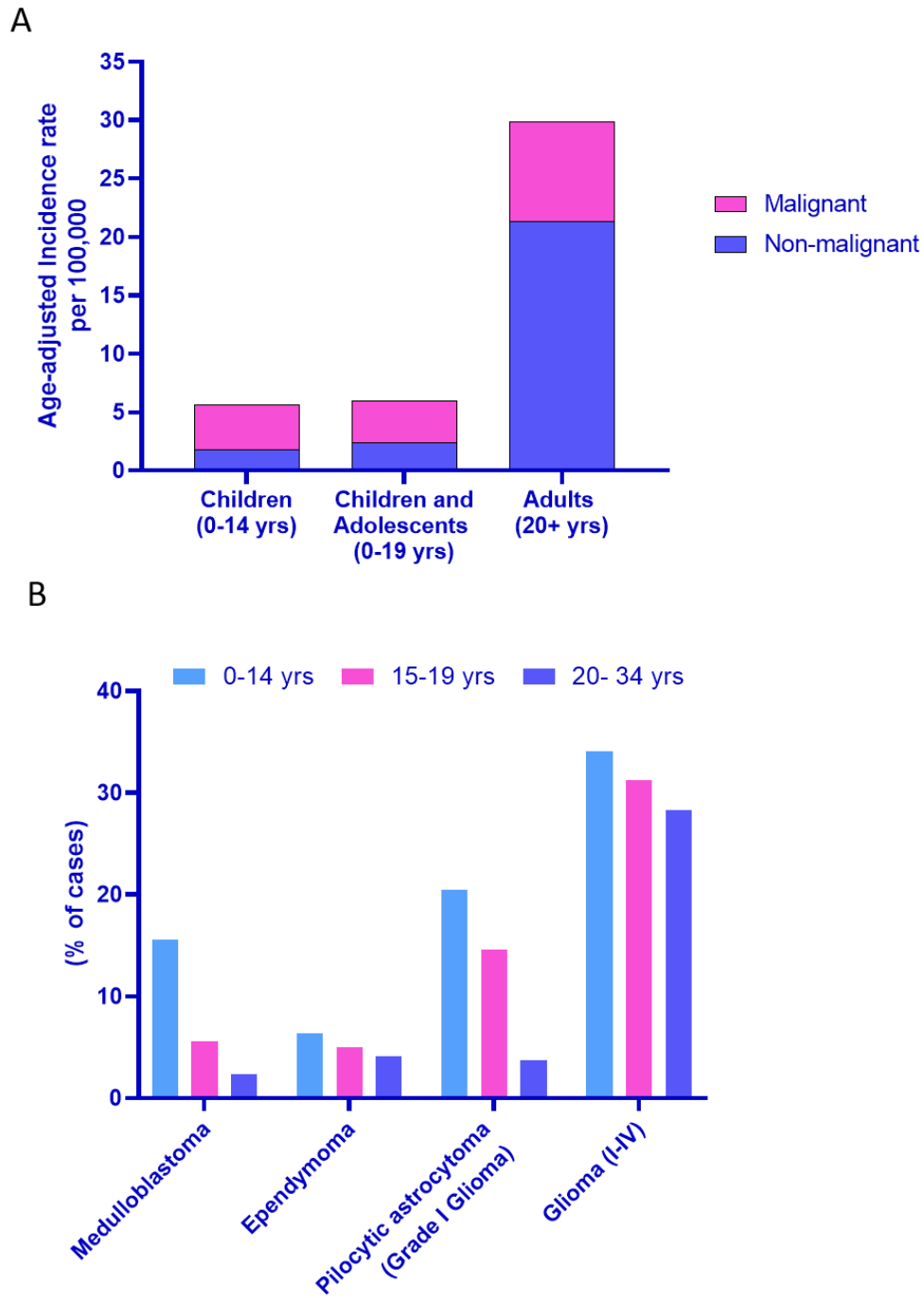


Figure 1.11 Age-associated malignancy of Brain tumours. A) Proportion of malignant and non-malignant brain tumours across an age spectrum. B) Age-related associations between malignant brain tumours. Data taken from Louis et al., 2018 (A) and Merchant et al., 2010 (B).

1.3.2.1 Differences in aetiology and mutational burden

Although cancers occur in both adult and paediatric populations, the aetiological factors contributing to disease differs. For cancer in adult, age is often a causal factor and additionally direct links between environmental exposures drive oncogenesis. Studies conducted by Genome-wide association (GWAS) of gliomas showed 25 common single nucleotide polymorphisms (SNP), which include SNPs associated with *TERT*, *EGFR*, *RTEL1* and *TP53* to be associated with increased risk in adult gliomas (Walsh et al., 2014, Melin et al., 2017, Rajaraman et al., 2012). There are very few studies performed which have conclusively associated genetic variants with childhood brain tumour risk since such studies are limited by low sample numbers (Ostrom et al., 2019, Spector et al., 2015). The causal factors in the paediatric setting remain unclear. However, it is thought that intrauterine genetic and environmental exposures may play a part. Exposure to high dose radiation and chemotherapy have been established as causal factors for some childhood brain cancers (also increases risk in adults) (Ron et al., 1988, Spector et al., 2015). Some studies have associated accelerated intrauterine growth, particularly a correlation between head circumference and risk of CNS tumours (Samuelsen et al., 2006).

Familial syndromes resulting from germline mutations, although they account for a small proportion of cases, are associated with increased cancer risk (Malkin, 2011). Beyond these, errors in developmental programmes are likely to contribute to the pathogenesis of childhood cancers. Interestingly, the mutation frequencies tend to be higher in adults compared to children: adult cancers are often attributed to acquisition of several mutations which drive cancer formation whereas childhood cancers are associated with putative driver genes (Grobner et al., 2018). The analysis conducted by Grobner and colleagues found that somatic mutational burden increased with patient age as did single nucleotide variants (SNV) and insertion/deletions (indels). The majority of children (~ 57%) were found to have only one mutated gene with 8% having a hereditary predisposition (Grobner et al., 2018). Ultimately the biology and nature of CNS tumours in adults and children population differ even when they are histologically similar (Sarkar et al., 2002). Uncovering the underlying driving events of tumourigenesis in these populations broaden our understanding but also may lead to opportunities for disease biomarkers and therapy development.

1.4 Malignant glioma

Gliomas are the most common primary adult-onset malignant intracranial tumours. The World Health Organisation (WHO) classifies gliomas based on histological features indicative of prognosis. Historical classification and tumour grading was based on histological resemblance to glial lineages (astrocytic, oligodendrocytic, ependymal etc.) and features indicative of disease aggressiveness (Weller et al., 2015). Low grade lesions (e.g. Grade I pilocytic astrocytoma) have a low proliferative capacity and are likely to be cured following tumour resection. Grade II lesions, which include diffuse astrocytomas and oligodendrogliomas, infiltrate normal brain parenchyma and have potential to develop into higher grade malignancies, in spite of their low proliferative capacity. Grade III are malignant lesions that are anaplastic and display mitotic activity (anaplastic astrocytoma). Additionally, tumours displaying microvascular proliferation, with or without necrosis are termed glioblastoma (grade IV astrocytoma, or GBM) (Louis et al., 2007). Malignant or high grade (grade III-IV) gliomas represent a high proportion of malignant brain tumour diagnoses. In particular, glioblastoma, the most lethal CNS tumour, accounts for 47.7% of all glioma cases (Ostrom et al., 2018). Although global incidence rates are low (5.3 in 100,000), the highly invasive nature of these tumours results in high morbidity and mortality rates (Ostrom et al., 2018).

1.4.1 Aetiology and epidemiology

There are few established contributing risk factors to the development of gliomas. Exposure to ionising radiation is the only conclusive risk factor that increases the likelihood of glioma formation. Although familial patterns of glioma are rare, heritable variants with higher risk are associated with rare genetic syndromes such as neurofibromatosis types 1 and 2, the Li–Fraumeni syndrome (germ-line *TP53* mutations associated with an increased risk of several cancers including glioma), and Turcot’s syndrome (intestinal polyposis and brain tumour (Malmer et al., 2007). Other genetic features associated with predisposition for glioma include certain variants of the *EGFR*, *TERT*, *CDKN2B* in astrocytomas and *CCDC26* in oligodendrogliomas. Malignant glioma is more prevalent in males who are 1.6 times more likely to develop GBM than their female counterparts. Malignant gliomas are also an age-associated disease. The occurrence of anaplastic astrocytoma and GBM increase with age, and peaks at around the 75-84 year group (Ostrom et al., 2018).

1.4.2 Clinical presentation

Patients with glioma often suffer from neurological deficits associated with tumour mass, increased intracranial pressure, surgical intervention and treatment response. Tumour associated epilepsy is a common manifestation in glioma patients albeit more so in low grade gliomas. Around 30% of patients present with epileptic seizures which require further intervention with antiepileptic drugs (Rajneesh and Binder, 2009).

1.4.3 Treatment strategies in glioblastoma

Current therapeutic interventions against GBM include maximal surgical resection, radiotherapy and/or temozolomide chemotherapy (Stupp et al., 2005). Tumour resection is often limited by infiltration into normal surrounding tissue. Due to a lack of removal of tumour bulk, disease progression and recurrence limits curative intervention (Wilson et al., 2014). Numerous studies have shown extent of surgical resection correlates with progression free and overall survival (Stummer et al., 2006, Mukherjee and Quinones-Hinojosa, 2011). The post-treatment survival outcome, with standard-of-care therapy, is 12-16 months for glioblastoma and 2-5 years for anaplastic astrocytoma. The challenges to the development of efficacious drugs is consequently affected by the heterogeneity of GBMs. In fact, the effectiveness and survival benefit of temozolomide, a DNA alkylating agent which is the primary chemotherapy drug used for glioma patients, is correlated with tumour MGMT promoter methylation status (Hegi et al., 2005).

1.4.4 Molecular classification and heterogeneity of glioblastoma

The advent of more genomic, epigenomic and molecular features of GBM have refined the diagnosis and prognostication of GBM. Previous limitations of histological classification presented challenges for prognostication particular when histologically similar tumours displayed varied survival outcomes even when clinicopathological features such as age and extent of tumour resection was accounted for (Perry and Wesseling, 2016). Recent advances have led to revision of diagnostic criteria and biomarkers for the disease (Louis et al., 2007, Louis et al., 2016a). The promoter methylation of O6-methylguanine-DNA methyltransferase (MGMT) has been shown to be a significant biomarker of temozolomide treatment response in GBM (Stupp et al., 2005, Hegi et al., 2005). MGMT is a suicide DNA repair enzyme which removes O6-methylguanine adducts induced by alkylating agents such as TMZ. Around 40% of GBMs have MGMT promoter methylation (Esteller et al., 2000) and where TMZ is used as part of upfront therapy, these patients have improved survival outcomes (Stupp et al., 2009). Surprisingly, MGMT promoter methylation is not a distinctive characteristic of a particular GBM subtype but nonetheless serves as useful prognostic marker (Chen et al., 2017).

Early gene expression and microarray studies identified distinct subgroups of GBM (Phillips et al., 2006). More comprehensive genomic characterisation by The Cancer Genome Atlas (TCGA) further unveiled the highly heterogeneous nature of GBMs (Verhaak et al., 2010). There are three core pathways (Receptor tyrosine kinase signalling, P53 and RB tumour suppressor pathways) forming an interconnected network of genetic abnormalities which drive tumourigenesis. The patterns of genomic alterations followed amplification of oncogenic signalling pathways and deletions in tumour suppressor pathways (Brennan et al., 2014). The TCGA analysis revealed four subtypes of GBM based on gene expression (Figure 1.12). The classical subtype was marked by *EGFR* amplifications which were not frequently observed in the other subtypes. The mesenchymal subtype was characterised by *NFI* mutations and presence of mesenchymal markers such as *CHI3LI* and *MET*. The proneural subtype strongly correlated with *PDGFRA* amplifications and mutations in *IDHI* which were almost exclusive to this subtype. Furthermore patients with *IDHI*-mutant GBMs had better prognostic outcomes and were associated with younger patients and secondary GBMs (Verhaak et al., 2010). The neural subtype was not distinguished by exclusive genomic alterations but by the expression of neural markers. The robustness of the neural subtype remains controversial,

since early and more recent classification studies failed to identify this subtype (Phillips et al., 2006, Sturm et al., 2012).

Using mutational status, DNA copy number alterations and gene expression signatures Sturm and colleagues identified six distinct subgroups of GBM. Some of the identified subgroups are supported by previous studies and the TCGA analysis with significant overlap (Phillips et al., 2006, Verhaak et al., 2010). The newly identified subgroups were termed RTK I (PDGFRA), RTK II (Classic), Mesenchymal, IDH1 and newly identified groups that correlated with K27 or G34 mutations of the H3F3A histone variant. Interestingly mutations of *H3F3A* and *IDH1* were mutually exclusive and also displayed age-associated distribution with K27 present in children, G34 in adolescents and IDH in young adults (Sturm et al., 2012).

The WHO have consolidated histological classification of gliomas with prognostic and molecular features in an attempt to group tumours that are likely to respond similarly to treatments (Table 1.3) (Louis et al., 2016a). The characterisation of differential molecular patterns and deregulated oncogenic and tumour suppressive pathways within GBM is informative of distinct tumour genotypes that may be of use in guiding development of novel therapeutics.

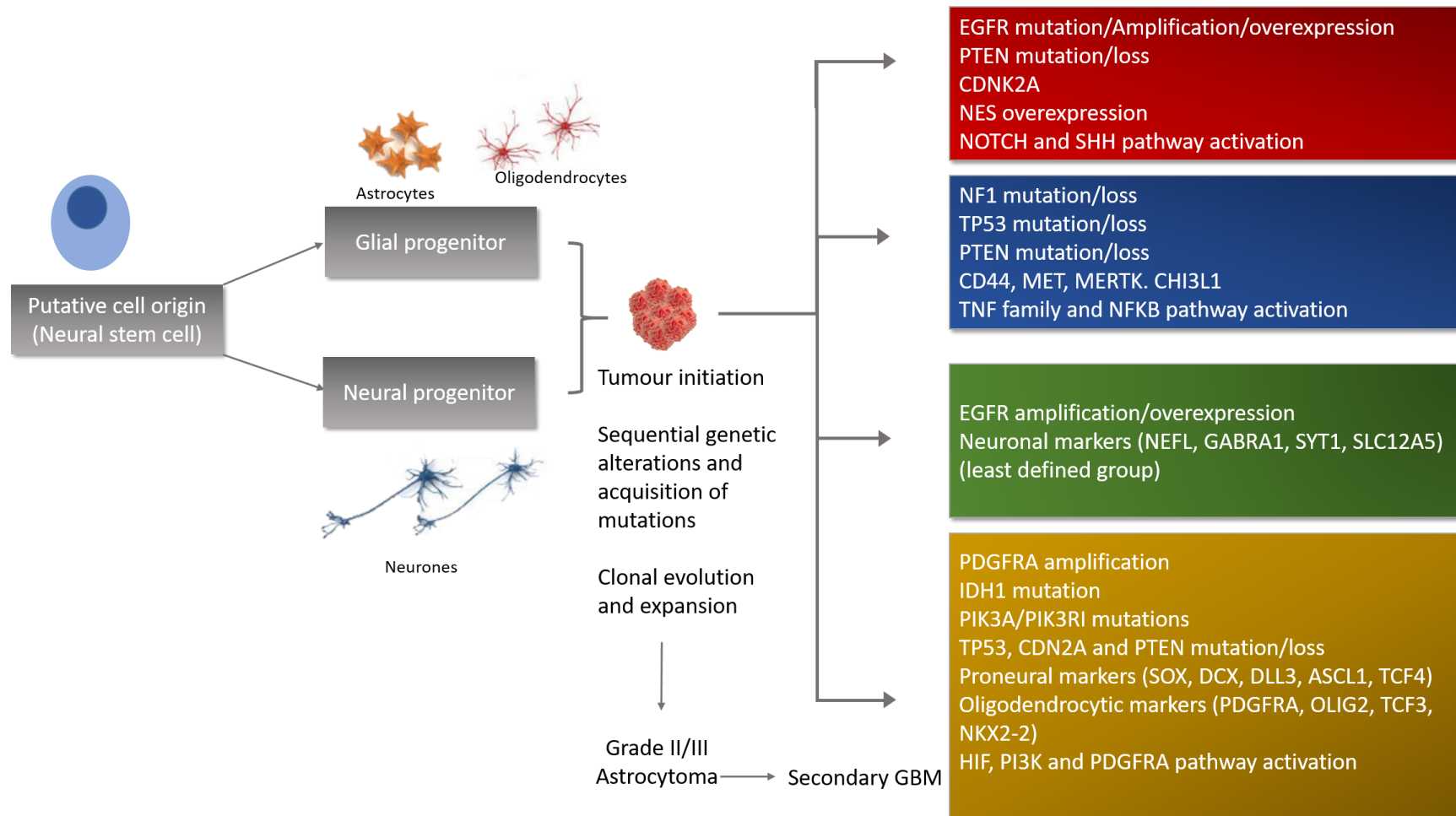


Figure 1.12 Molecular classification of Glioblastoma. Figure depicts evolution of GBM cell of origin, involvement of neuronal lineages and clonal evolution leading distinct subtypes. Classic (red); Mesenchymal (blue); Neural (green); Proneural (yellow). Adapted from (Verhaak et al., 2010)

Table 1.3 The WHO classification of Glioblastoma and clinicopathological characteristics

	IDH-wildtype GBM	IDH-mutant GBM
Synonym	Primary GBM, IDH-wildtype	Secondary GBM, IDH-mutant
Precursor lesion	Develops de novo	Diffuse astrocytoma Anaplastic astrocytoma
Proportion of GBM	~ 90 %	~ 10 %
Median age at diagnosis	62 years	44 years
Male : Female	1.42 : 1	1.05 :1
Mean length of clinical history	4 months	15 months
Median Overall survival		
Treatment protocol (Surgery and radiotherapy)	9.9 months	24 months
(Surgery, radiotherapy and chemotherapy)	15 months	31 months
Anatomical location	Supratentorial	Frontal
Necrosis	Extensive	Limited
TERT promoter mutations	72 %	26 %
TP53 mutations	27 %	81 %
ATRX mutations	Exceptional	71 %
EGFR amplification	35 %	Exceptional
PTEN mutations	24 %	Exceptional

1.4.5 Altered metabolism in glioma

1.4.5.1 Glycolysis and related pathways

Numerous studies have observed increased glycolysis as a feature of glioma (Zhou et al., 2011, Oudard et al., 1996). The use of FDG-PET which is an imaging modality dependent on the increased cancer cell uptake of glucose remains controversial for gliomas. Although certain reports have shown correlation of FDG uptake and increasing grade, there are still some limitations in distinguishing gliomas from normal brain tissue due to high physiological uptake of glucose (Strauss, 1996). Furthermore approximately 30% of

gliomas are FDG-PET negative and display low uptake for FDG-PET making tumour detection by this method unsuitable (Chen et al., 2005). It is often speculated that the increased glucose uptake is indicative of upregulation of glycolysis and ATP generation through this pathway.

GBMs display highly diverse inter- and intra-tumoural heterogeneity which is likely to impact on metabolic phenotypes. Studies have shown that distinct GBM cell populations display different metabolic phenotypes. For instance, cancer stem cell populations in GBM are often characterised by a higher oxidative capacity and are the most chemo- and radio-resistant populations within a tumour (Vlashi et al., 2011). In both immortalised and primary cultured cell lines, ATP production is not wholly accounted for by glycolysis which suggests that other metabolic pathways contribute to energy production. Warburg's observation of increased aerobic glycolysis whilst still relevant, does not capture the metabolic complexity of cancer cells. Several studies have observed the contribution diverse metabolic substrates which fuel energy production in cancer cells (Guppy et al., 2002, Bonnet et al., 2007, Michelakis et al., 2010). Although metabolic reprogramming serves ATP production in cancer cells, it provides the requirements for biosynthetic components. Cancer cells utilise a diverse range of substrates to supply fuel (ATP) and synthesis of macromolecules (Nucleic acids and lipids) which sustains aberrant proliferation and growth (DeBerardinis et al., 2008). While much of cancer cell metabolism research has concentrated on glucose utilization, other substrates, such as fatty acids, are increasingly being appreciated as major contributors to cancer cell bioenergetics. In fact, glioma cells engage in the β -oxidation of fatty acids and *de novo* fatty acid synthesis (Lin et al., 2016, Tao et al., 2013). This metabolic dependency may be exploited for clinical neuro-oncology, particularly biomarker discovery and drug development. Such novel approaches may give new promise to these patients, who currently have few therapeutic options.

1.4.5.2 Fatty acid oxidation in glioma

The brain is a highly lipid rich environment and lipids account for half of total brain mass (O'Brien and Sampson, 1965). Additionally, free fatty acids readily cross the BBB where they can be taken up by astrocytes and neurones and utilised for lipid biosynthesis and energy production. Whilst glucose is rapidly consumed in the brain, acetate is also widely available (Belanger et al., 2011). Glioma cells express fatty acid synthase (FASN), and indeed the expression of this enzyme increases with tumour malignancy (Tao et al., 2013). Inhibition of FASN and other enzymes involved in FAS is sufficient to slow tumour progression in GBM xenograft models (Guo et al., 2009, Gimple et al., 2019). Additionally, pharmacological inhibition of FASN was associated with decreased expression of stem cell markers nestin and Sox2 (Yasumoto et al., 2016). Additionally, upregulation of FAO enzymes, namely the acyl-dehydrogenases, correlate with worse patient outcomes (Strickland and Stoll, 2017). Although FAO is understudied in comparison to glycolysis, glutaminolysis and even FAS in tumour cells, there is increasing evidence of its importance in GBM. Previous results from Lin *et al.*, demonstrated that primary GBM stem-like cells (GSC) preferentially consumed and utilised fatty acids for ATP production (Lin et al., 2016). Specifically, human glioma cells primary-cultured under serum-free conditions require fatty acid oxidation to maintain both respiratory and proliferative activity. Several emerging lines of evidence directly or indirectly validate these findings using independent methods. *In vivo* radiolabelling studies conducted in orthotopic mouse models of malignant glioma using patient-derived cells showed that acetate is rapidly consumed and oxidised in TCA cycle supporting energetic and biosynthetic demands (Mashimo et al., 2014). Others have shown that acyl-CoA binding proteins support tumour growth by delivery of acyl-CoAs to mitochondria (Duman et al., 2019).

1.5 Medulloblastoma

Medulloblastoma (MB) is the most common primary malignant brain tumour occurring in children and incidence peaks around 4 to 7 years. It presents with 1.7: 1 male to female ratio (Pizer and Clifford, 2009). MB cases are also reported during infancy and adulthood but these cases are rarer and evidence suggests differences in pathogenesis especially in adult MB (Louis et al., 2016a). MB accounts for over 60% of embryonal tumours, a group encompassing histologically similar tumours which include atypical teratoid rhabdoid tumours (ATRT) and primitive neuroectodermal tumours (PNET) (Louis et al., 2016a). Molecular characteristics readily distinguish these embryonal tumours. MB arise in the posterior fossa region of the cerebellum. Additionally, a third of patients present with cerebrospinal fluid (CSF) infiltration and metastasis to other distal sites (Pizer and Clifford, 2008).



Figure 1.13 Medulloblastoma tumour. MR image of sagittal section of an in situ medulloblastoma in the posterior fossa. Case courtesy of Associate Prof Frank Gaillard, Radiopaedia.org, rID: 6494

1.5.1 Treatment of medulloblastoma

1.5.1.1 Clinical presentation of medulloblastoma

The symptoms manifested in patients with MB include increased intracranial pressure with frequent headaches, persistent vomiting and ataxia from breakdown of the cerebellar vermis (Bartlett et al., 2013). MB is diagnosed using both computed tomography (CT) and MRI. On CT, medulloblastoma is visualised as a hyper-attenuated mass in the cerebellum with oedema (Eran et al., 2010, Nelson et al., 1991). Using MRI, it appears as a hyper-intense mass in T1-weighted imaging in 80% of cases, obstruction of the fourth lateral ventricles is also observed. Gadolinium enhancement is achieved in the majority of tumours (Eran et al., 2010, Meyers et al., 1992). MRI is also extended to the craniospinal region for the purposes of staging. Staging of MB is based on the modified Chang system and is detailed in Table 1.4 (Chang et al., 1969).

Table 1.4 Staging of metastatic disease by Chang et al., 1969

Staging	Characteristics
M0	No metastases
M1	Presence of tumour cells in the CSF
M2	Intracranial metastases
M3	Spinal metastases
M4	Metastases outside of the CNS

1.5.1.2 Treatment regimen of Medulloblastoma

The current intervention against medulloblastoma includes maximal surgical resection and radiotherapy with adjuvant chemotherapy (Pizer and Clifford, 2008). Surgical removal of the tumour is the first line of treatment with the objective of achieving gross total resection where possible. Additionally, surgery aims to relieve intracranial pressure and re-establish normal CSF flow (Crawford et al., 2007, Pizer and Clifford, 2008). Development of posterior fossa syndrome following surgery is experienced in 20- 25% of MB cases. Symptoms includes ataxia, motor weakness, loss of speech and changes in mood (Bartlett et al., 2013, Gerber et al., 2014). Radiation is the next phase of curative treatment. Studies have shown that delay in receiving radiotherapy impacts survival

outcomes (Taylor et al., 2004). Currently, radiotherapy is delivered within 50 days post-surgery for average risk patients. Radiotherapy regimens also include craniospinal irradiation since over a third of MB patients present with metastasis to this site (Bartlett et al., 2013). The side effects of radiation therapy are immense and include decline in cognition, growth impediment, hearing loss, endocrine disorders and cardiomyopathy. For this reason, radiotherapy is avoided in MB patients less than 3 years old. Studies examining the benefits of hyper-fractionated radiotherapy found no survival benefits when compared to conventional therapy. Furthermore, the impact of both therapies on severe hearing loss were comparable (Lannering et al., 2012). However, hyper-fractionated accelerated radiotherapy resulted in more favourable outcomes in patients with metastatic disease (Gandola et al., 2009).

Adjuvant chemotherapy is included as a treatment strategy to further improve survival outcomes in standard risk patients. In infants (< 3 years old), it is used to delay or avoid radiotherapy (Bartlett et al., 2013, Grill et al., 2005). More recent studies have shown that a short intensive burst of chemotherapy eliminated the requirement for craniospinal irradiation in infants with non-metastatic disease (Dhall et al., 2008). The most frequently used regimen in standard risk patients currently combines lomustine, vincristine and cisplatin for up to 8 cycles. In high risk patients, it includes cisplatin, carboplatin, cyclophosphamide and vincristine (Bartlett et al., 2013, Stucklin et al., 2018).

1.5.2 Histopathological features of medulloblastoma

The histological classification of medulloblastoma has been long established. Prior to the advent of molecular classification, diagnosis of MB heavily relied on histological variants and informed prognosis. However, ambiguity in histological classification in some cases impacted diagnostic accuracy and prognostication. The classification of MB has evolved in the last decade and in particular since the 2007 WHO classification of CNS which only recognised MB entities resulting from histological analysis (Louis et al., 2007). Increasing understanding of the molecular pathology of MB has expanded the way in which MBs are diagnosed, and particularly since the 2012 consensus on molecular features, the 2016 WHO CNS classification has incorporated the expansive field of molecular pathology with histological variants (Louis et al., 2016b).

Four histological MB entities are recognised in the field and illustrated in Figure 1.14. The classic variant accounts for a large proportion of MBs (70%). They display increased cellularity with small round or oval cells that are undifferentiated, although neuronal

differentiation may be observed and these are typically organised as rosettes. Rosettes are characterised by tumour cells arranged circularly with fibrillary centre. Desmoplastic nodular (D/N) MB have nodular architecture or desmoplasia with permeation of reticulin fibres. The nodules however are reticulin free. Although Desmoplastic reactions may occur, without association with nodules they are not classified D/N. This histology is frequently associated with infants and has better prognosis. Overall D/N accounts for around 15% of MB with a small proportion classified further into histology subtype with higher nodularity (Ellison, 2010, Louis et al., 2007). MB with extensive nodularity (MBEN) have expansive nodularity with neurocytic differentiation. Patients with this histological variant tend to be in infancy and have better prognosis. MB with large cell anaplasia (LCA) have larger nuclei and are anaplastic with increased mitotic and apoptotic activity. LCA histology is found in 15% of MB cases. In particular, LCA histology is commonly associated with highly aggressive MB tumours and is associated with poorer survival (Eberhart and Burger, 2003, Stucklin et al., 2018).

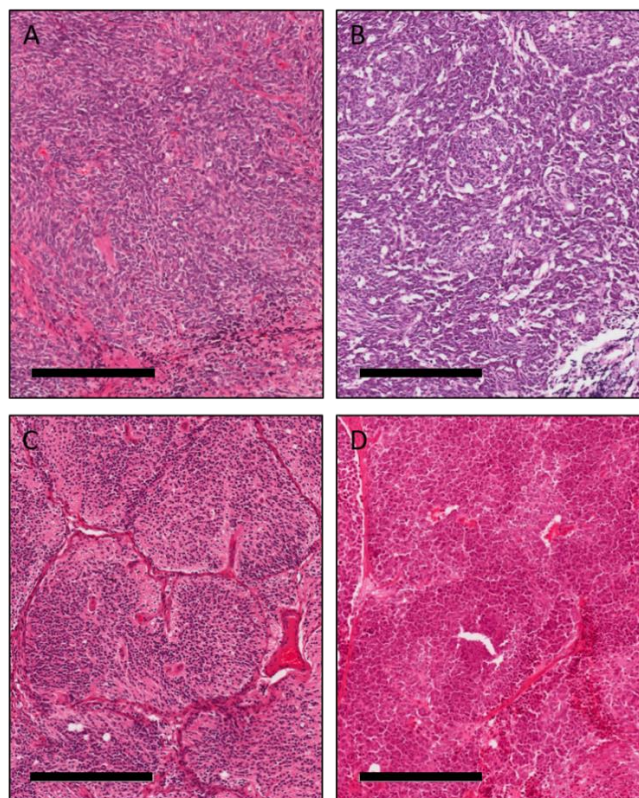


Figure 1.14 Histological variants of medulloblastoma. Haematoxylin and eosin staining of MB with A) Classic B) Desmoplastic nodular C) Extensive nodularity D) Large cell/anaplastic histology Scale bar = 300 μ M (H&E staining and images by Dr Steve Crosier).

1.5.3 Risk stratification of medulloblastoma

The traditional methods of risk stratification are based on clinicopathological features such as age at diagnosis, presence of metastatic disease, extent of surgical resection and histology (Table 1.5). With growing understanding of MB biology, molecular features are further contributing to MB risk stratification (Table 1.5) (Ramaswamy et al., 2016, Schwalbe et al., 2017b, Taylor et al., 2012). The 2016 WHO classification of CNS tumours has further incorporated genetic features in stratifying MB. These efforts were to improve and streamline both molecular and clinicopathological features to aid diagnosis and identification of patient risk (Table 1.6).

Table 1.5 Prognostic biomarkers and clinicopathological features of MB. Representation of current and planned biomarkers and associated clinical trials. Metastasis (M+), Recurrence (R+), Subgroup: Wingless (WNT) medulloblastoma (MBWNT), Sonic Hedgehog (SHH) medulloblastoma (MBSHH)

Risk Group	Clinical trials		
	Up to 2014	2014	2017
	-	SIOP-PNET5-MB	SIOP-PNET5-MB and SIOP-HR-MB
High risk (HR)	M+	M+	M+
	R+	R+	R+
	LCA pathology	LCA pathology	LCA pathology
		MYC or MYCN amplification	MYC or MYCN amplification MBSHH/TP53 mutation MBWNT with HR features (>16 years)
Standard risk (SR)	Negative for all HR factors	Non-MBWNT	Non-MBWNT
		Negative for all HR factors	Negative for all HR factors
			MBWNT without HR features (>16 years) MBWNT with HR features (<16 years)
Favourable risk (FR)	N/A	MBWNT	MBWNT (<16 years)
		Negative for all HR factors	Negative for all HR factors
Excluded	N/A	N/A	MBSHH with germline TP53, SUFU or PTCH1 mutations

Table 1.6 The WHO classification of Medulloblastoma. Wingless (WNT), Sonic hedgehog (SHH).

Genetic classification	Histology	Prognosis
MB, WNT activated	Classic	Low-risk tumour; Correlation of WNT activation and classic morphology
	LCA (very rare)	Uncertain clinicopathological significance
MB, SHH activated, TP53-mutant	Classic	Uncommon high risk
	LCA	High risk (ages 7-17 years)
	DN (very rare)	Uncertain clinicopathological significance
MB, SHH activated, TP53-wildtype	Classic	Standard risk
	LCA	Uncertain clinicopathological significance
	DN	Low risk in infants (< 3 years)
	MBEN	Low risk in infants (< 3 years)
MB, non-WNT/non-SHH. Group 3	Classic	Standard risk
	LCA	High risk
MB, non-WNT/non-SHH. Group 4	Classic	Standard risk; classic morphology found in almost all tumours
	LCA (rare)	Uncertain clinicopathological significance

1.5.4 Genetic abnormalities and subgroup classification of medulloblastoma

Familial predispositions associated with MB provided early insights and informed on genetic alterations found in MB. Although familial predispositions account for a small fraction of MBs (< 5%). Many of the genetic abnormalities found in familial syndromes play a role in sporadic MBs (Pizer and Clifford, 2009). Li Fraumeni's syndrome, which is characterised by germline mutations in *TP53*, is the most commonly reported hereditary association in MB (Pfister et al., 2010, Rausch et al., 2012).

Although less frequent, Gorlin's syndrome which is associated with germline mutations in transmembrane protein patched 1 (*PTCH1*), a tumour suppressor gene in the sonic hedgehog (*SHH*) signalling pathway, is observed in a proportion of MB patients. Loss of *PTCH1* results in high activity of the SHH pathway due to increased activity of smoothened (*SMO*). Interaction of SHH protein and PTCH1 causes release of SMO which triggers release of glioma-associated oncogene homologue (GLI) activating the transcription of several genes (Figure 1.15).

Turcot's syndrome predisposes individuals to several cancers, although it is less common in MB (Northcott et al., 2012b). The activity of transcriptional regulator adenomatous polyposis coli (*APC*) is lost due to germline mutations (Northcott et al., 2012b). The wingless (*WNT*) pathway of which *APC* is a regulator, is also implicated in MB. The Wnt pathway is a developmental pathway and in the brain, it is crucial for maturation of neurones and body axis patterning (Rosso and Inestrosa, 2013). *APC* is a critical component of WNT signalling cascade. WNT controls the intracellular localisation of β -catenin. Stimulation of the WNT pathway causes nuclear localisation of β -catenin which trans-activates the LEF/TCF transcriptional complexes which in turn, induces a pro-tumourigenesis programmes through the transcription of genes such as *MYC* (Figure 1.15). Missense mutations in *CTNNB1* (encoding beta-catenin) results in increased stability of protein which in turn leads to aberrant activity of the WNT pathway (Figure 1.15) (Clifford et al., 2006, Ellison et al., 2005, Northcott et al., 2019).

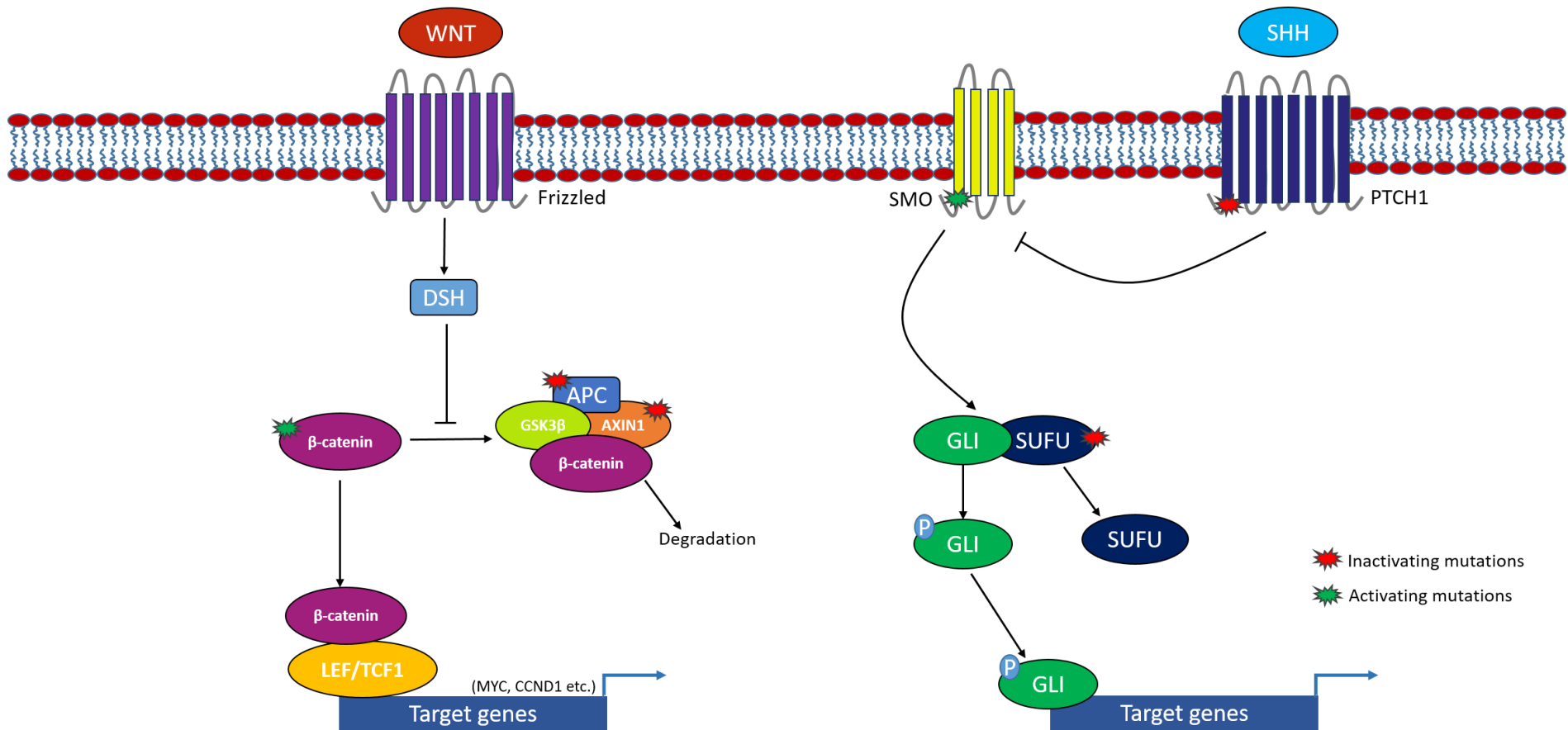


Figure 1.15 Overview of Wingless (WNT) and Sonic Hedgehog (SHH) signalling cascades in Medulloblastoma. Activation of pathway component is indicated by arrows and inhibition indicated by blunt arrows. Frequently observed mutations in WNT and SHH are indicated. Smoothed (SMO); patched (PTCH1); dishevelled (DSH); adenomatous polyposis coli (APC); Glycogen synthase kinase 3 beta (GSK3β); lymphoid enhancer factor/ T cell factor (LEF/TCF1); suppressor of fused (SUFU). Adapted from (Kool et al., 2014b)

The advancement of next generation sequencing (NGS) and genomic studies have expanded knowledge of the genetic features of MB (Pomeroy et al., 2002, Thompson et al., 2006, Kool et al., 2008, Northcott et al., 2011, Cho et al., 2011). It is now appreciated that MB consists of genetically distinct subtypes with distinguishable molecular features and survival outcomes (Taylor et al., 2012, Northcott et al., 2012a, Schwalbe et al., 2017a, Sharma et al., 2019). Genomic, transcriptomic and DNA methylation profiling has revealed four consensus subgroups with variations in genetic alterations, demographics and survival outcomes (Kool et al., 2008, Northcott et al., 2011, Schwalbe et al., 2017a, Taylor et al., 2012, Thompson et al., 2006). The four consensus subgroups of MB defined by DNA methylation profiling are termed MB_{WNT}, MB_{SHH}, MB_{GRP3}, and MB_{GRP4} which correlate with established molecular and clinic-pathological features (Figure 1.16 & Figure 1.17). Recent studies have further classified subtypes and distinctions within subgroups that even further delineates MB features and survival differences (Sharma et al., 2019). Interestingly several studies utilising single cell transcriptomics have highlighted that the separation of MB subgroups is influenced by the neuronal lineages and cerebellar compartments in which they arise (Hovestadt et al., 2019, Zhang et al., 2019).

Subgroup		MB _{WNT}	MB _{SHH}	MB _{GRP3}	MB _{GRP4}
Clinical features	% of Cases	10	30	25	35
	Age at Diagnosis				
	Gender ratio	1:1	1:1	2:1	3:1
	Anatomical location				
	Histology	Classic, Rarely LCA	Desmoplastic, Classic, LCA	Classic, LCA	Classic LCA
	Metastasis at Diagnosis (%)	5-10	15-20	40-45	35-40
	Recurrence pattern	Rare; Local or metastatic	Local	Metastatic	Metastatic
	Prognosis	Very good	Infants good, others intermediate	Poor	Intermediate
Molecular features	Putative cell of origin	Progenitor cells in the lower rhombic lip	Granule progenitor cells	Neural stem cells	Unipolar brush cells
	Recurrent SNVs	-	<i>MYCN</i> <i>GLI1</i> or <i>GLI2</i>	<i>MYC</i> <i>MYCN</i> <i>OTX2</i>	<i>KDM6A</i> <i>MYCN</i> <i>OTX2</i> <i>CDK6</i>
	Cytogenetics Loss Gain	6	3q,9p 9q,10q,17p	1q,7,18 8,10q,11,16q i17q	7,18q 8,11p, X i17q
	Other genetic events	-	-	GFI1 and GF1B Enhancer hijacking	PRDM6,GF1 and GF1B Enhancer hijacking



Figure 1.16 Summary of demographics, clinicopathological and molecular features of MB subgroups. Adapted from (Kyle and Michael, 2019) and data from (Kool et al., 2008, Northcott et al., 2017, Schwalbe et al., 2017a, Taylor et al., 2012)

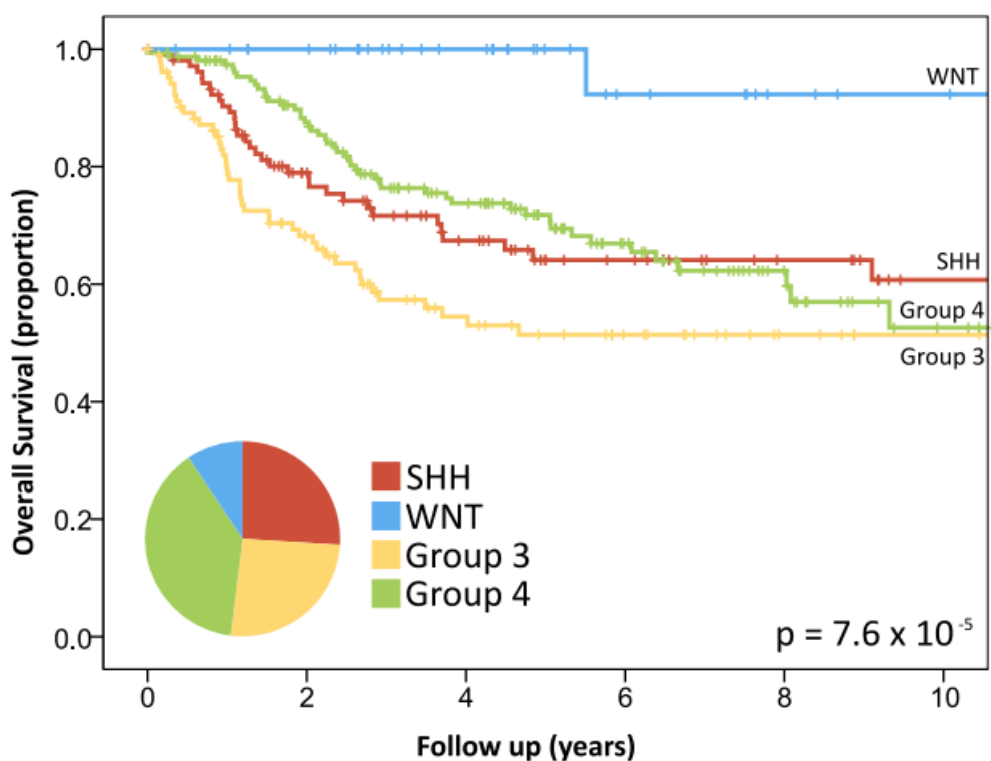


Figure 1.17 Overall survival of Medulloblastoma subgroups (Figure by Matt Selby)

1.5.4.1 WNT

The WNT MB (MB_{WNT}) subgroup accounts for 10% of MB cases. Favourable outcomes are observed for this group of patients with 95% surviving from disease. MB_{WNT} tumours predominantly have classic histology and very low frequency of metastatic cases (Kool et al., 2012). Activating mutations of *CTNNB1* are observed in WNT tumours (Clifford et al., 2006, Ellison et al., 2005). The main cytogenetic feature is frequent observation of monosomy of chromosome 6. Cell of origin studies suggest that these tumours arise from the progenitors of the lower rhombic lip (Gibson et al., 2010).

1.5.4.2 SHH

Several studies have pointed to the cell of origin of MB SHH (MB_{SHH}) tumours as the granule cell progenitors (Gibson et al., 2010, Hovestadt et al., 2019). Over-activation of the SHH pathway leads to an increase in transcriptional regulator *GLI2* which enacts a programme that drives uncontrolled proliferation which ultimately leads to development of cancer (Bai et al., 2002). Somatic or germline mutations of *PTCH1* and *SUFU* including missense mutations in *SMO* define the MB_{SHH} subgroup (Northcott et al., 2012b). Amplifications in *MYCN* and *GLI2* frequently co-occur and is characterised as a

high risk feature (Kool et al., 2014a). These additionally occur alongside inactivation of *TP53* and loss of tumour suppressor functions (Northcott et al., 2012b, Rausch et al., 2012). Age is an important discriminator in this subgroup. For instance alterations in *SUFU* are associated with infant MB_{SHH} whereas *GLI2* amplifications are linked with older children and adolescents (Northcott et al., 2011, Schwalbe et al., 2017b).

1.5.4.3 Group 3

The next MB subgroup is termed Group 3 (MB_{GRP3}) owing to the absence of a distinct abnormality in a molecular pathway. MB_{GRP3} accounts for 25 – 30% of all MB cases (Roussel and Robinson, 2013). There is a higher male to female frequency in this group. This subgroup is frequently found in children or infants however it rarely occurs in adults (Taylor et al., 2012). MB_{GRP3} is normally observed to have classic or LCA histology. A common genetic feature of group 3 MBs is *MYC* amplification and over-activation of the *MYC* pathway (Taylor et al., 2012). Although bonafide *MYC* amplifications account for around 15% of MB_{GRP3} tumours, transcriptomic analysis reveals a *MYC* signature in this group (Northcott et al., 2012b, Taylor et al., 2012). Additionally *PVT1-MYC* fusions are also found to stabilise *MYC* protein in this subgroup (Northcott et al., 2012b). Amplifications in the transcription factor, *OTX2*, are also observed and are thought to be a driver event in MB_{GRP3} pathogenesis (Boulay et al., 2017, Lu et al., 2017, Northcott et al., 2017). Interestingly, *OTX2* is a transcription factor involved in cell fate determination and differentiation of progenitors (Nishida et al., 2003). Patients in this subgroup have the worst survival outcome of all MB. Improved stratification of MB_{GRP3} has revealed two distinct subtypes with survival outcomes primarily based on the presence of high risk features which ultimately affect survival outcomes (Schwalbe et al., 2017b).

1.5.4.4 Group 4

Group 4 MB (MB_{GRP4}) accounts for the majority of MB cases however its molecular underpinnings remains very limited. MB_{GRP4} have intermediate survival outcomes with 75% of patients surviving in this subgroup. Frequent somatic mutations in histone H3 lysine 27 demethylases 6 A (KDM6A) are commonly reported. Amplifications in *MYCN* and *CDK6* are amongst the genetic characteristics of this subgroup (Taylor et al., 2012).

1.5.5 The role of *MYC* in cancer

1.5.5.1 *MYC* structure and function

The *MYC* family of transcription factors (*MYC*, *MYCN*, and *MYCL*) are basic helix-loop-helix leucine zipper (bHLH-LZ) proteins (Figure 1.18). *MYC* forms heterodimers with other bHLH-LZ proteins. Dimerisation is critical for its transcriptional function in response to mitogenic, apoptotic or oncogenic signalling. *MYC* forms heterodimers with its binding partner *MAX*, a small bHLH-LZ protein (Adhikary and Eilers, 2005, Cole and Nikiforov, 2006). The *MYC-MAX* complex binds to specific DNA consensus sequences CACGTG which are termed E-box sites (Blackwell et al., 1990). The binding of *MYC-MAX* transcriptional complex is associated with gene activation. Transcriptional repression by *MYC* is associated with binding to the bHLH-LZ proteins of the *MAD/MXI1* family. *Mad* proteins disrupt *MYC* dimerisation with *Max* thus disrupting transcriptional activation by *MYC-MAX* heterodimers. Additionally, *MAD* (*MXI1*) proteins also bind to *MYC/MAX* binding sites where they recruit transcriptional repressors (Schreiber-Agus and DePinho, 1998). The resulting heterodimers bind to the E-box regions enabling transcriptional repression instead of activation. *MYC*-dependent transcriptional repression may occur through the interference of other transcription factors such as *MIZ1* in transformed cells (Wiese et al., 2013). *MYC* has been found to bind around 15% of genomic loci supporting its activity in regulating numerous cellular processes.

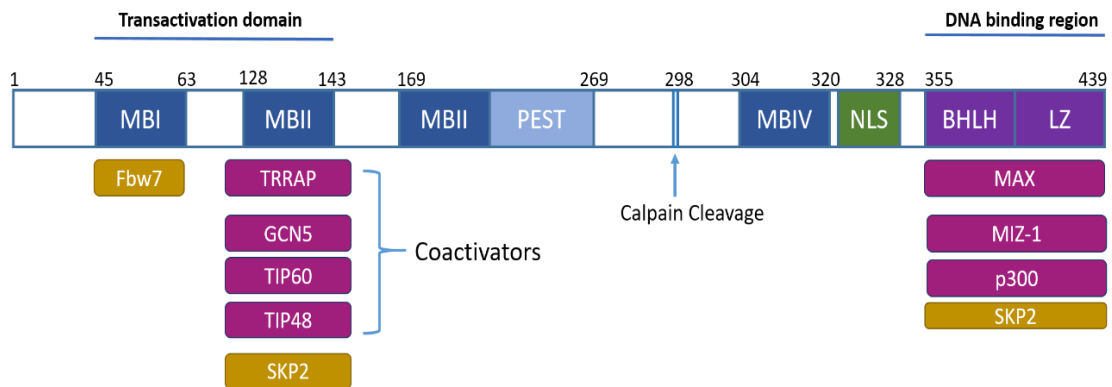


Figure 1.18 Protein structure of MYC. N-terminus contains the transactivation domain and three conserved elements referred to as MYC-boxes (MB). MBI can be targeted by the E3 ubiquitin ligases. MBII is required for all known MYC functions including the recruitment of HATs. MBIII regulates MYC stability and transcriptional activities. The C-terminal domain contains the BHLH/LZ motif responsible for DNA-protein interactions. In fuchsia, MYC interacting partners and in yellow major E3 ubiquitin ligases responsible for MYC turnover.

The transcriptional activity of MYC has been shown to be associated with histone modifications that control chromatin accessibility like ATP-dependent remodelling and histone acetylation. Histone acetylation levels are determined by the activity of histone acetyl-transferases (HAT) and HDACs. MYC was found to be associated with HATs through its interaction with transactivation transcriptional associated protein (TRRAP) and also GCN5 which are found in multi-subunit remodelling complexes. Other HATs known to interact with MYC include TIP60 and CBP/p300 (Vervoorts et al., 2003). MYC was also found to bind to INI1, a subunit of the SWI/SNF remodelling complex (Amati et al., 2001). The level of MYC binding at genomic loci has been shown to be correlated with H3K4 methylation which are active marks but not with H3K27 repressive marks (Guccione et al., 2006).

1.5.5.2 Regulation of *MYC*

The mRNA and protein expression levels of *MYC* are under tight regulation by various mechanisms. The mRNA half-life of *MYC* (~ 30 mins) reflects its high instability and influences the rate of translation of *MYC* proteins. Similarly the protein is rapidly degraded and has high turnover (15 – 20 mins). There are numerous transcription factors that regulated the expression of *MYC* including CNBP, FUSE-binding protein (FBP) and tubulin folding cofactor (TFC). The BET- domain containing transcription factor BRD4 has been shown to bind proximally to the *MYC* promoter and regulates its expression (Delmore et al., 2011).

Other mechanisms of regulating *MYC* expression involves changes in DNA conformation termed non-B DNA structures (Dang, 2012). Furthermore, PTMs of the *MYC* protein can further regulate its transcriptional activity and also protein stability. Two conserved phosphorylation sites found in the transactivation domain (TAD) of *MYC* exhibit this function. Phosphorylation of *MYC* at Ser-62 occurs in response to signalling such as that mediated by ERK or CDK (Bachireddy et al., 2005, Sears, 2004). Phosphorylation at Ser-62 is associated with an activated state and promotes the activity of *MYC*. Conversely, phosphorylation at Thr-58 has been shown to be a priming event for ubiquitin-mediated degradation of *MYC*. Phospho-Thr58 has been shown to correspond with activity of GSK3 β , which lies downstream of the PI3K pathway (Thomas and Tansey, 2011). There are numerous E3 ubiquitin ligases that are known to target *MYC* for proteosomal degradation of which FBW7 is the best characterised (Farrell and Sears, 2014). Other modifications at the Thr-58 site such as acetylation or O-GlcNACylation are thought to compete with phosphorylation and promote stability of *MYC* (Farrell and Sears, 2014, Makwana et al., 2019). *MYC* can be targeted for degradation by alternative pathways. For instance calpain-dependent cleavage of *MYC* results in partial degradation which results in “*MYC*-nick” which does not possess transcriptional activity (Conacci-Sorrell et al., 2010).

1.5.5.3 Oncogenic functions of *MYC*

The discovery of *MYC* came from studies focused on oncogenic retroviruses which was attributable to the expression of v-Myc (Duesberg and Vogt, 1979, Hu et al., 1979). However, the human paralogue *MYC* (C-*MYC*) functions differently and is not associated with oncogenic retroviral infections. Chromosomal translocations found in Burkitt lymphoma led to the identification of the oncogenic function of *MYC*. Unlike other oncogenes, mutations in *MYC* are limited. However its oncogenic functions are derived from mechanisms that lead to overexpression of *MYC* protein and also escape from normal regulatory controls. Genetic aberrations leading to increased *MYC* levels include, small and large focal amplification and also double-minute chromosomes. It is noteworthy that increased copy number does not always lead to *MYC* overexpression (Tansey, 2014). Although not frequently reported, mutations in *MYC* gene also occur. Around half of Burkitt lymphoma cases have reported altered coding sequence of *MYC*. However, in other cancers, it appears to occur as a consequence of other genetic rearrangements and does not drive tumourigenesis in these instances (Schaub et al., 2018, Tansey, 2014). Nevertheless a comprehensive analysis of *MYC* deregulation in human cancers found 50% of cancer to have deregulated *MYC* activity (Beroukhim et al., 2010). Interestingly, alterations in *MYC* is associated with worse patient outcomes in cancers such as ovarian, breast, gastric and some medulloblastoma subgroups (Vita and Henriksson, 2006, Schwalbe et al., 2017a). It has since been recognised that *MYC* amplifications occur in a variety of cancers and are one of the most frequently observed genetic aberrations in cancer (Beroukhim et al., 2010, Schaub et al., 2018). Additionally deregulated *MYC* activity can arise due to defects in other pathways such as the WNT-APC, SHH and NOTCH signalling pathways (He et al., 1998, Palomero et al., 2006). Remarkably, *MYC* in addition with Sox2, Oct4 and Klf4 can act in concert to reprogram fibroblast towards a pluripotent state highlighting its ability in altering cellular phenotypes (Kim et al., 2009, Takahashi and Yamanaka, 2006). Other experiments which employed the use of transgenic mouse models have established the role of *Myc* in driving tumour development (Dang, 2012).

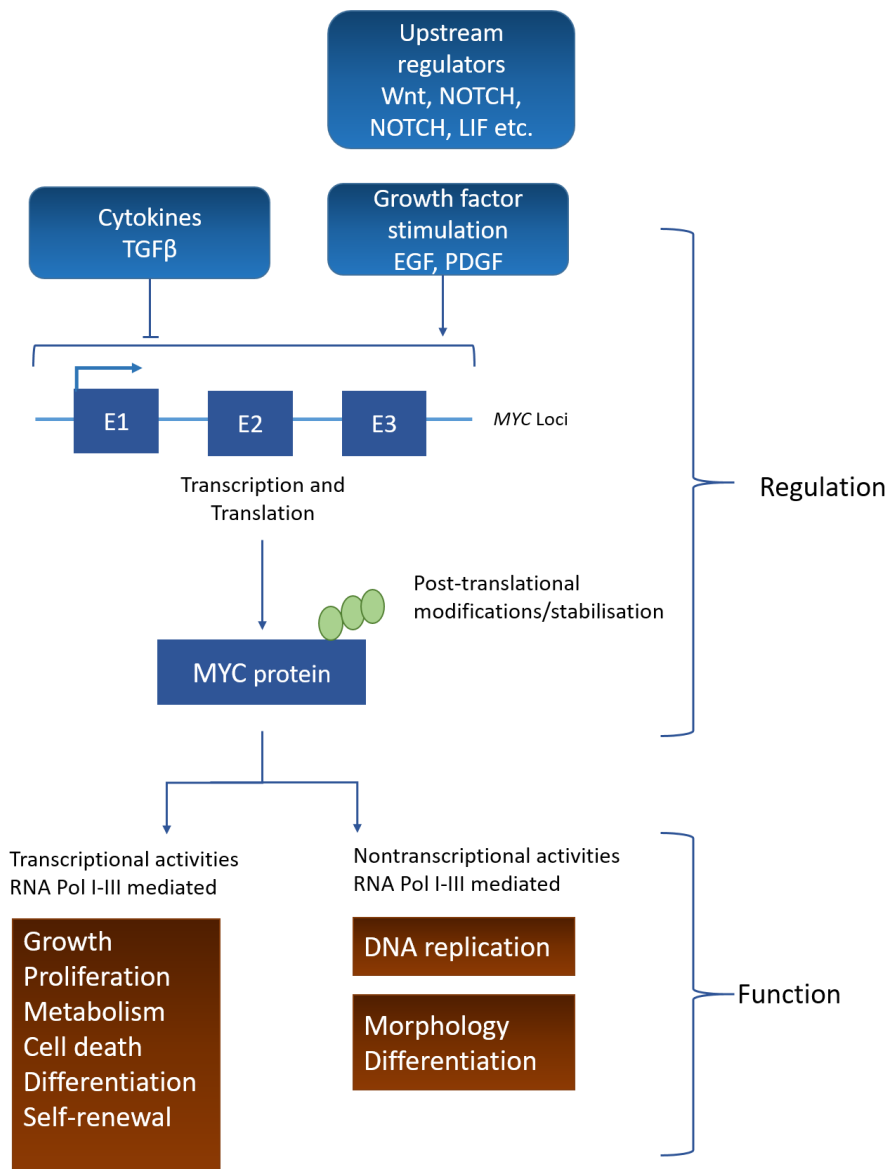


Figure 1.19 Overview of MYC pathway. A simplified diagram of signals leading to MYC expression changes. Subsequent cellular processes affected by the transcriptional and non-transcriptional activities of MYC are indicated.

Cell cycle progression and proliferation

The deregulated activity of MYC drives cellular transformation by altering a wide range of processes that contribute to tumourigenesis. Under normal physiological conditions, MYC orchestrates a transcriptional programme enabling growth by coordinating events in cellular metabolism, mitochondria and ribosome biogenesis which in concert increase biomass (Dang, 2012). MYC itself is not a direct cell cycle regulator however, it majorly influences the ability to enter the cell cycle and can impact the rate of progression through cell cycle phases. MYC activation is associated with changes in cyclins, CDK and CDK inhibitors (CDKI). It does so by tilting the balance towards increase in cyclin D1, CDK4 and CDK6 whilst reducing the expression of negative regulators such as p21. Together, cyclin Ds and CDK4/6 drive quiescent cells to enter cell cycle. Oncogenic MYC enables acceleration through G1 and G2 phase ensuring rapid cell cycle progression in a less restricted manner. Enforced MYC expression is sufficient to drive cell cycle re-entry in quiescent cells (Bretones et al., 2015, Shichiri et al., 1993).

Apoptosis

MYC paradoxically can also trigger apoptosis by regulating the expression or activity of pro-survival BCL2 proteins or pro-apoptotic p53 pathway. Triggering of apoptosis ultimately leads to perturbed mitochondrial function and release of apoptosis stimulating factors such cytochrome c. Release of cytochrome c and other pro-apoptotic proteins such as second mitochondria-derived activator of caspase (SMAC), apoptosis-inducing factor one (AIF1) engages the apoptotic machinery. The BCL2 proteins normally inhibit the function of pro-apoptotic functions of other BCL family proteins including BAX and BAK. MYC can also directly repress BCL2 expression thus enabling progression of apoptosis. MYC can also stimulate the expression of PUMA by P53-dependent or independent mechanisms and disrupting BCL2 function (Nilsson and Cleveland, 2003). MYC and BCL2 are found to be co-amplified in some leukaemias and lymphomas. In DLBCL, it is associated with higher frequency of CNS involvement and correlates with poorer survival (Li et al., 2018, Zou et al., 2017). Co-amplification of MYC and BCL2 family member MCL1 is implicated in drug resistance in TNBC. Overexpression of MYC and MCL1 in cancer stem cell population (CSC) increased OXPHOS and ROS production resulting in therapy resistance (Lee et al., 2017).

Differentiation

MYC plays a vital role in stem cell fate, deciding whether stem or progenitor cells expand or undergo differentiation. Differentiation has been shown to require DNA binding and transcriptional activity of *MYC* (Laverone and Losarella 2014). *Myc* is implicated in neural development where loss of *Myc* can lead to premature neuronal differentiation whereas *Myc* overexpression can 'lock' cells in an undifferentiated and hyper-proliferative state (Zhao et al., 2008). More recent findings have suggested that in distinct neuronal population such as radial glial precursors (RGP), *Myc* plays a varied role where interplay between *Myc* expression and *Notch* signalling dictates cell fate. In RGPs, *Myc* expression caused downregulation of *Notch* and induced differentiation. However, constitutively active *Notch* prevented *Myc* -induced neurogenesis (Zinin et al., 2014). The role *Myc* plays in differentiation is cell/tissue context specific. For instance in proliferative keratinocytes which have unlimited self-renewal capacity, activation of *Myc* stimulated terminal differentiation in these cells (Gandarillas and Watt, 1997). Elimination of *Myc* function in the bone marrow causes significant accumulation of haematopoietic stem cells (HSC). Here loss of *Myc* impairs differentiation in the bone marrow niche (Wilson et al., 2004).

Cellular metabolism

In its oncogenic function, MYC promotes cancer cell proliferation and induces changes in intermediary metabolism to support uncontrolled growth (Figure 1.20). Notably, it induces transcription of several enzymes in glycolysis such as HK2, PFKM, ENO1, LDHA and GLUT1 (Dang et al., 2009). Interestingly, MYC supports alternative splicing mechanisms of PKM generating PKM2 as the predominant isoform (Luan et al., 2015). LDHA is frequently overexpressed in *MYC*-driven tumours. The activity of LDHA is particularly important in regenerating NAD⁺ which sustains high glycolytic flux (Keith Chenault and Whitesides, 1989, Allison et al., 2014). *MYC* also plays a role in shunting glycolytic intermediates into anabolic pathways. To progress through cell cycle, cells must grow and duplicate DNA. MYC regulates the expression of enzymes involved in the oxidative and non-oxidative branch of the PPP. For example it promotes the expression of G6P dehydrogenase (G6PDH) which supports the biosynthesis of ribose sugars required for nucleotide synthesis (Morrish et al., 2009, Wang et al., 2011). Early studies in rat fibroblasts showed Myc induced expression of SHMT1 and SHMT2 (Nikiforov et al., 2002). Since then, MYC has been shown to regulate the expression of PHGDH, PSAT1 and PSPH in hepatocellular and liver cancer models (Sun et al., 2015, Anderton et al., 2017). Apart from directly regulating expression of enzymatic components of the glycolytic pathway, MYC impedes activity of transcriptional regulators of glycolysis. For instance MYC blocks activity of MondoA which in turn inhibits thioredoxin-interacting protein (TXNIP), a negative regulator of glycolysis (Tanner et al., 2018). Glycolysis also generates substrates used in PTMs such as GlcNACylation. *MYC* upregulation fuels these reactions of its target proteins. Interestingly, MYC itself is a target of O-GlcNACylation on its Thr-38 site and promotes stability of *MYC* protein. Introduction on GlcNAC moiety competes with phosphorylation which normally prepares MYC protein for proteosomal degradation (Itkonen et al., 2013).

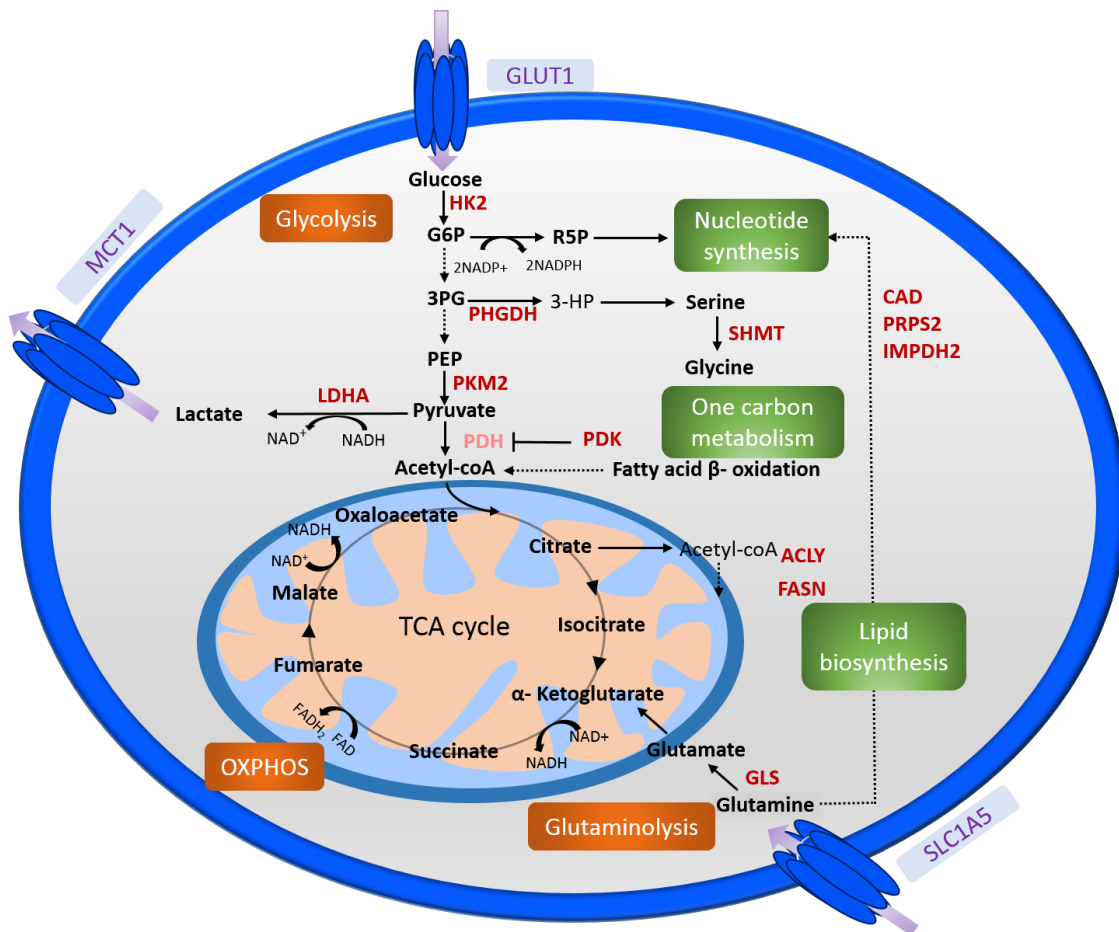


Figure 1.21 MYC-driven transcriptional regulation of metabolism. MYC directly regulates transcription of enzymes involved in bioenergetics and biosynthetic reactions (red). Indirectly targeted enzymes (orange). MYC also induces the expression of glucose, amino acid and monocarboxylate transporters.

Additionally, MYC expression is correlated with increased expression of the membrane transport proteins SLC1A5 (ASCT2) and SLC38A5 and increased glutamine consumption (Wise et al., 2008, Yuneva et al., 2007). These transporters also support the influx of amino acids serine and alanine which can be utilised in biosynthetic pathways. MYC-driven glutamine catabolism has been attributed to GLS1 through direct transcriptional regulation or indirectly by inhibiting micro-RNA 23 (miR-23) which normally inhibits GLS1 translation (Yuneva et al., 2012).

1.5.6 Role of *MYC* in medulloblastoma

The deregulated activity and oncogenic functions of *MYC* is well described for numerous cancers. In medulloblastoma, overexpression and amplifications of *MYC* (*C-MYC*) and its homologues *MYCN* and *MYCL* have been previously reported (Northcott et al., 2017, Taylor et al., 2012). In fact *MYC/MYCN* amplifications are utilised in MB risk stratification. Although deregulated activity of the *MYC* family members is reported across MB subgroups, differences in the role of *MYC* emerges in these distinct MB groups. For MB, the clinical and biological impact of *MYC* family overexpression/amplification is highly context dependent.

1.5.6.1 *MYC* in WNT

Moderate expression of *MYCN* and *MYCL1* can be observed in MB_{WNT} subgroup. However, high expression of *MYC* is observed in this subgroup and is comparable to levels seen in MB_{GRP3} tumours. Although *MYC* overexpression is linked to aggressive disease, this is not observed in the WNT subgroup. Overexpression of *MYC* in this subgroup is a consequence of over-activation of the WNT pathway. *MYC* is a downstream effector of the *WNT* signalling axis and its expression is increased via high activity of *CTNBB1* and its transcriptional interactions (He et al., 1998). Thus, *MYC* expression in MB_{WNT} is a marker of upregulated WNT signalling and not thought to be a primary driver of tumourigenesis. Indeed enforced expression of *MYC/MYCN* in distinct cell populations of the cerebellum does not recapitulate WNT tumours in mouse models (Zindy et al., 2007, Swartling et al., 2010, Swartling et al., 2012).

1.5.6.2 *MYC* in SHH

High expression of *MYCN* and *MYCL1* is observed in MB_{SHH} tumours compared to the other 3 MB subgroups. In this subgroup, overexpression of *MYCN* can occur through the SHH signalling or copy number gains of *MYCN* (Northcott et al., 2017, Northcott et al., 2011). These distinct mechanisms influences tumour biology and survival outcomes. *MYCN* amplifications occur in 8% of SHH cases and are associated with worse outcomes particularly when they occur in conjunction with LCA histology and *TP53* mutations (Rausch et al., 2012, Robinson et al., 2012). The development of SHH mouse models have also shed light on these modes of *MYCN* upregulation. The activation of SHH promotes *MYCN* protein stability in GEMM SHH model (Thomas et al., 2009). Additionally, enforced expression of *MYCN* in conjunction with *Ptch1* and *Cdkn2*, or *Tp53* and *Cdkn2* genetic backgrounds accelerates formation of SHH tumours in mice and

results in enhanced tumour aggression (Kawauchi et al., 2012, Zindy et al., 2007). Although high expression of *MYCN* is characteristic of MB_{SHH}, *MYCN* amplifications are a strong prognostic feature in this subgroup only and is included in MB risk stratification protocols (Roussel and Robinson, 2013).

1.5.6.3 *MYC* in Group 3

MYC is more closely linked with the MB_{GRP3} than any other MB subgroup. It has been shown to give rise to highly aggressive tumours and have the worst overall survival of MB (Schwalbe et al., 2017a). Amplification of *MYC* is observed more frequently in this subgroup (~20%). Typical expression of *MYC* exceeds all other subgroups with WNT being a notable exception. *MYC* amplification is also associated with LCA histology, two features which are established high risk features of MB and associated with much worse survival outcomes (Stearns et al., 2006). *MYCN* amplifications also occur in MB_{GRP3} but are less frequent (2-4% of cases) (Northcott et al., 2012b). Orthotopic mouse models and GEMMs of group 3 have previously been established. These models rely on loss of *TP53* in conjunction with enforced expression of *MYC/MYCN* to model Group 3 MBs. Although loss of P53 is not usually observed in human MBs, the resultant tumour from these mouse models recapitulate MB_{GRP3} tumours at the histological level and also model disease aggression (Swartling et al., 2012).

1.5.6.4 *MYC* in Group 4

The levels of *MYC* and *MYCN* in MB_{GRP4} is comparatively lower than the other MB subgroups. *MYCN* expression exceeds levels in the adult cerebellum but remarkably resembles expression levels observed in foetal cerebellum (Swartling et al., 2010). This suggests that *MYCN* expression may play a role in tumour maintenance. *MYCN* amplifications do not co-occur with epigenetic mutations in genes such as *KDM6A* and histone deacetylases (HDAC) or other amplifications. Although low frequency of *MYCN* amplifications is observed in group 4 tumours (~7%), it may exclusively drive tumourigenesis in subsets of group 4 tumours (Roussel and Robinson, 2013, Roussel and Stripay, 2018).

1.5.7 Challenges in treating *MYC*-amplified Group 3 MB

MYC amplifications and amplifications in family members occur across MB in varying frequencies as discussed in 1.5.5. However *MYC* amplifications are more closely associated with the MB_{GRP3} subgroup. This group of patients have dismal survival outcomes compared to other MB subgroups. There is an overwhelming need for more effective treatment and particularly more targeted approaches which rely on the biology of these tumours. The oncogenic activity of *MYC* regulates a broad range of biological processes and drives transformation (Figure 1.22). Currently, there are no targeted therapies for these high risk patients. Targeting *MYC* directly has so far not yielded convincing *in vivo* utility although there are anti-*MYC* therapies showing promising effects *in vitro* and *in vivo* (Beaulieu et al., 2019). Alternative strategies are required to treat patients with *MYC*-driven MB tumours effectively. One such example resulted from a high-throughput drug screening approach which identified Gemcitabine and Pemetrexed (two antimetabolite therapies) which in combination was selective against *MYC*-amplified MB_{GRP3} (Morfouace et al., 2014). Current clinical trials are assessing its use for high risk MB (NCT01878617).

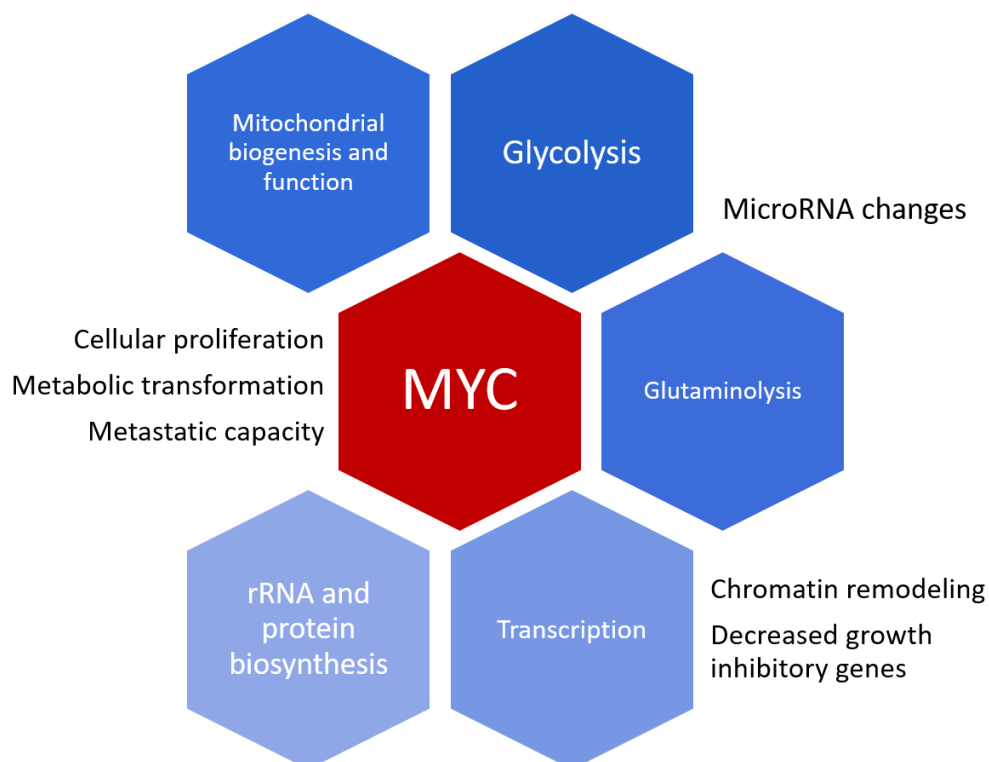


Figure 1.22 Pleiotropic effects of *MYC*. Molecular and cellular features contributing to *MYC*-driven transformation. *MYC*-driven changes occur in large gene sets and gene families which drive alterations in these cellular processes and pathways.

1.5.7.1 *MYC*-driven alterations in medulloblastoma metabolism: opportunities for therapeutic targeting

The regulatory control of *MYC* over various aspects on tumourigenesis, particularly sustained proliferation is served by altered metabolic functions and nutrient status (Dang, 2013a). Metabolic enzymes offers numerous druggable targets and present opportunities for targeting *MYC*-dependent metabolic reprogramming in MB_{GRP3} tumours. At present, the metabolic landscape of MB is not well understood. However, recent studies have shed light on metabolic phenotypes of *MYC*-driven MB_{GRP3} . Glutamine addiction has been suggested for several *MYC*-driven cancers (Yuneva et al., 2007). A recent study carried out by Tao and colleagues demonstrated *MYC* rewiring of metabolism in a model of *MYC*-driven MB_{GRP3} . Furthermore they showed that inhibition of LDHA was selectively toxic against *MYC*-amplified MB_{GRP3} cells compared to MB_{SHH} and normal cerebellar progenitors (Tao et al., 2019). The prodrug JHU-083 which inhibits GLS activity has been shown to impede in growth *MYC*-amplified MB cells *in vitro* and *in vivo* (Hanaford et al., 2019). These studies have highlighted metabolic features of MB_{GRP3} and also demonstrate opportunities to target altered metabolic phenotypes in MB.

1.6 Research background

Malignant brain tumours present in both adult and paediatric populations. Whilst the genesis of these cancers across the age spectrum is complex and affected by genetic, developmental and environmental factors, malignant brain tumours contribute significantly to cancer mortality in both populations. Glioblastoma (GBM) is a Grade IV astrocytoma and is the most commonly occurring primary adult brain tumour (Louis et al., 2018). Owing to aggressiveness and extent of tumour infiltration into normal brain regions, they are difficult to treat and are very lethal with only 5% of patients surviving up to 5 years. Further difficulties in treating these tumours is their intrinsic or acquired drug resistance to many therapies. Additionally, the BBB limits accessibility of drugs to the tumour site. GBM are thought to undergo several metabolic adaptations in order to sustain rapid proliferation. It is increasingly understood that GBM not only alter glucose metabolism, but they increase several aspects of metabolism such as lipid metabolism through a number of molecular mechanisms including growth factor signalling that regulates metabolic flux (Strickland and Stoll 2017). Fatty acid oxidation has been shown to contribute to acetyl-CoA pools that maintain ATP turnover through oxidative phosphorylation (Mashimo et al., 2015). Interrogating these alterations in lipid metabolism may provide useful insights into GBM tumour biology and subsequent viable therapeutic options for this group of patients.

In the paediatric population, MB is the most common primary brain malignancy and although survival outcomes are promising for MB overall, the MB subgroup MB_{GRP3} is a high risk tumour and patients with genomic amplifications of *MYC* have even worse prognosis (Taylor et al., 2012). Although molecular classification using NGS techniques has enlightened and revealed distinct subgroups and subtypes of MB, the underlying biology of these tumours are less defined. Recent efforts have sought to elucidate cell of origins of MB, and have highlighted different neural progenitors and lineages in which they may arise (Hovestadt et al., 2019). Since the neuronal population like NSCs, astrocytes and neurones have distinct metabolic requirements, it is vital to delineate any metabolic reprogramming of MB. Since metabolic alterations can relate to genomic features like *MYC* amplification, uncovering dependencies of MB_{GRP3} may give rise to novel candidates for therapeutic targeting which are needed to improve patient outcomes.

1.7 Aims of project

This project aims to explore metabolic dependencies that may contribute to the pathogenesis of malignant brain tumours, and to use these to identify potential therapeutic targets.

Aim 1: To investigate further, the dependence of gliomas on fatty acid oxidation and why this is the preferential metabolic pathway for fuel supply in GBM. I will investigate inhibition of energy metabolism with a new pharmaceutical intervention combining etomoxir with standard chemotherapeutic drugs for slowing GBM progression in a syngeneic mouse model of GBM. This project will also explore malignancy associated metabolic characteristics which drive progression of malignant gliomas. Findings are presented in Chapter 3.

Aim 2: To identify the metabolic changes associated with *MYC* amplification in Group 3 medulloblastoma using isogenic *MYC* regulable cell line models. I will explore the relationship between *MYC* and metabolic pathways and whether these interactions affords medulloblastomas the metabolic plasticity to sustain bioenergetics and biosynthetic requirements during progression. Findings are presented in Chapter 4 and Chapter 5.

Aim 3: To explore possible pharmaceutical interventions targeting *MYC* driven pathways and whether changes in metabolism may provide suitable biomarkers for identifying malignant features, subgroup classification and prognostic markers of *MYC* driven medulloblastoma. Findings are presented in Chapter 6.

Chapter 2 Materials and Methods

2.1 Methods used for Chapter 3

2.1.1 Mouse neural stem cell culture

Neural progenitor cells (NPCs) were previously isolated from adult wild type C57/B6 mice (Mikheev et al., 2009). NPCs were oncogenically transformed by an overexpression of HRas- (*Ha-RasV12*) and inhibition of *p53* and *p16/Rb* axis by human papillomavirus (*Hpv18 E6E7*) overexpression (previously carried out by Dr. Elizabeth Stoll). Transformed cells were maintained in serum-free Dulbecco's modified eagle's medium/F12 (Omega Scientific, USA) supplemented with 2 mM glutamine (Sigma Aldrich), 1% (v/v) N-2 supplement (Thermo Fisher) and 25 ng/mL EGF (Peprotech,UK) and 25 ng/mL FGF (Peprotech, UK). NPCs were routinely grown as neurospheres on poly-L-lysine (Sigma Aldrich) coated culture plates and were kept in a humidified incubator at 5% CO₂ and 37 °C. To coat plates with poly-L-lysine, a 1:6 dilution was made 0.1% (w/v) poly-Lysine solution and 1 x phosphate buffered saline (Sigma Aldrich, UK). The coating solution was added in a sufficient quantity to cover entire culture surface and incubated for at least 2 h prior to use. In between passages, cells were re-fed with growth factors (25 ng/mL EGF and 25 ng/mL FGF) in 2 mL of growth medium. Cells were passaged when they reached 80% confluence. To passage cells, 2 mL of accutase™ (Stemcell Technologies, UK) was directly added to 10 mL of growth medium containing neurospheres and incubated at room temperature for 5 – 10 minutes. To further dissociate neurospheres, cell suspension was pipetted up and down briefly to form a single cell suspension. Cell suspension was transferred to a conical tube (Corning®, UK) and centrifuged at 1000 rpm for 5 minutes. Supernatant was discarded and cells re-suspended in 5 mL of growth medium. NPCs were re-plated in a total 10 mL of fresh growth medium.

Table 2.1 Oncogenic NPCs and GBM initiating cells used in this thesis.

Cell line	Age of mice at NPC isolation	Culture medium
3month NPCs	3 month male C57/B6	DMEM/F12, 1% N2, 25 ng/mL EGF, 25 ng/mL FGF, 2mM glutamine
12 month NPCs	12 month male C57/B6	DMEM/F12, 1% N2, 25 ng/mL EGF, 25 ng/mL FGF, 2mM glutamine

2.1.2 Syngeneic mouse model of glioma

All *in vivo* experiments were carried out in accordance with Animals (scientific procedures) Act 1986 (UK Home office) and approved by the local ethics committee (AWERB). Oncogenically transformed NPCs isolated from adult-wild type C57BL/6 mice (Charles River laboratories, UK) were orthotopically transplanted into the striatum of male adult mice with the same genetic background (carried out by Dr. Elizabeth Stoll). A total of 1×10^4 cells/ μL was injected into two sites of striatum, AP +1.0, ML -1.0, DV -3.5 and -3.0. Animals were monitored daily and clinically scored according to a custom clinical scoresheet (Appendix 3.1).

Fourteen days subsequent to intracranial cell implantation, animals were treated with 67 mg/kg of temozolomide (TMZ) (Sigma Aldrich) or 10% DMSO/ PBS (v/v) (Sigma Aldrich, UK) solution once daily via intraperitoneal injection for 5 days (Robinson et al., 2010). Following this, animals were treated daily with 10 mg/kg of etomoxir (ETX) (MetaIQ, Denmark) or olive oil by oral gavage for the duration of the study. Animal drug groups: vehicle control n= 2 (10% DMSO/ PBS and olive oil), etomoxir n=2 (10% DMSO PBS and ETX), temozolomide n= 2 (TMZ and olive oil) and Combination n= 2 (10 mg/kg ETX and 67 mg/kg TMZ). Unfortunately, early loss of animals resulted in low sample numbers in drug groups which were originally assigned n= 5 for each drug treatment group in this pilot study. Once treatment commenced, all animals were kept on a soaked diet to ensure feeding whilst receiving daily dosing by gavage. Unfortunately, early loss of animals resulted in low sample numbers in drug experimental groups. A contraindication placed during the study was to switch animals that experienced any complications or difficulty due to gavaging to coconut pellet with ETX or vehicle which was voluntarily administered. Clinical monitoring and drug administration for this study was carried out independently.

2.1.3 *In vitro* ¹H NMR spectroscopy

Oncogenically transformed NPCs derived from 3 month and 12 month old mice (described in 2.1.1) were grown in serum-free growth culture medium in 10 cm culture dishes in the following drug conditions for 24 hours: Control (PBS and 10% (v/v) DMSO), 100 μ M etomoxir, 100 μ M temozolomide and combined (100 μ M ETX, 100 μ M TMZ) in duplicate. Cells were washed in PBS and centrifuged at 1500 rpm for 3 mins and pellets frozen until use. Cells were re-suspended in 500 μ l of deuterium oxide for signal locking (Sigma Aldrich, UK) and loaded into a 5mm NMR tube. One dimensional ¹H NMR spectra were acquired using a 700 MHz spectrometer (Bruker Biospin GbmH, Germany) at 294K. ¹H spectra were acquired with water suppression using pre-saturation, spin echo and TE = 8ms (Spectroscopy experiments carried out by Liam Mistry). Spectral processing was executed using Mestresnova version 11 (Mestrelabs Research S.L.). All spectra were baseline corrected using the ablative method and out of phase spectral regions corrected manually. Metabolites were assigned based on literature and the human metabolome database. The area under each peak was defined by their integral values which were normalised to the total area of spectrum and referenced to creatine at 3.03ppm. All data analysis of raw data was performed independently.

Statistical analysis.

Multivariate analysis using principal component analysis (PCA) was performed using Metaboanalyst software version 4 (<https://www.metaboanalyst.ca/>). Regions containing solvent peaks were discarded from the analysis.

2.1.4 *In vivo* magnetic resonance imaging and spectroscopy

2.1.4.1 MRI

All magnetic resonance experiments were acquired using a 7T Varian imaging system (Varian Inc., Palo Alto, USA) equipped with the Rapid 33mm volume coil (RAPID Biomedical GmbH, Germany) to transmit/receive MR signals. Animals were anaesthetised using a mixture of isoflurane/oxygen gas. Animals were fitted on a custom loading sled with pneumatic pillow for respiratory and surface temperature monitoring (SA instruments) and small animal system was used for physiological monitoring. Scout images were used to ensure animals were correctly orientated for brain imaging. A total of 4 imaging sequences were used to acquire brain images of different contrasts by altering repetition time (T_R) and echo time (T_E). Parameters for spin echo multi-slice

sequence (SEMS) were: SEMS 1 (TR 1000 ms TE 20ms), SEMS 2 (TR 1000 ms TE 20 ms with inversion recovery TI= 150 ms), SEMS 3 (TR 1100 ms TE 60ms) and SEMS 4 (TR 1600 TE 85ms). All image sequences were acquired using matrix 256 x 256, field of view 25 x 25 mm, and slice thickness 1 mm. To evaluate tumour development and progression, animals were imaged from day 50 and every 14 days subsequent to that.

2.1.4.2 MR Spectroscopy

Single voxel spectra were acquired from ipsilateral (intracranial injection site) and contralateral (normal brain) sites for each animal using point resolved spectroscopy sequence (PRESS). Selection of volume of interest was guided by previously acquired MR images. PRESS sequence parameters were: TR 2000ms, TE 8ms, 4096 real points and 100 averages. Localised manual shimming was performed for each cubic voxel (2 mm x 2 mm x 2 mm) resulting in an unsuppressed water signal with line width between 20-30Hz. Suppression of the water signal was optimised using variable RF pulse with optimised relaxation delays (VAPOR) water suppression. Proton NMR was performed at a short TE of 8 ms to acquire signal from a broad range of metabolites. All imaging and spectroscopy experiments and subsequent data analysis were carried out independently.

2.2 Methods used for Chapter 4

2.2.1 Medulloblastoma cell culture

2.2.1.1 Cell line authentication and handling

Cell lines used in this thesis were previously authenticated and identity confirmed by Dr Janet Lindsey. Validated stocks of these cell lines were maintained and used in subsequent generation of engineered cell lines and parental cell line experiments. Additionally, cell lines were routinely tested for mycoplasma contamination. Cells used in all experiments were negative for mycoplasma.

2.2.1.2 Cell lines and culture medium

MYC-amplified MB_{GRP3} cell lines D425, D283 and HDMB03 were previously engineered with a tetracycline (TET) inducible shRNA targeting *MYC* (Tet-pLKO-puro, Addgene plasmid #21915) (Cell lines were generated by Shanel Swartz, (Swartz, 2018)). The cell lines were transduced with two independent doxycycline inducible shRNA constructs targeting *MYC* for knockdown and a non-silencing (NS) shRNA construct which served as control (shRNA targeting sequences are outlined in Table 2.2). The two lentiviral vectors against bind *MYC* mRNA at different locations, For *MYC* 2 shRNA the *MYC* target sequence GATGAGGAAGAAATCGAT binds between 1180 to 1197bp. For the *MYC* 3 shRNA, *MYC* specific target sequence CCTGAGACAGATCAGCAACAA, binding occurs between 1404 to 1424bp. Addition of doxycycline to the growth medium triggers the expression of shRNA causing *MYC* knockdown (depicted in Figure 2.1). Isogenic cell lines were routinely cultured in Dulbecco's modified eagle medium (DMEM) (Sigma Aldrich, D6171) or Roswell Park Memorial Institute medium 1640 medium (RPMI) (Sigma Aldrich, R5886) and supplemented as described in table Table 2.3.

Table 2.2 Target sequences for shRNA constructs

Construct	Target sequence	Reference
NS	5'CCGGCAACAAGATGAAGAGCACCAATCGAGTTGGTG CTCTTCATCTTGTTGTTTTT3'	(Li <i>et al.</i> , 2010)
MYC 2	5'AATTAAAAACAACAAGATGAAGAGCACCAACTCGAG TTGGTGCTCTTCATCTTG TTG 3'	(Li <i>et al.</i> , 2010)
MYC 3	5'CCGGCCTGAGACAGATCAGCAACAACTCGAGTTGTT GCTGATCTGTCTCAGGTTTTT 3'	(Raeder <i>et al.</i> , 2013)
	5'AATTAAAAACCTGAGACAGATCAGCAACAACTCGAG TTGTTGCTGATCTGTCTCAGG 3'	

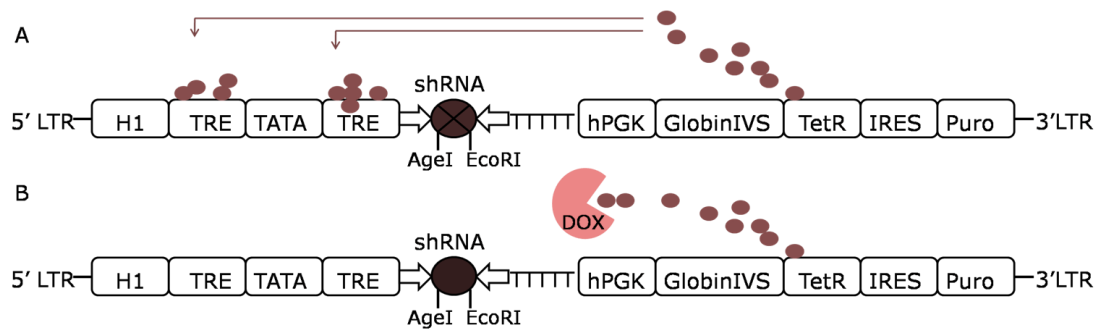


Figure 2.1 Schematic of pLKO-Tet-on inducible system. A) In the absence of doxycycline (DOX) the Tet repressor (TetR) (orange dots) bind to the Tet-response element (TRE) and inhibit the expression of the shRNA. B) In the presence of doxycycline, doxycycline binds the Tet repressor preventing it from binding the TRE enabling the expression of shRNA targeting MYC for Knockdown.

Table 2.3 MYC-inducible cell lines used in this thesis

Cell line	MYC status	shRNA construct	Culture medium
D425	Amplification	NS, MYC 2, MYC 3	DMEM, 10% TET free FBS, 2mM glutamine, 1 µg/mL puromycin
D283	Gain	NS, MYC 2, MYC 3	DMEM, 10% TET free FBS, 2mM glutamine, 1 µg/mL puromycin
HDMB03	Amplification	NS, MYC 2, MYC 3	RPMI, 10% TET free FBS, 2mM glutamine, 1 x NEAA, 1 µg/mL puromycin

2.2.1.3 Cell maintenance

Cells were routinely grown in T75 or T125 (Corning®, UK) flasks as a mixture of adherent cells and neurospheres and were kept in a humidified incubator at 5% CO₂ and 37 °C. Exponentially growing cells were sub-cultured routinely for maintenance or for cell based assays. To passage cells, growth medium containing neurospheres were collected into a 15 or 50 mL conical tube. The remainder of cells which had adhered to the culture flask were washed once with phosphate buffered saline (PBS) (Sigma Aldrich, UK) followed by addition of 2- 4 mL of Trypsin-EDTA (1x) (Sigma Aldrich, UK) to the culture flask and placed in humidified incubator for approximately 5 minutes. Trypsin was deactivated by adding 5 mL of growth medium which was collected and added to the previously collected cells. Cells were pelleted by centrifuging at 1000 rpm for 5 min. The supernatant was discarded and cells were re-suspended in 5 mL of fresh growth medium. Cells were split at 1: 3-6. All experiments were limited to cells with passage not exceeding 40.

2.2.1.4 Cell counting and seeding

Cell counting was carried out on a haemocytometer or an automated counter (Countess II, Invitrogen). Cells were harvested according to the protocol in 1.2.1.2. Following resuspension, 10 µL of the cell suspension was added to an equal amount of trypan blue (Invitrogen), an exclusion dye for assessing viability. 10 µL of the cell/trypan blue mixture was loaded into a haemocytometer chamber or onto a countess slide. For manual

counting, viable cells in the four corner squares were counted. Cell number was quantitated using the following equation:

$$\text{Cells per ml} = \frac{\text{Total number of cells}}{4} \times 2 (\text{dilution factor}) \times 10^4$$

2.2.1.5 Freezing and thawing

Following the protocol described in 1.2.1.2, a T75 or T125 of cells at 80-90% confluence were trypsinised and re-suspended in cold freezing medium (90% FBS, 10% DMSO (v/v)) and aliquoted in 2 mL cryovials which were placed in a Mr. Frosty and gradually frozen at -80 °C and later transferred to -150 °C for long term storage.

Cells were thawed in a 37 °C water bath and diluted in 20 mL of growth medium to dilute DMSO and plated in a T75 flask. Cells were allowed to acclimatise and passaged twice before use in an experiment.

2.2.2 Protein extraction and quantification

Protein was extracted from 5×10^5 cells using cold RIPA buffer (Sigma Aldrich) supplemented with protease and phosphatase inhibitors to a final concentration of 1x (Life Technologies, UK). Cells were vortexed briefly or sonicated for three cycles (10 seconds on, 10 seconds off). Cell debris was removed by centrifuging at 10,000 rpm for 10 mins at 4°C. Protein was quantified using the Pierce™ bicinchoninic acid (BCA) protein assay kit (23225, ThermoFisher Ltd.) according to manufacturer's instructions. Briefly, bovine serum albumin (BSA) was diluted to achieve BSA protein standards ranging from 20-2000 µg/mL. Working reagent was prepared by mixing 50 parts of BCA reagent A with one part BCA reagent B. In a 96 well microplate, 25 µL of each BSA standard is pipetted into a well, followed by duplicate wells with 10 µL of an unknown protein standard. Finally, 200 µl of working reagent is dispensed into each well and incubated at 37 °C for 30 minutes and absorbance measured at 562nm on a plate reader. A standard curve was generated from the BSA protein standards and used to determine protein concentration of each unknown sample. Protein samples were stored at -20°C until use.

2.2.3 Simple western immunoassays (WES)

WES is a capillary based automated size-based separation immunoassay (Proteintech, Biotechnie Ltd, UK). WES follows similar principle to traditional western blot. Samples are loaded onto assay plates and placed in the WES machine where it is automatically loaded into the capillary and separated by size as they migrate through a stacking/separation matrix. Separated proteins are immobilised to the capillary walls and target proteins detected using primary antibodies and immunoprobed using an HRP-conjugated secondary antibody and a chemiluminescent reagent. The signal is detected and quantitated (Figure 2.2). The protein lysates were loaded into WES plates at 0.8 µg per well. Assay plates were prepared according to manufacturer's instructions.

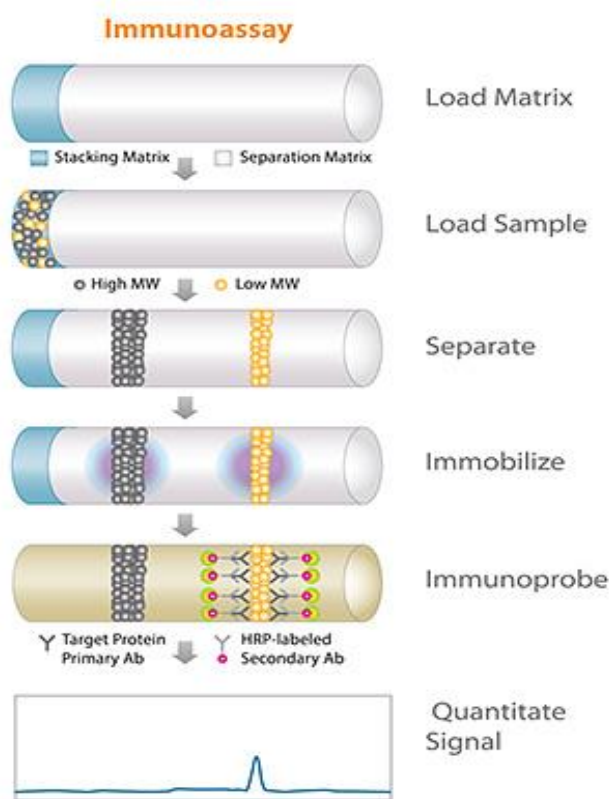


Figure 2.2 Schematic depicting the principles of simple western (WES).

2.2.4 Antibodies

Primary antibodies specific to protein of interest were obtained commercially. To obtain optimal signal from WES, primary antibodies were tested at serial dilutions and a concentration within the linear range of signal was chosen. Species specific secondary antibodies were supplied as part of the WES modules and used according to manufacturer's instructions. A detailed list of antibodies used in this project is provided in Table 2.4.

Table 2.4 List of antibodies used in this thesis

Target	Species	Dilution	Company
β -Actin	Mouse	1:10000	Abcam
GLDC	Rabbit	1:1000	Proteintech
GLS	Rabbit	1:1000	Proteintech
HK2	Rabbit	1:2000	Proteintech
LDHA-Specific	Rabbit	1:5000	Proteintech
MYC	Rabbit	1:5000	Cell signalling
PHGDH	Rabbit	1:8000	Proteintech
PSAT1	Rabbit	1:2000	Proteintech
PSPH	Rabbit	1:50	Proteintech
p-4EBP1	Rabbit	1:1000	Cell signalling
p-S6	Rabbit	1:100	Cell signalling
SHMT2	Rabbit	1:2000	Proteintech

2.2.5 Cell growth curves

Exponentially growing cells were passaged according to the procedure described in 1.2.1.2. The cells were plated at a density of 1×10^5 cells per well in a 6 well plate. Cell counts were performed between 1 and 7 days by counting on a haemocytometer. Doubling times and statistical significance were determined using linear regression on Graphpad Prism 8 (GraphPad).

2.2.6 Cell cycle analysis

To determine cell cycle distribution, cells were stained with a DNA content dye propidium iodide (PI) (Sigma Aldrich) and processed on a flow cytometer. Cells were harvested and pelleted in an appropriate manner and washed/resuspended in cold PBS before centrifuging at 1000 rpm. The supernatant was discarded and cells were fixed in 1 mL of cold 70% (v/v) ethanol. Ethanol was added dropwise to the cell pellet whilst vortexing to minimise clumping. Cells were fixed at 4 °C for at least 30 min. Ethanol was removed from the cells by pelleting cells and discarding the supernatant. Cells were washed twice in PBS and then re-suspended in 0.5 mL of PBS. Cells were treated with 50 μ L of Ribonuclease A (RNAase) (Thermo Fisher) to ensure DNA and not RNA was stained. The staining solution was prepared as a 1: 10 mix of PI/triton, and 250 μ L was added each sample. A list of reagents and preparations are listed in Table 2.5. PI

fluorescence was measured on a suitable band pass filter to determine its emission at 605 nm on an Attune NxT cytometer (Thermo Fisher). Analysis of cell cycle distribution was carried out by measuring forward and side scatter to identify the cell population. Pulse processing using pulse width vs. pulse area was carried out to exclude doublets from the analysis. A combination of the gating of cell population and doublet exclusion was used to generate a PI histogram plot displaying cell populations with 2n and 4n DNA content.

Table 2.5 Preparation of cell cycle analysis reagents

Reagent concentration	Preparation
50 µg/mL Propidium iodide	Prepared in PBS
100 µg/mL Ribonuclease A	Prepared in dH ₂ O and heated at 100°C for 10 minutes
5% Triton-x	Prepared in dH ₂ O

2.2.7 Cellular bioenergetics using XF analyser

To determine glycolytic and mitochondrial function of medulloblastoma cells, the Agilent seahorse XF analyser was used to determine extracellular acidification rate (ECAR) as a function of glycolysis and oxygen consumption rate (OCR) for OXPHOS (Nicholas et al., 2017). Cells were seeded at 8×10^5 cells per well in a XF microplate and incubated overnight. On the day of experiment, growth medium was removed from cells and replaced with assay medium (unbuffered DMEM supplemented with 3% (v/v)FBS, 25 mM glucose, and 2 mM glutamine) and incubated at 37 °C in a non-CO₂ incubator for 1 hour. OCR and ECAR were measured in the XF analyser at basal levels by the sequential injection of the following mitochondrial inhibitors; oligomycin (1 µM) an inhibitor of complex V allowing for the measurement of ATP-coupled OCR, FCCP (3 µM total) a protonophore and membrane potential uncoupler which drives maximal respiration, and finally addition of rotenone (0.5 µM) and antimycin (2.5 µM) to inhibit complex I and III simultaneously. Quantification of intracellular rates of glycolytic and oxidative ATP production were determined following the method described by Mookerjee *et al.*, 2017 using measurements derived from both OCR and ECAR (Mookerjee et al., 2017). The following calculations were used to determine glycolytic and oxidative ATP generation which was then normalised to total protein (µg).

$$Total\ OCR\ (OCR_{resp}) = OCR_{basal} - OCR_{Rot/AA}$$

$$OXPHOS\ OCR = OCR_{basal} - OCR_{OG}$$

$$ECAR_{total} = ECAR_{basal}$$

$$PPR_{total} = \frac{ECAR_{total}}{BP}$$

$$PPR_{resp} = (10^{(pH-pK1)}/1 + 10^{(pH-pK1)})(Max\ H^+/O_2)(OCR_{resp} - OCR_{Rot/AA})$$

$$PPR_{glycolysis} = PPR_{total} - PPR_{resp}$$

$$= \frac{ECAR_{total}}{(BP - (10^{(pH-pK1)}/(1 + 10^{(pH-pK1)})(Max\ H^+ / O_2)(OCR_{total} - OCR_{Rot/AA}))}$$

2.3 Methods used for Chapter 5

2.3.1 ¹H High resolution magic angle spectroscopy (HRMAS)

Cell preparation. D425 cells stably transduced with non-silencing construct and two independent doxycycline inducible *MYC* shRNA constructs were previously engineered (Swartz, 2018). The cells were grown in normal growth culture medium (25mM glucose, 2mM glucose, 10% (v/v) FBS, 1µg/mL puromycin) with/ or without 1µg/ml doxycycline for 72 hours. Cells were scraped, washed twice in ice cold PBS and centrifuged at 1500 rpm for 5 mins at 4°C. Cell pellets were flash frozen in dry ice. *High resolution magic angle spinning spectroscopy.* Cells were thawed and ~ 40 µL of cell pellet was placed into a zirconium oxide rotor and 5 µL of D₂O with TMSP (10mM) added for locking signal and providing a chemical shift reference for each sample, respectively. The rotor was inserted into 4mm 3 channel ¹H HRMAS z-PFG ban probe in a 500 MHz Bruker AVANCE spectrometer. ¹H NMR spectra were acquired at 54.7° magic angle at 4°C at rotor spin speed on 4 Khz. A standard NOESY sequence with water pre-saturation was acquired with a relaxation delay of 2s and repetition time of 4s. Each free induction decay (FID) was Fourier transformed, phased and baseline corrected (Mestresnova). Metabolites were assigned based on the literature and the human metabolome database. The area under each peak was defined by their integral values which were quantified and normalised to the total area of spectrum and referenced to creatine at 3.03ppm. *Statistical analysis.* Multivariate and clustering analysis was performed using Metaboanalyst

version 4. HRMAS experiments were performed by Dr Sarah Kohe (University of Birmingham). All subsequent analysis were performed independently.

2.3.1.1 Multivariate analysis of NMR spectra

Principal Component Analysis (PCA)

PCA is utilised for large and complex datasets to reduce dimensionality but with minimal loss of information. PCA is an unsupervised method meaning that clustering patterns are determined without knowledge of sample classification, treatment groups or phenotype. The goal of PCA is to summarise the data using limited set of variables defined as principal components. Principal components are a linear combination of original variables in the dataset. By looking at different principal components, variance in the data is accounted for. PCA generally performs well for establishing maximum variance of dataset but does not always achieve robust clustering.

Partial least squares-discriminant analysis (PLS-DA)

Like PCA, PLS-DA is also a dimensionality reduction tool however it achieves this with input from sample classification therefore making it a supervised method. Where principal components identify maximal variance, PLS identifies covariance between original data and class labelling. PLS-DA can also be adapted for feature selection however since over fitting of PLS-DA models can occur, it is important that models undergo 'cross validation' prior to use for feature selection. Validation of PLS-DA models ensures the knowledge of sample class does not give rise to false clustering or clustering that occurs by chance. A series of validation tests measure model accuracy and goodness of fit (R^2 and Q^2) of the original model against permuted models where Y (class) have been randomly assigned whilst maintaining X (bins/metabolites) observations. Another feature of PLS-DA is the variable importance projection (VIP) score which highlights the importance of a metabolite/bin region in the model. The VIP score is a weighted sum of squares correlations between PLS components and original variable. Higher VIP scores indicate greater contribution to the separation in the model.

2.3.2 ¹³C- Glucose labelling

The D425 MYC 2 cell line was plated in T75 flask in ± 1 $\mu\text{g/mL}$ of doxycycline for 48h. Cells (5×10^5) were plated in 6 well plates and further treated for $24\text{h} \pm 1$ $\mu\text{g/mL}$ doxycycline. Growth medium was removed from each well, washed with 1 x PBS and replaced with 10 mM D-glucose-¹³C (Sigma Aldrich, UK) containing medium for 6 or 24h. A control plate with unlabelled glucose and a plate for cell number determination was set up in parallel to labelling experiments. On the day of extraction, duplicate wells for each condition was counted. Labelled and unlabelled samples were washed once with ice cold PBS. For metabolite extraction, a mixture containing methanol: acetonitrile: water (50:30:20 vol/vol) was used and the volume used was adjusted to obtain 2×10^6 cells/mL. Cells were scraped into cold extraction mixture on wet ice and homogenised by pipetting. The lysates were transferred into Eppendorf tubes and centrifuged at 15000 g for 15 min at 4°C to pellet the cell debris. The supernatant was transferred to fresh tubes and stored at - 80°C. Labelling experiments were carried out independently.

2.3.2.1 Liquid chromatography- Mass spectrometry (LC-MS)

Analytes were separated using liquid chromatography with SeQuant ZIC pHILIC column (2.1 x 150 mM, 5 μM) coupled to a SeQuant ZIC pHILIC guard column (2.1 x 20 mM, 5 μM) and detected using high resolution MS with Orbitrap Exactive (Thermo Scientific) in line with a Aceela autosampler and Aceela 600 pump (Thermo Scientific). The Exactive operated using polarity switching mode with positive voltage at 4.5 kV and negative of 3.5 kV. Flow rate was 100 $\mu\text{l min}^{-1}$, buffers consisted of acetonitrile (CAN) for A and 20 mM (NH₄) CO₃ in addition with NH₄OH in dH₂O for B. Gradient ran from 80% (v/v) to 40% CAN in 20 min followed by was at 20% (v/v) CAN and re-equilibration at 80% (v/v) CAN. Metabolites were quantified using LCquan (Thermo Scientific). Positive identification of metabolites was on the basis of exact mass within 5 ppm and further validation by concordance with standard retention times and finally plotted as peak area for each metabolite. LC-MS, peak assignment and quantification were performed by Tong Zhang at the CRUK Beatson Institute (Glasgow, UK). Subsequent analysis were performed independently.

2.4 Methods used for Chapter 6

2.4.1 Gene expression analysis

2.4.1.1 R2 Genomics Analysis and Visualisation platform

Microarray data for medulloblastoma patient samples was obtained from the R2 genomics platform (<https://hgserver1.amc.nl/cgi-bin/r2/main.cgi>). The Cavalli *et al.*, cohort which comprises of 763 patient data including relevant clinical data and prognostic factors such as subgroup classification (Cavalli et al., 2017). Of these, there were 144 MB_{GRP3} samples which were used as the discovery dataset for determining significant gene expression changes that distinguished MB_{GRP3} subtypes according to the KEGG defined genes of the “serine_glycine_threonine” pathway.

2.4.1.2 Analysis of Newcastle MB_{GRP3} cohort

Previously generated RNA expression data from primary MB_{GRP3} patient samples (n= 36) which included both MYC-amplified (n=9) and non-amplified (n=27) were used as a validation cohort for gene expression changes in serine/glycine pathway in MB_{GRP3}. Hierarchical clustering and pathway analysis was performed using R statistical packages GSEA, fGSEA and PHeatmap. Data analysis was carried out by Dr Florence Burte.

2.4.2 Immunohistochemistry

2.4.2.1 Medulloblastoma patient tissue microarrays (TMA)

Construction of medulloblastoma patient TMA and immunohistochemical staining was conducted by Dr Stephen Crosier. Core tissue biopsies (1 mm diameter) were taken in duplicate from individual patient formalin fixed paraffin embedded (FFPE) MB tumours and arrayed unto a new paraffin recipient block (35 mm x 20 mm) using an automated tissue processor (Leica TP1020 semi-enclosed benchtop tissue processor). Additionally, samples from normal cerebellum, spleen, placenta and tumour samples from colon and prostate adenocarcinomas were added to each TMA to act as controls for immunohistochemical staining. In total, 199 MB specimens were included in the TMA cohort covering the four major MB subgroups and also diagnostic/relapse pairs. The overall cohort analysis was based on only diagnostic samples (n=183).

2.4.2.2 Immunohistochemical staining

Paraffin embedded TMA slide sections were dewaxed in xylene for 5 min and dehydrated in an ethanol gradient from 95- 50% followed by a 2 min wash in tap water. Heat induced antigen retrieval was performed using 10 mM citrate buffer (pH 6) and microwave heating for 15 min. Slides were briefly washed in tap water followed by three 5 min washes in TBS/Tween wash buffer (50 mM Tris-HCL pH 7.5, 150 mM sodium chloride (Sigma Aldrich, UK), 0.05% Tween 20 (Sigma Aldrich, UK)). The slides were incubated with PHGDH antibody (1:100) for one hour at RT followed by three 5 min washes in wash buffer. For antigen detection, the Menapath X-Cell plus HRP-polymer kit (A.Menarini diagnostics) was used. Slides were incubated with the HRP polymer for 30 min and washed briefly with water prior to a 2 min incubation with 3, 3'- diaminobenzidine. Slides were washed in water and counterstained with haematoxylin (Sigma Aldrich) by immersing in solution for 30- 60 sec and washing in Scott's solution for 2 min. Slides were dehydrated and mounted in DPX and allowed to dry. Analysis of PHGDH IHC staining intensity from slide sections were digitised using a Leica Scanscope Console (Aperio C52) and analysed using the Aperio software (version 12.3.1602, Leica Biosystems). Immunohistochemical staining and digitising was performed by Dr Stephen Crosier. All subsequent analysis of staining intensity was performed independently.

2.4.2.3 Statistical analysis

Cox proportional hazard modelling was used to determine the influence of known prognosticators (Subgroup, age, *MYC* amplification etc.) alongside PHGDH expression and their risk to disease progression. Furthermore, Kaplan Meier survival curves were plotted to study the association between PHGDH expression and survival outcomes. All statistical analysis was carried out on R statistical software using the survminer and ggplot packages.

2.4.3 Cell viability assays

2.4.3.1 Sulforhodamine B (SRB) assay

The SRB assay is a widely used cytotoxicity assay (Vichai and Kirtikara, 2006). The method relies on the ability of the SRB dye to bind stoichiometrically to proteins under mildly acidic conditions which is then extracted under basic conditions. The amount of dye bound is equivalent to cell mass/density which is then used to enumerate cell growth. Cells were plated between 2×10^4 cells/well in a clear 96 well microplate (Corning®, UK). Cells were treated with different growth medium conditions and pharmacological inhibitors which are specified within results chapters. At experiment endpoint, 50 μ L of cold 50% (w/v) trichloroacetic acid (TCA) (Sigma Aldrich, UK) was added to medium in each and incubated at 4 °C for 20 mins. Medium/TCA mixture was discarded and plates washed 3x by submerging in a tub of water with slow running tap water. Plates were dried overnight. Dried plates were stained with 100 μ L 0.04% (w/v) SRB in 1% (v/v) acetic acid for 15 mins. Unbound dye was removed and the plate washed with 1% (v/v) acetic acid then left to dry. Once dried, the dye was solubilised with 100 μ L 10 mM Tris base solution (pH 10.4) to each well and shaken in an orbital shaker for 5 min. The absorbance was measured at 570 nm in a plate reader. Background absorbance from media only wells were subtracted from all wells. Cell viability was normalised to a control/untreated wells using the following formula:

$$\% \text{ Cell viability} = \frac{\text{Absorbance of sample}}{\text{Absorbance of control/untreated}} \times 100$$

2.4.3.2 CellTiter-Glo® 2.0 luminescent assay

The CellTiter-Glo® 2.0 was used to determine cell viability by quantitating the amount of ATP present which is an indicator of metabolically active cells. Cells were plated between $0.5 - 1 \times 10^4$ cells/well in white 96 well microplate and under various experimental conditions. Upon endpoint, 25 μ L of CellTiter-Glo® 2.0 reagent was added to each well and placed on an orbital shaker for 5 min in the dark. Plates were kept at room temperature for 10 min to stabilise the relative light unit (RLU) signal was then read on a microplate reader using a luminescence filter. Cell viability was normalised to a control/untreated wells using the following formula:

$$\% \text{ Cell viability} = \frac{RLU \text{ of sample}}{RLU \text{ of control/untreated}} \times 100$$

2.4.4 Pharmacological inhibition of PHGDH

Two small molecule inhibitors of PHGDH were tested for their growth inhibitory capacity in MB cell lines. NCT503 which is an allosteric inhibitor of PHGDH binds to the NAD⁺ binding pocket of the enzyme and competitively inhibits PHGDH (Pacold et al., 2016). CBR5884 non-competitively inhibits PHGDH by disrupting oligomerisation of the enzyme (Mullarky et al., 2016). *MYC* isogenic cells were pre-treated with doxycycline as previously described in 1.2.14. Cells were then plated in a white 96 well microplate; cell numbers are summarised in (Table 2.6). Parental MB and *MYC* isogenic cell lines were treated with PHGDH inhibitors across a range of concentrations. Cell viability was determined using CellTiter Glo as described in 1.2.14

2.4.4.1 Parental MB cell lines

In addition to the *MYC* inducible cell lines, parental MB cell lines were used for pharmacological and phenotypic assessment. Altogether 9 MB cell lines with different *MYC* status were utilised for validation experiments. Two of the cell lines belonged to MB_{SHH} to further act as non-MB_{GRP3} and non-amplified *MYC* controls. Details of cells can be found in Table 2.6 and Appendix D.

Table 2.6 List of parental medulloblastoma used in this study.

Cell line	Culture medium	Cell density (cells/well)
CHLA-259	DMEM (D6171), 10% FBS, 2 mM glutamine	5.0×10^3
DAOY	DMEM (D6171), 10% FBS, 2 mM glutamine	2.0×10^3
D283	DMEM (D6171), 10% FBS, 2 mM glutamine	5.0×10^3
D425	DMEM (D6171), 10% FBS, 2 mM glutamine	5.0×10^3
D458	DMEM (D6171), 10% FBS, 2 mM glutamine	5.0×10^3
HDMB03	RPMI (D6171), 10% FBS, 2 mM glutamine, 1% NEAA	5.0×10^3
MED1	DMEM (D6171), 10% FBS (Gibco), 2 mM glutamine	5.0×10^3
MED8A	DMEM (D6171), 10% FBS, 2 mM glutamine	2.5×10^3
UW288.1	DMEM (D6171), 10% FBS, 2 mM glutamine	2.0×10^3

2.4.5 Molecular cloning

2.4.5.1 Plasmids

The pLentiCRISPR-PHGDH, a gift from David Sabatini (Addgene plasmid #83913) was supplied in bacterial hosts as an agar stab. Single colonies were obtained by streaking bacteria on Luria Bertani (LB) plate with 100 µg/mL ampicillin and incubated for 12-18 hours at 37°C. Plasmid DNA was purified according to the protocol described in 2.4.5.2. The pLentiCRISPR-non targeting control (NTC) a gift from Paul Sinclair, was supplied purified.

2.4.5.2 Plasmid DNA purification

Plasmid DNA were purified by inoculating a single bacterial colony into 30 mL of LB broth with 100 µg/mL ampicillin and placed in a shaking incubator for 12-18 hours at 37°C. Plasmid DNA was extracted using a miniprep kit (Qiagen) according to manufacturer's instructions (<https://www.qiagen.com/gb/products/discovery-and-translational-research/dna-rna-purification/dna-purification/plasmid-dna/qiaprep-spin-miniprep-kit/>).

2.4.6 Lentiviral preparation

2.4.6.1 Packaging vectors

HEK293T cells were seed at 2×10^6 cells in a 10 cm² tissue culture plates and incubated overnight. Lentivirus production was produced using the Calphos Mammalian transfection kit (Clontech, UK). Following manufacturer's instructions, solution A was prepared as shown in Table 2.7. Solution B was added dropwise to solution A with continuous mixing. The transfection mix was incubated for 15 minutes at room temperature. Following incubation, the transfection mix was added dropwise to plated HEK293T cells and gently swirled. Plates were placed in a humidified incubator (as described in 2.2.1.3) for 8 hours. Transfection medium was then replaced with fresh medium. Virus supernatant was collected 48 hours later by collecting medium and sterile filtering through 0.45 µM pore filter (Millipore). The supernatant was aliquoted and stored at -80 °C.

Table 2.7 Composition of solution A for transfection

Components	Concentration
10 g Plasmid DNA	-µL
10 µg psPAX2	-µL
5 µg pMD2.G-VSVG	-µL
2 M Calcium Phosphate	112 µL
dH2O made up to	900 µL

2.4.7 Titration of lentivirus

Lentiviral titration was performed using the Lenti-X GoStix assay (Takara Bio, UK) which tests for the presence of lentiviral p24 as per manufacturer's instructions. Briefly,

20 μ L of virus supernatant was applied to the sample well of a Lenti-X GoStix followed by 3 drops of chase buffer and incubated for 10 minutes to allow lateral flow and the appearance of a test and control band ensuring a properly functioning test. The bands are scanned digitally and a GoValue (GV) is obtained. To obtain infectious units (IFU)/mL for an unknown sample, a reference virus with known IFU/mL was tested on the Lenti-X GoStix to generate a GV score. The viral titer was determined using the following equation:

$$\text{Unknown IFU/mL} = \text{unknown GV} \times \frac{\text{reference IFU/mL}}{\text{reference GV}}$$

2.4.8 Generation of PHGDH knockout cell lines

To generate stable knockout of PHGDH in the medulloblastoma cell lines (D425, D458, D283, HDMB03 and DAOY), pLentiCRISPR PHGDH and pLentiCRISPR_v2 NTC vectors were transduced in the cell lines by lentiviral infection. Cells were seeded at 5×10^5 cells in 6 well tissue culture plates and incubated overnight. Virus containing medium for NTC or sgPHGDH was added to each well and incubated for 24h. The following day, virus containing media was removed and replaced in growth medium containing $1\mu\text{g/mL}$ puromycin for 7 days to select transduced cells. Knockdown of PHGDH protein was verified by WES as described in 1.2.3.

2.4.9 Clonogenic assays

To characterise the effect of PHGDH modulation on clonogenicity, MB_{GRP3} cells harbouring pLentiCRISPR PHGDH or pLentiCRISPR NTC were seeded at 5×10^2 in 6 well culture plates with three biological replicates for each cell line and condition. Following overnight incubation, growth culture media was switched to the serine/glycine deprived medium described in Table 2.8. Cells were incubated for up to 7 days to allow colony formation. To fix colonies, growth medium was gently removed from each well by aspiration. The wells were subsequently washed with 2 mL of 0.9% (v/v) saline. Colonies were fixed using cold neat methanol for 10 mins on wet ice. Colonies were then stained using 2 mL of 0.01% (w/v) crystal violet in dH₂O for 10 mins. Excess dye was washed with dH₂O and plates allowed to dry. Where appropriate, colonies were counted using a stereomicroscope. Digital images were obtained using a camera device.

Table 2.8 Media composition for serine and glycine deprivation experiments

Experimental condition	Media composition
Complete medium (CM)	Minimum essential medium, 10% dialysed FBS, 2 mM glutamine, 0.4 mM Serine, 0.4 mM Glycine
- Serine (-Ser)	Minimum essential medium, 10% dialysed FBS, 2 mM glutamine, 0.4 mM Glycine
- Glycine (-Gly)	Minimum essential medium, 10% dialysed FBS, 2 mM glutamine, 0.4 mM Serine
- Serine/Glycine (-Ser/Gly)	Minimum essential medium, 10% dialysed FBS, 2 mM glutamine

2.4.10 Incucyte™ growth assay

MB_{GRP3} cells harbouring pLentiCRISPR PHGDH or pLentiCRISPR NTC were plated at 5×10^4 cells in 96 well microplate in quadruplicate. For each condition, cells were adhered to poly-L-lysine coated plates overnight. The following day, growth medium was changed to serine/glycine deprived medium described in Table 2.8. Cells were allowed to grow for up to 7 days at 37°C with 5% CO₂ in an Incucyte incubator. Bright field images were captured at 100x magnification at 6 hr intervals from 4 independent locations of individual wells. Cell confluence in each resulting image was quantified using an adapted image mask defined with the Incucyte analysis software to recognise cells in the images. The confluence from independent well images and replicates were averaged for each condition and plotted over time.

Chapter 3 Investigating fatty acid oxidation in a syngeneic mouse model of Glioblastoma

3.1 Introduction

Glioblastomas (GBM) account for most malignant gliomas that occur in adults. Despite a harsh treatment strategy which involves surgical resection and adjuvant radio/chemotherapy, median survival is only improved from 12 months to 14.6 months with treatment. There is an unmet clinical need for novel therapies to improve survival of GBM patients. The TCGA and other subsequent studies characterised the heterogeneity of gliomas and identified genetic mutations in the P53, RTK and Rb signalling pathway as major contributors to GBM pathogenesis (Sturm et al., 2012, Verhaak et al., 2010, Phillips et al., 2006). Furthermore, IDH mutations which distinguishes a subset of GBM is a favourable prognostic marker and is associated with younger patients (Sturm et al., 2012, Verhaak et al., 2010). Although there has been great efforts to develop targeted therapies for the different molecular subsets of GBM, the infiltrative nature and drug resistance that persists in GBM makes this process challenging.

Although there is no firm consensus on the cell of origin of GBM, the putative candidate remains the neural stem cell (NSC) population. NSCs are localised to the subventricular zone (SVZ) of the lateral ventricles and subgranular zone (SGZ) of the dentate gyrus in the adult brain which give rise to neurones and glial cells (Gage and Temple, 2013, Lim and Alvarez-Buylla, 2016). Adult NSCs in the SVZ and SGZ have self-renewal capacity and multipotency and are identified in the SVZ and SGZ by the presence of glial fibrillary acidic protein positive (GFAP+) cells. These NSCs give rise to progenitors that have limited self-renewal and proliferative potential fated for differentiation into different neural cell types. This capacity supports the premise of NSCs being the likely cell type that undergoes oncogenic transformation and give rise to malignant gliomas. Using mouse models, some studies have shown lineage restriction of neuronal populations to give rise to GBM. More consistently, NSCs and progenitors have the most propensity to undergo malignant transformation and form high-grade GBMs (Alcantara Llaguno et al., 2019, Alcantara Llaguno et al., 2015, Zhu et al., 2005).

Cell lineage markers have been particularly useful for the determination of the cell of origin of GBMs. GFAP+ identifies quiescent NSCs, whereas Nestin stains for both NSCs and proliferative progenitors. Lineage specific cells like oligodendrocyte progenitors (OPCs) express specific proteins such as Olig1, NG2 and PDGFR α . Previous studies have shown that stereotactic injections of cre recombinase expressing adenovirus into the stem cell niche in adult mouse striatum directed against *Trp53*, *Pten* and *Nf1* is capable

of GBM formation (Alcantara Llaguno et al., 2009, Jacques et al., 2010). Although GFAP+ is not unique to NSCs and can be found in mature astrocytes, Gfap-creER mediated loss of *Pten*, *Trp53* and or *Rb* initiates high grade gliomas localised to the proliferative stem cell niche of the SVZ and SGZ suggesting that NSCs and not post mitotic astrocytes give rise to GBMs. Additionally, efforts initiating tumourigenesis by targeting astrocytes has proved largely unsuccessful (Alcantara Llaguno et al., 2009, Jacques et al., 2010). Targeted expression of *Ascl1*-creERTM mice carrying *Nf1*, *Trp53* and *Pten* also induces GBMs when OPCs are targeted (Galvao et al., 2014). This further supports self-renewal and proliferative capacity as necessary requirements for the initiation of GBM tumours. It is noteworthy that low grade gliomas almost certainly develop into malignant gliomas supporting the notion of a cell population that is maintained within the tumour that is capable of sustaining cancer growth.

The molecular landscape of GBMs has been extensively covered by transcriptomic profiling, mainly highlighting alterations in *TP53*, *PTEN*, *EGFR*, *NF1* and *RB* as the most commonly found driver mutations in primary GBMs. Despite this, there still remains a lack of targeted therapies implemented against malignant gliomas. For instance, preclinical evaluations using EGFR inhibitors Elortinib and Gefitinib only display weak sensitivity in GBM tumours (Vivanco et al., 2012). Adjuvant temozolomide chemotherapy remains a part of the standard treatment of GBMs despite only extending survival by two months on average (Stupp et al., 2005, Stupp et al., 2009). Furthermore, only a subset of patients benefit from TMZ therapy due to acquired resistance via the expression of O6-methylguanine-DNA-methyltransferase (MGMT), a suicide enzyme which alleviates DNA alkylation and counteracts the effect of alkylating therapies like TMZ (Bosnyak et al., 2017, Hegi et al., 2005). There still remains an unmet clinical need for more efficacious therapies against GBMs which requires further understanding the pathogenesis of GBM and other mechanisms that drive its aggressive and infiltrative phenotype.

Since the identification of GBM initiating NSCs, there has been numerous studies examining their contribution to GBM phenotypes. Not only have NSCs been shown to initiate gliomagenesis, they have been shown to facilitate resistance to chemotherapy and radiation therapy. Since GBM-populating NSCs are slow cycling, they evade TMZ-induced cytotoxicity and resurge the recurrence following chemo-selective pressure (Chen et al., 2012). Furthermore, glioblastoma neural stem-like cells (GSC), build multi-drug resistance through elevated expression of ATP-binding cassette transporters like

ABCB1 facilitating drug efflux and limiting accumulation of anticancer drugs (Eramo et al., 2006). Additionally, by selective activation of DNA damage response pathways, NSCs contribute to radioresistance and GBM recurrence following treatment (Bao et al., 2006). The lethality of GBM is also attributable to infiltration into nearby brain structures, limiting total surgical removal of tumour which supports recurrence. The infiltrative nature of GBMs has also been attributed to NSCs and is correlated with Wnt5A expression and activation. Comparison of recurrent GBM to primary patient samples revealed higher expression of Wnt5A in recurrent tumour samples supporting its role in GBM infiltration and recurrence (Binda et al., 2017, Hu et al., 2016).

NSCs also exhibit metabolic plasticity ensuring survival in temporal fluctuations in nutrient availability and oxygen concentrations ensuring survival and maintenance of NSC population. Stoll *et al.*, demonstrated that adult NSCs in the SVZ utilised fatty acids to maintain oxygen consumption rate and were less reliant on glucose unlike terminally differentiated neurones which exhibited differential metabolic signatures and enhanced lactate transport (Stoll et al., 2015). Remarkably, decreased mitochondrial content and oxidative phosphorylation is associated with reduced neurogenesis in aging NSCs underscoring the importance of this metabolic phenotype with self-renewal capacity and multipotency (Stoll et al., 2011). In the context of GBMs, NSCs have been shown to exhibit metabolic plasticity utilising glucose and fatty acids for energy production (Lin et al., 2016, Mashimo et al., 2014). Although the Warburg effect is reported for GBM, Marin-Valencia and colleagues reported metabolic complexity of glucose utilisation in GSCs. ¹³C -glucose labelling showed oxidation of glucose via the TCA cycle and glucose-derived anaplerosis even with large pools of glutamine. Furthermore, this oxidative phenotype was associated with GBM growth and aggression (Marin-Valencia et al., 2012). Notably specific GSC populations exhibit a higher propensity to undergo metabolic switch following inhibition of oxidative or glycolytic pathways and exposure to hypoxia. Remarkably, the metabolic adaptation to hypoxia was reversible when GSCs were re-oxygenated (Shibao et al., 2018).

The characterisation of intertumoural heterogeneity across GBM subtypes revealed numerous somatic mutations in growth factor- related and tumour suppressor pathways. Additionally, lineage specific markers contribute to the classification of these subgroups, like the neural subgroup being enriched for neuronal lineage markers but the impact of the cell of origin is not well understood. The use of multi-omics for GBM classification robustly clusters paediatric, adolescent and adult GBMs based on somatic mutations, copy number alterations and epigenetics (Verhaak et al., 2010, Sturm et al., 2012). These advances are promising in the efforts to reveal lineage specific origins of GBM. Subgroup classifications from medulloblastoma highlight the contribution of lineage specific tumour initiation events namely in the WNT and SHH subgroups which arise from mutations in these developmental pathways in dorsal brainstem progenitors and the granule neurone progenitors in the cerebellum, respectively (Gibson et al., 2010). The advent of more sophisticated NGS of DNA methylation, single nucleotide polymorphisms and copy number variations will aid work to establish the importance of lineage specific tumour initiating cells (TIC) and their contribution to the GBM biology and heterogeneity. GSCs also shunt glucose into anabolic pathways like the PPP suggesting alternative glucose utilisation in GBM contributing to rapid division. Owing to spatiotemporal variations in nutrient access and oxygen tensions, bulk tumours are characterised by hypoxic regions which ultimately influence the phenotype of GSCs. Tumour hypoxia upregulates glycolysis through stabilisation of HIF1 α and promotes migration of GBM cells whereas in the normoxia is associated with upregulation of anabolic pathways like PPP driving GSCs proliferation (Kathagen et al., 2013). The duality of GSC function in GBM undoubtedly contributes rapid proliferation and expansion of GBM cells under harsh conditions.

In order to facilitate the progression of drug development from ‘bench to bedside’, *in vitro* and preclinical studies must utilise more clinically relevant models of GBM. The artificialness of most *in vitro* culture conditions further potentiates this problem leading to many drug candidates that ultimately fail *in vivo*. Lee *et al.*, demonstrated that primary tumour-derived glioma stems cells recapitulated the gene expression patterns and biology of parental tumours when cultured in serum free medium (Lee et al., 2006). In fact, the addition of serum led to loss of stem cell-like characteristics including loss of lineage markers such as *Nestin* and *Sox2*. It is desirable for efficacy studies to be conducted in more sophisticated models that also resemble the primary disease.

A well-established GBM model exploits orthotopic transplantation of oncogenically transformed mouse neural progenitor cells (NPCs) in an immunocompetent mouse (Mikheev et al., 2009). Isolated NPCs from the SVZ of adult mice are transformed by over-expressing *Ha-Ras* and HPV18 E67 which inhibits both the *p53* and *p16/Rb* axis. The age of NPCs at time of transformation influenced the tumour biology where older NPCs (12 or 18 months) induced malignant gliomas characterised by increased cellularity, large-cell anaplasia, proliferation and infiltration into surrounding parenchyma. The maintenance of host immunity, an intact blood brain barrier and a dynamic tumour microenvironment make syngeneic models useful for evaluating tumour biology and testing of pharmacological compounds. Since metabolic reprogramming is thought to facilitate the GBM growth and aggressiveness, exploring alterations in these pathways may provide novel therapeutic opportunities. Of interest in particular, is the usage of alternative fuels such as fatty acids via the β -oxidation pathway in GBM. Lin *et al.*, provided evidence for utilisation of fatty acids by GBM stem cells to support growth and respiration (Lin et al., 2016). Importantly, the oxidative metabolic phenotype is consistently linked with the neurogenic capacity of normal NSCs and GSCs. Targeting this distinct population of GBMs in addition to other anti-proliferation agents may further regress GBM growth.

3.2 Aims

The aim of the study was to expand work previously carried out on targeting fatty acid oxidation as a therapeutic strategy in GBM. As a lipophilic drug, etomoxir crosses the BBB. For this study, the plan was to utilise a novel formulation of etomoxir with increased brain penetrance. The overarching aim was to establish whether combination of FAO inhibitor etomoxir and standard chemotherapeutic agent temozolomide, would be more effective for slowing tumour progression in a mouse model of GBM. In this chapter, a pilot *in vivo* study assessing tumour development and metabolic changes associated with combination therapy was explored using MR imaging and ^1H MR spectroscopy. The objectives of the study were to:

- Optimise imaging strategies for monitoring tumour progression in a mouse model of glioma.
- Determine tumour latency and progression using optimised MR imaging sequences
- Explore neurochemical changes associated with disease and treatment response using MRS.

3.3 Results

3.3.1 Monitoring tumour development in an *in vivo* mouse model of GBM

3.3.1.1 Generation of syngeneic mouse model of glioblastoma.

To investigate the effect of fatty acid oxidation inhibition in combination with the standard therapeutic agent temozolomide, we employed the syngeneic model of glioma described by Mikheev *et al.*, which involves orthotopic transplantation of transformed mouse progenitors into mice with the same genetic background (Mikheev *et al.*, 2009). This mouse model recapitulates the human disease and is a clinically relevant model for pharmaceutical testing. The pilot study followed previously established protocols for generating syngeneic mouse models, commencement of drug treatment and clinical monitoring. For this study, 12 month old oncogenically transformed NPCs were used for transplantation over younger aged NPCs due to associated age-related increase in malignancy and shorter tumour latency (Mikheev *et al.*, 2012). C57/BL6 mice were transplanted with NPC via stereotactic injection delivering cells to the striatum of mouse brain (performed by Dr. Elizabeth Stoll). Animals were allowed to recover and were clinically monitored daily until study endpoint (Illustrated in Figure 3.1 A). Clinical scoring was used as a measure of health that scored mice based on weight, posture and cognitive function (Appendix 8.1). After a 14 day period to allow the formation of dysplasia and recovery from surgery, mice were blindly assigned to the treatment groups: untreated n=2 (vehicle control); etomoxir n=2 (ETX); temozolomide n=2 (TMZ); and combination n=2 (ETX plus TMZ) group. Administration of the drugs was staggered to reduce potential toxicity and to reflect the cyclical nature of human TMZ dosage administration. Mice were given vehicle control or 67 mg/kg of TMZ which was administered intraperitoneally for 5 days before commencing on a daily gavage of vehicle control or 10 mg/kg of ETX (Figure 3.1 B). In order to limit gavage related injury in the cohort, gavage was limited to a 90 day period from which ETX, (which is lipophilic) was delivered by self-administration via solidified coconut oil pellets (Appendix 8.2).

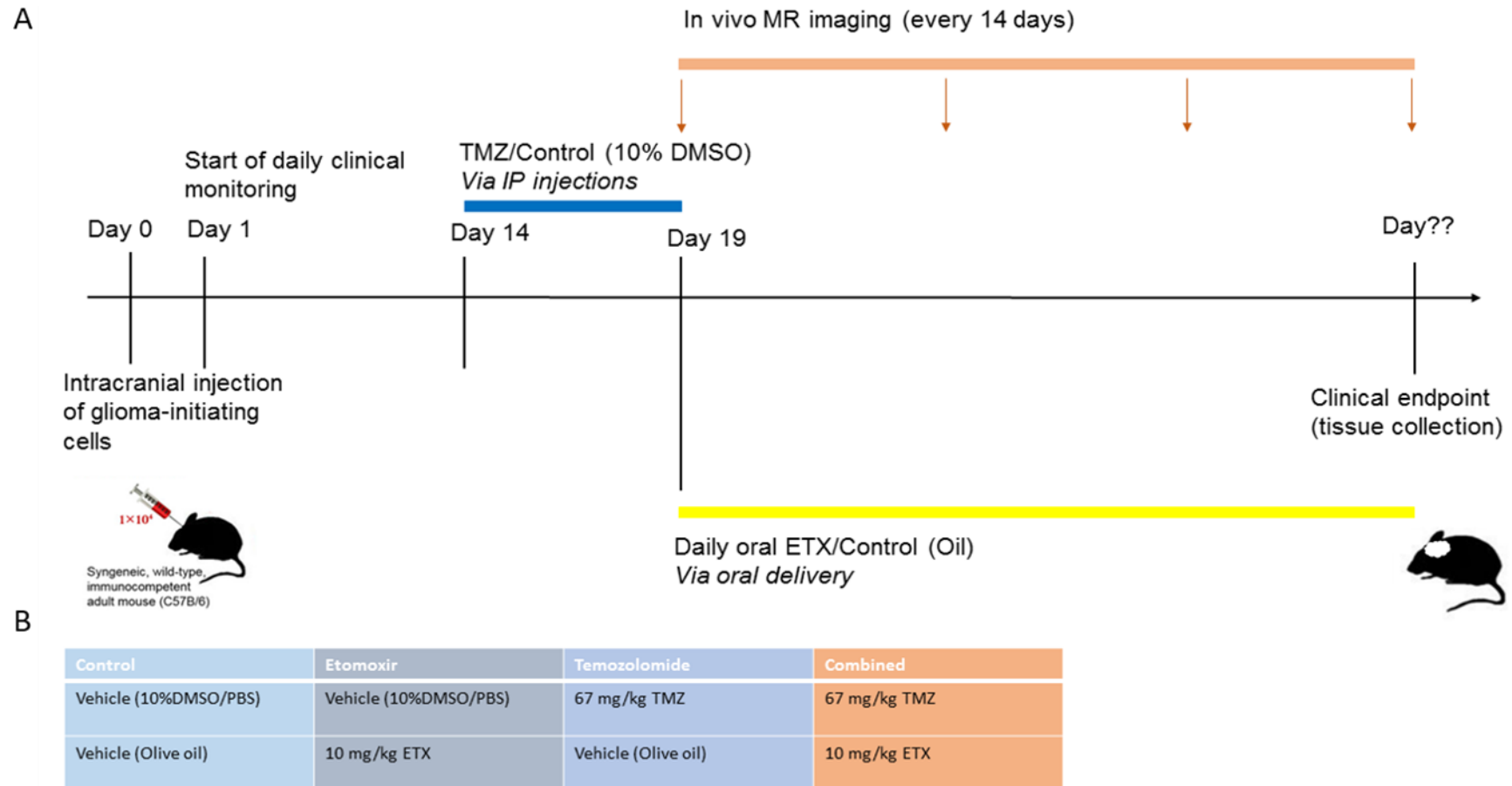


Figure 3.1 Illustration of in vivo study timeline. A) Oncogenic NPCs are orthotopically transplanted in the striatum. Animals are clinically scored and monitored for the duration of study. TMZ/Vehicle is administered for 5 days following a 14 day recovery period. ETX is administered orally for the duration of study via gavage or solidified oil pellets. In vivo MR images are acquired at 14 day intervals until clinical/study endpoint. B) Scheme of drug treatment group

3.3.1.2 Establishing and optimising imaging sequences for visualising brain structures

In this syngeneic model, oncogenic NPCs were implanted into a region of the striatum to generate GBMs. In order to detect and image structural changes associated with tumour formation within normal brain parenchyma, an array of MRI imaging sequences with different T1/T2 weightings were adopted and optimised to observe grey and white matter structures in the brain.

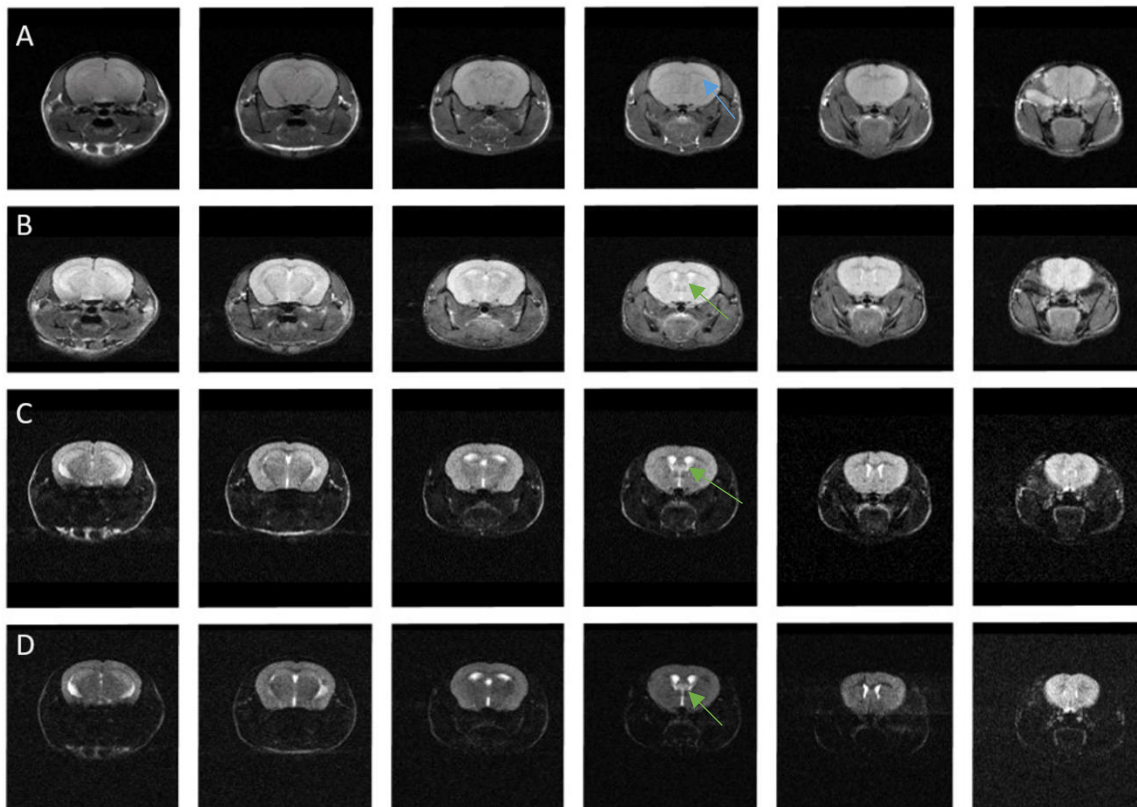


Figure 3.2 MRI images of coronal slice sections of mouse brain acquired using four SEMS sequences. Posterior to anterior (left to right) MR images of anatomical structures within mouse brain was acquired using the following SEMS sequences A) TR 1000 ms TE 20 ms B) TR 1000 ms TE 20 ms with inversion recovery C) TR 1100 TE 60 D) TR 1600 TE 85 ms. Blue arrow depicts corpus callosum. Green arrow depicts lateral ventricles.

The four separate spin-echo multi slice (SEMS) sequences were optimised and utilised in the study. As shown in Figure 3.2, images acquired from the different SEMS sequences achieved differences in tissue contrast. Sequence 1 (Figure 3.2A) had a higher signal to noise but provided limited information on brain structures. For instance, the most noticeable region observed is corpus callosum in lane 4. However, adding an inversion sequence to the sequence 1 led to more distinct brain regions being visualised (Figure 3.2B), particularly the lateral ventricles became more noticeable. The addition of sequence 3 and 4 resulted in regions of the brain with high CSF being visualised although this image type suffered from a loss of signal and high noise (Figure 3.2D, E). The contrast enhancement from sequence 3 and 4 highlighted tissue injury/scarring including surgical transplantation site. In combination, the 4 SEMS images were deemed appropriate for the detection of tumour growth due to the differences in image properties highlighting distinct brain regions and structures.

3.3.1.3 Monitoring tumour formation

The imaging protocol previously described was used to catalogue changes in brain structure that occurred over time following tumour initiation. During the course of this study, tumour development only occurred in untreated mice. Development of tumour was detected in control animals (M079, M095) across all MRI image sequences. Emergence of tumour, and distorted brain regions was detected at an earlier time point using the longer TE sequences (Sequence 3& 4) compared to shorter TE images with or without an inversion sequence (Appendix 8.3). Furthermore, the appearance of MRI visible tumour corresponded with clinical symptoms (e.g. weight loss and tumour associated seizure). Mice receiving any one of the treatment arms maintained normal brain architecture and no visible alterations were detected across MRI images during the course of the study (Figure 3.3).

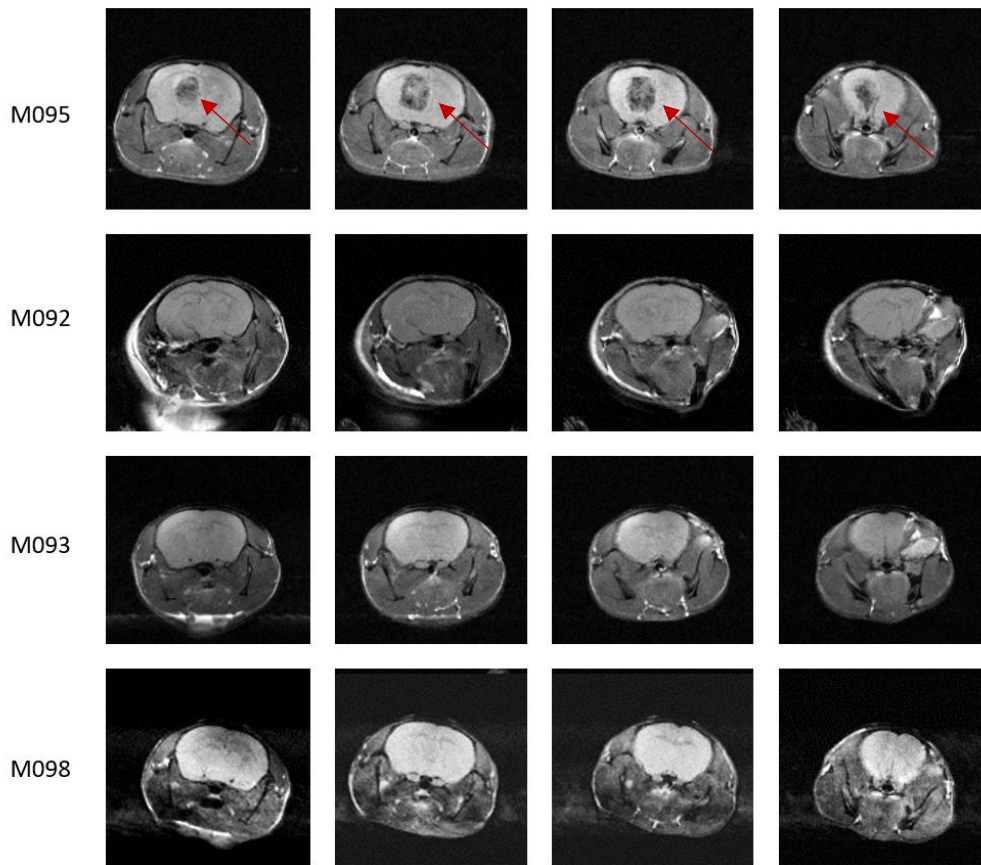


Figure 3.3 Comparison of tumour development across drug treatment groups. MRI images of coronal slice sections of mice treated with vehicle (M095), 100mg/kg ETX (M092), 67mg/kg TMZ, (M093) or combination (M098). Red arrows indicate presence of tumour across MRI slice sections.

3.3.1.4 Assessing tumour histology in tumour burdened animals

When mice reached euthanasia criteria or study endpoint, brain tissue samples were collected to evaluate clinical histology. Brain tissue was sectioned and stained with H&E to evaluate tumour/brain histology. Extensive tumour progression was visualised throughout coronal slice MRI images in control animals and histological assessment corresponded with these findings (Figure 3.4). Tumours resembled previous histological classification of high grade anaplastic astrocytoma (WHO Grade III or IV GBM). Although cells were transplanted into striatum, tumour cells had infiltrated surrounding cortices and across midline. Initial MR images of tumours revealed differences in contrast within the tumour suggesting differences in tissue characteristics. Histological evaluation further confirmed tumours were also characterised by necrotic and haemorrhaged regions

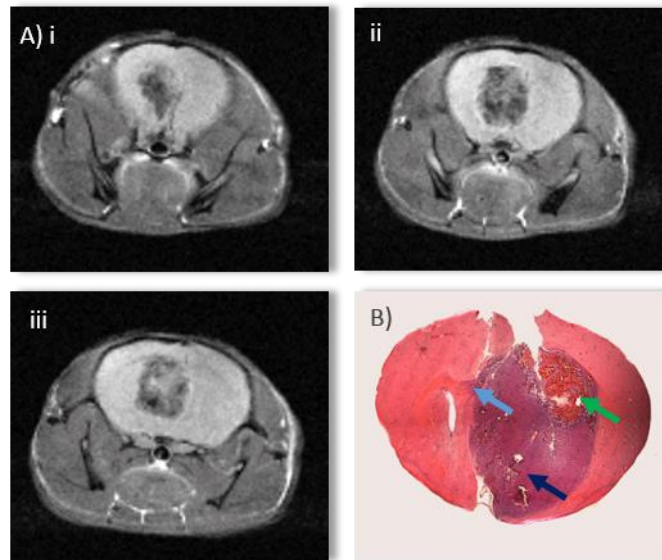


Figure 3.4 Histological confirmation of glioblastoma bearing mice identified by MRI. A) SEMS sequence 1 images of anterior to posterior coronal slices of tumour burdened M095 at day 109. B) Endpoint histology using H&E staining confirming presence of tumour (dark blue arrow) with haemorrhaged regions (green arrow) and infiltration across midline (light blue arrow).

3.3.1.5 Kaplan Meier curve of the four groups alongside clinical performance.

The primary aim of this study was to monitor the development of tumour progression in this model of GBM. Mice enrolled in the study underwent treatment in order to establish a suitable dosing regimen for maintaining a long term therapy cycle mimicking patient treatment protocols. Although the size of the cohort for this study was not sufficiently powered to determine differences in the efficacy of treatment, there was a clear difference between the untreated group and each of the drug treatments, i.e. disease progression in untreated mice was faster compared to animals treated with TMZ, ETX and in combination. Treatment delayed tumour onset and no MR visible tumours were observed in these groups (Figure 3.5). Mice that only received vehicle were euthanised due to tumour burden, decline in health and reaching euthanasia criteria determined by clinical score. It was not possible to determine differences between the treatment arms due to reaching study endpoint. For instance it was not determined whether etomoxir in combination with temozolomide improved survival when compared to monotherapies.

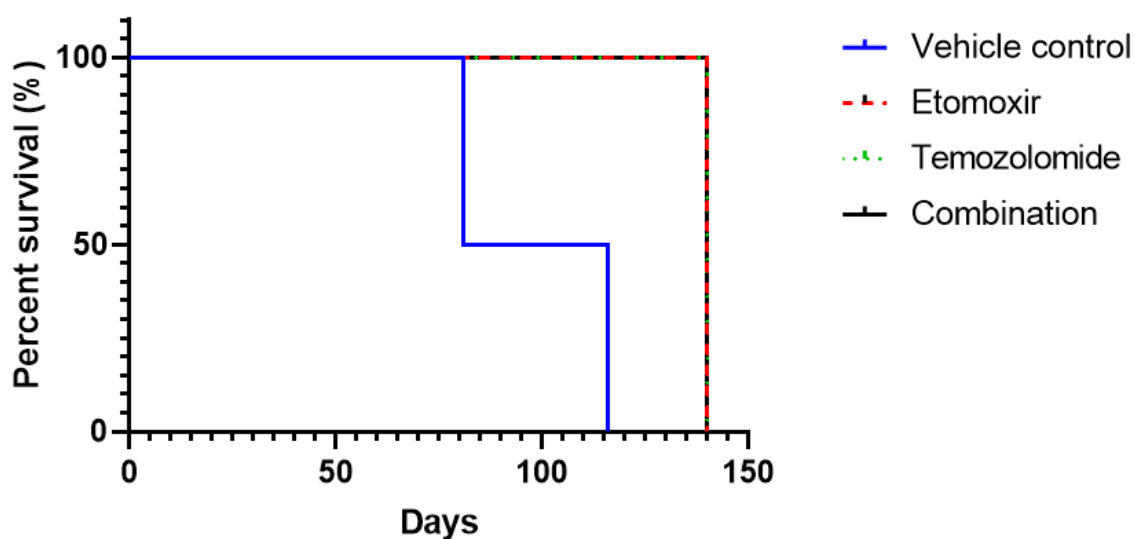


Figure 3.5 Comparison of survival across drug treatment groups. Kaplan Meier survival curve of glioma bearing mice treated with 100 mg/kg ETX, 67 mg/kg TMZ or combination. (n=2 per treatment group). Mice receiving vehicle control survived until day 81 and 116. One mouse in the TMZ group was euthanised for welfare reasons unrelated to tumour formation. The whole cohort was euthanised at day 138 at study endpoint.

3.3.2 Evaluating the feasibility of monitoring neurochemical changes during tumour development

MRS is a useful non-invasive technique for gathering biochemical information from tissues. It was hypothesised that the presence of dysplasia/tumour would alter brain metabolite abundances due to the differences in metabolic requirements and altered metabolic phenotype that is frequently observed in many cancers including GBM. In order to obtain *in vivo* MRS spectra, regions of interest (ROI) were selected based on SEMS sequence 1 images. ROIs were chosen directly on striatum and near transplantation side (ipsilateral) and on normal striatum (contralateral) hemispheres (Figure 3.6).

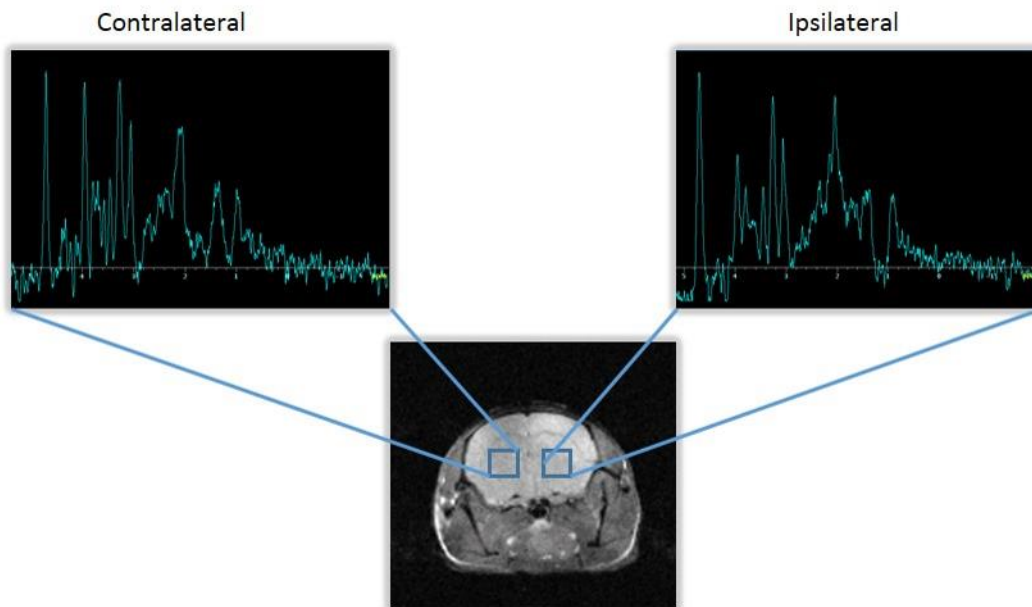


Figure 3.6 Scheme of ROI selection from SEMS sequence 1 MRI images. PRESS sequence TR= 2000 and TE= 8ms was acquired from 1mm voxel were placed in striatum on both brain hemispheres

3.3.2.1 Detection of brain metabolites

In vivo MRS was utilised in order to assess neurochemical changes in mouse striatum during development of GBM. Metabolite profiles in addition to MRI imaging could aid the early detection of tumours and monitoring treatment response. *In vivo* NMR spectra were acquired every 14 days across 2 ROIs (Figure 3.7). NMR spectra was pre-processed (phasing and baseline correction) and quantified using TARQUIN software. Analysis of metabolites were performed on metabolites detected in both ipsi-/contralateral hemispheres which had Cramer-Rao lower bound (CRLB) of <25%. CRLB thresholds have previously been used as an indicator of measurement precision and accuracy of fitted metabolites (Cavassila et al., 2001). Results for M079 are reported in Figure 3.7.

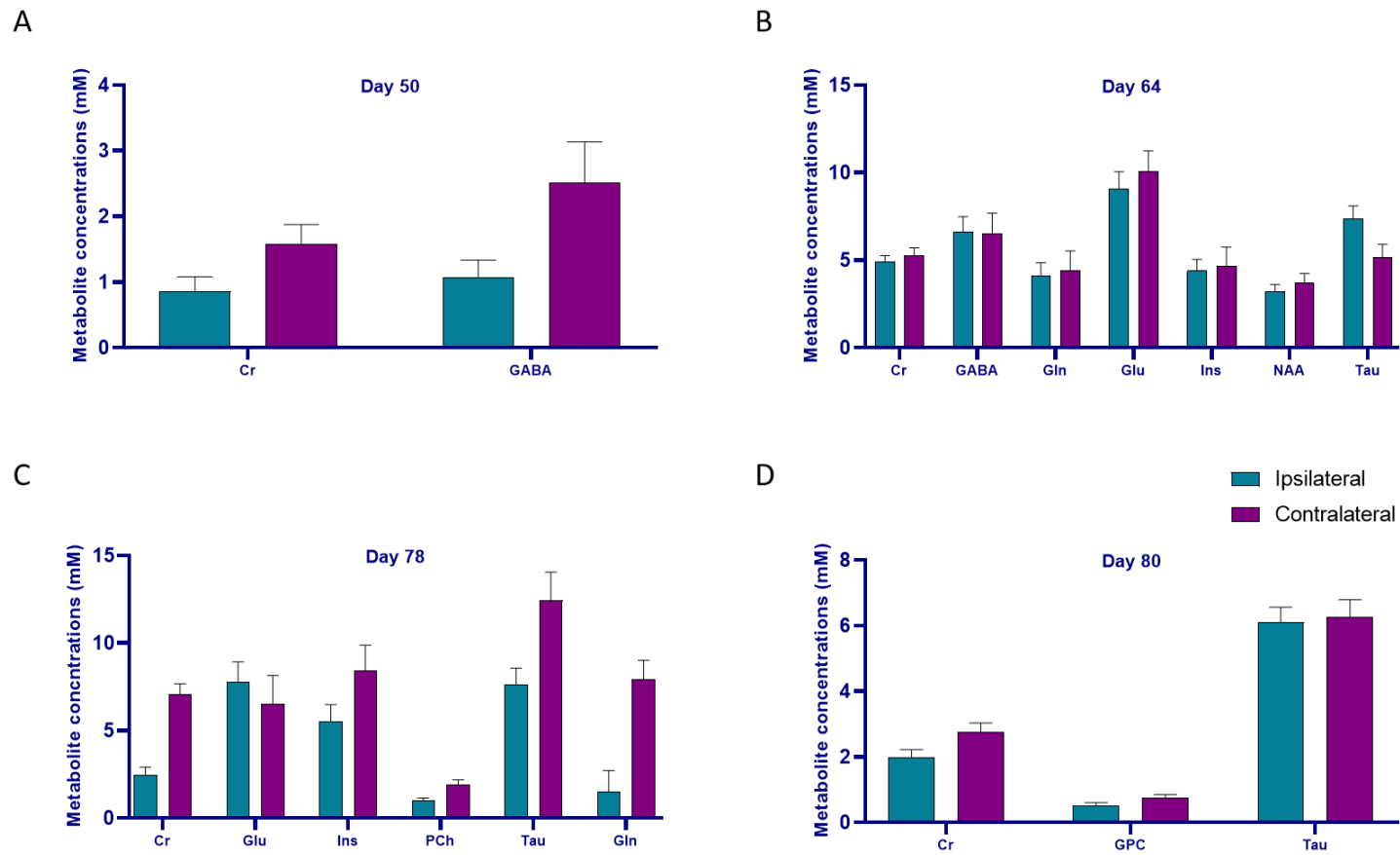


Figure 3.7 Concentrations of brain metabolites quantified by TARQUIN from NMR spectra for M079 (control). Creatine (Cr), glutamine (Gln), glutamate (Glu), inositol (Ins), N-acetyl aspartate (NAA), taurine (Tau), phosphocholine (PCh), glycerophosphocholine (GPC). Metabolites are an average of 100 scans, error bars = CRLB. Only metabolites that satisfy CRLB cutoffs are presented for each day.

Although several metabolites were detected in M079, there was a lack of consistency across days of acquisition. Creatine was consistently (confidently assigned in the 4 time points) detected in both ipsilateral (tumour bearing) and contralateral (normal striatum) hemispheres over time. The largest changes in brain metabolites was observed at day 78 (Figure 3.7). Creatine, inositol, taurine and glutamine were increased in the contralateral region. Additionally, an MR visible tumour was detectable at day 78 (Appendix 8.3). There were no observable differences at day 80 despite a visible MR tumour. Notably, the number of metabolites detected was less compared to day 78. With a lack of reliable metabolite detection, it cannot be concluded whether these changes are tumour associated or a result of day to day variation in MRS measurements.

3.3.3 Metabolic characteristics of oncogenically transformed mouse neural progenitor cells using one dimensional ^1H NMR

Due to the challenges of metabolite detection and quantification from *in vivo* MRS, we employed *in vitro* NMR spectroscopy to evaluate the biochemical changes that may occur in response to treatment with etomoxir and temozolomide. Furthermore, *in vitro* NMR has the advantage of improved signal resolution resulting in the identification of more metabolites.

Samples were not initially collected from animals for *ex vivo* metabolite assessment therefore, transformed mouse NPCs (3 month, 12 month), which are the cell of origin for this GBM syngeneic model were cultured *in vitro* and treated with 100 μM etomoxir, 100 μM temozolomide and combination of the two drugs for 24 h and cell pellets collected for *in vitro* ^1H NMR spectroscopy. Cell pellets were lysed in D_2O for metabolite extraction. NMR spectra was acquired at high field strength (16 T) on a 700 MHz instrument resulting in good quality spectra. Metabolites were detected in the upfield (5-12ppm) and downfield (0-5ppm) regions of the spectra. Metabolite identification was focused on the downfield region due to better characterisation of that region.

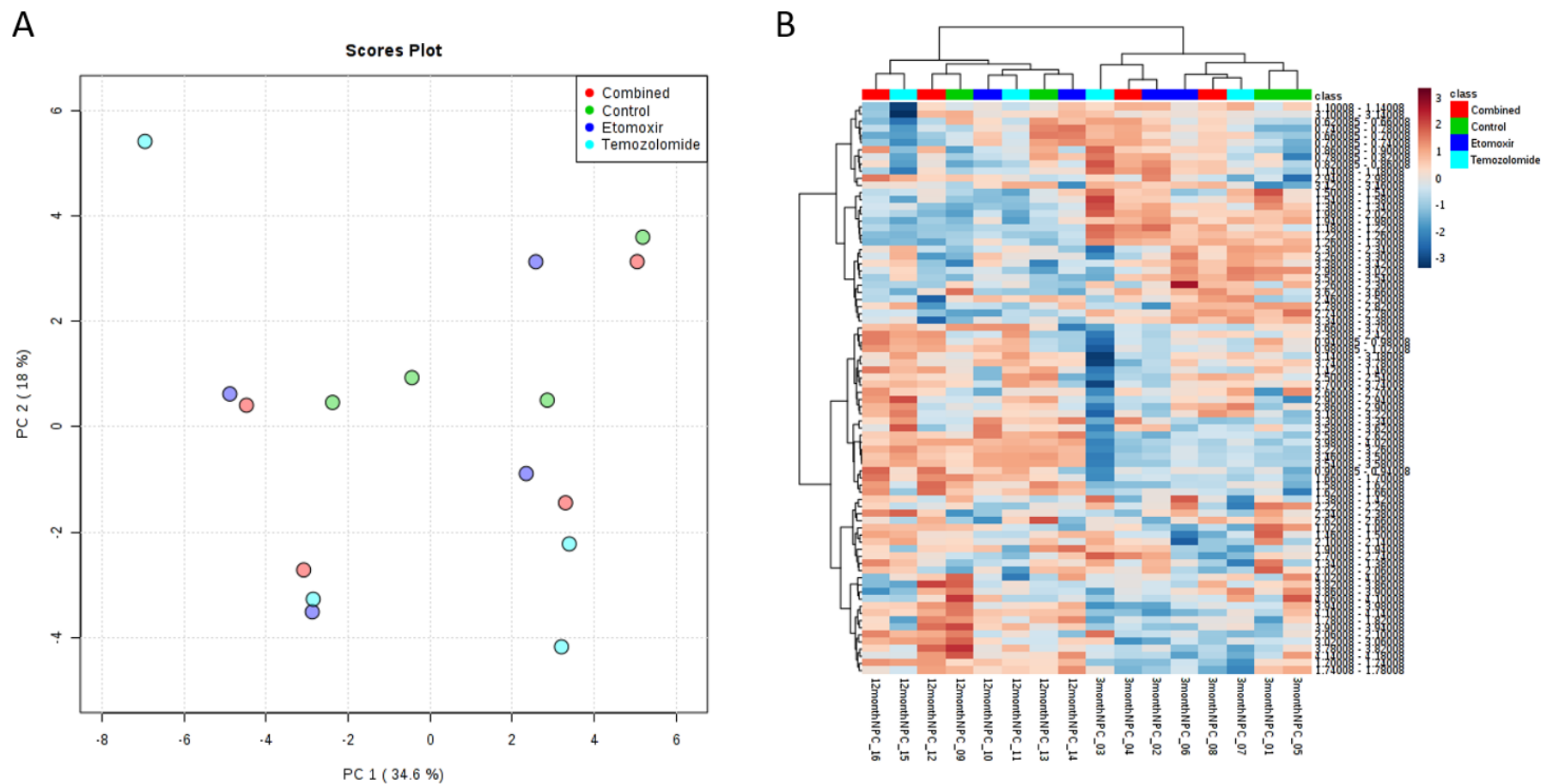


Figure 3.8 Multivariate analysis of ^1H NMR metabolite profiles of drug treated oncogenic NPCs. A) Unsupervised PCA analysis on the spectral bins of oncogenic NPCs treated with vehicle control, ETX, TMZ and combined groups ($n=4$ for each treatment condition). 3 month and 12 month NPCs were used as biological replicates ($n=2$ per drug condition). B) Clustered heatmap analysis of spectral bins for each treatment group. Red indicates an increased and blue a decrease in signal intensity. Spectral bins for each sample were normalised to the sum of total bins from the 0-5ppm spectrum region.

Following acquisition, spectra were pre-processed and binned into 0.04ppm regions. Multivariate analysis was carried out on the spectral bins from each sample to identify treatment related changes. Principal component analysis (PCA) revealed no obvious clustering patterns across the sample groups (Figure 3.8 A). To further elucidate variations between sample groups, spectral bins and their respective metabolite intensities were used to generate a clustered heatmap. As shown in Figure 3.8B, two clusters were apparent from this analysis. Surprisingly, the samples were ordered based on the different biological replicates. The two branches of the hierarchical cluster were related to the differently aged mouse NPCs (3 and 12 month NPCs). It is worth noting that the 3month NPCs were more ordered according to treatment group. With the knowledge in hand of possible variations with the samples, the PCA and more supervised clustering were revisited with class identifiers based on differently aged NPCs.

Distinct metabolic signatures were observed for 3 month and 12 month mouse derived oncogenic NPCs. The overview of PCA using 5 principal components revealed two distinct clusters with PC1 and PC2 accounting for around 66% of the variance (Appendix 8.4). The clusters were separated based on cell lines (i.e. 3 month or 12 month NPCs) and were independent of drug treatment (Figure 3.9). Inspection of the PCA loading plots revealed regions that contributed to separation. Elimination of these regions from spectral analysis reduced separation and resulted in no apparent clustering of the samples. Additionally, there were several bin regions that were significantly altered ($p < 0.05$) between the two biological cell lines (Appendix 8.5).

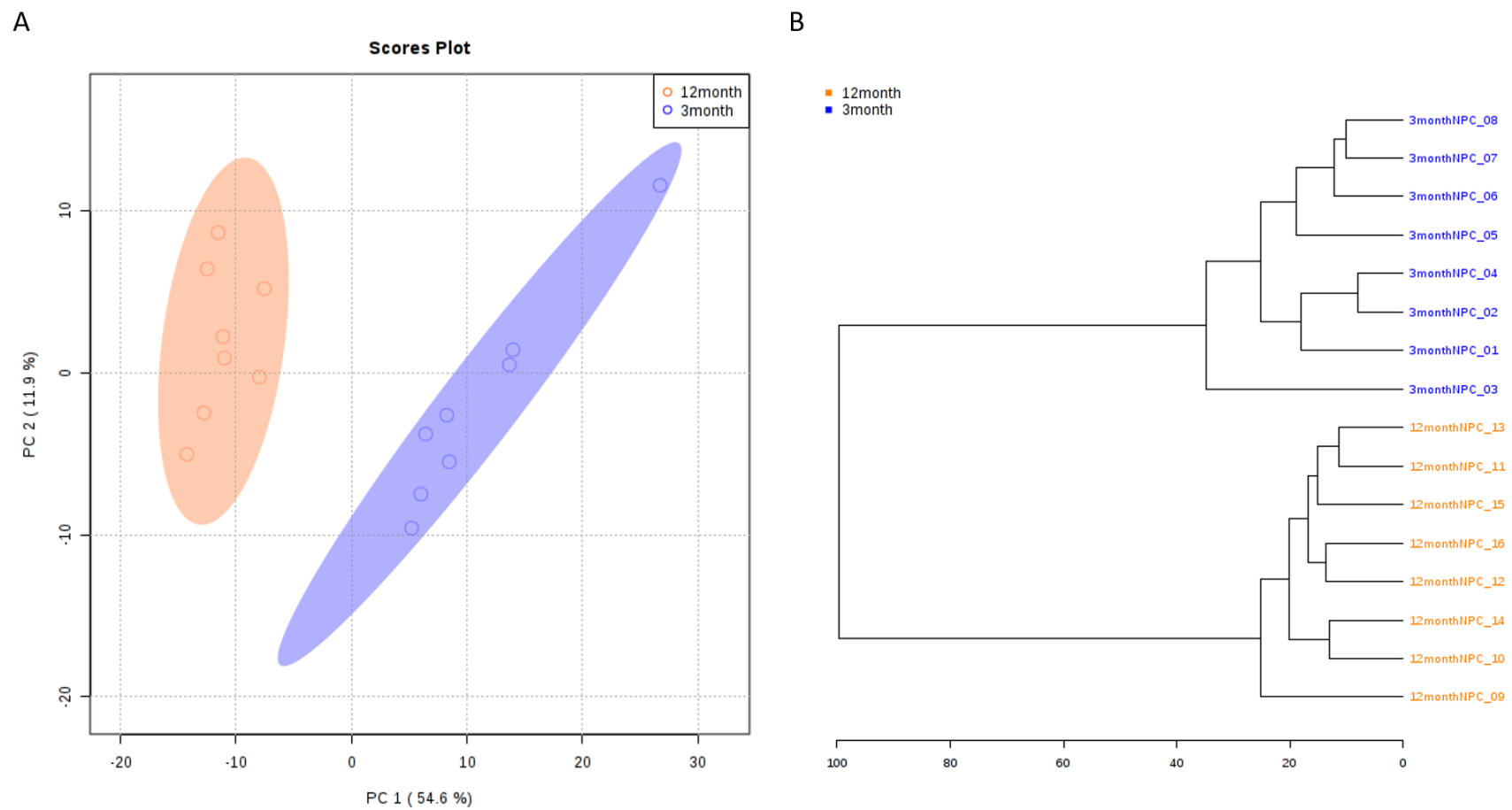
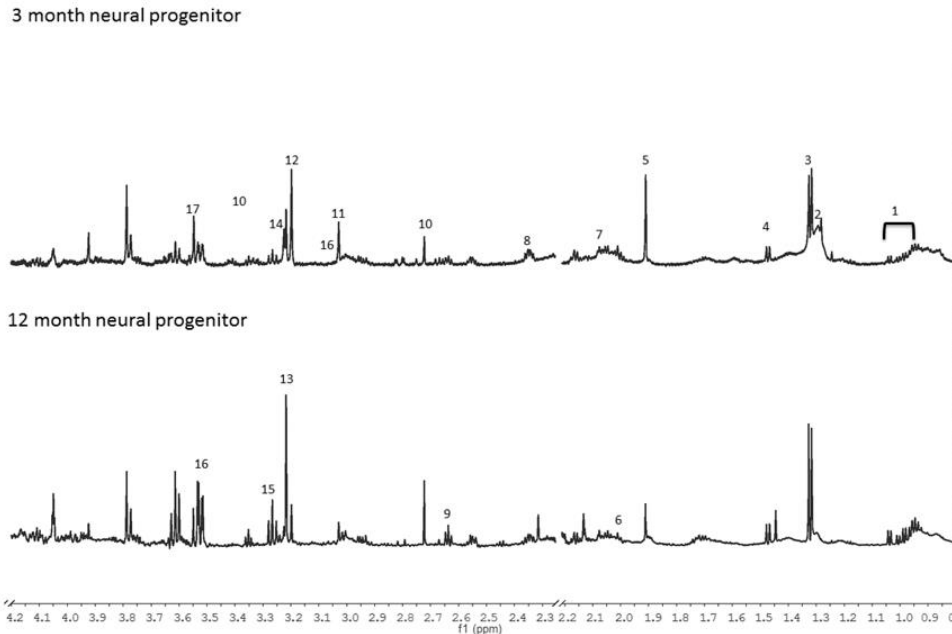


Figure 3.9 Unsupervised PCA analysis reveals variation in metabolic profiles of 3 and 12 month derived mouse NPCs. A) PCA score plot of 3 and 12 month NPCs treated with $100\ \mu\text{M}$ etomoxir, $100\ \mu\text{M}$ temozolomide, combined and vehicle control ($n=2$) B) Hierarchical clustering of samples.

To further characterise the metabolic differences between the differently aged mouse NPCs, concentrations of identifiable metabolites from untreated control NPCs were determined and normalised to NAA content (Figure 3.10). The 3 month NPCs were characterised by high creatine and signals from lipids. However, the 12 month NPCs had higher myo-inositol, taurine, alanine and branched chain amino acids; valine, leucine and isoleucine. The two differently aged NPCs had altered ratios of choline based metabolites. 12 month NPCs were characterised by high phosphocholine whereas 3 month NPCs had higher choline levels. Ratios of glutamine and glutamate were comparable in the NPCs.

A



B

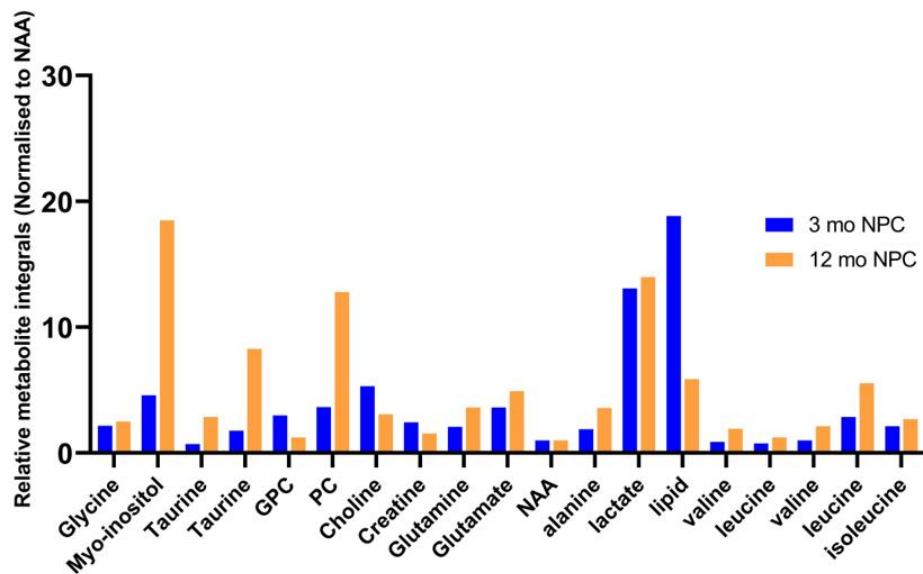


Figure 3.10 Metabolic profiles of differentially aged oncogenic NPCs. A) Representative ^1H NMR spectra of Oncogenically transformed mouse NPCs A) 12 month NPC B) 3 month NPC. The spectral regions 0.5- 4.5 ppm are shown. Regions containing solvent contamination were removed. Metabolite assignments (1); Valine, Leucine, Isoleucine (2); Lipid CH_2 (3); Lactate (4); Alanine (5); NAA (6); Glutamine (7); Glutamate (8); Hypotaurine (9); Dimethylamine (10); Creatine (11); Choline (12); Phosphocholine (13); Glycerophosphocholine (14); Taurine (15); Myo-inositol (16); Glycine B) Comparison of relative metabolite levels in 3 month and 12 month oncogenic NPCs. Metabolite signal integrals of control 3 month and 12 month ($n=2$) was normalised to NAA.

3.4 Discussion

This chapter employed an established mouse model of GBM to study the effect of FAO inhibition in combination with temozolomide in malignant gliomas. Tumour growth was monitored using MRI and MRS to capture changes in brain structure and metabolites. Furthermore, *in vitro* metabolite profiling of mouse oncogenic NPCs, the cell of origin used in the syngeneic model revealed age associated metabolic changes that were independent of drug treatment.

3.4.1 The syngeneic mouse model of GBM provides a tool for studying tumourigenesis and pharmacological testing

Animal models of GBM provide a useful tool for assessing pathology, identification of novel therapies and preclinical evaluations. In this study, the syngeneic model of GBM was employed as a model for monitoring tumour progression and also for pharmacological testing. Orthotopic transplantation of oncogenic mouse NPCs resulted in the formation of MR visible tumours with latency around 80 days (Figure 3.3). Using a 7T MRI, four SEMS sequences with different T1/T2 weightings were used to determine macroscopic anatomical changes from tumour development. Histological assessment confirmed presence of tumours along with clinically identifiable pathological features of human GBM including anaplasia, necrotic regions and infiltrating cells. Upon visualisation of MR visible tumours, there was rapid decline in clinical performance limiting the ability to gather more imaging data. It is worth considering other tools such as contrast enhancing agents to improve resolution of tumour visualisation and secondly imaging at shorter intervals, (e.g. 7 days) which could help earlier detection of tumour. This study also highlighted the benefit of different weighted MRI images in aiding in the detection of tumour at earlier time points.

In this study we tested the combination of etomoxir and temozolomide in our murine model of GBM. Although this study was not statistically powered to test the efficacy of treatment arms, for all of the treatments, the timing and dosage resulted in failure of any tumours to grow during the study time period: this meant it would be impossible to distinguish between the effects of ETX, TMZ and the combination (Figure 3.5). Possible considerations for a future efficacy study would be to commence treatment at a later time point where there was increased tumour burden which enables the determination of which treatment/combination decreases tumour progression or indeed causes regression. The dosing schedule adopted in this study sought to limit drug induced toxicity of the combination by adopting staggered delivery where TMZ dosing

mimicked clinical chemotherapy scheduling (5 days on, 25 days off). Although no immediate drug related toxicity issue arose in the combination group, TMZ in this study was only administered for one cycle and thus prolonged toxicity could not be assessed. Additionally, during the course of the study, mice receiving etomoxir administered continuously did not suffer any toxicity (ETX alone and Combination n = 4).

Etomoxir alone performed as well as temozolomide in delaying onset of MRI visible tumours. The study however did not determine whether combination of these drugs would further improve survival outcome. An efficacy study with larger cohort and alternative dosing regimens is required to establish whether inhibiting fatty acid oxidation in conjunction with standard GBM chemotherapy can prolong survival. Due to the aggressive nature of GBMs, development of resistance remains a caveat to treatment and often limits potential of monotherapies. Combinational strategies seeking to improve/potentiate the effect of temozolomide have been posited as strategy to overcome this. A recent phase 3 trial on the combination of lomustine and temozolomide in newly diagnosed GBM patients with MGMT promoter methylation and who had undergone tumour resection observed an improvement in overall survival (48.1 compared to 32.6 months with TMZ alone) (Herrlinger et al., 2019). Other advances in combination therapy also focus on drug delivery. Especially because drug discovery efforts are limited by blood brain barrier penetrance of pharmacological agents. Using tumour targeted nanoparticles for drug delivery, temozolomide and bromodomain inhibitor JQ1 showed enhanced efficacy and reduced systemic toxicity in an orthotopic/immunocompetent GBM mouse model (Lam et al., 2018).

Fatty acid catabolism is a major contributor to acetyl-coA pools and ATP production in malignant glioma. Although the notion of upregulated glycolysis has persisted as the predominant metabolic feature of GBM, emerging evidence suggest that this may not capture the biological diversity of GBMs. FDG-PET as an imaging modality is unsuitable for detection of gliomas due to the high uptake and glycolytic nature of neuronal cells which increases background. Early clinical studies and subsequent meta-analyses determined that FDG-PET as an imaging modality does not consistently detect presence of GBMs. In fact, 40% of recurrent GBMs do not show evidence of FDG uptake despite evidence of tumour from contrast enhanced MRI images (Chen et al., 2005). Previous studies have shown that only 50% of acetyl-coA was glucose derived in GBMs. Using ¹³C metabolic substrates, Mashimo *et al.*, showed using ¹³C infusions in human GBM patients that other fuel sources including acetate contributed to acetyl-CoA pools (Mashimo et al., 2014). Fatty acid oxidation has been reported in several cancers including breast cancer where *MYC* overexpression in triple negative breast cancer drives

upregulated fatty acid oxidation (Camarda et al., 2016). Pharmacological inhibition of CPT1 alters glioma metabolism and reduces proliferative capacity *in vitro* and *in vivo* (Lin et al., 2016). This feature is however observed in GBM stem cells not exposed to serum. It is likely that the use of serum may have limited this feature being observed by several studies.

There are several theories as to how targeting two very distinct pathways could lead to a more effective therapeutic intervention; firstly causing two injuries to cancer cells creates a larger hurdle to overcome, cooperation/synergistic effects and targeting distinct tumour cell populations. Previous studies have shown that inhibiting energy metabolism can potentiate the effects of genotoxic drugs. For instance, an increase in FAO and OXPHOS mediated by AMPK is observed as an adaptive response to DNA damage due to a decrease in NAD⁺ and ATP levels (Brace et al., 2016). Therefore it could be posited that, dual targeting using temozolomide and etomoxir could lead to crisis whereby ATP and biosynthetic products required in the repair process are limited and therefore leads to cell death due to unrepairable DNA damage.

3.4.2 Considerations for *in vivo* spectroscopy for the detection of brain metabolites

In vivo spectroscopy is an attractive tool for non-invasively profiling neurochemical changes associated with disease pathophysiology. Monitoring tumour-associated biochemical changes could inform or refine hypotheses regarding metabolites, in particular lipids and their role in GBM progression. In our study, MRI guided spectroscopy was utilised to gather such information however, metabolites were not consistently detected across imaging days to reliably inform on biochemical changes. At the occurrence of an MR visible tumour of M079 at day 78, there were corresponding changes in metabolites namely creatine, inositol and taurine which have been previously reported as indicators of malignant gliomas (Law et al., 2003, Yerli et al., 2007, Kousi et al., 2012). Other studies have used metabolite ratios to evaluate presence of tumour, tumour grading, image guided radiotherapy and also therapy response (Bluml et al., 2016, Choi et al., 2012, Guo et al., 2012, Kumar et al., 2014, Law et al., 2003, Mlynarik et al., 2012, Cao et al., 2017). For instance metabolite ratios of Cho/NAA or NAA/Cr have previously been used as malignancy markers of cerebral gliomas.

Although we identified some changes in metabolite profiles at some study time points, there was low confidence in the metabolite detection in this study. MRS has its inherent limitations which were not entirely addressed. The acquisition parameters used a very short TE (8ms) which although it captured various metabolites, the spectra contained overlapping peaks particularly in the lipid/lactate region. Shorter TE sequences require high magnetic field homogeneity in the tumour (or contralateral) region to reduce water contamination and

metabolite overlap. This depends on the consistent success of the shimming protocol and that can be difficult to achieve. In this study this caused increased baseline artefacts which decreased signal to noise ratio (SNR) resulting in a reduced number of metabolites that were confidently fitted/assigned by TARQUIN.

Various studies have utilised a 35 ms TE for short echo time acquisitions for *in vivo* MRS in preclinical and patient studies. Protocols tend to implement automated shimming like FASTMAP for field homogenisation in single voxel MRS acquisitions (Juchem and de Graaf, 2017). Another important factor for longitudinal metabolite profiling is voxel size and consistent placement. MR imaging does not capture the dysplasia following transplantation of oncogenic NPCs which made voxel placement and ROI selection early on in the study difficult. However, the voxel size of 1mm spanned a large region of striatum enabling profiling in a tumour associated region. In order to improve precision, voxel placement reliability could be assessed within a session acquiring two different spectra from a second voxel replacement to identify variations or overlap which may inform on consistency/reliability of metabolites profiled.

An alternative to an *in vivo* metabolite profiling could be *ex vivo* MRS which compares tumour metabolites to adjacent tissue metabolites. *In vitro* and *ex vivo* NMR acquisitions could benefit from higher field strength spectrometers, increased SNR and more metabolites detected. HRMAS is spectroscopic technique that allows solid state NMR acquisition therefore no extraction is required and lipids are retained in the sample. One dimensional ^1H NMR with D_2O lysis similarly achieves this and lipid moieties are observed. Future work is therefore required to optimise *in vivo* MRS and can be further validated by comparing to *ex vivo* analysis.

3.4.3 *In vitro* NMR spectroscopy reveals age-associated metabolic changes

Owing to the difficulties of *in vivo* MRS, we utilised *in vitro* spectroscopy at high field strength to inform on changes in intracellular metabolite abundances related to treatment in oncogenic NPCs (cell of origin in the syngeneic GBM model). Oncogenic NPCs were treated with etomoxir, temozolomide and combination for 24h. Initial analysis of the spectral bins using PCA did not reveal obvious clustering patterns suggesting little discernible differentiation in metabolite levels between drug treatment groups. However, hierarchical clustering and heatmap analysis revealed a distinct cluster between biological replicates which were NPCs derived from different aged mice.

Investigation of relative metabolite levels revealed that 12 month NPCs had high levels of taurine compared to 3 month NPCs. Taurine has previously been reported as a malignant feature of glioma cells. Although not entirely clear the role it plays in GBM, recent evidence suggest a role in regulating oxidative stress and possibly influencing the levels of classical ROS scavengers such as glutathione (Yildirim and Kilic, 2011). Differences in choline related metabolites were also observed in the different aged NPCs. Phosphocholine was markedly increased in 12 month NPCs. Others have shown a relationship between increasing ratios of choline-containing compounds to NAA and increasing tumour grade in glioma (Guo et al., 2012). Interestingly, 3 month NPCs had more detectable lipids which may be a result of increased fatty acid synthesis or slower catabolism. Increased lipids are normally associated with increasing glioma grade, in this context, the 3 month NPCs have a lower malignancy potential. It is noteworthy that only the lipid-CH₂ species at 1.28 ppm was quantified from NMR spectra. To further characterise lipid abundance in the NPCs, more sensitive lipidomics techniques would reveal the differences in a greater number of lipid species. Furthermore, staining for lipid droplets could highlight differences in abundance and also dynamics with other cellular components. For instance, whether lipid droplets in either NPCs localise to the mitochondria where FAO occurs.

Previous studies have highlighted alterations in protein expression of metabolic enzymes in aged NPCs. Notably, differences in the malignancy potential of aged NPCs is observed (Mikheev et al., 2012, Stoll et al., 2011). The differences in metabolite abundances in the differentially aged NPCs is likely a result of different metabolic programs, which ultimately lead to differences in tumour latency and malignancy following orthotopic transplantation. Changes in the expression and activity of key enzymes may underlie differences observed in metabolite levels. Other variations may result from post-translational modifications in key enzymes, impacting catalytic activity. Further work using more replicates is needed to confirm differences in the metabolic phenotype of these cells. Additionally, the untransformed aged NPCs could be profiled and matched to their oncogenic counterparts to establish whether metabolic features are maintained or lost during the transformation process.

Although our *in vitro* profiling did not reveal treatment associated changes, the experimental conditions may not have been optimised to detect this. Temozolomide is a DNA alkylating agent (prodrug) and so its effect may manifest at a later time point than 24h. To assess these changes, using multiple time points (i.e. 24, 48, 72h) may indeed highlight treatment related metabolic changes. Although the 3 and 12 month NPCs have differences in their metabolite profiles, it would be interesting to assess whether despite the difference in basal metabolite levels if treatment-induced changes displayed similar patterns.

Taken together, initial pharmacological testing of etomoxir and temozolomide in a syngeneic model of GBM has highlighted the promise of these agents as therapeutic intervention for GBM. Furthermore, the testing of agents in clinically relevant models of the disease is likely to aid the development of more translatable therapies for malignant gliomas. This study has highlighted the usefulness of NMR based metabolic profiling for features that are indicative of differences in metabolic and cellular phenotype. Altered metabolism is a hallmark of cancer and the utilisation of metabolic profiling may provide a useful tool for identifying biological/malignant features, subgroup differences and biomarkers of GBM and other brain malignancies. Differences in metabolites which are indicative of metabolic processes may provide novel opportunities for therapeutic targeting and assessment of therapy response. The usefulness of metabolic profiling in identifying phenotypic and metabolic characteristics led to its utilisation in characterising metabolic alterations associated with MYC amplification in medulloblastoma is covered in the subsequent chapters.

Chapter 4 Characterising the bioenergetics of *MYC*-amplified group 3 medulloblastoma

4.1 Introduction

MYC amplifications are the most notable genetic abnormalities in MB_{GRP3} (Taylor et al., 2012). Oncogenic *MYC* functions outside of the normal cellular regulatory mechanisms governed by growth factor stimulation and nutrient sufficiency. *MYC* exerts control over gene expression programmes through transcriptional activation/repression following binding to DNA regions termed E boxes or to non-consensus DNA binding sites. Deregulated activity of *MYC* may arise through amplification, translocations to enhancers and stabilisation of *MYC* protein itself (Boxer and Dang, 2001). There are numerous mechanisms by which *MYC* can drive transformation; by augmenting the existing gene expression programme within a cell-specific context without great specificity; or in a more refined manner which is driven by chromatin accessibility and interaction with other transcriptional regulators (Nie et al., 2012). Given the highly dynamic nature of metabolic pathways; responsiveness to micro-environmental changes and plasticity of metabolic networks, it is likely that *MYC* acts in between general amplification and specificity to ensure metabolic constraints do not persist to limit proliferation but respond dynamically to ensure survival in a harsh tumour microenvironment.

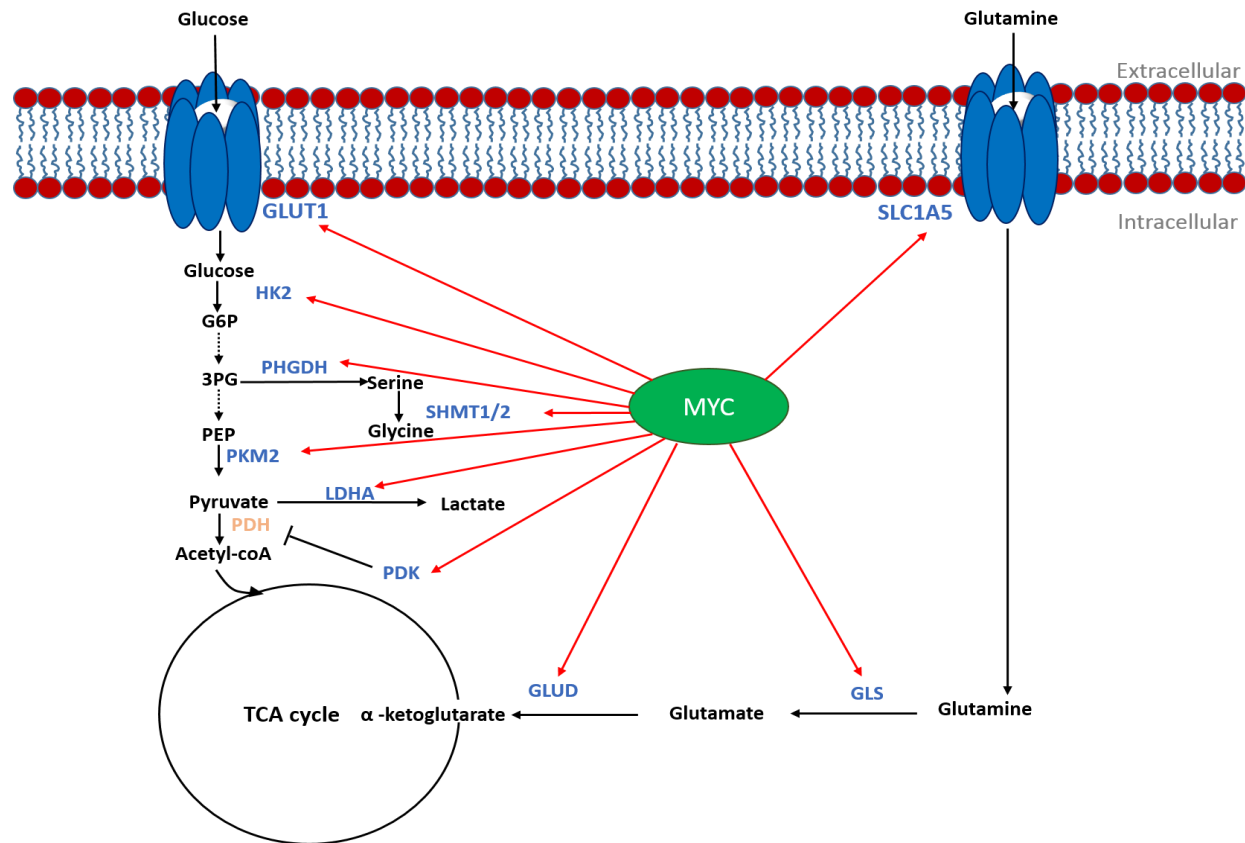


Figure 4.1 MYC-driven reprogramming of cellular metabolism to fuel rapid cancer cell growth. MYC promotes aerobic glycolysis (Warburg effect) by transcriptionally regulating several glycolytic enzymes and glucose transporters. MYC upregulates glutaminolysis as an alternative fuel source and to support TCA anaplerosis. Enzymes and transporters directly regulated by MYC are indicated in blue and indirectly regulated in orange. Adapted from Li and Simon, 2013.

Early indications of the ability of *MYC* to regulate the expression of metabolic enzymes were from the highly conserved E-boxes found in proximal promoter regions of the *LDHA* gene (Shim et al., 1997). Further work using RNAseq and ChIPseq has uncovered wide reaching regulation of several metabolic enzymes making up a diverse aspects of cellular metabolism (Dang et al., 2006). *MYC* driven cancers have been shown to have increased expression of enzymes involved in glycolysis and glutaminolysis (summarised in Figure 4.1). Particularly, *MYC* has been shown not only to increase expression but to increase specific mRNA splice variants as seen in the cases of PKM2 which is frequently associated with cancer phenotypes (Mazurek, 2011, Mazurek et al., 2005). In addition to altering the enzymatic landscape, *MYC* also upregulates nutrient transporters such as GLUT1 (SLC2A1) and ASCT2 (SLC1A5) to ensure continuous and adequate supply of nutrients to metabolic enzymes. Furthermore, transporters support the efflux of metabolic byproducts and in the case of increased glycolytic flux, upregulation of MCT1 and MCT4 is also observed. Expression of MCT4 is regulated by HIF1- α more commonly, however MCT1 is more commonly associated with *MYC* (Ullah et al., 2006, Pinheiro et al., 2012). The relationship between *MYC* and the glycolytic phenotype is further highlighted by RNAi and pharmacological studies targeting aspects of glycolysis which have been shown to be detrimental to *MYC*-driven cancers (Broecker-Preuss et al., 2017, He et al., 2015, Tateishi et al., 2016).

Glutamine addiction is frequently observed in *MYC* driven cancer *in vitro* and *in vivo*. Glutaminolysis is not a universal phenomenon of all cancer cells and is not directly linked to cellular growth but rather has been associated with oncogenic events. Overexpression of *Myc* in MEFs resulted in increased expression of glutamine transporters and glutaminases. Glutamine derived carbons are not necessarily used for biosynthetic requirements but to ensure TCA anaplerosis particularly since glucose is diverted away from being oxidised in the mitochondria. Glutamine derived α -ketoglutarate replenishes the TCA cycle ensuring mitochondria function. *MYC* transformed cells are particularly sensitive to glutaminase inhibition which has been suggested as a therapeutic strategy for these cancers. In fact, the specific function of glutamine utilisation has further been supported by experiments where GLS inhibition has been rescued using cell permeable α -KG (Wise et al., 2008, Yuneva et al., 2007).

MYC also regulates mitochondrial biogenesis and dynamics. *MYC* induces biogenesis by directly targeting genes such as peroxisome proliferator-associated gamma coactivator 1-beta (PGC-1 β) and transferrin receptor (TFRC) which transport haem and sulphur to support synthesis of mitochondrial proteins (Li et al., 2005). *MYC* also regulates mitochondria biogenesis through the mitochondria transcription factor A (TFAM) (Zhang et al., 2007). Several studies have shown *MYC* regulation of mitochondria fusion and fission events which govern mitochondria mass and cellular distribution (Li et al., 2005). *MYC* has also been shown to cooperate with other transcription factors such as MCL1 to increase mitochondria respiration and ROS production, which has been shown to contribute to maintenance of stem cell population and drug resistance in breast cancer (Lee et al., 2017).

Given the expansive gene expression programme governed by *MYC* in rewiring metabolic pathways, exploring *MYC* driven alterations in medulloblastoma may help to understand disease pathology and may provide avenues for novel therapies targeting *MYC*-driven metabolism.

4.2 Aims

The aim of this chapter was to characterise MYC-dependent changes in bioenergetics, using *MYC*-regulable MB_{GRP3} cell line models. In particular, the objective was to reveal *MYC*-driven metabolic phenotypes by:

- Assessing phenotypic changes associated with MYC knockdown in doxycycline inducible MB_{GRP3} cell lines (D425, D283 and HDMB03) with two independent shRNA constructs (MYC 2, MYC 3) and a control non-silencing construct (NS).
- Assessing changes in the protein expression of metabolic enzymes upon *MYC* knockdown.
- Determining the impact of MYC on bioenergetic function using the Seahorse XF bioanalyser to measure oxygen consumption rate and extracellular acidification rate.

4.3 Results

4.3.1 Phenotypic assessment of *MYC* modulation in MB_{GRP3} cell lines

4.3.1.1 Effective knockdown of *MYC* protein in doxycycline inducible MB_{GRP3} cell lines

MB_{GRP3} (D425, D283 and HDMB03) *MYC* inducible cell lines were previously established. For each MB cell line there were two independent shRNAs targeting *MYC* and a non-silencing (NS) control. Prior to commencing phenotypic assessment and characterisation of bioenergetic features, the knockdown efficiency for each cell line and construct was assessed. D425, D283 and HDMB03 (NS, MYC 2, MYC 3) cell lines were grown in the presence or absence of 1 µg/mL doxycycline for 72 h followed by cell pellet collection, protein extraction and quantification. Each sample was immunoblotted for *MYC* protein. For clarity, the absence or presence of doxycycline in the cell lines harbouring *MYC* constructs are referred to as “*MYC* (on)” and “*MYC* (off)” respectively. In the NS cell lines they are referred to as “NS (on)” and “NS Dox Ctrl (on)”.

In the D425 NS cell line, *MYC* expression levels were similar in the presence or absence of doxycycline (Dox) indicating uninterrupted expression of *MYC* when the NS construct was expressed following treatment with Dox (Figure 4.2). *MYC* knockdown in D425 was 80% in MYC 2 ($p=0.001$) and 30% in MYC 3 cell lines. Notably, *MYC* protein levels in the D425 MYC 3 (on) cell line was lower than in the NS (on) and MYC 2 (on) cells (Figure 4.2). Similar observations were made in D283 cell lines where, NS cell lines expressed *MYC* at comparable levels irrespective of doxycycline treatment. In the D283 MYC 2 cell line, prior to any genetic manipulation, starting levels of *MYC* was markedly higher in MYC 2 (on) compared to NS cell lines. The knockdown efficiency in the D283 cell line was 80% in MYC 2 ($p<0.001$) and 70% in MYC 3 ($p=0.003$) (Figure 4.3). The HDMB03 cell line was more variable in response to Dox. In HDMB03 NS, treatment with Dox caused a slight decrease in *MYC* expression although not significantly. In both HDMB03 MYC 2 and MYC 3 cell lines, 50% knockdown of the *MYC* protein was achieved (Figure 4.4).

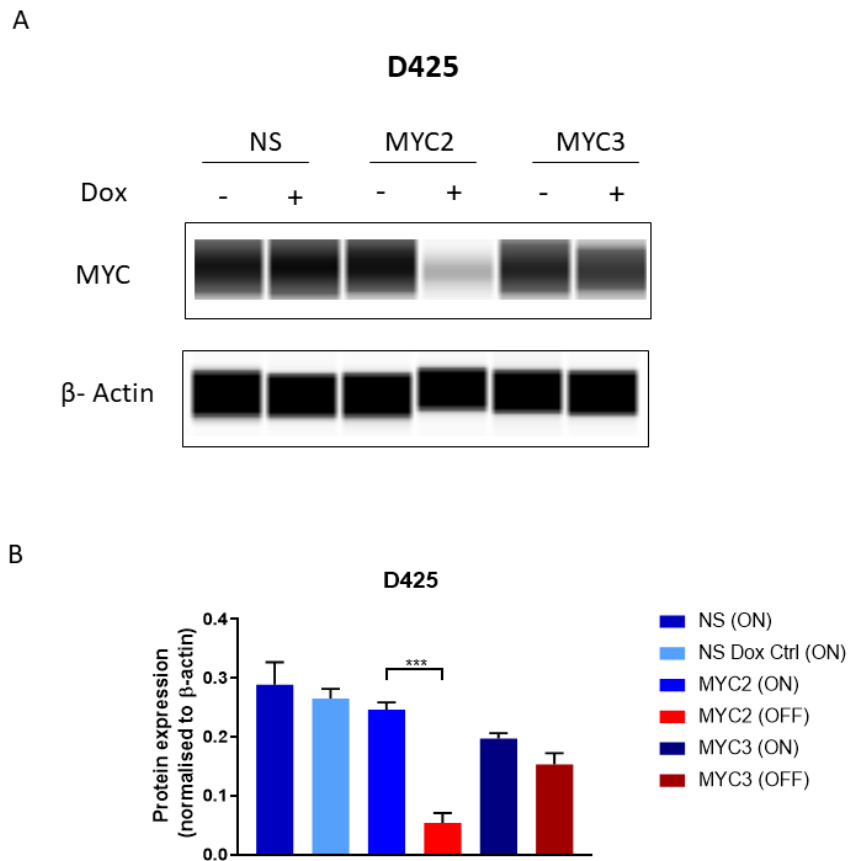


*Figure 4.2 Analysis of MYC expression levels in response to doxycycline treatment in the D425 NS, MYC 2 and MYC 3 cell lines. A) Representative WES image of MYC expression of D425 cells treated in the absence (- Dox, MYC on) or presence (+ Dox, MYC off) for 72 h. B) Quantitative analysis of MYC peak area normalised β- actin used as a loading control. Results are represented as mean ± SEM of three independent experiments. Significance denoted with * $p < 0.05$, ** $p < 0.01$, *** $p < 0.001$.*

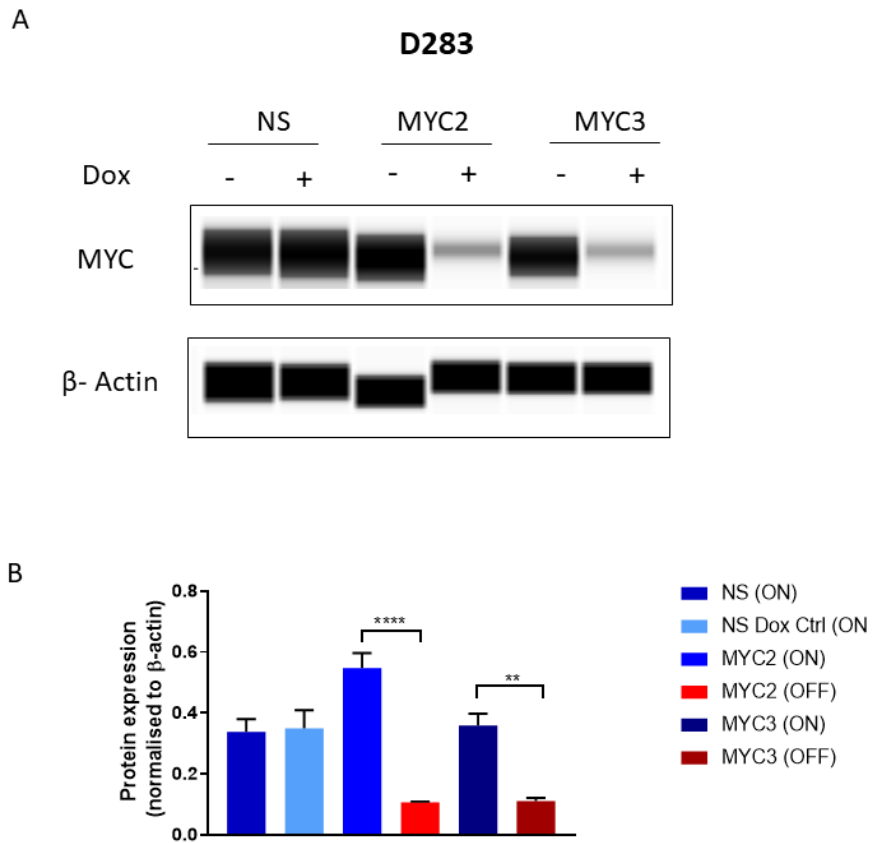


*Figure 4.3 Analysis of MYC expression levels in response to doxycycline treatment in the D283 NS, MYC 2 and MYC 3 cell lines. Representative WES image of MYC expression of D283 cells treated in the absence (- Dox, MYC on) or presence (+ Dox, MYC off) for 72 h. B) Quantitative analysis of MYC peak area normalised β -actin used as a loading control. Results are represented as mean \pm SEM of three independent experiments. Significance denoted with * $p < 0.05$, ** $p < 0.01$, *** $p < 0.001$.*

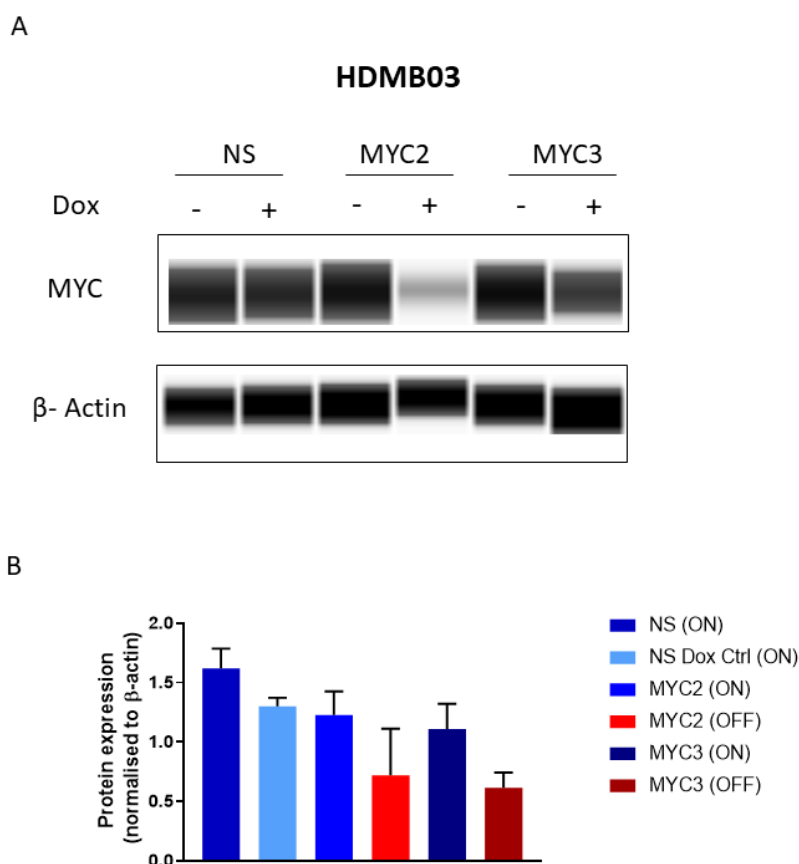


Figure 4.4 Analysis of MYC expression levels in response to doxycycline treatment in the HDMB03 NS, MYC 2 and MYC 3 cell lines. A) Representative WES image of MYC expression of HDMB03 cells treated in the absence (- Dox, MYC on) or presence (+ Dox, MYC off) for 72 h. B) Quantitative analysis of MYC peak area normalised β - actin used as a loading control. Results are represented as mean \pm SEM of three independent experiments. Significance denoted with * $p < 0.05$, ** $p < 0.01$, *** $p < 0.001$.

4.3.1.2 Effect of MYC knockdown on cell proliferation

The ability of MYC to drive increased proliferation has been well characterised. In order to determine the effect of MYC knockdown in the MYC isogenic cell lines, D425, D283 and HDMB03 (NS, MYC 2, MYC 3) cell lines were grown in the presence or absence of doxycycline and subjected to viable cell counting at 24, 72 and 120 h time points.

In the D425 NS cell line, proliferation was comparable between the D425 NS (on) cells D425 NS Dox Ctrl (on) cells (doubling time 30.76 and 37.96 h, respectively, $p > 0.05$). However, the growth curves showed marginal decrease in the D425 NS Dox Ctrl (on) cell numbers at 120 h following doxycycline treatment (Figure 4.5 A). In the D425 MYC 2 cell line however, MYC knockdown caused a significant reduction in proliferation that

was observable from 72 h and had a greater impact on doubling time (D425 MYC 2 (on) 30.57 versus D425 MYC 2 (off) 57.43 h, $p < 0.0001$) (Figure 4.5 B). Similarly, in the D425 MYC 3 cells, MYC knockdown markedly reduced proliferation although this was somewhat an intermediate phenotype compared to the observations in the D425 MYC 2 cells, $p < 0.0001$) (Figure 4.5C). Doubling times were 30.30 and 40.11 h in the D425 MYC 3 (on) and MYC 3 (off) cells respectively. The doubling times for the D425 MYC 3 harbouring cells were comparable to that seen in the D425 NS cell line thus making it difficult to differentiate whether the impact on proliferation was a result of lowered MYC knockdown efficiency or doxycycline induced effects (Figure 4.5). In order to further examine the doxycycline-induced compared to MYC-induced alterations in cell growth, cell number differences at 72 h were evaluated. Assessment of cell number differences at 72 h revealed divergence in cell numbers in the D425 MYC 2 and MYC 3 bearing cells but this was not observed in the D425 NS cell line post-treatment with doxycycline (Figure 4.2 D). These indicate that the effect of MYC knockdown occurred much earlier and that diverging proliferation rate in the D425 NS following doxycycline treatment may be attributable to prolonged exposure.

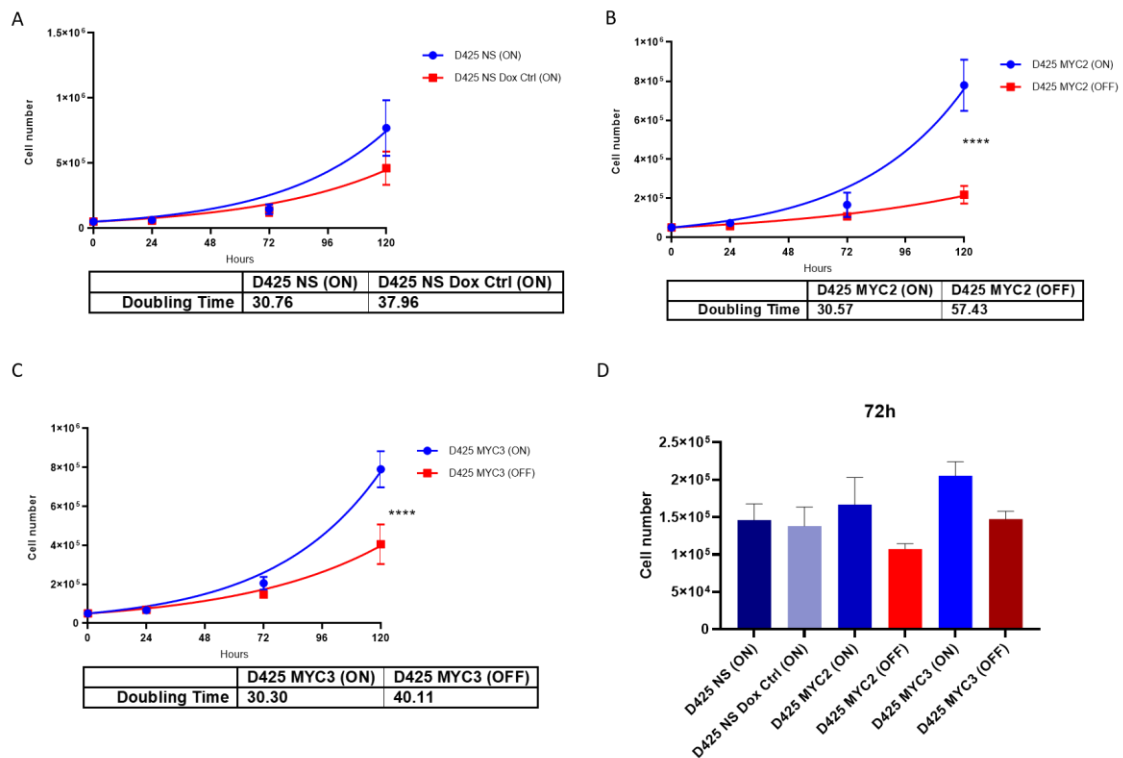


Figure 4.5 Effect of MYC knockdown on proliferation of D425 MYC-inducible cell lines.

A) Growth of curves of D425 NS B) D425 MYC 2 C) D425 MYC 3 cells grown $\pm 1 \mu\text{g/mL}$ Dox over 120 h. D) Comparison of cell counts across the 3 cell lines at 72h. Error bars represent \pm SEM of three independent experiments, **** $p < 0.0001$

In the D283 cell line, NS cells in the presence or absence of doxycycline proliferated similarly over 120h, although the doubling time was higher in the NS Dox Ctrl (on) cells which may be attributable to reduced cell numbers at 120h (Figure 4.6 A). In the D283 MYC 2 cells, knockdown of MYC impacted growth rate significantly ($p=0.0009$). This reduced proliferation was observable from 72h and doubling times were 39.54 and 44.53 in the D283 MYC 2 (on) and MYC 2 (off) cells, respectively (Figure 4.6 B). Notably, the doubling time of D283 MYC 3 (on) cells was observed to be higher than D283 MYC 2 (on) cells (30.05 h compared to 39.54 h). Nevertheless, MYC knockdown significantly impacted proliferation of the D283 MYC 3 (on) 30.05 compared to MYC 3 (off) 49.72 h, $p=0.002$) (Figure 4.6C). It is also noteworthy that in the MYC 3 harbouring cells, a decrease in cell number was observed after 72 h (Figure 4.6D).

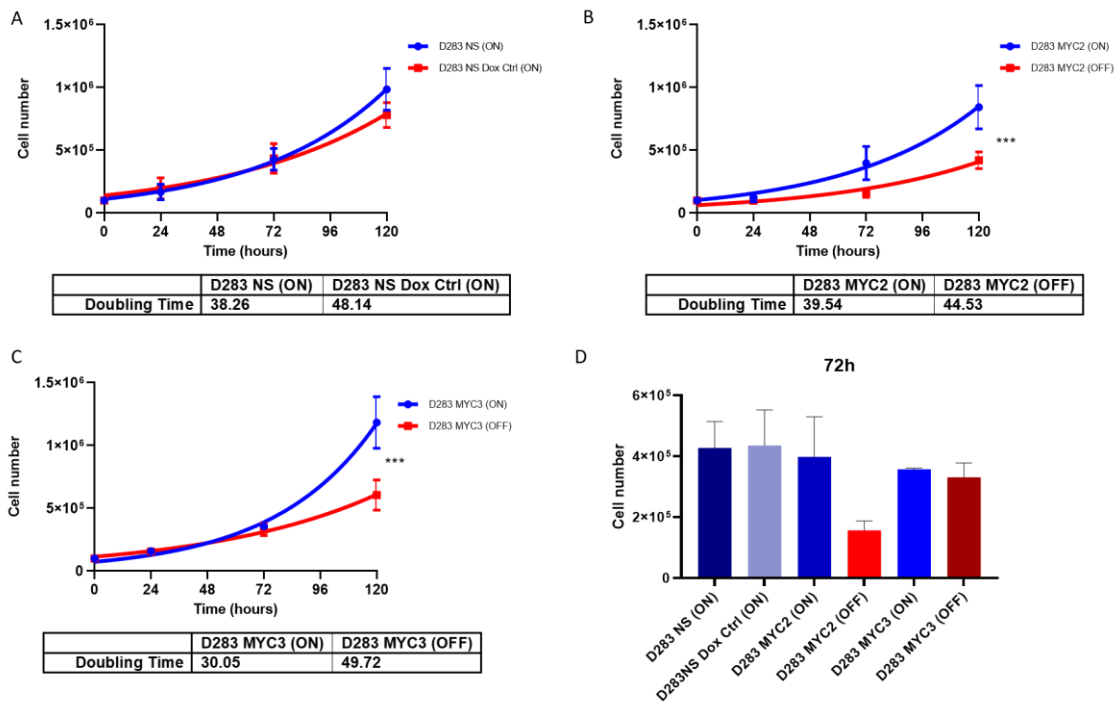


Figure 4.6 Effect of MYC knockdown on proliferation of D283 MYC-inducible cell lines.

A) Growth of curves of D283 NS (i), D283 MYC 2 (ii) and D283 MYC 3 (iii) cells grown \pm Dox over 120 h. B) Comparison of cell counts across the 3 cell lines at 72h. Error bars represent SEM of three independent experiments. *** $p < 0.001$

Similarly to D425 and D283 cell lines, HDMB03 NS cells grew consistently and were not responsive to the addition of Dox which was expected in the NS Dox control cell line (doubling time was 45.92 and 43.30 h in HDMB03 NS (on) and NS Dox Ctrl (on), respectively) (Figure 4.7 A). Proliferation was reduced considerably in the HDMB03 MYC 2 (doubling time MYC 2 (on) 61.53 and MYC 2 (off) 111.5 h, $p=0.003$) and HDMB03 MYC 3 (doubling time MYC 3 (on) 80.93 and MYC 3 (off) 179.4 h, $p=0.002$). However in these cell lines, in the absence of doxycycline, the doubling rate was dissimilar from the NS cell line which had doubling around 45.52 h compared to 61.53 and 80.83 h in HDMB03 MYC 2 (on) and MYC 3 (on) cells, respectively (Figure 4.7B, C). This difference in the doubling times would suggest that there was some leakiness of the MYC shRNA constructs in these cell lines particularly in the HDMB03 MYC 3 cell line which did not grow exponentially over the 120 h.

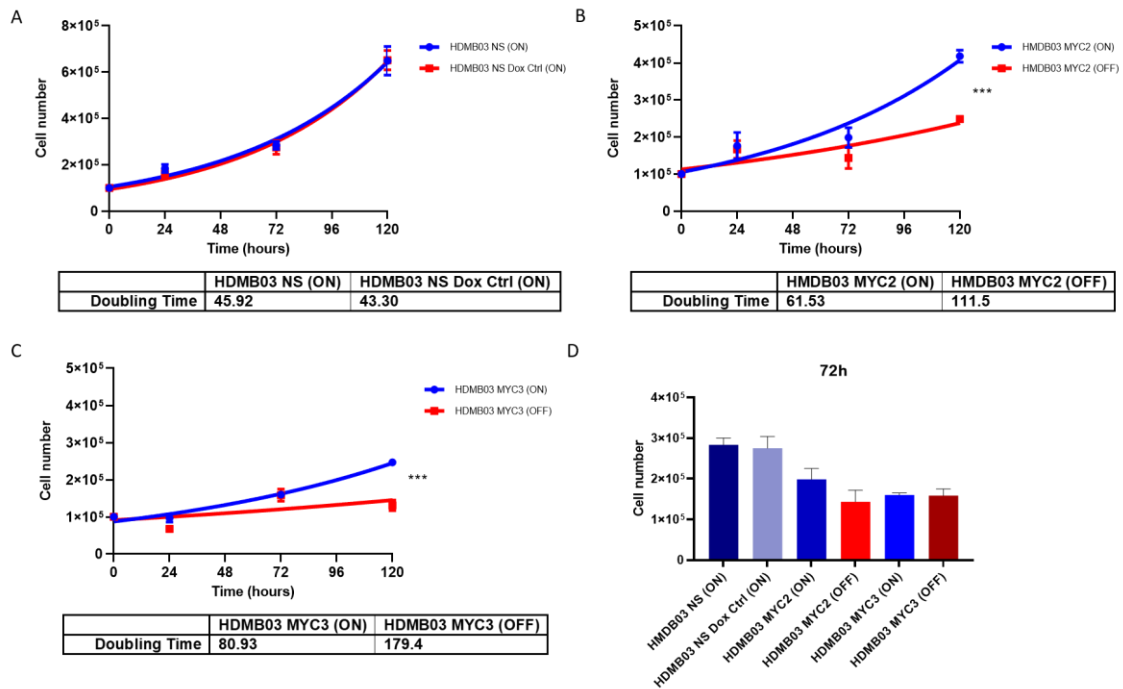


Figure 4.7 Effect of MYC knockdown on proliferation of HDMB03 MYC-inducible cell lines. A) Growth of curves of HDMB03NS (i), HDMB03 MYC 2 (ii) and HDMB03 MYC 3 (iii) cells grown \pm Dox over 120 h. B) Comparison of cell counts across the 3 cell lines at 72h. Error bars represent SEM of three independent experiments, * $p < 0.05$ by nonlinear regression analysis. *** $p < 0.001$

Assessment of proliferation in the MB_{GRP3} cell lines showed *MYC* addiction whereby knockdown affected proliferation and cell doubling times. This difference in proliferation was noticeable from 72 h in the MYC 2 harbouring cells in particular. In the MYC 3 cell lines, more modest effects were observed variations in cell numbers were observed at 72 h for D425 MYC 3 cells but this was not the case for D283 MYC 3 and HDMB03 MYC 3 cells following MYC knockdown. Earlier assessment on the protein expression of MYC in the MYC 3 cell lines suggested that there may be some “leakiness” of the construct i.e. high activity promoter resulting in the expression of shRNA targeting *MYC* in the absence of doxycycline treatment. Notably, MYC expression was lower in MYC 3 cell lines compared to their MYC 2 counterparts prior to the addition of doxycycline. With this in mind, experiments were restricted to 72 h to limit the impact of construct leakiness. Although it was also appreciated that subsequent phenotypic changes could be modest, particularly in the MYC 3 harbouring cells at this time point.

4.3.1.3 Effect of MYC knockdown on cell cycle progression

To further characterise the effect of MYC on cell growth, the effect of MYC knockdown on cell cycle progression was investigated in the MYC inducible cell lines. Cells were treated with doxycycline for 72 h and stained with propidium iodide and analysed using flow cytometry to determine cell cycle distribution. In the D425 MYC 2 cells, MYC knockdown caused a significant increase in the number of cells in G1 phase and decreased in cell G2/M (Figure 4.8A). Similarly, MYC knockdown resulted in G1 arrest in D283 (Figure 4.8B) and also in the HDMB03 MYC 2 cell lines where additionally the fraction of cells in G2/M were markedly reduced (Figure 4.8C). There were no discernible changes in cell cycle distribution in relation to the MYC 3 harbouring cell lines. Consistently, across all three cell lines there were no observable changes in the NS cell lines in the presence of doxycycline (Figure 4.8A-C).

Cell cycle related alterations were observed mostly in the MYC 2 harbouring cell lines at 72 h which was consistent with findings from analysis of cell number variations at 72 h in these cell lines (Figure 4.5-Figure 4.7). These early phenotypic data suggested that the most profound observations were likely to be observed in the MYC 2 harbouring cells with similar trends in the MYC 3 cell lines which suffered from lower knockdown efficiency resulting in milder phenotypic differences in the MYC 3 (on) compared to MYC 3 (off).

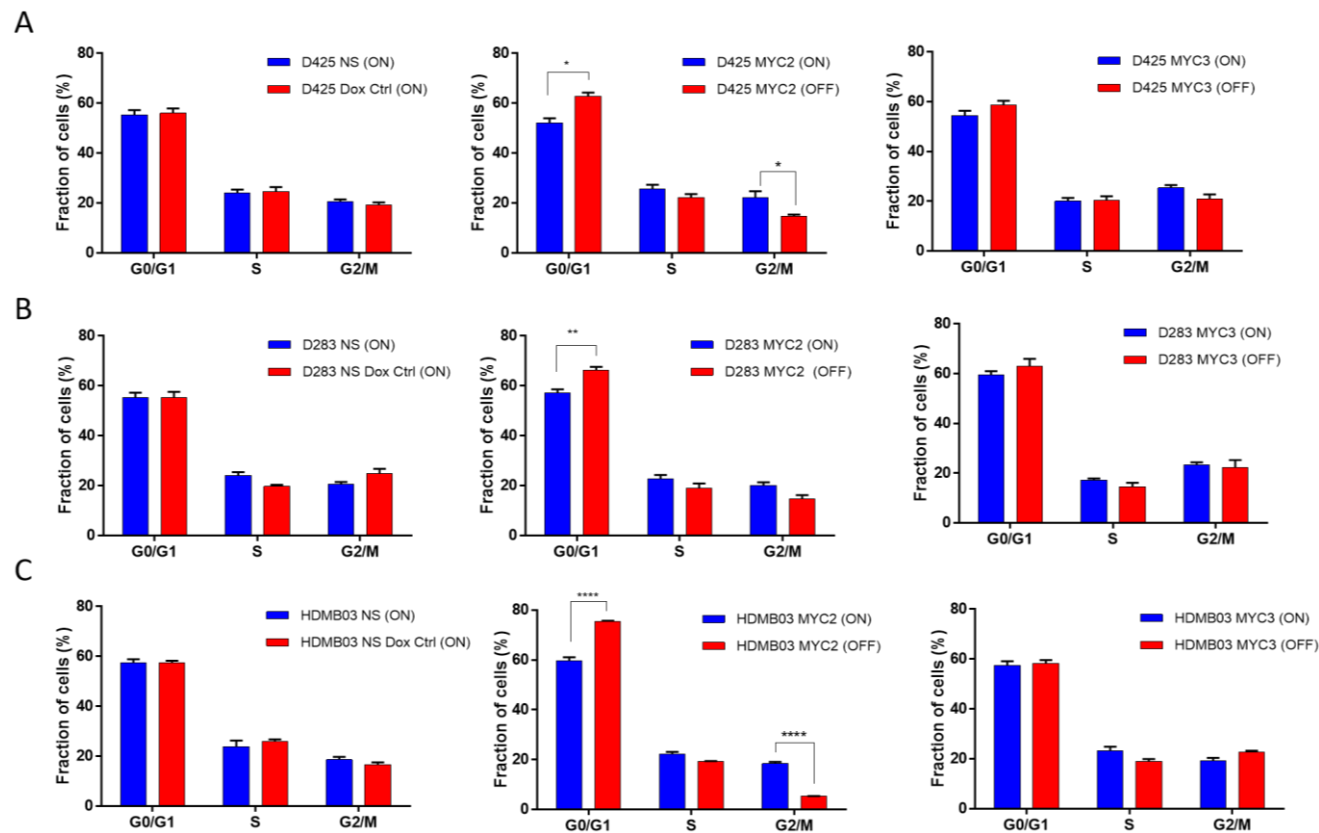


Figure 4.8 Impact of MYC knockdown on cell cycle distribution in MB_{GRP3} MYC regulable cell lines. Cells were treated in the absence or presence of doxycycline for 72 h, harvested and subjected to cell cycle analysis using flow cytometry. Cell cycle distribution between G0/G1, S and G2/M phases were assessed for A) D425, B) D283 and C) HDMB03 NS, MYC 2 and MYC 3 cell lines. Data is presented as mean \pm SEM of three independent experiments. * $p < 0.05$, ** $p < 0.01$, *** $p < 0.001$, **** $p < 0.0001$ as determined by one way ANOVA comparing NS (ON) v NS Dox Ctrl (ON), MYC 2 (ON) v MYC 2 (OFF) and MYC 3 (ON) v MYC 3 (OFF).

4.3.2 Alterations in metabolic enzymes in response to suppression of MYC

4.3.2.1 Alterations in the enzyme expression of the glycolytic pathway in response to MYC knockdown (Experiments by Yue Heng)

Since MYC regulates the expression of genes involved in numerous cellular processes, initial experiments focused on whether expression of metabolic enzymes were altered following MYC modulation. To assess this, the glycolytic enzymes HK2, PKM2 and LDHA were probed for using WES automated immunoblotting. These enzymes were selected due to well established evidence of MYC-dependent regulation (Shim et al., 1998, Shim et al., 1997, Mendez-Lucas et al., 2017). In addition to these glycolytic enzymes, PDH, an enzyme which routes pyruvate to oxidation in the TCA was probed for in its phospho-activated and total expression forms. PDH expression served as a determinant for alternative routes of pyruvate catabolism other than aerobic glycolysis. Briefly, *MYC* inducible cell lines were treated with/without 1µg/mL doxycycline for 72 h and protein lysates collected, quantified and protein expression examined by WES (full WES images are included in Appendix 8.6-Appendix 8.16).

In the D425 NS cells, similar expression of glycolytic enzymes was observed (Figure 4.9A& B). However in the D425 MYC 2 cell lines, reduced expression of *MYC* resulted in the trend of decreasing expression levels of all five glycolytic enzymes to varying degrees (Figure 4.9A&C). The most prominent effects were observed in the PKM2 and LDHA which are involved in later events of the glycolytic pathway. In the D425 MYC 3 cells, there were slight alterations in the expression of HK2 and phosphorylated PDH in MYC 3 (on) and (off) cells (Figure 4.9 A, D).

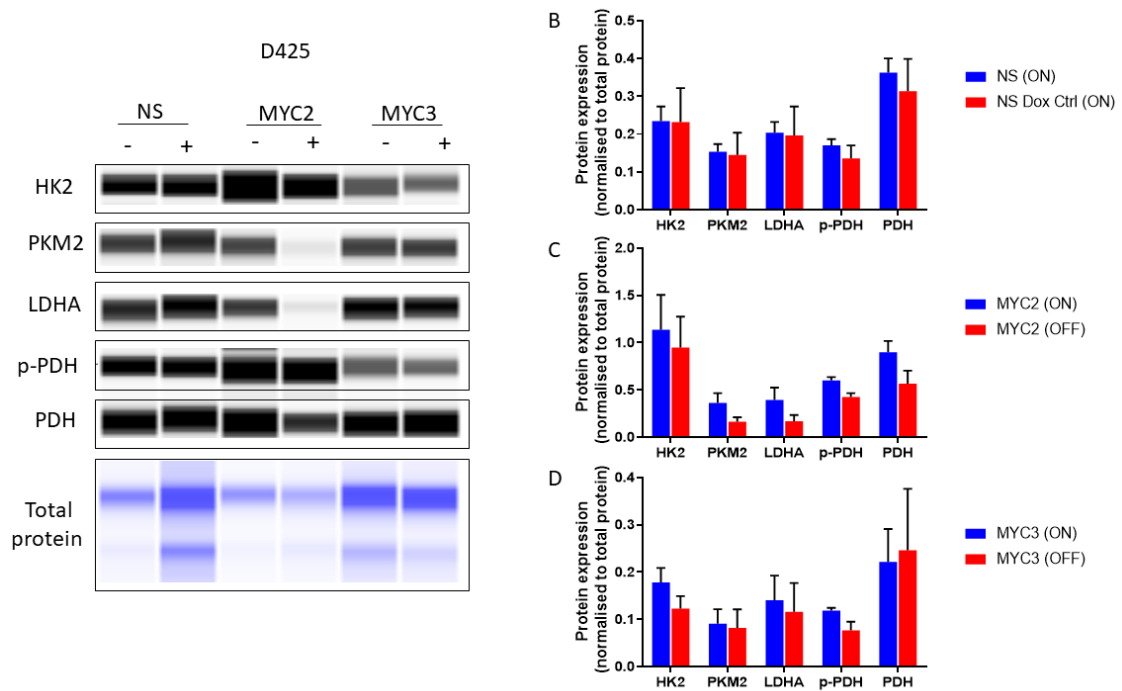


Figure 4.9 Effect of MYC knockdown on the glycolytic pathway in D425 MYC inducible cell lines. A) Representative WES image showing levels of HK 2, PKM 2, LDHA, phosphorylated PDH and total PDH from D425 NS, D425 MYC 2 and D425 MYC 3 cells treated \pm Dox for 72h. B-D) Quantitative analysis of glycolytic markers. Bars represent expression normalised to total protein. Data presented as mean \pm SEM of three independent experiments.

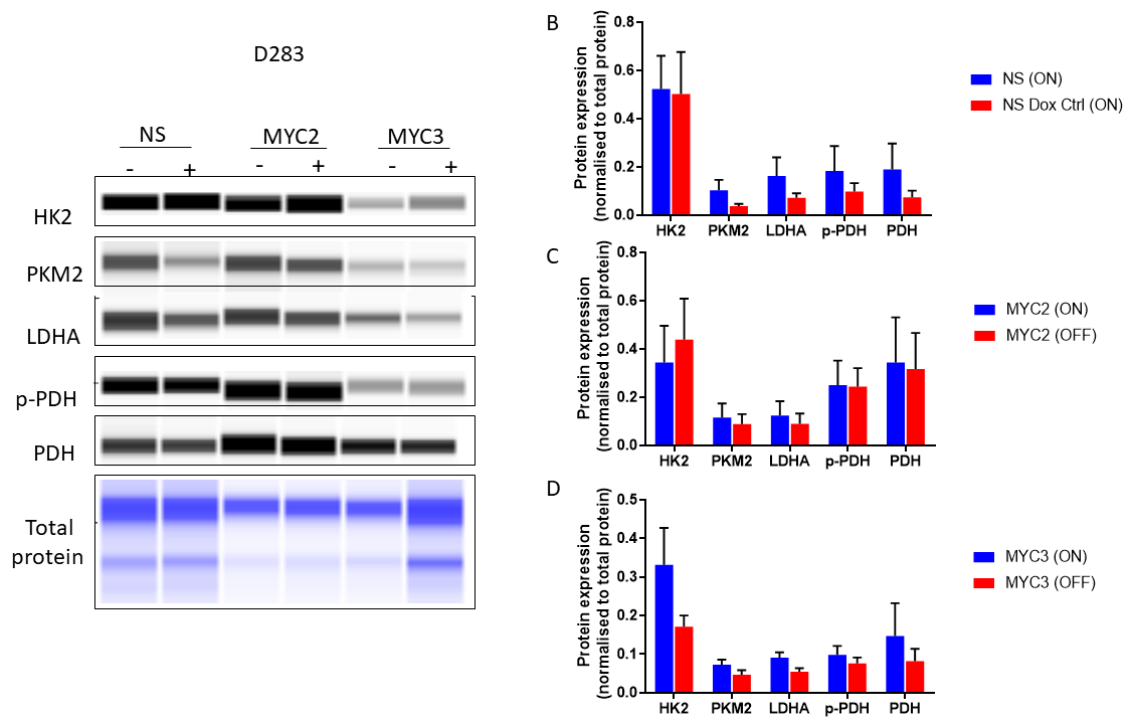


Figure 4.10 Effect of MYC knockdown on the glycolytic pathway in D283 MYC inducible cell lines. A) Representative WES image showing levels of HK 2, PKM 2, LDHA, phosphorylated PDH and total PDH from D283 NS, D283 MYC 2 and D283 MYC 3 cells treated \pm Dox for 72h. B-D) Quantitative analysis of glycolytic markers. Bars represent expression normalised to total protein. Data presented as mean \pm SEM of three independent experiments.

The D283 cell lines displayed large variations in expression levels between samples. Although HK2 expression was unaffected in the NS Dox control, the expression of other glycolytic enzymes showed a decreasing trend. D283 MYC 2 harbouring cells did not demonstrate any changes in the expression of glycolytic enzymes in contrast with MYC 3 harbouring D283 cells which showed observable differences in HK2, PKM2, LDHA and both forms of PDH (Figure 4.10A&C).

Similarly, in the HDMB03 NS cell lines, treatment with doxycycline caused slight alterations in the expression of glycolytic enzymes (Figure 4.11 A, B). In the HDMB03 MYC 2 cell lines, there were more pronounced alterations in the expression of enzymes particularly in HK2, LDHA and total PDH (Figure 4.11A, C). In contrast, increased expression of the glycolytic enzymes was observed in the HDMB03 MYC 3 cells (Figure 4.11 A, D).

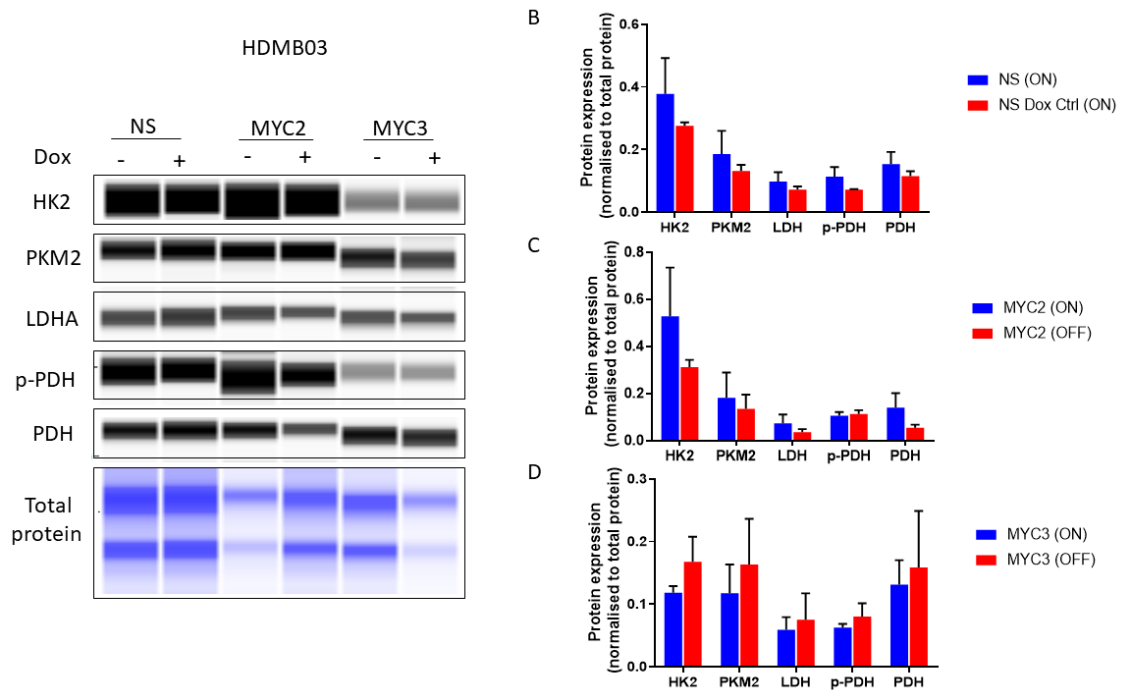


Figure 4.11 Effect of MYC knockdown on the glycolytic pathway in HDMB03 MYC inducible cell lines. A) Representative WES image showing levels of HK 2, PKM 2, LDHA, phosphorylated PDH and total PDH from HDMB03 NS, HDMB03 MYC 2 and HDMB03 MYC 3 cells treated \pm Dox for 72h. B-D) Quantitative analysis of glycolytic markers. Bars represent expression normalised to total protein. Data presented as mean \pm SEM of three independent experiments.

Data from enzyme expression suggests MYC knockdown affected the expression of glycolytic enzymes primarily, in the MYC 2 harbouring cells. However, these observable changes were confounded by the doxycycline-induced changes in enzyme expression, observable in the NS Dox Ctrl (on) cells. In an effort to clarify MYC-dependent changes and trends that were observed previously, the three cell lines were pooled according to shRNA constructs to increase sample size and statistical power. Analysis of enzyme expression across the NS cell lines reveal that expression levels did not remain stable following doxycycline treatment particularly for phospho-PDH and total PDH. In the MYC 2 cell lines, MYC knockdown significantly impacted glycolytic enzyme expression (Table 4.1).

Assessment of individual enzymes revealed robust decreases in PKM2 and LDHA ($p < 0.05$). In the MYC 3 cell lines however, alterations in glycolytic enzymes were minimal and this was likely affected by larger deviations and less consistent findings in enzyme expression in the MB_{GRP3} MYC 3 cell lines (Table 4.1). This data indicates that whilst MYC knockdown may impact the glycolytic pathway overall, MYC-dependent alterations in glycolytic enzyme expression was more intricately linked to PKM2 and LDHA in the glycolytic pathway in the context of MB_{GRP3}.

*Table 4.1 Log₂ (fold change) of metabolic enzyme following MYC knockdown in MBGRP3 cells. Significance determined using Two-way anova and Sidak test for multiple comparisons denoted by **

Enzyme	Construct	Log(FC)	Adjusted p-value
HK2	NS	-0.163	0.9343
	MYC 2	-0.048	0.9998
	MYC 3	-0.193	0.9861
PKM2	NS	-0.568	0.1005
	MYC 2	-1.085	0.0051*
	MYC 3	-0.030	>0.9999
LDHA	NS	-0.486	0.1820
	MYC 2	-1.146	0.0037*
	MYC 3	-0.153	0.9949
p-PDH	NS	-0.606	0.0759
	MYC 2	-0.408	0.3711
	MYC 3	-0.149	0.9955
PDH	NS	-0.584	0.0892
	MYC 2	-0.420	0.3464
	MYC 3	-0.060	>0.9999

4.3.2.2 Activation of the pyruvate dehydrogenase axis upon MYC knockdown

In addition to expression changes, involvement and activation of the PDH axis was investigated. As previously described, we observed trends of decreased levels of phosphorylated and total PDH when *MYC* was knocked down in some of the *MYC*-regulable cell lines (Figure 4.9, Figure 4.10 & Figure 4.11). Since we probed both total expression and phosphorylated forms of PDH, the ratios of these two markers were explored since that gave a better indication of pathway activity in the *MYC* isogenic cell lines. Interestingly, despite changes in expression levels, ratios of phosphorylated PDH to total PDH remained relatively constant across constructs in D425, D283 and HDMB03 cells (Figure 4.12A-C). This suggests that *MYC* knockdown, did not impact PDH activation and dynamics of this pathway

Phosphorylation of PDH is a crucial regulatory point coupling glycolysis to the TCA cycle which is highly conserved across eukaryotes(Gray et al., 2014).Our findings showed that activation of PDH was not *MYC*-dependent despite modest alterations in both phosphorylated and total expression levels. Importantly, ratios of p-PDH/PDH remained stable in the NS cell lines following Dox treatment. Since p-PDH/PDH ratios were largely comparable in the MB_{GRP3} cell lines following modulation of *MYC* expression, this data suggest activation of PDH and pathway activity, occurred independent of *MYC* and may be subject to regulation by other regulatory mechanisms.

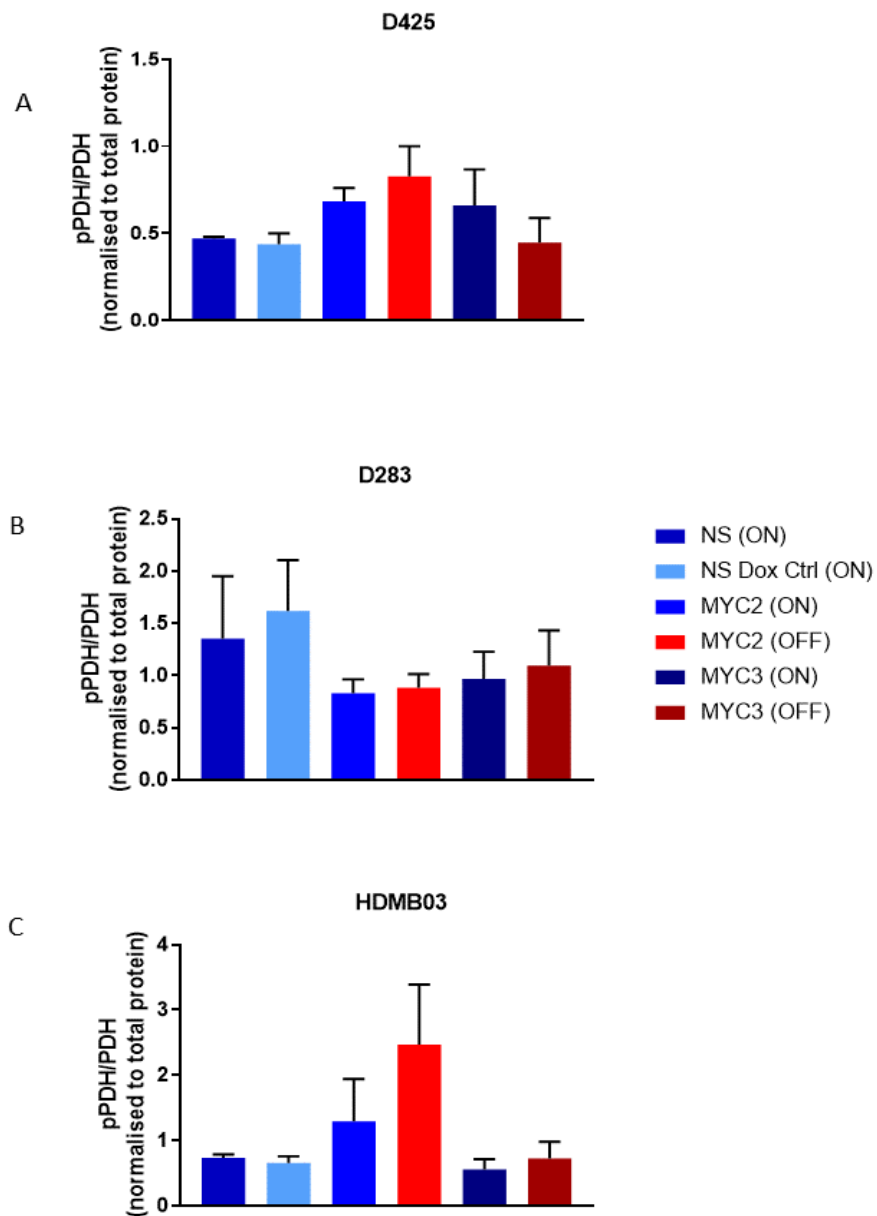


Figure 4.12 The ratios of phosphorylated PDH and total PDH in MB_{GRP3} doxycycline inducible cell lines. Protein levels of p-PDH and total PDH were assessed using WES following 72 h treatment in the absence or presence of Dox. The levels of p-PDH and PDH were normalised to total protein for A) D425, B) D283 and C) HDMB03 isogenic cell lines and represented as mean \pm SEM of three independent experiments.

4.3.2.3 Loss of MYC and the impact on glutaminase expression

The impact on glutaminase (GLS) expression following MYC knockdown was evaluated. MYC-driven cancers are associated with glutamine addiction. GLS which can be directly or indirectly regulated by MYC was chosen as a candidate enzyme for assessing alterations in this pathway (Gao et al., 2009). The GLS antibody used probes the kidney glutaminase (KGA), which localises to the cytosol, and also glutaminase C (GAC) which localises to the mitochondria. KGA and GAC are GLS1 isoforms produced from alternative splicing of the same gene (Elgadi et al., 1999). With localisation to the mitochondria, GAC has been shown to be the key isozyme and most efficient in glutamine catabolism and is more associated with cancer phenotypes (Cassago et al., 2012, van den Heuvel et al., 2012). Previous studies have shown the predominance of one isoform over the other occurs in a cell context-dependent manner (Daemen et al., 2018, Szeliga et al., 2016, van den Heuvel et al., 2012).

In the D425 NS, MYC 2 and MYC 3 cell lines, levels of KGA and GAC were comparable across cell lines irrespective of MYC status. Additionally, the expression of both isoforms were similar following MYC knockdown (Figure 4.13A). In the D283 cells however, KGA was highly expressed compared to GAC. Expression of KGA and GAC were relatively stable in the D283 NS cell lines. Both the expression of KGA and GAC glutaminases were reduced following MYC knockdown in the D283 MYC 2 harbouring cells but this was not observed in the D283 MYC 3 (Figure 4.13B). In the HDMB03 cell line, GAC appeared to be the predominant isoform. In the HDMB03 NS, MYC 2 and MYC 3 cell lines, there was a slight increase in the expression KGA isoform. For GAC however, there was decreased expression in the MYC 2 harbouring cells with no changes observed in MYC 3 and NS cell lines (Figure 4.13C).

These results suggests that glutaminase expression across the MB_{GRP3} cell lines varied and expression of glutaminase isoforms appeared to be cell-specific. The extent to which this may affect glutamine metabolism across the MB_{GRP3} cell lines was not determined. There were some indications of MYC-dependent alterations particularly in the D283 MYC 2 cells. Whilst these results remain interesting, further experimental repeats are required to confirm these findings reported here.

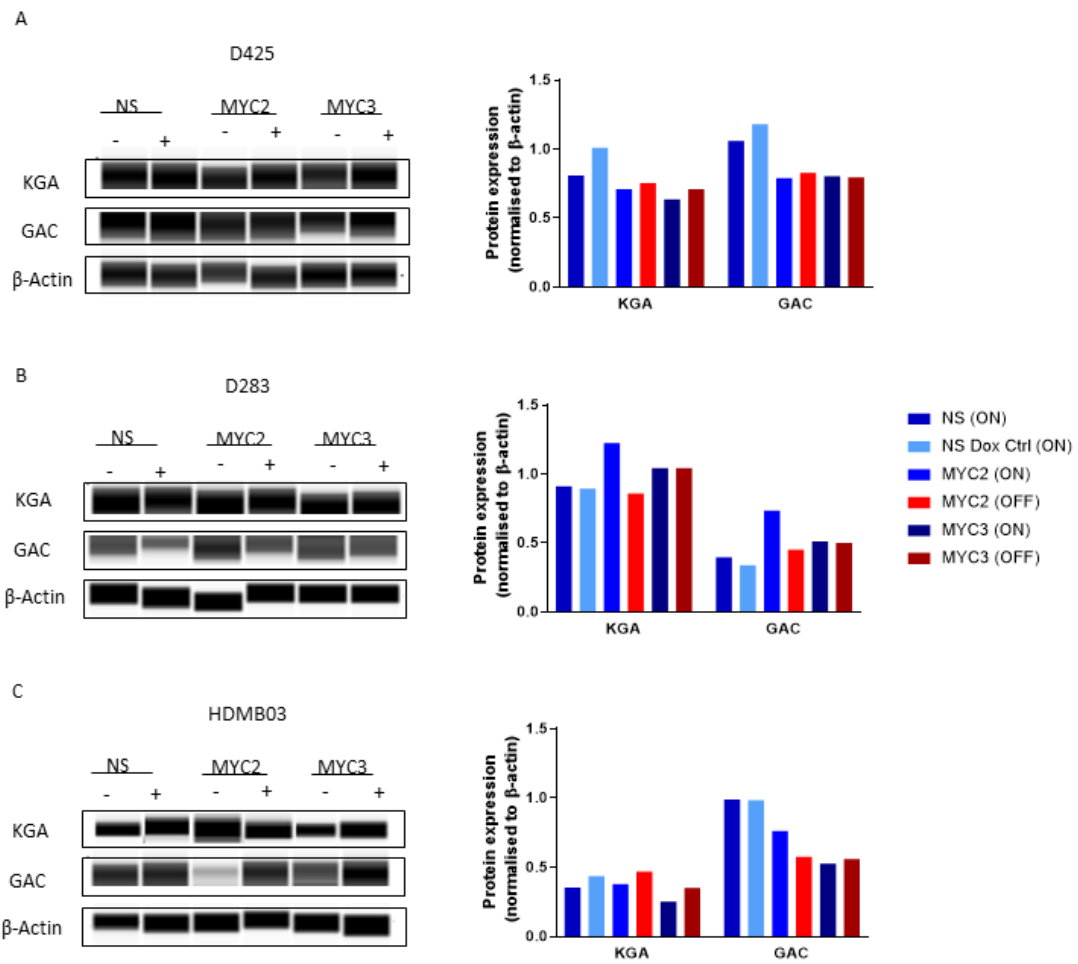


Figure 4.13 Effect of MYC knockdown on the glutaminase expression in the MB_{GRP3} cell lines. Representative WES image and densitometry showing levels of the glutaminase isoforms KGA and GAC in A) D425 B) D283 C) HDMB03 cells treated ± Dox for 72h.

4.3.3 Characterising changes in bioenergetics in response to MYC expression

The overarching aim of this study was to determine whether varying levels of MYC expression specifically affected metabolic activity and function. As previously described, MYC knockdown was capable of reducing the expression of enzymes involved in glycolysis but not PDH which is a key committing step in pyruvate oxidation in the TCA cycle. Owing to the fact that reduced enzyme expression does not always correlate with diminished pathway activity (Zdravlevic et al., 2018), a functional assay measuring oxygen consumption rate (OCR) and extracellular acidification (ECAR) in response to mitochondrial inhibitors (OG, FCCP, AM and ROT) was utilised to measure oxidative and glycolytic energetic output via OCR and ECAR measurements, respectively. MB_{GRP3} inducible cell lines were treated with or without doxycycline for 72 h and subsequently assayed on an XF bioanalyser. Although numerous aspects of bioenergetics can be ascertained from this assay, this study primarily focused on ATP production since it provided insights into both glycolytic- and OXPHOS-derived ATP. Additionally, spare respiratory capacity was reported as it informed on mitochondria capacity and performance (Experiment set up and calculations detailed in Chapter 2.2.7 and Appendix B).

4.3.3.1 ATP production

Mitochondria oxygen consumption is coupled to ATP production via complex IV which uses oxygen as the final electron acceptor. The proton motive force generated by the ETC complexes drives ATP production by the complex V ATPase. Glycolysis also generates ATP and here, extracellular acidification is linked with the activity of LDH which catalyses the conversion of pyruvate to lactate as the final step of aerobic glycolysis. Lactate efflux into the extracellular milieu results in acidification decreasing pH. It was previously observed that the expression of glycolytic enzymes were downregulated upon MYC knockdown. Here, we queried whether reduced enzyme expression affected the functional bioenergetic output in the MB_{GRP3} MYC-regulable models by measuring total ATP production. Total ATP production was quantified from OCR and ECAR-which enabled the quantification of ATP production from both pathways.

Firstly, across the MB_{GRP3} MYC isogenic cell lines, glycolysis remained the predominant pathway for ATP production compared to OXPHOS (Figure 4.14). In the D425 NS cell lines, glycolytic ATP generation was largely unaffected whereas a slight decrease in OXPHOS linked ATP was observed (Figure 4.14 A). In the D425 MYC 2 cells, total ATP production was significantly higher in MYC 2 (on) cells compared to MYC 2 (off) cells (p=0.040). The D425 MYC 2 (on) cells utilised OXPHOS to a greater extent to produce ATP compared to D425 MYC 2 (off) cells. In the D425 MYC 3 cell line however, there were no significant changes when MYC levels were reduced (Figure 4.14 A).

In the D283 NS cell line, there were no observable changes to bioenergetic output following doxycycline treatment (Figure 4.14 B). In the D283 MYC 2 and MYC 3 cell lines, there were modest reductions in total ATP production upon MYC knockdown although these were not significant. The D283 MYC 2 (on) and MYC 3 (on) cells were highly glycolytic and this was the primary pathway affected when MYC was knocked down; contributing to the slight decrease in total ATP observed in the D283 MYC 2 (off) and MYC 3 (off) cells (Figure 4.14 B).

For the HDMB03 NS cell lines, doxycycline treatment did not impact total ATP production (Figure 4.14 C). In contrast to the other MB_{GRP3} cell lines, slight increases in total ATP was observed when MYC was knocked down in the HDMB03 MYC 2 and MYC 3 cell lines. Glycolytic ATP production was higher in the HDMB03 2 (off) and HDMB03 (on) cells (Figure 4.14 C).

These experiments highlighted that glycolysis was the predominant ATP generating pathway in the MB_{GRP3} MYC-amplified cells even when MYC was knocked down. Findings presented here suggested that total ATP production in the D425 MYC 2 cells was impacted following MYC knockdown. Since no consistent observations were made in the cell lines, it is likely that ATP production was not strongly associated with MYC-dependent altered metabolism in the MB_{GRP3} cells.

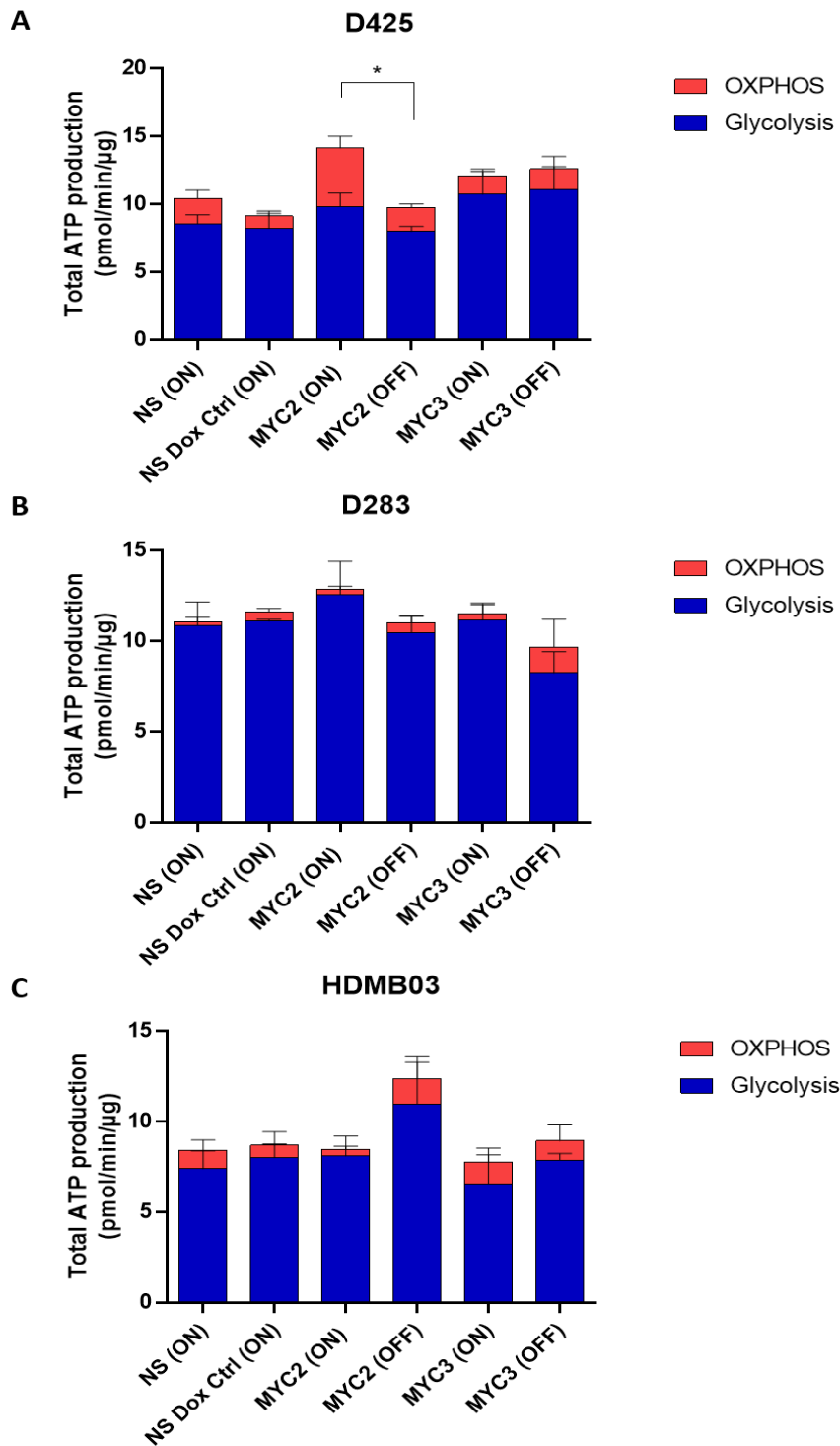


Figure 4.14 Impact of MYC knockdown on ATP production. OCR and ECAR measurements were used to determine glycolytic and OXPHOS derived ATP. ATP production in A) D425 B) D283 and C) HDMB03 MYC inducible cell lines treated with Dox for 72 h. Data represents mean measurements \pm SEM of 24- 48 biological replicates from 2-3 independent experiments. * $P < 0.05$ Significance determined by two way anova with Sidak multiple comparisons between NS (ON) v NS (ON), MYC 2 (ON) v MYC 2 (OFF) and MYC 3 (ON) v MYC 3 (OFF).

4.3.3.2 Spare respiratory function

Spare respiratory capacity (SRC) defines the ability of the mitochondria to respond to increased demand. It reflects the difference between basal respiration and maximal respiration. In these experiments, this measurement was detected after treatment with OG and treatment with the FCCP which uncouples oxygen consumption from ATP generation.

There was a slight decrease in SRC in the D425 NS cells following doxycycline treatment although this was negligible (Figure 4.15 A). This was also the case for the D425 MYC 2 and MYC 3 which had highly variable measurements. Knockdown of MYC was not observed to alter SRC in the D425 MYC 2 (on) and MYC 3 (on) compared to their MYC (off) equivalents (Figure 4.15 A).

D283 NS cells had comparable reserve respiratory capacity following doxycycline treatment and this was expected since MYC expression was not altered in the presence of doxycycline. In the D283 MYC 2 and MYC 3 cell lines, SRC increased although in varying degrees in the MYC (off) cells (Figure 4.15 B). In the D283 MYC 2 (on) cells SRC was 80% compared to 114% in the D283 MYC 2 (off) cells ($p=0.030$). Although a similar trend of increased SRC was observed in the D283 MYC 3 cells, this was not significant (D283 MYC 3 (on) 117% and D283 MYC 3 (on) 175%, $p=0.0509$) (Figure 4.15 B).

Like the D425 cells, doxycycline slightly impacted SRC in the HDMB03 NS cell lines. SRC was markedly increased in the HDMB03 MYC 2 (off) cells compared to the HDMB03 MYC 2 (on) cells (127% compared to 75% $p=0.049$). The HDMB03 MYC 3 cell line displayed similar trends to the NS harbouring cells where a slight decrease in SRC was observed (Figure 4.15 C).

In two of the three MB_{GRP3} isogenic cell lines, SRC was increased when MYC was knocked down. This was particularly evident in the D283 and HDMB03 MYC 2 harbouring cell lines. Mitochondria respiratory reserves is linked to mitochondria fitness and resilience. These results suggest *MYC* amplification may limit mitochondria reserve capacity which may ultimately impact ability to respond to oxidative stress creating a metabolic vulnerability in these cell lines. These results provide early indications of altered metabolic output linked to MYC expression. Further experiments are required to assess the source(s) of SRC from the individual mitochondrial complexes.

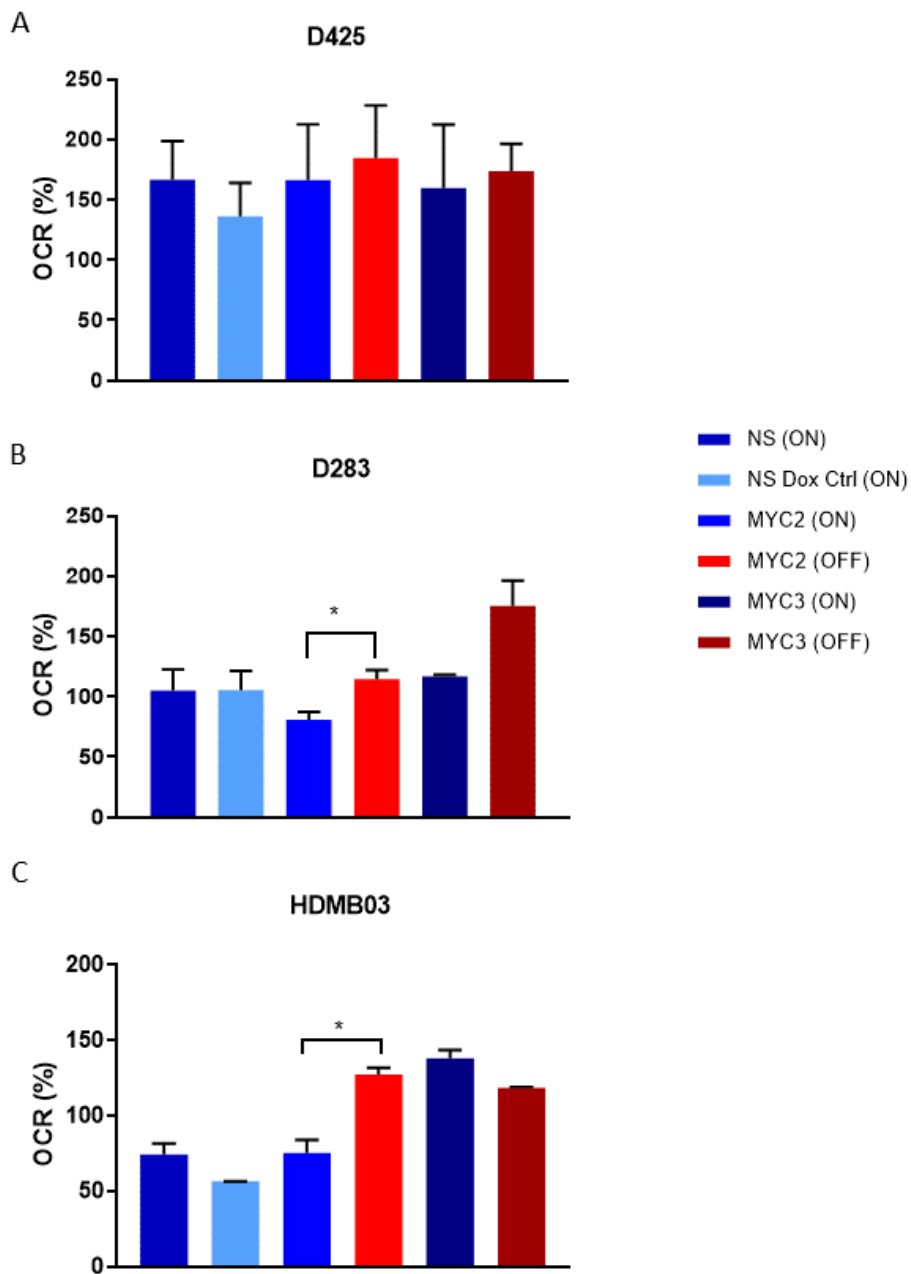


Figure 4.15 The effect of MYC knockdown on spare respiratory capacity in MB_{GRP3} cells. Spare respiratory capacity (%) was determined following treatment with Dox for 72h. A) D425 B) D283 C) HDMB03. Data represents mean measurements \pm SEM of 24- 48 biological replicates from 2-3 independent experiments. * $p < 0.05$ Significance determined by unpaired *t* test between NS (ON) v NS (ON), MYC 2 (ON) v MYC 2 (OFF) and MYC 3 (ON) v MYC 3 (OFF)

4.4 Discussion

MYC is a commonly deregulated oncogene in numerous cancers where it promotes transformation through increased growth, proliferation and also metabolic rewiring. *MYC* amplification is a common MB_{GRP3} subgroup feature and over-activation of *MYC* and downstream pathways are commonly described for this medulloblastoma subgroup. In this study, the aim was to utilise previously engineered *MYC* regulable MB_{GRP3} cell lines to further understand deregulated *MYC* in the context of MB_{GRP3} and more specifically the impact of *MYC* knockdown on MB metabolism. This current study demonstrated loss of *MYC* impacted proliferation and cell cycle progression in MB_{GRP3} cell lines. Furthermore, loss of *MYC* was accompanied by changes in the expression of glycolytic enzymes PKM2 and LDHA specifically. Further assessment of functional metabolism revealed cell-line specific alterations following *MYC* knockdown and implicated mitochondria spare reserve capacity.

4.4.1 *MYC* knockdown causes slowed proliferation and G1 arrest

Firstly, protein expression in the *MYC*-regulable cell lines demonstrated *MYC* knockdown in the *MYC*-targeting shRNA constructs in the D425, D283 and HDMB03. Assessment of *MYC* knockdown revealed the *MYC* 2 shRNA achieved higher knockdown efficiency compared to the *MYC* 3 shRNA construct. Furthermore, expression of *MYC* in the NS harbouring MB_{GRP3} cells were stable supporting their use as a control in this study. *MYC* knockdown was associated with reduced proliferation, accumulation of cells in G1 and fewer cells entering G2/M which was analogous to *MYC*-dependent cancer phenotypes (Wang et al., 2008). In these experiments, such changes were consistently seen across the D425, D283 and HDMB03 cell lines harbouring the *MYC* 2 shRNA construct. Although similar trends were observed in the *MYC* 3 cell line, they exhibited an intermediate phenotype compared to their *MYC* 2 counterparts. Additionally, there were several indications of shRNA construct leakiness particularly in the *MYC* 3 harbouring cell lines. Construct leakiness results in the expression of shRNA independent of doxycycline regulation. This ultimately would impact assessment and identification of phenotypic differences since they may have occurred prior to experimentation (summary of phenotypic alterations associated with cell lines depicted in Table 4.2).

In the NS cell line, there were no significant alterations in proliferation or cell cycle progression following treatment at 72 h in the MB_{GRP3} cell lines. This was consistent with the lack of MYC repression in the NS harbouring control cells. As previously mentioned, 72 h was sufficient to observe phenotypic changes in the MYC shRNA bearing cell lines. Although it was appreciated that longer time points (e.g. 96 h or 120 h) may have better distinguished MYC-dependent alterations, particularly in the MYC 3 harbouring cell lines.

Table 4.2 Summary of MYC-dependent phenotypic alterations in MB_{GRP3} MYC isogenic cell lines. Dashes represent stable phenotype in NS cell lines; Green ticks represent phenotypic alteration, red cross represent lack of phenotypic alteration.

Cell line	Construct	MYC protein KD	Cell proliferation over 120h	Cell cycle at 72 h
D425	NS	-	-	-
	MYC2	✓	✓	✓
	MYC3	✓	✓	✗
D283	NS	-	-	-
	MYC2	✓	✓	✓
	MYC3	✓	✓	✗
HDMB03	NS	-	-	-
	MYC2	✓	✓	✓
	MYC3	✓	✓	✗

It was important however to factor potential doxycycline-induced changes to metabolism independent of MYC modulation in the MB_{GRP3} MYC-regulable cell lines. Previous study by Ahler *et al.*, showed that doxycycline could induce alterations in cellular metabolism, particularly in mitochondrial function and oxidative metabolism *in vitro* (Ahler *et al.*, 2013). In this study, cell proliferation of NS (on) and NS Dox Ctrl (on) cells were highly similar up to 72h, after which cell proliferation began to drift. Although, ultimately, proliferation rate were not significantly different in the NS cell lines, it was important to consider indications from the proliferation data which suggested that long term exposure could cause doxycycline-induced phenotypic alterations (i.e. effect on proliferation at 120 h, Figure 4.2-4). These initial experiments, in conjunction with previous work carried out

in this cell line model suggested that 72 h was the ideal time point where there is sufficient MYC knockdown and limited off target effects of doxycycline (Swartz, 2018). Nevertheless, the NS cells were an important control in these experiments enabling the distinguishing of possible doxycycline induced effects and actual MYC-dependent effects.

Previous studies in MB_{GRP3} cell lines (D425 and D341) have shown loss of *MYC* via siRNA mediated silencing results in anti-proliferative effect on *MYC* overexpressing cell lines (von Bueren et al., 2009). Data presented in this chapter are concordant with findings from this study although different methods for MYC modulation was employed (siRNA versus shRNA). *MYC*-addiction renders cells reliant on constitutive expression of MYC such that repression of *MYC* leads to adverse phenotypic changes. MYC forms part of the regulatory control and response to growth factor stimulation enabling progression from G1 to S phase. Serum withdrawal triggers strong G1 arrest and ectopic expression of *MYC* can facilitate S phase re-entry in quiescent cells (Eilers et al., 1991). Additionally, loss of MYC is accompanied by alterations in the CDK/RB/E2F pathway. (Blagosklonny and Pardee, 2002). For medulloblastoma, *MYC* amplification is also frequently associated with the reduced expression of *CDKN1A*, a negative regulator of cell cycle progression. Previous experiments utilising the MB_{GRP3} inducible cell lines showed increased gene expression of *CDKN1* following MYC knockdown (Swartz, 2018). Loss of *MyC* has been shown to reduce the tumourigenic potential of NPC cells by limiting proliferation and division (Niu et al., 2015). Taken together, these experiments support *MYC*-addiction of MB_{GRP3} which were reliant on constitutive expression of *MYC* enabling rapid proliferation and cell cycle progression in the MB_{GRP3} *MYC* regulable cell lines. These cell lines thus provided MYC-dependent *in vitro* models and NS control which could be utilised in further experiments to assess other phenotypic alterations which were driven by MYC.

4.4.2 Expression of metabolic enzymes is impacted upon *MYC* knockdown

The protein expression levels of metabolic enzymes, some directly regulated by *MYC* were assessed following 72 h of doxycycline treatment which knocked down levels of MYC. Overall, decreased expression of *MYC* resulted in the downregulation of glycolytic enzymes in the MYC 2 shRNA harbouring cells. In this study, downregulation of specific glycolytic enzymes particularly, PKM2 and LDHA was observed. It is noteworthy to mention the variability and lack of reproducibility in the assessment on protein expression

of the MYC isogenic cell lines. MYC knockdown efficiency varied from one technical replicate to another, this ultimately impacted the severity of effects and introduced large variations in the dataset. Pooling of the cell line samples from D425, D283 and HDMB03, and their corresponding NS, MYC 2 and MYC 3 harbouring cells was adopted to mitigate against the large variations, increase sample size and statistical power which enabled the realization of the impact on PKM2 and LDHA expression upon MYC knockdown. Although high expression of PKM2 is frequently associated with MYC-driven tumours, it remains to be elucidated whether it drives tumour progression. A study by Mendez-Lucas *et al.*, revealed decreased pyruvate kinase activity upon PKM2 loss but this was inconsequential to tumour development. Interestingly, this study found that MYC could indeed upregulate both PKM1 and PKM2 however, increased PKM1/2 ratios diverted glucose intermediates away from serine biosynthesis and the TCA cycle (Mendez-Lucas *et al.*, 2017). These findings shed light on PKM2 as an important regulator of glucose catabolism. Several studies have demonstrated the ability of serine to allosterically regulate PKM2 activity. Under serine deprived conditions, the activity of PKM2 is reduced causing reduced glucose flux to lactate, a buildup of glucose intermediates upstream enhanced shunting into the *de novo* serine synthesis pathway to meet anabolic demands (Chaneton *et al.*, 2012, Kung *et al.*, 2012, Ye *et al.*, 2012). This adaptation involving PKM2 affords metabolic plasticity to growing cancer cells and more importantly, it has been shown to maintain mTORC1 activity in nutrient limiting conditions. Hence, MYC-induced PKM2 expression could provide MB cells with a growth advantage by enabling diversion to biosynthetic pathways to support aberrant growth.

LDHA is a well described MYC regulated gene containing a consensus E box binding site (Shim *et al.*, 1997). Abrogation of LDHA in MYC transformed cells impacts their tumourigenic potential and leads to reduced lactate production and colony forming ability in rat fibroblasts (Shim *et al.*, 1997). In pancreatic cancer, concomitant expression of MYC and LDHA is associated with histological stage, metastasis and poorer prognosis (He *et al.*, 2015). A recent study by Tao *et al.*, revealed that MYC could transform astrocyte progenitors to form histologically identical LCA MB_{GRP3} tumours (Tao *et al.*, 2019). Furthermore, this particular study showed that inhibition of LDHA markedly reduced growth of MYC-driven MB cells. Overall, there was a downregulation of the glycolytic enzymes, namely PKM2 and LDHA in the MB_{GRP3} cell lines resulting from

reduced *MYC* expression which suggests *MYC* may drive the high expression of these enzymes and may contribute to altered metabolism in *MYC*-amplified MB_{GRP3} cells.

The loss of *MYC* in the MB_{GRP3} cell lines appeared to alter the expression of GLS1 isoforms in the D283 *MYC* 2 cells particularly. However, further experimental repeats are required to determine *MYC*-dependent regulation of GLS1 protein expression. Glutamine addiction in cancer cells can occur through an oncogenic driver such as *MYC* which enacts a transcriptional programme enabling glutamine uptake and catabolism. *MYC* regulates the expression of GLS by two distinct mechanisms: by increased mRNA expression and repression of mir-23a/b which is a repressor of GLS (Gao et al., 2009). Surprisingly, breakdown of glutamine is not thought to support protein or nucleotide synthesis but supports the TCA cycle. Whilst glucose-derived pyruvate is diverted away from oxidative metabolism, TCA anaplerosis driven by glutamine which is PI3K/AKT independent, supports normal mitochondria function (Wise et al., 2008). Glutamine catabolism was shown to provide a mechanism to support TCA cycling during glucose deficiency by maintaining fumarate and citrate which in turn supported B cell survival (Le et al., 2012). Activation of GLUD has been shown to be a crucial mechanism for diverting glutamine-derived carbons into the TCA when mitochondria pyruvate carrier is inhibited (Yang et al., 2014). GLS is also seen as critical enzyme during G2 phase of cell cycle where there is a determination of nutrient sufficiency prior to progression into the mitotic phase of the cell cycle (Morrish et al., 2009).

Higher expression of GLS1 observed in the D283 *MYC*-amplified compared to *MYC* KD cells corresponds with observations of previous studies. Probing glutaminolysis further by determining the expression of other enzymes such as GLS2 and GLUD across the MB_{GRP3} cell lines to assess impact of *MYC* on this pathway.

An important observation made from this study was probing activated/phosphorylated PDH and total PDH. Although there were slight decreases in both phosphorylated and total PDH upon *MYC* knockdown, the ratios of the two forms of PDH remained unchanged in the majority of MB_{GRP3} cell lines. This would suggest that overall pathway activity was unaffected despite alterations in total expression of PDH and that activity of this pathway is maintained despite *MYC* knockdown. Pyruvate decarboxylation by PDH generates acetyl-CoA which subsequently enters the TCA and is converted to citrate. Citrate can be shunted back into the cytoplasm where it may be utilised in fatty acid synthesis. Assessing the downstream utilisation of PDH-derived acetyl-CoA in the *MYC* isogenic cell lines may provide further details into the metabolic activities of *MYC*-

amplified cells compared to KD equivalents. Together, examination of protein expression changes revealed MYC-dependent alterations in metabolic enzymes expression and pathways unaffected by reduced expression of MYC. These initial experiments highlighted specific pathways which may be MYC-dependent and influence altered metabolism in the *MYC*-amplified MB_{GRP3} cell lines.

4.4.3 Functional changes in mitochondria function and cellular energetics upon MYC knockdown

It was important to characterise alterations in the activity of both glycolytic and oxidative metabolism to identify functional changes in metabolism associated with decreased expression of MYC. Particularly since alterations in enzyme expression does not always limit pathway activity. Evaluation of pathway utilisation for ATP production revealed that MYC-amplified MB_{GRP3} cells were highly glycolytic and produced the majority of ATP using this pathway. Reduction in ATP production was observed only in the D425 MYC 2 cell line following MYC knockdown. Since this effect was only observed in one of the MB_{GRP3} cell lines, this may indicate that MYC expression does not significantly impact ATP production and that indeed ATP production is not the limiting factor in MB_{GRP3} proliferation.

One of the characteristics identified was that upon loss of MYC, the D283 MYC 2 (off) and HDMB03 MYC 2 (off) cells retained more of a reserve of respiratory capacity compared to their MYC (on) counterparts. This was similar to the observations made by Anso *et al.*, in osteosarcoma cells (Anso *et al.*, 2013). These findings suggest that MYC-amplified cells did not tolerate bioenergetic stress compared to their MYC knockdown counterparts. Others have shown that MYC-overexpression colorectal cancer cells are sensitive to inhibition of anti-oxidant pathways but can be rescued by repression of MYC. Oncogenic activity of MYC thus conferred dependence on AMPK-related kinase 5 (ARK5) which sustains ETC complexes and regulated respiratory capacity. Inhibition of ARK5 depleted ATP and triggered apoptosis in a MYC-dependent manner *in vitro* and *in vivo* (Liu *et al.*, 2012). A further study in MYC-overexpressing melanoma found oncogenic MYC caused reliance on AMPK to maintain energy and redox homeostasis. Inhibition of AMPK in these cells caused apoptosis whereas activation of AMPK promoted survival under oxidative stress (Kfoury *et al.*, 2018). Since the aim of this study was to identify consistent MYC-dependent alterations across the three MB_{GRP3} engineered cell lines, this line of investigation was not carried further. However, these

studies provide rationale for further investigating susceptibility to oxidative stress and nutrient limiting conditions in our MYC-amplified MB_{GRP3} cell lines in light of findings from SRC measurements.

Taken together, the phenotypic and metabolic assessment carried out in this chapter provided insights into the MYC-dependent alterations in cell growth and metabolic reprogramming in the MB_{GRP3} cell lines. Findings showed MYC-dependency of the MB_{GRP3} cell lines, where knockdown of MYC resulted in marked reduction in proliferation and also caused G1 arrest which were analogous with MYC-dependent cancer phenotypes (Wang et al., 2008). Although it was important to have independent shRNA targeting MYC, data presented here showed more robust phenotypic alterations in the MYC 2 harbouring cells owing to their higher MYC knockdown efficiency and lack of construct leakiness which was evident in the MYC 3 cell lines. To overcome construct leakiness associated with inducible shRNA expression, observed particularly in the MYC 3 bearing cell lines, future experiments could select for single clones where this characteristic is not observed. Others have previously shown that by engineering two Tet operators flanking the TATA box of the U6 promoter resulted in a more tightly regulated variant (Lin et al 2004). These strategies could be utilised to achieve more stable expression of the shRNA in response to doxycycline treatment. Assessment of glycolytic enzyme expression highlighted MYC-dependent alterations in PKM2 and LDHA in the MB_{GRP3} MYC-amplified cell lines suggesting that overexpression of MYC was associated with glycolytic enzyme expression. However, whilst MYC-driven alterations in enzyme expression occurred, they were not always associated with consistent repression of pathway activity as determined by the bioenergetic functional testing. Assessment of bioenergetics revealed glycolytic pathway to be the main ATP producing pathway in the MB_{GRP3} MYC isogenic cell lines.

Whilst these initial data showed promising alterations in metabolic pathways of *MYC*-amplified MB_{GRP3} cells, there was a need for more comprehensive assessment of *MYC*-dependent metabolic reprogramming. With the aim of identifying *MYC*-dependent vulnerabilities of the MB_{GRP3} cells, an experimental strategy which focused on metabolic output would more likely reveal these *MYC*-dependent alterations. To achieve this, metabolite profiling was employed as a strategy in unravelling *MYC*-driven metabolite alterations. Since metabolites are indicative of the pathways that generate them, identifying variations in metabolite profiles that distinguished *MYC*-amplified MB cells from their *MYC* knockdown counterparts would allow the determinations of metabolic pathway which are *MYC*-dependent and could potentially lead to increased sensitivity to pathway inhibition.

Chapter 5 Metabolic profiling of *MYC*-inducible MB_{GRP3} cell lines using high resolution magic angle spectroscopy

5.1 Introduction

Metabolomics is a continually expanding field that has been extensively used in drug discovery, toxicology, biomarker discovery and defining novel metabolic pathways. Metabolomics is typically characterised by the profiling of the low molecular weight metabolites often relying on analytical techniques such as nuclear magnetic resonance (NMR) spectroscopy (also referred to as MRS) and mass spectrometry (MS). The study of the metabolome is crucial as it enables a measurement of chemical responses attributable to specific genotypes and phenotypes (Fiehn, 2002). Most metabolomic studies employ just one analytical platform and the goal of capturing alterations or discovering metabolites within a specific biological context is often achieved. Despite that, information may be partially lost, depending on the specific -omics technology used. NMR spectroscopy enables the deduction of chemical structures based on their nuclear spins under a strong magnetic field. NMR spectra typically informs on chemical shifts which informs on the composite atomic groups within a molecule. Furthermore, it also reveals information regarding to adjacent atoms and molecular dynamics (Emwas et al., 2019). The benefit of NMR is that the signal intensity directly relates to quantity. Other strengths associated with NMR spectroscopy include minimal sample handling, non-destructive acquisition and its inherent quantitative nature make it highly useful for metabolic profiling (Emwas et al., 2019). However, NMR is also limited by significant peak overlap and although sensitivity has improved with higher magnetic field strengths, there is limited peak dispersion which makes capturing of all metabolites unlikely. Additionally NMR is capable of detection of metabolites in the micromolar range resulting in spectra with only the most abundant metabolites (Pan and Raftery, 2007)

MS is an analytical tool used to measure the mass-to-charge (m/z) ratio of molecules of a given sample. The MS instrumentation is made up of three components namely the ionisation source which converts molecules into gas-phase ions, the mass analyser which sorts and separates ions based on their m/z ratios and lastly the ion detection system. MS has great resolution and a higher dynamic range capable of detecting metabolites in the femtomolar range. Detection of metabolites using MS relies on how ionisable metabolites are and this, remarkably, leaves around 40% of chemical libraries undetectable using this platform (Copeland et al., 2012). Furthermore, ion suppression agents which may be present from external sources (e.g. buffers and materials used) could further reduce ionisation of compounds which can lead to loss of chemical information from complex

biological samples. Additionally the use of chromatography to reduce peak overlap introduces new sources of variations including metabolite decomposition and misaligned retention times. Although NMR and mass spectrometry have their strengths and weaknesses, these tend not to overlap, making the usage of these two platforms complementary in metabolomics studies. Although the use of multiple analytical tools remains limited in most studies, it is increasingly recognised that utilisation of multiple analytical tools and software for handling both datasets is likely to improve coverage of metabolic information (Bhinderwala et al., 2018, Marshall and Powers, 2017).

Other complementary advances to the NMR and MS analytical platforms involve the use of stable isotopes in metabolomics. Stable isotope resolved metabolomics (SIRM) differs from the untargeted metabolomics approach which normally samples global metabolite changes, SIRM however requires the use of heavy isotopes (^{13}C , ^2H , ^{15}N) compounds to profile pathway dynamics and fluxes of metabolites based on isotopologue distributions. These compounds are 1 Dalton heavier and therefore have different mass to charge ratios (m/z) in MS and different spectral properties in NMR spectroscopy. SIRM coupled to NMR can also reveal positions of isotopes further detailing chemical information and metabolic activity (Hoffman and Rasmussen, 2019).

In the previous chapter MYC-dependent bioenergetics in the regulable cell-based models of MYC-amplified Group 3 MB was evaluated. These experiments showed alterations in the glycolytic pathway, particularly in the MYC 2 harbouring cell lines. Furthermore, cell line-specific alterations were observed in mitochondrial function and ATP production when MYC expression levels were modulated. Further insights into MYC-dependent changes in metabolic processes were not fully explored. Numerous studies have utilised metabolite profiling to explore and characterise metabolic features of cancer cells highlighting the interconnectivity of metabolism and genomic abnormalities (Ortmayr et al., 2019, Reznik et al., 2018, Li et al., 2019). Utilising High Resolution Magic Angle NMR Spectroscopy (HRMAS), a form of solid state NMR allowing improved resolution of frozen samples, enabled others to determine unique metabolite features of medulloblastoma that distinguished them from other embryonal tumour samples (Bennett et al., 2018, Kohe et al., 2018). This distinction has also been achieved using *in vivo* MRS, further underlining how metabolic profiles can provide tumour specific information that may be advantageous for diagnosis and prognostication in a clinical setting (Kovanlikaya et al., 2005, Panigrahy et al., 2006).

More recent studies have explored the use of metabolic profiling in distinguishing subgroups of MB which have achieved classification of Group3/4 tumours from SHH MBs (Bluml et al., 2016). In addition, metabolic profiling has been utilised in elucidating alterations resulting from genetic abnormalities such as the production of 2-hydroxyglutarate in IDH mutant gliomas compared to IDH wildtype gliomas (Choi et al., 2012, Natsumeda et al., 2014). The number of studies on the impact of *MYC* amplification on metabolic reprogramming in medulloblastoma has not been extensively covered so far. Thus, understanding how aberrant *MYC* expression affects MB metabolism will provide further understanding of the biology of these tumours and aid the development of novel and targeted therapies.

5.2 Aims

The aim of this chapter was to profile changes in metabolite abundances in response to *MYC* modulation using ^1H HRMAS. Since alterations in metabolite levels are indicative of pathway activity, it was hypothesised that profiling the metabolome would enable the identification of important pathways/networks which *MYC*-amplified MB cells rely on. The objectives of this study were to:

- Profile the metabolite abundances of *MYC* regulable MB_{GRP3} cell lines using HRMAS.
- Identify consistent *MYC*-dependent changes across the three cell lines D425, D283 and HDMB03
- Validate any *MYC*-dependent changes observed using ^{13}C stable isotope resolved metabolic tracing.

5.3 Results

5.3.1 Experimental design and analysis pipeline

Following phenotypic assessment and characterisation of bioenergetics in the MB_{GRP3} *MYC* modulable cell lines (Chapter 4), alterations in the metabolome of these engineered cell lines were further evaluated following genetic manipulation of *MYC* expression levels. ¹H HRMAS, a high resolution solid state spectroscopy tool was employed for this study. This method was utilised over conventional (liquid state) ¹H NMR due to minimal sample handling required, wider range of polar and non-polar chemicals captured and minimal solvent effects. The three MB_{GRP3} *MYC* isogenic cell lines D425, D283 and HDMB03 (each containing NS, *MYC* 2, *MYC* 3 constructs) were treated in the presence or absence of 1 µg/mL doxycycline for 72 h to induce *MYC* knockdown. This time point was chosen for profiling experiments due to achieving effective *MYC* knockdown in most cell lines and minimal doxycycline effects observed in the NS harbouring cell lines (Chapter 4). Although the construct leakiness was a characteristic observed in the *MYC* 3 harbouring cells particularly in the HDMB03 *MYC* 3 cell line, previous phenotypic assessment such as cell proliferation, cell cycle analysis and expression of metabolic enzymes following *MYC* KD revealed some intermediate effects that were concordant with observations found in the *MYC* 2 harbouring cells. In light of this, these cell lines were profiled to ascertain whether *MYC*-dependent metabolite alterations could still be detected despite construct leakiness. Cell pellets were collected for ¹H HRMAS. NMR spectra were acquired on a 500 MHz instrument fitted with a MAS probe. Spectra were visually inspected, pre-processed and subjected to subsequent analysis (detailed in Chapter 2.3). Metabolites within the downfield region of the ¹H NMR spectrum (0- 5 ppm) are reported.

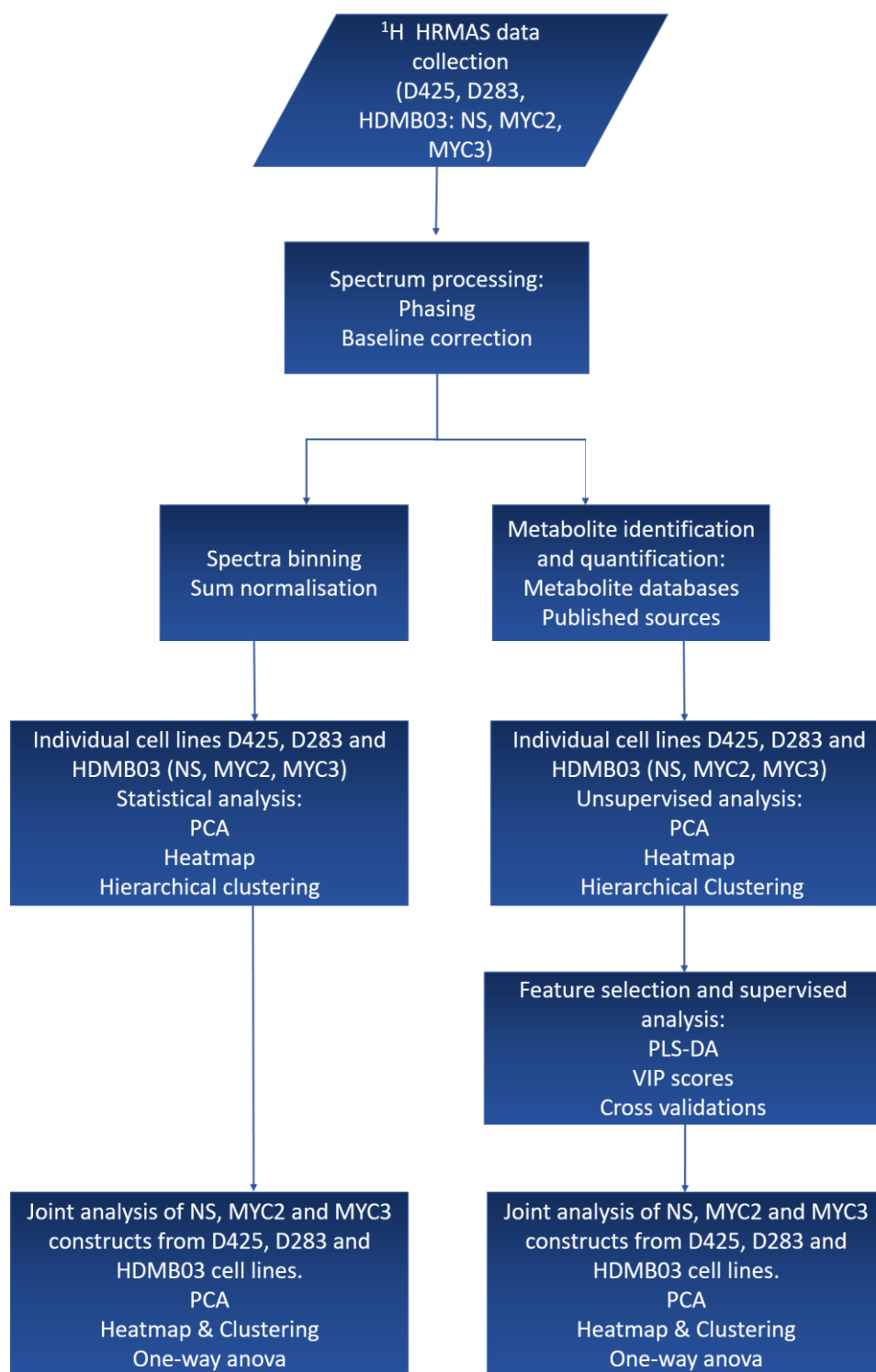


Figure 5.1 Flowchart of the analysis pipeline used for metabolite profiles of MYC-regulable *MB_{GRP3}* cell lines

The analysis strategy employed in this chapter focused on two methods of analysis for NMR spectra. First, binning a method which involves uniform division of each spectrum into smaller regions or ‘bins’ which integrate signal intensity of the bin regions with variable reduction. Although loss of resolution occurs, particularly affecting low intensity signals the overall dimensionality reduction and removal of baseline noise makes this advantageous for determining class separation using chemometrics. Second, metabolite identification and quantification provides great information and relationships of metabolic pathways and biological alterations within conditions. Changes in metabolite concentrations are even more powerful when coupled with statistical validation which enable feature selection and identification of characteristic changes associated with an experimental condition.

The analysis used for the metabolic profiling of the *MYC*-regulable cell lines to evaluate metabolite changes following *MYC* knockdown is outlined in (Figure 5.1). The use of spectral binning enables unbiased and unsupervised analytical approach in determining clusters and patterns within complex datasets. In this study, the aim would be to establish separation of NS, MYC 2 and MYC 3 in the *MYC* (on) and *MYC* (off) states individually for each cell line (D425, D283 and HDMB03) and as combined pool of cell lines. This latter step would increase statistical power, enable identification of important spectral features and also early indication of differences in the performance of the *MYC*-targeting shRNA constructs (i.e. MYC 2 and MYC 3).

The second branch of the analysis pipeline focused on metabolite identification and quantification of relative concentration in order to obtain biologically meaningful data and metabolite information associated with pathways. Once obtained, metabolite profiles were treated similarly to binned profiles undergoing statistical analysis using chemometric methods. Additionally, supervised discriminant analysis was used to enable feature selection and identification of metabolites associated with modulation of *MYC* expression. Consistent metabolite changes across the cell lines and their corresponding constructs were realised by overlapping changes identified from individual cell lines.

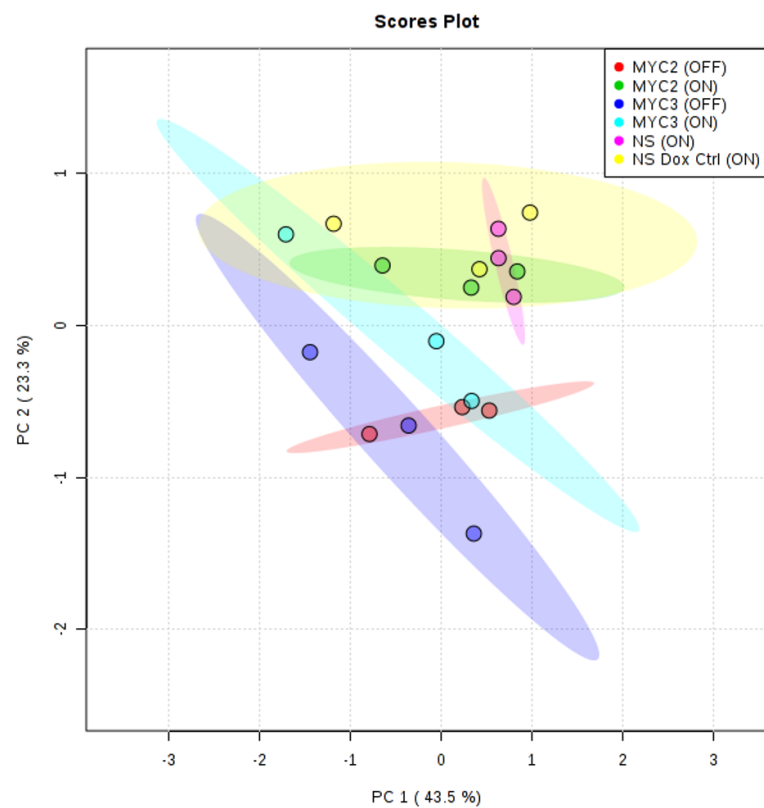
5.3.2 Analysis of ^1H NMR spectra of MB_{GRP3} *MYC*-regulable cell lines using spectral binning

5.3.2.1 Assessing impact of *MYC* knockdown on spectral profiles of MB_{GRP3} cell lines

Multivariate analysis was used to evaluate changes in the NMR spectra of the MB_{GRP3} cell lines following *MYC* knockdown. Firstly, spectra were binned into 0.01 ppm regions and normalised to the sum of the spectra (0- 5ppm) to enable comparison between samples. PCA was used to assess the separation of *MYC* (on) and *MYC* (off) cells based on the signal intensities of each bin region. It was expected that since *MYC* knockdown caused phenotypic changes in the D425, D283 and HDMB03 cell lines, these would be accompanied by alterations in metabolic pathways leading to variations in metabolite abundances. In a perfect statistical model, the NS (on) and NS Dox Ctrl (on) would have similar metabolite profiles, since *MYC* expression levels were similar. Furthermore this pair would also highlight possible doxycycline induced effects. In the *MYC*-specific shRNA and their *MYC* (on) and *MYC* (off) pairs, differing metabolite concentrations/ pathway activity would give rise to distinctive metabolite features. Additionally it was hypothesised that *MYC* (on) would have similar profiles to NS (on) and NS Dox Ctrl (on) counterparts in the absence of construct leakiness and doxycycline-induced metabolic effects.

Analysis of the D425 cell lines showed that, PC 1 and PC 2 accounted for almost 70% of the variation observed in the spectra (Figure 5.2 A). In the D425 cell line, the NS cells and MYC 2 (on) cells remain relatively unseparated. The MYC 2 (off) cells formed a distinct cluster suggesting alterations in the spectral regions compared to MYC 2 (on) cells. The D425 MYC 3 (on) were slightly separated from the NS and MYC 2 (on) cells suggesting some alterations prior to doxycycline treatment and MYC knockdown. The D425 MYC 3 (off) further separate from the MYC 3 (on) cells suggesting alterations compared to its *MYC* expressing equivalent. Further visualisation of the 3D PCA plot accounts for more variance between the sample groups however no further separation was observed although it provides a better representation of the projection of individual samples (Figure 5.2 B). Subsequent analysis using heatmap analysis coupled with hierarchical clustering of the relative bin intensities, aided the visualisation of changes and clustering patterns (Figure 5.3). The hierarchical clustering further supported separations already highlighted from the PCA score plots. The NS (on) and NS Dox Ctrl form a family, followed closely by the MYC 2 (on) and MYC 3 (on) in subfamilies. Contrastingly, the MYC 2 and MYC 3 (off) cells form a distinct branch with highly noticeable changes in metabolite profiles compared to all of the *MYC* (on) groups (Figure 5.3).

A



B

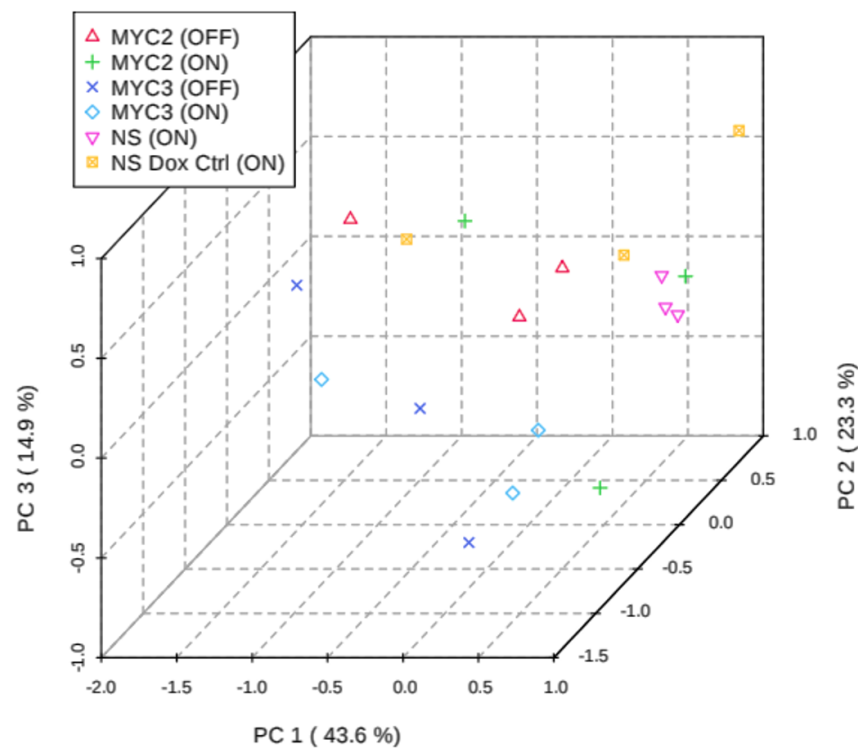


Figure 5.2 Principal component analysis of metabolic profiles from D425 cell lines indicating variances in spectra. D425 cells were treated with or without doxycycline for 72 h and HRMAS profiling performed. PCA of the first two principal components from the D425 NS, MYC 2 and MYC 3 harbouring cells, labelled by construct and MYC status. PCA was performed on binned spectra. Spectra data was sum normalised. Symbols refer to individual samples and colours indicate sample groups. 95% confidence regions are illustrated by ellipses surrounding sample groups. Data represents 3 independent biological replicates.

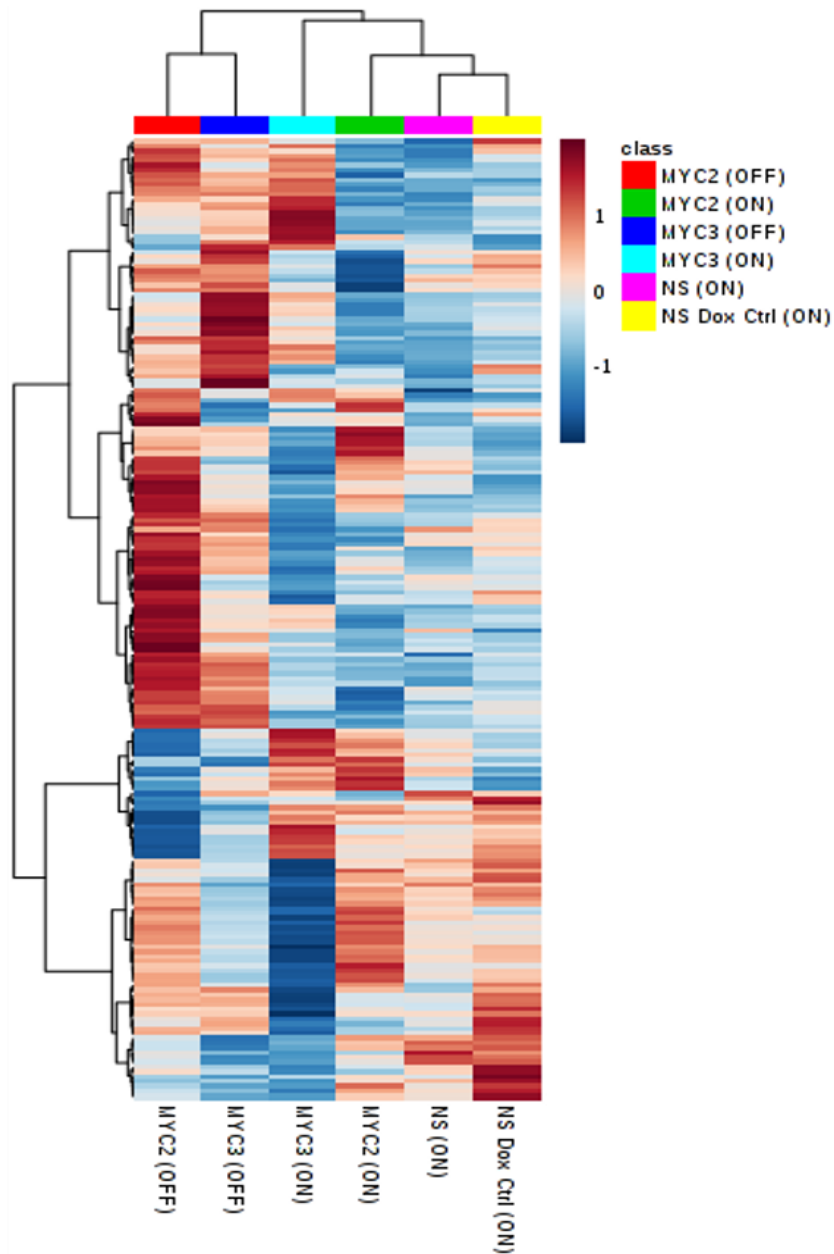


Figure 5.3 Clustered heatmap of spectral bins of D425 Cell lines. D425 NS, MYC 2, and MYC 3 harbouring cells were clustered using the Ward clustering algorithm. The colours represent the relative spectral bin intensity. Averaged group samples ($n=3$) are depicted along the vertical axis and bins across the horizontal axis. Group is indicated at the top of the figure by fuchsia and yellow (NS On and NS Dox Ctrl On respectively), green and red (MYC 2 on and MYC 2 Off respectively), light blue and dark blue (MYC 3 on and MYC 3 Off respectively).

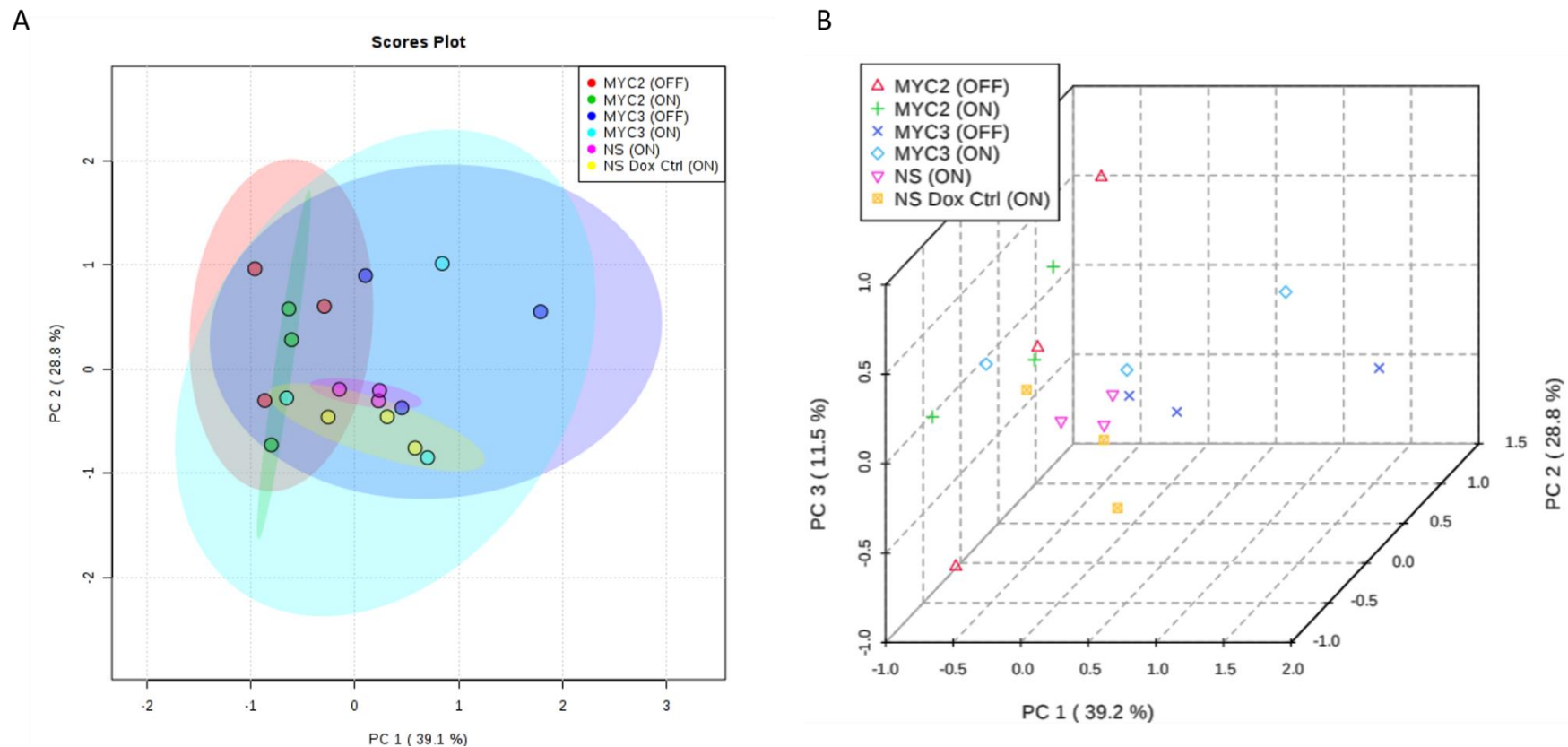


Figure 5.4 Principal component analysis of metabolic profiles from D283 cell lines indicating variances in spectra. D283 cells were treated with or without doxycycline for 72 h and HRMAS profiling performed. PCA of the first two principal components from the spectral bins of D283 NS, MYC 2 and MYC 3 harbouring cells, labelled by construct and MYC status. PCA was performed on binned spectra. Spectra data was sum normalised. Symbols refer to individual samples and colours indicate sample groups. 95% confidence regions are illustrated by ellipses surrounding sample groups. Data represents 3 independent biological replicates.

Like the D425 cell lines, PCA using the first two principal components displayed separation between sample groups of the D283 cell (Figure 5.4 A). PCA analysis of the D283 cell line did not reveal robust clusters equivalent to those observed in the D425 cell line. The D283 NS (on) and NS Dox Ctrl (on) overlap on the PCA score plot suggesting similar metabolite profiles. The D283 MYC 2 harbouring cell lines were however slightly separated from the NS cell lines however, there was significant overlap of the MYC 2 (on) and MYC 2 (off) cells. The D283 MYC 3 cells displayed more variability across individual samples (as shown in PCA score plot, Figure 5.4 A) and again revealed no separation of the MYC 3 (on) and MYC 3 (off) groups. This was further supported when 3D PCA was evaluated (Figure 5.4 B). Inspection of the heatmap clusters showed comparable profiles for the NS (on) and Dox control cells. Interestingly in this cell line the MYC 3 harbouring cells cluster closely to the NS cell lines than the MYC 2 cell line (Figure 5.5). There were some variations in the MYC 2 and MYC 3 (on) cells compared to their MYC (off) equivalents however these differences were not as striking as previously seen in the D425 cell line (Figure 5.3). Although the MYC KD observed in the D283 MYC 2 and MYC 3 bearing cells in this cell line were comparable, it is noteworthy that the D283 cell line has gain of three MYC copies as supposed to the high level amplification in the D425 cell line.

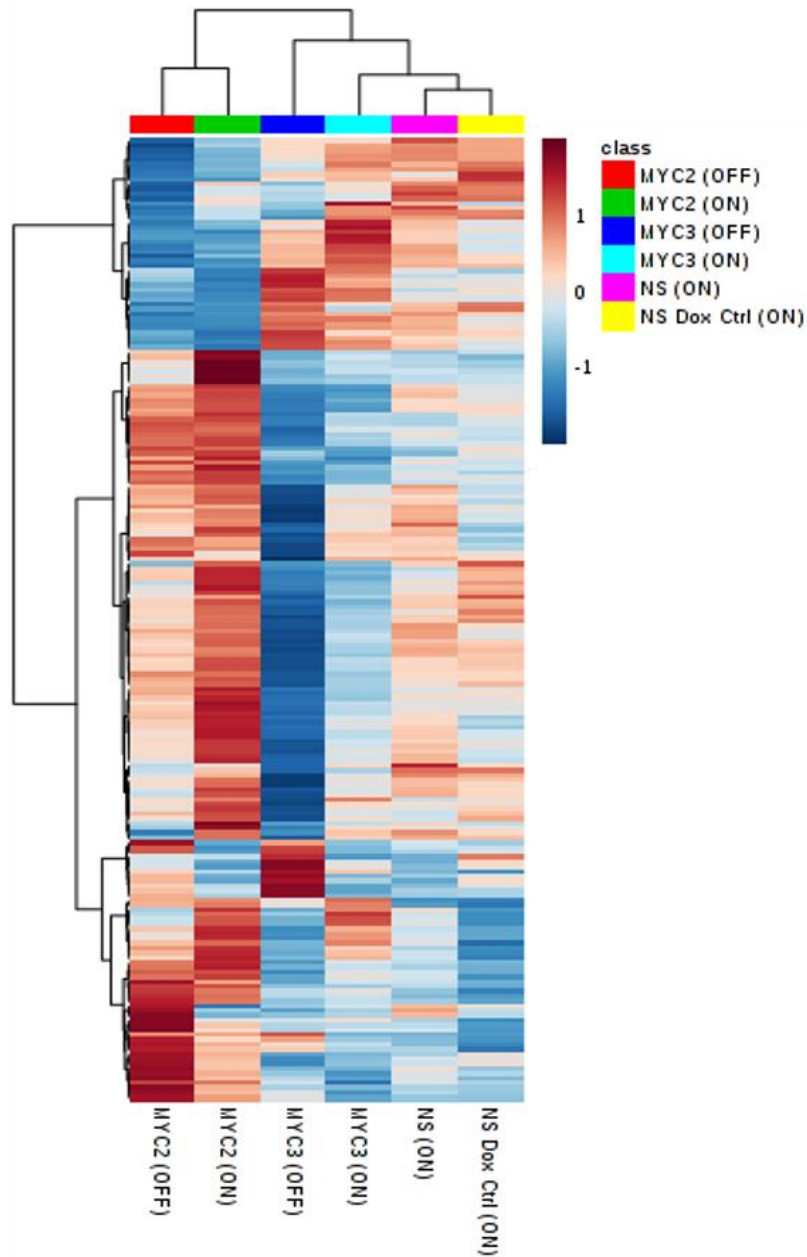


Figure 5.5 Clustered heatmap of spectral bins of D283 Cell lines. D283 NS, MYC 2, and MYC 3 harbouring cells were clustered using the Ward clustering algorithm. The colours represent the relative spectral bin intensity. Averaged group samples ($n=3$) are depicted along the vertical axis and bins across the horizontal axis. Group is indicated at the top of the figure by fuchsia and yellow (NS On and NS Dox Ctrl On respectively), green and red (MYC 2 on and MYC 2 Off respectively), light blue and dark blue (MYC 3 on and MYC 3 Off respectively).

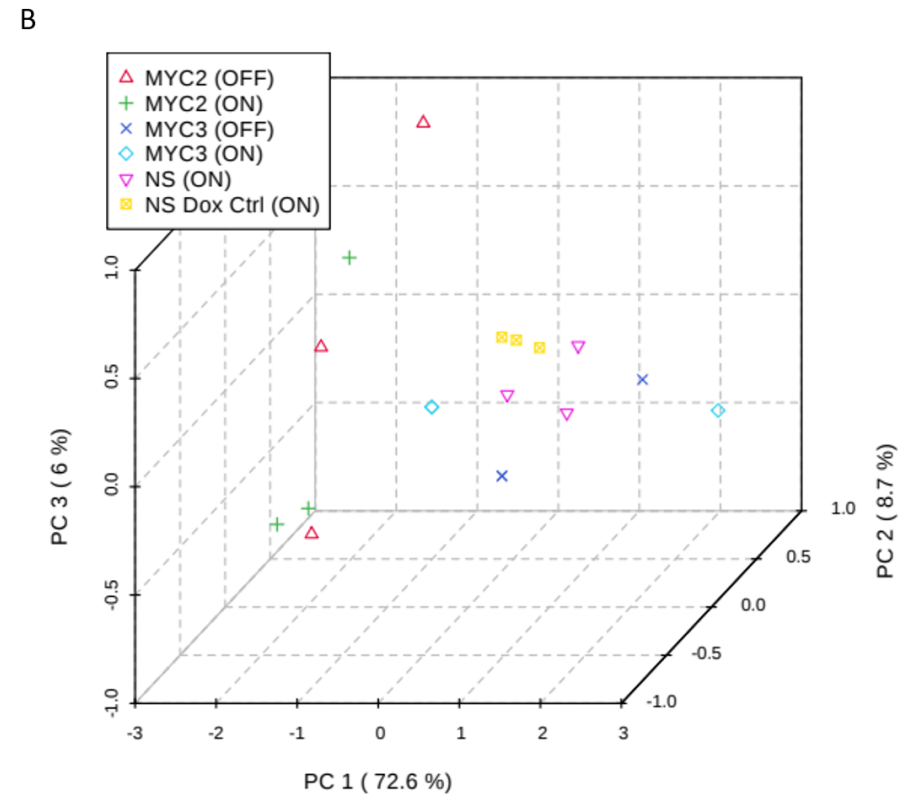
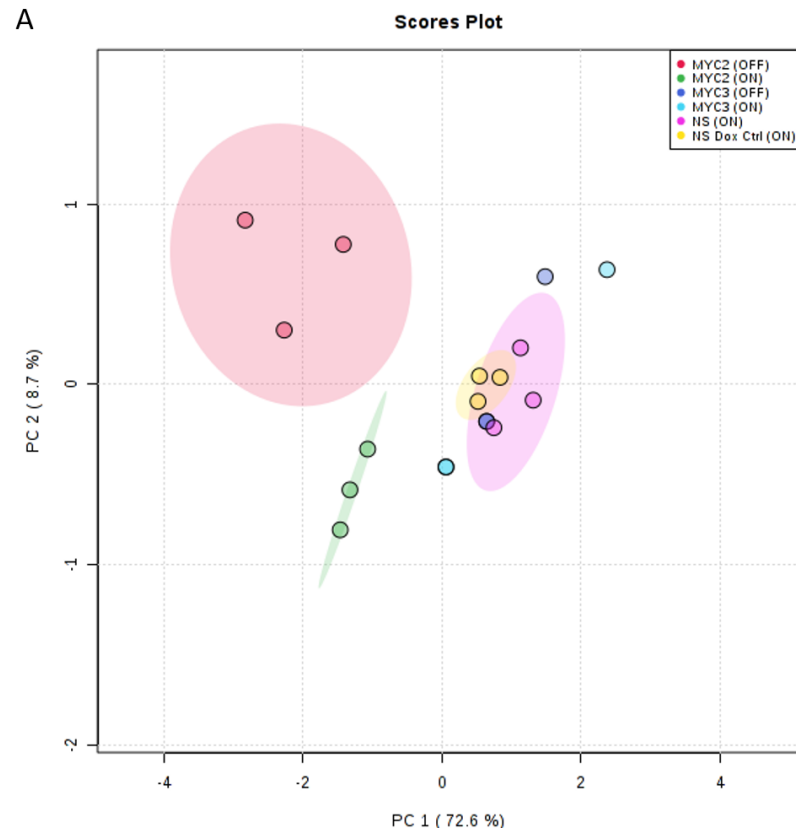


Figure 5.6 Principal component analysis of metabolic profiles from HDMB03 cell lines indicating variances in spectra. HDMB03 cells were treated with or without doxycycline for 72 h and HRMAS profiling performed. PCA of the first two principal components from the HDMB03 NS, MYC 2 and MYC 3 harbouring cells, labelled by construct and MYC status. PCA was performed on binned spectra. Spectra data was sum normalised. Symbols refer to individual samples and colours indicate sample groups. 95% confidence regions are illustrated by ellipses surrounding sample groups. Data represents 3 independent biological replicates.

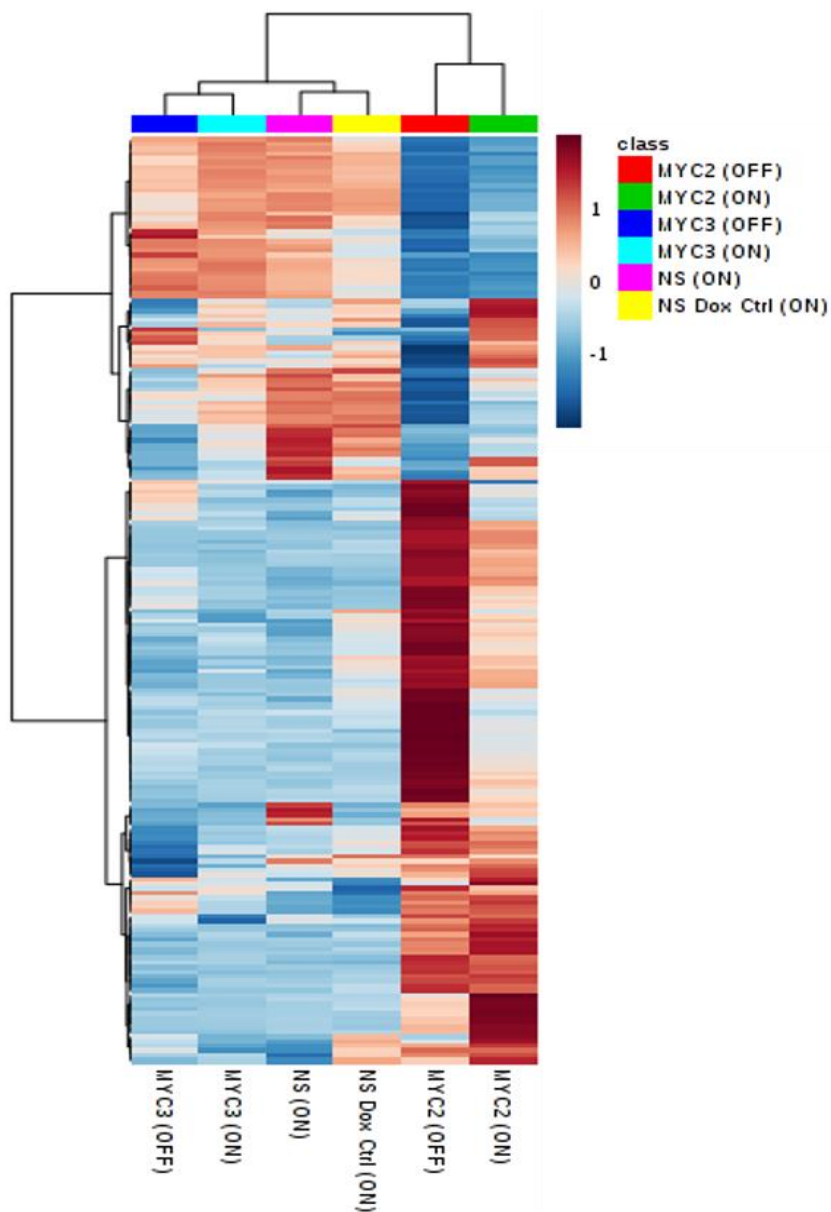


Figure 5.7 Clustered heatmap of spectral bins of HDMB03 Cell lines. HDMB03 NS, MYC 2, and MYC 3 harbouring cells were clustered using the Ward clustering algorithm. The colours represent the relative spectral bin intensity. Averaged group samples ($n=3$) are depicted along the vertical axis and bins across the horizontal axis. Group is indicated at the top of the figure by fuchsia and yellow (NS On and NS Dox Ctrl On respectively), green and red (MYC 2 on and MYC 2 Off respectively), light blue and dark blue (MYC 3 on and MYC 3 Off respectively).

Inspection of the PCA score plot for the HDMB03 cell lines revealed consistency in the NS, and MYC 2 samples in particular. Overall, there was less between-sample variation in the HDMB03 cell lines replicates compared to the D425 and D283 cell lines and is

indicated by how closely samples of experimental groups sit together on the PCA score plot. Additionally PC 1 and PC 2 accounted for over 80% of variance (Figure 5.6 A). Evaluation of the PCA score plot of the HDMB03 cell lines revealed closer clustering of the NS cell lines than observed in the D425 and D283 NS cell lines. The HDMB03 MYC 2 (on) cells however formed a distinct cluster from the NS (on) cells. Irrespective of this, the HDMB03 MYC 2 (off) cells were separated from MYC 2 (on) cluster suggesting an effect of *MYC* knockdown on alterations in the spectral profiles. Unfortunately only two samples of HDMB03 MYC 3 (on) and (off) cells were used and thus a confidence region of clusters could not be determined. Nonetheless, both MYC 3 (on) and MYC 3 (off) cells were proximate to the HDMB03 NS cluster (Figure 5.6 A). Notably, 3D PCA captured almost 90% of the variability of the spectral profiles between the HDMB03 MYC (on) and MYC (off) groups (Figure 5.6 B).

Hierarchical clustering and heatmap analysis of HDMB03 NS, MYC 2 and MYC 3 revealed distinct profiles (Figure 5.7). The heatmap profiles of HDMB03 NS and MYC 3 shared similar features but the HDMB03 MYC 2 profile was highly distinctive and differed from its sister cell lines. Further inspection of individual HRMAS spectra did not reveal spurious differences between NS, MYC 2 and MYC 3 samples. As highlighted in the PCA of HDMB03 samples (Figure 5.6), HDMB03 MYC 2 (on) were separated from the HDMB03 NS (on) and MYC 3 (on) which could suggest changes in this cell prior to the addition of doxycycline and may indicate construct leakiness. Nonetheless when the overall heatmap profiles of MYC (on) and MYC (off) cell were assessed, subtle alterations in profiles were observed in the HDMB03 MYC 2 cell lines but not HDMB03 NS which was expected. However the spectral profiles of MYC 3 (on) and MYC (off) cells were very similar. This is in line with previous findings of limited knockdown and phenotypic alterations in this particular cell line.

Altogether, the analysis of the individual MYC-modulable cell lines revealed alterations in the spectral profiles of MYC (on) and MYC (off) cell lines. In this initial analysis, shRNA-specific differences emerged and in particular revealed the MYC 2 harbouring cell lines had more variations in NMR spectra when comparing MYC expressing and MYC knockdown cells. Additionally, analysis of spectral profiles of NS engineered cell lines revealed similarities although some cell lines appeared less susceptible to doxycycline induced effects. Subsequent analysis should highlight further alterations associated with doxycycline and whether they are comparable or distinctive to *MYC*-driven metabolite changes.

5.3.2.2 Joint analysis of MB_{GRP3} cells to interrogate the effect of *MYC* knockdown on NMR spectral profiles

The overview of individual analysis of the MB_{GRP3} cell lines (i.e. D425, D283 and HDMB03) separately highlighted alterations in the metabolite profiles of *MYC* (off) cells compared to their *MYC* (on) equivalents. Additionally, minimal changes in NS cell lines following doxycycline treatment were observed. This was crucial as it improved confidence of categorising *MYC* specific changes in metabolites and associated metabolic pathways. Analysis combining the cell lines, across the *MYC*-specific and NS shRNA constructs was utilised to establish *MYC*-specific changes. Pooling of the samples was advantageous as it increased sample number for each shRNA bearing cell line thus improving power for subsequent analysis. Joint analysis of the spectral bins was used in the first instance due to there being a greater number of spectral features (~ 500) compared to assigned metabolites (~ 30) although the latter was used to validate and confirm alterations identified by spectral bin analysis (discussed in greater detail in following sections).

PCA was performed for the combined cell lines. However, the separation was dominated by the distinct metabolite features of the individual MB_{GRP3} cell lines rather than *MYC* status i.e. MB_{GRP3} cell lines formed three distinct clusters irrespective of shRNA construct (Appendix 8.19). To address this, samples were pooled according to shRNA constructs, which although this still displayed clusters of the individual cell lines, highlighted the separation between *MYC* (on) and *MYC* (off) cells when it occurred. Inspection of the PCA score plots and hierarchical clustering of NS (on) samples showed nominal separation within distinct MB_{GRP3} cell lines. In fact, in the NS cell lines, the clustering was ordered according to cell lines forming three major families (Figure 5.8). In the *MYC* 2 samples however, there was clear separation between the *MYC* 2 (on) and *MYC* 2 (off) cells which was clear in two out of three cell lines, namely the D425 and HDMB03 cells (Figure 5.9 A). Hierarchical clustering further showed the similarities between the D425 *MYC* 2 (off) and HDMB03 *MYC* 2 (off) which formed a cluster away from other samples (Figure 5.9 B). This is noteworthy since both the D425 and HDMB03 cell lines have high level *MYC* amplification and the *MYC* 2 shRNA construct achieved greater *MYC* knockdown. There was greater spread in the *MYC* 3 cell line samples, although some separation was observed, they did not form robust clusters as observed in the *MYC* 2 cell lines (Figure 5.10).

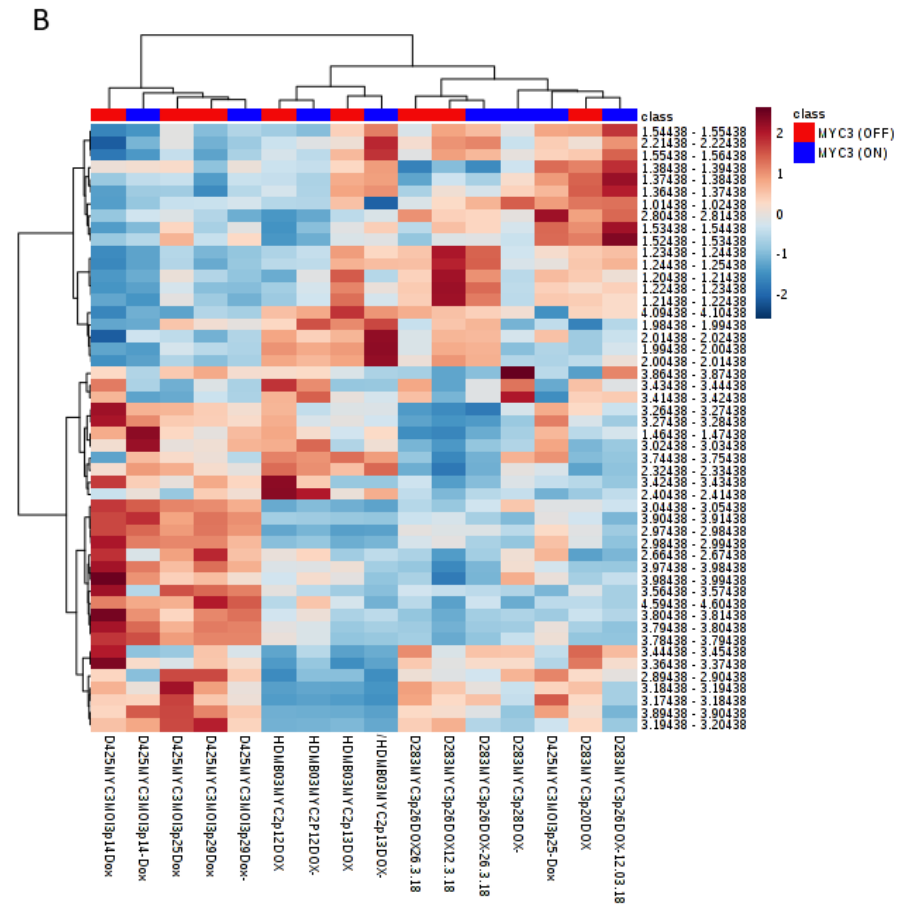
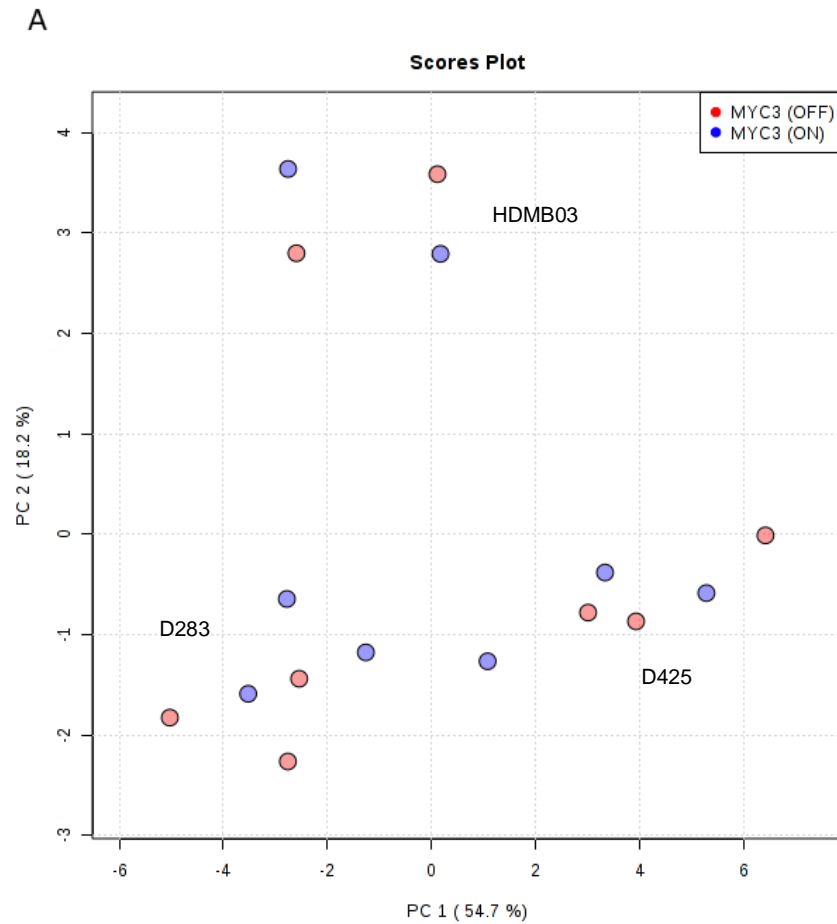


Figure 5.10 Pooled multivariate analysis of MB_{GRP3} MYC 3 cell lines metabolite profiles. A) PCA score plot of spectral bins from D425, D283 and HDMB03 MYC 3 cell lines following treatment with or without doxycycline for 72 h. PCA of sum normalised and pareto scaled spectral bins showing the first two principal components. B) Hierarchical clustering and heatmap analysis of the top 50 spectral bins of the MYC 3 (on) versus MYC 3 (off) cells.

To assess the overall characteristics of metabolite profiles, hierarchical clustering combined with heatmap analysis of the pooled cell lines was performed. This method also enabled comparison of the performance of the pooled NS, MYC 2 and MYC 3 bearing cell lines against patterns previously observed in individual cell lines.

The MYC 2 bearing cell lines demonstrated the best separation following MYC knockdown (Figure 5.11). In the MYC 3 cell lines, there were minimal changes in features consistent with lower levels of knockdown for this construct. For this particular shRNA construct, lower knockdown efficiency and leakiness of the construct was speculated as the reason for more subtle changes observed in previous experiments. Data from metabolomics experiments demonstrated the MBGRP3 cell lines were affected in distinct ways. For instance in the D425 cell line, it appeared that indeed leakiness of MYC 3 shRNA may have affected the metabolite profile of the MYC 3 (on) cells since they exhibited altered spectral profile from the MYC 2 (on) and NS cell lines. However despite this, observable differences and separation were observed in this cell line (Figure 5.3). This follows from previous findings where the most profound effects of MYC knockdown were observed in the D425 cell line which has higher copy number of MYC compared to the other cell lines which may in turn, overcome the effects of construct leakiness where lower knockdown sufficiently gives rise to phenotypic changes (Siu et al., 2003).

The D283 MYC 3 (on) on the PCA score plot cluster closely to NS cell line suggesting construct leakiness an unlikely candidate. The similarity of the MYC 3 (on) and MYC 3 (off) metabolic profiles would suggest that the knockdown achieved may not have reached a sufficient threshold to impact metabolite levels or give rise to stark variations equivalent to those evident in the D425 cell lines. The HDMB03 MYC 3 bearing cells were previously reported to display atypical growth characteristics and inconsistencies in earlier experiments. Although there may be some off target effects in this cell line in addition to construct leakiness, assessing global metabolites could further enable conclusion of these effects. From metabolite experiments, the NS and MYC 2 bearing cells behaved according to the expected alterations in MYC expression following addition of doxycycline, which was reflected in their respective metabolite profiles.

Although it was important to inspect global alterations in spectral profiles, assessing individual spectral features would reveal specific alterations associated with reduced MYC expression. In this instance, univariate analysis was used to examine the significantly altered spectral regions across the dataset including all three MB_{GRP3} cell lines and corresponding shRNA construct cell line pairs. Pooling of samples resulted in more statistical power, enabling identification of common changes across the MYC-regulable cell lines. Four bin regions were emphasised across the MB_{GRP3} isogenic cells lines (Figure 5.12 A). The regions highlighted are routinely assigned to NAA (2.01-2.02), taurine (3.43 -3.44 ppm) and glycine (3.56- 3.57 ppm). The bin region 2.02-2.03 was found to be significantly altered but confident assignment could not be made due to multiple peaks adjacent to the region arising from resonance of glutamine. An artefact of binning could result in splitting of peak regions of metabolites of NMR spectra, although plausible in this scenario, this bin region could also represent an unknown metabolite peak. Comparison across the groups largely revealed significant variations in the MYC 2 (on) compared to MYC 2 (off) cells (Figure 5.12 B, Appendix 8.20).

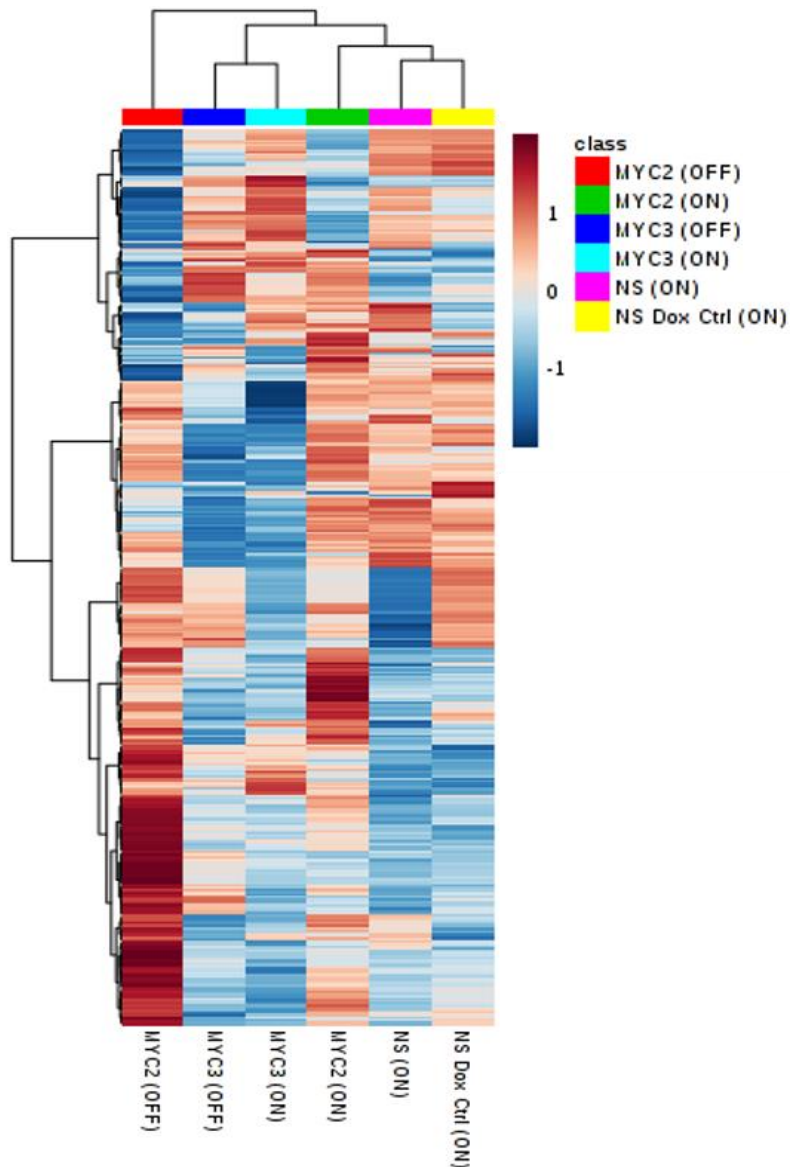


Figure 5.11 Clustered heatmap of spectral bins of MB_{GRP3} MYC inducible cell lines. D425, D283 and HDMB03 NS, MYC 2, and MYC 3 harbouring cells pooled ($n=9$ for each condition) according to constructs and then clustered using the Ward clustering algorithm. The colours represent the relative spectral bin intensity. Sample groups are depicted along the vertical axis and bins across the horizontal axis. Group is indicated at the top of the figure by fuchsia and yellow (NS On and NS Dox Ctrl On respectively), green and red (MYC 2 on and MYC 2 Off respectively), light blue and dark blue (MYC 3 on and MYC 3 Off respectively).

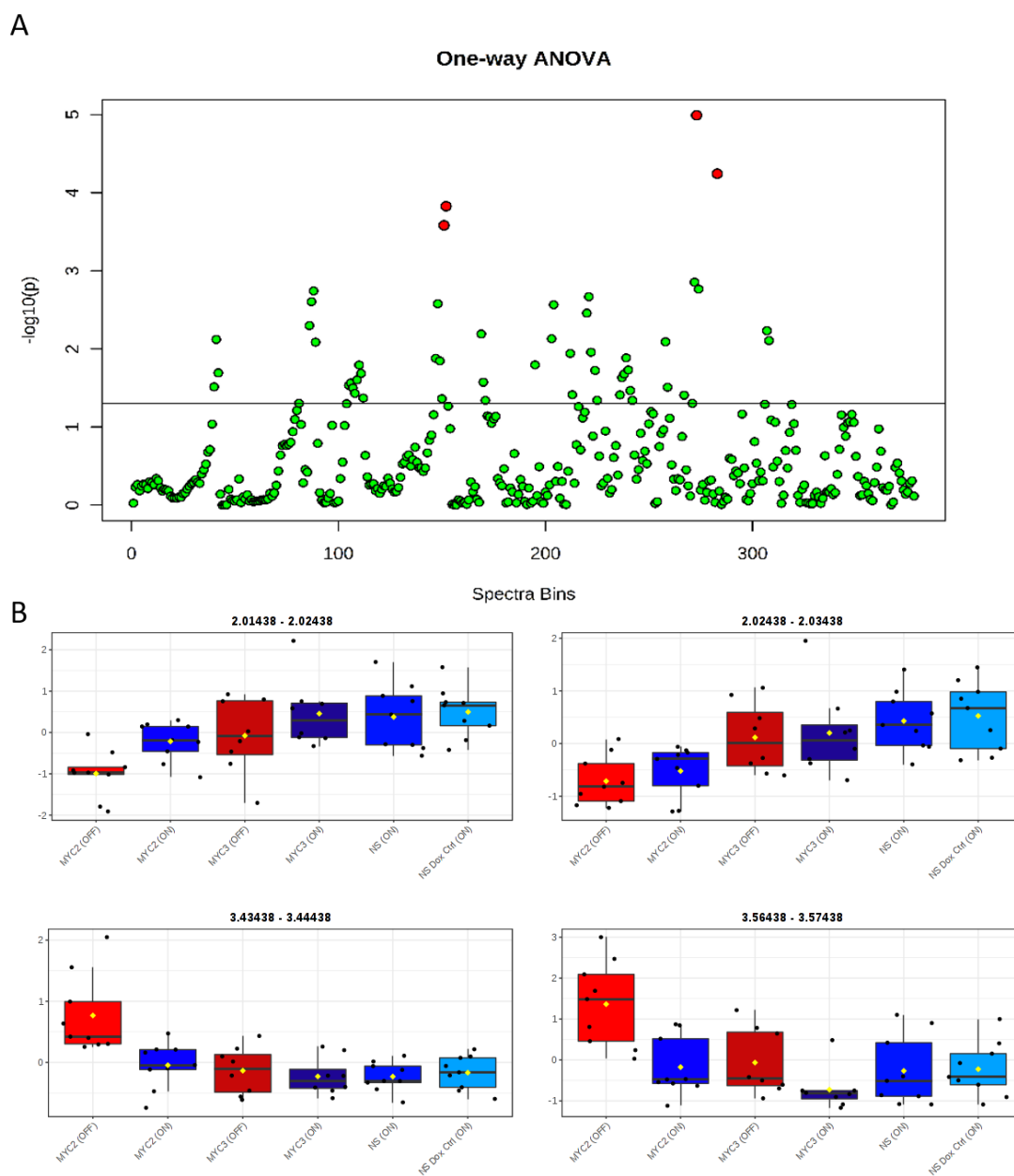


Figure 5.12 Significantly altered spectral features in MB_{GRP3} cell lines. A) Scatter plot showing mean difference of spectral bins of the D425, D283 and HDMB03 NS, MYC 2 and MYC 3 cell lines following MYC knockdown determined by One-way ANOVA. Red dots indicate p-value <0.05. Y-axis is automatically adjusted by Metaboanalyst using $-\log_{10}(p)$. Line on scatter plot shows the $-\log_{10}(0.05)$ value on y-axis. B) The four highlighted altered spectral bins regions following MYC knockdown. Boxplots display individual samples (black dots) and represent lower and upper quartiles with middle line indicating median.

5.3.3 Analysis of metabolite concentrations derived from ¹H NMR spectra

5.3.3.1 Multivariate analysis on the impact of *MYC* knockdown on global metabolite profiles of MB_{GRP3} *MYC*-regulable cell lines

As previously outlined in Figure 5.1, the second analysis carried out on the ¹H NMR spectra of MB_{GRP3} cell lines was to identify and quantify metabolites detected and follow similar analysis pipeline previously used. Analysis utilising spectral bins indicated on a global level how *MYC* knockdown impacted detectable metabolites and also highlighted regions which significantly distinguished the *MYC* (on) and *MYC* (off) cells. Binning suffers from loss of resolution and additionally may induce artificial splitting of metabolites with multiplet peaks. Thus analyses using metabolite quantitation may highlight changes missed in the spectra binning analysis and also corroborate previous observations. Furthermore biological relevance isn't immediately obvious in spectral binning underscoring the further need for evaluation of relative metabolite concentrations. Details of metabolite/lipid assignments are listed in Appendix 8.22 and Appendix 8.23. Altogether 21 metabolites and 5 lipid species were identified from HRMAS spectra. For each cell line, metabolites reported were consistently found within cell lines harbouring NS, *MYC* 2 and *MYC* 3 constructs.

Metabolic profiling of D425, *MYC* 2 and *MYC* 3 following *MYC* knockdown showed altered metabolite abundances (Figure 5.13). Similarly to analysis of spectral bins, clustering of metabolite abundances showed a distinct subfamily and branch of the D425 *MYC* 2 and *MYC* 3 (off) cells compared to the *MYC* (on) cells. Furthermore the distance between D425 *MYC* 2/3 (on) versus *MYC* 2/3 (off) were increased, highlighting these distinct changes. It is worth noting that although there were slight variations in the profiles of the D425 NS (on) and Dox control (on) cells, these alterations largely differed from those observed in the *MYC* shRNA bearing cells following addition of doxycycline. However, additional supervised analysis further established and distinguished these alterations.

Examination of metabolite profiles of the D283 cell lines revealed similarities to previous analysis conducted on spectral bins. As previously observed, the D283 *MYC* 2 cell lines clustered distinctly from the D283 NS and *MYC* 3 cells (Figure 5.14; Figure 5.5). There were some alterations in metabolite abundances observed which were not immediately highlighted from spectral bin analysis between the D283 *MYC* 2 (on) and *MYC* 2 (off) cells. In the D283 *MYC* 3 also, distinctions between the *MYC* 3 (on) and *MYC* 3 (off)

were more pronounced. In fact, MYC 3 (off) formed a sub-branch away from the MYC 3 (on) which clusters closely to the D283 NS (on) and Dox control (on) cells (Figure 5.14).

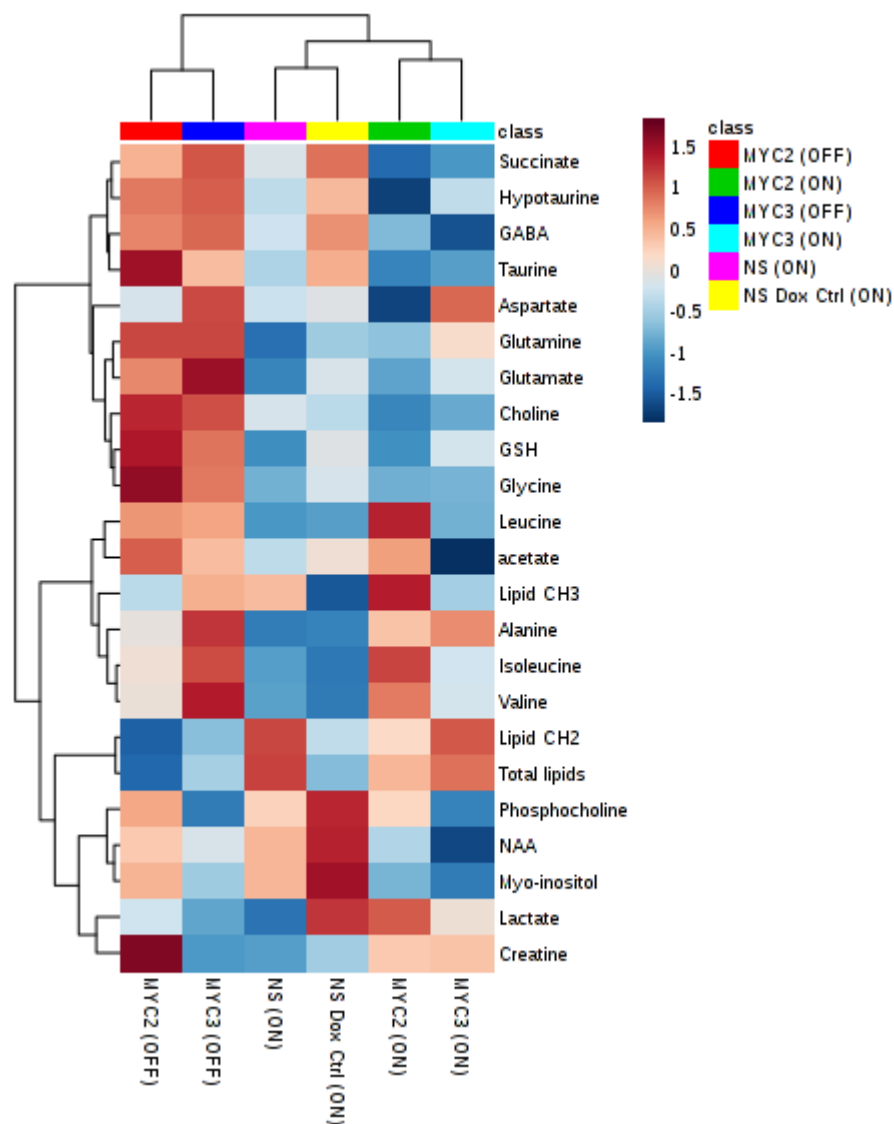


Figure 5.13 Metabolite profiles of D425 cell lines following MYC knockdown. D425 NS, MYC 2, and MYC 3 harbouring cells were treated in the presence or absence of doxycycline for 72h and subjected to metabolic profiling. Metabolites were clustered using the Ward clustering algorithm. The colours represent the relative metabolite levels (Red for high, Blue for low). Individual samples are depicted along the vertical axis and metabolites across the horizontal axis. Group is indicated at the top of the figure by fuchsia and yellow (NS On and NS Dox Ctrl On respectively), green and red (MYC 2 on and MYC 2 Off respectively), light blue and dark blue (MYC 3 on and MYC 3 Off respectively). Data represents mean of 3 replicates.

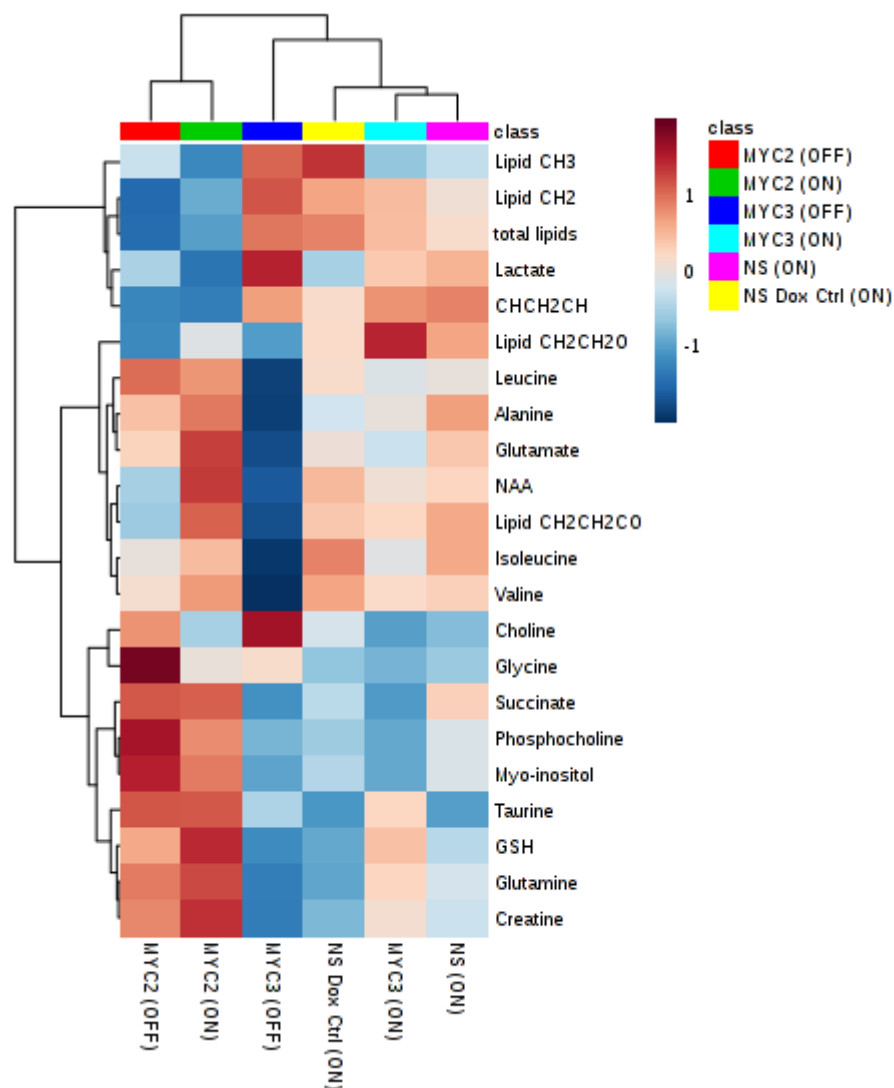


Figure 5.14 Metabolite profiles of D283 cell lines following MYC knockdown. D283 NS, MYC 2, and MYC 3 harbouring cells were treated in the presence or absence of doxycycline for 72h and subjected to metabolic profiling. Metabolites were clustered using the Ward clustering algorithm. The colours represent the relative metabolite levels (Red for high, Blue for low). Individual samples are depicted along the vertical axis and metabolites across the horizontal axis. Group is indicated at the top of the figure by fuchsia and yellow (NS On and NS Dox Ctrl On respectively), green and red (MYC 2 on and MYC 2 Off respectively), light blue and dark blue (MYC 3 on and MYC 3 Off respectively). Data represents mean of 3 replicates.

Similar clustering patterns to the D283 cell lines were observed in the HDMB03 cell lines. It was previously observed that metabolite profiles for the HDMB03 MYC 2 (on) cells were in contrast to the NS and MYC 3 (on) cells (Figure 5.7). These characteristics remained observable when metabolite abundances were considered (Figure 5.15).

Although the HDMB03 MYC 2 (on) and MYC 2 (off) clustered closely together, there were subtle differences in metabolites within this cell line following MYC knockdown. The NS (on) and Dox control (on) cells had highly similar profiles which was anticipated as MYC knockdown was not expected in this cell line. The HDMB03 MYC 3 (on) cells cluster narrowly to the NS cell lines. Additionally the HDMB03 MYC 3 (off) cells form a subfamily, slightly separated from the HDMB03 NS and MYC 3 (on) cells (Figure 5.15).

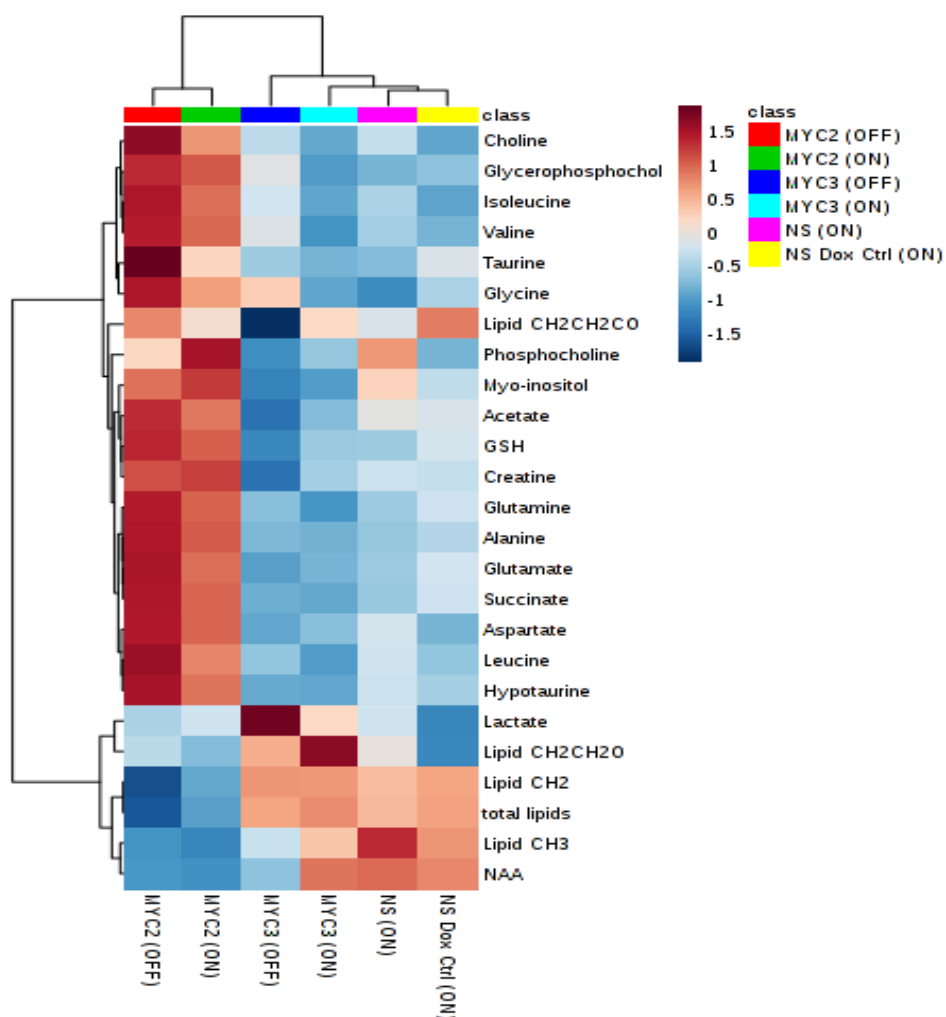


Figure 5.15 Metabolite profiles of HDMB03 cell lines following MYC knockdown. HDMB03 NS, MYC 2, and MYC 3 harbouring cells were treated in the presence or absence of doxycycline for 72h and subjected to metabolic profiling. Metabolites were clustered using the Ward clustering algorithm. The colours represent the relative metabolite levels (Red for high, Blue for low). Individual samples are depicted along the vertical axis and metabolites across the horizontal axis. Group is indicated at the top of the figure by fuchsia and yellow (NS On and NS Dox Ctrl On respectively), green and red (MYC 2 on and MYC 2 Off respectively), light blue and dark blue (MYC 3 on and MYC 3 Off respectively). Data represents mean of 3 replicates.

5.3.3.2 Supervised discriminant analysis for identifying metabolite altered following modulation of *MYC* expression

So far, we have employed PCA alongside heatmap analysis as a tool for reducing dimensionality of the ¹H NMR spectra dataset when assessing the impact of *MYC* knockdown in the MB_{GRP3} cell lines. Although PCA is an unbiased method, it is still prone to within-group sample variation which can impact the analysis of between group variations. PLS-DA, like PCA, is dimensionality reduction tool however it does so by relying on class membership. In order to identify *MYC*-driven metabolite alterations, supervised analysis using PLS-DA was utilised. The purpose of PLS-DA here was to utilise feature selection and is the primary focus of this section. Prior to use in identifying important metabolites which distinguished *MYC* (on) cells from *MYC* (off) cells, PLS-DA models were cross-validated. This ensured PLS model accuracy and statistical significance. Variable important projections (VIP) scores were used as a feature selection method to identify impacted metabolites when *MYC* expression was reduced. VIP scores greater than 1 were used as a cut-off for relevant metabolites as previously described (Akarachantachote et al., 2014).

Individual feature selection using PLS-DA with VIP scores were used to determine metabolites distinguishing *MYC* (on) and *MYC* (off) pairs in addition with NS (on) and NS Dox Ctrl (on) pairs (Appendix 8.24- Appendix 8.32). The primary focus was to ensure metabolites that were consistently altered across the three MB_{GRP3} cell lines in response to *MYC* loss were highlighted. It was appreciated that cell line-specific metabolic changes may occur, however the consistent changes across MB_{GRP3} cell lines with varying genetic backgrounds were likely to result in the identification of the most profound *MYC*-induced alterations. For this reason, similar sample pooling and joint analysis techniques previously used were employed, such that PLS-DA models were generated for the pooled NS, *MYC* 2 and *MYC* 3 harbouring MB_{GRP3} cell lines.

PLS-DA was cross validated to ensure models accurately fitted data; this confirmed cross-validated PLS-DA models for *MYC* 2 and *MYC* 3 samples (Appendix 8.36- Appendix 8.36). In the *MYC* 2 cell lines, elevation in choline, glycine and taurine in the *MYC* 2 (off) distinguished these samples from the *MYC* 2 (on) cells (Figure 5.16, Figure 5.17). In the *MYC* 3 cell lines, decrease in creatine levels accompanied by elevations in choline and glycine distinguished *MYC* 3 (off) cells from their *MYC* 3 (on) counterparts (Figure 5.18, Figure 5.19). The model generated for the NS cell lines failed cross validation, meaning that PLS-DA model was relying on class membership and artificially clustered

the NS (on) and NS Dox Ctrl (on). Since ‘goodness of fit’ of the model was invalid, this meant NS (on) and NS Dox Ctrl (on) could not be distinguished and attempts to do so using VIP scores was statistically insignificant (Appendix 8.36 A). Indeed when metabolite levels were interrogated, only minimal variations were observed (Figure 5.20, Figure 5.21).

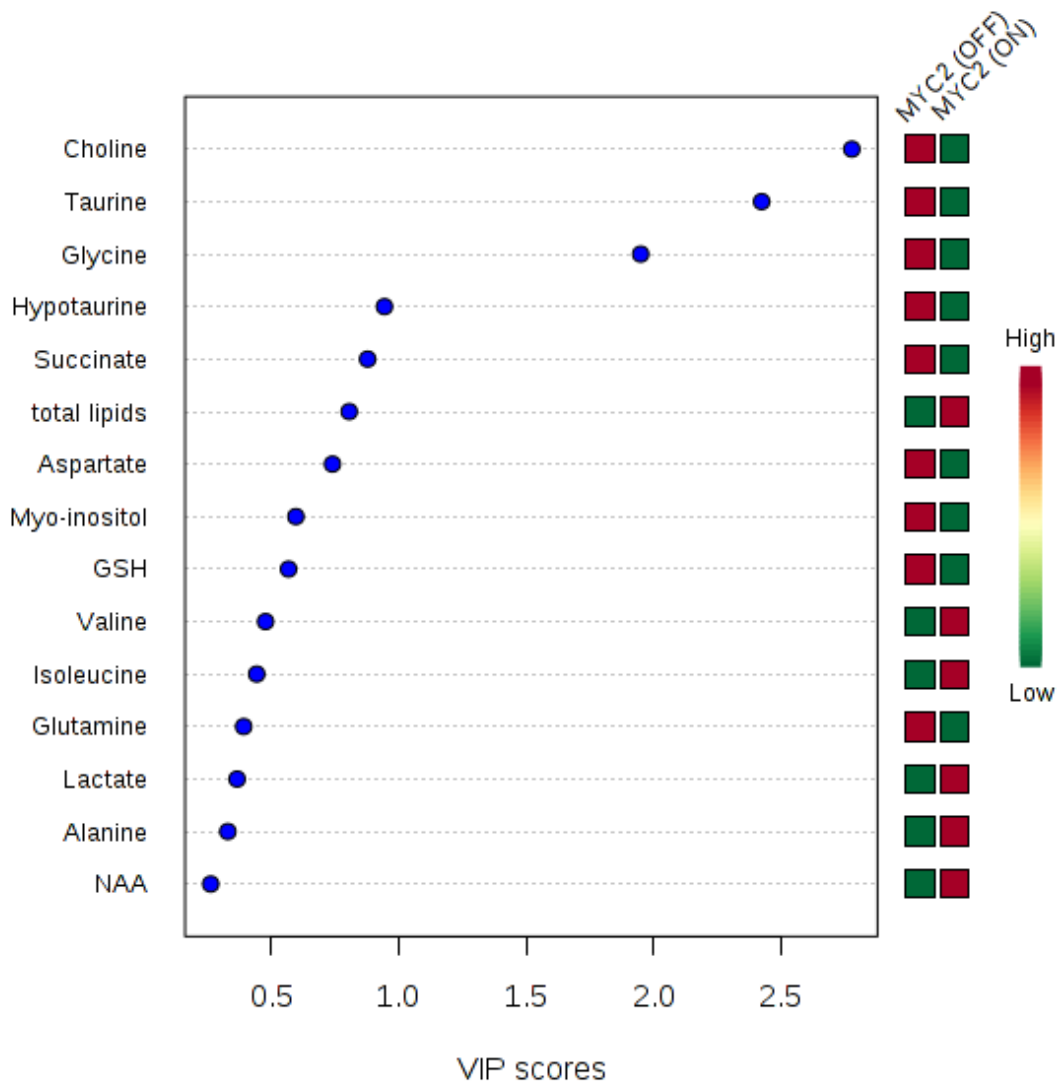


Figure 5.16 Discriminant metabolites in the pooled MB_{GRP3} MYC 2 (on) compared to MYC 2 (off) cells. Variable importance in projection (VIP) scores displaying top 15 metabolites that are altered following MYC knockdown as identified by PLS-DA. VIP score is weighted sum of squares correlations between PLS components and original variable. Higher VIP scores indicate greater contribution to the separation in the model. The red and green boxes to the right indicate whether a metabolite is increased (red) or decreased (green) when MYC was knocked down.

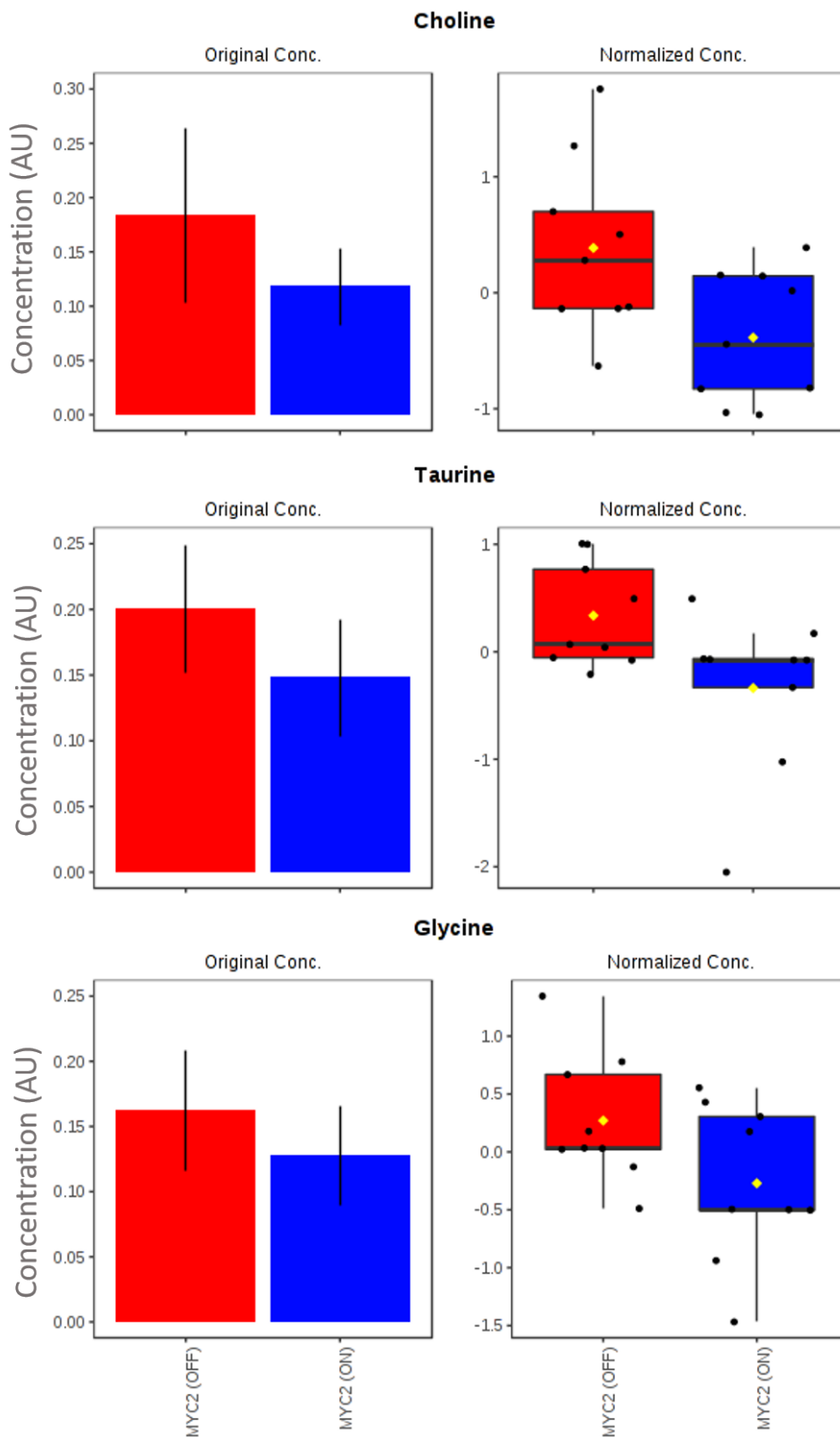


Figure 5.17 Top 3 discriminant metabolites in the pooled MB_{GRP3} MYC 2 cell lines. The data indicates original concentrations (bar plot \pm SD) and normalised concentrations (boxplots) of the top metabolites according to VIP score between MYC 2 (on) v MYC 2 (off) MB_{GRP3} cell lines. Arbitrary units (AU).

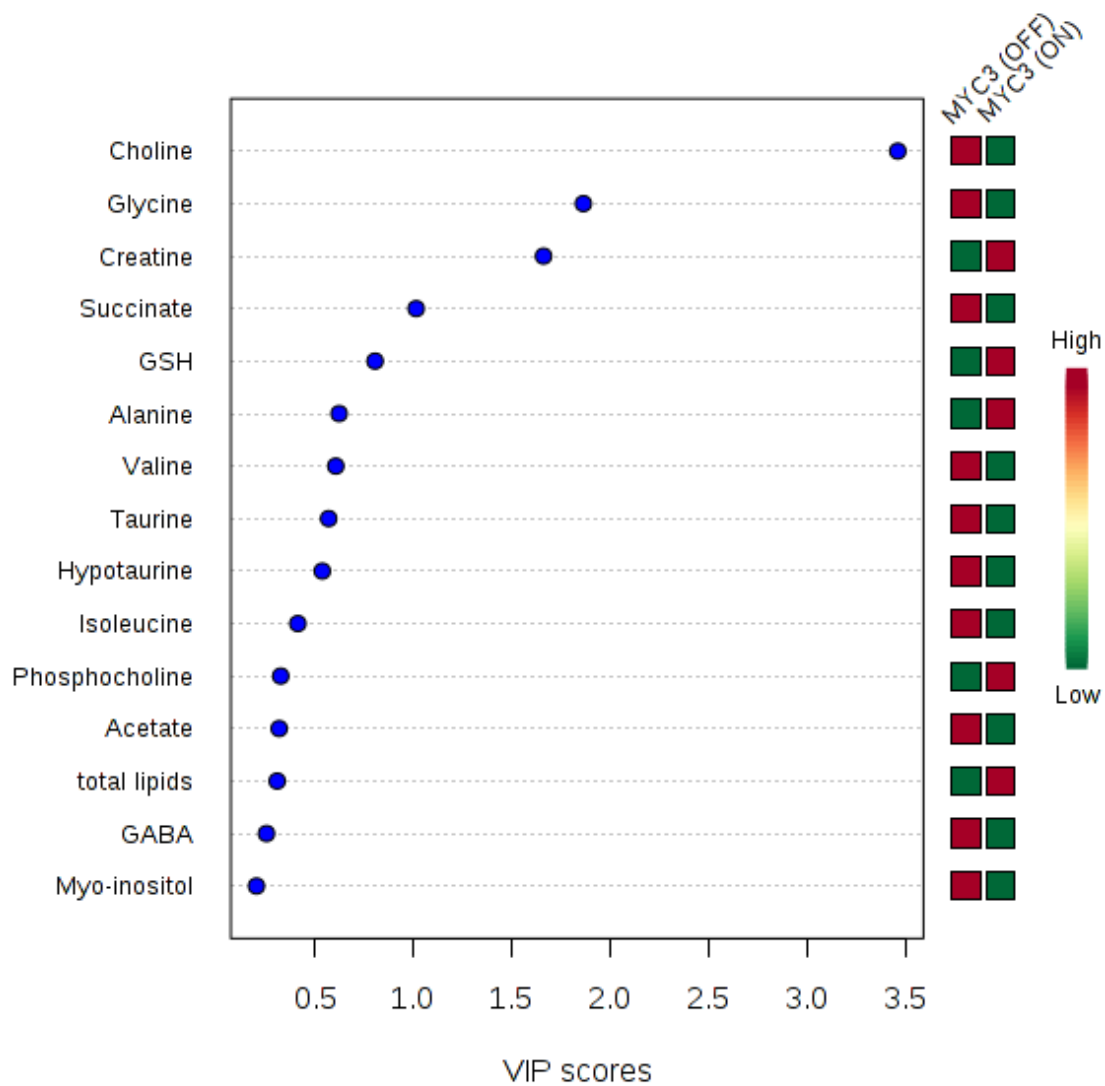


Figure 5.18 Discriminant metabolites in the pooled MB_{GRP3} MYC 3 (on) compared to MYC 3 (off) cells. Variable importance in projection (VIP) scores displaying top 15 metabolites that are altered following MYC knockdown as identified by PLS-DA. VIP score is weighted sum of squares correlations between PLS components and original variable. Higher VIP scores indicate greater contribution to the separation in the model. The red and green boxes to the right indicate whether a metabolite is increased (red) or decreased (green) when MYC was knocked down.

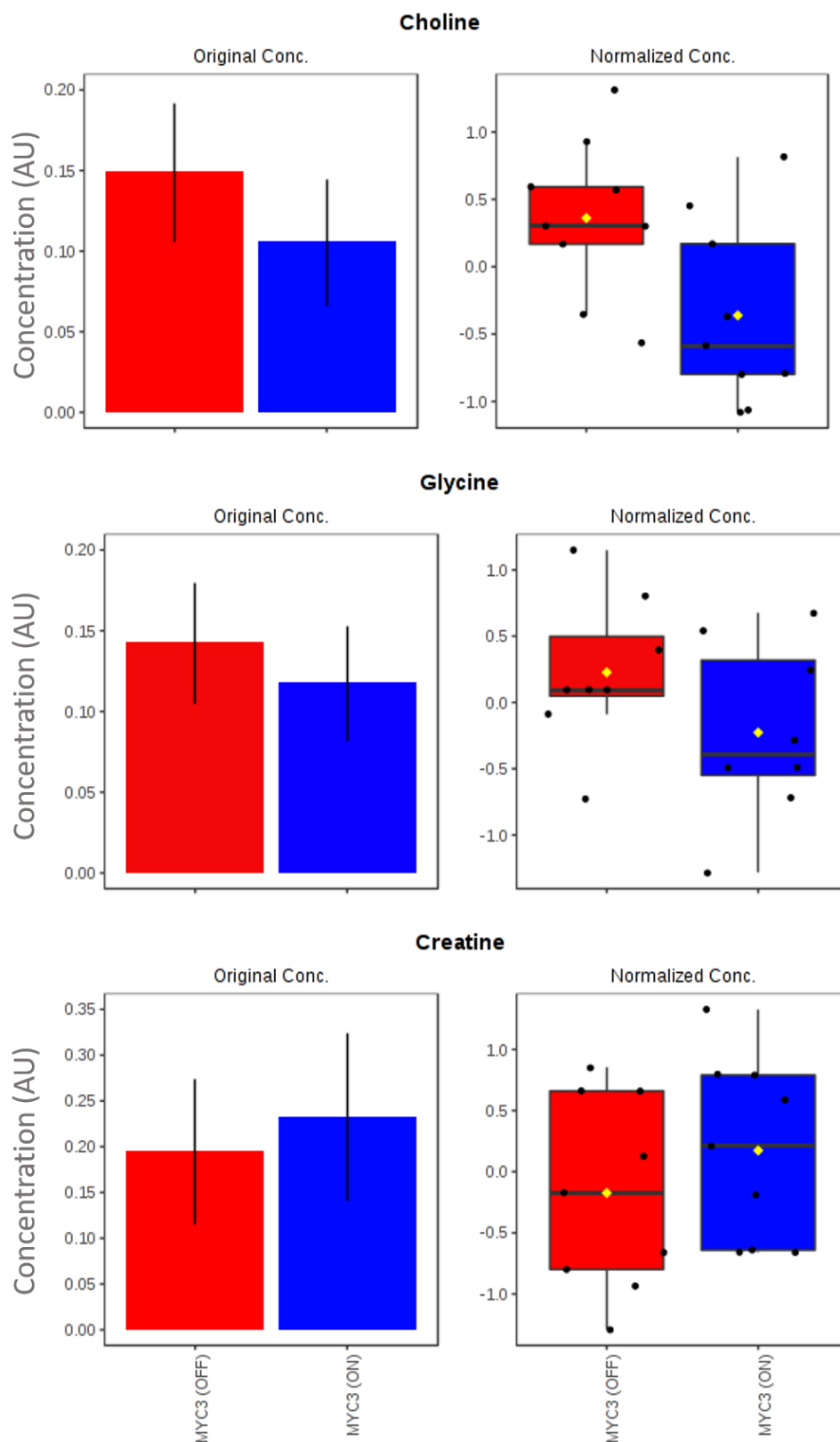


Figure 5.19 Top 3 discriminant metabolites in the pooled MB_{GRP3} MYC 3 cell lines. The data indicates original concentrations (bar plot $\pm SD$) and normalised concentrations (boxplots) of the top metabolites according to VIP score between MYC 3 (on) v MYC 3 (off) MB_{GRP3} cell lines. Arbitrary units (AU).

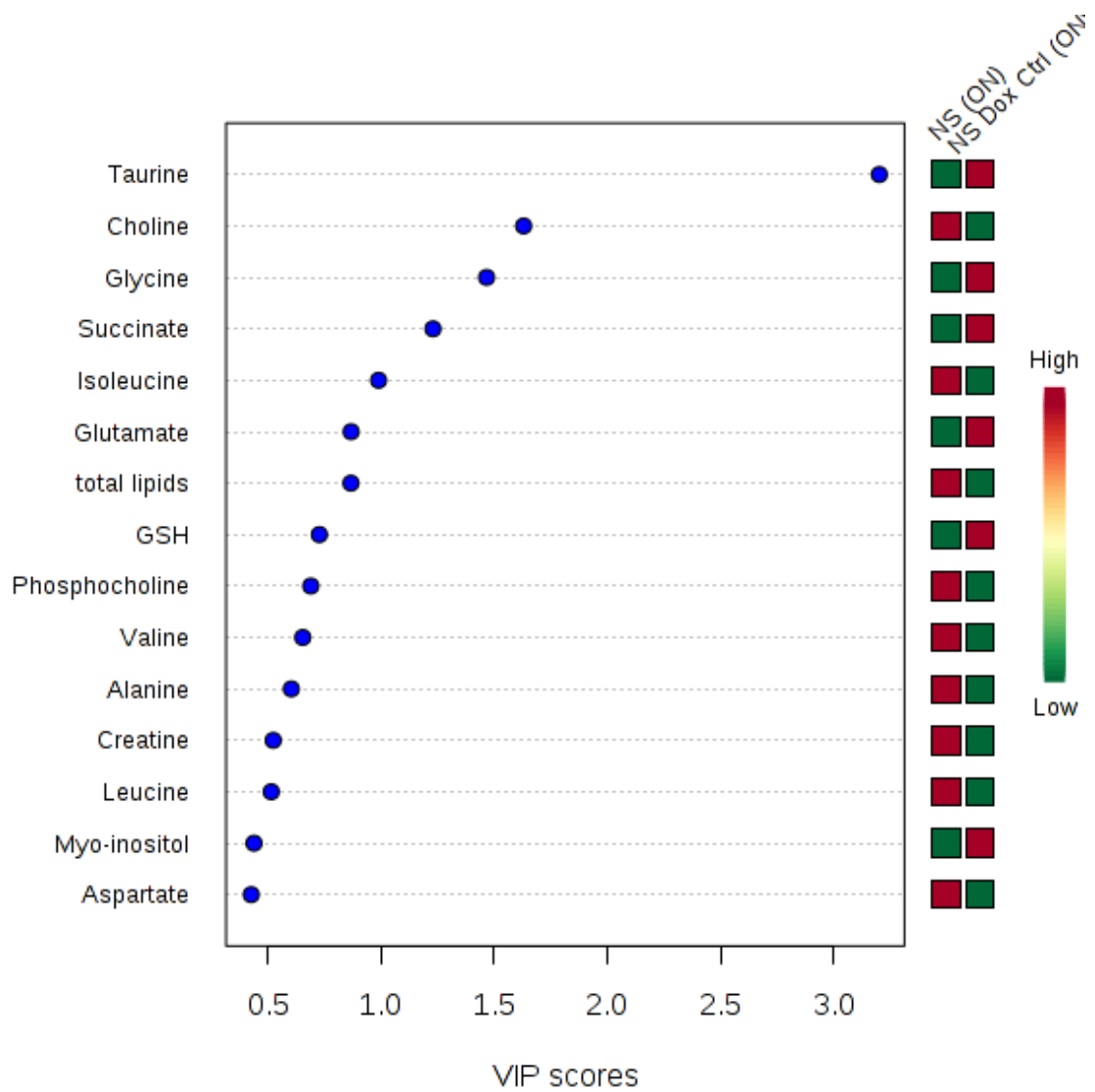


Figure 5.20 Discriminant metabolites in the pooled MB_{GRP3} NS (on) compared to NS Dox Ctrl (on) cells. Variable importance in projection (VIP) scores displaying top 15 metabolites that are altered following MYC knockdown as identified by PLS-DA. VIP score is weighted sum of squares correlations between PLS components and original variable. Higher VIP scores indicate greater contribution to the separation in the model. The red and green boxes to the right indicate whether a metabolite is increased (red) or decreased (green) when MYC was knocked down.

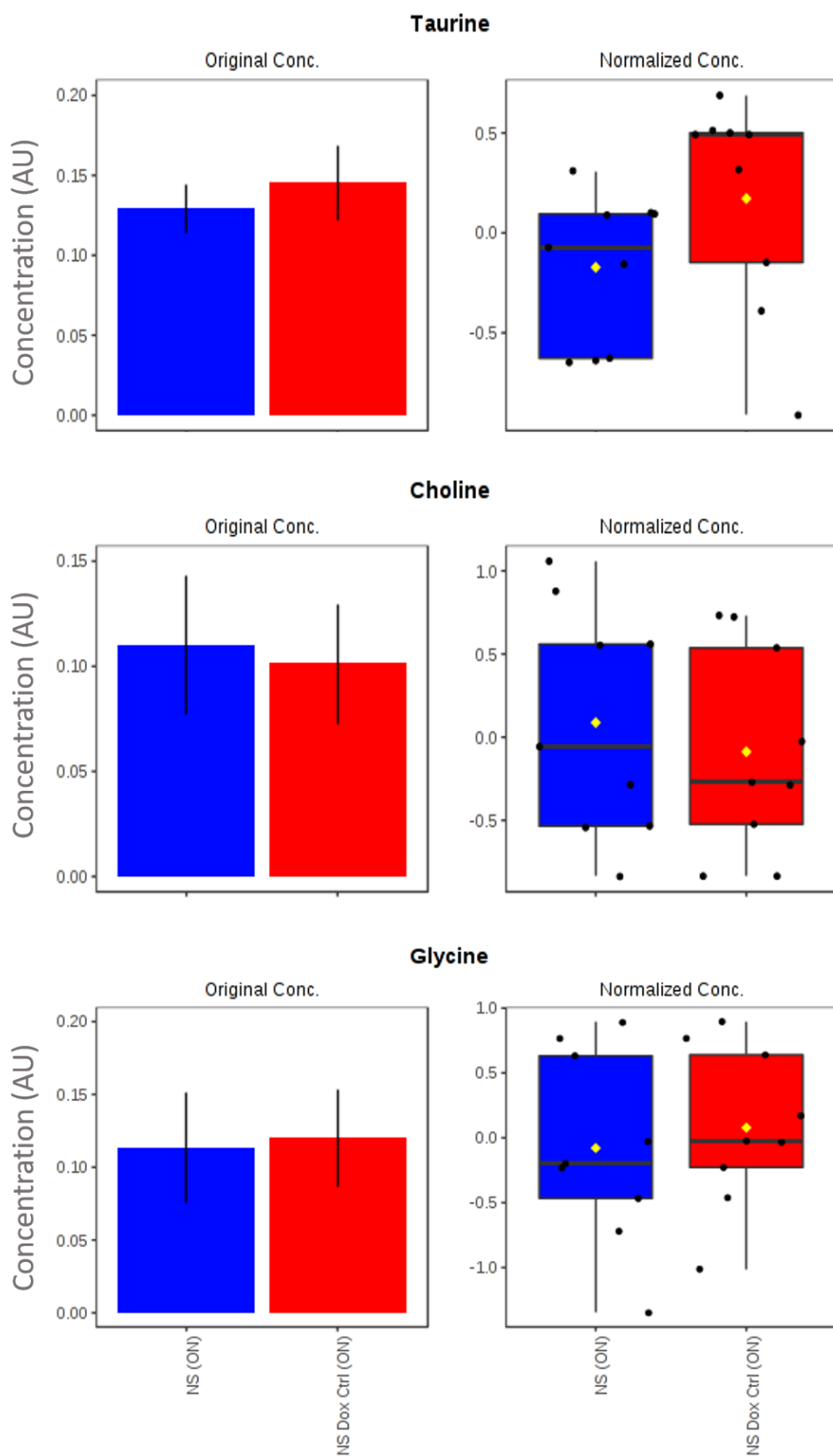


Figure 5.21 Top 3 discriminant metabolites in the pooled MB_{GRP3} NS cell lines. The data indicates original concentrations (bar plot \pm SD) and normalised concentrations (boxplots) of the top metabolites according to VIP score between NS (on) v NS Dox Ctrl (on) MB_{GRP3} cell lines. Arbitrary units (AU).

5.3.3.3 Overlap of metabolites in the MB_{GRP3} MYC-regulable cell lines

Using PLS-DA and VIP scores for feature selection highlighted metabolites that were altered following *MYC* knockdown in the MB_{GRP3} cell lines. Although pooling of samples improved power for statistical analysis, it was important to ensure that these results were not being influenced by a subset of samples or that other features weren't masked. The discriminant metabolites for each *MYC*-specific shRNA construct in the MB_{GRP3} cell lines were overlapped to corroborate previous findings and also assess individual cell line behaviour. For the *MYC* 2 bearing cell lines, glycine and choline were the 2 shared metabolites that distinguished the *MYC* 2 (on) and *MYC* 2 (off) cells across the D425, D283 and HDMB03 cell lines. It is also worth noting that the D425 and HDMB03 *MYC* 2 cell lines also had taurine and hypotaurine species as common metabolites that were impacted following *MYC* knockdown (Figure 5.22). Additionally there was at least 1 metabolite that was unique to each cell line for discriminant analysis. Glycine and choline similarly were identified in the *MYC* 3 bearing cell lines (Figure 5.23).

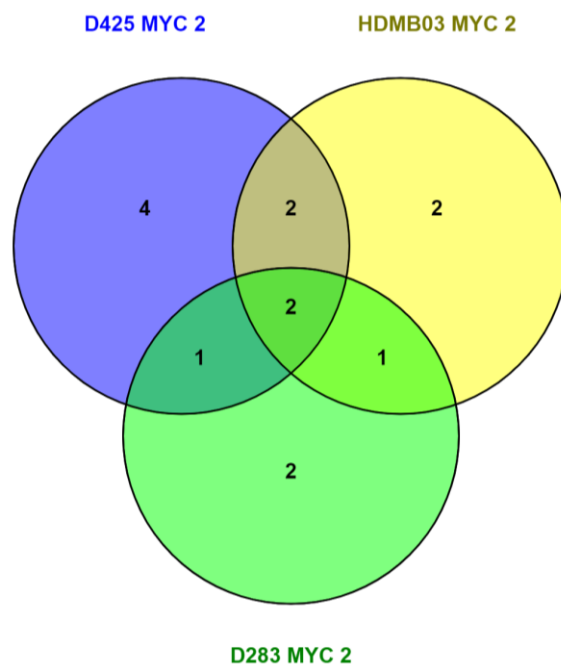


Figure 5.22 Venn diagram of common discriminant metabolites between the MYC 2 harbouring cell lines following MYC knockdown. The diagram indicates altered metabolites with $VIP > 1$ in the PLS-DA model.

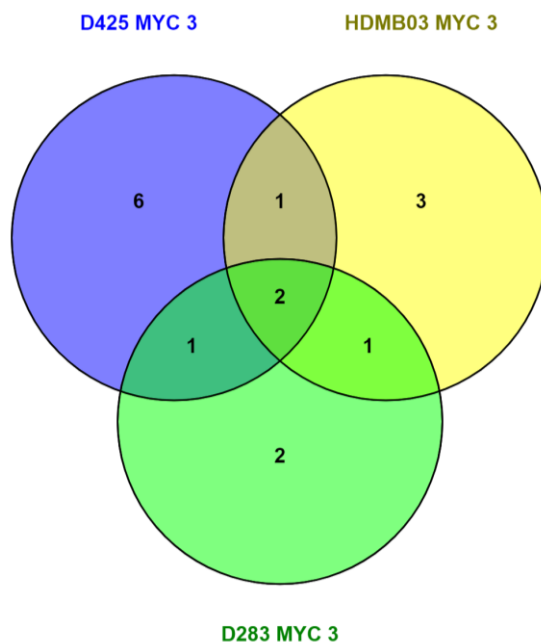


Figure 5.23 Venn diagram of common discriminant metabolites between the MYC 3 harbouring cell lines following MYC knockdown. The diagram indicates altered metabolites with $VIP > 1$ in the PLS-DA model.

5.3.4 Utilising ^{13}C -glucose tracing to understand pathway dynamics of *MYC*-amplified medulloblastoma cells

Overall, metabolic profiling revealed novel metabolite changes associated with *MYC* amplification in MB. Previous experiments (Section 5.3.3) have highlighted *MYC*-dependent changes in metabolites levels, namely alterations in the intracellular abundance of glycine and choline which were highly concordant across MB_{GRP3} cell lines. Interestingly both metabolites provide one-carbon units that feed into the folate and methionine cycles. Although metabolic pathways affected can be deduced from metabolic profiling, it is difficult to understand the dynamics of these highlighted metabolites. For instance, in the case of choline, increased levels were observed which may be attributable to increased uptake or decreased activity of choline kinase which converts choline to phosphocholine. In the case of glycine is it increased *de novo* synthesis or uptake from the extracellular medium?

The utility of both NMR and MS in metabolomics studies to further clarify information where one platform was limited was previously discussed (Chapter 5.1). For this study, the use of ^{13}C tracing could provide more context for the alterations observed in these metabolites. Since ^{13}C tracing is not widely utilised for choline, this portion of the study focused on the dynamics of glycine which could be assessed using ^{13}C glucose as a tracer. The *de novo* synthesis of glycine and its precursor serine is derived from the glucose intermediate 3-phosphoglycerate. Both serine and glycine are important biosynthetic precursors and important contributors to one carbon metabolism. Although serine was not detectable in the HRMAS profiling, it links glucose metabolism to biosynthetic pathways and thus provides a rationale for evaluating its role in *MYC*-regulable MB cell lines in addition to glycine. The D425 *MYC* 2 cell lines performed consistently in most experiments and thus were utilised for ^{13}C tracing analysis. D425 *MYC* 2 cells were treated in the presence or absence of doxycycline for 48 h in growth medium with unlabelled glucose to induce *MYC* KD prior labelling. Subsequently, media was replaced with growth medium with ^{13}C glucose alongside doxycycline treatment and cells were cultured for 6 and 24 h to determine pathway activity.

Pathway activity was determined by assessing the labelling patterns of isotopologue and overall abundance of a particular metabolite over the two time points. Since ^{13}C has an additional mass to ^{12}C , metabolites with labelled with ^{13}C heavy isotopes are denoted with + n, where n is the number of heavy isotopes found in the metabolite/isotopologue. As illustrated in Figure 5.24 A, uniformly labelled ^{13}C -glucose gives rise to a 3-carbon unit metabolite, 3PG, which is utilised for the *de novo* synthesis of serine and glycine. In this scenario, phosphoserine and serine, which are uniformly labelled with three ^{13}C atoms are denoted as M+3, here M represents mass. For glycine this would be M+2 since glycine is a two-carbon metabolite. Once introduced into the system, numerous labelling patterns of metabolites may arise from various metabolic sources to generate mixed labelled metabolites as shown in Figure 5.24 B. Since phosphoserine is a direct product of glycolytic metabolism, only two labelling patterns are observed. Serine and glycine are however more complex, since they can be generated from metabolic sources in addition to interconversion. Conventional MS analysis derives mass changes and does not inform on position of heavy isotopes which require more sophisticated MS techniques. Figure 5.24 B depicts possible isotopologues (i.e. M+1, M+2, M+3) of serine and glycine with no reference to proximity to amide or carboxyl terminals of these AAs.

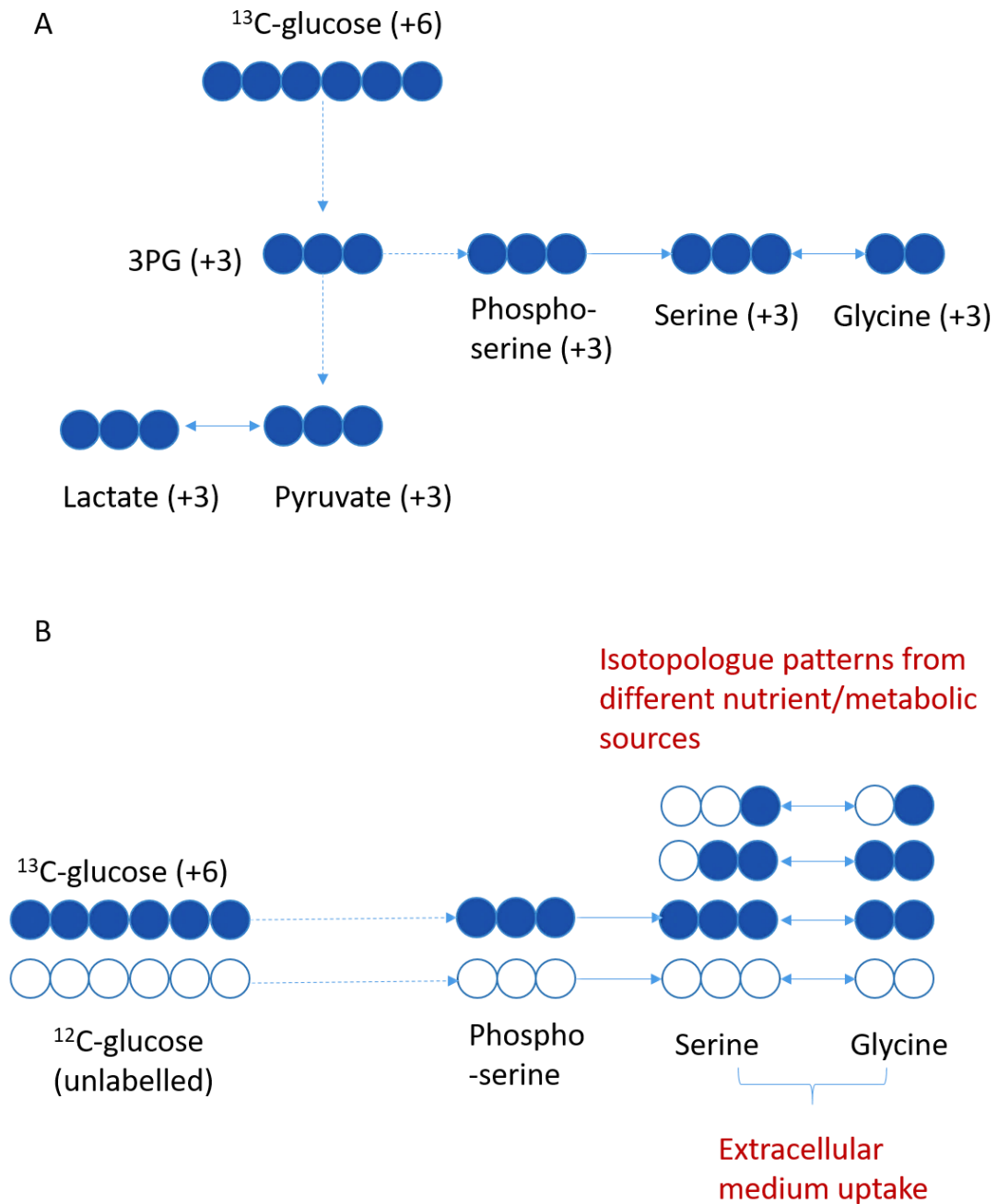


Figure 5.24 Schematic of isotopologues following ^{13}C -glucose labelling in glycolysis and de novo serine and glycine synthesis pathway. A) Uniformly labelled glycolytic intermediates and serine/glycine related metabolites, solid blue indicates ^{13}C atoms. B) Simplified evolution of serine and glycine metabolites giving rise to metabolites with both ^{13}C -labelled (Blue) and ^{12}C -unlabelled (white).

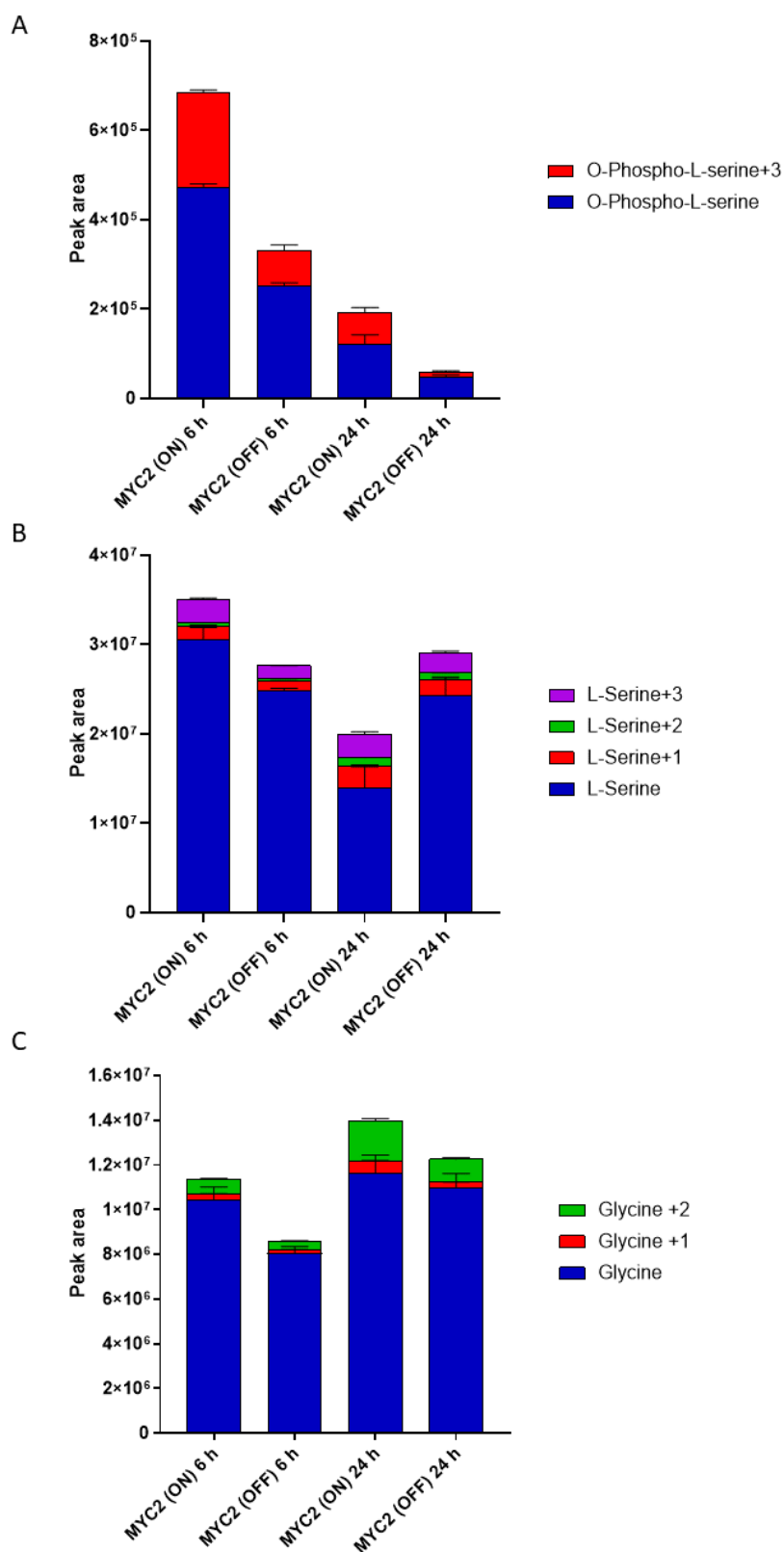


Figure 5.25 Effect of MYC knockdown on the ¹³C -glucose labelling patterns of the de novo serine and glycine synthesis pathways. Isotopologue distribution of A) O-Phospho-3-serine B) Serine C) glycine in D425 MYC 2 (on) and MYC 2 (off) cells over 24 h. Data represents ± SD of three biological replicates. Metabolites are denoted with +1, +2, +3 to indicate number of heavy isotopes. Data represents mean ± SD of three biological replicates.

Table 5.1 Mean differences in unlabelled and ^{13}C labelled metabolites in the D425 MYC 2 (on) and MYC 2 (off) cells. Significance was determined using two-way ANOVA

Metabolite	Mean difference at 6 h	Adjusted p-value	Mean difference at 24 h	Adjusted p-value
Phosphoserine	2.22×10^5	0.0001	4.82×10^4	0.0001
Phosphoserine +3	1.32×10^5	0.0001	1.17×10^4	0.0001
Serine	5.77×10^6	0.0001	-1.03×10^6	0.0001
Serine + 1	4.20×10^5	0.9925	5.43×10^5	0.9721
Serine + 2	1.06×10^5	0.9999	2.40×10^6	0.9997
Serine + 3	1.17×10^6	0.4992	3.07×10^5	0.9987
Glycine	2.40×10^6	0.0001	6.67×10^5	0.1674
Glycine + 1	1.04×10^5	0.9995	2.65×10^5	0.9366
Glycine + 2	2.58×10^5	0.9438	8.03×10^5	0.061

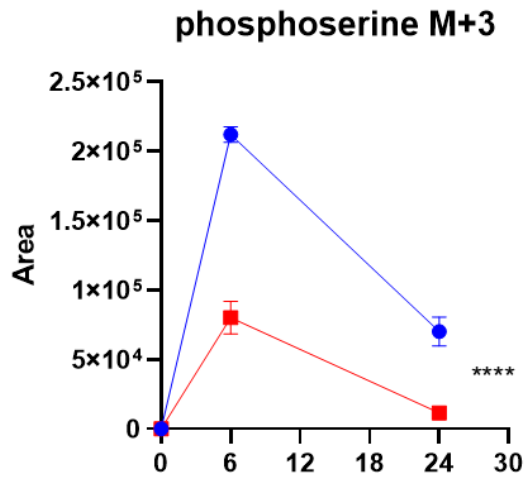
Examining the labelling patterns of the de novo serine/glycine metabolites revealed a decrease in total levels of phosphoserine at 6 and 24 h when MYC expression levels were reduced. Crucially, the levels of M+3 phosphoserine were reduced following MYC knockdown. In both MYC 2 (on) and MYC 2 (off), higher levels of phosphoserine were observed at the earlier time point (Figure 5.25 A). The total levels of serine were higher in the D425 MYC 2 (on) cells at 6 h although the reverse was true at 24 h where total levels of serine were greater in the D425 MYC 2 (off) cells. Isotopologue distributions of labelled serine in the D425 MYC 2 (on) cells showed greater levels of labelled serine species at both 6 and 24 h suggesting greater rate of de novo synthesis. The increase in total serine observed in the D425 MYC 2 (off) cell line was attributable to a rise in unlabelled serine suggesting uptake from the extracellular medium (Figure 5.25 B). Across both time points, total glycine levels were lower in the D425 MYC 2 (off) cells

when compared to their MYC expressing counterparts. Additionally, the levels of M+1 and M+2 glycine were higher in MYC 2 (on) cells.

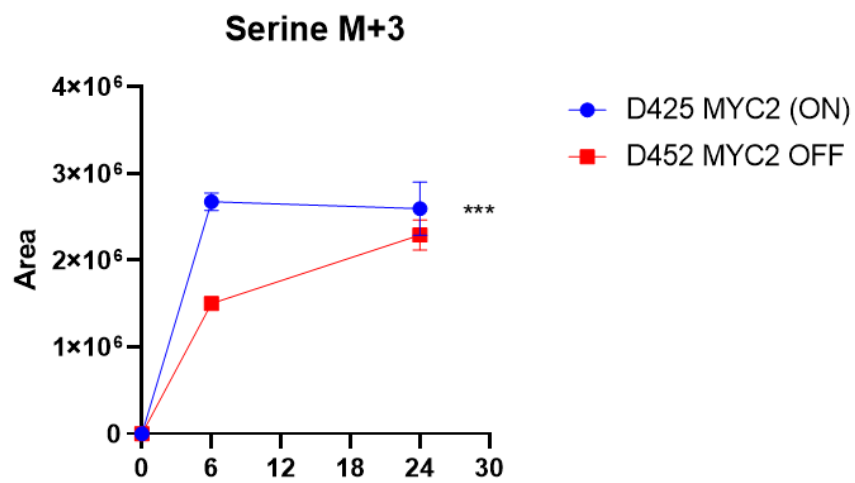
Notably, of the three metabolites measured within this pathway, total glycine was the only metabolite to increase at the 24 h time point in both MYC 2 (on) and MYC 2 (off) cell lines suggesting a more stable pool of this metabolite (Figure 5.25 C). Appreciating the rise in levels of unlabelled serine in the MYC 2 (off) cells at 24 h, evaluation of whether this phenomenon occurred in unlabelled glycine was considered. At 6 h, there was a marked difference in unlabelled glycine between MYC 2 (on) and MYC 2 (off) cells however this is diminished at 24 h. This observation would suggest the rate of uptake of glycine was in fact higher in MYC 2 (off) cells. To quantify this change, the difference in peak area of unlabelled glycine between the MYC 2 (on) and MYC 2 (off) cells were determined. Since peak area corresponds to intensity of metabolite signal and concentration, this would indicate whether unlabelled glycine was being accumulated from extracellular medium. The difference in peak area was 2.36×10^6 and 6×10^5 at 6 h and 24 h respectively (Figure 5.25 C). The diminishing difference between the MYC isogenic cell lines indicated acquisition of glycine through uptake or alternative sources.

Exploring the isotopologue distributions of uniformly labelled metabolites across the two time points enabled assessment of flux and labelling dynamics. The levels of M+3 phosphoserine peaked at 6h and fell dramatically in both cell lines (Figure 5.26 A). More importantly, labelling indicated higher turnover of M+3 phosphoserine in D425 MYC 2 (on) cells compared to MYC 2 (off) cells ($p < 0.0001$). Similarly, there was a sharp increase in M+3 serine in the first 6h, and this reached isotopic steady state in the MYC 2 (on) cells (Figure 5.26 B). In contrast, there was a steadier rise to similar M+3 serine levels in the D425 MYC 2 (off) cells indicating significantly lower flux of ^{13}C -glucose into the de novo pathway compared to the D425 MYC 2 (on) ($p = 0.0008$). Unlike its precursor metabolites, there was a slower rise in fully labelled M+2 glycine in the both conditions. The difference in M+2 glycine was more pronounced at 24 h (8.03×10^5) than at 6 h (2.58×10^5) which was in contrast trends observed in M+3 phosphoserine and M+3 serine. Nonetheless, MYC knockdown caused markedly lower M+2 glycine levels in the D425 MYC 2 (off) compared to D425 MYC 2 (on) ($p < 0.0001$) (Figure 5.26 C). Taken together, these findings detail upregulated de novo serine and glycine synthesis in the D425 MYC 2 (on) cells compared to its MYC 2 (off) counterpart. Labelling showed ^{13}C -glucose-derived serine and glycine was reduced in response to MYC knockdown suggesting MYC expression regulates flux of glucose intermediates into this biosynthetic branch.

A



B



C

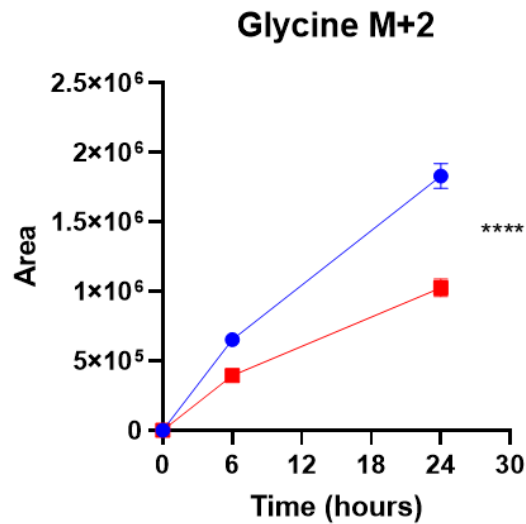


Figure 5.26 Time course on fully labelled serine related metabolites in D425 MYC 2 cell lines. Isotopologue distribution over 6 and 24 h in the D425 MYC 2 (on) and MYC 2 (off) cells A) O-Phospho-3-serine B) Serine C) Glycine. . Data represents \pm SD of three biological replicates. *** $p < 0.001$ and **** $p < 0.0001$ as determined by a Two-way ANOVA.

5.4 Discussion

5.4.1 HRMAS based metabolomics for the identification of novel MYC-driven changes

In this chapter, extensive analysis of *MYC*-driven rewiring of metabolism in MB_{GRP3} cell lines was undertaken. To my knowledge, this is the first study to interrogate the associations of *MYC*-amplification in MB_{GRP3} and cellular metabolism using metabolic profiling. Untargeted metabolomics using NMR spectroscopy and MS-based isotope labelling was used to elucidate changes in the metabolite profiles of *MYC*-amplified MB cells compared to isogenic equivalents with *MYC* knockdown. Distinct profiles were achieved between these groups in the three independent MB_{GRP3} cell line models used in this study. Furthermore, the identification of *MYC*-driven changes were validated by interrogating pathway dynamics and flux. Importantly, the upregulation of the *de novo* serine and glycine pathway as a feature across *MYC*- amplified MB cell lines was identified.

A key benefit of utilising this technique was that variations in a wide range of metabolites were quantified. HRMAS has been utilised for *ex vivo* profiling studies to establish tumour associated metabolic characteristics. In particular HRMAS profiling has previously highlighted distinct features of normal brain tissue compared to malignant transformed cancer cells (Fuss and Cheng, 2016). Furthermore, other studies have utilised this technique for correlating tumour grade with metabolite changes. Although this study focused on *in vitro* profiling of MB_{GRP3} cell lines, there remains scope and compatibility of coupling findings found here with *ex vivo* profiling of *MYC*-amplified patient samples to establish more clinically relevant signatures. It also provides motivation for validating *in vivo* MRS measurement of specific metabolites.

Untargeted metabolomics using HRMAS identified alterations in the metabolic profiles of *MYC*-amplified MB cell lines when *MYC* levels were modulated and this was particularly noticeable in the *MYC* 2 bearing cell lines. Several multivariate techniques analysing both spectral bins and relative metabolite concentrations were used to identify the underlying metabolic alterations that were dependent on *MYC* expression. Utilising both individual analysis and joint analysis of both data types aided in the identification of consistent metabolite changes between *MYC* (on) and *MYC* (off) cell lines. Spectral binning requires very little processing and provides an unbiased method extrapolating

differences in the metabolite information contained within spectra when comparing different sample groups. However, the relative metabolite concentrations enable biological extrapolation and identifiable pathway associations. These two different methods enabled discovery and validation of these novel metabolite changes.

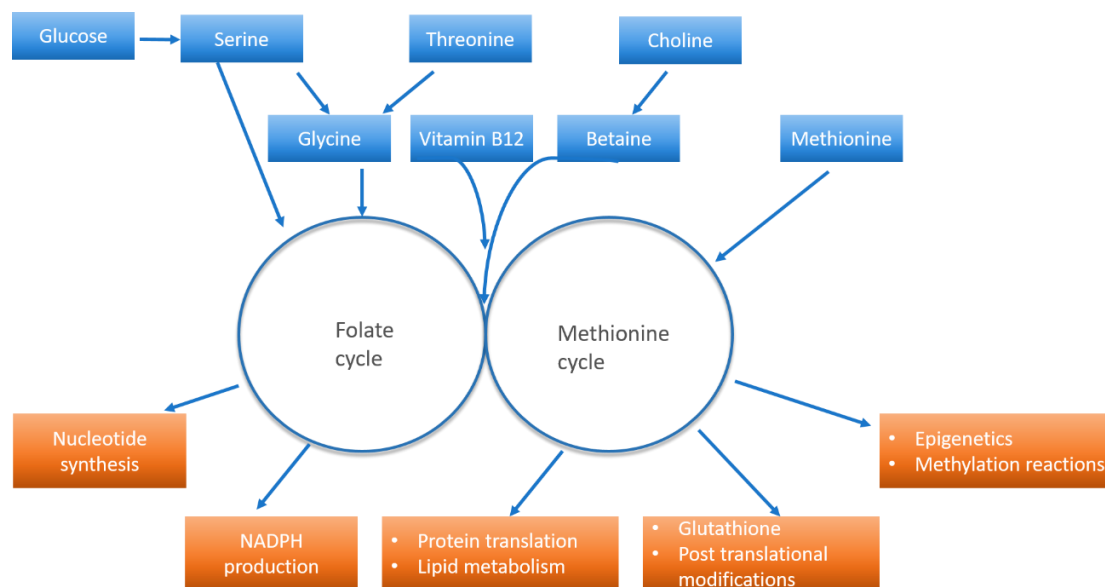


Figure 5.27 Schematic of simplified one carbon metabolism.

In this study, elevation of glycine and choline was detected when MYC expression was knocked down in D425, D283 and HDMB03 cell lines. Metabolic profiling in combination with SIRM carried out in this chapter, has highlighted MYC-dependent dysregulation of the de novo serine and glycine synthesis pathway in MYC-amplified MB_{GRP3} cell lines. Glycine and choline are highly interconnected in sustaining one carbon pools required for folate and methionine cycles (Figure 5.27). These downstream pathways provide anabolic substrates required for nucleotide synthesis and methylation reactions. The conversion of serine to glycine by SHMT1/2, and subsequent cleavage by the glycine cleavage system provides methyl donors for the methylated forms of tetrahydrofolate (THF) required for biosynthesis of purines and thymidylate. Pemetrexed is an antifolate that acts on dihydrofolate reductase (DHFR) and thymidylate synthase (TYMS) and exerts antineoplastic activity. Unlike its predecessor methotrexate, Pemetrexed acts directly on the aforementioned enzymes to reduce THF-dependent reactions rather than depleting cofactors required for these reactions (Chattopadhyay et al., 2007). Interestingly, the combination of Pemetrexed and gemcitabine has been shown to be more effective against MYC-amplified medulloblastoma over SHH

medulloblastoma in orthotopic mouse models, consistent with the over-activation of this pathway as a distinctive feature of *MYC*-amplified Group 3 MB (Morfouace et al., 2014). Phase II clinical evaluation of this combination therapy is on-going (NCT01878617) (Bautista et al., 2017). Whilst, earlier studies have highlighted anti-metabolite drug combination strategies that are effective at targeting *MYC*-amplified MB_{GRP3}, this study reveals pathway dysregulation of serine and glycine biosynthesis associated with *MYC* which provides supportive and mechanistic evidence to the therapeutic efficacy of these inhibitors. Furthermore, although methotrexate is not extensively used in paediatric oncology settings, recent studies have highlighted improved risk stratification and adaptation which has aided its clinical utility and improved outcomes in carefully selected patients (Pompe et al., 2015). Together these investigations support our findings and highlight the potential therapeutic targeting of these pathways in medulloblastoma and in particular *MYC*-amplified tumours.

In this study, higher levels of choline were observed in MB cells upon *MYC* knockdown. In fact, this signature was the most profound of the metabolite alterations observed in the study. The degradation of choline also provides one carbon units through the production of betaine which then facilitates the remethylation of homocysteine to generate methionine. The regeneration of methionine is particularly important to sustain substrates for the enzyme S-adenosylmethionine synthetase which produces SAM, the major methyl donor for DNA, RNA and lysine/arginine protein methylation reactions (Ducker and Rabinowitz, 2017). In addition to its role as a one carbon donor, choline is an important nutrient in maintaining phospholipid biosynthesis. Although phospholipid membrane turnover is increased in cancer cells due to increased proliferation, it is not the only physiological process that accounts for the rise in choline metabolites observed in cancer. Interestingly, stimulation of proliferation in non-malignant cells does not recapitulate the abnormal choline phenotype observed in cancers cells (Aboagye and Bhujwala, 1999). The tumour microenvironment has been shown to influence choline metabolism. Choline kinase α is a HIF1 responsive enzyme and the rise in phosphocholine levels during hypoxia is attributable to its activity in a prostate cancer model (Glunde et al., 2008).

It was not entirely clear the reason for increased levels of choline in our model. In the MB_{GRP3} *MYC*-regulable cell lines, although choline is elevated and most abundant choline-containing metabolite in *MYC* (off) cells, phosphocholine and glycerophosphocholine (only observed in the HDMB03 cell lines) levels vary in the cell lines. For instance, in the D425 *MYC* 2 (off) cells, phosphocholine is reduced whereas

the reverse is true for the D283 MYC (off) cells. In the HDMB03 MYC (off) cells, phosphocholine levels remained relatively unchanged however, glycerophosphocholine levels increased when MYC was knocked down. There may be differences in the intermediary metabolism of choline or sources of choline, either from breakdown of phosphatidylcholine from lipid droplet sources or uptake from extracellular sources which may account for the differences observed in the three cell lines. Due to the rise in SIRM in metabolomics, there are various stable isotope tracers that are becoming readily available which is enabling evaluation of more metabolic pathways. The use of ^{13}C choline could illuminate the alterations and pathway activity that may be associated with MYC in MB. Choline is also readily detectable using *in vivo* MRS which has highlighted upregulated choline metabolism as a feature of numerous human cancer types including brain, breast and prostate (Glunde et al., 2011). Understanding its role in MYC-driven MB could offer opportunities as a biomarker, diagnostic tool and for prognostication. Additionally therapeutic targeting of choline metabolism could benefit treatment of MYC-amplified MB. Indeed, one study has linked the overexpression of MYC to aberrant choline metabolism in lymphoma through its transcriptional regulation of PCYT1A which was targetable in a MYC-dependent manner (Xiong et al., 2017). Additionally, targeting of CK α in GBM reduced invasiveness and expression of EMT genes particularly in the stem cell population which was associated with the choline phenotype observed (Koch et al., 2016).

5.4.2 MYC expression influences usage of the *de novo* serine and glycine pathway

The dynamics of the *de novo* serine and glycine pathway was further interrogated using ^{13}C glucose tracer analysis. By probing this pathway, the partitioning of glucose into the *de novo* serine and glycine pathway was observed to be greater in MYC expressing cells compared to when MYC was knocked down. The significance of endogenous production of both serine and glycine is now widely established in cancer metabolism. For instance, consumption of glycine was highly correlated with proliferative rates in cancer (Jain et al., 2012). However, others have shown that it is serine levels which are important in fuelling the folate cycle and thus providing substrates required for nucleotide synthesis (Labuschagne et al., 2014). In the initial untargeted profiling, elevated levels of glycine following MYC knockdown were detected. Conversely, isotopic labelling revealed greater levels of glycine in the MYC (on) cells which was notably different from HRMAS profiling results. Although the two techniques might initially appear contradictory,

sources of glycine were indistinguishable in the untargeted profiling. It was proposed that the uptake of exogenous glycine was higher in the MYC (off) cells despite overall glycine levels being lower. Although the overall doxycycline treatment was carried out for 72 h in both types of metabolomics studies, isotopic tracing was limited to 24 h. An extended labelling time period is needed to further establish whether total glycine levels in MYC (off) surpass that of the MYC (on) cells and particularly whether this is driven by uptake from extracellular medium. Importantly, further time points would allow for isotopic steady state of glycine to be reached, if indeed it could as seen in the case of serine (Figure 5.26). Interestingly, uptake of exogenous serine was also greater in the MYC (off) cells which actually increased overall levels of serine even with reduced flux of the *de novo* serine pathway. This observation suggests distinct mechanisms/ sources for intracellular levels of serine and glycine.

Our data suggests that overexpression of *MYC* is associated with the amplification of the *de novo* serine and glycine synthesis pathway. The switch from *de novo* synthesis to extracellular uptake was evident when *MYC* was knocked down and may be associated with a differentiated phenotype. Upon loss of *MYC*, MB_{GRP3} cells were more adherent, and expressed genes associated with a differentiated state (Swartz, 2018). This feature is supported by several other studies which have associated *MYC* with stemness and self-renewal capacity alongside repression of differentiation genes (Smith et al., 2010, Varlakhanova et al., 2010). The hypothesis of exogenous uptake being more closely associated with a differentiated state is highlighted by the supply and availability of serine and glycine in the brain microenvironment. Glycine is an important neurotransmitter in the brain and functions additionally as a co-agonist of NMDA receptors. D-serine is an even more potent a co-agonist of NMDA receptors and its generation is dependent on L-serine. During foetal development, there is high activity of the *de novo* serine and glycine pathway due to the requirement for biosynthetic substrates essential for the intense burst of proliferation required during early development. With the formation of the blood brain barrier in the latter stages of foetal development, the brain occludes various metabolites including serine and glycine and is reliant on *de novo* synthesis of these metabolites. In the case of L-serine, *de novo* synthesis is predominantly restricted to astrocytes which supply terminally differentiated neurones with L-serine required for D-serine synthesis.

Although the cell lineage for MB_{GRP3} had remained elusive, advances in single cell transcriptomics is aiding in delineating the developmental architecture and features of medulloblastomas. Particularly for MB_{GRP3}, the current consensus suggests that these tumours likely originate from an early cerebellar progenitor which is nestin positive and can give rise to the various glial and neuronal lineages (Hovestadt et al., 2019, Vladoiu et al., 2019). Interestingly, *MYC* amplification is thought to potentiate this undifferentiated state characterised by a high proportion of cells displaying this phenotype (Hovestadt et al., 2019). The characteristics of MB_{GRP3} tumours may resemble features of their cell of origin. This could explain why under reduced expression of *MYC*, MB cells revert to being dependent on the availability of serine and glycine from extracellular sources. From these results the hypothesis generated was that *MYC*-amplified MB_{GRP3} tumours would be more susceptible to the targeting of the *de novo* serine and glycine pathway, which is required to maintain the hyper-proliferative state observed in these tumours which is explored in the next chapter.

5.4.3 Study limitations

Although this study has shed light on the metabolic pathways associated with overexpression of *MYC*, there were some constraints on experiments. HRMAS profiling would benefit from additional samples, such as in the case of HDMB03 *MYC* 3 cell lines to conclusively define impact on metabolites. One of the difficulties encountered in this study was attributed to leakiness of the *MYC* 3 shRNA. One of the benefits of inducible shRNA systems is that they allow direct association of a particular phenotype to expression of a specific protein. Whilst stable shRNA knockdown or CRISPR-mediated knockouts provide efficient mechanisms of reducing/depleting expression levels, long-term depletion of *MYC* could result in deleterious effects such as induction of apoptosis or senescence. This would limit the opportunity to determine some phenotypic or metabolic consequences of *MYC* perturbation and as such was not considered appropriate for this study. Possible experiments, which could further improve association of *MYC* KD with metabolite alterations, could be rescue experiments where doxycycline treatment is removed enabling re-expression of *MYC* and profiling the metabolic consequences. Timepoint studies could also be beneficial in evaluating the dynamics of alterations in metabolism, although the high cell number requirement of HRMAS may not be the ideal and other technologies such as MS could be considered. Although HRMAS profiling provided the opportunity to profile clinically detectable metabolites, MS with its greater coverage of the metabolome could further magnify the metabolic reprogramming in the MB_{GRP3} *MYC*-regulable cell lines. While using ¹³C -labelling enabled evaluation of pathway activity, definitive conclusions of isotopologues could not always be established. In the case of serine M+1 or M+2, the specific origin of these metabolites could not be determined. Since MS only informs on mass, position of ¹³C could not be identified and pathway of origin of these labelled species could not be deciphered. ¹³C -labelling coupled with NMR spectroscopy could further shed light on this.

Chapter 6. Exploiting upregulation of the *de novo* serine and glycine synthesis pathway as a novel therapeutic strategy for *MYC*-amplified medulloblastoma

6.1 Introduction

In the previous chapter, we uncovered upregulation of the *de novo* synthesis (i.e. glucose derived) of serine and glycine to be a feature of *MYC*-amplified MB_{GRP3} cells. Metabolic reprogramming has expanded beyond the two most studied nutrients namely glucose and glutamine to explore the contributions of other metabolic substrates and their impact on oncogenesis. Recent advances demonstrate the requirement for not only glucose but various amino acids and vitamins to fuel several cellular outputs including synthesis of nucleotides, proteins, maintenance of redox balance and genetic and epigenetic landscape of cancer cells through nucleic acid and protein methylation (Ducker and Rabinowitz, 2017). One carbon metabolism encompasses the folate and methionine cycle in addition to the trans-sulphuration pathway, and is a vital integrator of nutrient status coupling input of one carbon units derived from several metabolites which in turn, fuels a series of chemical reactions that supports anabolic metabolism (Ducker and Rabinowitz, 2017, Newman and Maddocks, 2017, Lukey et al., 2017).

Serine and glycine provide methyl donors that enable maintenance of cycling of these systems and their importance is highlighted in autosomal recessive inborn errors of amino acid metabolism characterised by deficiencies either in synthesis or cleavage systems (de Koning et al., 2003, Razak et al., 2017). In the case of serine, genetic defects in PHGDH, PSAT and PSPH are the hallmarks of low plasma and cerebrospinal serine concentrations that lead to neurological symptoms including seizures and microcephaly (van der Crabben et al., 2013). Neuro-metabolic disorders arising from abnormal glycine metabolism are often associated with defects in the glycine cleavage system resulting in elevated glycine concentrations in CSF. Similarly to serine, this typically leads to seizures and various other neurocognitive deficits (Hennermann et al., 2012). These very rare disorders highlight the importance of the synthesis and subsequent utilisation of serine and glycine in normal physiological processes.

Although earlier studies revealed associations between the serine and glycine synthesis pathway (SGP) and cancer, recent advances in SIRM are putting this pathway at the forefront of abnormal metabolism observed in cancer. Early studies in rat carcinomas highlighted imbalances of enzymes involved in serine and glycine metabolism (Snell, 1984, Snell and Weber, 1986). In particular these studies highlighted how tumour cells co-opted the *de novo* serine and glycine synthesis pathway (SGP) to enable proliferation, a characteristic not observed in non-neoplastic tissues (Snell et al., 1987). Extensive

profiling of metabolism performed by Jain and colleagues, underscored the requirements of tumour cells for glycine. Using the NCI-60 cancer cell panel and utilising metabolite consumption and release profiling, they found high consumption and synthesis rates of glycine correlated with rapid proliferation. Importantly, compartmentalisation of glycine biosynthesis influenced its association with proliferation with the mitochondrial pathway involving SHMT2, MTH1DL and MTHD2 correlating to proliferation and not their cytosolic equivalents (Jain et al., 2012). Subsequent studies demonstrated serine availability as the crucial determinant of glycine utilisation. These studies showed the consumption of serine and not glycine was intricately linked with proliferation and the maintenance of nucleotide pools (Labuschagne et al., 2014).

In the absence of exogenous serine, glycine cleavage alone does not sustain nucleotide pools. Moreover, PHGDH amplified cells with high activity of SGP are less reliant on exogenous sources of serine and glycine, and in fact have high glycine efflux rates (Labuschagne et al., 2014). In addition to sustaining cellular nucleotide pools, serine availability maintains the epigenetic landscape of cancer cells. Serine starvation reduced *de novo* ATP synthesis, disrupting the methionine/SAM ratio and reducing supply of methyl units required for methylation of DNA and RNA (Maddocks et al., 2016). It is likely that usage of serine and glycine is context dependent and is influenced by genetic background and microenvironment cues.

As previously discussed, *MYC* regulates several nodes of cellular metabolism. Transcriptomic profiling and ChIP-seq studies have demonstrated its ability to bind to E box regions of several enzymes involved in the SGP including PHGDH, PSAT, PSPH, SHMT2 and GLDC. Aside from direct *MYC*-dependent regulation of SGP, *MYC* acts in concert with other transcription factors to regulate the activity of this pathway. NFR2 functions as a mediator of the antioxidant response by targeting antioxidant response element (ARE)-driven and SGP including PHGDH and SHMT2, which in turn support glutathione production (DeNicola et al., 2015). ATF4 is implicated in *MYC*-driven responses. Interestingly, ATF4 has been found to co-occupy promoter regions of *MYC* targets, particularly those involved in amino acid metabolism and protein synthesis (Tameire et al., 2019). *MYC* has also been shown to facilitate a feedforward regulatory mechanism which sees the upregulation of AA transporters SLC7A5 and SLC43A1 import and cause elevations in essential AAs. This in turn promotes *MYC* mRNA translation which cycles back to promote *MYC*-dependent transcriptional programmes. Depletion of SLC7A5 or SLC43A1 disrupts both *MYC* and *MYCN* expression in Daudi

and BE-2C cells (Yue et al., 2017). Additionally, the activity of *MYC* enables progression under difficult growth environments. For instance, depletion of glucose or glutamine activated SGP via a *MYC*-dependent stress induced response to support nucleotide synthesis, cell cycle progression and glutathione generation (Sun et al., 2015). *MYC* is therefore capable of enhancing the activity of SGP to promote tumour progression. Interestingly, the usage of serine or glycine in proliferating tumour cells differs from that of non-cancerous cells. Using *ex vivo* matched resected samples from NSCLC patients, Fan and co-workers demonstrated a preference for glucose-derived carbons for purine synthesis via the *de novo* SGP pathway in NSCLC tumours compared to their corresponding normal lung tissue which also displayed lower expression of *MYC* (Fan et al., 2019). PHGDH has been shown to be responsible for diverting glycolytic flux to the SGP pathway (Locasale et al., 2011). Understanding these differences that exist between cancer cells and untransformed cells could benefit cancer therapy targeting the *de novo* SGP and one carbon metabolism.

It is clear that the metabolic pathways associated with serine and glycine play an important role in cancer cell proliferation. Targeting these pathways which tumour cells rely on, must be approached taking into account the dynamics of the tumour microenvironment and substrate availability. For some cancers, dietary restriction of serine and glycine has been shown to slow tumour progression and prolong survival (Maddocks et al., 2017). *MYC* activated lymphomas respond to serine/glycine deprivation *in vivo* however, *KRAS*-driven intestinal tumour do not. This is chiefly a result of upregulated expression of SGP enzymes which combats the lack of exogenously available serine and glycine (Maddocks et al., 2013, Maddocks et al., 2017). The capacity to upregulate enzymes of the SGP is not always a determinant of response to serine/glycine deprivation. For instance activated T cells increase expression of enzymes involved in the SGP and one carbon metabolism however, diet restriction of serine impacted the pathogen-dependent T-cell expansion without affecting immune cell homeostasis *in vivo* (Ma et al., 2017). Furthermore, genetic background modulates response to serine and glycine restriction. Particularly, activation of p53 promotes cell survival attributable to prolonged G1, activation of the SGP and diversion of carbons towards glutathione synthesis thus maintaining anti-oxidant capacity (Maddocks et al., 2013).

Another method for modulating serine and glycine availability is to directly inhibit the activity of enzymes involved in the pathway. Upregulation of PHGDH has been shown

to be beneficial to tumours arising in locations with low physiological concentrations of serine and enables faster tumour growth (Sullivan et al., 2019). The first committed step of *de novo* serine synthesis is via the activity of PHGDH which oxidises the glycolytic intermediate 3-phosphoglycerate diverting it into the biosynthesis pathway. Previous studies have highlighted a direct role for PHGDH in cancer. A large scale analysis of frequent copy number variation revealed a region not previously attributable to any known oncogenes with high focal amplifications belonging to the locus harbouring PHGDH gene (Beroukhim et al., 2010). Overexpression of PHGDH has been correlated with worst prognostic outcomes in several tumours including breast, lung and neuroblastomas (Noh et al., 2014, Zhang et al., 2017, Zhu et al., 2016)(Liu *et al.*, 2016). High proportions of ER-negative breast cancer have been observed to have copy number gains of PHGDH and this characteristic is associated with aggressiveness and stemness (Possemato et al., 2011). Furthermore, overexpression of PHGDH has also been correlated with tumour staging and metastasis in lung cancer (Zhu et al., 2016).

Direct targeting of SGP has been facilitated by inhibitors of PHGDH and has energised efforts to target this pathway for therapeutic interventions (Mullarky et al., 2016, Pacold et al., 2016, Wang et al., 2017). Several small molecule inhibitors with varying modes of inhibition now exist and are continually being developed. The PHGDH inhibitor NCT503 is an allosteric inhibitor, targeting the NAD⁺ binding domain of the PHGDH enzyme that has been shown to be effective against PHGDH amplified breast cancer *in vitro* and *in vivo* (Pacold et al., 2016). Similarly, the compound CBR5884 which disrupts oligomerisation state of PHGDH has shown similar effects in PHGDH-amplified breast cancer cell lines (Mullarky et al., 2016). ¹³C tracers have shown that inhibition of PHGDH causes a reduction in glucose-derived serine accompanied by decrease in growth and proliferation. Remarkably, PHGDH inhibition by NCT503 caused a decline in one-carbon units assimilated into the nucleotide from both glucose (i.e. *de novo* synthesis) and exogenous serine (Pacold et al., 2016). Furthermore, inhibition of PHGDH appears to affect other aspects of cellular metabolism, namely central carbon metabolism and the TCA cycle. Kinetic flux profiling following ¹³C -glucose labelling revealed a reduction in PPP-derived ribose and a decrease in nucleobases generated from TCA anabolism which further disrupted nucleotide synthesis. Additionally, a combination of ribose and α -ketoglutarate rescued PHGDH inhibited cells (Reid et al., 2018). Although direct targeting of PHGDH has yielded positive outcomes in a myriad of cancer contexts, others have shown effective targeting of PHGDH via other mechanisms.

Indeed, targeting co-factor generating pathways have also revealed similar findings to direct targeting. The activity of PHGDH relies on NAD⁺ and inhibition of the NAD⁺ salvage pathway in PHGDH amplified breast cancer cell lines has been shown to disrupt serine synthesis (Murphy et al., 2018). A recent study has demonstrated *MYCN*-dependent sensitivity towards PHGDH inhibition. Upregulation of SGP enzymes due to the *MYCN*/ATF4 axis renders *MYCN*-amplified neuroblastoma susceptible to targeting of the *de novo* SGP (Xia et al., 2019). Furthermore, overexpression of PHGDH and other SGP enzymes are associated with HIF-dependent acquisition of drug resistance. Treatment with PHGDH inhibitors restored sensitivity to Erlotinib in EGFR-activated lung carcinomas and increased response to HIF2 α antagonists in renal cell carcinoma (Dong et al., 2018, Yoshino et al., 2017). It has been demonstrated that the inhibition of SGP via targeting of PHGDH may prove useful to PHGDH amplified cancers and other genetic backgrounds that upregulate serine and glycine synthesis.

Further efforts into targeting other enzymes in the SGP yielded a dual inhibitor of SHMT1/2 which was particularly potent against DLBCL cell lines with defective glycine import (Ducker et al., 2017). Others have identified more hit compounds against both SHMT isoforms although these compound are not yet widely available (Bartosik et al., 2018, Nonaka et al., 2019). Nevertheless, with increasing evidence of how crucial the contribution of serine and glycine metabolism is to tumourigenesis, targeting these pathways could provide novel therapeutic strategies for many cancers.

Experiments carried out in Chapter 5 of this study highlighted differences in serine and glycine utilisation in our engineered *MYC*-amplified MB_{GRP3} cell lines following *MYC* knockdown. In this chapter I probed whether *MYC*-driven reprogramming of the SGP provides a distinctive metabolic vulnerability to *MYC*-amplified MB_{GRP3} cells which may render these cell vulnerable to therapeutic targeting.

6.2 Aims

Results from metabolic profiling indicated that the *de novo* serine and glycine production may be a characteristic of *MYC*-amplified MB_{GRP3} cells. This feature was abrogated following *MYC* knockdown suggesting *MYC*-amplification contributed to this phenotype. The aim of this chapter was to explore therapeutic targeting of the *de novo* serine and glycine pathway as a novel strategy for *MYC*-amplified MB_{GRP3}. The objectives are outlined as follows:

- To examine the gene expression of serine and glycine metabolism related genes in MB_{GRP3} patient cohorts.
- To investigate PHGDH expression across MB subgroups and their correlation with survival outcomes
- To investigate pharmacological and genetic manipulation of PHGDH in MB_{GRP3} cell lines
- To elucidate the phenotypic effects and stress responses associated with PHGDH manipulation.

6.3 Results

6.3.1 Establishing clinical relevance of the serine and glycine pathway in medulloblastoma patient cohorts

6.3.1.1 Gene expression changes in the serine and glycine pathway in MB_{GRP3}

It was previously highlighted that significant differences exist in the *de novo* SGP in the engineered MB_{GRP3} cell line models. In order to establish the importance of this pathway, gene expression signatures of the SGP were investigated in MB patient samples to establish clinical relevance of the pathway. This undertaking was critical as it would indicate whether our previous observations of changes within the SGP were an *in vitro* phenomenon or whether indeed it was a feature of primary MB_{GRP3} *MYC*-amplified tumours which could further support the rationale of targeting this pathway as a therapeutic intervention.

To determine altered SGP in MB_{GRP3}, the RNA expression data from two primary MB_{GRP3} cohorts were analysed; Newcastle cohort data generated from RNA-seq (n= 36) and the Cavalli cohort generated from gene expression microarrays (n= 144)(Cavalli et al., 2017). Using the Cavalli *et al.*, dataset, differential gene expression analysis of the SGP was conducted between the MB_{GRP3} subtypes (subtypes and *MYC* abnormalities detailed in Appendix 8.38). Of the 40 genes involved in the SGP according to the Kyoto encyclopaedia of genes and genomes (KEGG), 17 were found to be significantly altered in the MB_{GRP3} subtypes. Subsequent heatmap and clustering analysis highlighted the striking differences in the SGP signatures of MB_{GRP3} tumours according on subtypes (Figure 6.1). A cluster family containing largely Group 3 α samples is separated from the Group 3 β and 3 γ samples. Interestingly, these latter groups contain more *MYC*-amplifications and *MYC* gain samples compared to Group 3 α .

Since the Cavalli *et al.*, cohort did not definitively classify *MYC* amplification status, these results were validated with this SGP signature in the Newcastle cohort with known *MYC*-amplification status in the MB_{GRP3} tumour samples. As illustrated by Figure 6.2, most *MYC*-amplified MB_{GRP3} samples cluster distinctly from the non-amplified samples. Furthermore, upregulation of SGP genes was observed in *MYC*-amplified tumours compared to their non-amplified counterparts. Of the genes that were upregulated in *MYC*-amplified tumours, *PHGDH*, *PSAT1*, *SHMT2* and *GLDC* were identified amongst other genes. In contrast, non-amplified tumours highly expressed *MAOA*, *SARDH*, *PIPOX* and *BPGM*. It is noteworthy to highlight *SARDH* and *PIPOX* which are capable of generating glycine from sarcosine, a metabolite involved in choline metabolism. Furthermore *MYC*-amplified tumours had elevated expression of CBS which commits serine to the transulphuration pathway which ultimately generates glutathione. These observations highlighted variations in serine glycine metabolism in MB_{GRP3} tumours.

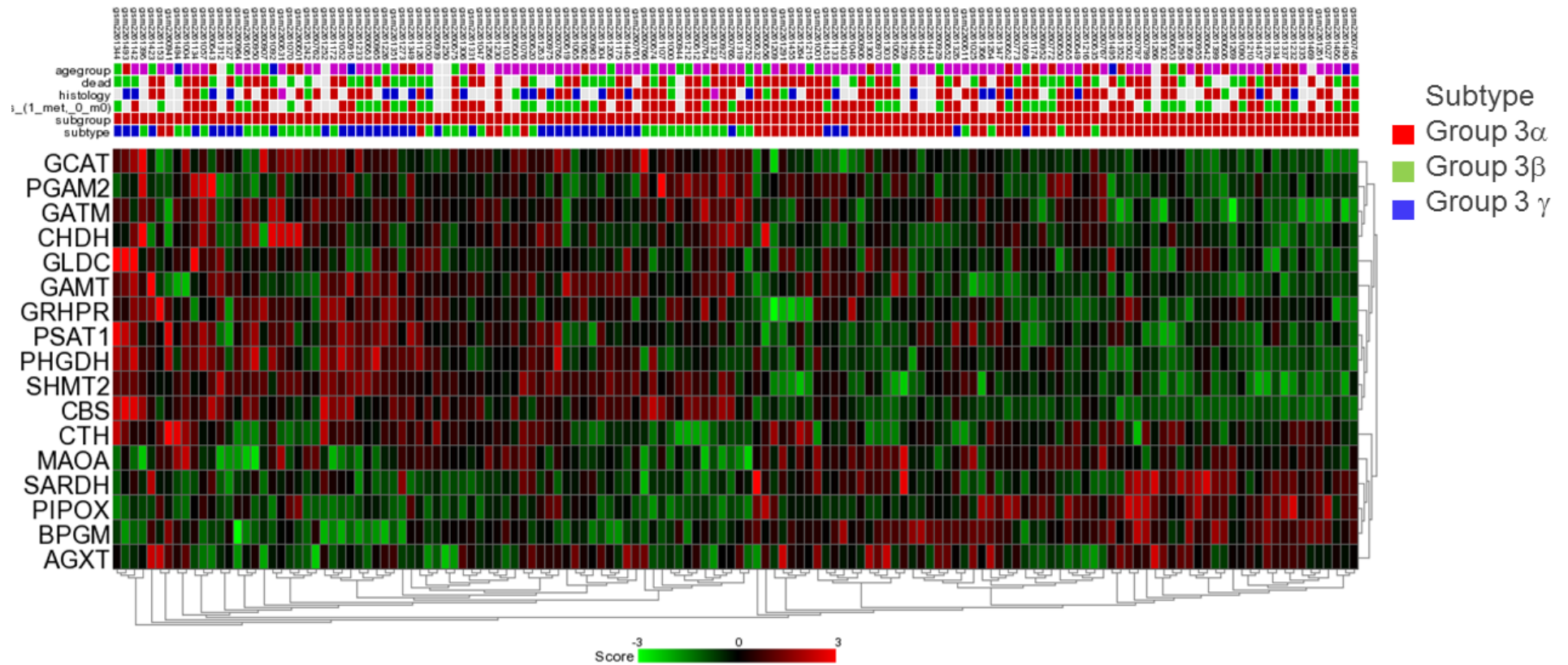


Figure 6.1 Gene expression profiling of the serine and glycine metabolism in the Cavalli et al., MB_{GRP3} dataset. Hierarchical clustering and heatmap visualisation of the 17 differential genes in the serine and glycine pathway in MB. Heatmap was generated using R2 genomic analysis and visualisation platform. Expression values are z-score transformed and hierarchical clustering performed using Euclidean distances. Z-score ranges are indicated by green, black and red colour keys. MB_{GRP3} are further classified in the Cavalli cohort into 3 subtypes based on MYC features.

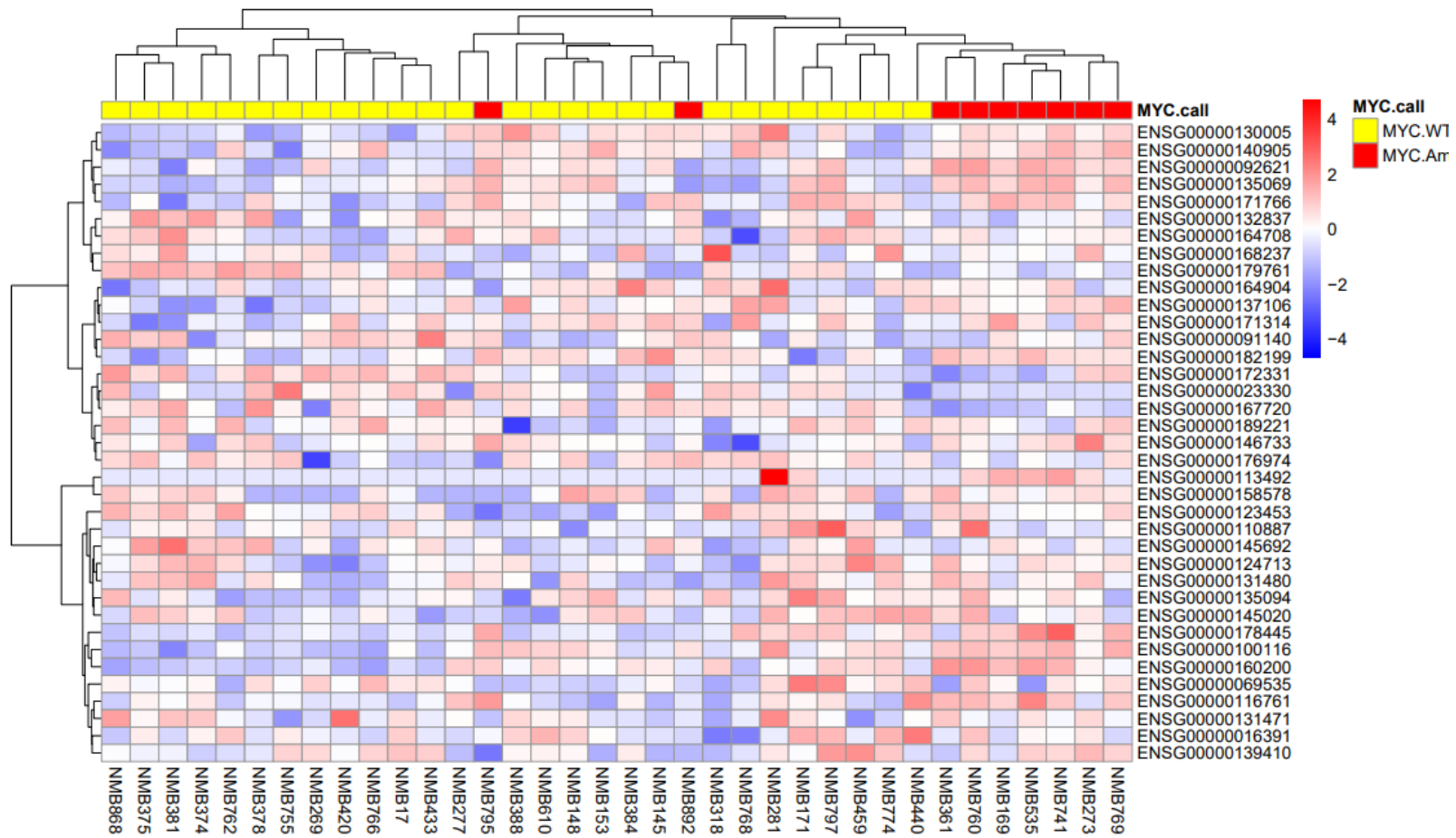


Figure 6.2 Gene expression profiling of serine and glycine metabolism-associated genes in MYC-amplified and non-amplified MB_{GRP3} patients in the Newcastle dataset. Hierarchical clustering and heatmap visualisation of the 17 differential SGP genes signature from Cavalli et al., dataset.. Expression values are z-score transformed and hierarchical clustering performed using Ward distances. Z-score ranges are indicated by red, white and blue colour keys.

6.3.1.2 Assessing protein expression of PHGDH in a tissue microarray cohort of medulloblastomas

Gene expression analysis has highlighted differential signatures of the SGP in *MYC*-amplified MB_{GRP3} compared to their non-amplified counterparts, highlighting that this pathway may provide an opportunity for clinically-relevant therapeutic targeting. Although gene expression programmes are important for highlighting pathway changes, it was important to examine protein expression of potential targets for drug targeting. The expression of PHGDH was probed using tissue microarrays (TMA) comprising all four MB groups. Construction of TMA and immunohistochemical staining of PHGDH was performed by Dr Steve Crosier and subsequent analysis of intensity staining performed independently. The TMAs used in this study included 183 unique patient samples with clinicopathological annotation shown in Table 6.1. These covered the four molecular subgroups of MB (MB_{GRP3}, MB_{Grp4}, MB_{SHH}, and MB_{WNT}). Importantly, the TMA cohort was highly concordant with, and representative of previously established clinical and histological features of MB (Table 6.1).

As previously mentioned, PHGDH is the rate limiting and committing step of *de novo* serine and glycine synthesis. Furthermore, currently the most widely available targeting of SGP is via small molecule inhibition of PHGDH, thus making this an appropriate candidate for interrogating at protein expression level (Wang et al., 2017, Mullarky et al., 2016, Pacold et al., 2016). Immunohistochemical staining for PHGDH was performed on 4 TMAs (n= 183 patient samples) containing duplicate samples from two discrete tumour regions originated from a tumour sample. TMAs included cerebella samples (n=9) and to assess differences between tumour samples and normal cerebellar in addition to several staining controls used to assess quality of immunohistochemical staining (Appendix 8.39). A PHGDH intensity score was determined for each patient sample (Intensity scoring details summarised in Chapter 2) and matched to their clinicopathological measures for subsequent analysis.

Table 6.1 Clinicopathological features of TMA cohort compared to Schwalbe et al., 2017 medulloblastoma cohort.. Data presented as n(%) where appropriate.

		TMA cohort	Schwalbe et al., 2017
Cohort size		n=183	n=428
Age at diagnosis (median)		5.36	6.34
Sex	M	119 (66%)	278 (65%)
	F	60 (34%)	150 (35%)
Resection	GTR	134 (83%)	285 (74%)
	STR	27 (17%)	98 (26%)
Histology	CLA	104 (62%)	276 (70%)
	DN/MBEN	41 (24%)	58 (15%)
	LCA	21 (13%)	60 (15%)
	MBNOS	2 (1%)	34
MYC	Amplified	12 (7%)	22 (5%)
	Non-amplified	171 (93%)	404 (95%)
MYCN	Amplified	15 (8%)	29 (7%)
	Non-amplified	168 (92%)	397 (93%)
Metastatic stage	M+	47 (28%)	104 (27%)
	M0	123 (72%)	285 (73%)
Subgroup	WNT	12 (7%)	33 (8%)
	SHH	58 (32%)	109 (26%)
	GRP3	59 (32%)	130 (31%)
	GRP4	53 (29 %)	153 (36%)

Firstly, median PHGDH intensity scores of the MB tumours were compared to cerebella samples to examine whether PHGDH expression differed from normal tissue and also to establish a baseline for PHGDH expression in the brain. Median expression was utilised since this parameter was less sensitive to outliers and more accurately represents the distribution of data. This comparison revealed MB tumour overall had higher PHGDH staining compared to cerebella, with median intensity score of 178 and 157 respectively ($p=0.016$). The caveat here was that these are non-matched comparisons as the cerebella samples were obtained post-mortem. Nonetheless, our analysis suggests tumour-specific alterations in PHGDH protein expression in MB.

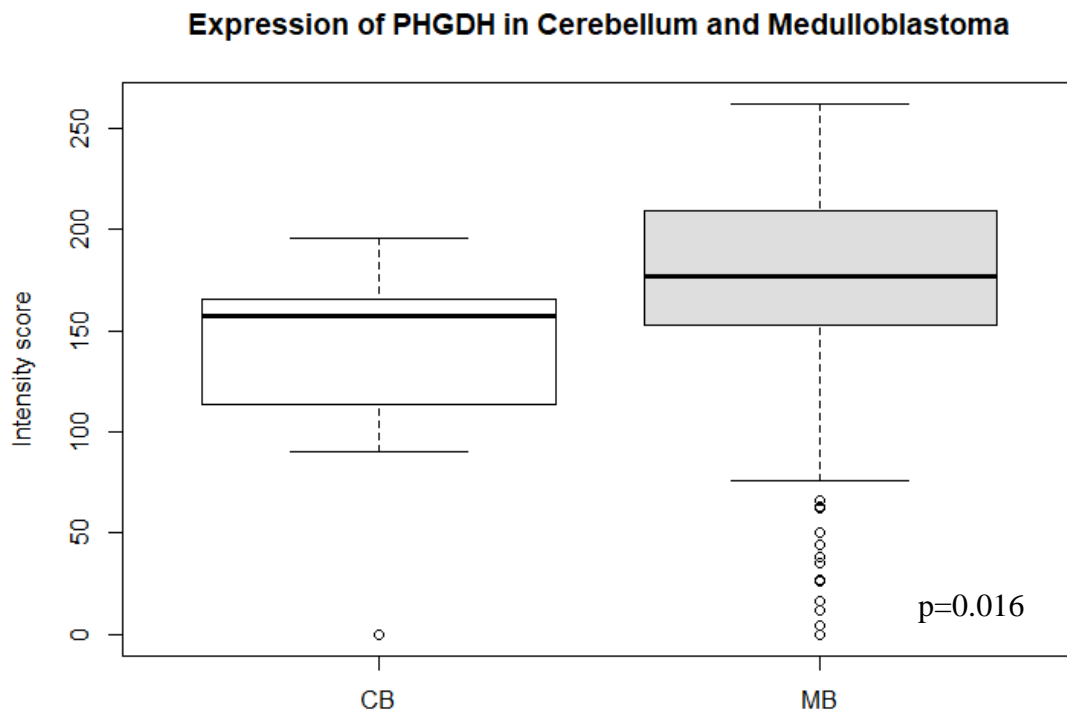


Figure 6.3 Comparison of PHGDH expression in cerebellum and medulloblastoma tumour samples. Boxplots displaying upper and lower quartiles and median of PHGDH intensity scores across cerebellum ($n=9$) and MB tumours including MB_{GRP3} , MB_{Grp4} , MB_{SHH} and MB_{WNT} tumours ($n=183$). Significance was determined by t test.

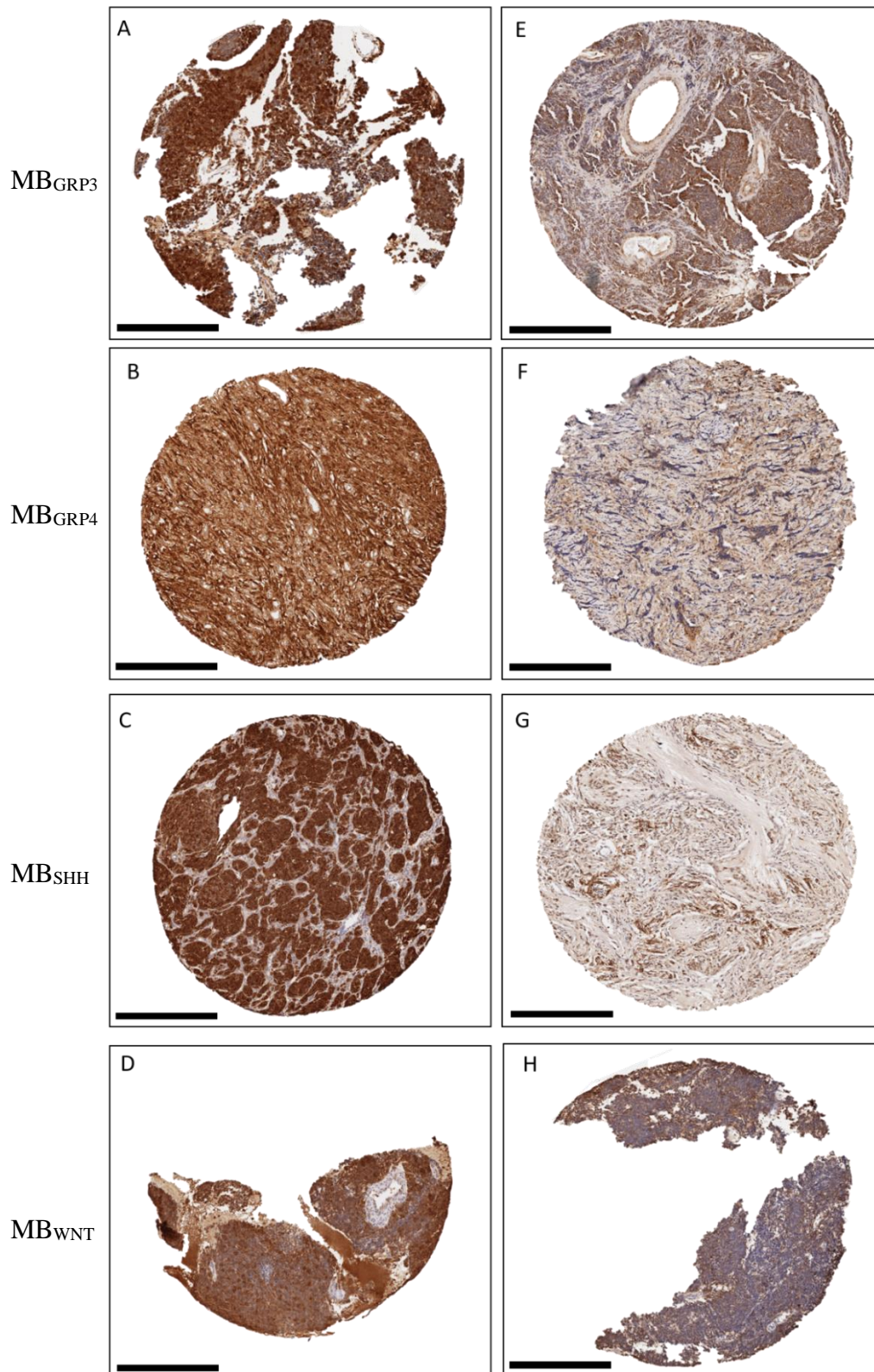


Figure 6.4 Immunohistochemical staining of PHGDH across primary medulloblastoma patient samples. Representative micrographs of TMA cores from MB subgroups. MB_{GRP3} , MB_{GRP4} , MB_{SHH} and MB_{WNT} tumour samples. A-D) Strong staining of PHGDH. E-H) Weak staining. PHGDH staining is indicated in brown and nuclei staining in blue. Scare bar = 100 μM

The subgroup-specific variations in PHGDH expression in the TMA cohort were examined. This analysis would also form the basis of subsequent Kaplan Meier survival analysis described in 6.3.1.4. As highlighted in Figure 6.4, there was a range of PHGDH expression across the four MB subgroups which consisted of samples with high immunostaining of PHGDH in tumour regions compared to samples with low intensity staining and more cellularity. MB_{GRP3} tumours had the lowest median intensity of PHGDH compared to the remaining subgroups (median score= 158, $p < 0.05$) (Figure 6.5). MB_{GRP4} tumours had comparable PHGDH expression and intensity to MB_{GRP3} (median= 169). MB_{SHH} had the highest PHGDH staining followed by MB_{WNT} (median= 211 and 200, $p < 0.05$ respectively) (Figure 6.5).

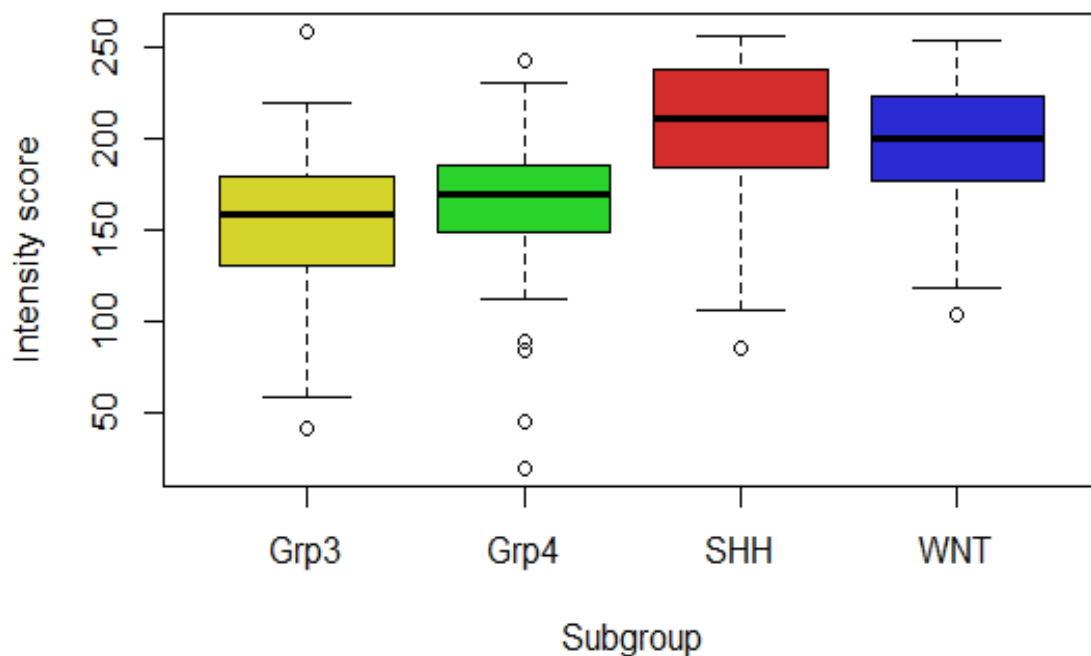


Figure 6.5 Expression of PHGDH across medulloblastoma subgroups. Boxplots of PHGDH intensity scores of MB_{GRP3} (n=59), MB_{GRP4} (n=53), MB_{SHH} (n=58) and MB_{WNT} (n=12). Boxplots show upper and lower quartiles and median intensity score values. Significance determined by one-way anova.

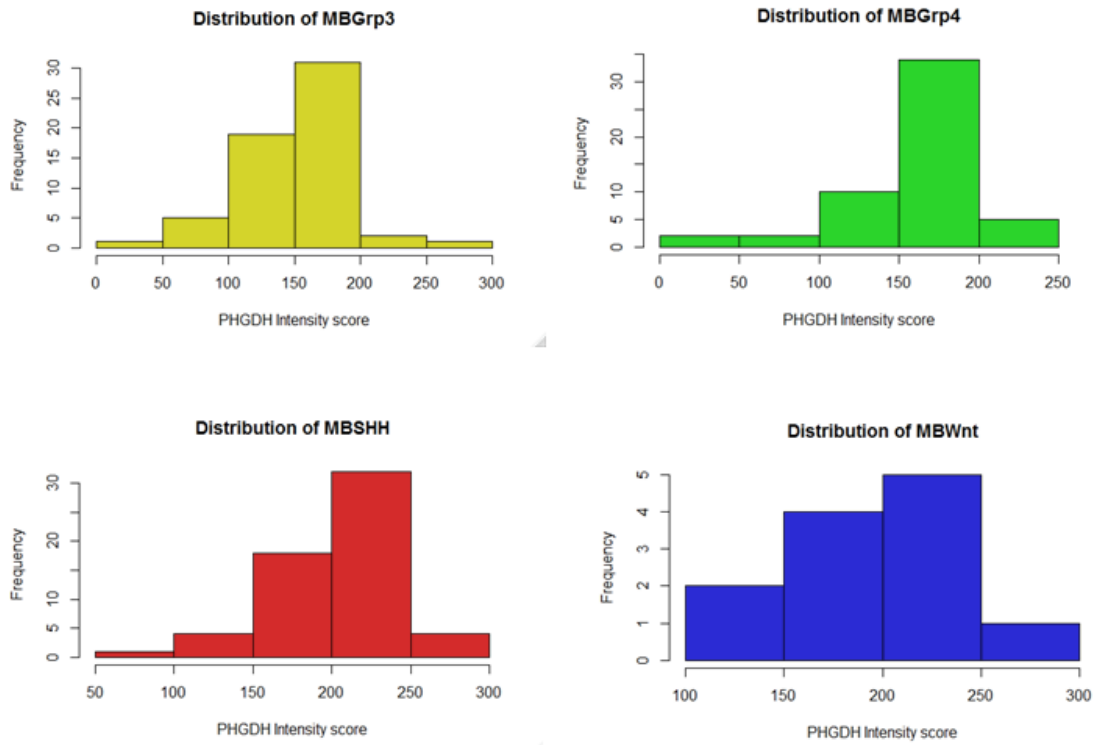


Figure 6.6 Distribution of PHGDH intensity scores across medulloblastoma subgroups. Histograms depicting distribution of PHGDH intensity scores in MB_{GRP3} ($n=53$), MB_{GRP3} ($n=55$), MB_{SHH} ($n= 58$) and MB_{WNT} ($n=12$).

These findings suggested differential expression of PHGDH across MB subgroups. Subsequently, the distribution of PHGDH staining was examined in the subgroups to reveal subgroup-specific expression patterns. PHGDH expression was normally distributed across MB_{GRP3} samples with the bulk of samples falling between score of between 100-200 intensity (Figure 6.6 A). Again MB_{GRP4} samples displayed comparable patterns to MB_{GRP3} tumours although there was no representation of MBGrp4 samples within the highest PHGDH intensity range of 250-300 (Figure 6.6 B). In MB_{SHH} however, PHGDH expression was skewed to the right, with most tumour samples categorised by PHGDH intensity ranging from 150-250 (Figure 6.6 C). Although MB_{WNT} had fewer samples available compared to the other MB subgroups, a similar skewed distribution towards higher expression was evident (Figure 6.6 D).

Since the previous gene expression analysis focused solely on MB_{GRP3} tumours, there was a need to validate whether these subgroup-specific patterns could be corroborated by gene expression data. Subsequent differential gene expression analysis of the SGP in MB

subgroups using the Cavalli *et al.*, cohort which in total consisted of 763 individual patient data was performed. Indeed this revealed similar subgroup expression patterns of PHGDH and other SGP enzymes at the gene expression level (Appendix 8.42). Taken together, these results highlight subgroup specific variation of PHGDH expression.

6.3.1.3 Differential expression of PHGDH in non-amplified and *MYC*-amplified MB_{GRP3}

A normally distributed pattern of expression of PHGDH was observed in the MB_{GRP3} tumours and this subsequently led to assessment of whether *MYC* amplification influenced or correlated with PHGDH expression. Overall, higher PHGDH expression was attributable to the *MYC*-amplified MB_{GRP3} tumours (Figure 6.7). The median expression levels for *MYC*-amplified and non-amplified were 185 and 154 respectively ($p=0.008$). Notably, there was less variation in PHGDH expression in *MYC*-amplified cases and particularly, only 2 out of 9 tumour samples fell under the overall MB_{GRP3} median score of 158. These results suggests that *MYC*-amplified tumours were accompanied by high PHGDH expression in MB_{GRP3} .

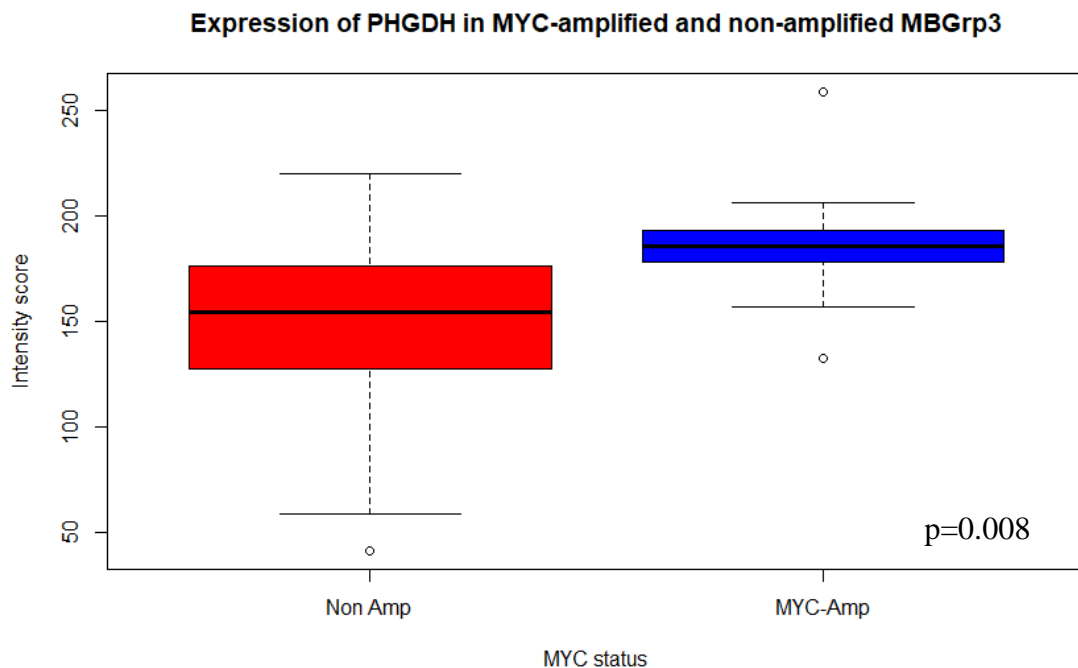


Figure 6.7 Expression of PHGDH of *MYC*-amplified versus non-amplified MB_{GRP3} . Boxplots showing PHGDH intensity scores of MB_{GRP3} tumour samples with *MYC* amplification ($n=9$) and non-amplified ($n=50$) status. Boxplots display median intensity scores with upper and lower quartiles. Significance was determined using *t* test.

Although upregulation of *MYC* is more intricately linked with MB_{GRP3}, only a small number of MB_{GRP3} patients have bona fide *MYC* amplifications and this was the case in the MB_{GRP3} tumour samples in the TMA cohort. Since the non-amplified cases account for the majority of MB_{GRP3}, differential PHGDH in this group was further explored. The advancement of molecular classification and subgrouping of MB beyond the four consensus subgrouping has further highlighted high risk groups within MB subgroups. In particular, Schwalbe *et al.*, identified seven novel subgroups and focussing solely on the MB_{GRP3}, this study identified MB_{GRP3} low risk (LR) and MB_{GRP3}-high risk (HR) and *MYC* amplifications were not exclusive to one risk group (Schwalbe *et al.*, 2017a). Subsequent analysis focused on whether PHGDH expression differed in non-amplified MB_{GRP3} LR and HR cases. Median expression of MB_{GRP3} HR was higher compared to MB_{GRP3} LR although these results were not statistically significant (PHGDH score 163 compared to 148 respectively, $p > 0.05$).

Since the TMA had clinical annotations for *MYCN* amplifications, I interrogated the relationship between with this *MYC* family member and PHGDH expression. Amplification of *MYCN* was reported for both MB_{GRP4} (~13% of cases) and MB_{SHH} (~14% of cases) therefore enabling similar evaluations assessing PHGDH expression in patients with *MYCN* amplifications compared to non-*MYCN* amplified cases exclusively in both subgroups. In the MB_{SHH}, there was disparity between median expressions of PHGDH in *MYCN*-amplified compared to non-amplified cases (Figure 6.8). Here *MYCN*-amplification correlated with higher expression of PHGDH which bore similarities to *MYC*-amplified MB_{GRP3} samples. Interestingly, this phenomenon was not evident in *MYCN*-amplified MB_{Grp4} tumours (Figure 6.9). Both non-amplified and *MYCN*-amplified had similar distribution and median expression of PHGDH. These observations highlight the context dependency of PHGDH expression in MB subgroups and also the influence of amplifications of *MYC* family members which also appear to be subgroup dependent. In the MB_{GRP3} and MB_{SHH} subgroups, *MYC* and *MYCN* amplifications respectively, correlate with higher PHGDH expression.

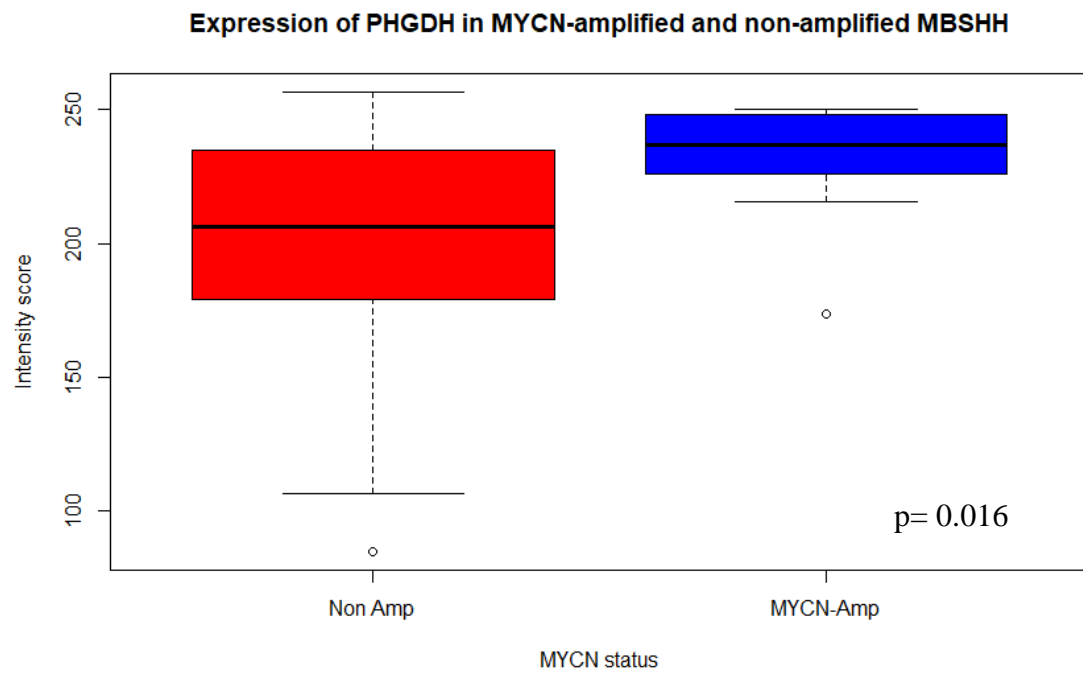


Figure 6.8 Expression of PHGDH of MYCN-amplified versus non-amplified MB_{SHH} tumour samples.. Boxplots showing PHGDH intensity scores of MB_{SHH} tumour samples with MYCN amplification (n=8) and non-amplified (n=50) status.Boxplots display median intensity scores with upper and lower quartiles. Significance was determined using t test.

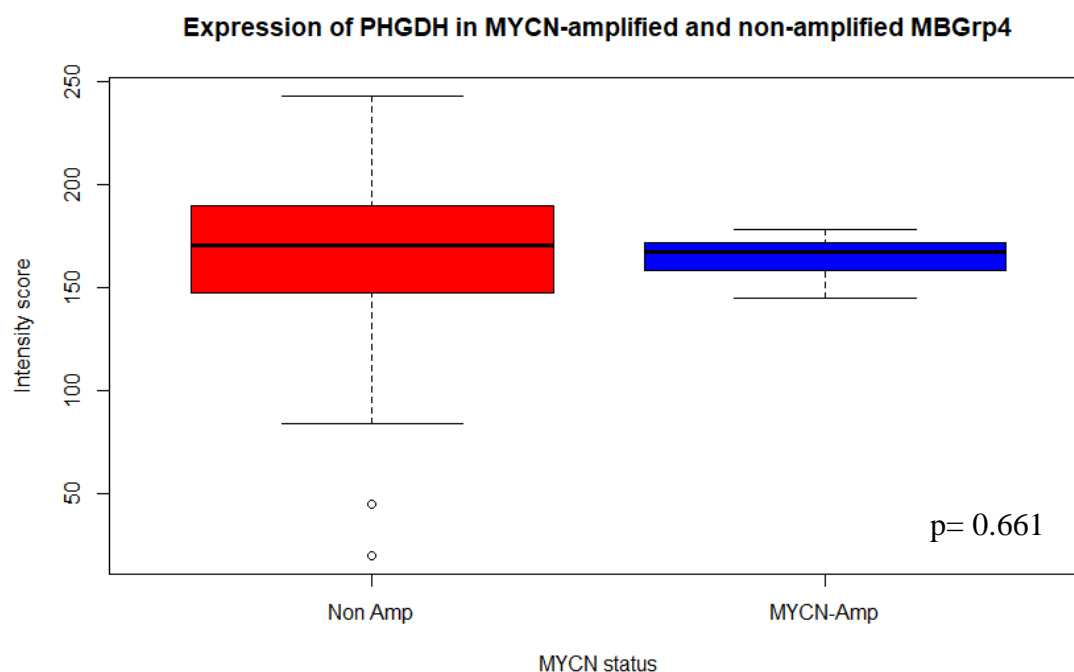


Figure 6.9 Expression of PHGDH of MYCN-amplified versus non-amplified MBGrp4 tumour samples.. Boxplots showing PHGDH intensity scores of MBGrp4 tumour samples with MYCN amplification (n=7) and non-amplified (n=49) status. Boxplots display median intensity scores with upper and lower quartiles. Significance was determined using t test.

6.3.1.4 Survival analysis of PHGDH expression in MB

Kaplan-Meier survival analysis was utilised to determine the impact of PHGDH on overall survival in MB subgroups and exclusively for MB_{GRP3} patients. For this MB wide analysis, classification of PHGDH-low and PHGDH-high was based on median expression cut-off. The median of PHGDH expression was used as a cut-off/separator as it was considered a simple and unbiased approach which is supported in the literature (Asciutto et al., 2015).

PHGDH scores were classified low or high based on the median score of the entire TMA cohort which was determined to be 176. Patients with scores below 176 were classified low PHGDH expressing and above classified high PHGDH expressing. For subgroup-specific analysis, low or high groups were similarly categorised based on median score of the subgroup (MB_{GRP3} median score = 158).

As illustrated in Figure 6.10, overall survival rates in the MB wide patient cohort showed that patients with high PHGDH expression had significantly worse outcomes compared to patients with low PHGDH expression. Cox proportional hazards analysis was carried out and included various clinicopathological parameters including PHGDH expression and other clinical features that are currently used in risk stratification (Figure 6.11). Previously identified prognostic factors were highlighted from this analysis suggesting that the TMA cohort was representative of the established high risk features of MB. For instance favourable prognosis for MB_{WNT} was observed (HR = 0.21 p = 0.041). High risk features such as *MYC* and *MYCN* amplification were also observed (HR= 6.55 p = 0.001, HR= 2.44 p = 0.031 respectively). PHGDH expression over the median score (i.e. high PHGDH) was associated with increased risk and worse outcomes in this cohort (HR = 2.31 = 0.007).

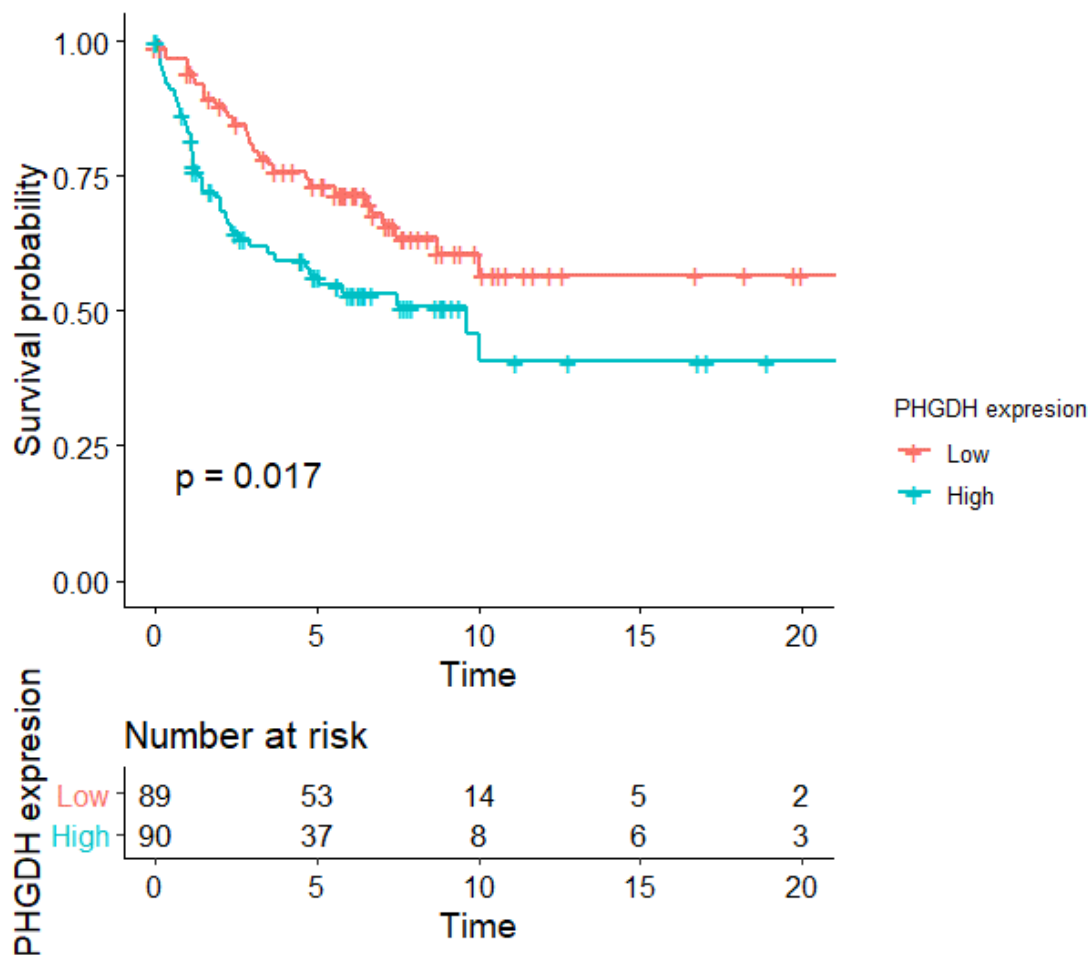


Figure 6.10 Kaplan Meier survival analysis of PHGDH expression in the TMA medulloblastoma wide cohort. Overall survival of patients with PHGDH low (orange) and PHGDH high (green) with table depicting number of patients at risk at a given time period. Significance was tested using log rank test.

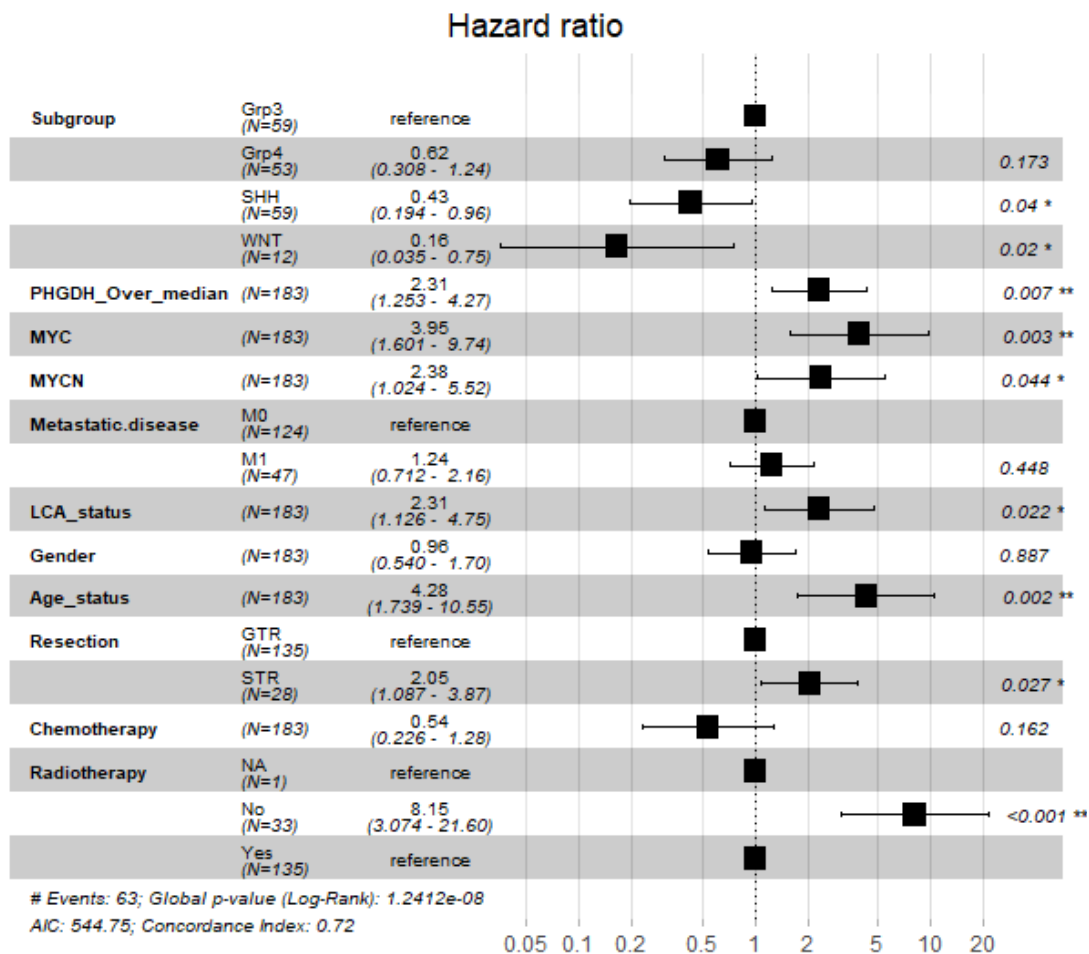


Figure 6.11 Forest plots of Cox proportional hazard models for the TMA cohort assessing PHGDH expression and other clinicopathological parameters. Estimation of overall survival hazard ratios. Hazard ratios of covariates > 1 and over the unity line are associated with increased risk of death whereas hazard ratios between 0 and 1 represent decreased risk of death. Significance of hazard ratio estimates was evaluated by log rank test with * $p < 0.05$, *** $p < 0.001$.

In the MB_{GRP3} subgroup, high expression of PHGDH was associated with the MYC-amplified subtype (MYC-amplified 185 PHGDH score compared to 154 in non-amplified, $p=0.008$). When survival was examined, patients with high PHGDH expression had worse prognostic outcomes which was more pronounced within first 5 years (Figure 6.12). Multivariate analysis showed that increased PHGDH correlated with worse survival outcomes in a MB wide cohort analysis. Our analysis has highlighted subgroup-specific differences in expression levels and also its association with MYC expression

particularly in the MB_{GRP3} subgroup. Without the possibility of matched tumour and normal samples, it is difficult to ascertain whether subgroup level expression of PHGDH are associated with tumour location and cell of origin and explain the variations in PHGDH expression across the MB subgroups. In summary, this analysis has demonstrated a division in MB_{GRP3} PHGDH expression where a distinction was made between PHGDH low and PHGDH high patients when overall survival was examined. This is important as it highlights the possibility of distinct phenotypes associated with the SGP pathway with respect to non-amplified and *MYC*-amplified MB_{GRP3} patients.

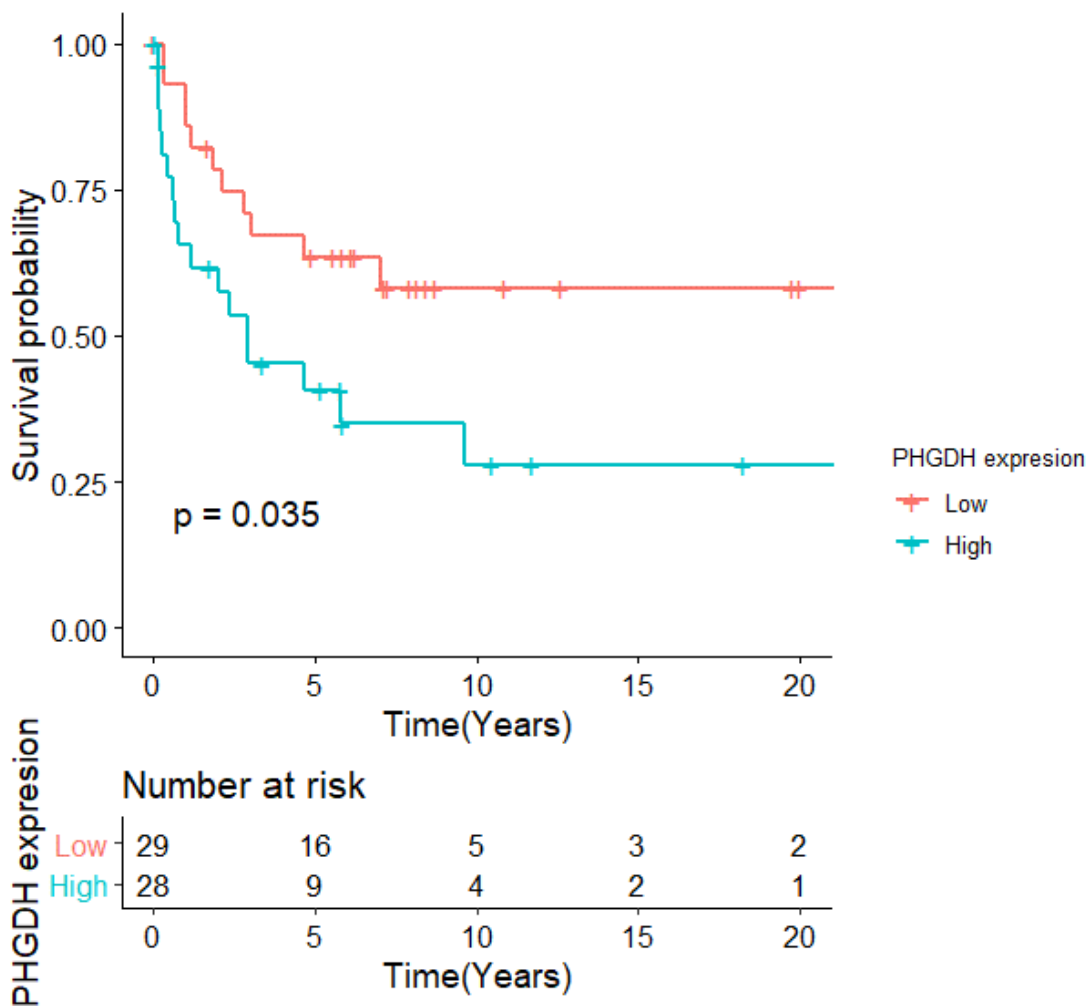


Figure 6.12 Kaplan Meier survival analysis of PHGDH expression in MB_{GRP3} tumours.. Overall survival of patients with PHGDH low (orange) and PHGDH high (green) with table depicting number of patients at risk at a given time period. Significance was tested using log rank test.

6.3.2 MYC-dependent alterations in the *de novo* serine and glycine pathway

6.3.2.1 Effect of MYC knockdown on the protein expression of SGP enzymes in the MB_{GRP3} MYC-regulable cell lines

Having established clinically significant differences in the expression of PHGDH in primary MB_{GRP3} tumour samples, the following part of this study focused on the MYC-regulable MB_{GRP3} isogenic cell lines. The D425, D283 and HDMB03 NS and MYC 2 bearing cells were treated in the presence or absence of doxycycline for 72 h to induce MYC knockdown. Cell pellets were collected and protein extracted and subjected to immunoblotting to evaluate protein expression changes in the SGP pathway.

MYC knockdown in the D425 MYC 2 cell line caused downregulation of all SGP enzymes tested with varying degrees of severity (Figure 6.13). Crucially, PHGDH levels reduced in the MYC 2 (off) cells compared to MYC 2 (on) cells. Additionally, there was robust knockdown in GLDC which is at the lower branch of the serine and glycine metabolism. The D425 NS (on) and NS Dox control (on) cells had similar expression levels of SGP enzymes. In the D283 MYC 2 cells, MYC knockdown negatively affected expression on PHGDH, PSPH and SHMT 2. Conversely, expression of PSAT1 and GLDC were modestly increased in the MYC 2 (off) cells. The expression of SGP enzymes were relatively unaffected in the D283 NS cells (Figure 6.14). Although there was more variation in the HDMB03 MYC 2 cells, the upstream enzymes of the SGP, PHGDH and PSAT1 displayed slightly reduced expression in the HDMB03 MYC 2 (off) cells compared to the MYC (on) counterparts. However, the expression PSPH, SHMT 2 and GLDC were unaffected by MYC knockdown in the HDMB03 MYC 2 cell lines (Figure 6.15). Although there were modest changes in the expression of SGP enzymes in the HDMB03 NS cell lines, they displayed alterations to lesser magnitude to the HDMB03 MYC 2 cells (Figure 6.15). Taken together, MYC knockdown causes downregulation of the SGP pathway albeit with cell line-specific differences and variations in the protein expression arising from individual replicates. Importantly however, MYC 2 (on) cells have elevated expression of PHGDH compared to MYC 2 (off) cells.

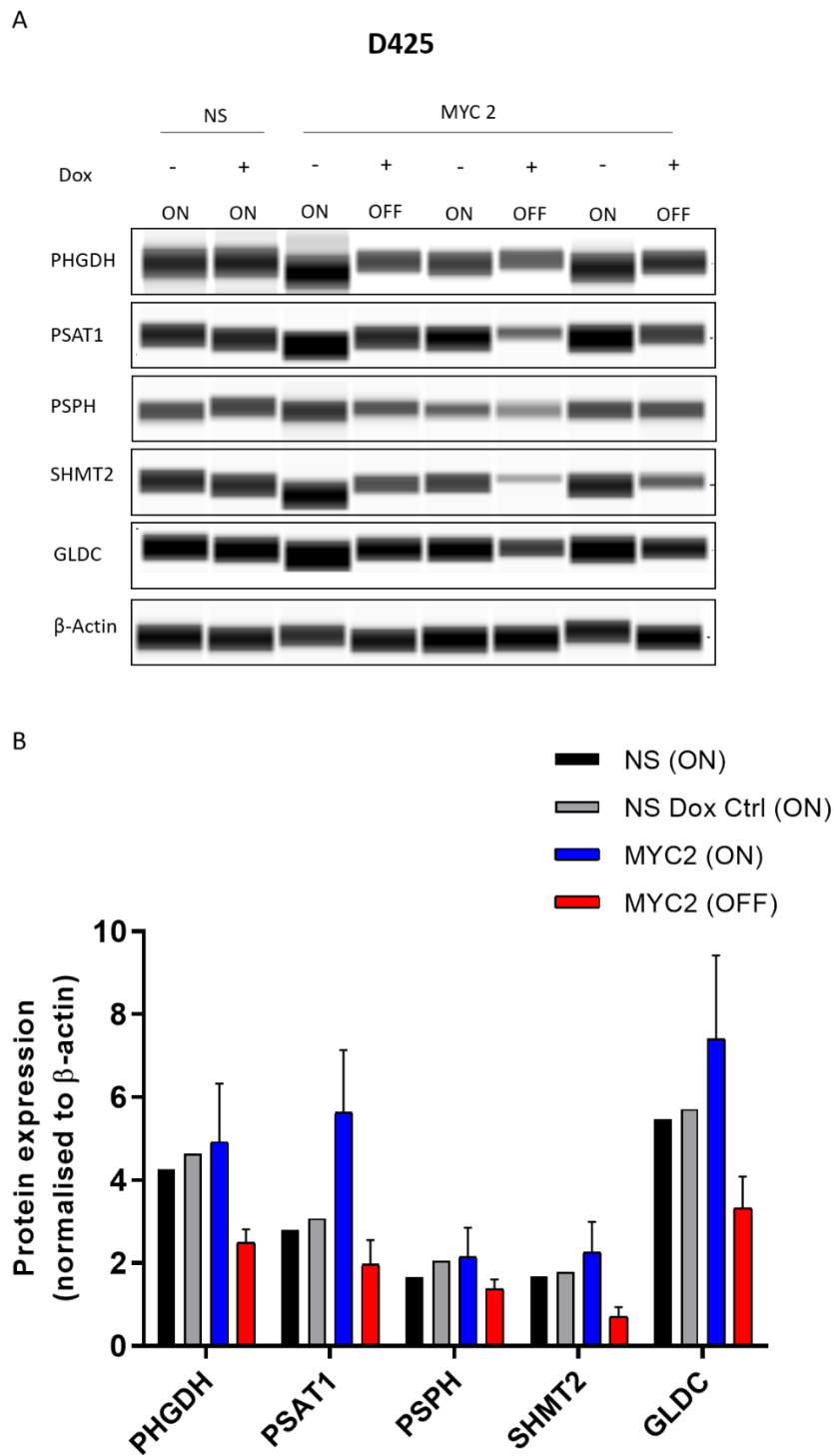


Figure 6.13 Examining protein expression of the de novo serine and glycine pathway in D425 MYC-regulable cell lines. D425 NS and MYC 2 cells were treated with 1 $\mu\text{g}/\text{mL}$ of doxycycline for 72 h. Cell lysates and proteins quantified and immunoprobed for PHGDH, PSAT1, PSPH, SHMT2 and GLDC. A) Representative WES images of D425 NS (on) and NS Dox Ctrl (on) and MYC 2 (on) and (off) cells. B) Quantitative analysis protein expression of the SGP enzymes. Protein expression was normalised to loading control, β -actin. Bars \pm SEM.

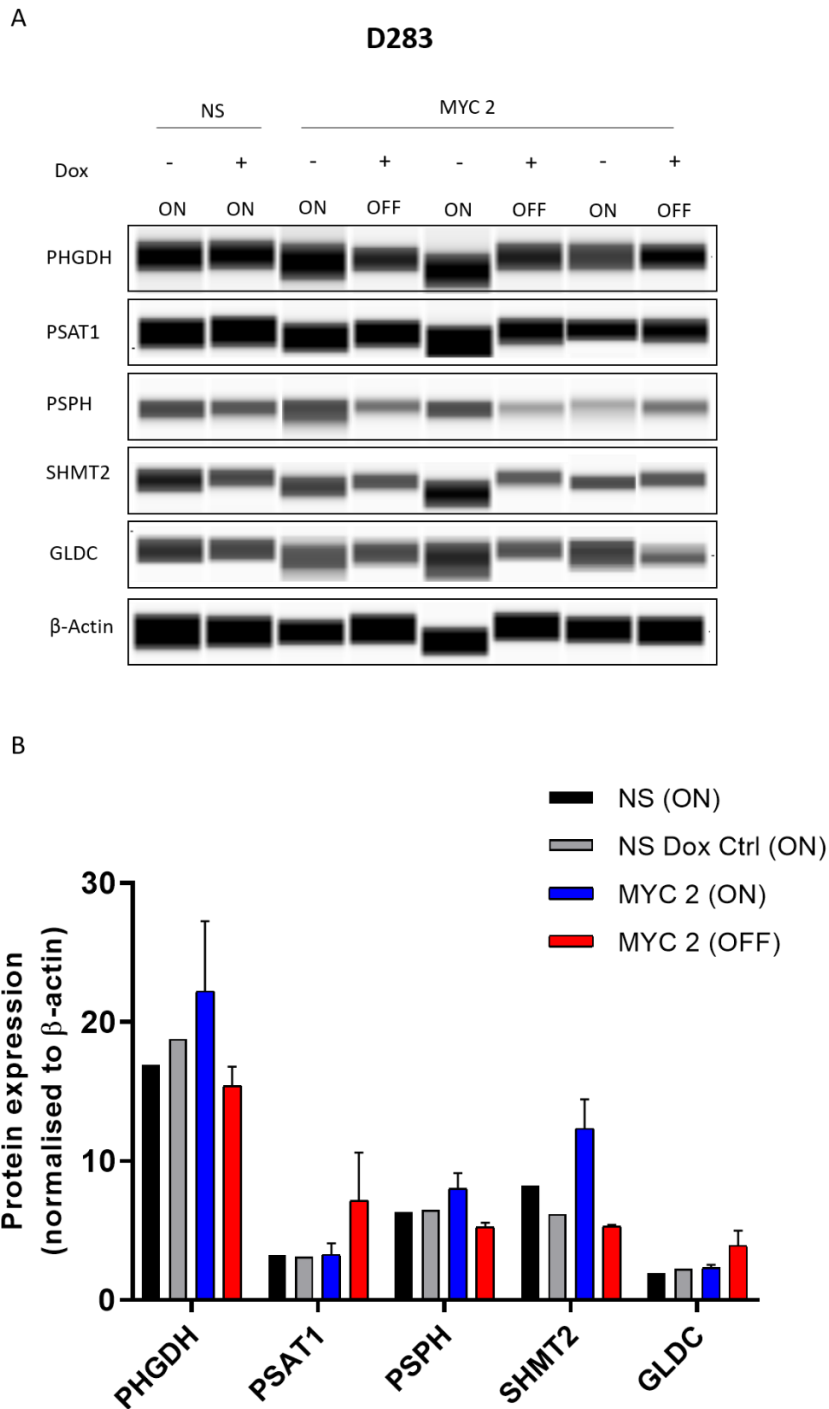
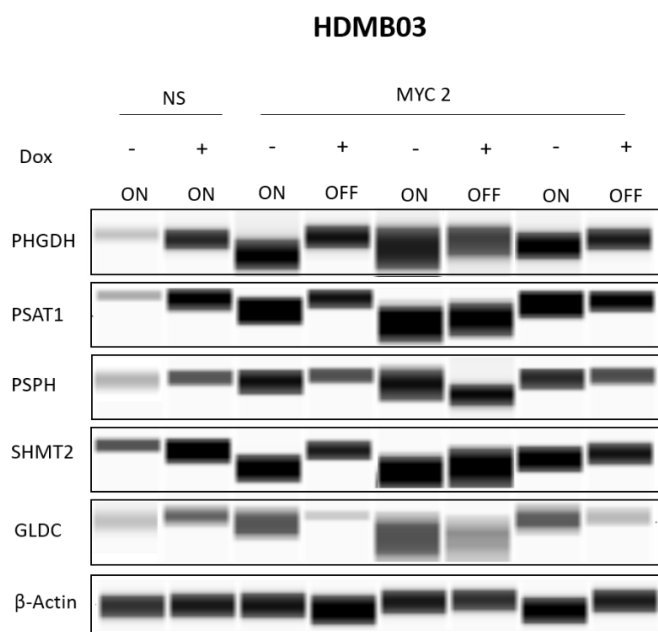


Figure 6.14 Examining protein expression of the de novo serine and glycine pathway in D425 MYC-regulable cell lines. D283 NS and MYC 2 cells were treated with 1 $\mu\text{g}/\text{mL}$ of doxycycline for 72 h. Cell lysates and proteins quantified and immunoprobed for PHGDH, PSAT1, PSPH, SHMT2 and GLDC. A) Representative WES images of D283 NS (on) and NS Dox Ctrl (on) and MYC 2 (on) and (off) cells. B) Quantitative analysis protein expression of the SGP enzymes. Protein expression was normalised to loading control, β -actin. Bars \pm SEM.

A



B

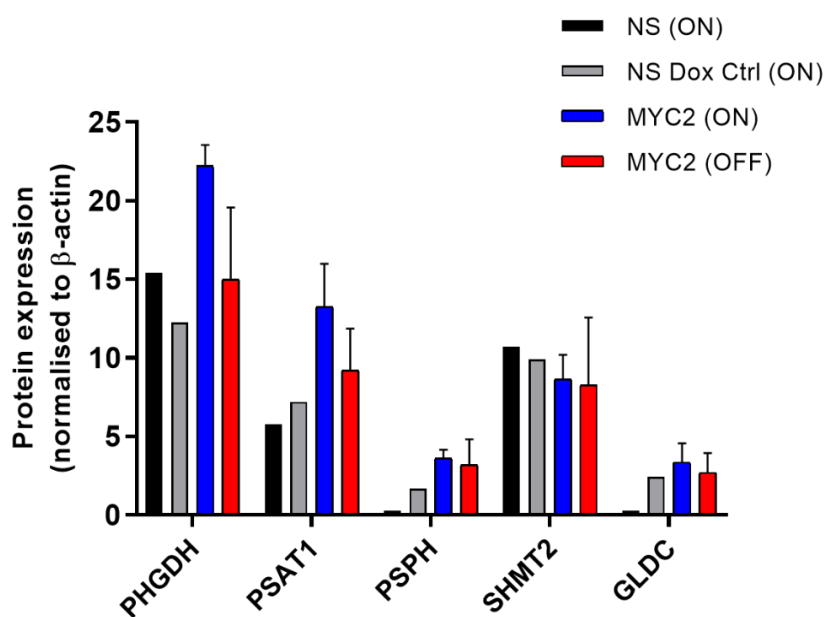


Figure 6.15 Examining protein expression of the de novo serine and glycine pathway in D425 MYC-regulable cell lines. HDMB03 NS and MYC 2 cells were treated with 1 μ g/mL of doxycycline for 72 h. Cell lysates and proteins quantified and immunoprobed for PHGDH, PSAT1, PSPH, SHMT2 and GLDC. A) Representative WES images of HDMB03 NS (on) and NS Dox Ctrl (on) and MYC 2 (on) and (off) cells. B) Quantitative analysis protein expression of the SGP enzymes. Protein expression was normalised to loading control, β -actin. Bars \pm SEM.

6.3.2.2 Response of MB_{GRP3} MYC-regulable cell lines to PHGDH inhibition

Previous HRMAS profiling and ¹³C -glucose tracing analysis suggested increased utilisation of the de novo SGP as feature of MYC-amplified MB_{GRP3} cells compared to their MYC knockdown counterparts. Analysis of protein expression of enzyme components of the SGP further revealed the downregulation of this pathway following loss of MYC. I next examined whether relative sensitivities to the PHGDH inhibitor NCT503, in the MB_{GRP3} MYC-regulable cells. Firstly the D425, D283 and HDMB03 MYC 2 cell lines were treated with or without doxycycline for 48 h to induce MYC knockdown prior to drug treatment. Cells were then treated with a range concentrations of NCT503 for a further 72 h. Cell viability was measured using two distinct methods: CellTiter Glo™ and SRB staining which measured ATP and protein content respectively.

Since MYC-amplified cells displayed higher levels of de novo serine and glycine, which potentially resulted in proliferative advantage, it was postulated that MYC-amplified cells would exhibit greater sensitivity to the inhibition of PHGDH activity. Treatment with NCT503 resulted in a dose-dependent reduction of cell viability in the MB_{GRP3} isogenic cell lines. MYC-dependent sensitivity to NCT503 was observed across all three MB_{GRP3} cell lines (Figure 6.16). Notably, varying responses to NCT503 was observable in the individual MB_{GRP3} cell lines. In the D425 MYC 2 cells, the sensitivity of MYC 2 (on) cells was around three times less than that of and MYC 2 (off) cells ($p < 0.0001$). The D425 MYC 2 (on) cells had an IC₅₀ of 15.10 μ M compared to its knockdown equivalent of 42.94 μ M (Figure 6.16 A). The D283 MYC 2 (on) were the most sensitive towards NCT503 with a sensitivity towards NCT503 almost four times than that of D283 MYC 2 (off) cells (IC₅₀ 9.57 versus 41.94 μ M, respectively, $p < 0.0001$) (Figure 6.16 B). Although the HDMB03 was the least sensitive cell line to NCT503 treatment, there was still a measurable difference in the response of HDMB03 MYC 2 (on) cell to HDMB03 MYC 2 (off) cells (IC₅₀ 23.52 μ M versus 43.90 μ M, respectively ($p < 0.0001$) Figure 6.16 C).

Altogether, NCT03 elicited a profound cytotoxic response against MYC overexpressing cells within an IC₅₀ range of 9 – 23 µM compared to MYC knockdown cells which had concordant IC₅₀ in the three MB_{GRP3} cell lines (~ 40 µM) when measured with CellTiter Glo™. Additionally, IC₅₀ determination from SRB cell viability measurements supported a MYC-dependent response to NCT503 treatment albeit with varying IC₅₀ values (Appendix 8.48). The IC₅₀ of NCT503 in MB_{GRP3} cell lines were comparable to similar observations in breast cancer cell lines with PHGDH amplification with sensitivities ranging from 8 – 14 µM in the Pacold et al., study which utilised CellTiter Glo™ as a viability measurement with 96 h NCT503 treatment. In this particular study, NCT503 insensitive cell lines had IC₅₀ over 100 µM (Pacold et al., 2016). Although dampened response to PHGDH inhibition was expected in the MYC (off) cells, IC₅₀ for our ‘insensitive’ MYC (off) cells were lower than those seen in the non-PHGDH amplified breast cancer cell lines with minimal expression of PHGDH in the Pacold et al., study. Additionally, Dox-induced MYC knockdown did not entirely diminish the expression of MYC and SGP pathway components (Figure 6.13). So, whilst decreased flux into the SGP was observed in our MYC-amplified cell line models following MYC knockdown, they remain reliant on this pathway albeit to a lesser extent than MYC-amplified counterparts. Taken together, our results demonstrate in vitro MYC-dependent sensitivity to NCT503 treatment in MB_{GRP3} MYC-amplified cells.

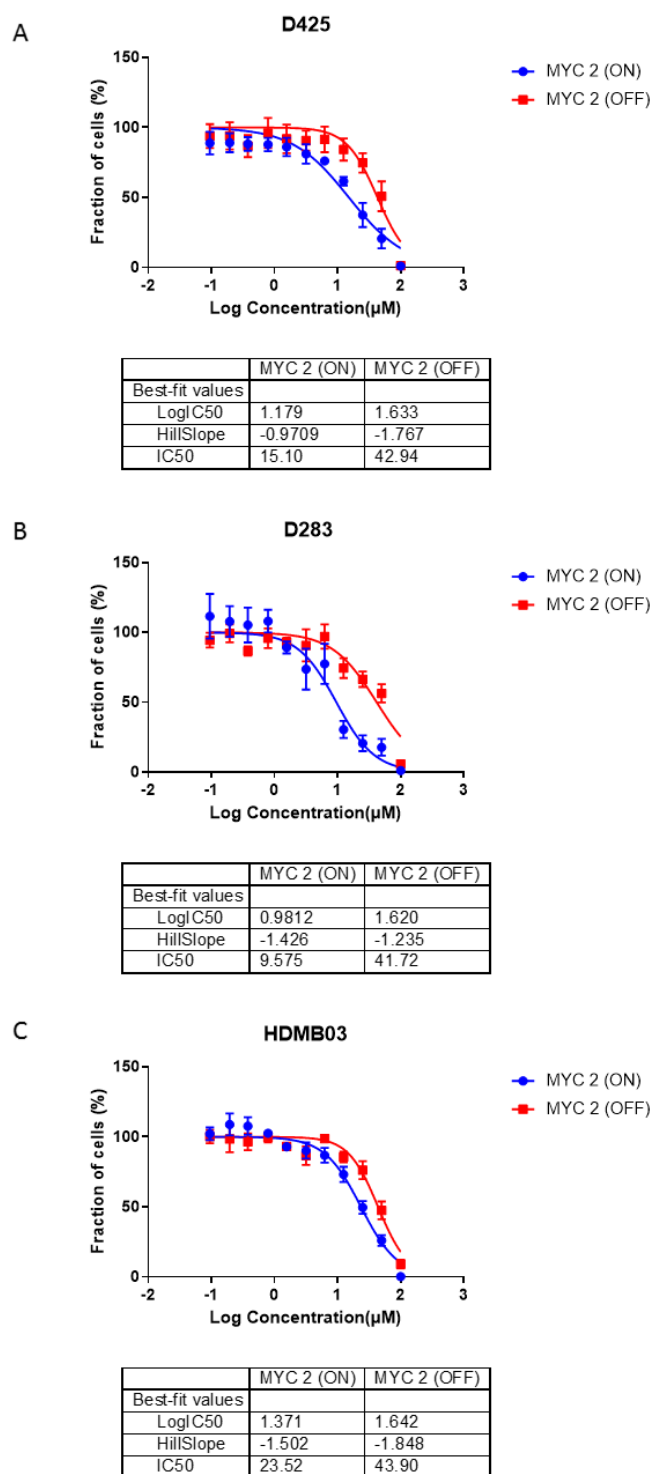


Figure 6.16 Response of MYC-regulable *MB_{GRP3}* isogenic cells to NCT503 treatment. A) D425 MYC 2 B) D283 MYC 2 C) HDMB03 MYC 2 were treated in the presence or absence of 1 $\mu\text{g/mL}$ of doxycycline for 48 h. Subsequently cells were plated in 96 well microplates and treated with varying concentrations of NCT503 for 72 h. Cell viability measured with CellTiter Glo™. Data was normalised to vehicle control and log transformed (NCT503 concentrations ranges from 1.56 μM to 100 μM). Data represents mean of five independent experiments \pm SEM.

6.3.3 Response of MB parental cell lines with varying *MYC* expression to PHGDH inhibition

6.3.3.1 Correlation of *MYC* and PHGDH expression MB cell lines

In order to further investigate *MYC*-associated sensitivity to PHGDH inhibition, the consequence of PHGDH inhibition was investigated in 9 MB parental cell lines. To our knowledge, non-amplified MB_{GRP3} cell lines are not routinely cultured therefore a direct comparison between *MYC*-amplified and non-amplified MB_{GRP3} could not be evaluated. However, there are numerous MB cell lines available with varying *MYC* expression and subgroup classifications. A range of these cell lines were utilised for pharmacological testing (details of cells lines are reported in the Appendix 8.49). Prior to commencing drug testing, the protein expression of *MYC* and SGP enzymes was evaluated in these cell lines. Cell lysates were collected, quantified and immunoblotted for *MYC*, PHGDH, PSAT1, PSPH, SHMT2 and GLDC.

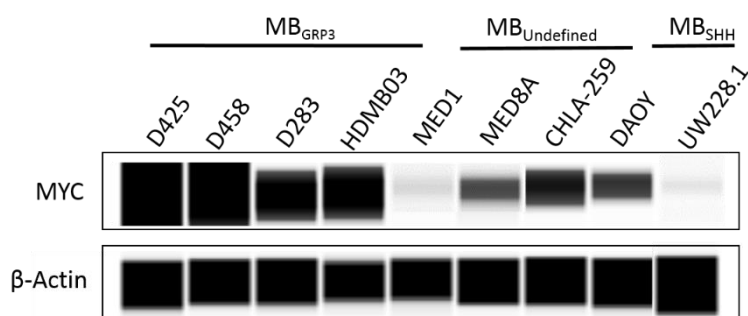


Figure 6.17 Protein expression of *MYC* across parental MB cell lines. β -actin was used as a loading control and normalisation of *MYC* expression.

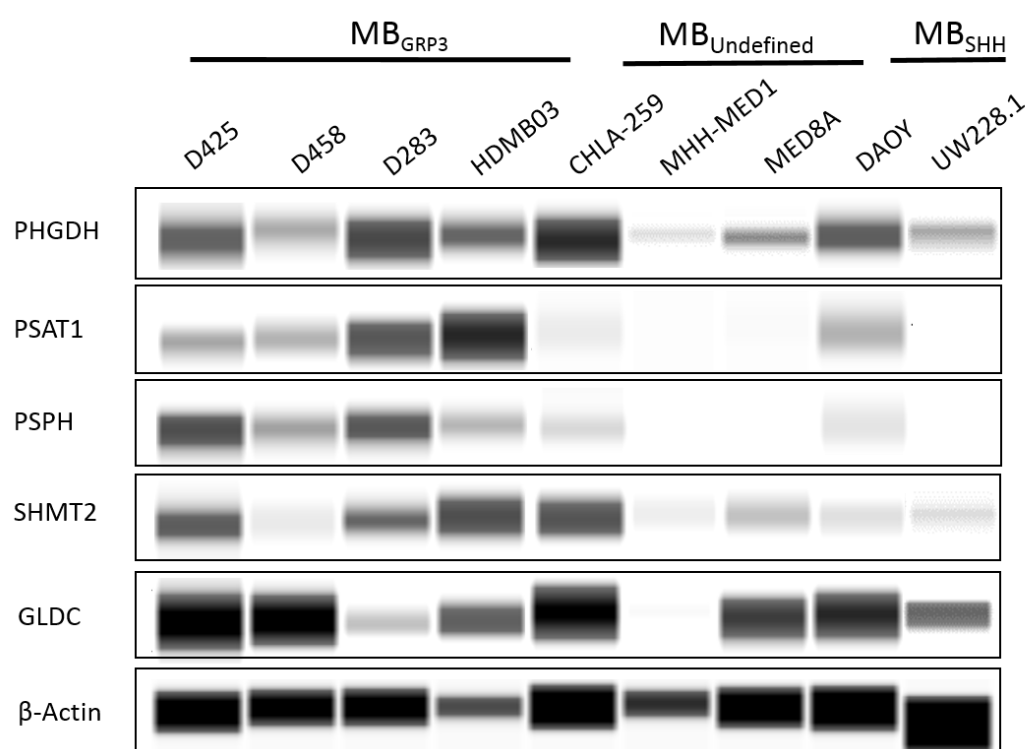


Figure 6.18 Protein expression of the *de novo* serine and glycine enzymes in parental MB cell lines. Representative WES immunoblots of PHGDH, PSAT1, PSPH, SHMT2 and GLDC. β -actin was used as a loading control.

WES analysis of the *de novo* SGP pathway revealed variations in enzyme expression across MB cell lines (Figure 6.18). Our results revealed high expression of SGP enzymes in the D425, D458, D283 and HDMB03 *MYC*-amplified MB_{GRP3} cell lines. The remainder of the cell lines had lower expression and varying expression of SGP components. Our previous analysis in the *MYC* isogenic cell lines revealed knockdown of *MYC* negatively impacted SGP enzyme expression. It was queried whether *MYC* influenced expression of the various enzymatic components of the SGP. Correlation analysis of *MYC* and individual SGP revealed significant correlations in two out of five SGP enzymes (Figure 6.19). High *MYC* expression positively correlated with PHGDH ($R^2=0.581$, $p=0.0169$) and GLDC ($R^2=0.781$, $p=0.0016$). Our data show that *MYC* expression is associated with specific SGP enzymes in these MB cell lines.

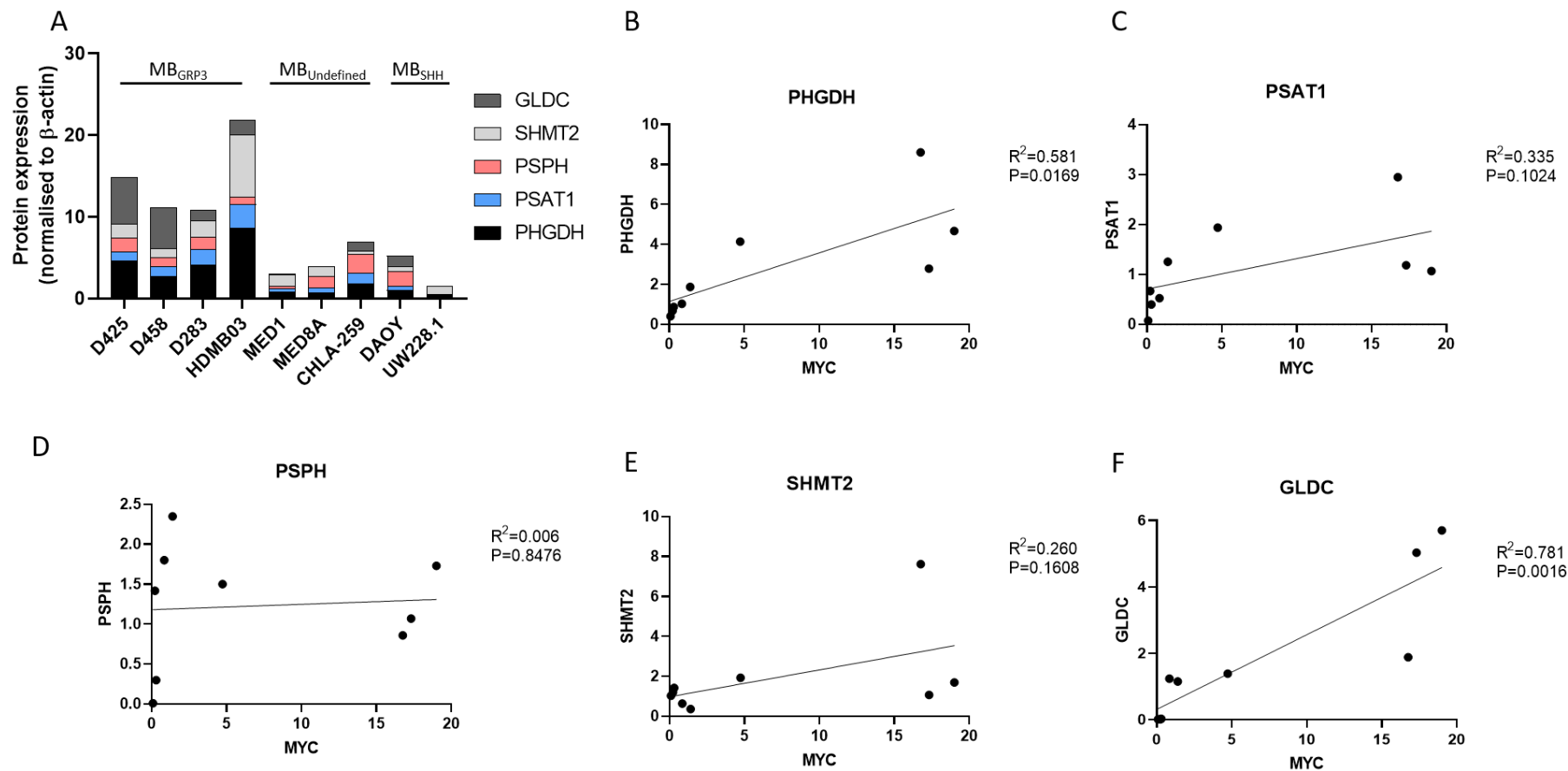


Figure 6.19 Relationship between MYC expression and de novo serine and glycine pathway in medulloblastoma cell lines. A) Quantitative analysis of the immunoblotted SGP enzymes in the 9 medulloblastoma cell lines (MB_{GRP3}: D425, D458, D283, HDMB03; Subgroup-undefined: CHLA-29, MED1, MED8A; MB_{SHH}: DAOY, UW228.1). B-F) Correlation analysis of MYC and individual SGP enzymes. Pearson correlation coefficients were computed with two tailed significance testing.

6.3.3.2 Response of parental MB_{GRP3} and MB_{SHH} cell lines to PHGDH inhibition

PHGDH inhibition in the MB parental cell lines was assessed using two small molecule inhibitors: NCT503 and CBR5884 the addition of a second compound with distinct mechanisms of inhibitory action towards PHGDH is likely to inform on target specificity. The 9 MB parental cell lines were treated with NCT503 or CBR5884 for 72 h and cell viability measured using CellTiter Glo™. For ease and clarity, D425, D458, D283 and HDMB03 were assigned as the *MYC*-amplified MB_{GRP3} cell lines; MED1, MED8A and CHLA-259 as subgroup-undefined cell lines; DAOY and UW288.1 which are the MB_{SHH} cell lines.

Although differences in potency was observed between the two inhibitor compounds, response of each cell line were consistent between the inhibitors. For instance, when a cell line was observed to be sensitive to NCT503, it was also sensitive to CBR5884 demonstrating reliability and specificity of target engagement despite different mode of inhibition. In general, the classical *MYC*-amplified and subgroup-undefined cell lines were more sensitive to PHGDH inhibition by NCT503 or CBR5884 (Figure 6.20). Examination of IC₅₀ revealed the MED1 and MED8A cell lines to be the most sensitive cell lines (2.52 μM and 5.33 μM respectively). Although CHLA-259 were rather sensitive to PHGDH inhibition (NCT503 IC₅₀ = 13.33 μM, CBR5884 IC₅₀ = 6.32 μM), increasing concentrations of either NCT503 or CBR5884 did not result in a reduction in cell viability (Figure 6.20 B). The order of sensitivity for the classical *MYC*-amplified MB_{GRP3} cell lines went as follows D458, D283, D425 and finally HDMB03 (Table 6.2). The MB_{SHH} were the least sensitive to PHGDH inhibition with both DAOY and UW288.2 IC₅₀ values exceeding 50 μM for NCT503 (Figure 6.20) and IC₅₀ for CBR5884 being around twice that of the least sensitive MB_{GRP3} cell line (Figure 6.20, Table 6.2). Although directed comparison of non-amplified and *MYC*-amplified MB_{GRP3} cell lines was not possible, analysis in several MB parental cells lines suggests sensitivity of *MYC*-amplified MB_{GRP3} cells compared to non-amplified MB_{SHH}. Interestingly, pharmacological testing highlighted other cell lines in which NCT503/ CBR5884 is effective. These cell lines may be susceptible to PHGDH inhibition owing to high rates of de novo synthesis.

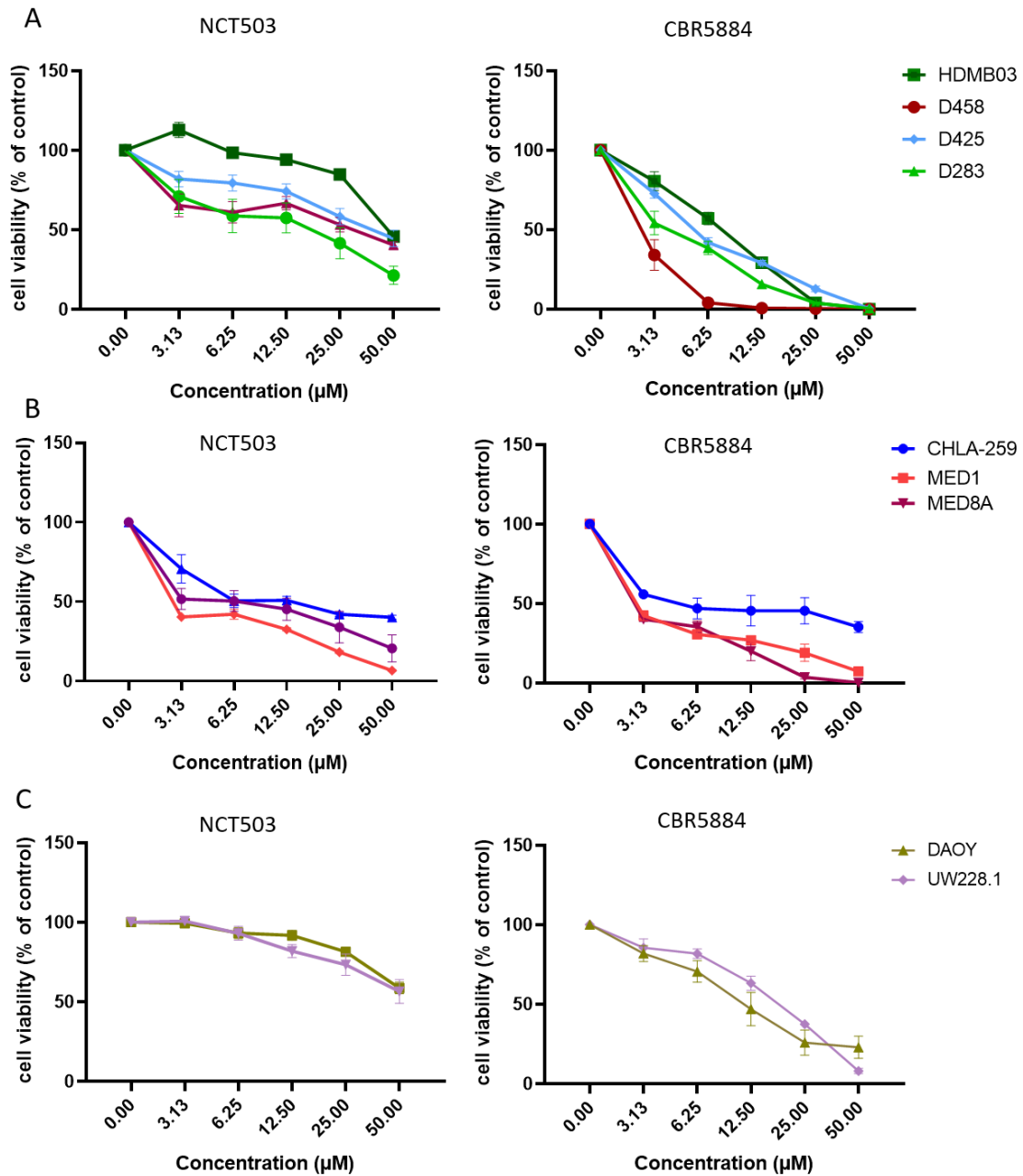


Figure 6.20 Pharmacological inhibition of PHGDH in medulloblastoma cell lines. Dose response curves of MB cell lines following treatment with NCT503 or CBR5884 for 72 h. Cell viability was measured with CellTiter Glo™. A) MB_{GRP3} MYC-amplified D425, D458, D283, HDMB03 B) Subgroup-undefined CHLA-259, MED1, MED8A and C) MB_{SHH}: DAOY and UW228.1. Error bars represent mean \pm SEM of three independent experiments.

Table 6.2 Table of IC_{50} values for NCT503 and CBR5884 following 72 h exposure in medulloblastoma cell lines. IC_{50} were determined using non-linear regression analysis.

Cell line	NCT503 IC_{50} (μ M)	95 % CI (μ M)	CBR5884 IC_{50}	95 % CI (μ M)
D425	40.69	7.907 - 22.47	5.75	5.158 - 6.418
D458	12.85	1.653 - 3.833	2.59	2.126 - 3.167
D283	30.22	14.10 - 64.76	2.52	1.774 - 3.59
HDMB03	47.09	2.403 - 11.82	7.18	6.386 - 8.086
CHLA259	13.33	27.05 - 61.21	6.32	2.000 - 19.99
MED1	2.518	7.626 - 21.65	1.95	1.191 - 3.207
MED8A	5.33	42.00 - 52.78	3.83	3.202 - 4.593
DAOY	65.26	52.13 - 81.69	12.02	8.858 - 16.32
UW288.1	61.62	39.21 - 96.84	16.43	14.35 - 18.81

6.3.4 Phenotypic assessment of MB_{GRP3} cells following PHGDH inhibition using NCT503 and CBR5884

6.3.4.1 Effect of PHGDH inhibition on Clonogenic survival

Subsequent to determination IC_{50} values for the 9 MB cell lines, more in depth characterisation of phenotypic consequences following disrupted PHGDH activity was undertaken. The 4 classical *MYC*-amplified MB_{GRP3} cell lines were used in this portion of the study owing their bona fide *MYC* amplification/ overexpression status and their wider use in the literature. The MB_{GRP3} *MYC*-amplified cell lines were poly-L-lysine adhered to tissue culture plates and treated with two concentrations of NCT503 or CBR5884 for 10 days. Subsequently, cells were fixed, colonies stained with crystal violet and number of colonies counted.

In the D425 cell lines, treatment with NCT503 impacted colony forming ability when treated with the 50 μ M concentration and not the lesser concentration (Figure 6.21 A & D). This result was expected since the IC_{50} for this cell line was around 40 μ M. Treatment with NCT503 in the D458 and D283 cell lines exhibited a dose-dependent reduction in number of colonies formed (Figure 6.21 A, B & D). This supports previous data which suggested these two cell lines as the more sensitive classical MB_{GRP3} cell lines. Similarly to the D425 cells, the colony forming ability was only impacted in the HDMB03 cells when treated with the higher concentration of NCT503 (Figure 6.21 A & D). Contrary to the effect of CBR5884 on cell viability, the D425 cells and indeed the other 3 *MYC*-amplified cell lines displayed a more modest effect on clonogenic survival when

compared to NCT503 response despite both concentrations used being over IC_{50} dosage for most cell lines. Nevertheless, inhibition of PHGDH via CBR5884 did also impact the clonogenicity of the MB_{GRP3} cells (Figure 6.22). Treatment using CBR5884 however did not exhibit striking effects on colony forming ability in the D425 cell lines (Figure 6.22 B). The maximal response to CBR5884 treatment in the D458, D283 and HDMB03 cells resulted in 80%, 60% and 50% reduction in colony forming ability respectively (Figure 6.22 C-D). These experiments highlighted that impairment of PHGDH activity reduced colony forming capacity and thus viability of the *MYC*-amplified MB_{GRP3} cells.

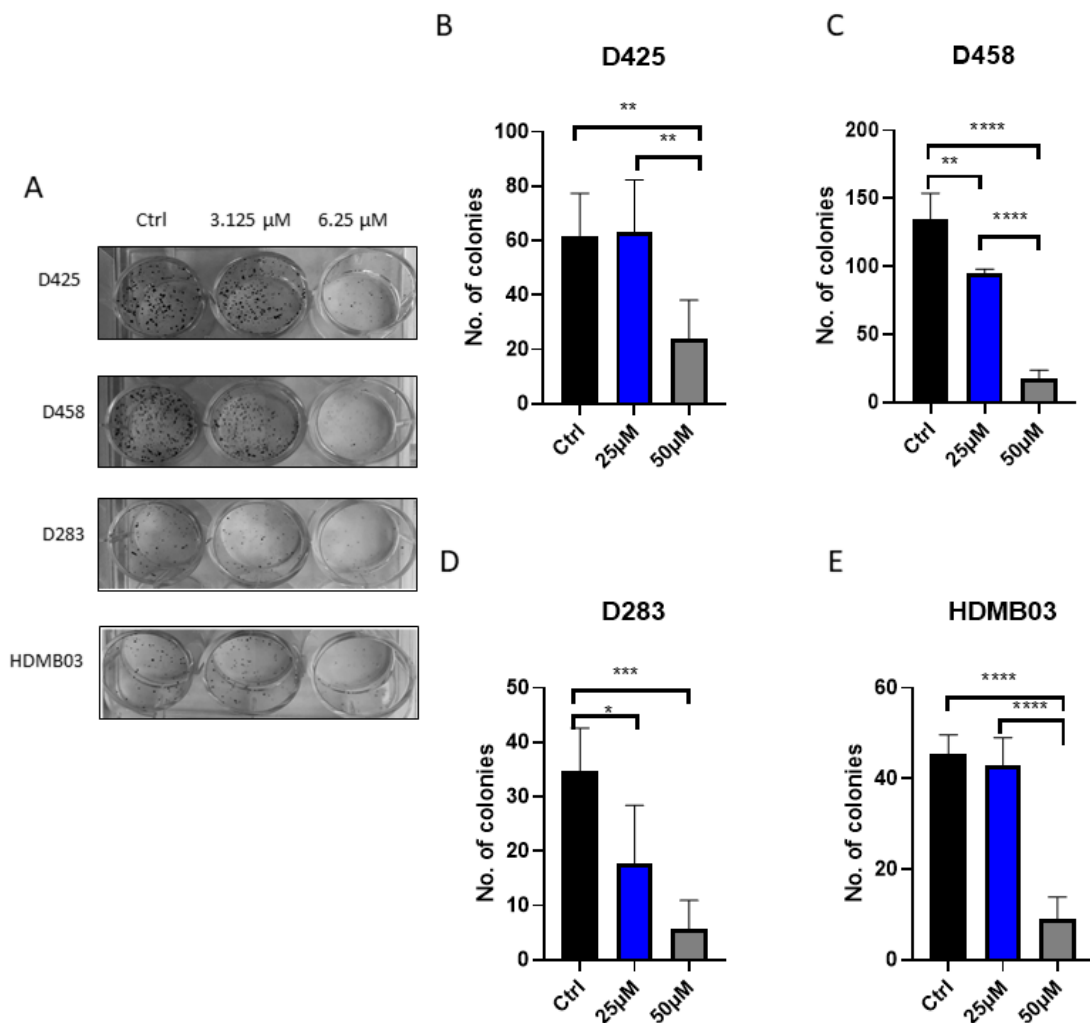


Figure 6.21 Effect of NCT503 on clonogenic survival in *MYC*-amplified MB_{GRP3} parental cells. A) Representative images of clonogenic assay in D425, D458, D283 and HDMB03 cell lines following 10 day treatment with 25 μ M and 50 μ M NCT503.. Histogram representation of colony numbers post-treatment in B) D425 C) D458 D) D283 and E) HDMB03 cells. Data represents mean of three biological replicates \pm SEM. Significance determined by one-way ANOVA. * $p < 0.05$, ** $p < 0.01$, *** $p < 0.001$, **** $p < 0.0001$.

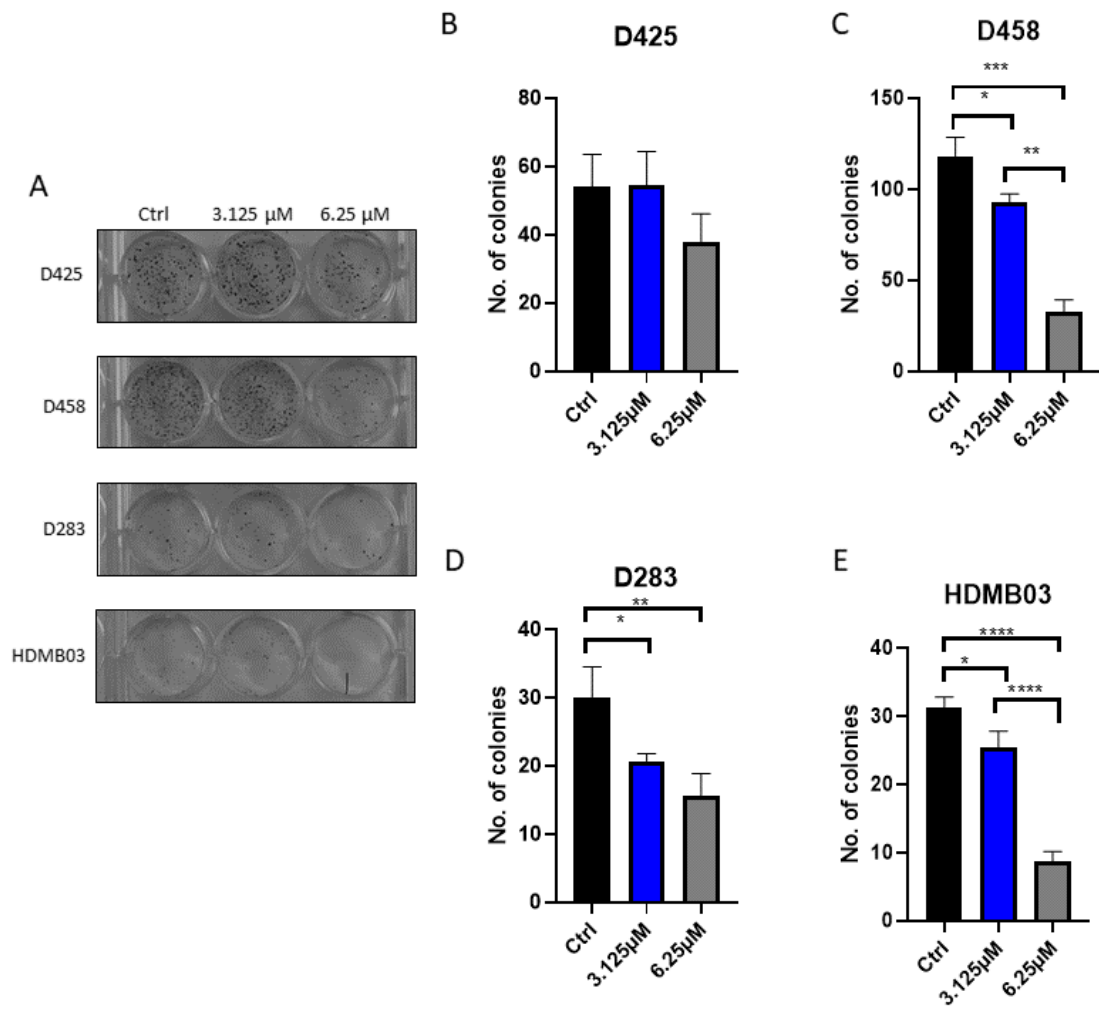


Figure 6.22 Effect of CBR5884 on clonogenic survival in MYC-amplified MB_{GRP3} parental cells. A) Representative images of clonogenic assay in D425, D458, D283 and HDMB03 cell lines following 10 day treatment with 3.125 μ M and 6.25 μ M CBR5884 .. Histogram representation of colony numbers post-treatment in B) D425 C) D458 D) D283 and E) HDMB03 cells. Data represents mean of three biological replicates \pm SEM. Significance determined by one-way ANOVA. * $p < 0.05$, ** $p < 0.01$, *** $p < 0.001$, **** $p < 0.0001$.

The clonogenicity of MYC-regulable cell lines was also evaluated following pharmacological inhibition of PHGDH. The objective was to establish whether MYC knockdown could abrogate the effect of NCT503 on colony formation. The D425 MYC 2 cells were treated with two concentrations of NCT503 in the presence or absence of doxycycline and measured the effect on colony formation. The impact of MYC knockdown on number of colonies formed in D283 and HDMB03 meant that assessment of NCT503 on colony formation was not possible (data not shown). Notably, MYC knockdown alone severely impacted colony number in the D425 MYC 2 cells (Figure 6.23 A & B) but did not completely diminish colony formation. In fact, knockdown of MYC resulted in a 90% reduction of D425 MYC 2 (off) colonies. A dose-dependent reduction of colonies was observed in D425 MYC 2 (on) cells post NCT503 treatment (Figure 6.23 A & B). However colony numbers were still significantly higher in D425 MYC 2 (on) cells to their equivalent D425 MYC 2 (off) cells at each dosage of NCT503. Although NCT503 affected colony numbers in D425 MYC 2 (off) cells, these appeared less dramatic. To capture NCT503 treatment effects we looked at relative alterations in colony number for the MYC (on) and MYC (off) cells relative to their untreated control. This analysis suggested that MYC knockdown abrogated the response to NCT503 treatment (Figure 6.23 C). Although NCT503 displayed dose-dependent effects on colony formation, it was a greater magnitude in D425 MYC 2 (on) cells and this was more pronounced when cells were treated with 12.5 μ M NCT503 (Figure 6.23 C). These results suggests that diminished MYC expression blunted the effect of NCT503 on colony forming ability.

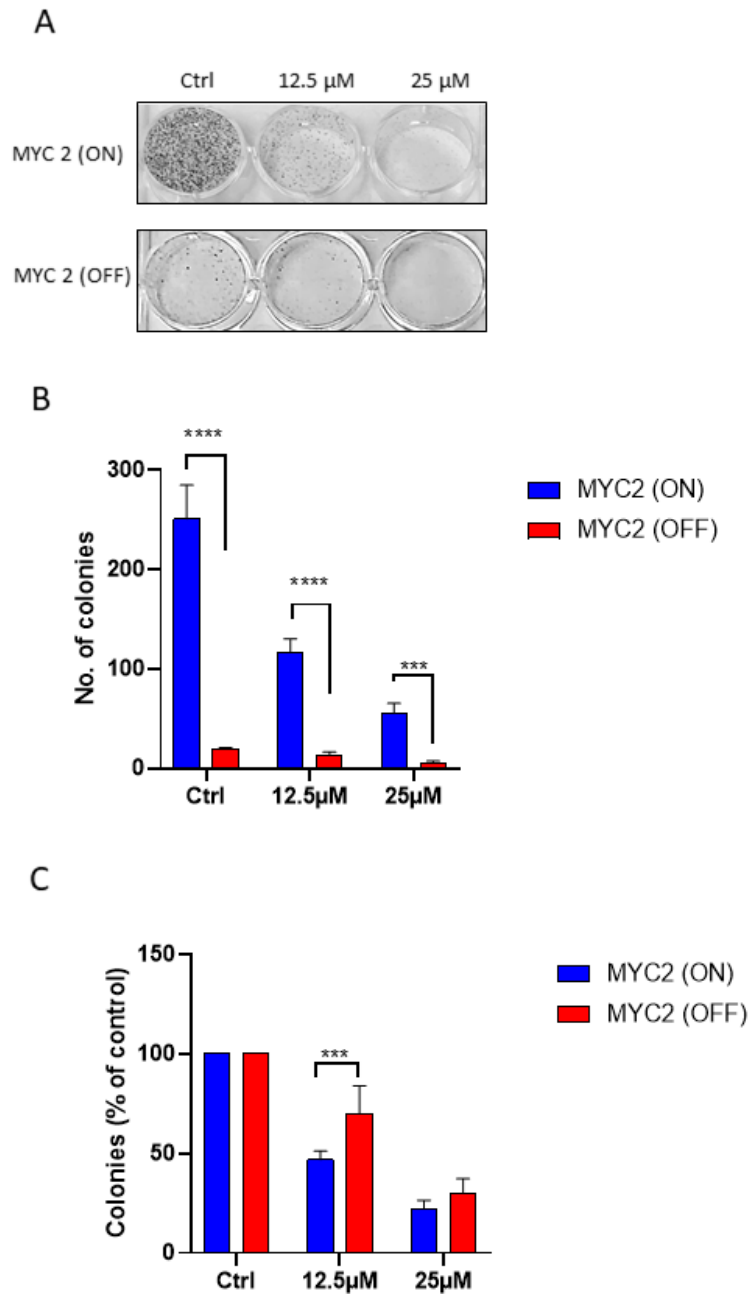


Figure 6.23 Effect of NCT503 on clonogenic survival in D425 MYC 2 cells.. A) Representative images of clonogenic assay in D425 MYC 2 (on) and MYC 2 (off) cells following 10 day treatment with 12.5 μM and 25 μM NCT503 treatment. B) Quantification of colony numbers post-treatment in MYC 2 (on) and MYC 2 (off) cells C) Colony numbers normalised to their respective untreated controls. Data represents mean of three biological replicates \pm SEM. Significance determined by one-way ANOVA. *** $p < 0.001$, **** $p < 0.0001$.

6.3.4.2 Cell cycle progression upon PHGDH inhibition

Analysis of clonogenicity revealed treatment with NCT503 or CBR5884 caused a reduction in colony formation and consequently proliferation of MB_{GRP3} cell lines. It was addressed whether PHGDH inhibition would alter progression through the cell cycle. MB_{GRP3} cells were treated with 25 μ M or 50 μ M NCT503 for 72 h including appropriate DMSO controls. Following treatment, cells were collected and prepared according to protocols detailed in Chapter 2. Cells were stained with propidium iodide and subjected to flow cytometry analysis.

Treatment with NCT503 caused alterations in cell cycle progression of MB_{GRP3} cells. Following treatment with NCT503 in the D425 cells, there was a dose-dependent increase in the fraction of cells in sub-G1 phase, which is associated with apoptotic cell populations. This was accompanied by a decrease in the percentage of cells in G0/G1 phase indicating that NCT503 may cause G0/G1 arrest, which ultimately results in cell death (Figure 6.24, Table 6.3). This was also observed in the D458 cells in addition to a significant decrease in the proportion of cells in S phase (Figure 6.24, Table 6.3). Although marked reductions in cells at S and G2/M were observed in the D283 cells, the effect of NCT503 treatment was more pronounced at the sub-G1 and G0/G1 phases of the cell cycle (Figure 6.24, Table 6.3). In the HDMB03 cells, a dose-dependent rise in the G0/G1 population was observed. Additionally, the fraction of cells in S phase was markedly reduced in the HDMB03 cells. At 72 h, there were more cells in G2/M in control cells compared to when cells were treated with 50 μ M NCT503 (Figure 6.24, Table 6.3). Overall, NCT503 caused a profound increase in cells in sub-G1 or G0/G1. These results demonstrate that PHGDH inhibition via NCT503 impacts cell cycle progression and may lead to apoptotic cell death in MB_{GRP3} MYC-amplified cells.

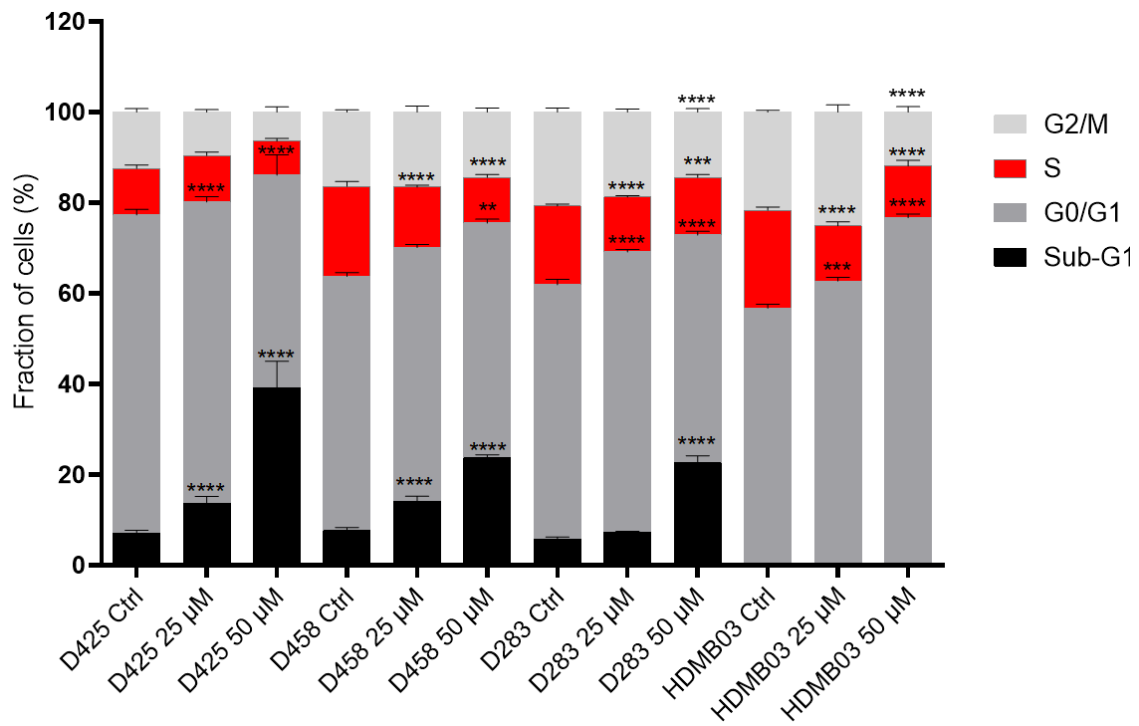


Figure 6.24 Effect of NCT503 on cell cycle progression in MYC-amplified MB_{GRP3} parental cells. D425, D458, D283 and HDMB03 cells were treated with 25 μM or 50 μM for 72 h and subjected to flow cytometry analysis to determine cell cycle progression. Data indicates fraction of cells in each cell cycle phase. Data represents mean ± SEM from three biological replicates. Significance was tested using a Two-way anova for each cell line. * $p < 0.05$, ** $p < 0.01$. *** $p < 0.001$, **** $p < 0.0001$

Table 6.3 Cell cycle analysis in MB_{GRP3} cells treated with NCT503

Cell line	Treatment (vs Ctrl)	Sub-G1	G0/G1	S	G2/M
D425	25 μM	-6.72	3.85	-0.01	2.88
	50 μM	-32.16	23.38	2.70	6.08
D458	25 μM	-6.41	0.02	6.55	-0.16
	50 μM	-16.09	4.37	9.72	1.99
D283	25 μM	-1.55	-5.69	5.25	1.99
	50 μM	-16.81	5.87	4.62	6.32
HDMB03	25 μM		-5.97	9.44	-3.47
	50 μM		-19.96	10.21	9.75

6.3.4.3 Impact on mitochondrial and glycolytic function following PHGDH inhibition

The *de novo* serine and glycine pathway has been demonstrated to contribute to cellular nucleotide pools through its supply of one carbon units to the folate cycle. The supply of nucleotides and other substrates is particularly important during the growth phases of the cell cycle thus predictably NCT503 treatment reduced proliferation and caused G0/G1 arrest in the MB_{GRP3} cell lines. The function of the SGP has also been shown to support mitochondria function. It was queried whether inhibition of PHGDH would impact bioenergetics and mitochondrial function. Following treatment with 25 μ M and 50 μ M NCT503 for 24 h in the MB_{GRP3} cell lines, mitochondrial function and bioenergetics were assessed using the Seahorse Bioanalyser to measure OCR and ECAR.

Firstly, the effect on mitochondrial activity following NCT503 was determined. In general, a dose dependent reduction in basal OCR post-treatment in the MB_{GRP3} cell lines was observed (Figure 6.25). Basal OCR was not affected by treatment with 25 μ M in the D425 cells however was reduced when treated with 50 μ M ($IC_{50} \sim 40 \mu$ M). Treatment with both concentrations of NCT503 significantly perturbed basal OCR in the D458 cells ($IC_{50} \sim 13 \mu$ M) (Figure 6.25 B). This trend was similarly observed in the D283 ($IC_{50} \sim 30 \mu$ M) and HDMB03 ($IC_{50} \sim 47 \mu$ M), although only significant in the former (Figure 6.25 B & C). These results reveal a metabolic response to PHGDH inhibition via NCT503, mechanisms for this observation may be related to a stress response or an early indicator of insufficient substrates for mitochondria function.

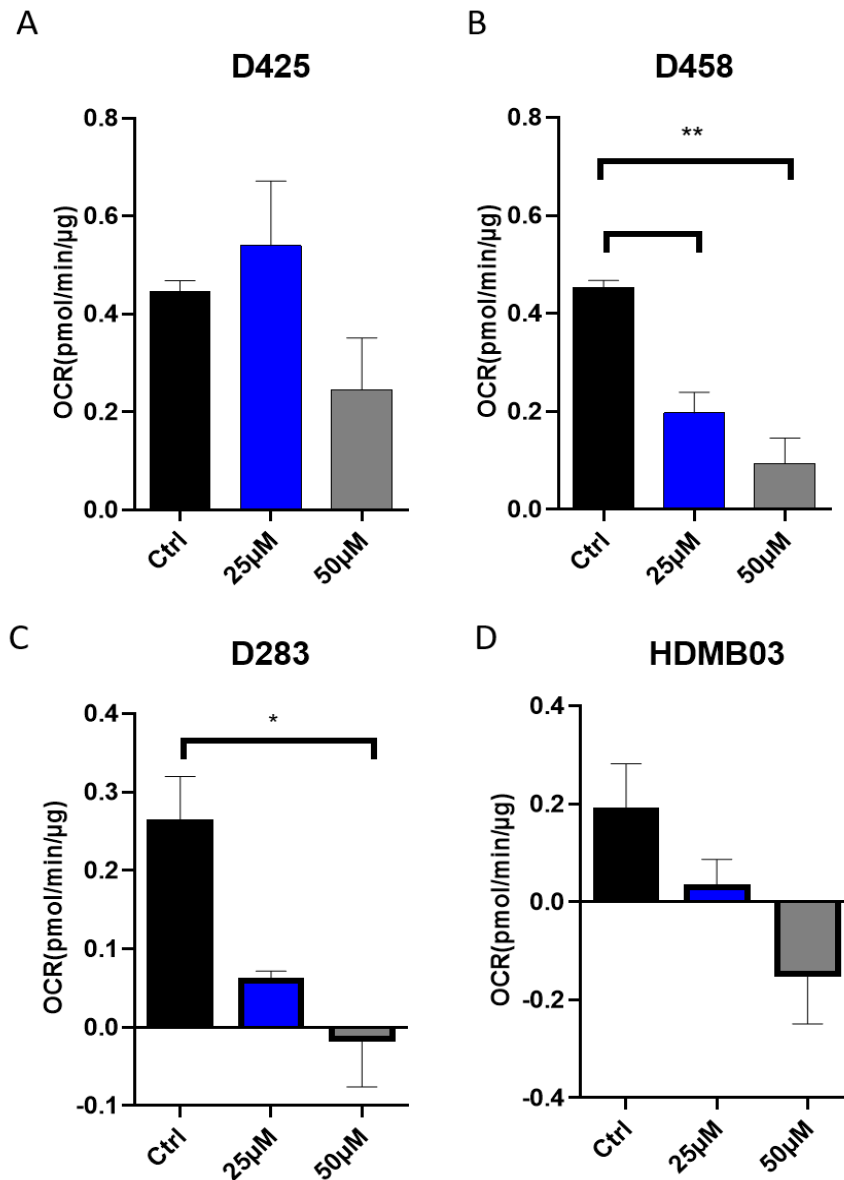


Figure 6.25 Effect of NCT503 on mitochondrial function in MYC-amplified MB_{GRP3} parental cell lines. A) D425 B) D458 C) D283 D) HDMB03 cells were treated with 25 μ M or 50 μ M NCT503 for 24 h and bioenergetic output determined using a Seahorse Bioanalyser to measure oxygen consumption rate (OCR). OCR was normalised to protein content (μ g) to account for cell number variations. Data represents three independent experiments with 8 technical replicates each. Bars show mean \pm SEM. Significance was determined using a one-way ANOVA. * $p < 0.05$, ** $p < 0.01$.

The effect of NCT503 on glycolysis via ECAR measurements was also determined (Figure 6.26). PHGDH shunts glycolytic intermediates into the SGP and diverts glucose-derived carbons from generating acetyl-CoA which can then be utilised for ATP production resulting from lactate production and OXPHOS. In 3 of the 4 MB_{GRP3} cells,

treatment of NCT503 caused an increase in ECAR ($p < 0.05$). A dose-dependent rise in ECAR was observed in the D425 and D458 cells post-treatment. In the HDMB03 cells, at 25 μM there was a rise in ECAR although a striking drop in ECAR was measured at 50 μM . Conversely, NCT503 treatment augmented ECAR in the D283 cells. Together our results suggest that whilst NCT503 may impact mitochondria function and reduce OXPHOS derived ATP, the opposing effect is observed in glycolytic derived ATP where there was a noticeable rise in ECAR and presumably lactate production.

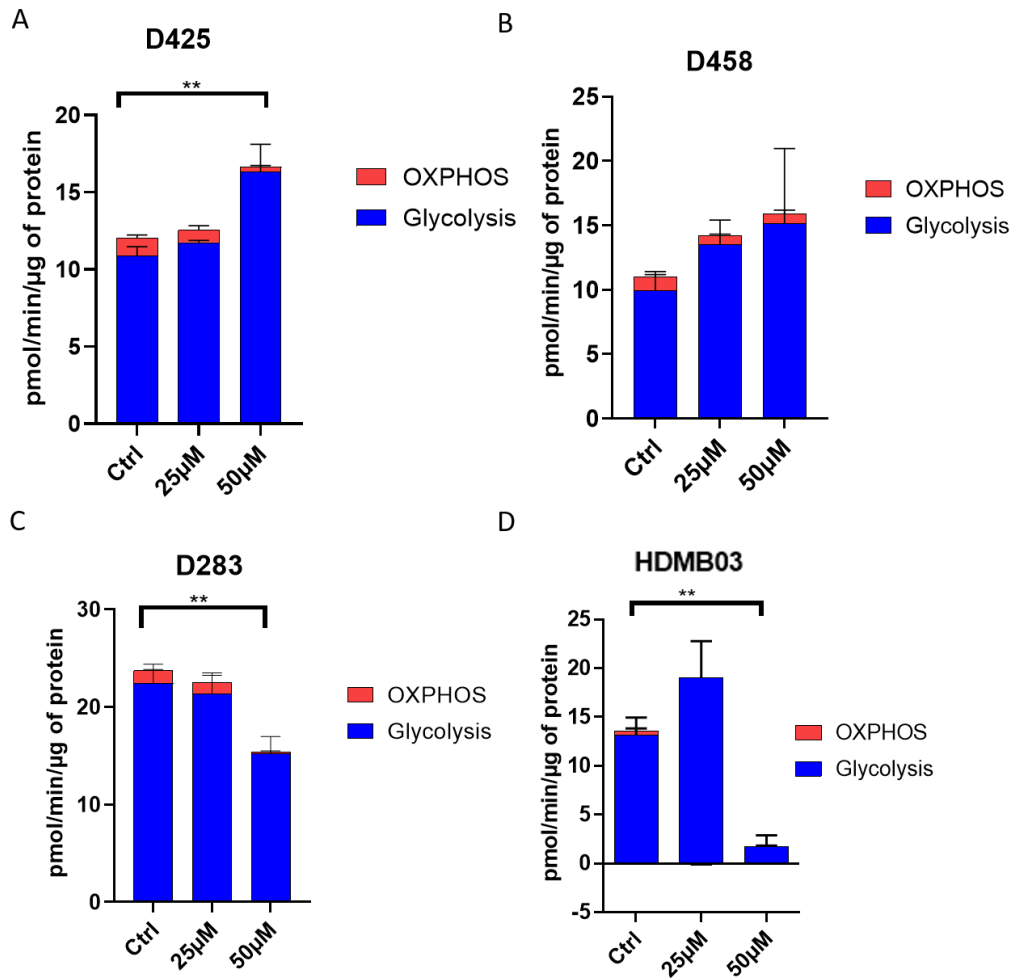


Figure 6.26 Effect of NCT503 on glycolytic and OXPHOS dependent ATP production in MYC-amplified MB_{GRP3} parental cell lines. A) D425 B) D458 C) D283 D) HDMB03 cells were treated with 25 μM or 50 μM NCT503 for 24 h and bioenergetic output determined using Seahorse Bioanalyser to measure OCR and ECAR. OCR and ECAR was normalised to protein content (μg) to account for cell number variations. Data represents three independent experiments with 8 technical replicates each. Bars show mean \pm SEM. Significance was determined using a one-way ANOVA. * $p < 0.05$, ** $p < 0.01$.

6.3.4.4 Impact on nutrient sensing pathway following PHGDH inhibition

Treatment with NCT503 caused an observable reduction in cell viability, clonogenicity, G0/G1 cell cycle arrest and mitochondrial function. NCT503 inhibits the activity of PHGDH, the enzyme which is the committing step of *de novo* serine synthesis and serine derived from glucose. Inhibition of its activity is likely to affect intracellular levels of serine and glycine causing metabolic imbalances likely leading to metabolic stress and concomitant activation of nutrient sensing pathways. This notion is particularly emphasised in our experiments assessing mitochondrial output following NCT503 treatment. Within the first 24 h of NCT503 mediated PHGDH inhibition, there was a loss of basal mitochondrial OCR in response to treatment indicating metabolic stress which may indeed impact nutrient signalling pathways. In particular, the activity of mTOR senses nutrients and growth factors and integrates cellular conditions to downstream pathways which ultimately balance anabolism and catabolism. The activity of the mTORC1 complex is interconnected with the protein synthesis machinery through the regulation of its downstream effectors 4EBP1 and S6K. Phosphorylation of 4EBP1 by mTORC1 releases it from the cap binding protein eIF4Ea, a key component of the multi-protein eIF4F complex, a transcription factor whose activity is the rate-limiting step to translation initiation. The phospho-activated S6K phosphorylates the ribosomal protein S6 (RPS6) and this processes has been linked as a determinant of cell size (Ruvinsky et al., 2005).

I therefore evaluated whether NCT503 treatment induced alterations in mTOR signalling. MB_{GRP3} cells were treated with 12.5 μ M, 25 μ M or 50 μ M NCT503 for 24h, cell pellets were collected and protein extracted. Immunoblotting of phospho-4EBP1 and phospho-RPS6 were used as indicators of mTOR pathway activity in the D425, D458, D283 and HDMB03 cell lines. *MYC* expression was also probed to establish whether NCT503 affected *MYC* protein expression or stability (Figure 6.27). Treatment with NCT503 caused minimal but dose-dependent reduction in *MYC* expression in the D425, D458 and HDMB03 cell lines. *MYC* levels remained constant in the D283 cells although there was an increase at 50 μ M NCT503 (Figure 6.28A). There was marked loss of phospho-RPS6 post-treatment in a dose-responsive manner across the *MYC*-amplified MB_{GRP3} cell lines (Figure 6.28B). WES examination of phospho-4EBP1 (T36/T47) sites resolved two distinguishable bands/peaks across the cell lines. These were therefore assessed as individual bands and the impact of NCT503 treatment evaluated. There was a differential effect on the two phosphorylated peaks of 4EBP1. A general incremental reduction in peak 1 and a rise in peak 2 post-treatment was observed (Figure 6.28C & D).

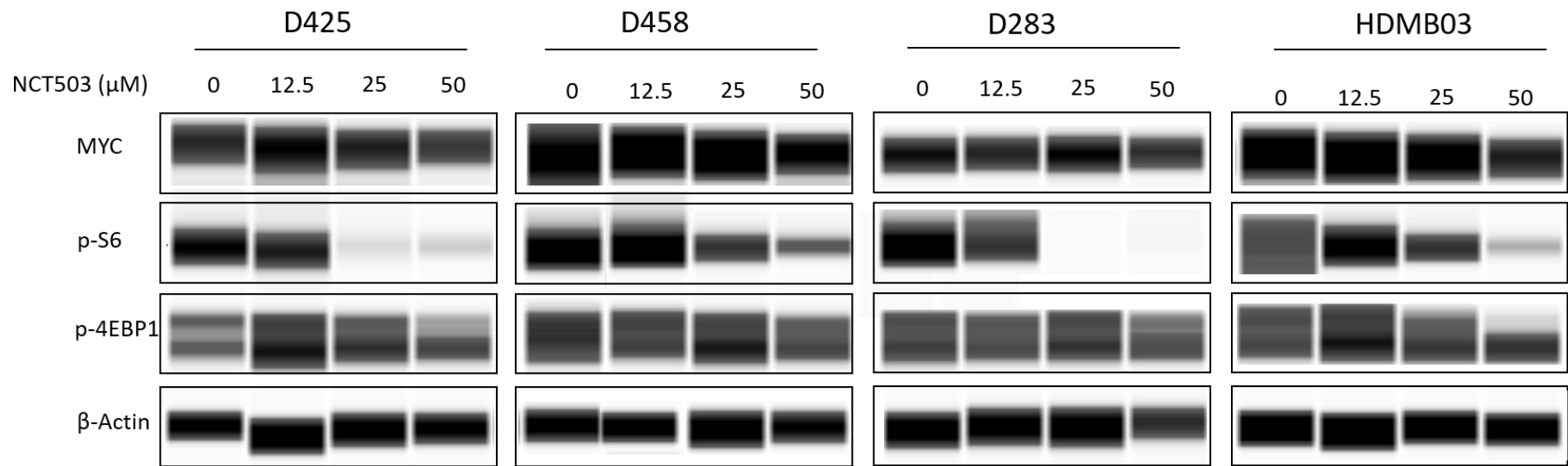


Figure 6.27 Impact of NCT503 treatment on mTOR signalling in MYC-amplified MB_{GRP3} parental cell lines. Cell lines were treated with a range of NCT503 concentrations for 24 h and cell lysates collected. Samples were probed for MYC and phosphorylated ribosomal protein S6 and 4EBP1. β -Actin was used as a loading control. 0.8 μ g of protein lysate was loaded for each sample.

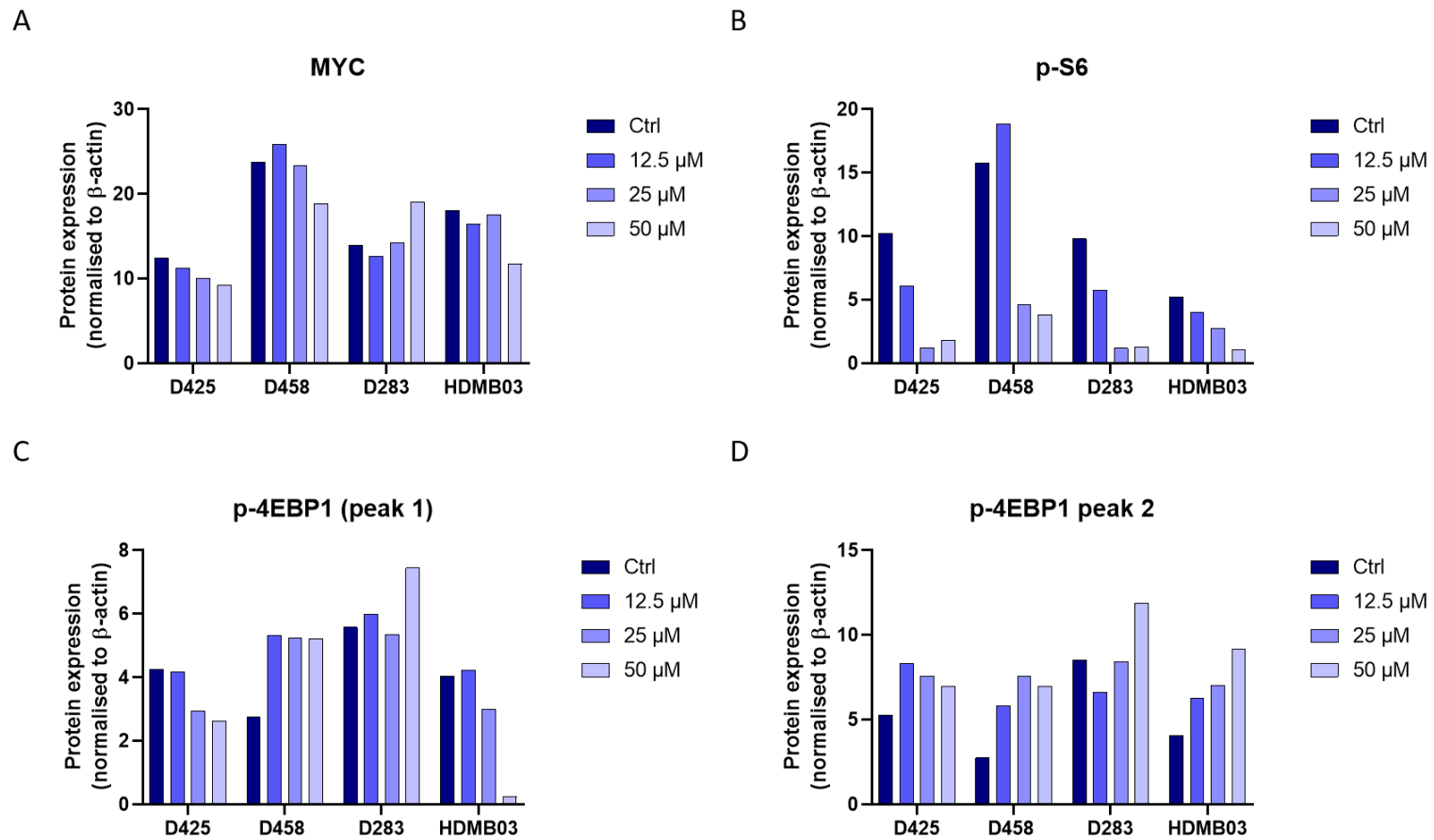


Figure 6.28 Quantitative analysis of the mTOR pathway in MYC-amplified MB_{GRP3} parental cell lines. D425, D458, D283 and HDMB03 cells were treated with a range of NCT503 concentrations for 24 h and cell lysates collected. Samples were probed for MYC and phosphorylated ribosomal protein S6 and 4EBP1. Protein expression was normalised to a β -actin loading control.

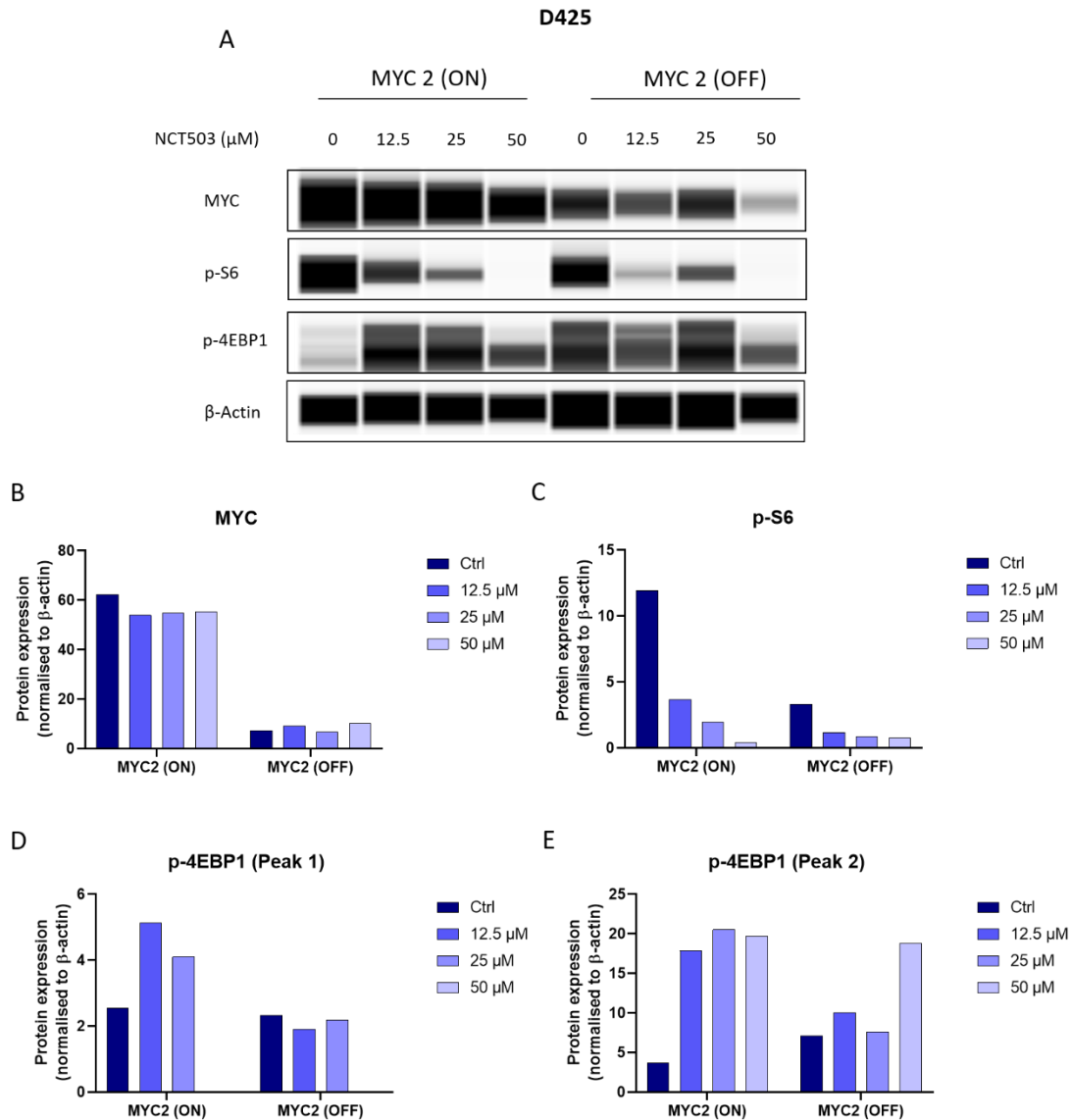


Figure 6.29 Impact of NCT503 on mTOR signalling pathway in D425 MYC 2 isogenic cells. Cells were doxycycline induced for 48 h prior to treatment with varying concentrations of NCT503 for 24 h. A) Typical WES image of MYC, phospho-S6 and phospho-4EBP1 in D425 MYC 2 (on) and MYC 2 (off) cells. B) Quantitative analysis of WES immunoblotting of MYC and mTOR downstream effectors. Protein expression was normalised to β -actin control.

The D425 MYC 2 cell line was utilised to further understand the influence of MYC expression on the mTOR response observed in the parental cell lines. In contrast to parental cell lines, a proportional decrease in MYC expression was not observed in the D425 MYC 2 (on) cells following NCT504. Although doxycycline reduced MYC expression in the D425 MYC 2 (off) cells, this was not further reduced with subsequent treatment of NCT503 (Figure 6.29A & B). Phosphorylated levels of ribosomal protein S6 decreased in a dose-dependent manner in the

D425 MYC 2 (on) cells. Although an initial decrease in phospho-S6 in the D425 MYC 2 (off) cells when treated with 12.5 μM NCT503, levels remain relatively similar at higher doses of NCT503 (Figure 6.29 C). With regards to peak 1 of phospho-4EBP1, there was an initial rise in levels following 12.5 μM NCT503 treatment however this is completely diminished by 50 μM NCT503 in the D425 MYC 2 (on) cells. This supports our initial findings in the MB_{GRP3} parental cell lines which also displayed reductions in this phospho-4EBP1 peak. However, levels of phospho-4EBP1 (peak 1) remain near constant in the D425 MYC 2 (off) cells with the exception of 50 μM NCT503 which similarly reduced phosphorylation (Figure 6.29 D). When phospho-4EBP1 (peak 2) was evaluated, there was a sharp rise in its levels at 12.5 μM NCT503 which was maintained when dose was increased in the D425 MYC 2 (on) cells. This event was observed much later in the D425 MYC 2 (off) cells, specifically at 50 μM NCT503 treatment. Taken together, these results suggest that NCT503 induces a response in the mTOR pathway following NCT503 inhibition albeit with differential effects on the two distinct branches of the S6 and 4EBP1 effector pathways. Particularly, decreased MYC expression abrogated mTOR-dependent response.

6.3.5 CRISPR-mediated loss of PHGDH in parental MB_{GRP3} cell lines

Some studies have demonstrated through genetic knockout models that PHGDH is essential to cancer survival and tumour progression, particularly in PHGDH amplified cancers like certain breast cancer subtypes, melanoma and colon cancers. To my knowledge, its role in MB tumorigenesis has not been studied. I investigated whether the loss of PHGDH had a functional consequence on MB_{GRP3} cells. Certainly the dynamics of genetic manipulation could differ from pharmacological inhibition since the latter would not impact PHGDH expression at either mRNA or protein level rather the functional activity of the enzyme. For this study, CRISPR-mediated gene editing was utilised for loss of function study of PHGDH in MB. CRISPR gene editing was achieved using single guide RNA (sgRNA) specific for PHGDH and a non-targeting control. The sgRNA directs the CAS9 endonuclease to its complementary site where the CAS9 induces double strand DNA breaks which is repaired by non-homologous end joining (NHEJ). NHEJ introduces indels which disrupt open reading frame of the gene effectively creating a functional knockout (Ran et al., 2013). PHGDH KD models was engineered in 3 out of 4 MB_{GRP3} MYC-amplified cells PHGDH KD could not be established for the D283 as considerable cell death occurred post-selection.

6.3.5.1 Confirmation of PHGDH knockdown at the protein expression level

Prior to experimentation using the PHGDH KD cell lines, loss of expression in the D425, D458 and HDMB03 was confirmed at the protein expression level. Following 7 days of antibiotic selection and establishment of an adequate cell population, cell pellets were collected, protein extracted and samples subjected to immunoblotting for PHGDH using WES. Overall, efficient knockdown of PHGDH was achieved in the three MB_{GRP3} cell lines. For the D425 cells, 90% reduction in PHGDH expression levels were achieved. Similarly, 80% and 70% knockdown was reached in the D458 and HDMB03 cell lines respectively (Figure 6.30).

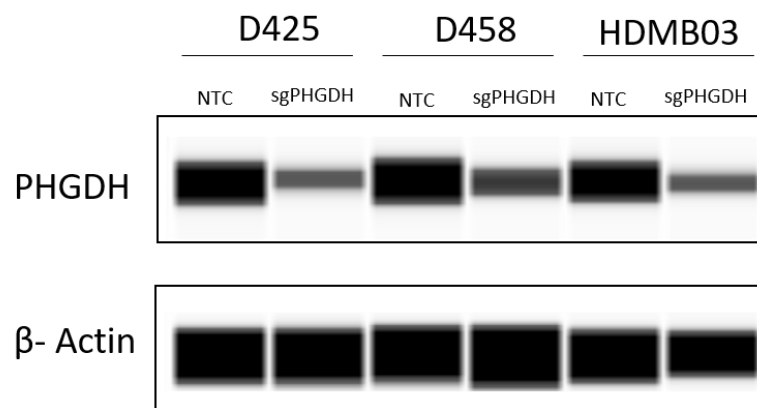


Figure 6.30 PHGDH expression in MB_{GRP3} cells following CRISPR mediated knockdown of PHGDH. WES images of D425, D458 and HDMB03 non-targeting controls (NTC) and sgPHGDH cells.

6.3.5.2 The effect on cellular growth following PHGDH loss

The activity of PHGDH sequesters glucose-derived carbons into anabolic pathways by fuelling one carbon metabolism which supports growth and proliferation of cancer cells. It was examined whether loss of PHGDH in MB_{GRP3} cell lines impacted cellular proliferation. Cell growth was measured using trypan-blue dye exclusion to perform viable cell counting at 24, 72, 120 and 168 h.

Reduced expression of PHGDH inhibited proliferation of *MYC*-amplified MB_{GRP3} cell lines (Figure 6.31). In the D425 cells, NTC and sgPHGDH grew similarly in the first 72 h however, D425 sgPHGDH cells lagged behind their NTC counterparts from 120 h onwards (doubling time D425 NTC (36.85 h) versus sgPHGDH (40.54 h)). There was a slight but significant reduction in proliferation of the D425 cell following PHGDH knockdown ($p < 0.05$, Figure 6.31A). A more divergent effect on proliferation was observed at earlier time points in the D458 and HDMB03 cell lines following loss of PHGDH. The doubling rate of D458 NTC compared to the D458 sgPHGDH cells were 45 and 47.59 h, respectively ($p < 0.01$, Figure 6.31 B). Impairment in the proliferation of HDMB03 cells was observed following PHGDH knockdown. The proliferation of HDMB03 NTC was exponential over the time course however in the case of HDMB03 sgPHGDH cells, proliferation slowed after 72 and the estimated doubling rates differed by ~20 hrs in this cell line (doubling time HDMB03 NTC 61.4 versus sgPHGDH 85.23 h) (Figure 6.31 C). In summary, loss of PHGDH was not detrimental to cell survival however, it noticeably caused a decline in proliferation of *MYC*-amplified MB_{GRP3} cells. Notably, differences in proliferation were observed following 72 h and diverged from this time point onwards.

It is noteworthy that in the D283 cell line, knockdown of PHGDH could not be established for this study despite two attempts to do so owing to cell death post-selection. Previous genome-wide CRISPR analysis identified PHGDH as a cell essential gene in the D283 cell line but not D425 or HDMB03 cell lines. The D458 were not included in these CRISPR experiments (Unpublished data from Matt Selby thesis, Appendix). These experiments in conjunction with the genome-wide CRISPR analysis, suggest differential response to PHGDH loss and cell line-specific effects following reduced expression of PHGDH.

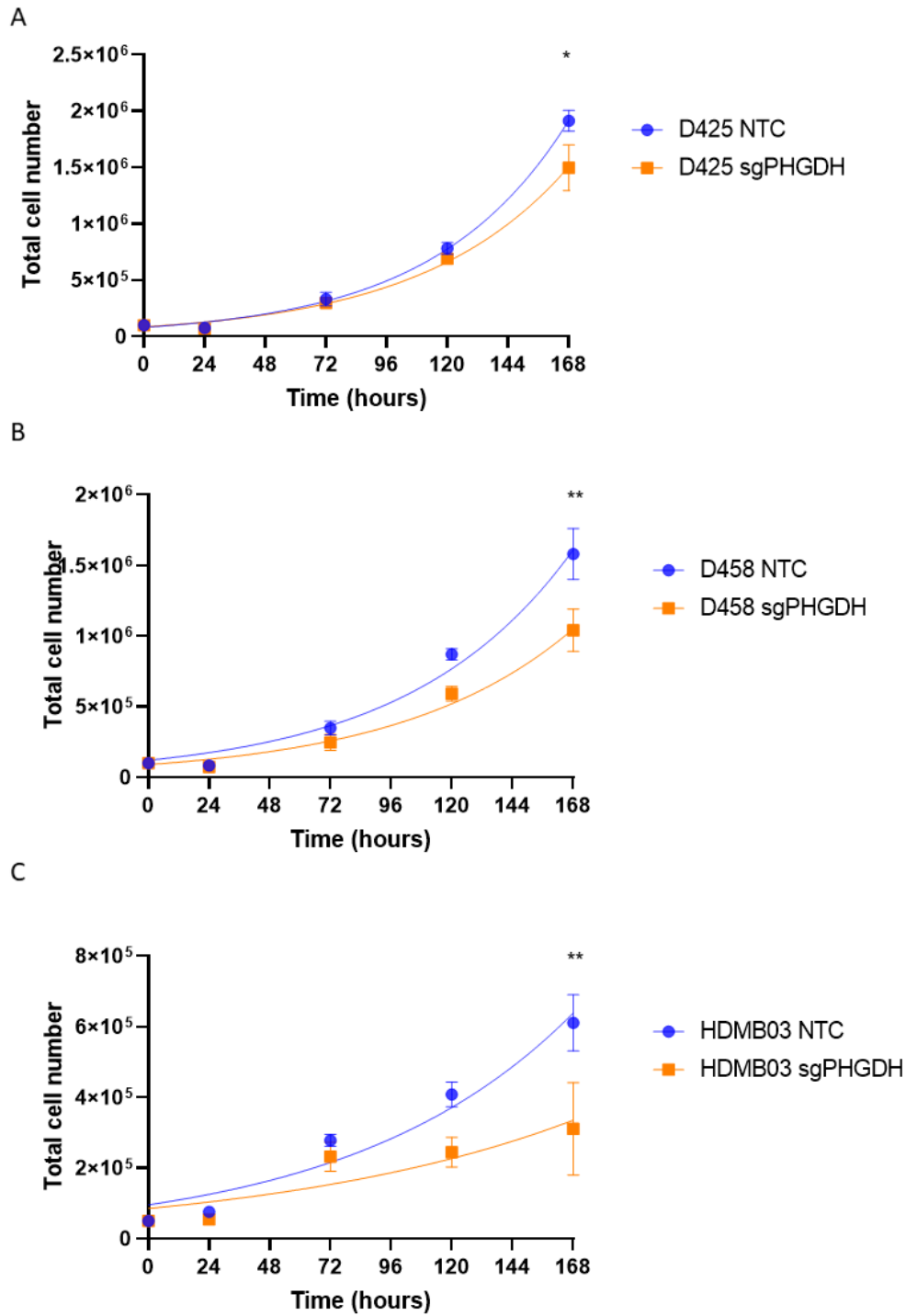


Figure 6.31 Consequence of PHGDH loss on proliferation of MB_{GRP3} MYC-amplified cells. D425, D458 and HDMB03 were subjected to viable cell counting at indicated time points. Cell proliferation and curve of best fit plotted using linear regression. Data represents three biological experiments and data shows mean \pm SEM. Significance was determined using linear regression comparison of lines of best fit.

6.3.5.3 Impact on MB_{GRP3} proliferation in serine and glycine replete conditions upon PHGDH loss

Knockdown of PHGDH in the MB_{GRP3} *MYC*-amplified cell lines affected proliferation in nutrient abundant growth culture medium. Notably, the growth impairment was more noticeable at late-stage culture suggesting the interplay of nutrient sufficiency and the growth deficiency observed. PHGDH is the crucial node in *de novo* serine and glycine biosynthesis and loss of expression could render cellular reliance on exogenous sources of serine and glycine. It was hypothesised that loss of PHGDH would cause serine auxotrophy and render MB_{GRP3} dependent on exogenous serine. Since glycine can be synthesised from exogenous serine by SHMT, reliance on exogenous glycine alone was not anticipated. Incucyte live cell imaging was utilised to measure proliferation (i.e. confluence) when serine and/or glycine was deprived from the growth medium. In addition, effect on colony formation was assessed by clonogenicity under nutrient limiting conditions.

Serine deprivation caused marked reduction in growth of PHGDH knockdown cells. Under –SER and –SER/GLY conditions, proliferation was impaired in the D425 sgPHGDH compared D425 NCT cells (Figure 6.32). This effect was even more pronounced in the D458 sgPHGDH cells under serine limiting conditions where proliferation was reduced (Figure 6.33). In the HDMB03 sgPHGDH cells, there was a similar decrease in proliferation in –SER or –SER/GLY growth culture conditions (Figure 6.34). As previously postulated, glycine deprivation alone was insufficient to cause a significant reduction in growth of the 3 MB_{GRP3} cells when PHGDH was knocked down. Notably, there was a slight cumulative effect when both serine and glycine was removed from growth culture medium. As predicted, these results reveal a reliance on exogenous sources of serine and not glycine when PHGDH expression was diminished.

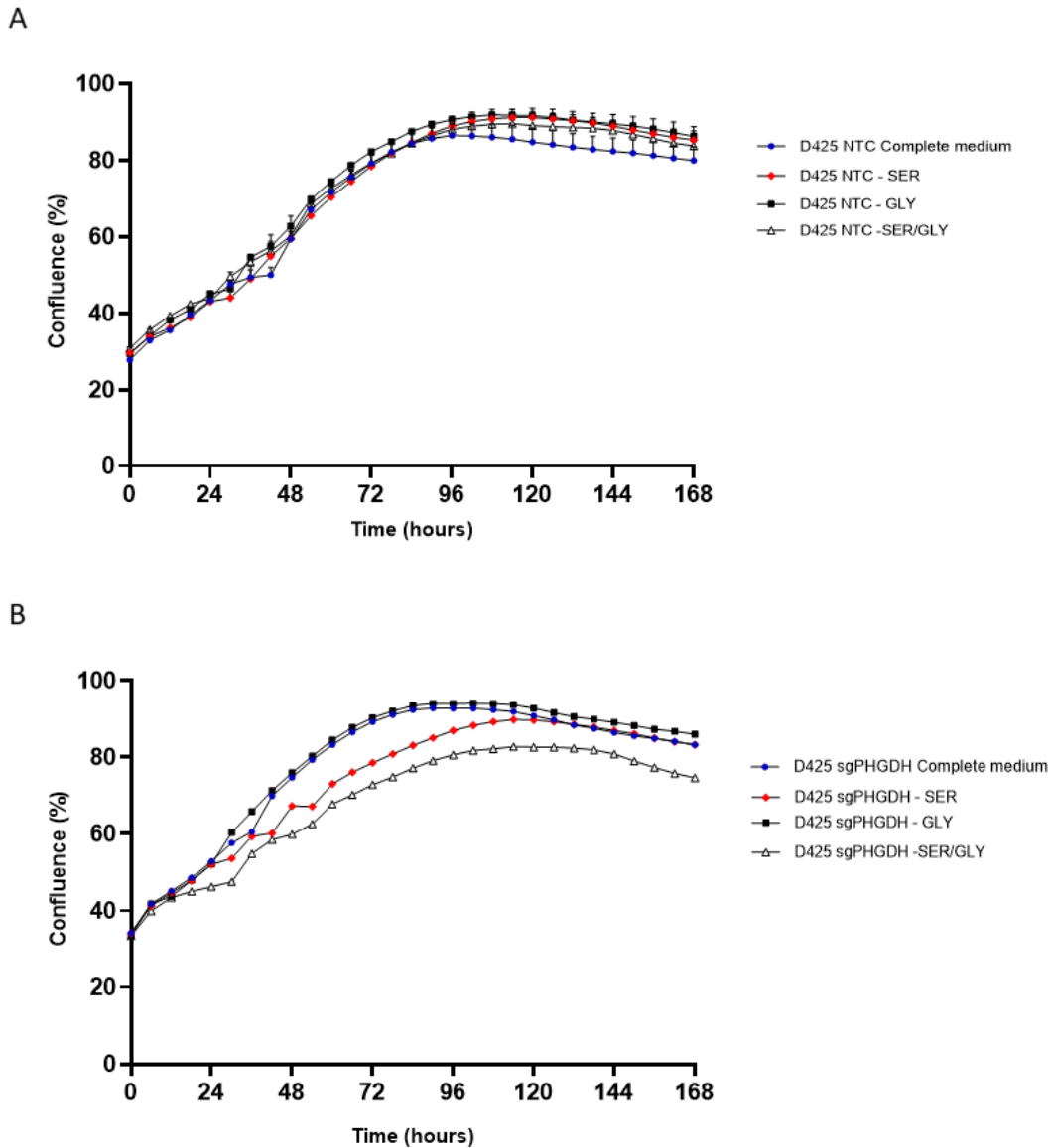
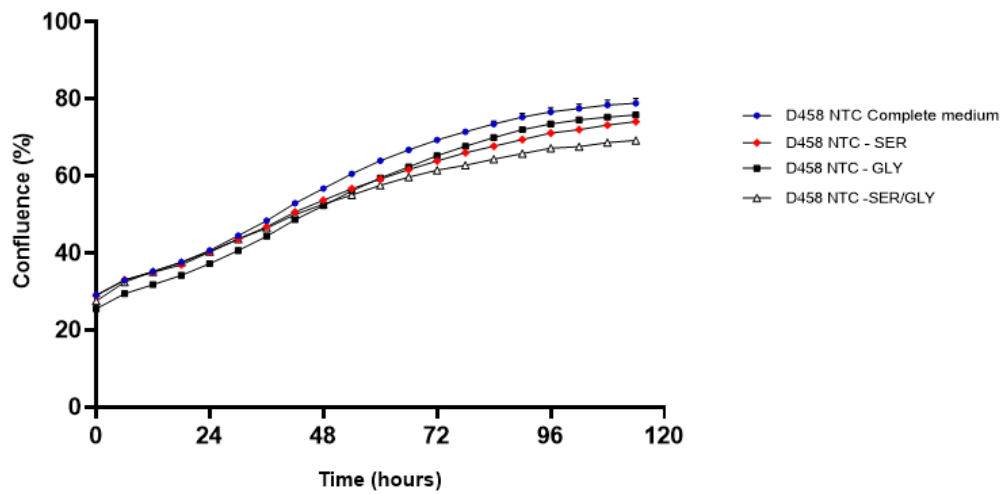


Figure 6.32 Response of D425 cells to serine and glycine depleted conditions. Incucyte live cell imaging analysis. A) D425 NTC and B) sgPHGDH cells were seeded in a 96 well microplate at 1×10^4 cells per well and allowed to adhere to poly-L-lysine coated plates overnight. Cells were subjected to medium deprived of serine or glycine, or both nutrients in addition to nutrient replete minimal essential growth medium. The mean confluence \pm SEM of four individual wells with 9 fields of images from a representative experiment is shown.

A



B

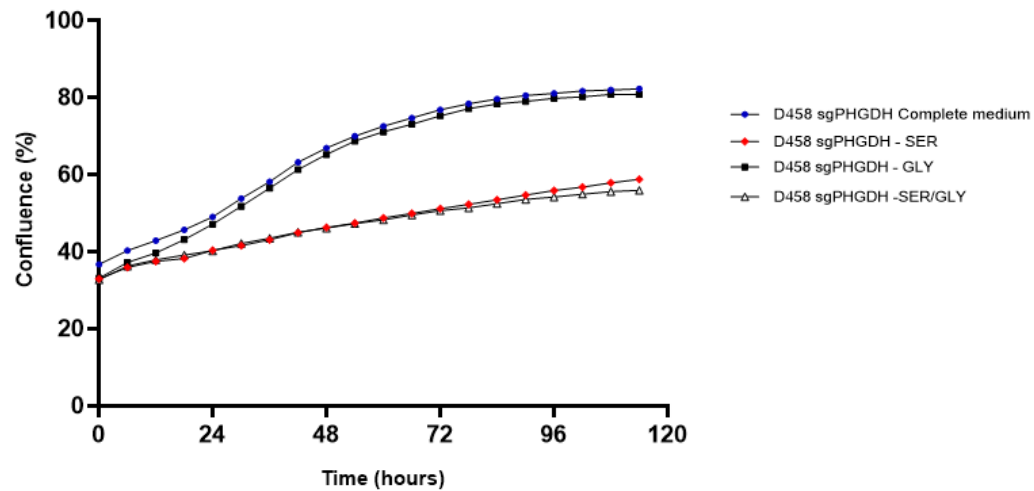


Figure 6.33 Response of D458 cells to serine and glycine depleted conditions. Incucyte live cell imaging analysis. A) D458 NTC and B) D458 sgPHGDH cells were seeded in a 96 well microplate at 1×10^4 cells per well and allowed to adhere to poly-L-lysine coated plates overnight. Cells were subjected to medium deprived of serine or glycine, or both nutrients in addition to nutrient replete minimal essential growth medium. The mean confluence \pm SEM of four individual wells with 9 fields of images from a representative experiment is shown.

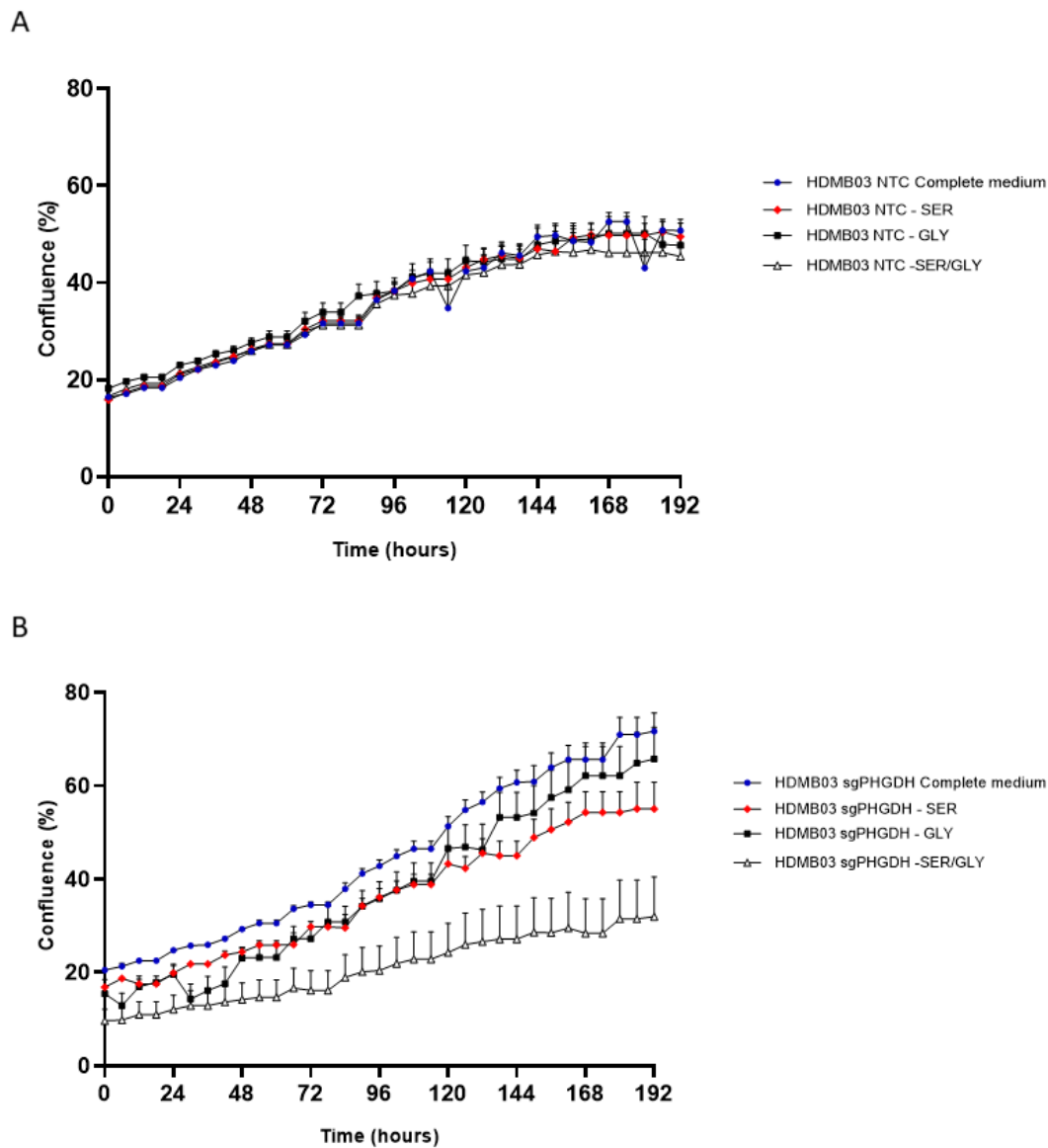


Figure 6.34 Response of HDMB03 cells to serine and glycine depleted conditions. Incucyte live cell imaging analysis. A) HDMB03 NTC and B) HDMB03 sgPHGDH cells were seeded in a 96 well microplate at 1×10^4 cells per well and allowed to adhere to poly-L-lysine coated plates overnight. Cells were subjected to medium deprived of serine or glycine or both nutrients in addition to nutrient replete minimal essential growth medium. The mean confluence \pm SEM of four individual wells with 9 fields of images from a representative experiment is shown.

6.3.5.4 Impact PHGDH knockdown on clonogenic survival following serine and glycine depletion

Results from clonogenic survival assays corresponded with Incucyte growth analysis suggesting that PHGDH loss conferred a reliance on exogenously available serine. In the D425 NTC cells, only removal of both serine and glycine from growth medium impacted number of colonies formed. However in the D425 sgPHGDH, serine depletion alone or in conjunction with glycine caused a marked decrease in number of colonies formed. Depletion of glycine alone was not sufficient to cause a marked reduction in colony forming ability. Similar observations were made in the D458 and HDMB03 sgPHGDH and NTC cells albeit in varying degrees of severity. Taken together, these results show loss of PHGDH impacts the ability of *MYC*-amplified MB_{GRP3} cells to proliferate and survive in serine limiting conditions.

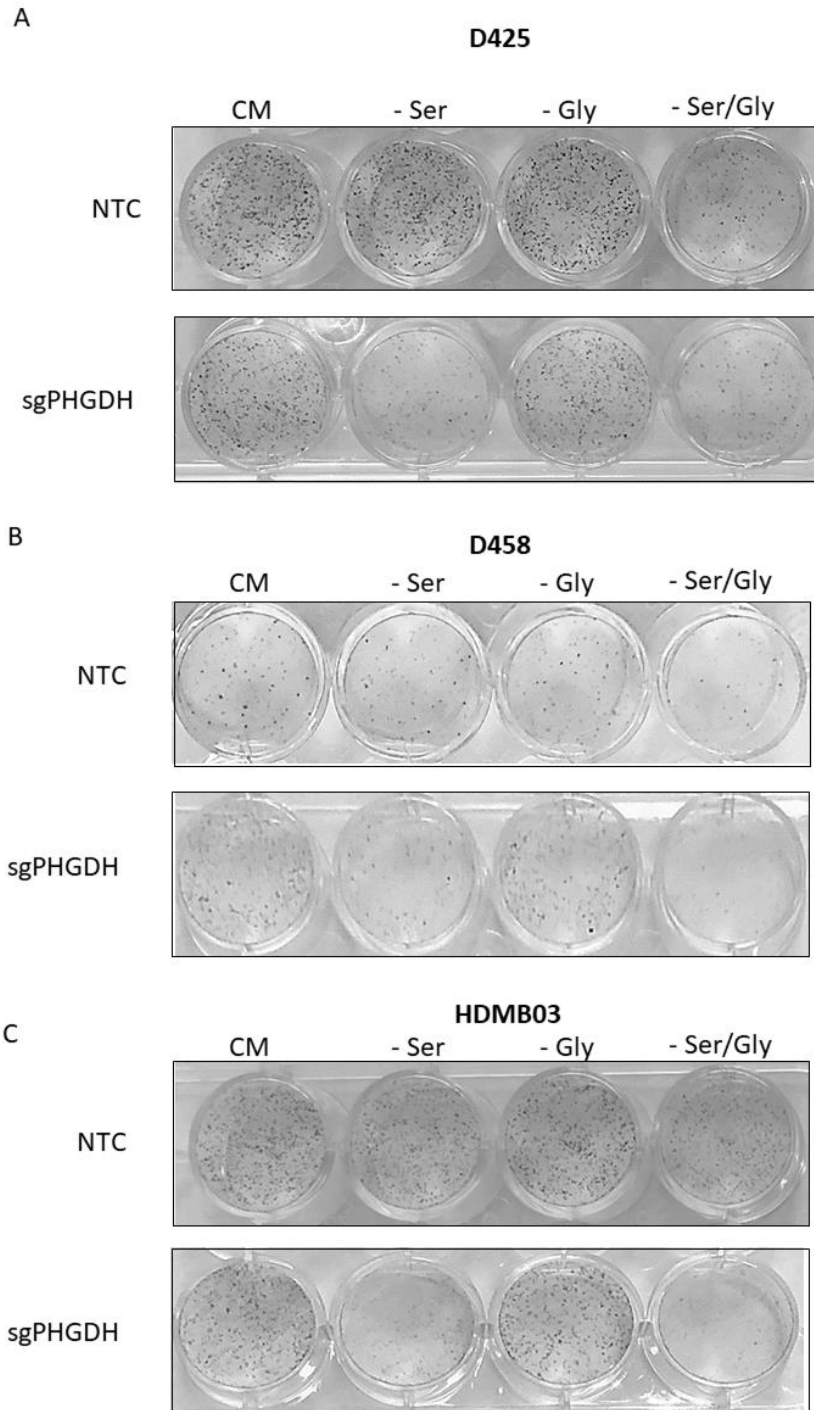


Figure 6.35 Effect on serine and glycine deprivation on clonogenic survival of MB_{GRP3} MYC-amplified cells following PHGDH knockdown. D425, D458 and HDMB03 NTC and sgPHGDH cells were poly-l-lysine adhered to 12 well plates and grown in complete medium (CM), serine depleted (-Ser), glycine depleted (-Gly) or serine and glycine depleted (-Ser/Gly) for 10 days. Colonies were fixed and stained with crystal violet. Representative images of clonogenic assay in A) D425 B) D458 C) HDMB03 cells following nutrient starvation.

6.4 Discussion

6.4.1 Primary MB_{GRP3} display upregulated expression of SGP enzymes

For this chapter, I sought to determine the relevance of the SGP in primary MB in order to establish whether targeting this pathway would be of any clinical relevance. Here it was shown that primary MB_{GRP3} have altered SGP between subtypes and in particular, gain/amplification of *MYC* is associated with upregulation of SGP enzymes at the gene expression level. It was also determined whether PHGDH, a key component of the SGP conferred worst outcomes in MB patients. PHGDH expression was associated with worse prognosis in the MB wide cohort. Evaluating the distribution of PHGDH expression between the subgroups revealed skewed distribution in the MB_{SHH} group in particular, this hinted a differential expression of PHGDH across the MB subgroups with MB_{SHH} samples having higher expression of PHGDH compared to other subgroups. Matched samples are not typically available from surgical resections since the ultimate goal is to limit injury to normal tissue, it was therefore not possible to determine differences in PHGDH expression in surrounding tissues. Additionally it would be useful to establish whether different cells of origin for the MB subgroups are associated with different levels of expression of SGP enzymes. Higher expression of PHGDH was associated with *MYC*-amplified MB_{GRP3} patients. Additionally, high expression of PHGDH was associated with worse overall survival in MB_{GRP3}. A caveat of this analysis, owing to small number of samples was that it could not further evaluate survival differences between low PHGDH, *MYC*-amplified cases against high PHGDH, *MYC*-amplified tumours.

6.4.2 Response of MB_{GRP3} cell lines to modulation of PHGDH function using NCT503

I then explored whether therapeutically targeting PHGDH would display *MYC*-dependent sensitivity in *MYC*-amplified MB_{GRP3} cells. Results from these experiments showed that *MYC*-amplified MB_{GRP3} cells were more sensitive to NCT503 treatment whereas *MYC* knockdown blunted this response. Indeed in the D425 *MYC* 2 cell lines, colony formation was severely affected in the D425 *MYC* 2 (on) cells. Although *MYC* knockdown itself impacted clonogenicity, there was no further cumulative effect of *MYC* knockdown and NCT503 treatment in the D425 *MYC* 2 (off) cells. This supports my previous finding of higher activity of *de novo* serine and glycine pathway highlighted by ¹³C -glucose tracing analysis (Chapter 5) and higher expression of SGP enzymes in *MYC*-amplified cells compared to *MYC* knockdown cells. These data reveal a dependence of *MYC*-amplified MB_{GRP3} cells on the

activity of PHGDH, which supports assimilation of glucose-derived carbons into the SGP and fuels downstream pathways supporting growth and proliferation.

This MYC-dependent sensitivity to PHGDH inhibition was further corroborated using numerous MB_{GRP3} MYC-abnormal cells compared to MB_{SHH} cell lines. PHGDH inhibition using small molecule inhibitors with distinct modes of action revealed sensitivity of MB_{GRP3} cells to NCT503 or CBR5884 treatment compared to non-amplified MB_{SHH} cell lines. The use of the two inhibitors demonstrate target specificity as consistent corresponding effects were observed for each cell line. Phenotypic assessment demonstrated that treatment with NCT503 caused G0/G1 arrest and led to a higher proportion of sub-G1 cells 72 h post-treatment. Furthermore, treatment with NCT503 also led to a significant reduction in basal mitochondria OCR and limited OXPHOS-derived ATP production. Contrastingly, glycolytic function and ATP production was slightly increased in some MB_{GRP3} cells. Inhibition of PHGDH has been shown to cause metabolic stress owing to reduction of glucose-derived serine and glycine and disrupt central carbon metabolism by disrupting PPP-derived ribose and availability of TCA cycle intermediates to anabolic pathways (Pacold *et al.*, 2016; Reid *et al.*, 2018). Interestingly, serine deprivation in conjunction with NCT503 did not cause a further decrease in cell viability suggesting that availability of exogenous serine does not limit effectiveness of PHGDH inhibition mediated by NCT503 (Xia *et al.*, 2019). This was in line with observations made by Pacold *et al.*, which demonstrated that PHGDH inhibition led to wasting of exogenous glycine by SHMT1 which prioritised the reverse reaction of generating serine from glycine and meTHF preventing their incorporation into downstream metabolic pathways (Pacold *et al.*, 2016). Furthermore Reid *et al.*, showed that in addition to nucleoside supplementation in culture medium, α -ketoglutarate and ribose could partially rescue PHGDH inhibition (Reid *et al.*, 2018). These studies in addition to our study support that PHGDH inhibition caused metabolic stress that potentially occurs as a result of imbalances of SGP and other metabolic pathways.

6.4.3 Nutrient sensing pathway response to post NCT503 treatment

PHGDH inhibition via NCT503 caused several phenotypic changes in the MB_{GRP3} cells. The mTOR pathway represents a major pathway for nutrient sensing and coordinates nutrient availability with metabolism and other cellular processes including protein synthesis. The ribosomal protein S6, is phosphorylated by the S6 kinase (S6K), is an effector of the mTORC1 signalling axis (Dennis *et al.*, 2001). Numerous studies have shown that inhibition of mTORC1 by rapamycin suppresses S6 phosphorylation (Biever *et al.*, 2015, Holz and Blenis, 2005).

Assessment of the downstream effectors showed a robust response in the S6 branch which showed decrease in phospho-S6 in a dose-dependent manner. Previous studies have shown S6 phosphorylation may impact global protein synthesis although this remains ambiguous and may be tissue/ context dependent (Biever et al., 2015). Two distinct phospho-4EBP1 peaks were detected using WES analysis. When examined, peak 1 showed diverging trends in the MB_{GRP3} cell lines. Levels were relatively steady in the D458 and D283 cells post-treatment however in the D425 and HDMB03 cell lines, phospho-4EBP1 levels (peak 1) decreased. When the second peak was assessed across the four cell lines, phospho-4EBP1 (peak 2) levels increased in a dose-dependent manner. In the D425 isogenic cells, MYC 2 (on) cells here was a dose-dependent decrease in phospho-4EBP1 (peak 1) which is diminished at highest NCT503 concentration. In the D425 MYC 2 (off) cells however, only 50 μ M treatment with NCT503 impacts phosphorylation levels. Similarly, there was a rise in phosphorylated 4EBP1 (peak 2) in the D425 MYC 2 (on) cells however only the highest dose of NCT503 invokes a change in phospho-4EBP1 in the D425 MYC 2 (off) cells. Since treatment with NCT503 in the MYC 2 (off) cells did not elicit changes in mTOR signalling pathway (except at 50 μ M), this would further support that loss of MYC reduces sensitivity and did not engage mTOR signalling at lower concentrations. It is noteworthy that total expression of s6 and 4EBP1 were not assessed in this study. To fully contextualise and assess the impact of these changes, it is important to determine whether ratios of phospho/total expression were altered following NCT503 in the MYC-amplified and isogenic cell lines.

The divergent effects observed in the phosphorylation of 4EBP1 is intriguing. Studies have previously shown that phosphorylation of Thr37 and Thr46 can be priming events for phosphorylation of other 4EBP1 Ser/Thr sites (Gingras et al., 1999, Gingras et al., 2001, Wang et al., 2003). Phosphorylation of 4EBP1 releases it from eIF4E enabling the interaction of eIF4E/eIF4G which leads to the formation of eIF4F translation initiation complex (Silvera et al., 2010). Although the P13K/Akt/mTOR is implicated in the regulation of 4EBP1, knockdown of both of mTOR or Akt repressed phosphorylation of S6 kinase but had no functional consequence on 4EBP1 suggesting mTOR-independent regulation of 4EBP1 (Nawroth et al., 2011). Others have shown maintenance of 4EBP1 hyper-phosphorylation using mTOR inhibitor RAD001 although it successfully inhibited differentiation of C2C12 myoblast along with decreased phosphorylation of S6 kinase (Willett et al., 2009).

These studies suggest alternative routes of 4EBP1 phosphorylation which may account for some of the observations made in this study. Although WES distinguished two separate peaks

of phospho-4EBP1 at Thr37/46, further clarification of the impact of NCT503 treatment on these sites is required. Using phospho-specific antibodies may distinguish the varying effect of NCT503 on 4EBP1 more clearly. Further experiments evaluating total protein levels of both 4EBP1 and S6 would also enable assessments of whether changes in the ratios of phosphorylated to total protein occur. Going further, assessing whether other nutrient sensing pathways such as the GCN2/eIF2 α may also be implicated and whether interaction of 4EBP1 and eIF4E is disrupted and does indeed impede translation initiation and protein synthesis in the *MYC*-amplified MB_{GRP3} cells

6.4.4 Loss of PHGDH is detrimental to MB_{GRP3} cells under serine limiting conditions

In this study it was determined whether PHGDH loss would impact the growth of MB_{GRP3} cells. PHGDH was found to be essential for growth under normal culture conditions. During periods of serine depletion however, PHGDH loss led to deficiency in proliferation and colony formation. Interestingly, glycine depletion alone did not severely impact growth which is supported by other studies which have shown, serine and not glycine is required during proliferation (Labuschagne et al., 2014). Notably, in the absence of exogenous glycine, glycine can still be synthesised from serine via SHMT 1/2 once imported from extracellular sources. The results of our CRISPR-mediated knockdown of PHGDH are in contrast with small molecule inhibition results which showed pharmacological inhibition of PHGDH resulted in decreased viability irrespective of the availability of exogenous serine. Although CRISPR-mediated knockdown of PHGDH reduced proliferation of *MYC*-amplified MB_{GRP3} cells, this effect was observed at latter stages of cell culture (i.e. post 72 h). This late-stage effect was likely attributable to decreasing concentrations of serine in culture medium. Consistently, depletion of serine in culture medium caused dramatic decrease in colony forming ability in cells lacking PHGDH. These experiments perhaps demonstrate the differences in the kinetics of pharmacological loss of function compared to genetic loss of expression. NCT503 or CBR5884 inhibit the activity of PHGDH without affecting mRNA or protein expression levels whereas the reverse was true for CRISPR-mediated loss of PHGDH (Mullarky et al., 2016, Pacold et al., 2016).

Although similar effects were noticeable from treatment with either NCT503 or CBR5884, off target effects of these small molecule inhibitors cannot be ruled out. Pacold and colleagues provided evidence of lack of inhibitory capacity of NCT503 against other dehydrogenases such as lactate and malate dehydrogenase (Pacold et al., 2016). In contrast to small molecule

inhibition, CRISPR or shRNA-targeted knockdown results in loss of protein expression which may disrupt formation of protein complexes and remove functional domains not explicitly targeted by inhibitors (Weiss et al., 2007, Knight and Shokat, 2007). PHGDH has been shown to interact with the translation initiating factors eIF4A1 and eIF4E. Intriguingly, PHGDH knockdown was associated with reduced phosphorylation of eIF4E, eIF4G1, 4EBP1 and disassembly of the eIF4F multicomplex resulting in reduced translation initiation (Ma et al., 2019). A recent study has shown the oncogenic activity of *MYC* leads to increased endoplasmic reticulum (ER) stress through increased translational activity and activates the GCN2/ATF4/eIF4E axis as part of an adaptive response to balance *MYC*-dependent translation activity with bioenergetic status (Tameire et al., 2019). In the absence of PHGDH, is translational capacity impeded through reduced phosphorylation of translational initiation factors in the *MYC*-amplified MB cells? Does the inhibition of *MYC*-driven translation facilitate an adaptation to PHGDH loss through ATF4? One study in *MYCN*-amplified neuroblastoma suggests that *MYC* dependence of the SGP is mediated via ATF4 (Xia et al., 2019). Although results from small molecule inhibition and CRISPR-mediated loss of PHGDH are not congruent, loss of PHGDH may in fact phenocopy *MYC* knockdown in *MYC*-amplified MB_{GRP3} cells. Loss of *MYC* results in reduced proliferation and increased uptake of serine and glycine from extracellular medium which is also observed in PHGDH knockdown cells. Further experiments are required to confirm this notion. Although a general hypothesis from data reported in previous chapters and this chapter would suggest reliance of *MYC* (off) cells on exogenous serine and glycine as opposed to *MYC*-amplified MB cells which maintain high rates of *de novo* serine and glycine synthesis.

Nevertheless, data presented here showed that loss of PHGDH resulted serine in auxotrophy causing reliance on exogenous sources of serine rendering cells sensitive towards serine depletion. A question which still remains is, whether the utilisation of serine synthesised *de novo* differs from serine that is taken up from extracellular medium in *MYC*-amplified cells following *MYC* ablation? Inhibition of PHGDH has been shown to induce uptake of serine; import of serine is not utilised in downstream pathways but instead maintains intracellular pools (Pacold et al., 2016). Data presented in this chapter showed that although *MYC*-amplification drives upregulation of the *de novo* SGP, and that this may be targeted pharmacologically using PHGDH inhibitors. PHGDH itself was not required for the survival of MB_{GRP3} cells in serine replete conditions.

Chapter 7 Discussion

7.1 Overview

Glioblastoma and medulloblastoma are the most common malignant CNS tumours to occur in adults and children respectively. Glioblastoma is less commonly occurring compared to other adult solid cancers such as lung, breast and prostate cancer however, it significantly contributes to adult cancer mortality. Median survival of GBM is around a year and only 13% of patients survive up to 5 years (NICE statistics). Outcomes for medulloblastoma are more promising, however there remains a subset of patients with difficult to treat tumours. Although CNS tumours are second in frequency to blood malignancies in childhood cancers, they account for a higher proportion of childhood cancer deaths. Specifically for MB, overall survival is around 70% however for a subset of MBs with amplification of the *MYC* oncogene, 5-year survival is < 50% and 10-year survival as low as 20% of cases (Schwalbe et al., 2017a). There is an urgent clinical need for more effective treatments to improve survival outcomes of GBM and *MYC*-amplified MB patients. To assist this process, better understanding of tumour biology is required to develop more efficacious and targeted therapies. In MB, treatment strategies that limits therapy-induced side effects that may impact future development is of great need.

Altered metabolism of cancer is a well-documented feature of cancer. The best characterised metabolic phenotype is where cancer cells repress mitochondrial oxidative phosphorylation and preferentially use aerobic glycolysis as a major energetic pathway (Warburg effect). The benefit of increased glycolysis is faster ATP turnover and supply of glycolytic intermediates into biosynthetic pathways which support growth of cancer cells (Heiden et al., 2009). Alterations in oncogene and tumour suppressor function are linked to these metabolic alterations. For instance, *MYC*, *TP53* and *HIF1* are implicated in metabolic reprogramming observed in cancer. *MYC* has been shown to upregulate glycolysis and glutaminolysis and mitochondrial biogenesis in several cancer contexts (Dang, 2013a, Shim et al., 1997, Stine et al., 2015, Terunuma et al., 2014, von Eyss et al., 2015, Wise et al., 2008). Loss of normal regulatory function of *P53* on glycolysis further leaves glycolysis unchecked. *P53* negatively regulates glycolysis by repressing GLUT expression and upregulating TIGAR which lowers the glycolytic rate and favours OXPHOS by facilitating expression of components of the ETC such as *SCO2* (Matoba et al., 2006). Under hypoxia, *HIF1 α* , upregulates glycolytic enzymes and represses mitochondrial respiration by upregulating PDKs which inhibit PDH activity which converts glycolysis generated pyruvate to acetyl-CoA enabling entry into the TCA. Instead *HIF1 α* promotes upregulation of LDH (Dengler et al., 2014, Tanimoto et al., 2000,

Zhang et al., 2007). It is increasingly appreciated that aberrant metabolic activity can itself drive alterations in the genomic and epigenomic landscape of tumours and additionally accumulation of metabolites can be intricately associated with genetic abnormalities such as copy number alterations, activation of oncogenes and loss of tumour suppressor genes (Li et al., 2019, Sciacovelli and Frezza, 2016).

Advancing our understanding of metabolic alterations of malignant brain tumours and understanding underlying tumour biology is essential in developing novel targeted therapies which could contribute to improved clinical outcomes. This thesis thus examined metabolic vulnerabilities of glioblastoma and medulloblastoma. In particular, this thesis explored whether alterations in metabolic pathways could be exploited for treatment and treatment monitoring through *in vitro* and *in vivo* metabolic profiling. The findings presented here support previous studies on FAO inhibition as a means of targeting glioblastoma with the potential for etomoxir in combination with temozolomide chemotherapy as a novel strategy for GBM. In MYC-driven MB_{GRP3} tumours, using HRMAS profiling, altered metabolism driven by overexpression of MYC was highlighted. MYC was shown to confer a dependence on *de novo* serine and glycine synthesis which rendered MB_{GRP3} cells sensitive to PHGDH inhibition.

7.2 Summary

7.2.1 Inhibition of fatty acid oxidation in malignant gliomas: Exploring combination therapy and metabolic profiling

Glioblastoma is a highly aggressive disease and standard therapies only marginally increase overall survival rates. It remains the leading cause of death in adult brain malignancies. The TCGA classification identified four distinct subtypes with common driver mutations in *EGFR*, *P53* and loss of *PTEN*. Overall survival remains poor for GBM regardless of molecular classification and so far it is not fully understood how subtypes influence treatment response (Teo et al., 2019, Verhaak et al., 2010)}. GBMs are highly infiltrative which often limits total surgical resection which leaves opportunity for disease recurrence from residual disease. GBMs are thought to arise from the NSC population of the SVZ in the adult brain (Singh SK *et al.*, 2004). NSCs retain self-renewal capacity and give rise to several neuronal lineages. Indeed, tumour recurrence is thought to arise from the stem-like cell population of tumour, which repopulate tumours following removal of treatment selective pressures. In addition, GBM stem-like cells are thought to contribute to therapy resistance attributable to poor survival

(Bao et al., 2006). Targeting these cells in combination with other anti-proliferative therapies are likely to eradicate distinct tumour populations. NSCs in the SVZ have been shown to rely on the oxidation of fatty acids to support proliferation and neurogenesis (Stoll et al., 2015). Inhibition of CPT1A or lipid droplet utilisation reduces NSC pools and limits self-renewal (Stoll et al., 2015, Xie et al., 2016).

A previously established syngeneic mouse model was utilised for use in preclinical testing of etomoxir and temozolomide as a combination therapy. Our findings suggest that treatment with etomoxir alone or in combination with temozolomide performed as well as temozolomide alone and delayed tumour onset, although these concepts must be tested with greater samples and a longer endpoint to empirically determine this. Currently, multi-drug therapies are seen as the most effective approach for improving clinical outcomes, with several combinations of temozolomide therapy in conjunction with tyrosine kinase inhibitors, mTOR inhibitors and immune-stimulants under clinical investigation in phase I-II trials (Ghosh et al., 2018). To our knowledge, the combination of temozolomide and etomoxir is a newly proposed combination therapy for GBM treatment. Others have shown using combinations of etomoxir with radiotherapy improved radiation efficacy in lung adenocarcinoma 3D models (Dheeraj et al., 2018). Flaig and colleagues found that CPT1 inhibitors combined with anti-androgen therapy (enzalutamide) resulted in robust growth inhibitory effects even in enzalutamide-resistant cells (Flaig et al., 2017). Since GBM treatment resistance and recurrence is thought to arise from the stem cell-like population, the question remains whether targeting these via inhibiting FAO combined with anti-proliferative therapies could result in more efficacious therapies against GBM (Figure 7.1).

This study focused on aberrant fatty acid metabolism in GBM and as such, *in vivo* and *in vitro* metabolic profiling of GBM in response to treatment was carried out. Consistent measurements of brain metabolites were not achieved in the *in vivo* metabolite profiling study. *In vitro* investigations yielded surprising results following drug treatment with etomoxir and temozolomide as single agents or in combination in the oncogenic mouse NPCs. Although the objective of this study was to profile treatment related changes in the oncogenic NPCs, our study highlighted the differences in metabolite abundances in 3 month NPCs compared to 12 month NPCs. Stoll *et al.*, identified an age-dependent malignancy potential of NPCs. Older NPCs (12 or 18 month), when implanted orthotopically, exhibited shorter latency and resulted in more aggressive GBM tumours. Of note, IDH-mutant GBM which is closely associated with younger patients have better survival outcomes. So far, the molecular mechanisms of this are

not fully understood(Verhaak et al., 2010). Probing the differences in oncogenic NSCs and the resultant tumours formed, may benefit the understanding of age-associated malignant features of GBM.

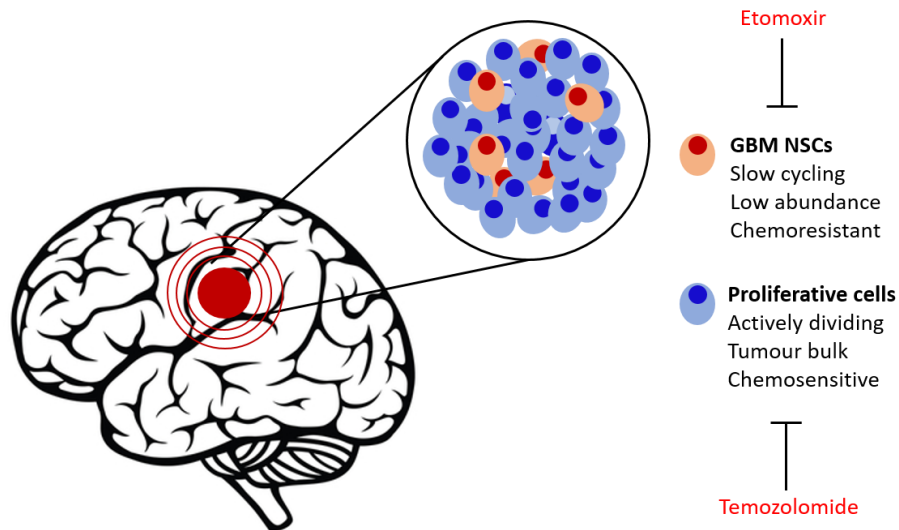


Figure 7.1 Novel treatment strategy for targeting Glioblastoma. Proposed mechanism of combination of fatty acid oxidation inhibition (etomoxir) and standard chemotherapy (Temozolomide). Glioblastoma (GBM); Neural stem-like cells (NSC)

7.2.1.1 Limitations of GBM study

We utilised the syngeneic mouse model of GBM to conduct preclinical assessment, and for *in vivo* MRI and MRS. This model enabled the testing of drug combinations in the relevant tumour anatomical location and also under an immunocompetent background. The drug administration of the *in vivo* testing of etomoxir in combination with temozolomide occurred 14 days post-transplantation of oncogenic NSCs. Previous studies have shown the presence of anaplasia at this time point; our study did not explore or confirm this. Our *in vivo* study timeline may potentially have modelled recurrent GBM since drug treatment commenced with animals not presenting MRI visible tumours which is the case for primary GBM cases. The lack of tumour burden prior to drug testing may therefore not recapitulate clinical settings.

7.2.2 Exploring metabolic dependencies of *MYC*-amplified MB_{GRP3}

Amplification of *MYC* is a notable feature of MB_{GRP3} tumours. Patients with *MYC*-amplification have the worst prognosis of all MB subgroups. 10-year survival is as low as 22% in this subgroup (Schwalbe et al., 2017b, Sharma et al., 2019, Taylor et al., 2012). Furthermore MB_{GRP3} are more likely to present with metastatic disease further limiting curative therapeutic interventions. Development of novel personalised therapy is required to improve survival outcomes. Since direct targeting of *MYC* remains elusive (discussed in detail in chapter 1), targeting *MYC*-dependent alterations in cellular processes may provide effective therapeutic interventions for these tumours. The data presented in this thesis highlights *MYC*'s role in supporting growth and proliferation of MB_{GRP3} cells. Additionally, *MYC* expression is linked with expression of various enzymes involved in glycolysis and glutaminolysis. Loss of *MYC* in the '*MYC*-addicted' MB_{GRP3} cell lines altered their bioenergetics and increased mitochondrial function. Finally, metabolite profiling highlighted the *de novo* serine and glycine pathway as a *MYC*-driven feature of MB_{GRP3} cells and rendered cells sensitive to disruption of pathway activity. Investigations into the metabolic landscape of MB in general is quite limited and there are even fewer studies on the metabolism of MB_{GRP3} tumours.

Although the Warburg effect remains the best characterised metabolic phenomenon in cancer cells, it is now widely established that several nodes in cellular metabolism are rewired in cancer cells to sustain aberrant proliferation and expansion of cancer cells. *MYC*'s reach on metabolism and its impact on altered cancer metabolism is well documented (Dang, 2013b, Dang et al., 2009). Deregulated *MYC* promotes proliferation and alters metabolism to provide anabolic substrates required to support enhanced growth. This feature is also extended to the *MYC* family members *MYCN* and *MYCL* (Roussel and Robinson, 2013, Swartling et al., 2010).

Notably, *MYC* regulates the expression of many glycolytic enzymes. LDHA was one of the earliest identified downstream targets of *MYC* (Dang, 2013b, Morrish et al., 2009, Shim et al., 1997, Tateishi et al., 2016). *MYC* also regulates the influx of metabolic substrates such as glucose and glutamine via upregulation of transmembrane transporters such as GLUTs and SLC1A5. The oncogenic functions of *MYC* on metabolic regulation were evidenced in data presented in this project which showed *MYC* expression correlated with enzymes in glycolysis (PKM2 and LDHA), and SGP enzymes (PHGDH and GLDC) (Chapter 4 and Chapter 6). Previous characterisation of *MYC* in inducible systems in immortalised proliferating cells revealed its links with oxygen consumption rates, mitochondria mass and function (Li et al.,

2005). However, it appears *MYC*'s role in metabolism in tumour cells differs from that in untransformed cells (Anso et al., 2013). Although loss of *MYC* repressed oxygen consumption in rat fibroblasts, *MYC* repression in osteogenic sarcoma cells leading to undifferentiated osteocytes, led to increase in oxygen consumption and increased mitochondrial reserve capacity suggesting context dependent activity of *MYC* (Anso et al., 2013, Li et al., 2005). Data presented in this study suggested that reduction in *MYC* expression conserved mitochondria spare capacity in concordance with the Anso *et al.*, study.

The consequences of *MYC*-driven metabolic reprogramming can lead to reliance on certain metabolic pathways and a continuous supply of nutrients. For instance, *MYC*-driven cancer cells can be particularly sensitive to glutamine deprivation and inhibition of GLS (Wise et al., 2008, Yuneva et al., 2007). Although overexpression of *MYC* drives proliferation and changes in intermediary metabolism, the dual function of *MYC* in growth and cell death can sensitise and programme cells for apoptosis in nutrient limiting conditions. Qing and colleagues showed that glutamine starvation induced ATF4-dependent PUMA and NOXA driven apoptosis in *MYCN*-amplified neuroblastoma cells (Qing et al., 2012). ATP depletion resulting from altered glutamine metabolism has been shown to activate the AMPK-P53 axis and trigger apoptosis via BAK-dependent mechanisms (Nieminen et al., 2013). It would be of interest to determine whether glutamine addiction is a consequence of *MYC*-dependency in the MB_{GRP3} cell lines. In medulloblastoma, p73 expression has been shown to sustain proliferation through the regulation of glutamine catabolism. Additionally, subgroup analysis found p73 to be elevated in MB_{GRP3} and MB_{GRP4} primary tumour samples (Niklison-Chirou et al., 2017).

Although not unique to *MYC*-driven cancers, glucose deprivation has been shown to induce apoptosis in *MYC* overexpressing rat fibroblasts (Shim et al., 1998). In the P439 *MYC*-inducible Burkitt lymphoma cell line, glutamine-dependent TCA anaplerosis was heightened and sustained TCA cycling under glucose deprivation and hypoxic conditions (Le et al., 2012). These results suggests that increased glutamine consumption driven by *MYC* may maintain important TCA cycle function, particularly under nutrient deprived and stress-inducing conditions further highlighting to probe altered metabolism in the MB_{GRP3} *MYC*-amplified cell lines.

Metabolic profiling of the MB_{GRP3} *MYC*-amplified cell lines revealed novel insights into *MYC*-driven metabolic features of MB. Combination of NMR spectroscopy and MS-based SIRM assessed global metabolite changes and pathway activity respectively. Assessment of metabolic alterations in MB remain limited and this is especially the case for MB_{GRP3}. Thus, this study contributes to the expanding field of MB metabolomics. Previous studies involving metabolic profiling have shown that MB metabolism differs from other embryonal tumours such as retinoblastoma and ependymomas. Since childhood tumours tend to have lower mutational burdens, identifying other features characteristic of the disease may aid development of more targeted and effective therapies. Findings from this study have revealed metabolic phenotypes that correlate with a genetic abnormality, *MYC*-amplification. HRMAS profiling revealed one carbon metabolism related metabolites glycine and choline as specific *MYC*-dependent metabolites which were impacted following reduced *MYC* expression. ¹³C -labelling further supported HRMAS data and reinforced upregulated *de novo* SGP as a feature of *MYC*-amplified cells. Furthermore, *MYC*-amplified cells were more susceptible to perturbation of the SGP via PHGDH compared to knockdown counterparts and MB_{SHH} cells (Figure 7.2). PHGDH expression was found to correlate with *MYC*-expression indicating *MYC*-dependent sensitivity likely due to *MYC*-driven alterations in the *de novo* SGP which was governed by PHGDH. These findings together implicate serine and glycine metabolism in *MYC*-driven metabolic reprogramming and provide a rationale for targeting this pathway as a novel therapeutic strategy for *MYC*-amplified MB_{GRP3}.

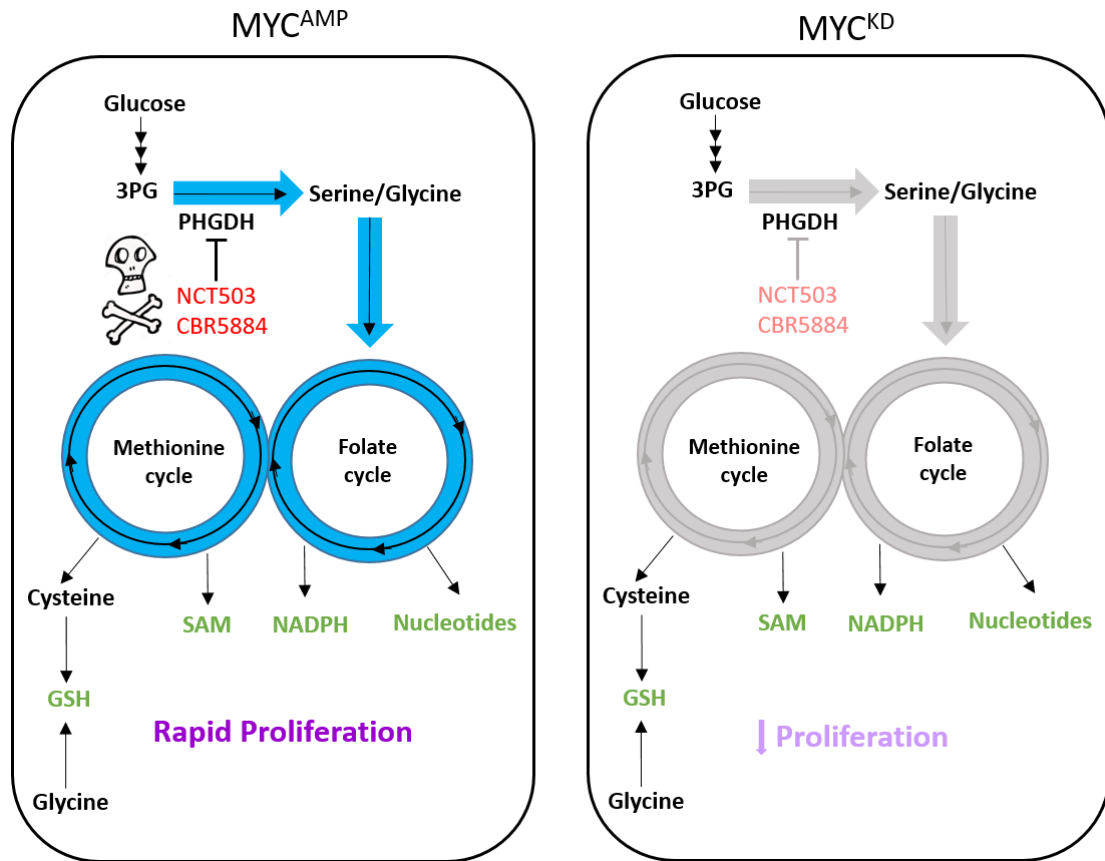


Figure 7.2 Summary of drug strategy for MYC-amplified MB_{GRP3}. Schematic demonstrating upregulated de novo serine and glycine synthesis in MYC-amplified MB_{GRP3} which was demonstrated in this thesis. MYC-driven reliance on this pathways caused increased sensitivity to PHGDH inhibition which may affect downstream pathways such one-carbon metabolism through folate and methionine cycles. One-carbon metabolism supports nucleotide synthesis, redox balance and methylation reactions supporting rapid proliferation and increased survival. MYC-amplified (MYC^{AMP}); MYC knockdown (MYC^{KD})

7.2.2.1 Limitations of MB study

We investigated the role of MYC in altered metabolism of *MYC*-amplified MB_{GRP3} using doxycycline-inducible isogenic cell line models for this project. One of limitation of this study was attributable to leakiness of shRNA constructs. The HDMB03 cell line was particularly affected by this since inconsistent results were obtained from the MYC 3 shRNA harbouring cells. Minimising leakiness is crucial to avoid *MYC* knockdown prior to experiments and measurements. Construct leakiness could be overcome by generating cell populations from single cell colonies and selecting for populations that do not exhibit this feature. Doxycycline has been shown to affect cellular metabolism albeit in a context dependent manner. We sought to control for these alterations by utilising non-silencing controls for experiments. Although *MYC*-dependent effects on metabolism were striking and could be discriminated from NS cells, doxycycline did impact NS cells particularly cell growth and expression of metabolic enzymes at later time points. Owing to the lack of MB_{GRP3} non-amplified cell lines, it was not possible to conduct experiments comparing non-amplified and *MYC*-amplified MB_{GRP3} cell lines.

We utilised HRMAS to profile alterations in metabolites as a consequence of *MYC* knockdown in the MB_{GRP3} *MYC*-regulable cell lines. Although HRMAS-based metabolic profiling enabled the identification of clinically detectable metabolites, only a small range of metabolites are detected using this method. It also required a large number of cells (greater than 1×10^7 cells). MS-based profiling is capable of detecting a far greater number of metabolites (hundreds) and requires less cells to do so (Bhinderwala et al., 2018, Emwas et al., 2019, Zhang et al., 2013). With the requirement on cell number lowered, metabolic assessment over several time points could also be achieved. Since the commencement of this project, RNAseq and proteomic data has been generated for the MB_{GRP3} *MYC* isogenic cell lines. Integration of this multi-omics data will aid the discovery of *MYC*-dependent metabolic changes and highlight several other pathway alterations not detectable from our HRMAS profiling.

7.3 Future directions

7.3.1 Etomoxir in combination with temozolomide: a promising treatment strategy for Glioblastoma?

In GBM, FAO has been highlighted as a vital bioenergetic pathway and is associated with GBM stem cell proliferation and survival. As previously mentioned, the pilot *in vivo* GBM study highlighted the potential effectiveness of FAO inhibition in conjunction with standard chemotherapy in GBM. Undertaking a preclinical assessment of etomoxir in combination with temozolomide in a sufficiently powered blinded study would enable the evaluation of the efficacy of this combination strategy. It is also important to assess the efficacy of this combination strategy in other *in vivo* models with varied genetic backgrounds to assess the impact of this combination across models that reflect the inter-tumoural heterogeneity of GBM. Although the syngeneic model enables pharmacological assessment in an immunocompetent and BBB intact setting, it is also important to evaluate treatment response in a human genetic background. The use of orthotopic PDX models could address this (Irtenkauf et al., 2017, William et al., 2017). A further consideration of assessing FAO inhibition in GBM could be to explore other inhibitors of the pathway. Phase I/II clinical trials assessing the use of etomoxir for use in congestive heart failure was discontinued owing to severe liver toxicity in 4 out of 226 patients. This risk was deemed significant to halt further assessment of etomoxir in this context. However, assessment of the anti-cancer in a clinical setting remains untested although observed toxicity may limit clinical evaluation of etomoxir in GBM. However, there are other CPT1 inhibitors that have been developed such as the reversible inhibitor compound, ST1326 (Gianessi et al 2003) which has shown promising effects in slowing progression of leukaemia and lymphoma *in vivo* (Riciardi et al 2015, Pacili et al 2013). The repurposing of other inhibitors such as perhexiline which is currently used to treat chronic heart failure and refractory angina could provide further alternatives to etomoxir (Phan et al 2009). Perhexiline inhibits CPT1 and to a lesser extent CPT2. It has shown anti-tumour effects in prostate cancer and CLL (Itkonen et al 2017, Liu et al 2016). So whilst the inhibition of fatty acid oxidation remains a potential therapeutic strategy for GBM, exploration of other compounds may provide a suitable route into clinical evaluation.

Although temozolomide chemotherapy remains a part of standard care for GBM patients, combinations of etomoxir and other novel targeted therapies could be explored *in vitro* and *in vivo* to determine whether potentiation, or synergy could be achieved. Appropriate cell line

models of GBM, particularly the non-serum exposed cells which retain their stem-like characteristics could be utilised for *in vitro* testing as they more accurately model human disease in comparison to their serum exposed counterparts (Pollard et al., 2006, Stoll et al., 2016). Functional profiling of drug combinations with etomoxir using GBM NSCs and/or PDX-derived cell lines could highlight novel interventions against GBM.

7.3.2 Imaging and monitoring therapy response using advanced imaging techniques

Monitoring tumour progression could provide insights into characteristics of tumour development, discovery of disease associated biomarkers and opportunities for monitoring therapy response. With the advancement of MR imaging techniques, opportunities for monitoring microscopic and macroscopic changes associated with tumour formation and development could be further explored in the syngeneic model of GBM. Some studies have utilised dynamic susceptibility contrast MR perfusion imaging to characterise difference between low-grade and high-grade gliomas which correlated with survival outcomes. Law *et al.*, demonstrated that low-grade tumours that are highly perfused had worse outcomes compared to high-grade gliomas with low perfusion (Law et al., 2003). Furthermore combination of MR imaging and multiple voxel spectroscopy could further illuminate structural and metabolic alterations associated with tumour development. A potential strategy for monitoring tumour response, may be to undertake *ex vivo* metabolic profiling of tumour samples from control and treatment groups and evaluate metabolite changes that differentiate these groups. Metabolites of interest could be monitored *in vivo* by optimising spectroscopy sequences which improve resolution of acquisition and thus lead to reliable and accurate measurements which can inform on response to treatment.

7.3.3 Exploring metabolic features of Glioblastoma

GBM have been observed to demonstrate metabolic plasticity utilising both glucose, fatty acids and other substrates to generate acetyl-CoA which can be utilised in energy production and biosynthesis. In particular, acetyl-CoA through the TCA generates substrates and reducing agents required by the ETC and ultimately, ATP production. Previous studies have shown a significant contribution of fatty acids to acetyl-CoA pools of GBM, particularly GBM NSCs which maintain tumour populations. Targeting oxidative metabolism remains an interesting approach to targeting GBM. Metformin is a clinically approved drug used in the treatment of type 2 diabetes. Metformin and other derivatives like phenformin has been shown to inhibit the

activity of Complex I thereby decreasing mitochondrial derived ATP (Kasznicki et al., 2014). Since upregulated FAO provides acetyl-CoA which can be utilised for ATP production, it would be important to assess whether survival of FAO-dependent GBM NSCs could be impacted by inhibiting downstream bioenergetic pathways.

Metabolic alterations of age-associated malignant transformation

Furthermore, exploring the age-dependent metabolic alterations associated with GBM stem-like cells could shed light on the metabolic reprogramming acquired during malignant transformation and may reveal targetable metabolic vulnerabilities of GBM. We would propose a multi-omics approach utilising NMR/MS metabolic profiling in conjunction with proteomics to identify metabolite alterations associated with differently aged oncogenic NSCs (3, 12 and 18 month NSCs alongside their non-transformed counterparts. This would enable comparison of age-related alterations in tumour biology and metabolism in addition to malignancy-specific changes.

7.3.4 Cellular response of fatty acid oxidation inhibition in oncogenic mouse NSCs and human NSCs: Metabolic plasticity of GBM cells

Previous work by Randle *et al.*, established a dynamic biochemical mechanism which controls fuel selection and adapts substrate supply (Randle, 1981). The glucose-fatty acid cycle (Randle effect) describes a functional antagonism between fatty acids and glucose as substrates of oxidation. Inhibition of glucose of oxidation by fatty acids contributes to the so called glucose sparing effect, spares pyruvate and lactate, both being gluconeogenic precursors. The interaction between the two metabolic substrates is highly complex, involving allosteric control by pathway specific substrates, expression of key enzymes (including PDH and PDK) and finally by metabolic regulators such as AMPK and SREBP (Randle, 1998, Strickland and Stoll, 2017). Although the Randle effect is more clearly defined in other disease contexts i.e. type 2 diabetes, fatty acid syndrome etc., its role in cancer remains largely unexplored. Furthermore understanding these pathway dynamics and how one energetic pathway impacts the other, would enable assessment of possible mechanisms of therapy resistance.

Future experiments could assess the metabolic response of etomoxir (FAO inhibitor) or glycolytic inhibitors on either pathway in non-serum exposed human GBM NSCs using the Seahorse Bioanalyser to evaluate the effect on ATP production, OCR and ECAR. Additional experiments to examine impact on metabolites could utilise ^{13}C -glucose labelling to determine

the fate of glucose when FAO is inhibited i.e. is glucose oxidised in the TCA or fermented producing lactate? The reverse for glucose inhibition and impact on FAO could also be determined. An alternative approach could be to use RNAi to ablate the expression of component enzymes of FAO and evaluate the impact of glycolytic enzymes or fate determining enzymes like PDH and PDK. These experiments would aim to uncover the metabolic adaptations of GBMs and whether they can be counteracted using pharmacological agents to prevent 'switch on' of alternative pathways that could sustain GBM progression.

7.3.5 Inhibition of PHGDH as a novel therapeutic strategy to counteract MYC-driven tumourigenesis in MB

Pharmacological inhibition of PHGDH impeded cell proliferation and mitochondrial function in MYC-amplified MB_{GRP3} cells. Alterations in gene expression networks which coordinate response to PHGDH inhibition was not characterised in this study. Genome-wide assessment using RNAseq could be utilised to correlate phenotypic changes with alterations in gene expression. Additionally interrogating response of MYC-amplified cells compared to MYC KD may reveal biomarkers of drug sensitivity or resistance to PHGDH inhibition.

Pharmacological inhibition focused on PHGDH which shunts glucose-derived 3PG into the serine biosynthesis pathway. Further exploration of targeting of the different enzyme components of the SGP should be considered especially if stronger inhibitory effects could be achieved. Of particular interest are SHMTs and GLDC which are further downstream in the pathway and dictate fate of carbon units. A small inhibitor of SHMT, SHIN1 displayed anti-tumour effects in BCL (Ducker et al., 2017). Inhibition of GLDC using genetic manipulation has been shown to disrupt pyruvate to lactate conversion and slow tumour growth (Woo et al., 2018). Additionally inhibition of GLDC was found to cause glycine accumulation which later caused cytotoxicity resulting from toxic by-products generated from alternative catabolism of glycine in GBM cells (Kim et al., 2015). RNAseq data generated by the Clifford lab showed profound downregulation of GLDC following MYC KD in MB_{GRP3} cell lines. Findings from HRMAS profiling also suggested glycine accumulation in these cell lines. These data further implicate serine and glycine in MYC-dependent alterations in metabolism which should be explored further.

This study also provides proof-of-concept for targeting the *de novo* SGP in MYC-amplified MB *in vivo*. In depth preclinical efficacy assessment is required to validate this specific metabolic phenotype as a potential clinically actionable therapeutic strategy for MYC-amplified MB. Genetically engineered mouse models (GEMMs) and PDX models are indispensable tools for understanding tumour biology and drug interactions in whole-organism system. *In vivo* characterisation is important for understanding metabolic alterations, appropriate models which recapitulate human disease enable assessments in appropriate anatomical location mimicking environments experienced by tumour. Since metabolic adaptations may occur in response to long term culture of cell lines in growth medium that does not accurately reflect physiological nutrient availability, it is important to assess effectiveness of targeting *de novo*

serine and glycine synthesis in mouse models of MB. The GTML mouse model which is an *MYCN*-driven MB mouse model recapitulates high risk features associated with MB_{GRP3} such as LCA histology (Swartling et al., 2010). The *MYCN*-gene is doxycycline regulable in the GTML model and has been previously utilised to uncover the pleiotropic role of *MYC* family members in MB tumourigenesis and recurrence (Swartling et al., 2010, Hill et al., 2015). Furthermore, recent efforts have characterised and made available a biobank of PDX mouse models for *MYC*-amplified and non-amplified MB_{GRP3} (Brabetz et al., 2018). Pharmacokinetic data supports the BBB penetrance of the tool compound, NCT503 which was utilised in this study (Pacold et al., 2016). Initial efforts would be to first validate whether treatment with NCT503 could slow tumour progression *in vivo*. In addition to preclinical evaluations efficacy evaluations, pharmacokinetic and pharmacodynamic evaluations to further understand drug interactions and effect on the brain. The ideal experiment would be to test this under differing *MYC* backgrounds to replicate isogenic cell line experiments.

Additional *in vivo* experiments could explore combination of NCT503 with conventional chemotherapeutic drugs. Using a four-arm study assessing effect of monotherapy in contrast with combination treatment. Although the aims of our study was to explore novel targeted therapies for *MYC*-amplified MB and potentially limit the use of agents with high systemic toxicities, developing synergistic/ cumulative effect from combined therapy could limit use of radiation therapy which is linked with late effects in MB patients.

7.3.5.1 Identifying a serine and glycine pathway signature for MB using immunohistochemical analysis

In order to evaluate the clinical relevance of serine and glycine in *MYC*-amplified MB, we probed the expression of PHGDH in primary MB samples using TMAs. In order to establish the interplay of other pathway enzymes in the upregulated *de novo* serine, characterising enzymes such as PSAT1, PSPH, SHMT2 and GLDC much like experiments carried out in the *MYC*-inducible cell lines could enable the derivation of an expression signature of the SGP pathway and how it correlates with survival outcomes. This, in turn, could further provide rationale for targeting other components of the SGP pathway.

7.3.6 The role one carbon metabolism in *MYC*-amplified Group 3 MB

The present study explored metabolic alterations of MB_{GRP3} that could potentially be targeted therapeutically. HRMAS profiling showed accumulation of glycine and choline, two important metabolites contributing to one carbon metabolism following downregulation of *MYC*. Increased *de novo* serine and glycine synthesis was validated as a *MYC*-driven characteristic but in light of changes in other one carbon supporting metabolites, further investigation is required to understand the role of one carbon metabolism, and particularly the folate and methionine cycles in *MYC*-driven transformation. The use of ¹³C -glucose tracing in the MB_{GRP3} *MYC*-inducible cell models confirmed increased glucose-derived serine and glycine. Characterising how this pathway contributes to *MYC*-driven transformation not only advances the understanding of MB tumour biology, but may reveal more therapeutic targets. Using ¹³C serine and glycine labelling to determine metabolic activity can inform on downstream activities and contributions to one carbon metabolism.

Not only does ¹³C -labelling allow determination of metabolic activity, it can also evaluate methylation marks found on DNA and RNA. Previous studies have highlighted crosstalk of serine metabolism and the epigenome. Depletion of serine decreased levels of SAM, the predominant source of cellular methyl donor which in turn, decreased methylation of DNA and RNA (Maddocks et al., 2016). Others have shown direct tumour suppressor and oncogene contribution to increased SAM mediated by serine metabolism and upregulation of methyltransferases that are recruited to retrotransposons associated with gene silencing (Kottakis et al., 2016). Since *MYC* plays a role in chromatin remodelling, it is necessary to delineate how adaptations of the *de novo* serine and glycine pathway may influence epigenetic status in *MYC*-amplified MB.

7.3.7 Comprehensive analysis of Group 3 MB altered bioenergetics. Integration of ‘omics’ data and generation of genome scale models to characterise MB-specific metabolic alterations

Currently, this study is one of the earliest characterisations of MYC-driven metabolism in MB. Although findings presented in this thesis have shed light on alterations in bioenergetics and metabolite profiles in association with *MYC*-amplification, further work is required to comprehensively cover altered metabolism in MB. With the rise of NGS and the accumulation of ‘omics’ data for MB in particular, there is a wealth of data characterising molecular features of MB which can be further integrated into additional analytical pipelines for the discovery of novel metabolic features. Additionally, our lab has generated transcriptomic and proteomic data for the *MYC*-inducible MB_{GRP3} models which may be utilised for further validation studies. There is increasing interest in altered metabolism and holistic approaches such as the use of genome scale mathematical models to decipher underlying nature of alterations in cellular metabolism (Dai et al 2019, Gu et al., 2019, Lewis et al., 2013). To provide representation of global metabolic networks, genome scale models use metabolomics, gene expression and proteomic data to provide mechanistic and interconnections of genotype and phenotype (Nilsson and Nielsen, 2017, Adiamah and Schwartz, 2012).

To determine these *MYC*-specific metabolic alterations, previously generated omics data derived from patient samples will be utilised. Since these datasets cover MB subgroups, it would be interesting to note variation in metabolism between distinct MB subgroups with different genetic/molecular features and cell of origin. Particularly useful to this study would be comparison of metabolic alterations of *MYC*-amplified MB in contrast to non-amplified cases. Parallel modelling using MB_{GRP3} *MYC*-inducible cell line data could also be performed in order to evaluate whether these *in vitro* cell line models recapitulate primary MB. Furthermore, the isogenic cell lines provide a method for validation of findings and exploration of therapeutic targets.

7.4 Concluding remarks

The aims of this study was to characterise metabolic dependencies of malignant brain tumours, as a foundation for novel therapeutic strategies against these lethal cancers. The initial aims of this study were to explore combination of FAO inhibition in conjunction with temozolomide chemotherapy in a syngeneic mouse model of GBM. Findings from our pilot study supported previous findings that FAO inhibition delayed tumour onset. *In vivo* MRI detected alterations in brain structures that accompanied tumour formation and clinical symptoms. Histological assessment supported formation of high grade astrocytoma lesions. Further metabolic profiling of transformed NSCs revealed potential malignancy and age-associated variations in metabolism of differently aged NSCs.

The aim for MB_{GRP3} was to characterise novel metabolic features associated with *MYC* amplification which is a high risk feature of MB. This investigation has contributed to the understanding of *MYC*-driven metabolic reprogramming in MB. Observations made are also supported by findings in other *MYC*-driven cancer contexts. This study additionally implicated *de novo* serine and glycine synthesis as a druggable feature of *MYC*-amplified MB. Disruption of the *de novo* SGP impeded proliferation, cell cycle progression and mitochondrial respiration. Most importantly, PHGDH, a critical component of glucose-derived serine and glycine was found to correlate with increased risk in MB patients.

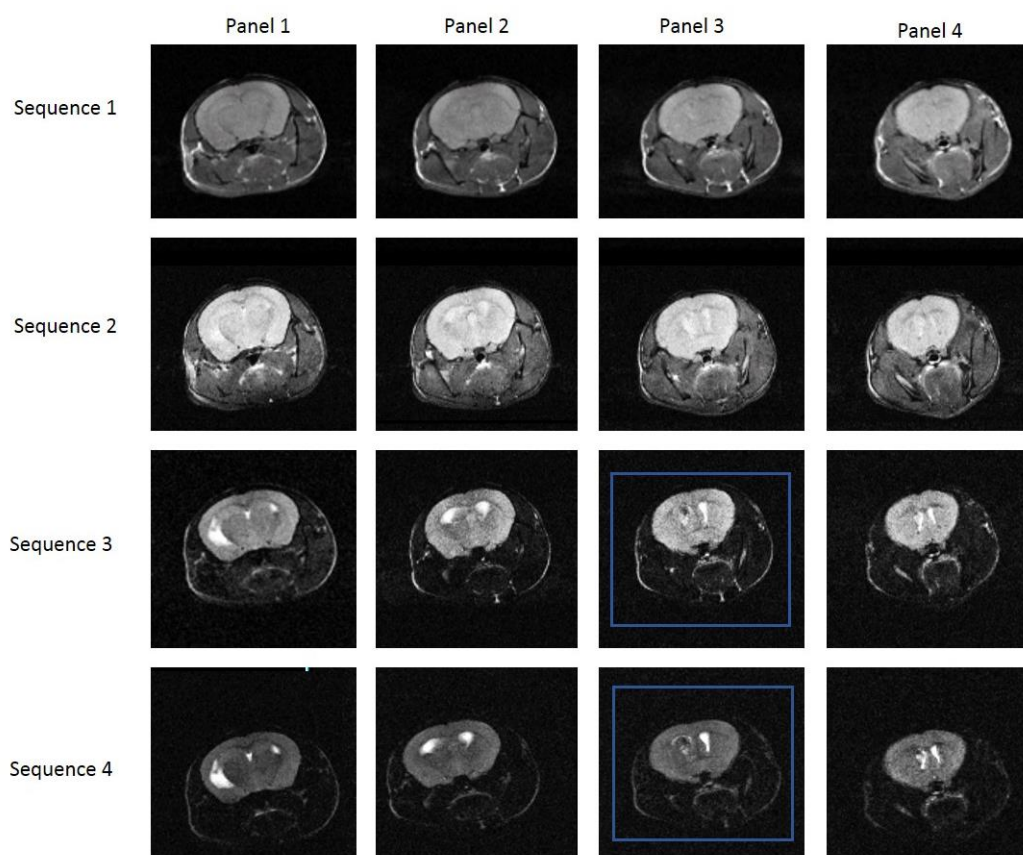
Ultimately these investigations have highlighted metabolic vulnerabilities of GBM and MB using *in vivo* and *in vitro* models. These findings lay the foundation for exploiting fatty acid oxidation and *de novo* serine and glycine which have been identified as important metabolic pathways in GBM and MB respectively.

Appendices

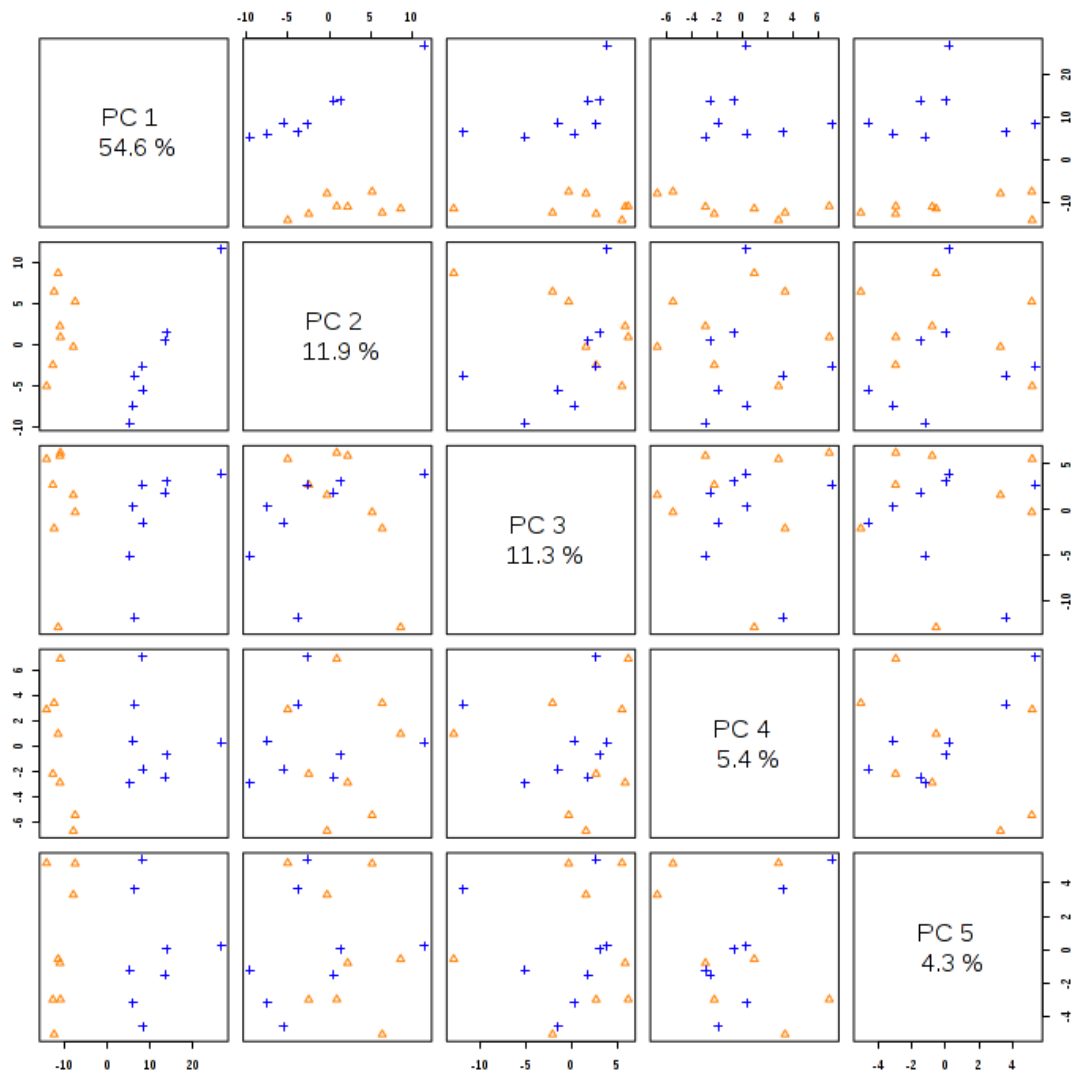
A. Appendix for Chapter 3



Appendix 8.2 Voluntary oral administration. The vehicle (coconut oil)-drug mixture is supplied as a pellet for delivery. Mice ingested vehicle-drug mixture from a polystyrene culture dish containing soaked diet food.



Appendix 8.3 Detection of tumour in M079 identified by sequence 3 and 4 at day 78.

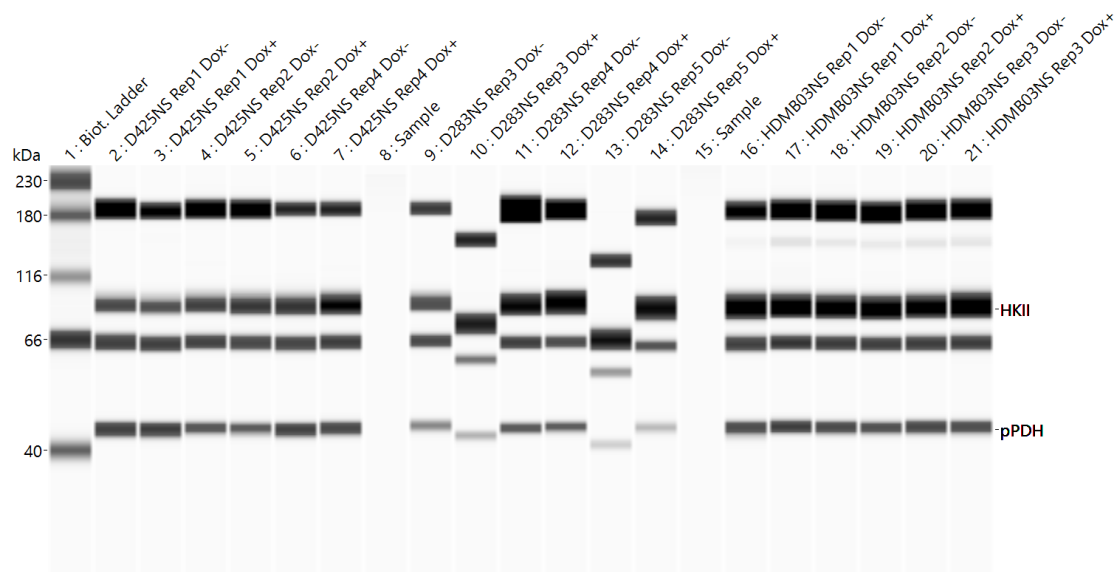


Appendix 8.4 Overview of PCA of spectral bins in 3 month and 12 month oncogenic NPCs

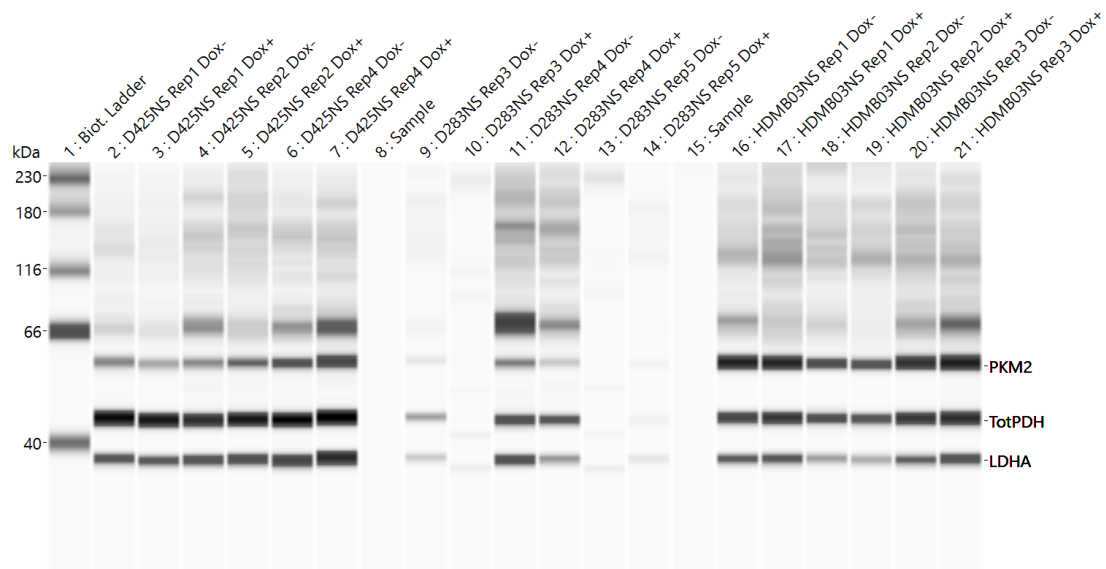
Appendix 8.5 Significantly altered spectral bin regions between 3 month and 12 month oncogenic NPCs.

	t.stat	p.value	LOG10(p)	FDR
1.22008 - 1.26008	-10.347	6.12E-08	7.2136	4.89E-06
3.22008 - 3.26008	8.6097	5.77E-07	6.2392	2.31E-05
3.54008 - 3.58008	7.9798	1.41E-06	5.8506	3.08E-05
3.98008 - 4.02008	7.9186	1.54E-06	5.8118	3.08E-05
1.26008 - 1.30008	-7.6793	2.20E-06	5.6581	3.52E-05
3.46008 - 3.50008	7.2868	3.99E-06	5.399	5.32E-05
2.58008 - 2.62008	6.8917	7.42E-06	5.1295	8.48E-05
2.74008 - 2.78008	-6.3894	1.68E-05	4.7737	0.000168
1.94008 - 1.98008	-6.1111	2.69E-05	4.57	0.000239
1.98008 - 2.02008	-5.8752	4.04E-05	4.3938	0.000323
1.18008 - 1.22008	-5.7251	5.25E-05	4.2799	0.000382
1.66008 - 1.70008	5.4888	7.98E-05	4.0979	0.000513
1.30008 - 1.34008	-5.465	8.33E-05	4.0794	0.000513
1.70008 - 1.74008	5.0504	0.000177	3.7516	0.001013
4.10008 - 4.14008	4.8421	0.000261	3.5832	0.001393
1.58008 - 1.62008	4.6976	0.000343	3.4651	0.001714
3.34008 - 3.38008	-4.1544	0.000973	3.0118	0.004579
1.54008 - 1.58008	-3.6856	0.002446	2.6115	0.010872
1.62008 - 1.66008	3.491	0.003599	2.4439	0.015153
3.02008 - 3.06008	3.3699	0.004579	2.3392	0.017593
3.94008 - 3.98008	3.3656	0.004618	2.3355	0.017593
3.50008 - 3.54008	-3.284	0.005432	2.265	0.019754
3.78008 - 3.82008	3.0926	0.007948	2.0998	0.027645
3.90008 - 3.94008	2.8759	0.01221	1.9133	0.040701
0.820085 - 0.860085	-2.8404	0.013094	1.8829	0.041267
3.30008 - 3.34008	2.807	0.013987	1.8543	0.041267
4.14008 - 4.18008	2.7945	0.014334	1.8436	0.041267
0.900085 - 0.940085	2.7907	0.014443	1.8403	0.041267
3.62008 - 3.66008	-2.7282	0.016327	1.7871	0.045041

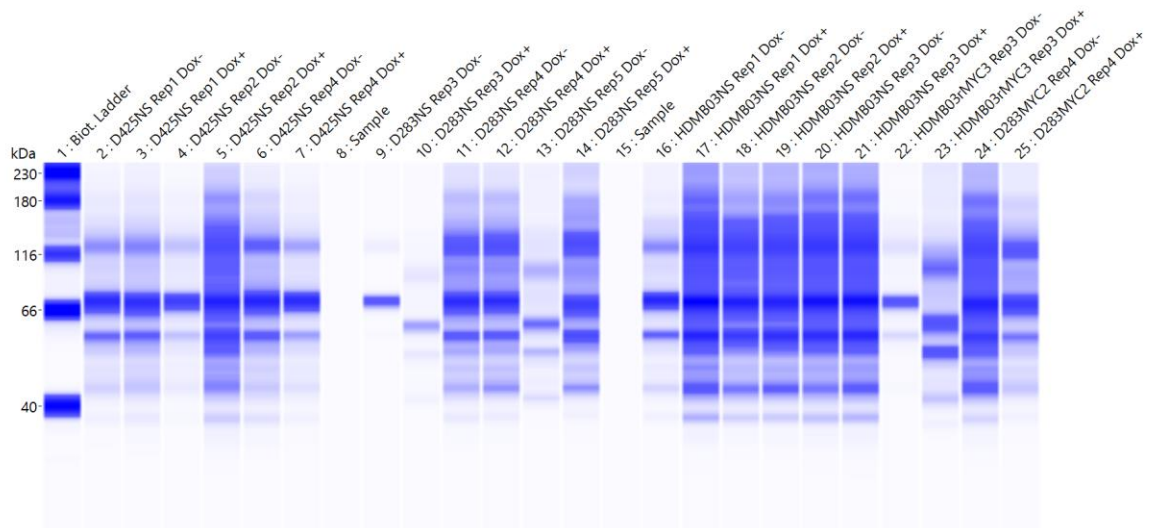
B. Appendix for Chapter 4



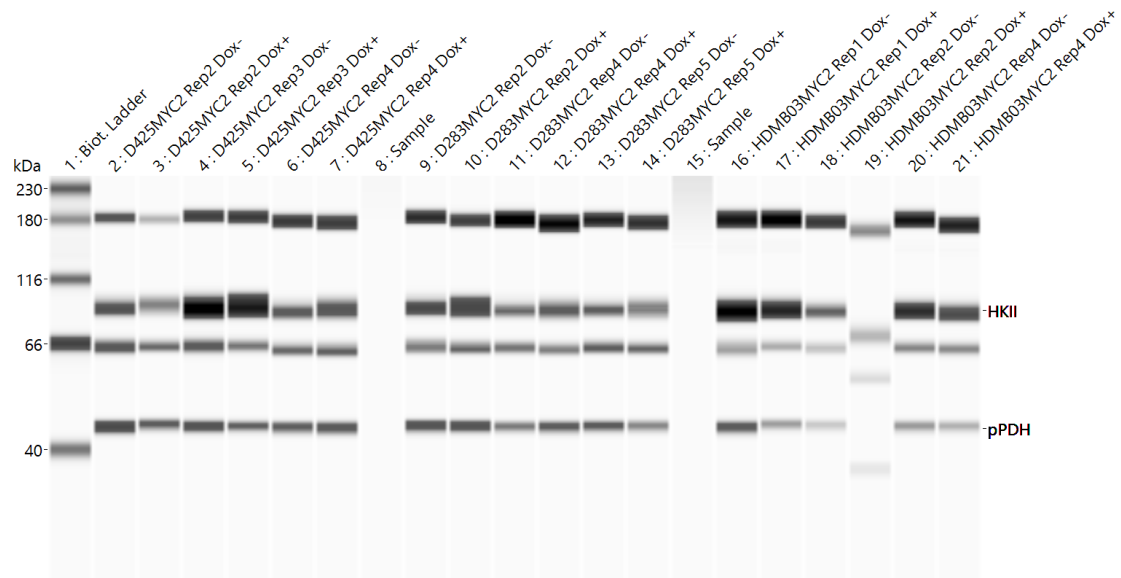
Appendix 8.6 Effect of MYC knockdown on metabolic enzymes in MYC inducible cell lines. WES image showing levels of HK2 and phosphorylated PDH in D425, D283 and HDMB03 NS cells treated \pm Dox for 72h.



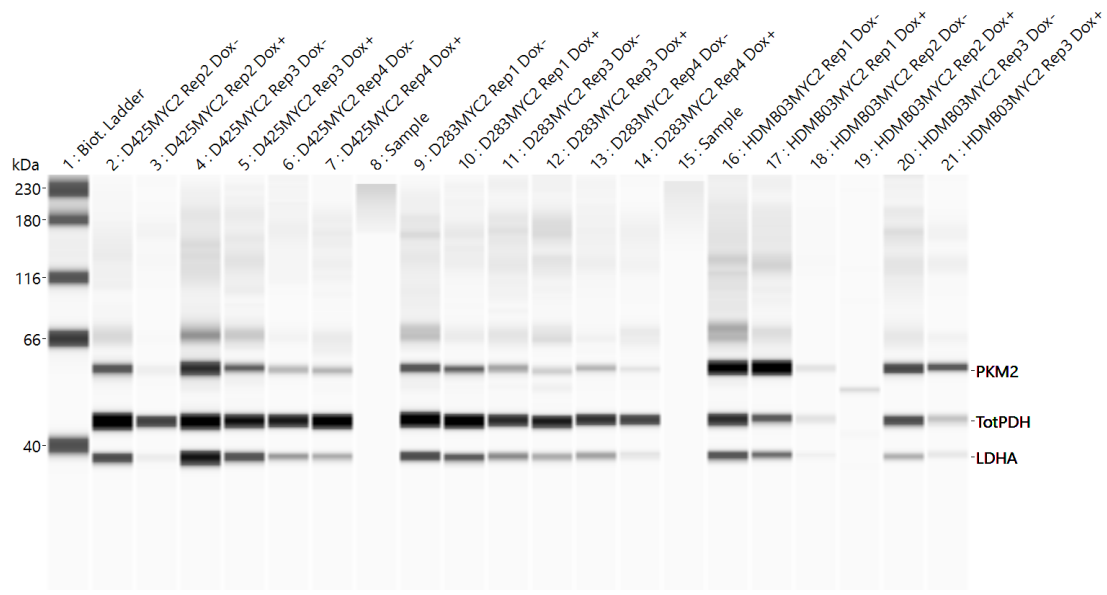
Appendix 8.7 Effect of MYC knockdown on metabolic enzymes in MYC inducible cell lines. WES image showing levels of PKM2, LDHA and total PDH in D425, D283 and HDMB03 NS cells treated \pm Dox for 72h.



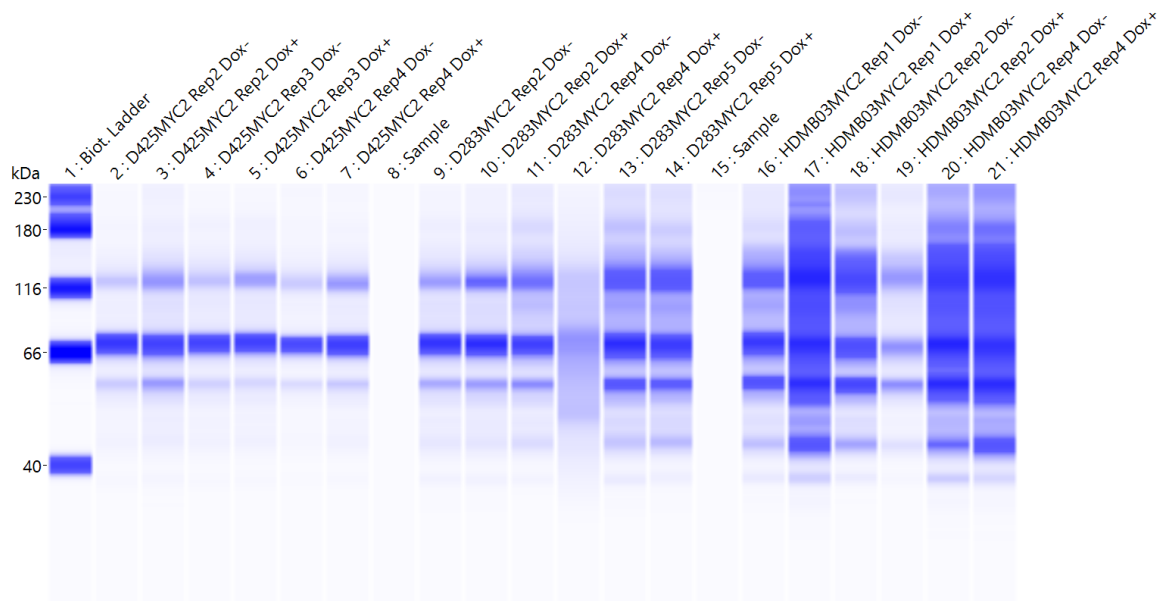
Appendix 8.8 Effect of MYC knockdown on metabolic enzymes in MYC inducible cell lines. WES image showing total protein levels in D425, D283 and HDMB03 NS cells treated \pm Dox for 72h.



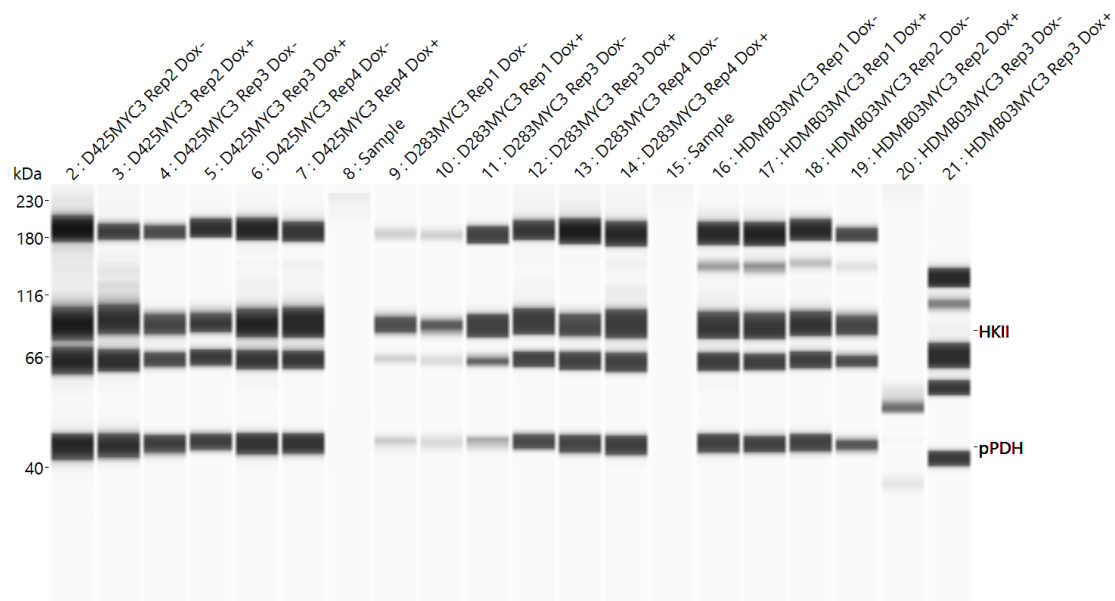
Appendix 8.9 Effect of MYC knockdown on metabolic enzymes in MYC inducible cell lines. WES image showing levels of HK2 and phosphorylated PDH in D425, D283 and HDMB03 MYC 2 cells treated \pm Dox for 72h.



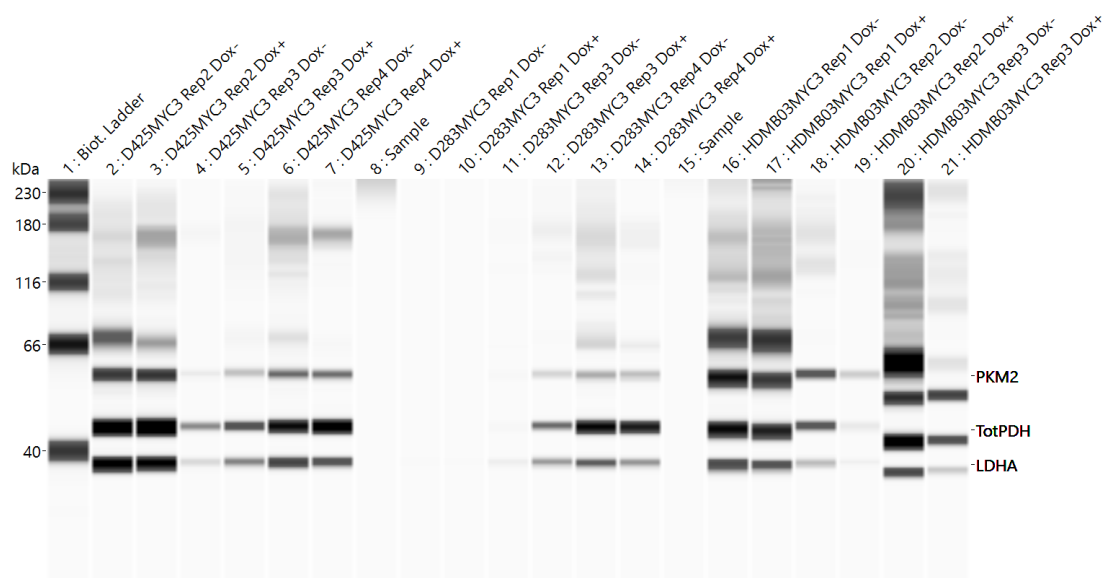
Appendix 8.10 Effect of MYC knockdown on metabolic enzymes in MYC inducible cell lines. WES image showing levels of PKM2, LDHA and total PDH in D425, D283 and HDMB03 MYC 2 cells treated \pm Dox for 72h.



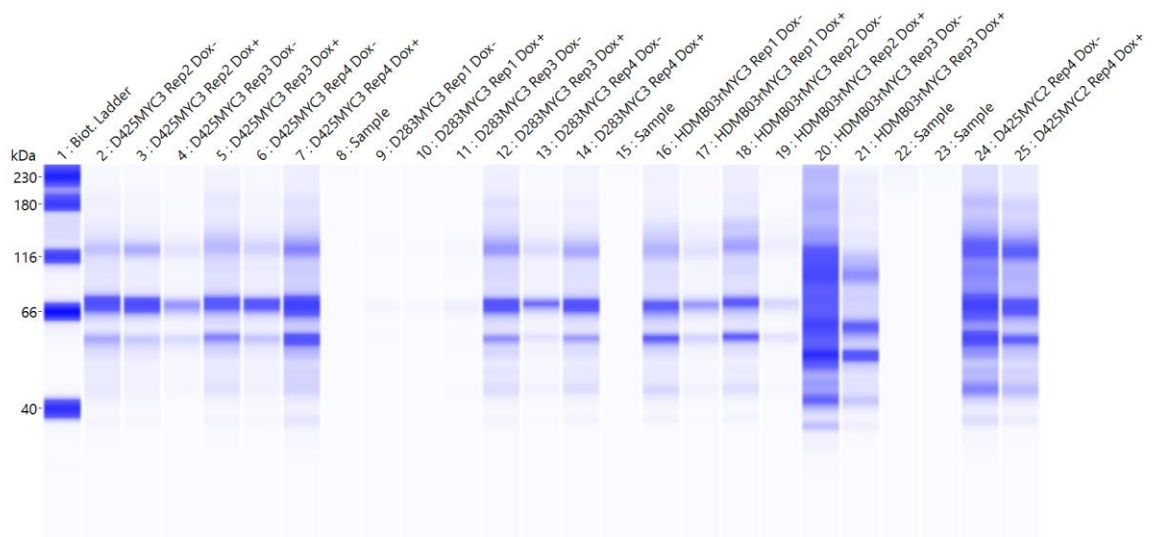
Appendix 8.11 Effect of MYC knockdown on metabolic enzymes in MYC inducible cell lines. WES image showing total protein levels in D425, D283 and HDMB03 MYC 2 cells treated \pm Dox for 72h.



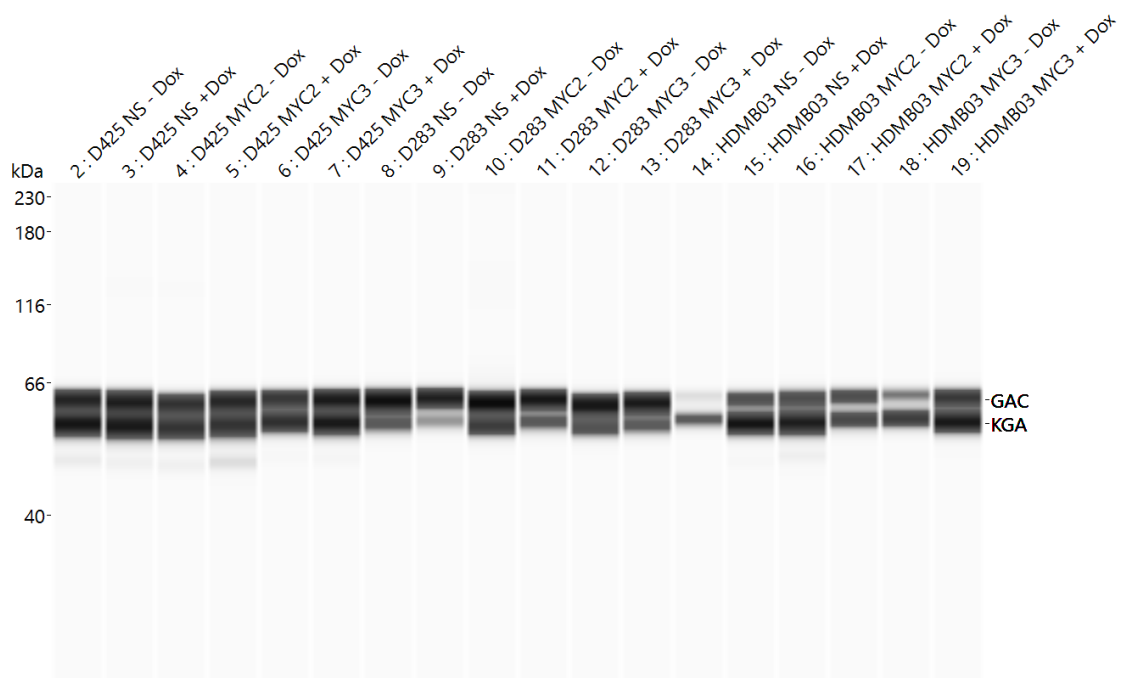
Appendix 8.12 Effect of MYC knockdown on metabolic enzymes in MYC inducible cell lines. WES image showing levels of HK2 and phosphorylated PDH in D425, D283 and HDMB03 MYC 3 cells treated \pm Dox for 72h.



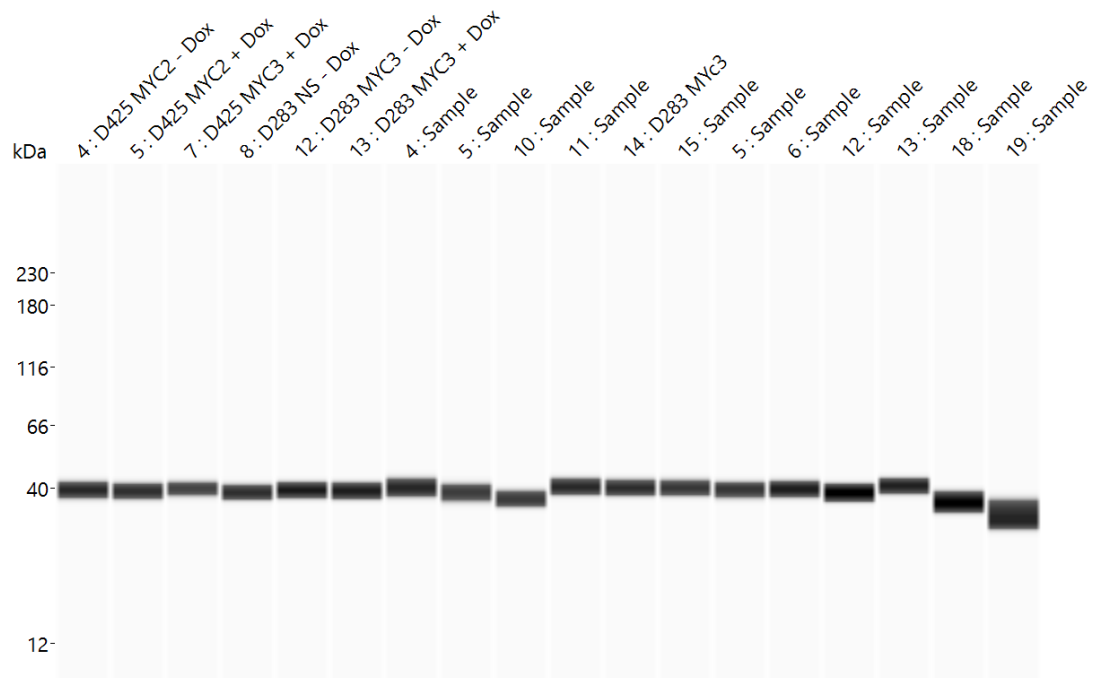
Appendix 8.13 Effect of MYC knockdown on metabolic enzymes in MYC inducible cell lines. WES image showing levels of PKM2, LDHA and total PDH in D425, D283 and HDMB03 MYC 2 cells treated \pm Dox for 72h.



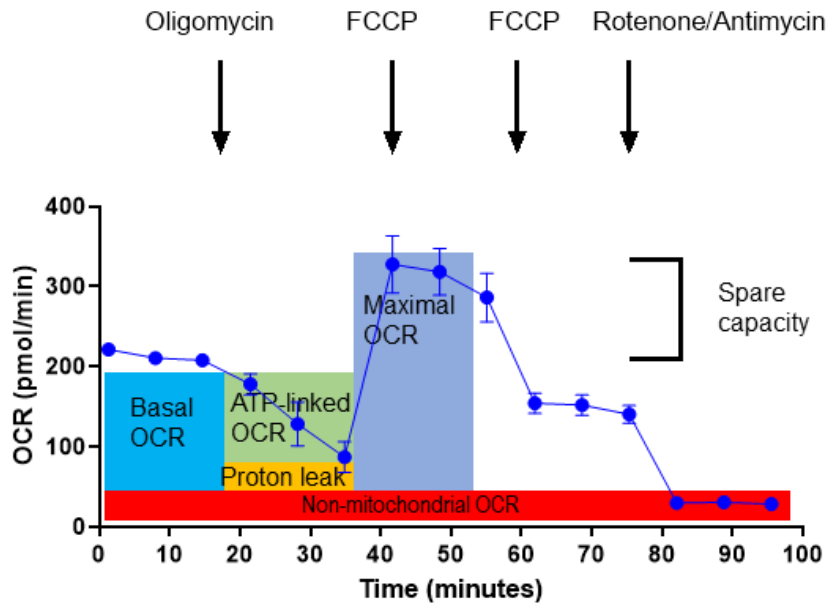
Appendix 8.14 Effect of MYC knockdown on metabolic enzymes in MYC inducible cell lines. WES image showing total protein levels in D425, D283 and HDMB03 MYC 3 cells treated \pm Dox for 72h.



Appendix 8.15 Effect of MYC knockdown on GLS isoforms in MYC inducible cell lines. WES image showing levels of GAC and KGA in D425, D283 and HDMB03 (NS, MYC 2, MYC 3) cells treated \pm Dox for 72h.



Appendix 8.16 Effect of MYC knockdown on GLS isoforms in MYC inducible cell lines. WES image showing levels of β -actin in D425, D283 and HDMB03 (NS, MYC 2, MYC 3) cells treated \pm Dox for 72h.



Appendix 8.17 Representative OCR profile of seahorse bioenergetics assay using D425 NS cells. Baseline OCR is measured prior to injection. Measurements for each parameter is taken in triplicate in 2 min wait and 3 min measurement cycles. Mitochondria inhibitors into each well followed by wait/measurement cycles. Data represents mean \pm SEM.

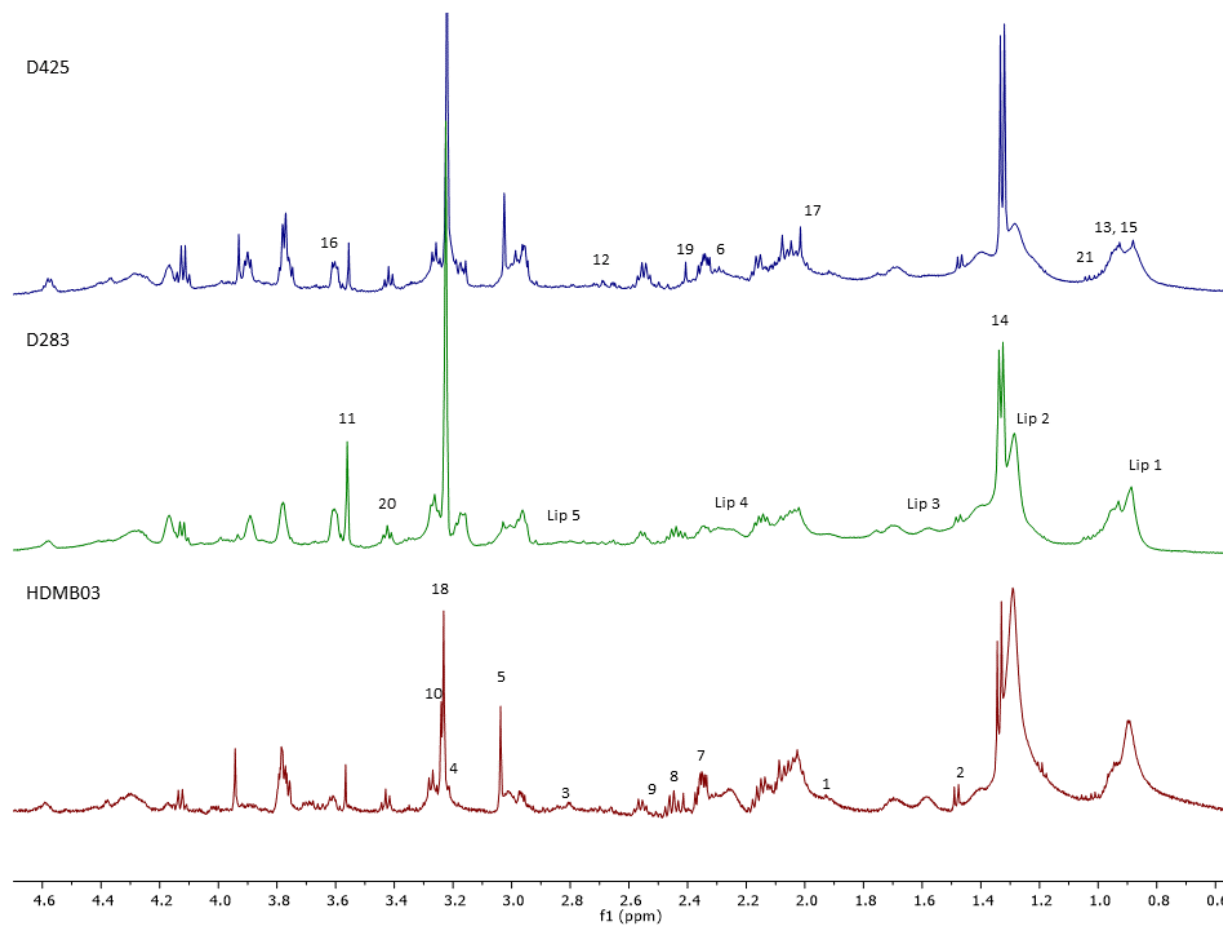
Appendix 8.18 Parameter calculations for seahorse bioenergetics assay

Parameter value	Equation
Non-mitochondrial oxygen consumption	Minimum rate measurement after rotenone/ antimycin injection
Basal respiration	(Last rate measurement before first injection) – (Non-mitochondrial oxygen consumption)
Maximal respiration	(Maximum rate measurement after FCCP injection) – (Non-mitochondrial oxygen consumption)
Spare respiratory capacity	(Maximal respiration) – (Basal respiration)
Spare respiratory capacity as a %	(Maximal respiration)/ (Basal respiration) x 100

C. Appendix for Chapter 5

Appendix 8.20 Table of significantly altered spectral bin regions from the pooled MB_{GRP3} cell lines.

Bin region	f.Value	p.Value	-log10(p)	FDR	Fisher's LSD
3.43438 - 3.44438	8.4238	1.02E-05	4.9914	0.003855	MYC2 (OFF) - MYC2 (ON); MYC2 (OFF) - MYC3 (OFF); MYC2 (OFF) - MYC3 (ON); MYC2 (OFF) - NS (ON); MYC2 (OFF) - NS Dox Ctrl (ON)
3.56438 - 3.57438	7.0596	5.71E-05	4.2437	0.010784	MYC2 (OFF) - MYC2 (ON); MYC2 (OFF) - MYC3 (OFF); MYC2 (OFF) - MYC3 (ON); MYC2 (OFF) - NS (ON); MYC2 (OFF) - NS Dox Ctrl (ON)
2.02438 - 2.03438	6.337	0.000149	3.8265	0.018789	MYC3 (OFF) - MYC2 (OFF); MYC3 (ON) - MYC2 (OFF); NS (ON) - MYC2 (OFF); NS Dox Ctrl (ON) - MYC2 (OFF); MYC3 (OFF) - MYC2 (ON); MYC3 (ON) - MYC2 (ON); NS (ON) - MYC2 (ON); NS Dox Ctrl (ON) - MYC2 (ON)
2.01438 - 2.02438	5.9249	0.000262	3.5816	0.024767	MYC2 (ON) - MYC2 (OFF); MYC3 (OFF) - MYC2 (OFF); MYC3 (ON) - MYC2 (OFF); NS (ON) - MYC2 (OFF); NS Dox Ctrl (ON) - MYC2 (OFF); MYC3 (ON) - MYC2 (ON); NS Dox Ctrl (ON) - MYC2 (ON)



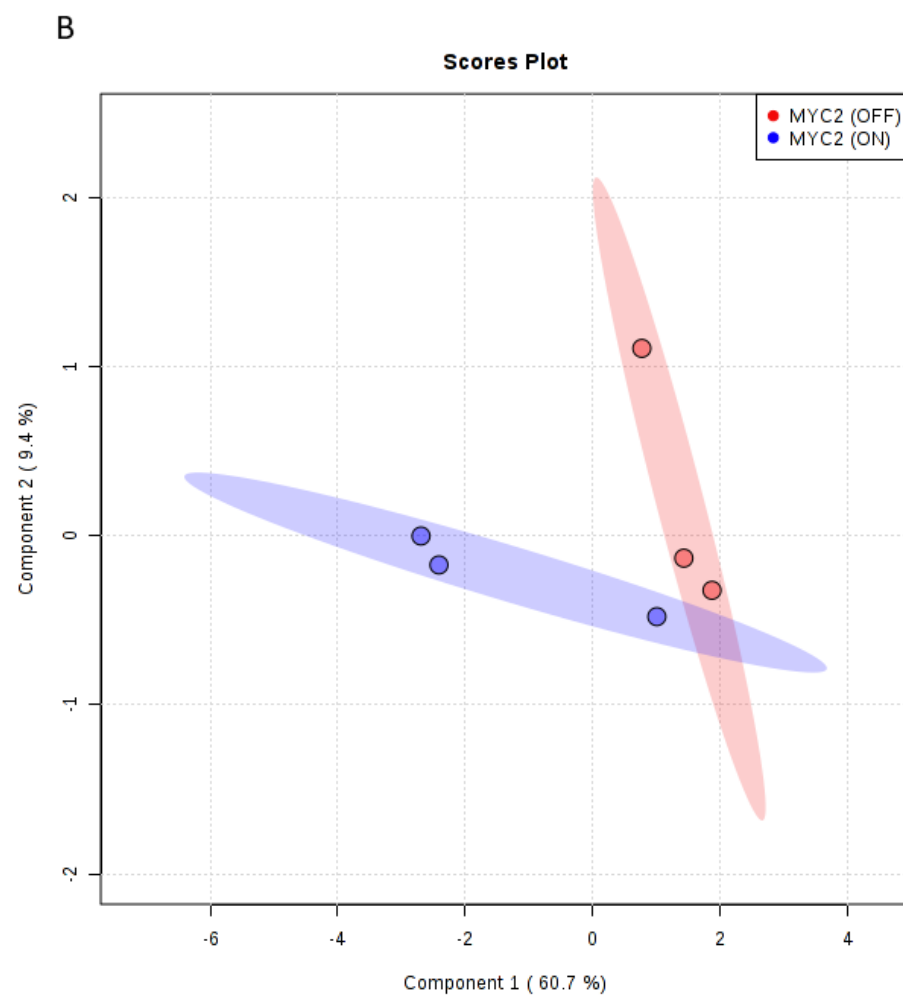
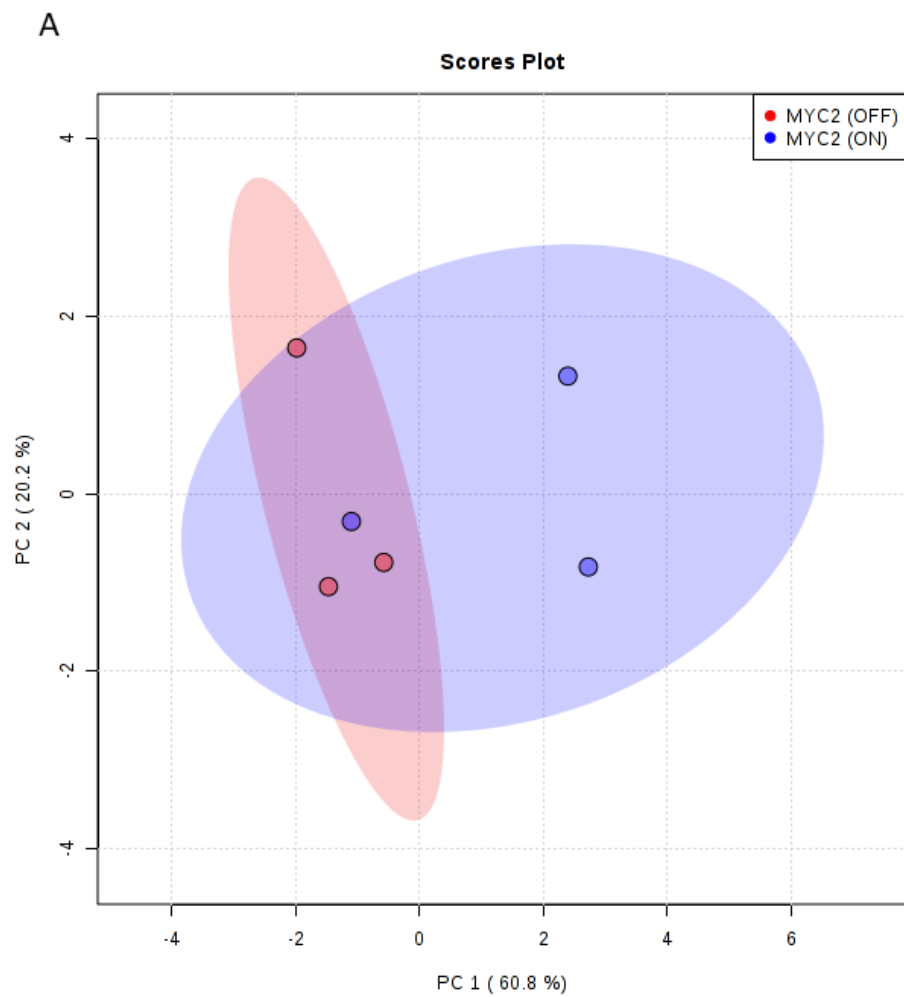
Appendix 8.21 Representative HRMAS spectra of A) D425 B) D283 C) HDMB03 the MB_{GRP3} cell lines. Assigned metabolites are as follows: Acetate (1), Alanine (2), Aspartate (3), Choline (4), Creatine (5), GABA (6), Glutamate (7), Glutamine (8), Glutathione (9), Glycerophosphocholine (10), Glycine (11), Hypotaurine (12), Isoleucine (13), Lactate (14), Leucine (15), Myo-inositol (16), NAA (17), Phosphocholine (18), Succinate (19), Taurine (20), Valine (21)

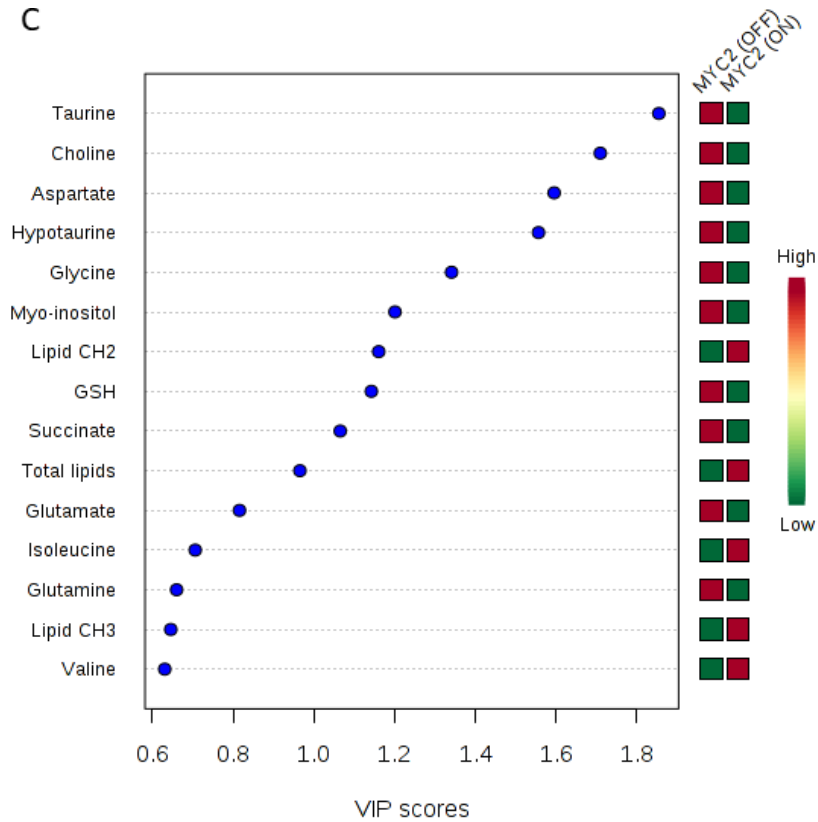
Appendix 8.22 Assignment of metabolite peaks in HRMAS spectra.

Identified metabolite	Chemical shift (ppm)
Acetate (1)	1.92 (s)
Alanine (2)	1.48 (d)
Aspartate (3)	2.83 (dd)
Choline (4)	3.20 (s)
Creatine (5)	3.03 (s)
GABA (6)	2.30 (t)
Glutamate (7)	2.34 (m)
Glutamine (8)	2.44 (m)
Glutathione (9)	2.55 (m)
Glycerophosphocholine (10)	3.23 (s)
Glycine (11)	3.56 (s)
Hypotaurine (12)	2.65 (t)
Isoleucine (13)	1.01 (d)
Lactate (14)	1.32 (d)
Leucine (15)	0.95 (t)
Myo-inositol (16)	3.62 (t)
NAA (17)	2.02 (s)
Phosphocholine (18)	3.22 (s)
Succinate (19)	2.40 (s)
Taurine (20)	3.42 (t)
Valine (21)	1.07 (d)

Appendix 8.23 Assignment of lipids in HRMAS spectra.

Identified lipid group	Chemical shift (ppm)
Lipid 1: CH ₃	0.90
Lipid 2: CH ₂)n	1.29
Lipid 3: CH ₂ -CH ₂ =O	1.59
Lipid 4: CH ₂ CH ₂ C=O	2.26
Lipid 5: =CH-CH ₂ -CH=	2.80





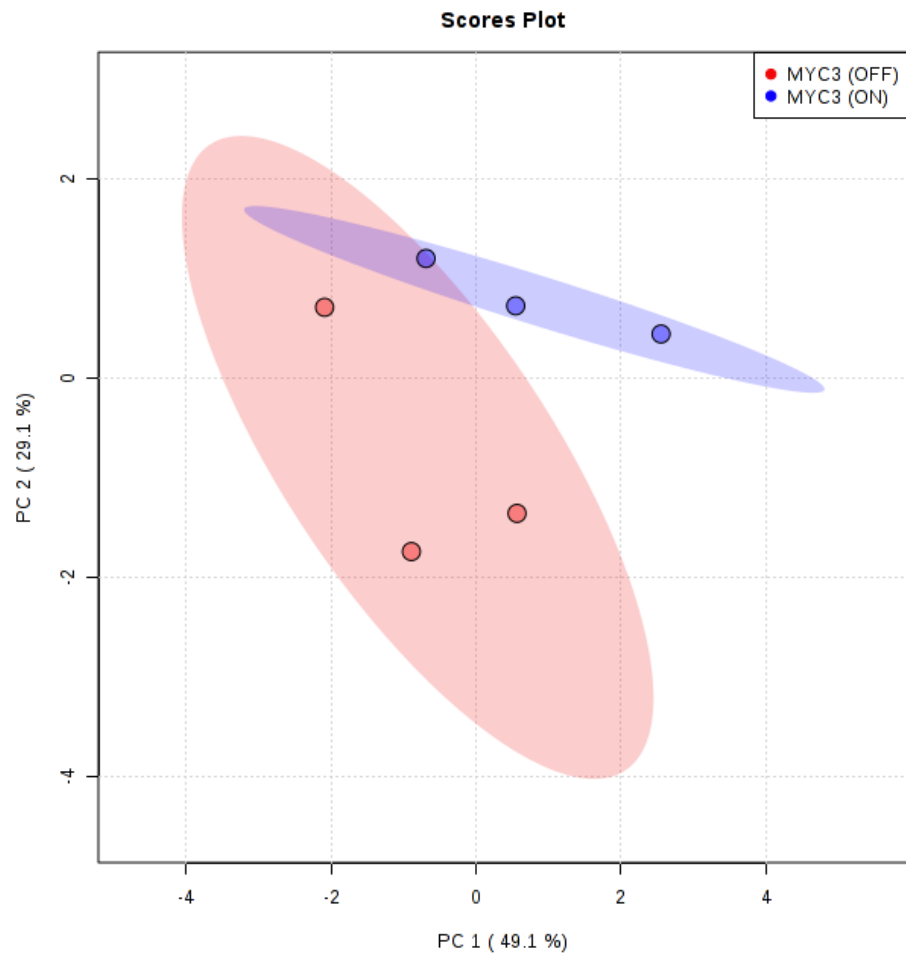
D

PLS-DA cross validation details:

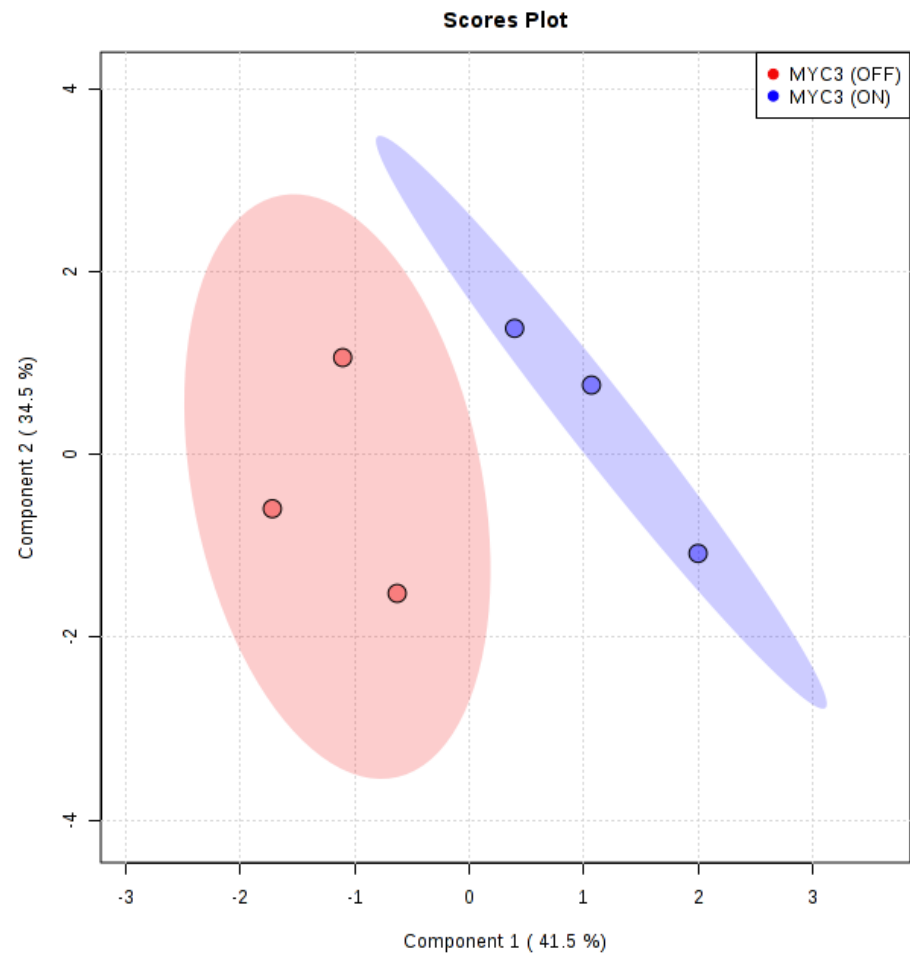
Measure	1 comps	2 comps	3 comps
Accuracy	0.66667	0.33333	0.33333
R2	0.55028	0.72689	0.85174
Q2	0.038606	-2.0381	-4.2185

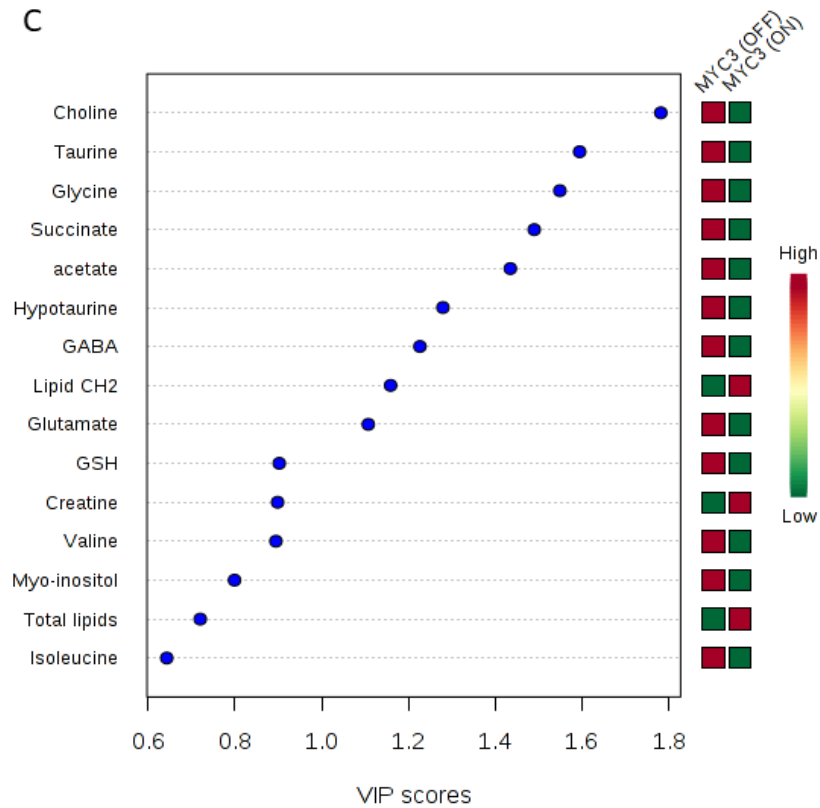
Appendix 8.24 A) PCA score plot of metabolite concentrations of the D425 MYC 2 cells following treatment in the presence or absence of doxycycline to induce MYC knockdown. PCA shows the first two principal components. B) Supervised PLS-DA score plot showing group variations. C) VIP score from PLS-DA showing top 15 metabolites contributing to separation of the MYC 2 (on) and MYC 2 (off) groups. The red and green boxes to the right indicate whether a metabolite is increased (red) or decreased (green) when MYC was knocked down. D) Cross validation of the PLS-DA showing model accuracy, R2 and Q2 values.

A



B





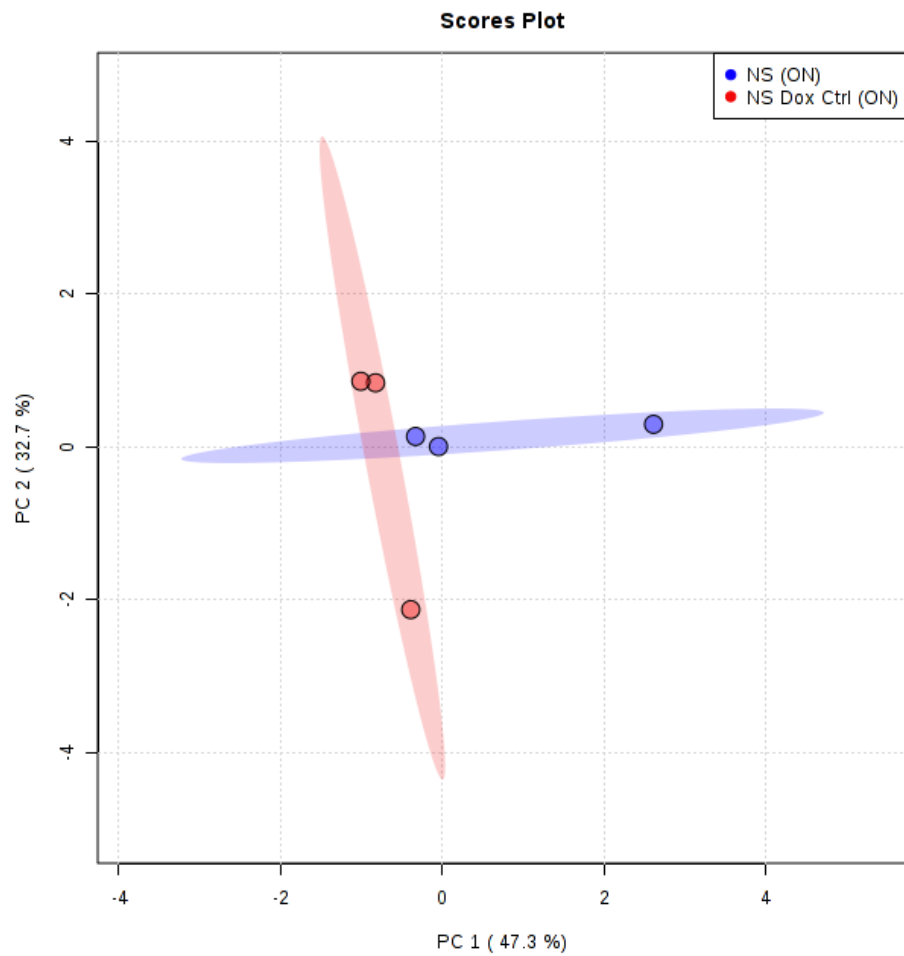
D

PLS-DA cross validation details:

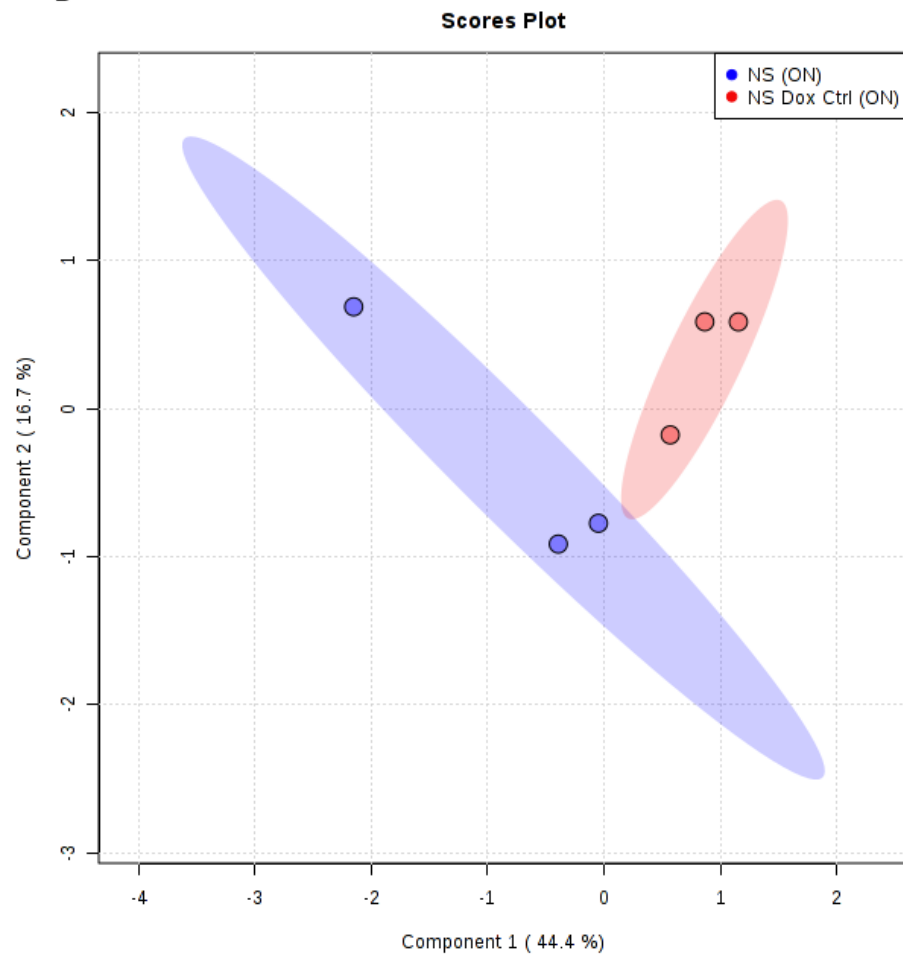
Measure	1 comps	2 comps	3 comps
Accuracy	0.5	0.83333	0.66667
R2	0.80822	0.90799	0.97965
Q2	0.24824	0.32315	0.23356

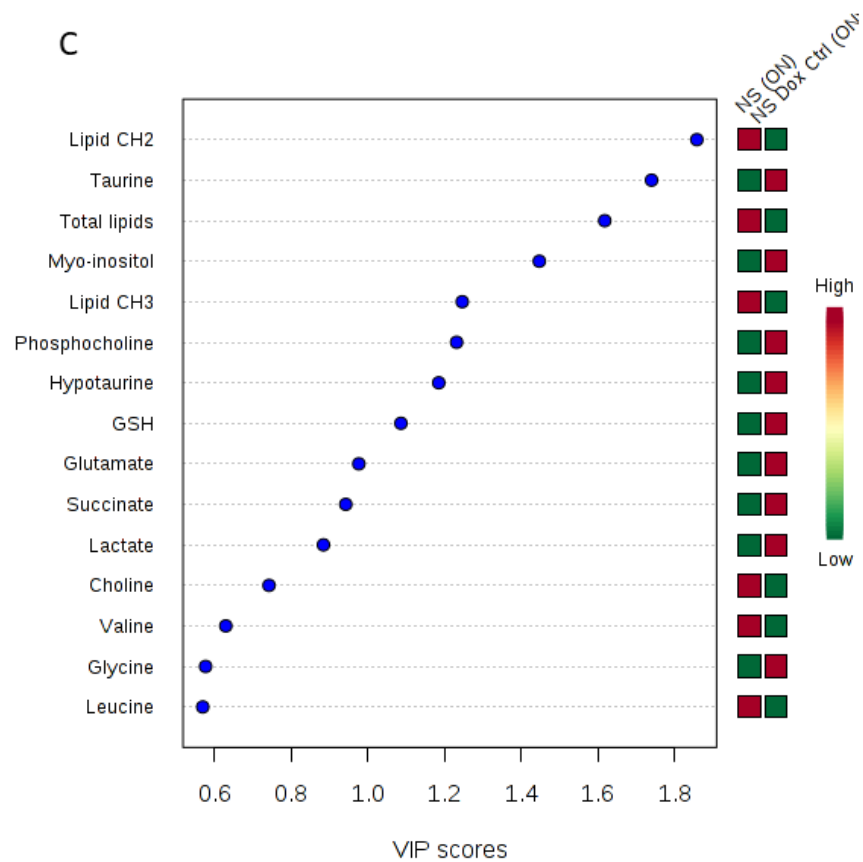
Appendix 8.25 PCA score plot of metabolite concentrations of the D425 MYC 3 cells following treatment in the presence or absence of doxycycline to induce MYC knockdown. PCA shows the first two principal components. B) Supervised PLS-DA score plot showing group variations. C) VIP score from PLS-DA showing top 15 metabolites contributing to separation of the MYC 3 (on) and MYC 3 (off) groups. The red and green boxes to the right indicate whether a metabolite is increased (red) or decreased (green) when MYC was knocked down. D) Cross validation of the PLS-DA showing model accuracy, R2 and Q2 values.

A



B





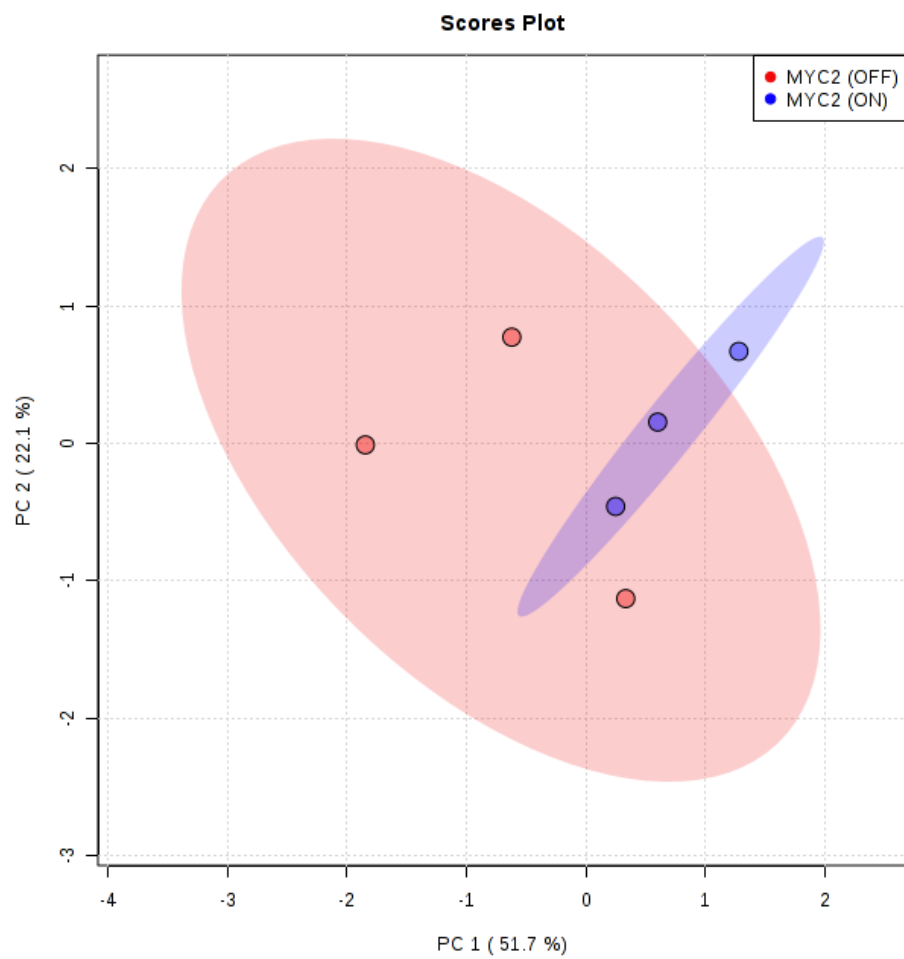
D

PLS-DA cross validation details:

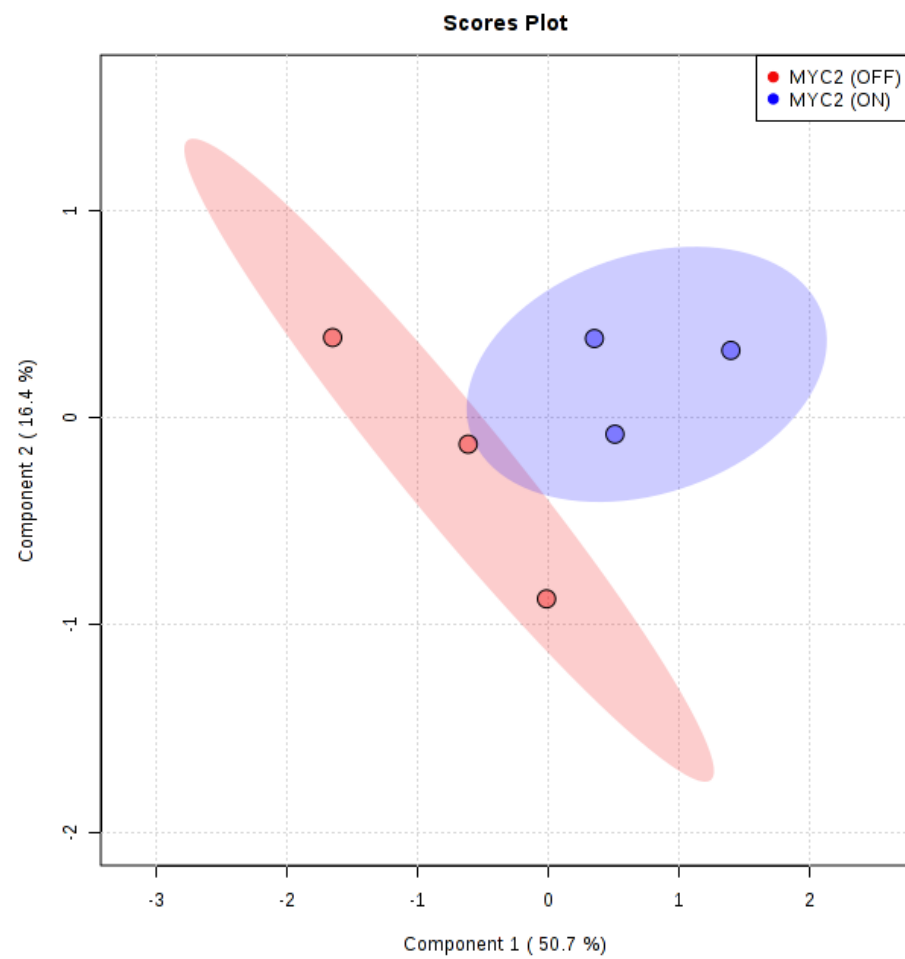
Measure	1 comps	2 comps	3 comps
Accuracy	0.33333	0.5	0.5
R2	0.62222	0.87492	0.93042
Q2	-0.10822	-0.3623	-1.0069

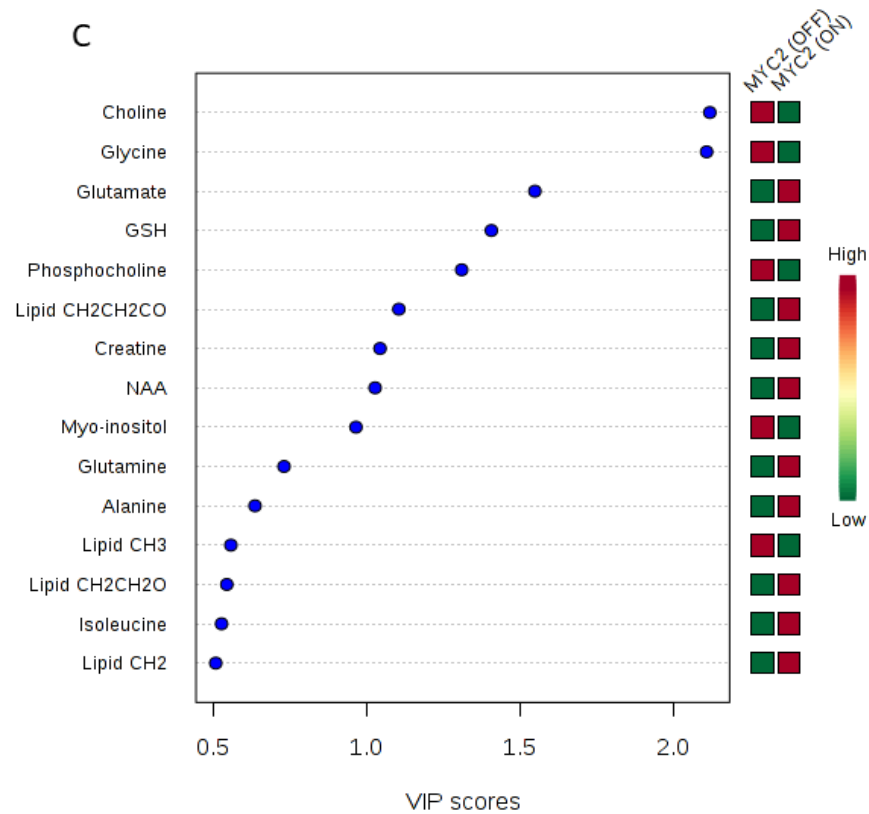
Appendix 8.26 PCA score plot of metabolite concentrations of the D425 NS cells following treatment in the presence or absence of doxycycline to induce MYC knockdown. PCA shows the first two principal components. B) Supervised PLS-DA score plot showing group variations. C) VIP score from PLS-DA showing top 15 metabolites contributing to separation of the NS (on) and NS Dox Ctrl (on) groups. The red and green boxes to the right indicate whether a metabolite is increased (red) or decreased (green) when MYC was knocked down. D) Cross validation of the PLS-DA showing model accuracy, R2 and Q2 values.

A



B





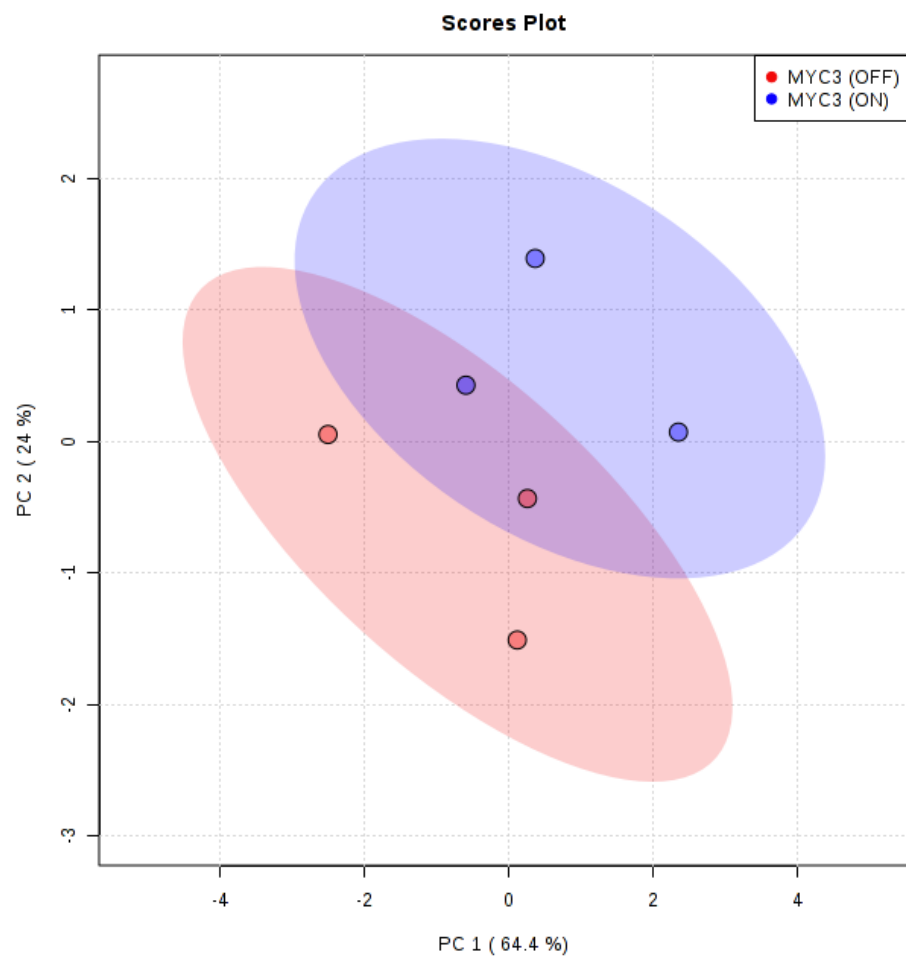
D

PLS-DA cross validation details:

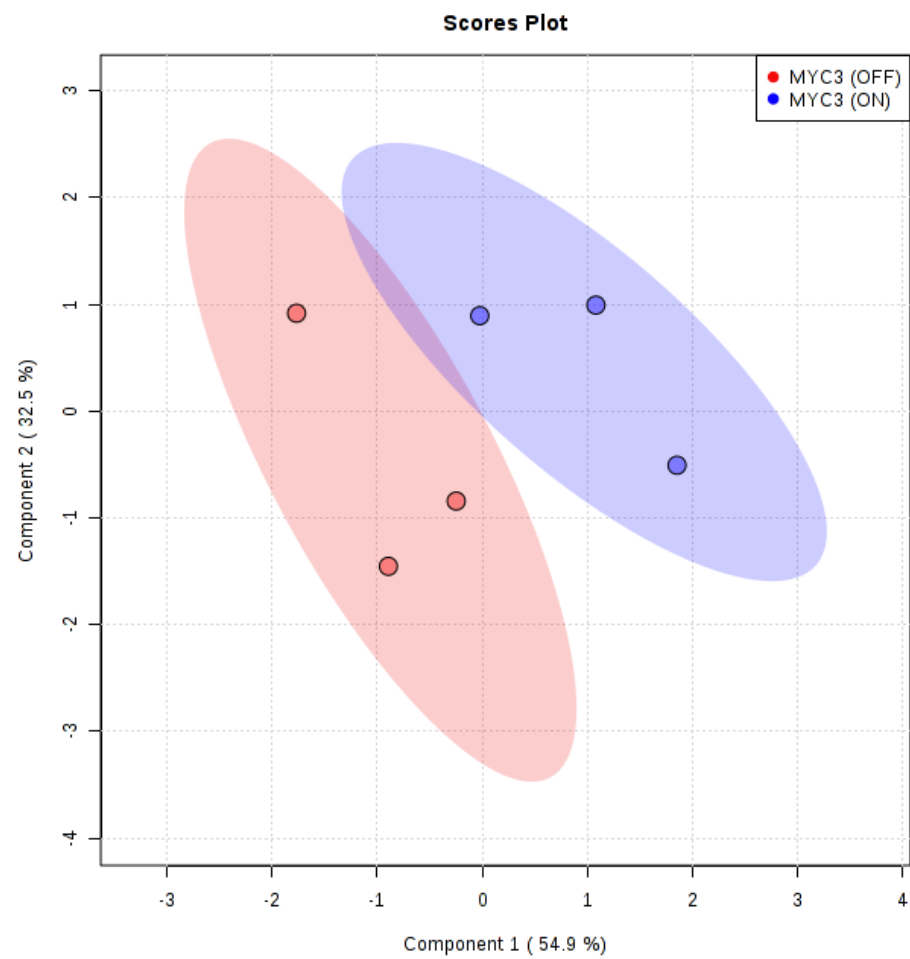
Measure	1 comps	2 comps	3 comps
Accuracy	0.5	0.33333	0.33333
R2	0.63107	0.84777	0.99493
Q2	0.020702	-1.1286	-1.1478

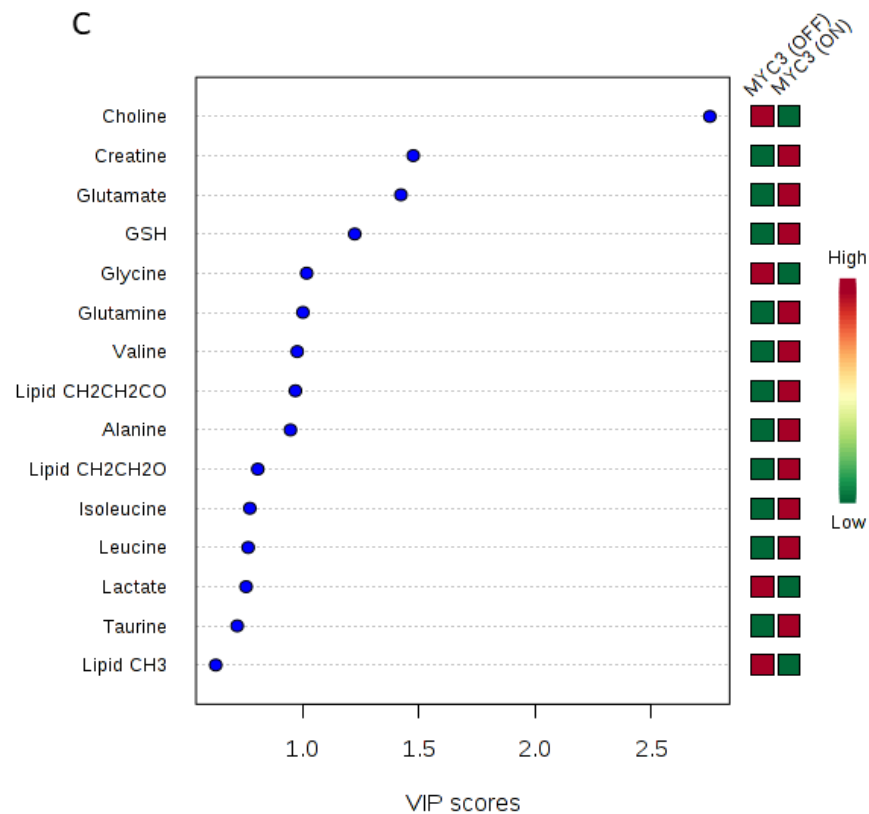
Appendix 8.27 PCA score plot of metabolite concentrations of the D283 MYC 2 cells following treatment in the presence or absence of doxycycline to induce MYC knockdown. PCA shows the first two principal components. B) Supervised PLS-DA score plot showing group variations. C) VIP score from PLS-DA showing top 15 metabolites contributing to separation of the MYC 2 (on) and MYC 2 (off) groups. The red and green boxes to the right indicate whether a metabolite is increased (red) or decreased (green) when MYC was knocked down. D) Cross validation of the PLS-DA showing model accuracy, R² and Q² values.

A



B





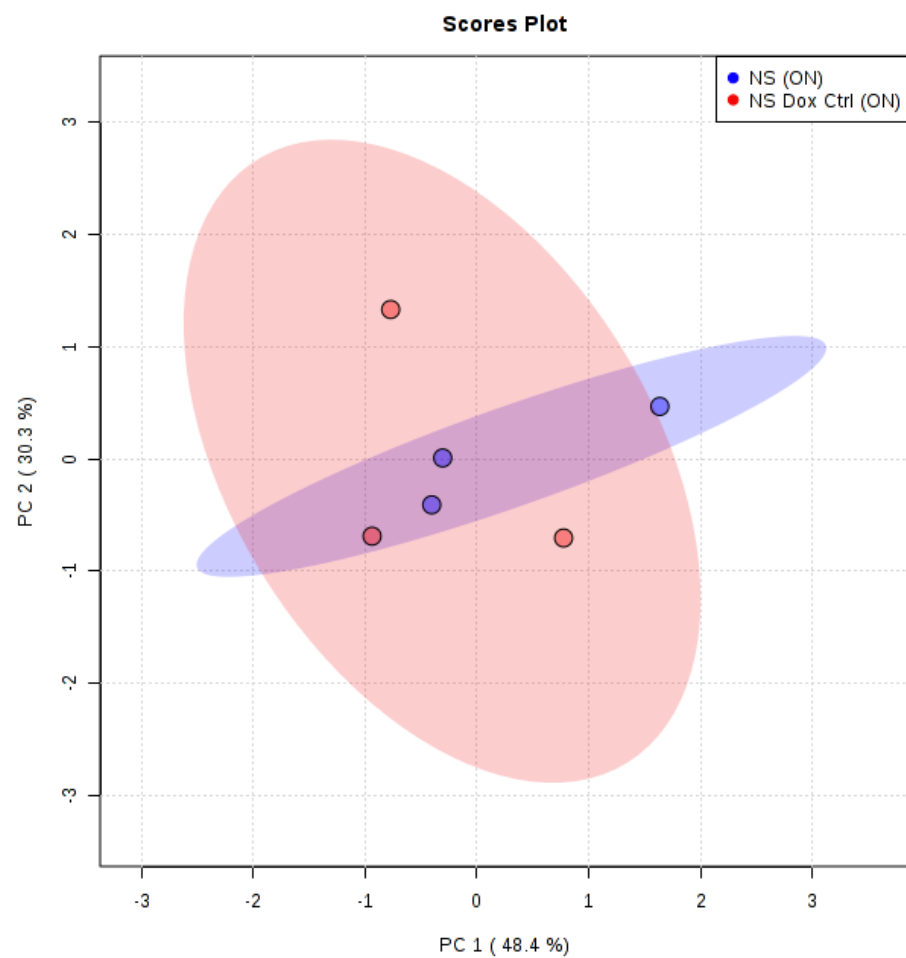
D

PLS-DA cross validation details:

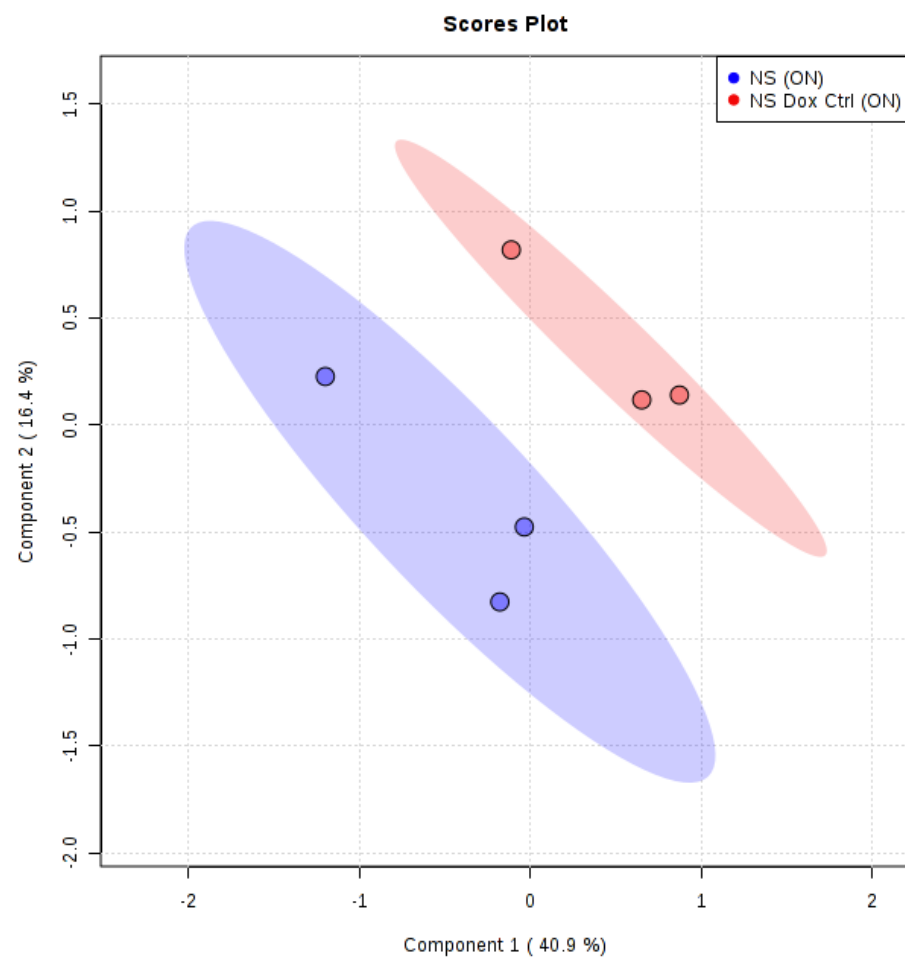
Measure	1 comps	2 comps	3 comps
Accuracy	0.66667	0.66667	0.83333
R2	0.65728	0.87962	0.96406
Q2	0.18318	0.35144	0.50669

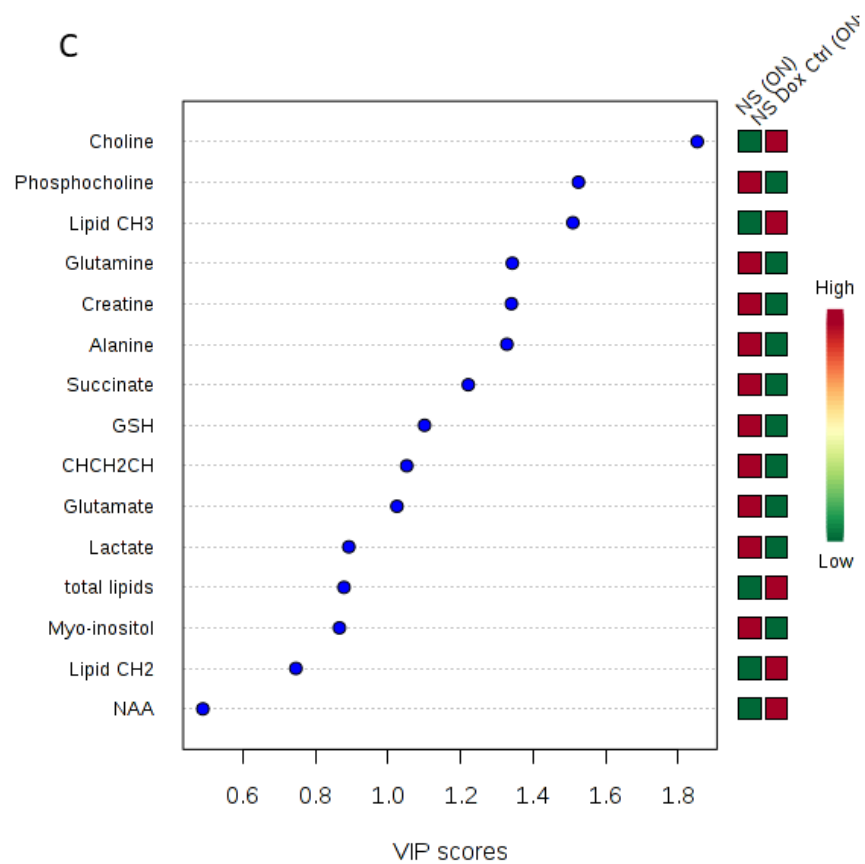
Appendix 8.28 PCA score plot of metabolite concentrations of the D283 MYC 3 cells following treatment in the presence or absence of doxycycline to induce MYC knockdown. PCA shows the first two principal components. B) Supervised PLS-DA score plot showing group variations. C) VIP score from PLS-DA showing top 15 metabolites contributing to separation of the MYC 3 (on) and MYC 3 (off) groups. The red and green boxes to the right indicate whether a metabolite is increased (red) or decreased (green) when MYC was knocked down. D) Cross validation of the PLS-DA showing model accuracy, R2 and Q2 values.

A



B



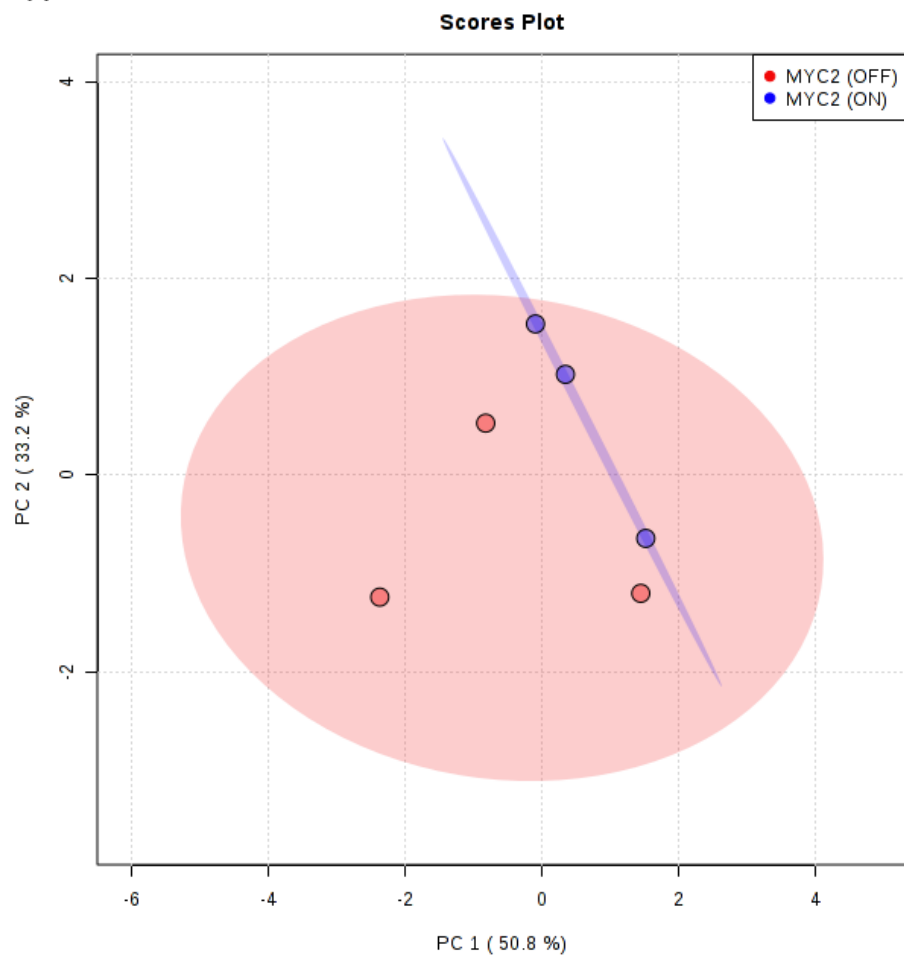
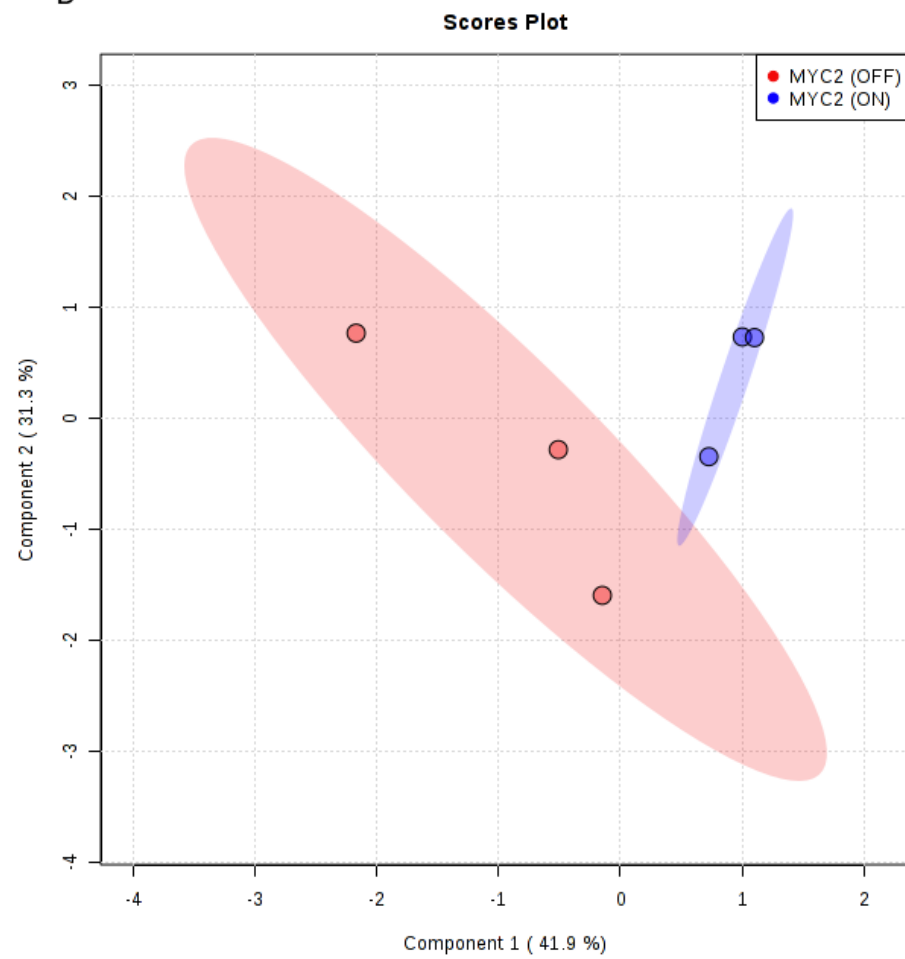


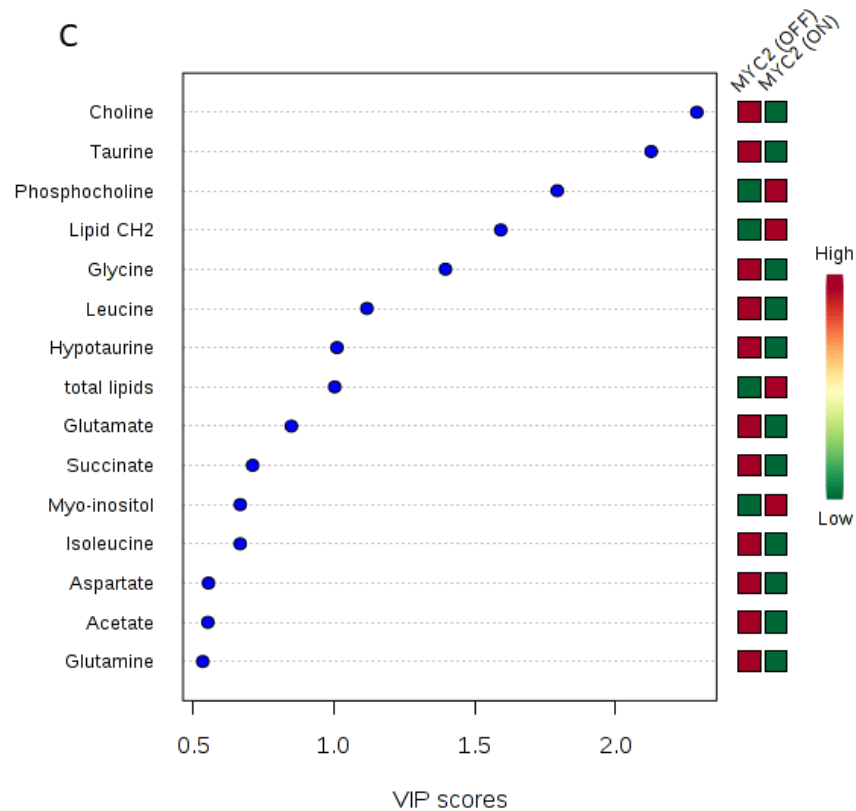
D

PLS-DA cross validation details:

Measure	1 comps	2 comps	3 comps
Accuracy	0.0	0.16667	0.16667
R2	0.49848	0.96224	0.98113
Q2	-1.4367	-1.9907	-1.6135

Appendix 8.29 PCA score plot of metabolite concentrations of the D283 NS cells following treatment in the presence or absence of doxycycline to induce MYC knockdown. PCA shows the first two principal components. B) Supervised PLS-DA score plot showing group variations. C) VIP score from PLS-DA showing top 15 metabolites contributing to separation of the NS (on) and NS Dox Ctrl (on) groups. The red and green boxes to the right indicate whether a metabolite is increased (red) or decreased (green) when MYC was knocked down. D) Cross validation of the PLS-DA showing model accuracy, R2 and Q2 values.

A**B**



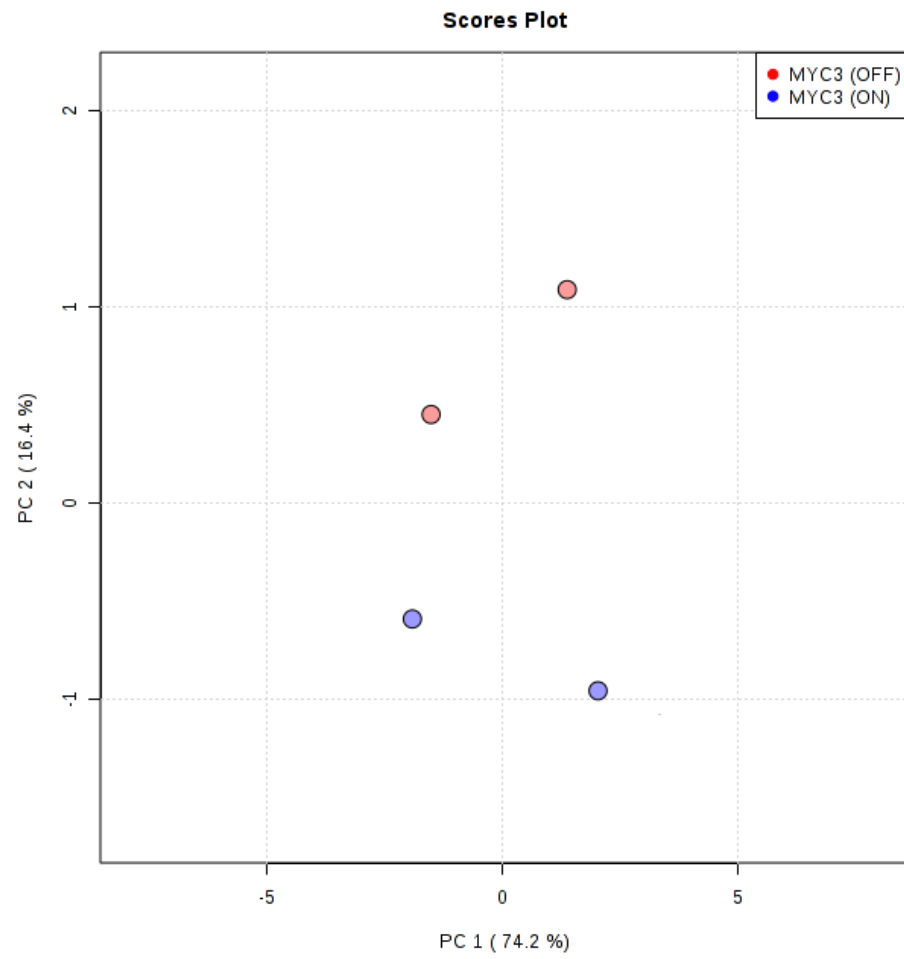
D

PLS-DA cross validation details:

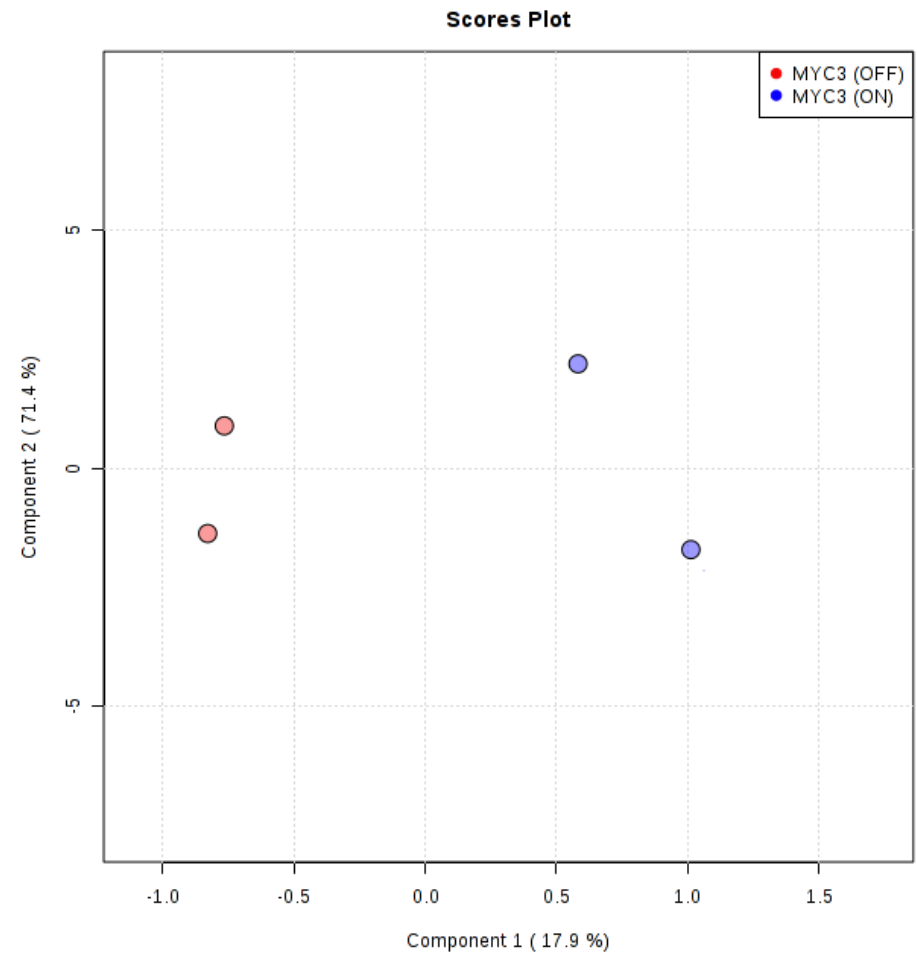
Measure	1 comps	2 comps	3 comps
Accuracy	0.5	0.5	0.83333
R2	0.68967	0.87729	0.98101
Q2	-0.09796	0.042796	0.47748

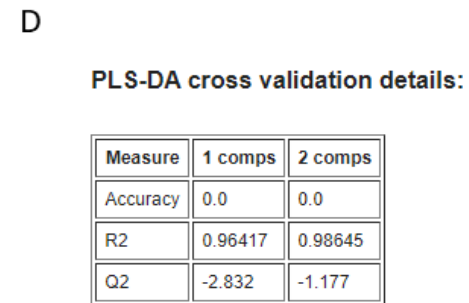
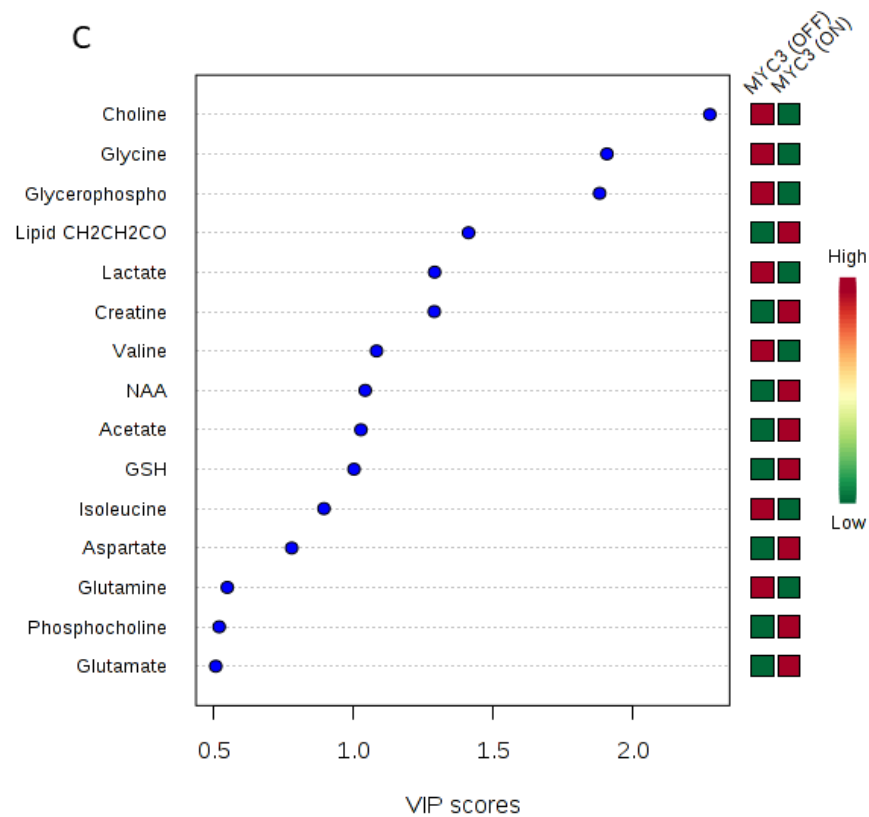
Appendix 8.30 PCA score plot of metabolite concentrations of the HDMB03 MYC 2 cells following treatment in the presence or absence of doxycycline to induce MYC knockdown. PCA shows the first two principal components. B) Supervised PLS-DA score plot showing group variations. C) VIP score from PLS-DA showing top 15 metabolites contributing to separation of the MYC 2 (on) and MYC 2 (off) groups. The red and green boxes to the right indicate whether a metabolite is increased (red) or decreased (green) when MYC was knocked down. D) Cross validation of the PLS-DA showing model accuracy, R2 and Q2 values.

A



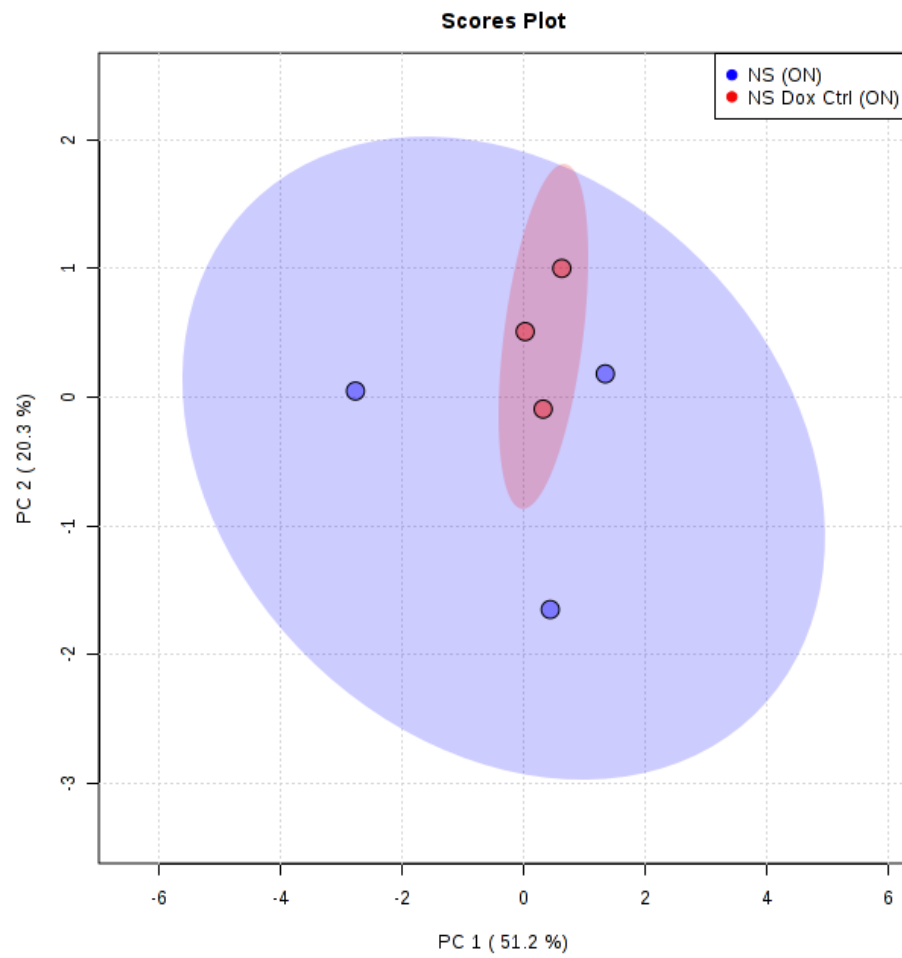
B



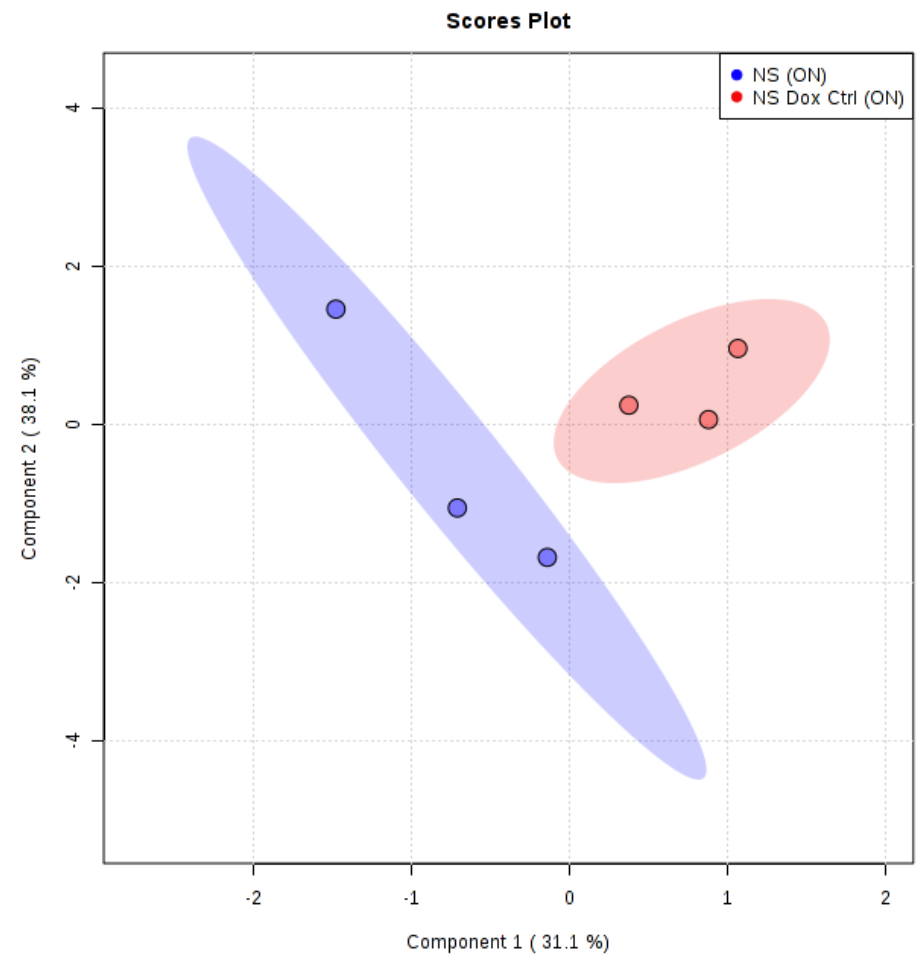


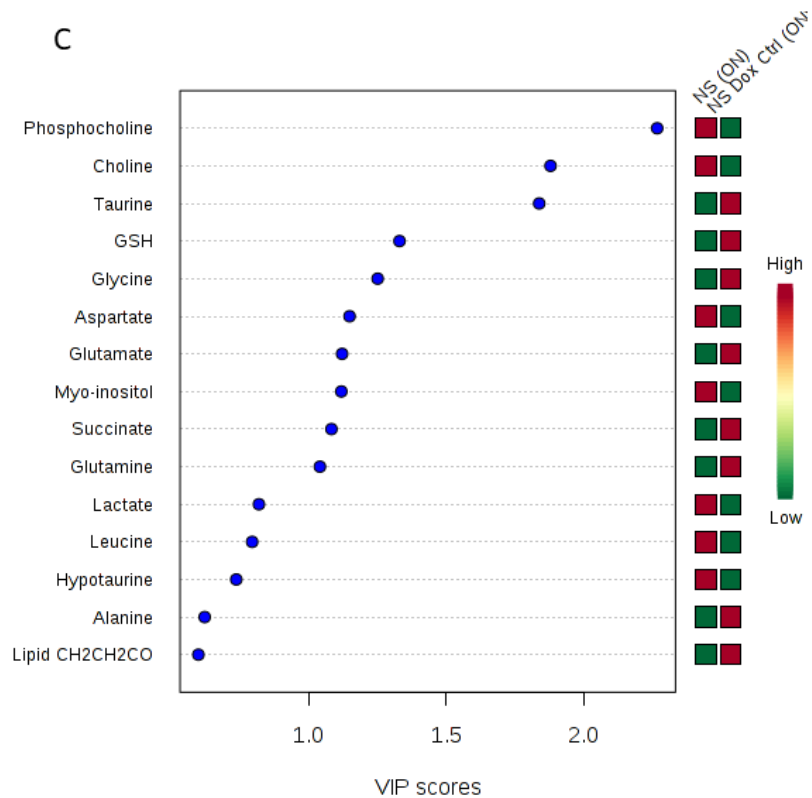
Appendix 8.31 PCA score plot of metabolite concentrations of the HDMB03 MYC 3 cells following treatment in the presence or absence of doxycycline to induce MYC knockdown. PCA shows the first two principal components. B) Supervised PLS-DA score plot showing group variations. C) VIP score from PLS-DA showing top 15 metabolites contributing to separation of the MYC 3 (on) and MYC 3 (off) groups. The red and green boxes to the right indicate whether a metabolite is increased (red) or decreased (green) when MYC was knocked down. D) Cross validation of the PLS-DA showing model accuracy, R2 and Q2 values.

A



B



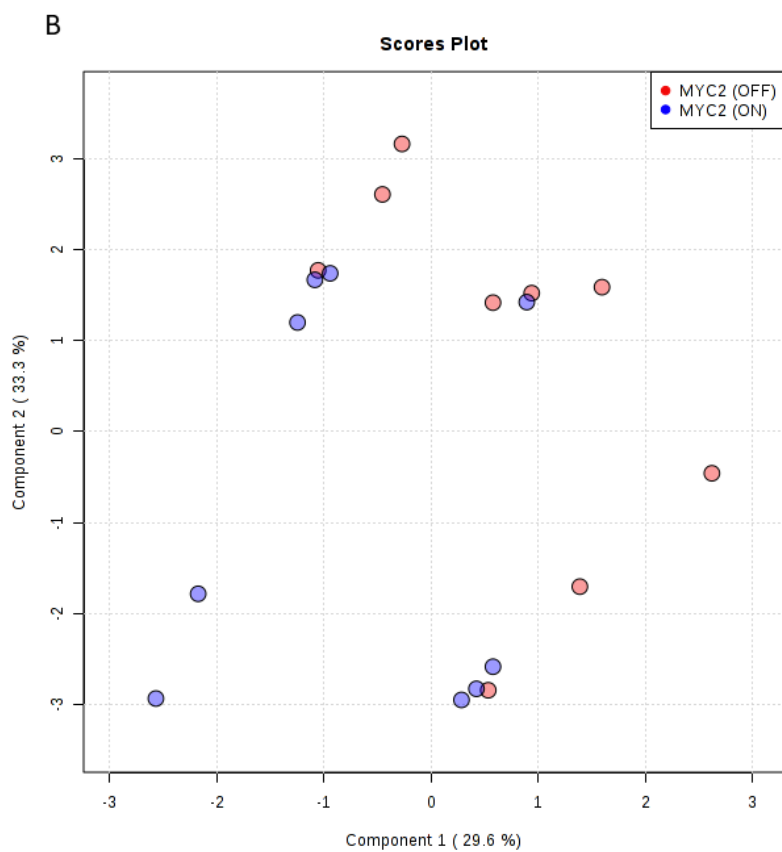
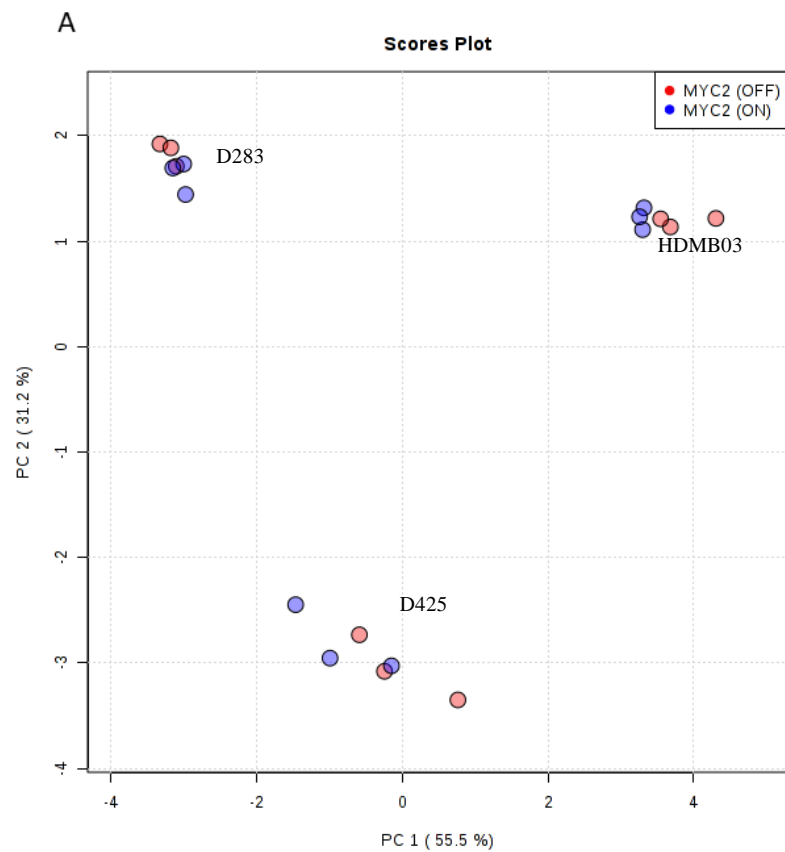


D

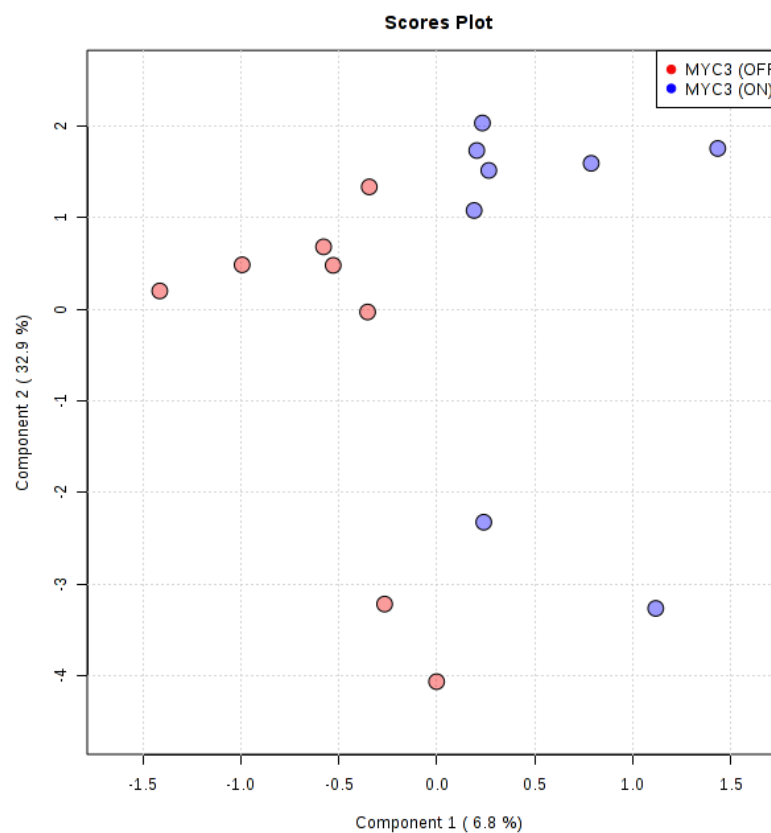
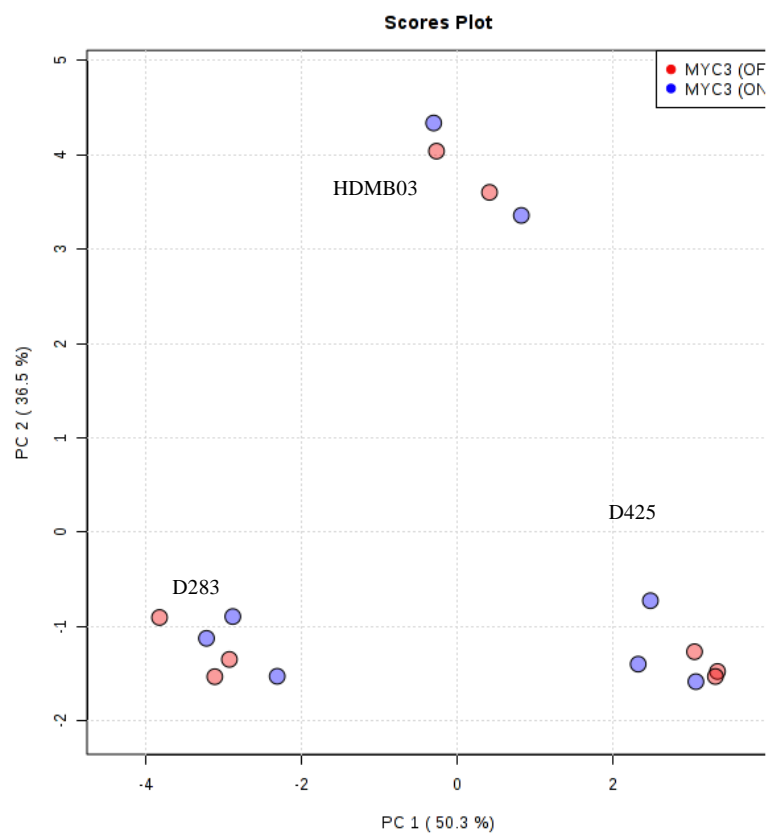
PLS-DA cross validation details:

Measure	1 comps	2 comps	3 comps
Accuracy	0.33333	0.33333	0.33333
R2	0.75702	0.91007	0.96977
Q2	-0.88424	-0.98903	-1.2262

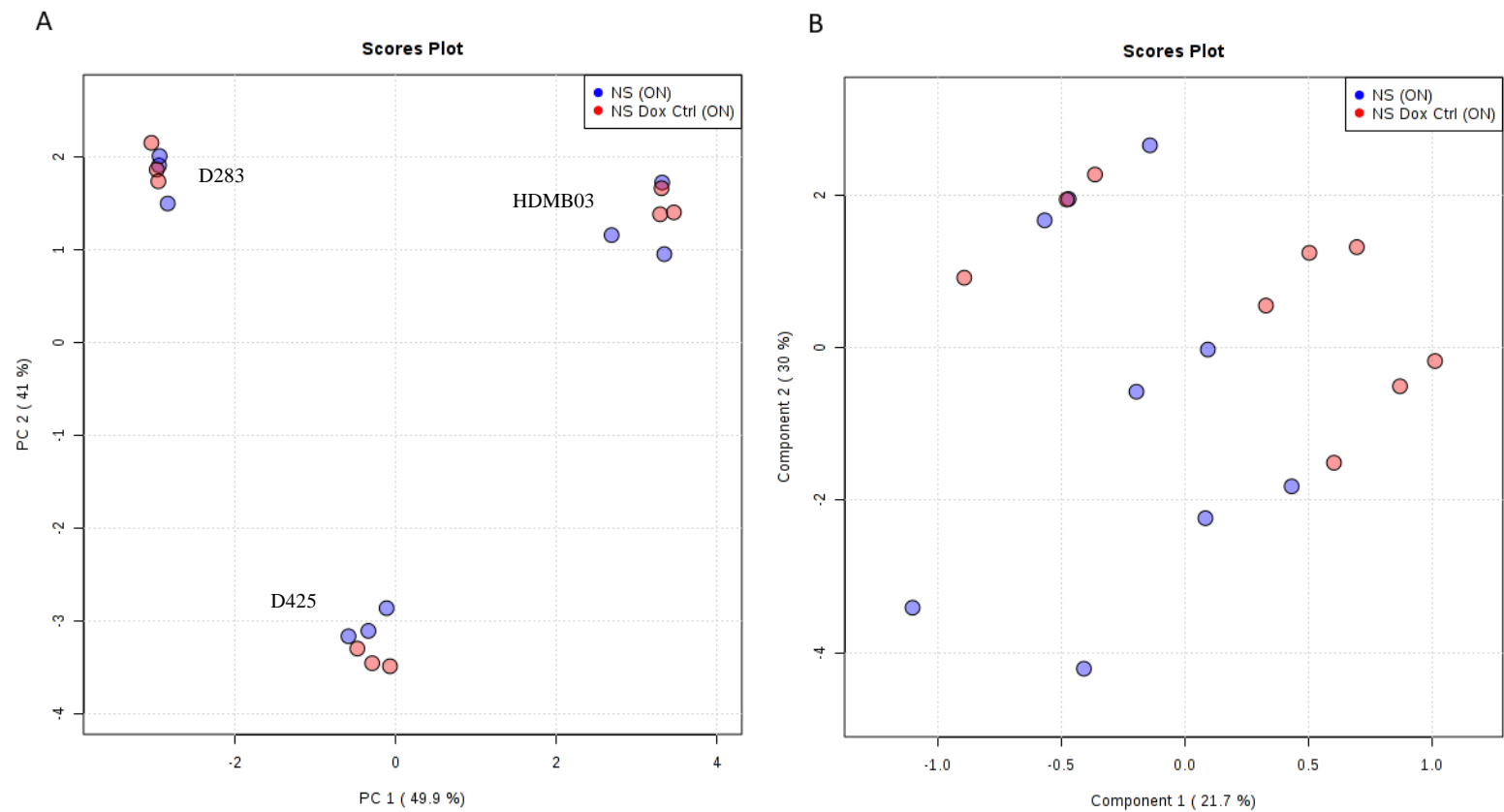
Appendix 8.32 PCA score plot of metabolite concentrations of the HDMB03 NS cells following treatment in the presence or absence of doxycycline to induce MYC knockdown. PCA shows the first two principal components. B) Supervised PLS-DA score plot showing group variations. C) VIP score from PLS-DA showing top 15 metabolites contributing to separation of the NS (on) and NS Dox Ctrl (on) groups. The red and green boxes to the right indicate whether a metabolite is increased (red) or decreased (green) when MYC was knocked down. D) Cross validation of the PLS-DA showing model accuracy, R2 and Q2 values.



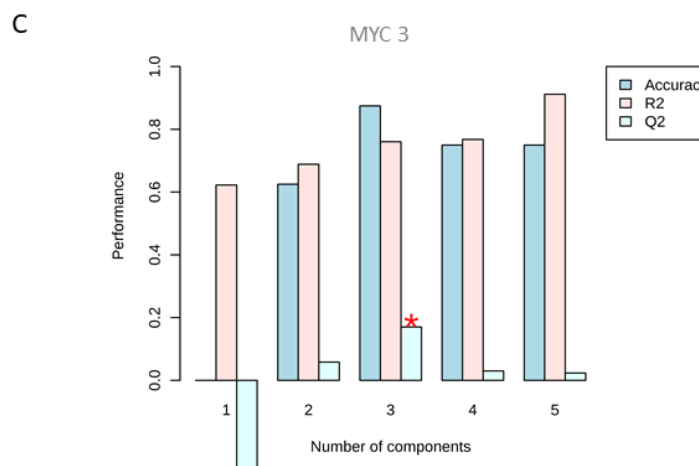
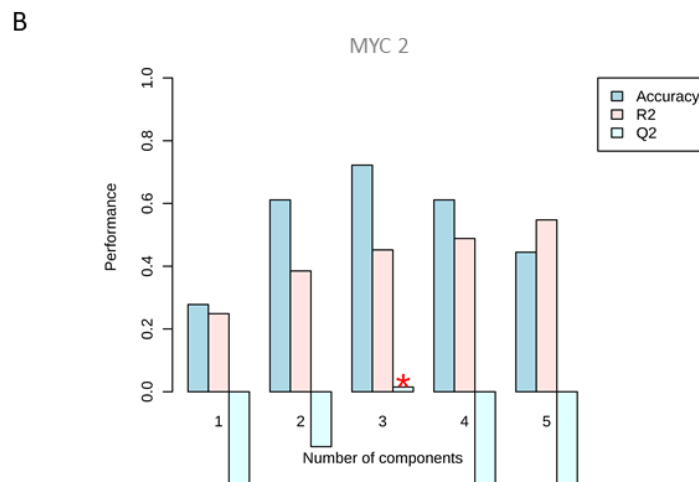
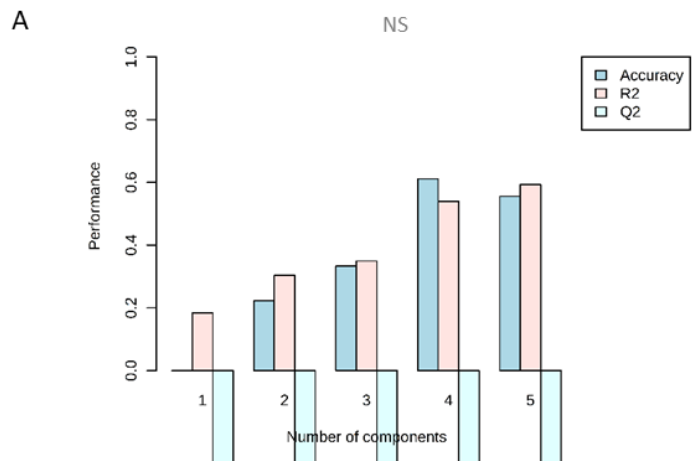
Appendix 8.33 Pooled multivariate analysis of MB_{GRP3} MYC 2 cell lines metabolite profiles. A) PCA score plot of metabolite concentrations from D425, D283 and HDMB03 MYC 2 cell lines following treatment with or without doxycycline for 72 h. PCA shows the first two principal components. B) PLS-DA score plot of the pooled MYC 2 bearing MB_{GRP3} cell lines.



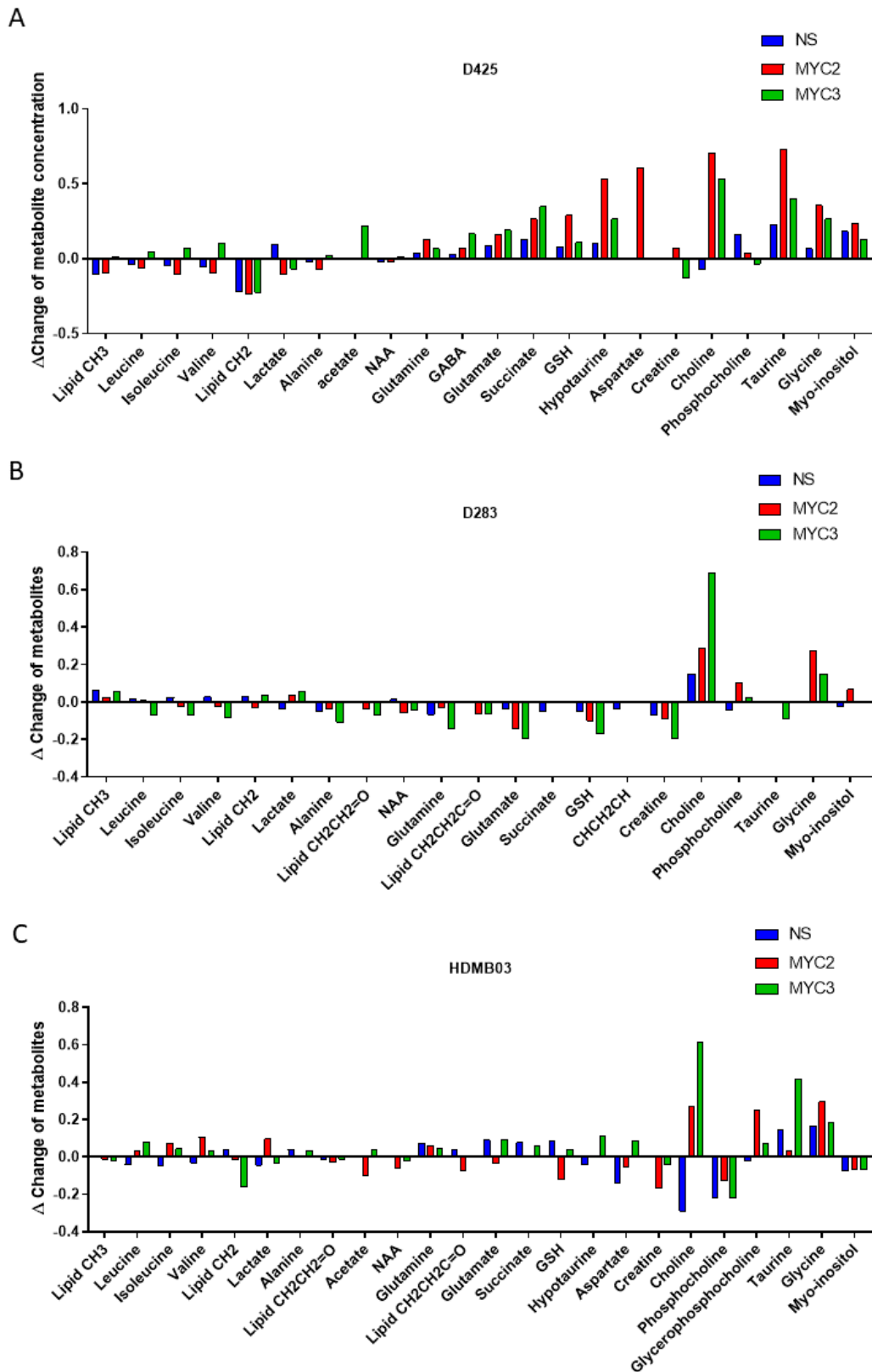
Appendix 8.34 Pooled multivariate analysis of MB_{GRP3} MYC 3 cell lines metabolite profiles. A) PCA score plot of metabolite concentrations from D425, D283 and HDMB03 MYC 3 cell lines following treatment with or without doxycycline for 72 h. PCA shows the first two principal components. B) PLS-DA score plot of the pooled MYC 3 bearing MB_{GRP3} cell lines.



Appendix 8.35 Pooled multivariate analysis of MB_{GRP3} NS cell lines metabolite profiles. A) PCA score plot of metabolite concentrations from D425, D283 and HDMB03 NS cell lines following treatment with or without doxycycline for 72 h. PCA shows the first two principal components. B) PLS-DA score plot of the pooled NS bearing MB_{GRP3} cell lines.

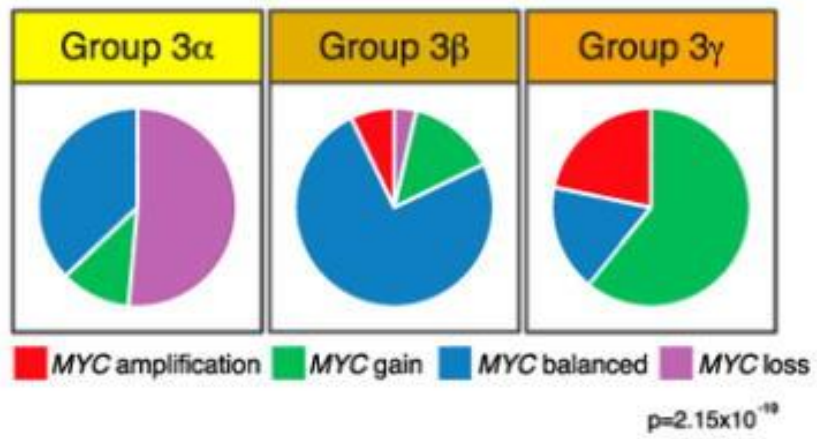


*Appendix 8.36 Cross validations of PLS-DA models for the pooled MB_{GRP3} cell lines generated from random permutations showing accuracy, R2 and Q2 values from analysis. * indicates significance of permutations test. Graph cutoffs automatically adjusted by Metaboanalyst.*

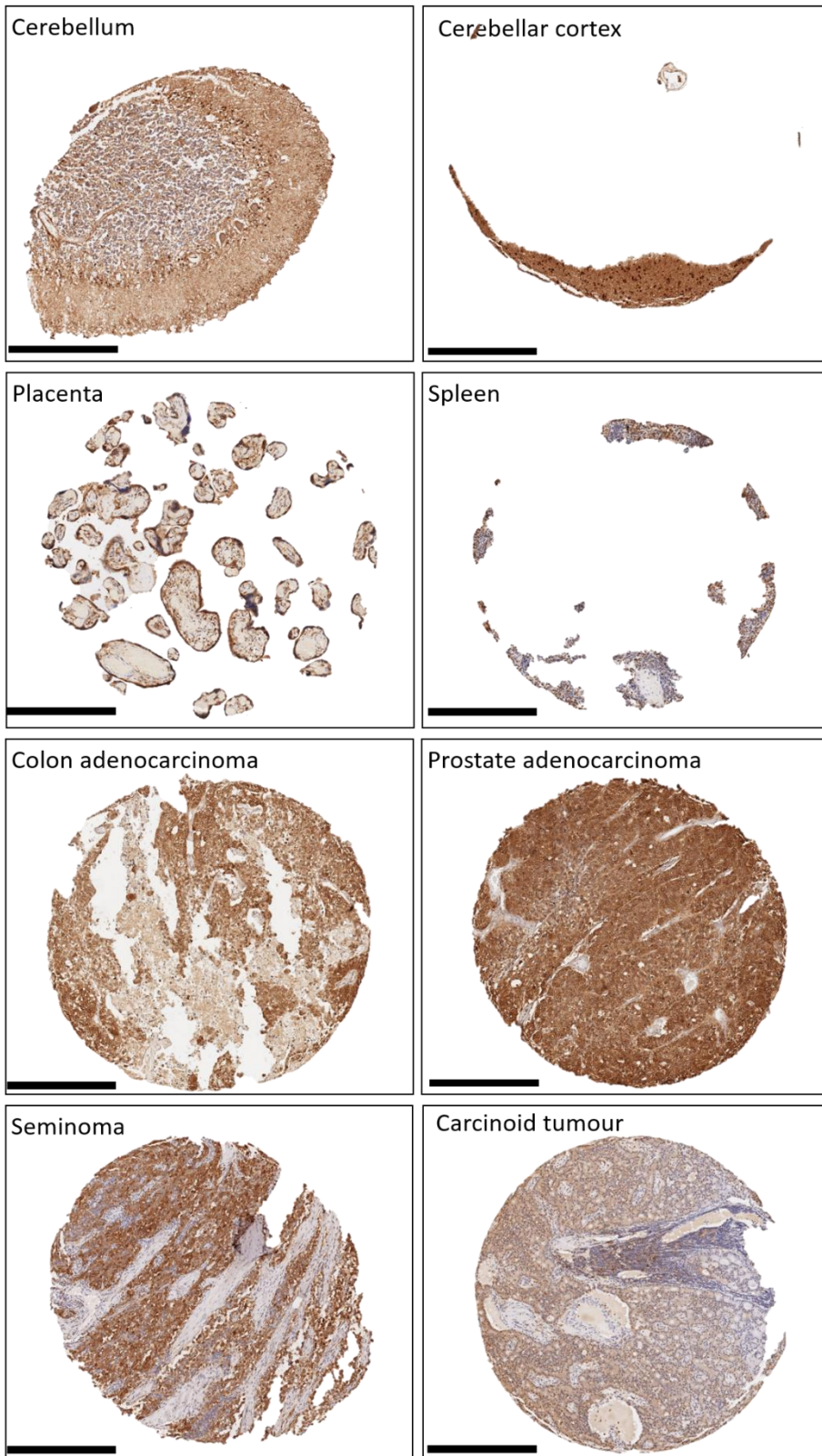


Appendix 8.37 Differential metabolites in the MB_{GRP3} cell lines. Horizontal axis represents metabolites and vertical axis shows fold change between each construct pair following doxycycline treatment for 72 h.

D. Appendix for Chapter 6



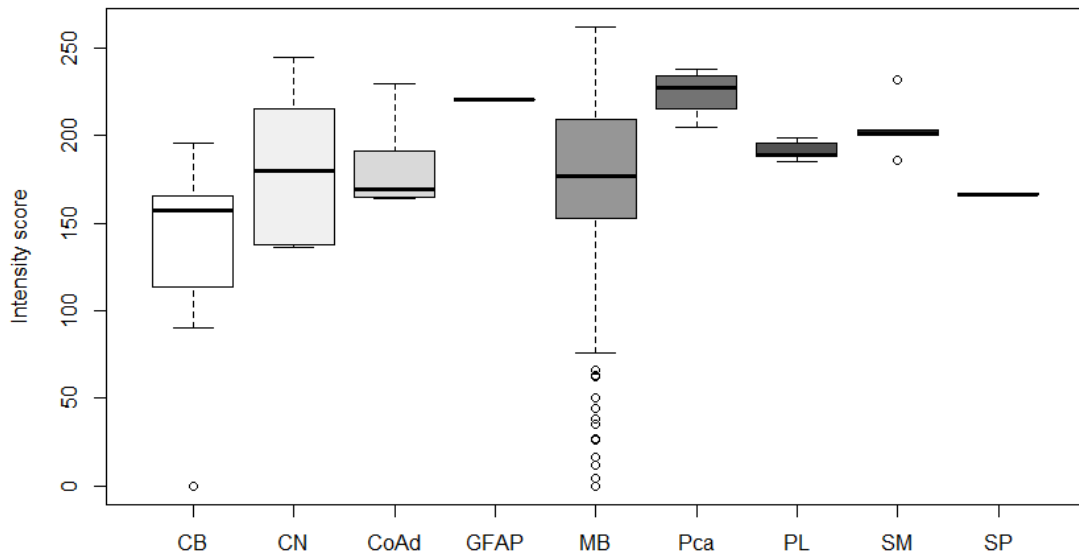
Appendix 8.38 Subtype definitions for the Cavalli MB_{GRP3} dataset



Appendix 8.39 Immunohistochemical staining of PHGDH in control tissues.

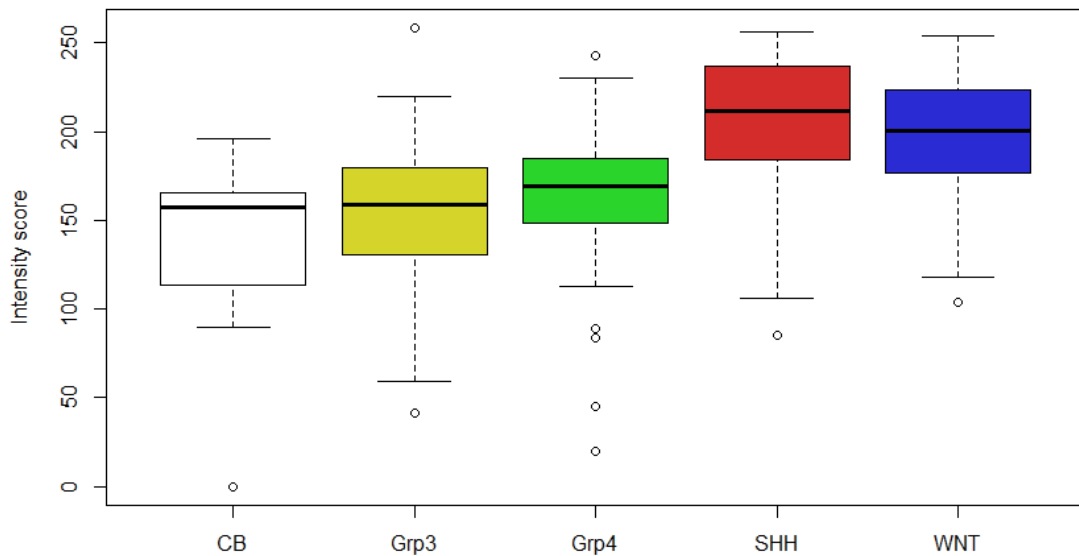
Scale bar = 100 μ M

Expression of PHGDH across control tissues and tumours

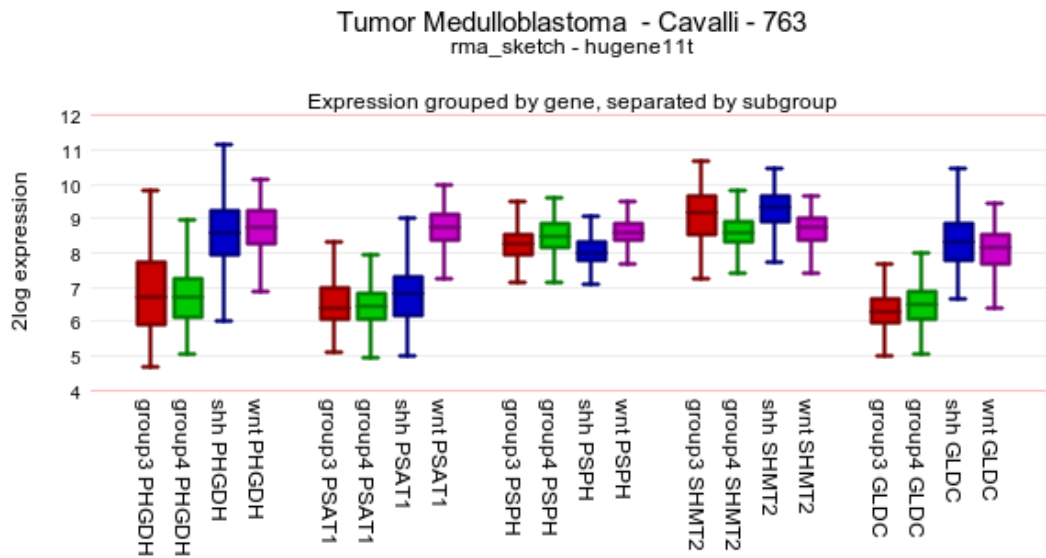


Appendix 8.40 PHGDH intensity scores for control samples. Cerebellum (CB); Carcinoid tumour (CN); Colon Adenocarcinoma (CoAd); GFAP positive sample; Medulloblastoma (MB); Prostate cancer (PCa); Placenta (PL); Semimoma (SM); Spleen (SP).

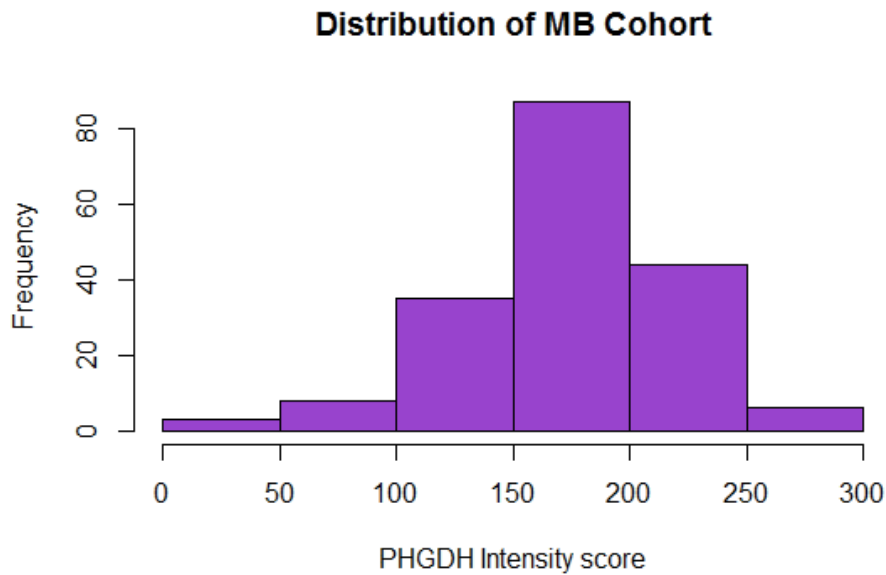
PHGDH expression in normal cerebellum and MB Subgroups



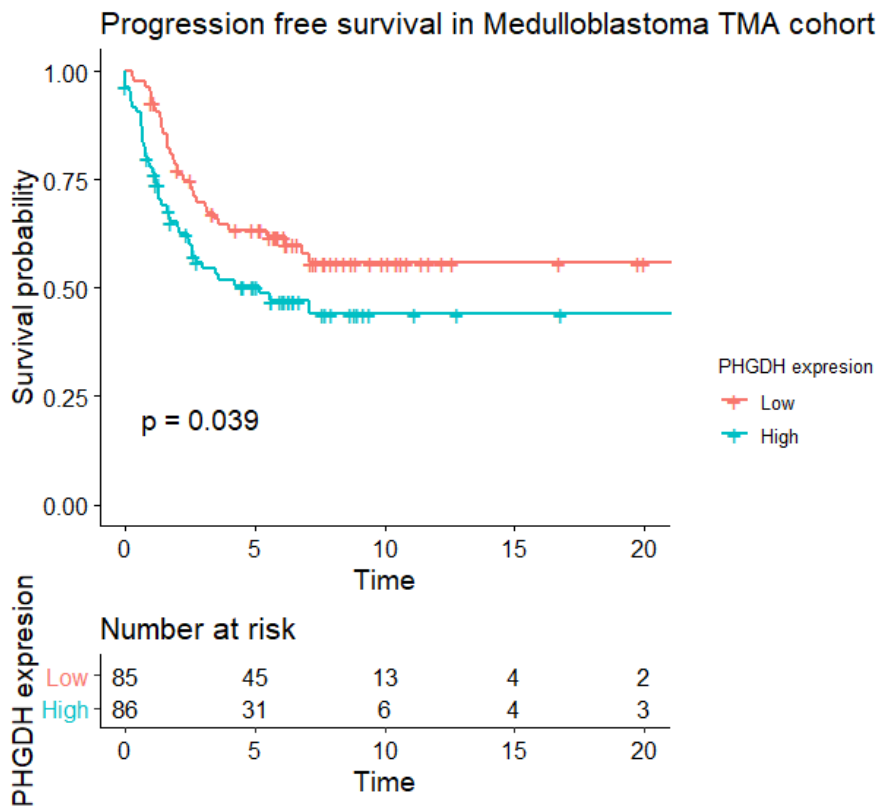
Appendix 8.41 Comparison of PHGDH expression in cerebellum and MB subgroups



Appendix 8.42 Expression of SGP enzymes in MB subgroups from Cavalli dataset generated from R2 genomics.



Appendix 8.43 Distribution of PHGDH intensity score in TMA cohort

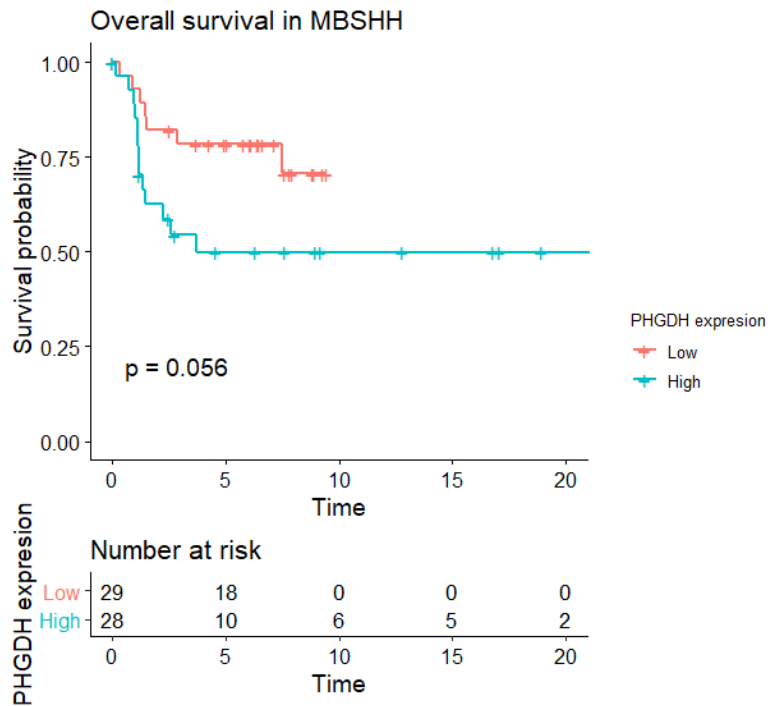


Appendix 8.44 Progression free survival of TMA cohort.

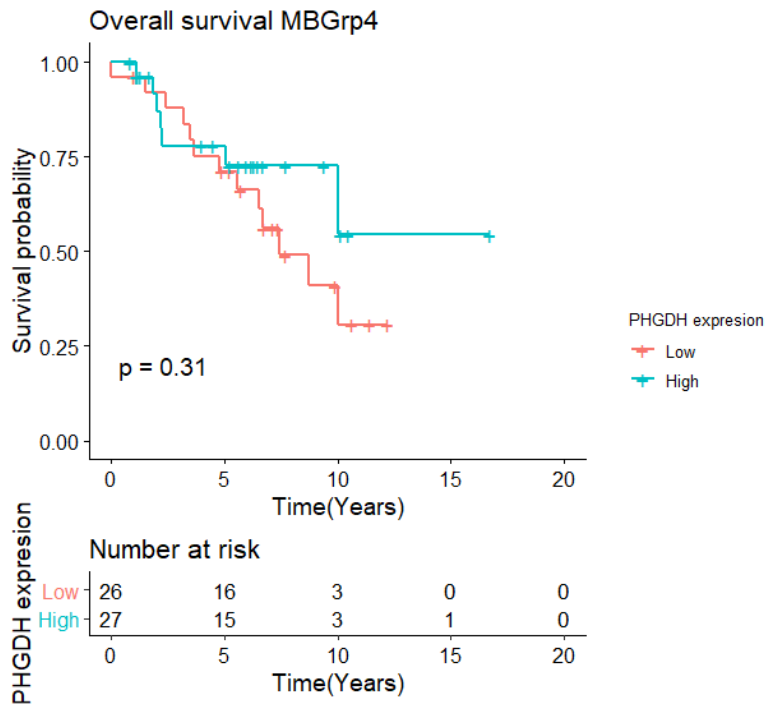
Appendix 8.45 Coefficients from Cox proportional hazard modelling of TMA cohort

	Exp (coef)	Exp(-coef)	95% CI	
Subgroup MB _{GRP4}	0.6166	1.6218	0.30758	1.2361
Subgroup MB _{SHH}	0.4315	2.3175	0.19374	0.961
Subgroup MB _{WNT}	0.1624	6.1568	0.03514	0.7507
PHGDH > 176	2.3135	0.4322	1.25304	4.2715
MYC	3.9488	0.2532	1.60055	9.7423
MYCN	2.3785	0.4204	1.02397	5.5249
Metastatic disease	1.2395	0.8068	0.71204	2.1576
LCA	2.3125	0.4324	1.12628	4.7479
Gender (Male)	0.9592	1.0425	0.54046	1.7024
Age > 3	4.282	0.2335	1.73852	10.5468
Resection (STR)	2.0501	0.4878	1.08685	3.8671
Chemotherapy	0.5381	1.8584	0.22591	1.2817
Radiotherapy (None)	8.1491	0.1227	3.07387	21.6039

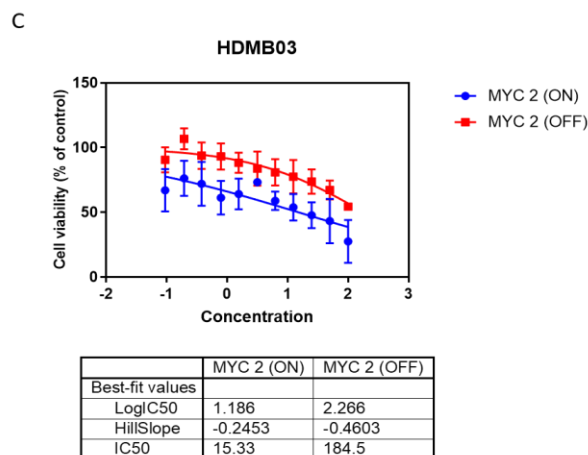
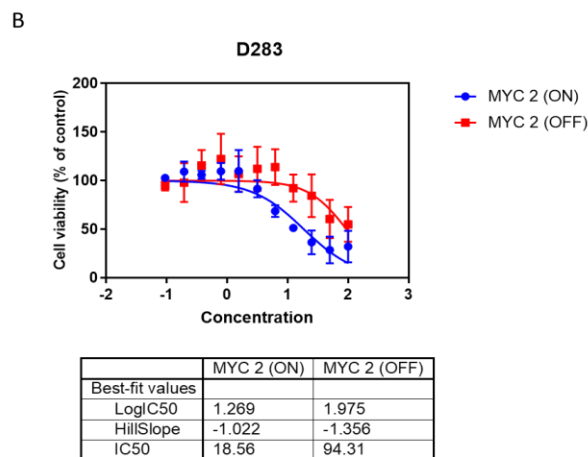
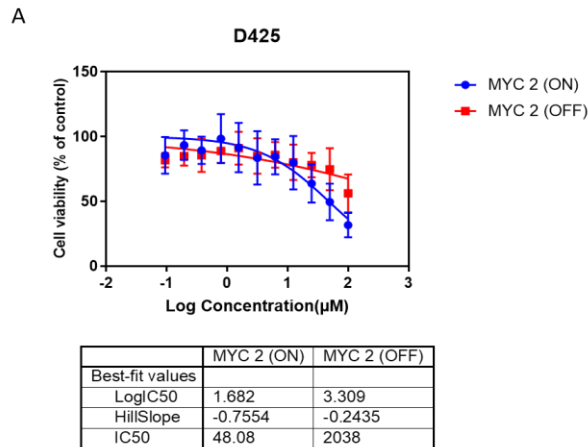
Concordance = 0.723 (se = 0.038)
 Rsquare = 0.338 (max possible= 0.977)
 Likelihood ratio test = 63.48 on 13 df, p=1.241e-08
 Wald test = 62.94 on 13 df, p=1.559e-08
 Score (log rank) test = 84.81 on 13 df, p=1.363e-12



Appendix 8.46 Kaplan Meier survival analysis of PHGDH expression in MB_{SHH} . Overall survival of patients with PHGDH low (orange) and PHGDH high (green) with table depicting number of patients at risk at a given time point. Significance was tested using log rank test. MYCN amplification in MB_{SHH} was found to correlate with higher PHGDH and survival analysis suggest that it may impact survival.



Appendix 8.47 Kaplan Meier survival analysis of PHGDH expression in MB_{SHH}. . Overall survival of patients with PHGDH low (orange) and PHGDH high (green) with table depicting number of patients at risk at a given time point. Significance was tested using log rank test. MYCN amplification in MB_{GRP4} was not associated with PHGDH expression and here it does not impact survival outcomes in this subgroup.



Appendix 8.48 Response of MYC-regulable MB_{GRP3} isogenic cells to NCT503 treatment. A) D425 MYC 2 B) D283 MYC 2 C) HDMB03 MYC 2 were treated in the presence or absence of 1 µg/mL of doxycycline for 48 h. Subsequently cells were plated in 96 well microplates and treated with varying concentrations of NCT503 for 72 h. Cell viability measured with CellTiter Glo™. Data was normalised to vehicle control and log transformed (NCT503 concentrations ranges from 1.56 µM to 100 µM). Data represents mean of five independent experiments ± SEM. IC₅₀ were determined using non-linear regression analysis using log (inhibitor) versus response (variable slope).

Appendix 8.49 Subgroup definition and MYC status of MB parental cell lines

Cell lines	Subgroup	MYC
D425	MBGrp3	Amplified
D458 (recurrence from D425)	MBGrp3	Amplified
D283	MBGrp3	Gain (3 copies) Overexpression
HDMB03	MBGrp3	Amplified
CHLA-259	Undefined	Non-amp MYCN amplification (*)
MED1	Undefined	Gain (2 copies) (*)
MED8A	Undefined	Amplified PVT1-MYC fusion (*)
DAOY	Sonic hedgehog (SHH)	Non-amp
UW228.1	Sonic hedgehog (SHH)	Non-amp

Asterisks denotes characteristic reported in (Ivanov et al., 2016)

Appendix 8.50 CRISPR screen data for D283 cell line.

D283	Num of guides	Neg score	Neg p-value	Neg fdr	Neg rank	Neg goodsgr rna	Pos score	Pos p-value	Pos fdr	Pos rank	Pos goodsgr na
MYC	6	0.000293	0.000434	0.110016	82	6	0.99971	0.99996	0.999999	21786	0
RPL6	6	0.002686	0.004391	0.263043	364	3	0.59114	0.94986	0.999999	16892	3
RPL3	6	0.003352	0.005871	0.278998	439	4	0.86308	0.98597	0.999999	19974	2
PHGDH	6	0.00514	0.009281	0.281243	633	2	0.10639	0.61342	0.999999	6076	4
CAD	6	0.005915	0.009718	0.281243	714	5	0.6817	0.9651	0.999999	17947	1
SLC16A1	6	0.013493	0.020057	0.31667	1380	5	0.97255	0.99658	0.999999	21111	1
YWHAZ	6	0.020602	0.028866	0.325279	1827	4	0.68525	0.96569	0.999999	17978	1
RPL12	6	0.047668	0.074657	0.477542	3345	5	0.30822	0.85478	0.999999	12055	1
SLC2A1	6	0.084257	0.13121	0.562829	5081	4	0.52852	0.93287	0.999999	15838	2
NCL	6	0.11508	0.18205	0.626324	6160	3	0.73556	0.97139	0.999999	18476	2
PGK1	6	0.12513	0.1892	0.626324	6484	3	0.4373	0.90425	0.999999	14303	2
EIF4E	6	0.14094	0.2031	0.626324	6973	4	0.64665	0.96098	0.999999	17599	2
RPS12	6	0.14851	0.21069	0.626324	7225	4	0.17805	0.72438	0.999999	8401	2
CDK4	6	0.17266	0.23369	0.639444	7951	3	0.10196	0.60648	0.999999	5919	3
RPS20	6	0.20172	0.26195	0.642176	8801	3	0.42382	0.89964	0.999999	14071	3
HPRT1	6	0.26699	0.32306	0.656911	10609	4	0.5808	0.9474	0.999999	16738	1
LDHA	6	0.31037	0.3672	0.682692	11675	3	0.052223	0.43793	0.999999	3504	3
ODC1	6	0.33165	0.38263	0.688685	12028	2	0.28808	0.83877	0.999999	11554	4
PTMA	6	0.3328	0.38449	0.688685	12048	1	0.004352	0.10324	0.999999	438	5
SLC1A5	6	0.53761	0.52514	0.735226	15544	3	0.093899	0.58855	0.999999	5619	3
HK2	6	0.56793	0.54296	0.737356	16048	3	0.28073	0.83279	0.999999	11389	3
SHMT2	6	0.56817	0.54301	0.737356	16053	3	0.46608	0.9149	0.999999	14811	3
PDK1	6	0.99585	0.9597	0.963884	21708	0	0.004151	0.10133	0.999999	413	6

References

- ABOAGYE, E. O. & BHUJWALLA, Z. M. 1999. Malignant transformation alters membrane choline phospholipid metabolism of human mammary epithelial cells. *Cancer Res*, 59, 80-4.
- ADHIKARY, S. & EILERS, M. 2005. Transcriptional regulation and transformation by Myc proteins. *Nat Rev Mol Cell Biol*, 6, 635-45.
- ADIAMAH, D. A. & SCHWARTZ, J. M. 2012. Construction of a genome-scale kinetic model of mycobacterium tuberculosis using generic rate equations. *Metabolites*, 2, 382-97.
- AHLER, E., SULLIVAN, W. J., CASS, A., BRAAS, D., YORK, A. G., BENSINGER, S. J., GRAEBER, T. G. & CHRISTOFK, H. R. 2013. Doxycycline alters metabolism and proliferation of human cell lines. *PLoS One*, 8, e64561.
- AKARACHANTACHOTE, N., CHADCHAM, S. & SAITHANU, K. 2014. Cutoff Threshold of Variable Importance in Projection for Variable Selection. *International Journal of Pure and Applied Mathematics*, 94.
- ALCANTARA LLAGUNO, S., CHEN, J., KWON, C. H., JACKSON, E. L., LI, Y., BURNS, D. K., ALVAREZ-BUYLLA, A. & PARADA, L. F. 2009. Malignant astrocytomas originate from neural stem/progenitor cells in a somatic tumor suppressor mouse model. *Cancer Cell*, 15, 45-56.
- ALCANTARA LLAGUNO, S., SUN, D., PEDRAZA, A. M., VERA, E., WANG, Z., BURNS, D. K. & PARADA, L. F. 2019. Cell-of-origin susceptibility to glioblastoma formation declines with neural lineage restriction. *Nat Neurosci*, 22, 545-555.
- ALCANTARA LLAGUNO, S. R., WANG, Z., SUN, D., CHEN, J., XU, J., KIM, E., HATANPAA, K. J., RAISANEN, J. M., BURNS, D. K., JOHNSON, J. E. & PARADA, L. F. 2015. Adult Lineage-Restricted CNS Progenitors Specify Distinct Glioblastoma Subtypes. *Cancer Cell*, 28, 429-440.
- ALDAPE, K., BRINDLE, K. M., CHESLER, L., CHOPRA, R., GAJJAR, A., GILBERT, M. R., GOTTARDO, N., GUTMANN, D. H., HARGRAVE, D., HOLLAND, E. C., JONES, D. T. W., JOYCE, J. A., KEARNS, P., KIERAN, M. W., MELLINGHOFF, I. K., MERCHANT, M., PFISTER, S. M., POLLARD, S. M., RAMASWAMY, V., RICH, J. N., ROBINSON, G. W., ROWITCH, D. H., SAMPSON, J. H., TAYLOR, M. D., WORKMAN, P. & GILBERTSON, R. J. 2019. Challenges to curing primary brain tumours. *Nat Rev Clin Oncol*, 16, 509-520.
- ALLISON, S. J., KNIGHT, J. R. P., GRANCHI, C., RANI, R., MINUTOLO, F., MILNER, J. & PHILLIPS, R. M. 2014. Identification of LDH-A as a therapeutic target for cancer cell killing via (i) p53/NAD(H)-dependent and (ii) p53-independent pathways. *Oncogenesis*, 3, e102-e102.
- ALMUHAIDEB, A., PAPATHANASIOU, N. & BOMANJI, J. 2011. 18F-FDG PET/CT imaging in oncology. *Ann Saudi Med*, 31, 3-13.
- AMATI, B., FRANK, S. R., DONJERKOVIC, D. & TAUBERT, S. 2001. Function of the c-Myc oncoprotein in chromatin remodeling and transcription. *Biochim Biophys Acta*, 1471, M135-45.
- ANASTASIOU, D., POULOGIANNIS, G., ASARA, J. M., BOXER, M. B., JIANG, J. K., SHEN, M., BELLINGER, G., SASAKI, A. T., LOCASALE, J. W., AULD, D. S., THOMAS, C. J., VANDER HEIDEN, M. G. & CANTLEY, L. C. 2011. Inhibition of pyruvate kinase M2 by reactive oxygen species contributes to cellular antioxidant responses. *Science*, 334, 1278-83.

- ANDERSON, M., MARAYATI, R., MOFFITT, R. & YEH, J. J. 2017. Hexokinase 2 promotes tumor growth and metastasis by regulating lactate production in pancreatic cancer. *Oncotarget*, 8, 56081-56094.
- ANDERTON, B., CAMARDA, R., BALAKRISHNAN, S., BALAKRISHNAN, A., KOHNZ, R. A., LIM, L., EVASON, K. J., MOMCILOVIC, O., KRUTTWIG, K., HUANG, Q., XU, G., NOMURA, D. K. & GOGA, A. 2017. MYC-driven inhibition of the glutamate-cysteine ligase promotes glutathione depletion in liver cancer. *EMBO Rep*, 18, 569-585.
- ANDRONESI, O. C., ARRILLAGA-ROMANY, I. C., LY, K. I., BOGNER, W., RATAI, E. M., REITZ, K., IAFRATE, A. J., DIETRICH, J., GERSTNER, E. R., CHI, A. S., ROSEN, B. R., WEN, P. Y., CAHILL, D. P. & BATCHELOR, T. T. 2018. Pharmacodynamics of mutant-IDH1 inhibitors in glioma patients probed by in vivo 3D MRS imaging of 2-hydroxyglutarate. *Nat Commun*, 9, 1474.
- ANDRONESI, O. C., LOEBEL, F., BOGNER, W., MARJANSKA, M., VANDER HEIDEN, M. G., IAFRATE, A. J., DIETRICH, J., BATCHELOR, T. T., GERSTNER, E. R., KAELIN, W. G., CHI, A. S., ROSEN, B. R. & CAHILL, D. P. 2016. Treatment Response Assessment in IDH-Mutant Glioma Patients by Noninvasive 3D Functional Spectroscopic Mapping of 2-Hydroxyglutarate. *Clin Cancer Res*, 22, 1632-41.
- ANSO, E., MULLEN, A. R., FELSHER, D. W., MATES, J. M., DEBERARDINIS, R. J. & CHANDEL, N. S. 2013. Metabolic changes in cancer cells upon suppression of MYC. *Cancer Metab*, 1, 7.
- APPLING, D. R. 1991. Compartmentation of folate-mediated one-carbon metabolism in eukaryotes. *Faseb j*, 5, 2645-51.
- ASCIUTTO, G., DIAS, N. V., EDSFELDT, A., NITULESCU, M., PERSSON, A., NILSSON, M., DUNER, P., NILSSON, J. & GONCALVES, I. 2015. Low elastin content of carotid plaques is associated with increased risk of ipsilateral stroke. *PLoS One*, 10, e0121086.
- ASHTON, T. M., MCKENNA, W. G., KUNZ-SCHUGHART, L. A. & HIGGINS, G. S. 2018. Oxidative Phosphorylation as an Emerging Target in Cancer Therapy. *Clin Cancer Res*, 24, 2482-2490.
- ASTUTI, D., LATIF, F., DALLOL, A., DAHIA, P. L., DOUGLAS, F., GEORGE, E., SKOLDBERG, F., HUSEBYE, E. S., ENG, C. & MAHER, E. R. 2001. Gene mutations in the succinate dehydrogenase subunit SDHB cause susceptibility to familial pheochromocytoma and to familial paraganglioma. *Am J Hum Genet*, 69, 49-54.
- AVRAMIS, V. I. & TIWARI, P. N. 2006. Asparaginase (native ASNase or pegylated ASNase) in the treatment of acute lymphoblastic leukemia. *Int J Nanomedicine*, 1, 241-54.
- BACHIREDDY, P., BENDAPUDI, P. K. & FELSHER, D. W. 2005. Getting at MYC through RAS. *Clin Cancer Res*, 11, 4278-81.
- BAI, C. B., AUERBACH, W., LEE, J. S., STEPHEN, D. & JOYNER, A. L. 2002. Gli2, but not Gli1, is required for initial Shh signaling and ectopic activation of the Shh pathway. *Development*, 129, 4753-61.
- BAO, S., WU, Q., MCLENDON, R. E., HAO, Y., SHI, Q., HJELMELAND, A. B., DEWHIRST, M. W., BIGNER, D. D. & RICH, J. N. 2006. Glioma stem cells promote radioresistance by preferential activation of the DNA damage response. *Nature*, 444, 756-60.
- BAR-EVEN, A., FLAMHOLZ, A., NOOR, E. & MILO, R. 2012. Rethinking glycolysis: on the biochemical logic of metabolic pathways. *Nat Chem Biol*, 8, 509-17.
- BARTLETT, F., KORTMANN, R. & SARAN, F. 2013. Medulloblastoma. *Clin Oncol (R Coll Radiol)*, 25, 36-45.

- BARTOSIK, A., GUZIK, P., SOWINSKA, M., GLUZA, K., KROL, M., WROBEL, A., DREAS, A., IWANSKA, F., ZASTAWNA, M., KULESZA, U., BOUTARD, N., SCHULTZ, D., WUJKOWSKA, J., PYZIAK, K., SROKA-PORADA, A., PRZYBYLOWICZ, A., ADAMUS, A., SIEPRAWKA-LUPA, M., GOLIK, P., KOWALCZYK, P., BRZOZKA, K., RZYMSKI, T. & NOWAK, M. 2018. Abstract 3516: Discovery of novel SHMT small molecule inhibitors for cancer treatment. *Cancer Research*, 78, 3516-3516.
- BAUTISTA, F., FIORAVANTTI, V., DE ROJAS, T., CARCELLER, F., MADERO, L., LASSALETTA, A. & MORENO, L. 2017. Medulloblastoma in children and adolescents: a systematic review of contemporary phase I and II clinical trials and biology update. *Cancer Medicine*, 6, 2606-2624.
- BAYSAL, B. E., FERRELL, R. E., WILLETT-BROZICK, J. E., LAWRENCE, E. C., MYSSIOREK, D., BOSCH, A., VAN DER MEY, A., TASCHNER, P. E., RUBINSTEIN, W. S., MYERS, E. N., RICHARD, C. W., 3RD, CORNELISSE, C. J., DEVILEE, P. & DEVLIN, B. 2000. Mutations in SDHD, a mitochondrial complex II gene, in hereditary paraganglioma. *Science*, 287, 848-51.
- BEAULIEU, M. E., JAUSET, T., MASSO-VALLES, D., MARTINEZ-MARTIN, S., RAHL, P., MALTAIS, L., ZACARIAS-FLUCK, M. F., CASACUBERTA-SERRA, S., SERRANO DEL POZO, E., FIORE, C., FORADADA, L., CANO, V. C., SANCHEZ-HERVAS, M., GUENTHER, M., ROMERO SANZ, E., OTEO, M., TREMBLAY, C., MARTIN, G., LETOURNEAU, D., MONTAGNE, M., MORCILLO ALONSO, M. A., WHITFIELD, J. R., LAVIGNE, P. & SOUCEK, L. 2019. Intrinsic cell-penetrating activity propels Omomyc from proof of concept to viable anti-MYC therapy. *Sci Transl Med*, 11.
- BELANGER, M., ALLAMAN, I. & MAGISTRETTI, P. J. 2011. Brain energy metabolism: focus on astrocyte-neuron metabolic cooperation. *Cell Metab*, 14, 724-38.
- BENJAMIN, D., ROBAY, D., HINDUPUR, S. K., POHLMANN, J., COLOMBI, M., EL-SHEMERLY, M. Y., MAIRA, S. M., MORONI, C., LANE, H. A. & HALL, M. N. 2018. Dual Inhibition of the Lactate Transporters MCT1 and MCT4 Is Synthetic Lethal with Metformin due to NAD⁺ Depletion in Cancer Cells. *Cell Rep*, 25, 3047-3058.e4.
- BENNETT, C. D., KOHE, S. E., GILL, S. K., DAVIES, N. P., WILSON, M., STORER, L. C. D., RITZMANN, T., PAINE, S. M. L., SCOTT, I. S., NICKLAUS-WOLLENTEIT, I., TENNANT, D. A., GRUNDY, R. G. & PEET, A. C. 2018. Tissue metabolite profiles for the characterisation of paediatric cerebellar tumours. *Sci Rep*, 8, 11992.
- BEROUKHIM, R., MERMEL, C. H., PORTER, D., WEI, G., RAYCHAUDHURI, S., DONOVAN, J., BARRETINA, J., BOEHM, J. S., DOBSON, J., URASHIMA, M., MC HENRY, K. T., PINCHBACK, R. M., LIGON, A. H., CHO, Y. J., HAERY, L., GREULICH, H., REICH, M., WINCKLER, W., LAWRENCE, M. S., WEIR, B. A., TANAKA, K. E., CHIANG, D. Y., BASS, A. J., LOO, A., HOFFMAN, C., PRENSNER, J., LIEFELD, T., GAO, Q., YECIES, D., SIGNORETTI, S., MAHER, E., KAYE, F. J., SASAKI, H., TEPPER, J. E., FLETCHER, J. A., TABERNERO, J., BASELGA, J., TSAO, M. S., DEMICHELIS, F., RUBIN, M. A., JANNE, P. A., DALY, M. J., NUCERA, C., LEVINE, R. L., EBERT, B. L., GABRIEL, S., RUSTGI, A. K., ANTONESCU, C. R., LADANYI, M., LETAI, A., GARRAWAY, L. A., LODA, M., BEER, D. G., TRUE, L. D., OKAMOTO, A., POMEROY, S. L., SINGER, S., GOLUB, T. R., LANDER, E. S., GETZ, G., SELLERS, W. R. & MEYERSON, M. 2010. The landscape of somatic copy-number alteration across human cancers. *Nature*, 463, 899-905.

- BHINDERWALA, F., WASE, N., DIRUSSO, C. & POWERS, R. 2018. Combining Mass Spectrometry and NMR Improves Metabolite Detection and Annotation. *J Proteome Res*, 17, 4017-4022.
- BIEVER, A., VALJENT, E. & PUIGHERMANAL, E. 2015. Ribosomal Protein S6 Phosphorylation in the Nervous System: From Regulation to Function. *Front Mol Neurosci*, 8, 75.
- BINDA, E., VISIOLI, A., GIANI, F., TRIVIERI, N., PALUMBO, O., RESTELLI, S., DEZI, F., MAZZA, T., FUSILLI, C., LEGNANI, F., CARELLA, M., DI MECO, F., DUGGAL, R. & VESCOVI, A. L. 2017. Wnt5a Drives an Invasive Phenotype in Human Glioblastoma Stem-like Cells. *Cancer Res*, 77, 996-1007.
- BIRSOY, K., POSSEMATO, R., LORBEER, F. K., BAYRAKTAR, E. C., THIRU, P., YUCEL, B., WANG, T., CHEN, W. W., CLISH, C. B. & SABATINI, D. M. 2014. Metabolic determinants of cancer cell sensitivity to glucose limitation and biguanides. *Nature*, 508, 108-12.
- BLACKWELL, T. K., KRETZNER, L., BLACKWOOD, E. M., EISENMAN, R. N. & WEINTRAUB, H. 1990. Sequence-specific DNA binding by the c-Myc protein. *Science*, 250, 1149-51.
- BLAGOSKLONNY, M. V. & PARDEE, A. B. 2002. The restriction point of the cell cycle. *Cell Cycle*, 1, 103-10.
- BLOUIN, M. J., ZHAO, Y., ZAKIKHANI, M., ALGIRE, C., PIURA, E. & POLLAK, M. 2010. Loss of function of PTEN alters the relationship between glucose concentration and cell proliferation, increases glycolysis, and sensitizes cells to 2-deoxyglucose. *Cancer Lett*, 289, 246-53.
- BLUML, S., MARGOL, A. S., SPOSTO, R., KENNEDY, R. J., ROBISON, N. J., VALI, M., HUNG, L. T., MUTHUGOUNDER, S., FINLAY, J. L., ERDREICH-EPSTEIN, A., GILLES, F. H., JUDKINS, A. R., KRIEGER, M. D., DHALL, G., NELSON, M. D. & ASGHARZADEH, S. 2016. Molecular subgroups of medulloblastoma identification using noninvasive magnetic resonance spectroscopy. *Neuro Oncol*, 18, 126-31.
- BONNET, S., ARCHER, S. L., ALLALUNIS-TURNER, J., HAROMY, A., BEAULIEU, C., THOMPSON, R., LEE, C. T., LOPASCHUK, G. D., PUTTAGUNTA, L., HARRY, G., HASHIMOTO, K., PORTER, C. J., ANDRADE, M. A., THEBAUD, B. & MICHELAKIS, E. D. 2007. A mitochondria-K⁺ channel axis is suppressed in cancer and its normalization promotes apoptosis and inhibits cancer growth. *Cancer Cell*, 11, 37-51.
- BOSNYAK, E., MICHELHAUGH, S. K., KLINGER, N. V., KAMSON, D. O., BARGER, G. R., MITTAL, S. & JUHASZ, C. 2017. Prognostic Molecular and Imaging Biomarkers in Primary Glioblastoma. *Clin Nucl Med*, 42, 341-347.
- BOULAY, G., AWAD, M. E., RIGGI, N., ARCHER, T. C., IYER, S., BOONSENG, W. E., ROSSETTI, N. E., NAIGLES, B., RENGARAJAN, S., VOLORIO, A., KIM, J. C., MESIROV, J. P., TAMAYO, P., POMEROY, S. L., ARYEE, M. J. & RIVERA, M. N. 2017. OTX2 Activity at Distal Regulatory Elements Shapes the Chromatin Landscape of Group 3 Medulloblastoma. *Cancer Discov*, 7, 288-301.
- BOWKER, S. L., YASUI, Y., VEUGELERS, P. & JOHNSON, J. A. 2010. Glucose-lowering agents and cancer mortality rates in type 2 diabetes: assessing effects of time-varying exposure. *Diabetologia*, 53, 1631-7.
- BOXER, L. M. & DANG, C. V. 2001. Translocations involving c-myc and c-myc function. *Oncogene*, 20, 5595-610.
- BRABETZ, S., LEARY, S. E. S., GROBNER, S. N., NAKAMOTO, M. W., SEKER-CIN, H., GIRARD, E. J., COLE, B., STRAND, A. D., BLOOM, K. L., HOVESTADT, V., MACK, N. L., PAKIAM, F., SCHWALM, B., KORSHUNOV, A., BALASUBRAMANIAN, G. P., NORTHCOTT, P. A.,

- PEDRO, K. D., DEY, J., HANSEN, S., DITZLER, S., LICHTER, P., CHAVEZ, L., JONES, D. T. W., KOSTER, J., PFISTER, S. M., KOOL, M. & OLSON, J. M. 2018. A biobank of patient-derived pediatric brain tumor models. *Nat Med*, 24, 1752-1761.
- BRACE, L. E., VOSE, S. C., STANYA, K., GATHUNGU, R. M., MARUR, V. R., LONGCHAMP, A., TREVINO-VILLARREAL, H., MEJIA, P., VARGAS, D., INOUE, K., BRONSON, R. T., LEE, C. H., NEILAN, E., KRISTAL, B. S. & MITCHELL, J. R. 2016. Increased oxidative phosphorylation in response to acute and chronic DNA damage. *NPJ Aging Mech Dis*, 2, 16022.
- BRENNAN, C. W., VERHAAK, R. G. W., MCKENNA, A., CAMPOS, B., NOUSHMEHR, H., SALAMA, S. R., ZHENG, S. Y., CHAKRAVARTY, D., SANBORN, J. Z., BERMAN, S. H., BEROUKHIM, R., BERNARD, B., WU, C. J., GENOVESE, G., SHMULEVICH, I., BARNHOLTZ-SLOAN, J., ZOU, L. H., VEGESNA, R., SHUKLA, S. A., CIRIELLO, G., YUNG, W. K., ZHANG, W., SOUGNEZ, C., MIKKELSEN, T., ALDAPE, K., BIGNER, D. D., VAN MEIR, E. G., PRADOS, M., SLOAN, A., BLACK, K. L., ESCHBACHER, J., FINOCCHIARO, G., FRIEDMAN, W., ANDREWS, D. W., GUHA, A., IACOCCA, M., O'NEILL, B. P., FOLTZ, G., MYERS, J., WEISENBERGER, D. J., PENNY, R., KUCHERLAPATI, R., PEROU, C. M., HAYES, D. N., GIBBS, R., MARRA, M., MILLS, G. B., LANDER, E., SPELLMAN, P., WILSON, R., SANDER, C., WEINSTEIN, J., MEYERSON, M., GABRIEL, S., LAIRD, P. W., HAUSSLER, D., GETZ, G., CHIN, L. & NETWORK, T. R. 2014. The Somatic Genomic Landscape of Glioblastoma (Vol 155, pg 462, 2013). *Cell*, 157, 753-753.
- BRETONES, G., DELGADO, M. D. & LEON, J. 2015. Myc and cell cycle control. *Biochim Biophys Acta*, 1849, 506-16.
- BROECKER-PREUSS, M., BECHER-BOVELETH, N., BOCKISCH, A., DÜHRSEN, U. & MÜLLER, S. 2017. Regulation of glucose uptake in lymphoma cell lines by c-MYC- and PI3K-dependent signaling pathways and impact of glycolytic pathways on cell viability. *Journal of translational medicine*, 15, 158-158.
- CABODEVILLA, A. G., SANCHEZ-CABALLERO, L., NINTOU, E., BOIADJIEVA, V. G., PICATOSTE, F., GUBERN, A. & CLARO, E. 2013. Cell Survival during Complete Nutrient Deprivation Depends on Lipid Droplet-fueled beta-Oxidation of Fatty Acids. *Journal of Biological Chemistry*, 288, 27777-27788.
- CAMARDA, R., ZHOU, A. Y., KOHNZ, R. A., BALAKRISHNAN, S., MAHIEU, C., ANDERTON, B., EYOB, H., KAJIMURA, S., TWARD, A., KRINGS, G., NOMURA, D. K. & GOGA, A. 2016. Inhibition of fatty-acid oxidation as a therapy for MYC-overexpressing triple-negative breast cancer. *Cancer Research*, 76.
- CAO, Y., TSENG, C.-L., BALTER, J. M., TENG, F., PARMAR, H. A. & SAHGAL, A. 2017. MR-guided radiation therapy: transformative technology and its role in the central nervous system. *Neuro-Oncology*, 19, ii16-ii29.
- CARO, P., KISHAN, A. U., NORBERG, E., STANLEY, I. A., CHAPUY, B., FICARRO, S. B., POLAK, K., TONDERA, D., GOUNARIDES, J., YIN, H., ZHOU, F., GREEN, M. R., CHEN, L. F., MONTI, S., MARTO, J. A., SHIPP, M. A. & DANIAL, N. N. 2012. Metabolic Signatures Uncover Distinct Targets in Molecular Subsets of Diffuse Large B Cell Lymphoma. *Cancer Cell*, 22, 547-560.
- CASSAGO, A., FERREIRA, A. P., FERREIRA, I. M., FORNEZARI, C., GOMES, E. R., GREENE, K. S., PEREIRA, H. M., GARRATT, R. C., DIAS, S. M. & AMBROSIO, A. L. 2012. Mitochondrial localization and structure-based phosphate activation mechanism of Glutaminase C with implications for cancer metabolism. *Proc Natl Acad Sci U S A*, 109, 1092-7.

- CAVALLI, F. M. G., REMKE, M., RAMPASEK, L., PEACOCK, J., SHIH, D. J. H., LUU, B., GARZIA, L., TORCHIA, J., NOR, C., MORRISSY, A. S., AGNIHOTRI, S., THOMPSON, Y. Y., KUZAN-FISCHER, C. M., FAROOQ, H., ISAEV, K., DANIELS, C., CHO, B. K., KIM, S. K., WANG, K. C., LEE, J. Y., GRAJKOWSKA, W. A., PEREK-POLNIK, M., VASILJEVIC, A., FAURE-CONTER, C., JOUVET, A., GIANNINI, C., NAGESWARA RAO, A. A., LI, K. K. W., NG, H. K., EBERHART, C. G., POLLACK, I. F., HAMILTON, R. L., GILLESPIE, G. Y., OLSON, J. M., LEARY, S., WEISS, W. A., LACH, B., CHAMBLESS, L. B., THOMPSON, R. C., COOPER, M. K., VIBHAKAR, R., HAUSER, P., VAN VEELLEN, M. C., KROS, J. M., FRENCH, P. J., RA, Y. S., KUMABE, T., LOPEZ-AGUILAR, E., ZITTERBART, K., STERBA, J., FINOCCHIARO, G., MASSIMINO, M., VAN MEIR, E. G., OSUKA, S., SHOFUDA, T., KLEKNER, A., ZOLLO, M., LEONARD, J. R., RUBIN, J. B., JABADO, N., ALBRECHT, S., MORA, J., VAN METER, T. E., JUNG, S., MOORE, A. S., HALLAHAN, A. R., CHAN, J. A., TIRAPELLI, D. P. C., CARLOTTI, C. G., FOULADI, M., PIMENTEL, J., FARIA, C. C., SAAD, A. G., MASSIMI, L., LIAU, L. M., WHEELER, H., NAKAMURA, H., ELBABAA, S. K., PEREZPENA-DIAZCONTI, M., CHICO PONCE DE LEON, F., ROBINSON, S., ZAPOTOCKY, M., LASSALETTA, A., HUANG, A., HAWKINS, C. E., TABORI, U., BOUFFET, E., BARTELS, U., DIRKS, P. B., RUTKA, J. T., BADER, G. D., REIMAND, J., GOLDENBERG, A., RAMASWAMY, V. & TAYLOR, M. D. 2017. Intertumoral Heterogeneity within Medulloblastoma Subgroups. *Cancer Cell*, 31, 737-754.e6.
- CAVASSILA, S., DEVAL, S., HUEGEN, C., VAN ORMONDT, D. & GRAVERON-DEMILLY, D. 2001. Cramer-Rao bounds: an evaluation tool for quantitation. *NMR Biomed*, 14, 278-83.
- CHAN, D. A., SUTPHIN, P. D., NGUYEN, P., TURCOTTE, S., LAI, E. W., BANH, A., REYNOLDS, G. E., CHI, J. T., WU, J., SOLOW-CORDERO, D. E., BONNET, M., FLANAGAN, J. U., BOULEY, D. M., GRAVES, E. E., DENNY, W. A., HAY, M. P. & GIACCIA, A. J. 2011. Targeting GLUT1 and the Warburg effect in renal cell carcinoma by chemical synthetic lethality. *Sci Transl Med*, 3, 94ra70.
- CHANETON, B., HILLMANN, P., ZHENG, L., MARTIN, A. C. L., MADDOCKS, O. D. K., CHOKKATHUKALAM, A., COYLE, J. E., JANKEVICS, A., HOLDING, F. P., VOUSDEN, K. H., FREZZA, C., O'REILLY, M. & GOTTLIEB, E. 2012. Serine is a natural ligand and allosteric activator of pyruvate kinase M2. *Nature*, 491, 458-462.
- CHANG, C. H., HOUSEPIAN, E. M. & HERBERT, C., JR. 1969. An operative staging system and a megavoltage radiotherapeutic technic for cerebellar medulloblastomas. *Radiology*, 93, 1351-9.
- CHATTOPADHYAY, S., MORAN, R. G. & GOLDMAN, I. D. 2007. Pemetrexed: biochemical and cellular pharmacology, mechanisms, and clinical applications. *Mol Cancer Ther*, 6, 404-17.
- CHEN, J., LI, Y., YU, T. S., MCKAY, R. M., BURNS, D. K., KERNIE, S. G. & PARADA, L. F. 2012. A restricted cell population propagates glioblastoma growth after chemotherapy. *Nature*, 488, 522-6.
- CHEN, R., SMITH-COHN, M., COHEN, A. L. & COLMAN, H. 2017. Glioma Subclassifications and Their Clinical Significance. *Neurotherapeutics*, 14, 284-297.
- CHEN, W., CLOUGHESY, T., KAMDAR, N., SATYAMURTHY, N., BERGSNEIDER, M., LIAU, L., MISCHEL, P., CZERNIN, J., PHELPS, M. E. & SILVERMAN, D. H. S. 2005. Imaging proliferation in brain tumors with F-18-

- FLT PET: Comparison with F-18-FDG. *Journal of Nuclear Medicine*, 46, 945-952.
- CHO, Y. J., TSHERNIAK, A., TAMAYO, P., SANTAGATA, S., LIGON, A., GREULICH, H., BERHOUKIM, R., AMANI, V., GOUMNEROVA, L., EBERHART, C. G., LAU, C. C., OLSON, J. M., GILBERTSON, R. J., GAJJAR, A., DELATTRE, O., KOOL, M., LIGON, K., MEYERSON, M., MESIROV, J. P. & POMEROY, S. L. 2011. Integrative genomic analysis of medulloblastoma identifies a molecular subgroup that drives poor clinical outcome. *J Clin Oncol*, 29, 1424-30.
- CHOI, C., GANJI, S. K., DEBERARDINIS, R. J., HATANPAA, K. J., RAKHEJA, D., KOVACS, Z., YANG, X. L., MASHIMO, T., RAISANEN, J. M., MARIN-VALENCIA, I., PASCUAL, J. M., MADDEN, C. J., MICKY, B. E., MALLOY, C. R., BACHOO, R. M. & MAHER, E. A. 2012. 2-hydroxyglutarate detection by magnetic resonance spectroscopy in IDH-mutated patients with gliomas. *Nat Med*, 18, 624-9.
- CLIFFORD, S. C., LUSHER, M. E., LINDSEY, J. C., LANGDON, J. A., GILBERTSON, R. J., STRAUGHTON, D. & ELLISON, D. W. 2006. Wnt/Wingless pathway activation and chromosome 6 loss characterize a distinct molecular sub-group of medulloblastomas associated with a favorable prognosis. *Cell Cycle*, 5, 2666-70.
- COLE, M. D. & NIKIFOROV, M. A. 2006. Transcriptional activation by the Myc oncoprotein. *Curr Top Microbiol Immunol*, 302, 33-50.
- CONACCI-SORRELL, M., NGOUENET, C. & EISENMAN, R. N. 2010. Myc-nick: a cytoplasmic cleavage product of Myc that promotes alpha-tubulin acetylation and cell differentiation. *Cell*, 142, 480-93.
- COPELAND, J. C., ZEHR, L. J., CERNY, R. L. & POWERS, R. 2012. The applicability of molecular descriptors for designing an electrospray ionization mass spectrometry compatible library for drug discovery. *Comb Chem High Throughput Screen*, 15, 806-15.
- CORY, J. G. & CORY, A. H. 2006. Critical roles of glutamine as nitrogen donors in purine and pyrimidine nucleotide synthesis: asparaginase treatment in childhood acute lymphoblastic leukemia. *In Vivo*, 20, 587-9.
- CRAWFORD, J. R., MACDONALD, T. J. & PACKER, R. J. 2007. Medulloblastoma in childhood: new biological advances. *Lancet Neurol*, 6, 1073-85.
- DAEMEN, A., LIU, B., SONG, K., KWONG, M., GAO, M., HONG, R., NANNINI, M., PETERSON, D., LIEDERER, B. M., DE LA CRUZ, C., SANGARAJU, D., JAOCHICO, A., ZHAO, X., SANDOVAL, W., HUNSAKER, T., FIRESTEIN, R., LATHAM, S., SAMPATH, D., EVANGELISTA, M. & HATZIVASSILIOU, G. 2018. Pan-Cancer Metabolic Signature Predicts Co-Dependency on Glutaminase and De Novo Glutathione Synthesis Linked to a High-Mesenchymal Cell State. *Cell Metab*, 28, 383-399.e9.
- DANG, C. V. 2012. MYC on the path to cancer. *Cell*, 149, 22-35.
- DANG, C. V. 2013a. MYC, metabolism, cell growth, and tumorigenesis. *Cold Spring Harb Perspect Med*, 3.
- DANG, C. V. 2013b. MYC, Metabolism, Cell Growth, and Tumorigenesis. *Cold Spring Harbor Perspectives in Medicine*, 3.
- DANG, C. V., LE, A. & GAO, P. 2009. MYC-induced cancer cell energy metabolism and therapeutic opportunities. *Clin Cancer Res*, 15, 6479-83.
- DANG, C. V., O'DONNELL, K. A., ZELLER, K. I., NGUYEN, T., OSTHUS, R. C. & LI, F. 2006. The c-Myc target gene network. *Semin Cancer Biol*, 16, 253-64.

- DE KONING, T. J., SNELL, K., DURAN, M., BERGER, R., POLL-THE, B. T. & SURTEES, R. 2003. L-serine in disease and development. *Biochem J*, 371, 653-61.
- DEBERARDINIS, R. J. & CHANDEL, N. S. 2016. Fundamentals of cancer metabolism. *Sci Adv*, 2, e1600200.
- DEBERARDINIS, R. J., LUM, J. J., HATZIVASSILIOU, G. & THOMPSON, C. B. 2008. The biology of cancer: Metabolic reprogramming fuels cell growth and proliferation. *Cell Metabolism*, 7, 11-20.
- DELMORE, J. E., ISSA, G. C., LEMIEUX, M. E., RAHL, P. B., SHI, J., JACOBS, H. M., KASTRITIS, E., GILPATRICK, T., PARANAL, R. M., QI, J., CHESI, M., SCHINZEL, A. C., MCKEOWN, M. R., HEFFERNAN, T. P., VAKOC, C. R., BERGSAGEL, P. L., GHOBRIAL, I. M., RICHARDSON, P. G., YOUNG, R. A., HAHN, W. C., ANDERSON, K. C., KUNG, A. L., BRADNER, J. E. & MITSIADES, C. S. 2011. BET bromodomain inhibition as a therapeutic strategy to target c-Myc. *Cell*, 146, 904-17.
- DEMICHELE, A., HARDING, J. J., TELLI, M. L., MUNSTER, P. N., MCKAY, R., ILIOPOULOS, O., ORFORD, K. W., BENNETT, M. K., MIER, J. W., OWONIKOKO, T. K., PATEL, M. R., CARVAJAL, R. D., MERIC-BERNSTAM, F. & INFANTE, J. R. 2016. Phase 1 study of CB-839, a small molecule inhibitor of glutaminase (GLS) in combination with paclitaxel (Pac) in patients (pts) with triple negative breast cancer (TNBC). *Journal of Clinical Oncology*, 34, 1011-1011.
- DENGLER, V. L., GALBRAITH, M. & ESPINOSA, J. M. 2014. Transcriptional regulation by hypoxia inducible factors. *Crit Rev Biochem Mol Biol*, 49, 1-15.
- DENICOLA, G. M., CHEN, P. H., MULLARKY, E., SUDDERTH, J. A., HU, Z., WU, D., TANG, H., XIE, Y., ASARA, J. M., HUFFMAN, K. E., WISTUBA, II, MINNA, J. D., DEBERARDINIS, R. J. & CANTLEY, L. C. 2015. NRF2 regulates serine biosynthesis in non-small cell lung cancer. *Nat Genet*, 47, 1475-81.
- DENNIS, P. B., JAESCHKE, A., SAITOH, M., FOWLER, B., KOZMA, S. C. & THOMAS, G. 2001. Mammalian TOR: a homeostatic ATP sensor. *Science*, 294, 1102-5.
- DHALL, G., GRODMAN, H., JI, L., SANDS, S., GARDNER, S., DUNKEL, I. J., MCCOWAGE, G. B., DIEZ, B., ALLEN, J. C., GOPALAN, A., CORNELIUS, A. S., TERMUHLEN, A., ABROMOWITCH, M., SPOSTO, R. & FINLAY, J. L. 2008. Outcome of children less than three years old at diagnosis with non-metastatic medulloblastoma treated with chemotherapy on the "Head Start" I and II protocols. *Pediatr Blood Cancer*, 50, 1169-75.
- DHEERAJ, A., AGARWAL, C., SCHLAEPFER, I. R., RABEN, D., SINGH, R., AGARWAL, R. & DEEP, G. 2018. A novel approach to target hypoxic cancer cells via combining β -oxidation inhibitor etomoxir with radiation. *Hypoxia (Auckland, N.Z.)*, 6, 23-33.
- DIEHN, M., CHO, R. W., LOBO, N. A., KALISKY, T., DORIE, M. J., KULP, A. N., QIAN, D., LAM, J. S., AILLES, L. E., WONG, M., JOSHUA, B., KAPLAN, M. J., WAPNIR, I., DIRBAS, F. M., SOMLO, G., GARBEROGLIO, C., PAZ, B., SHEN, J., LAU, S. K., QUAKE, S. R., BROWN, J. M., WEISSMAN, I. L. & CLARKE, M. F. 2009. Association of reactive oxygen species levels and radioresistance in cancer stem cells. *Nature*, 458, 780-3.
- DONG, J. K., LEI, H. M., LIANG, Q., TANG, Y. B., ZHOU, Y., WANG, Y., ZHANG, S., LI, W. B., TONG, Y., ZHUANG, G., ZHANG, L., CHEN, H. Z., ZHU, L. & SHEN, Y. 2018. Overcoming erlotinib resistance in EGFR mutation-positive lung

- adenocarcinomas through repression of phosphoglycerate dehydrogenase. *Theranostics*, 8, 1808-1823.
- DUCKER, G. S., GHERGUROVICH, J. M., MAINOLFI, N., SURI, V., JEONG, S. K., HSIN-JUNG LI, S., FRIEDMAN, A., MANFREDI, M. G., GITAI, Z., KIM, H. & RABINOWITZ, J. D. 2017. Human SHMT inhibitors reveal defective glycine import as a targetable metabolic vulnerability of diffuse large B-cell lymphoma. *Proc Natl Acad Sci U S A*, 114, 11404-11409.
- DUCKER, G. S. & RABINOWITZ, J. D. 2017. One-Carbon Metabolism in Health and Disease. *Cell Metab*, 25, 27-42.
- DUESBERG, P. H. & VOGT, P. K. 1979. Avian acute leukemia viruses MC29 and MH2 share specific RNA sequences: evidence for a second class of transforming genes. *Proc Natl Acad Sci U S A*, 76, 1633-7.
- DUMAN, C., YAQUBI, K., HOFFMANN, A., ACIKGOZ, A. A., KORSHUNOV, A., BENDSZUS, M., HEROLD-MENDE, C., LIU, H. K. & ALFONSO, J. 2019. Acyl-CoA-Binding Protein Drives Glioblastoma Tumorigenesis by Sustaining Fatty Acid Oxidation. *Cell Metab*, 30, 274-289.e5.
- DUNPHY, M. P. S., HARDING, J. J., VENNETI, S., ZHANG, H., BURNAZI, E. M., BROMBERG, J., OMURO, A. M., HSIEH, J. J., MELLINGHOFF, I. K., STATON, K., PRESSL, C., BEATTIE, B. J., ZANZONICO, P. B., GERECITANO, J. F., KELSEN, D. P., WEBER, W., LYASHCHENKO, S. K., KUNG, H. F. & LEWIS, J. S. 2018. In Vivo PET Assay of Tumor Glutamine Flux and Metabolism: In-Human Trial of (18)F-(2S,4R)-4-Fluoroglutamine. *Radiology*, 287, 667-675.
- EBERHART, C. G. & BURGER, P. C. 2003. Anaplasia and grading in medulloblastomas. *Brain Pathol*, 13, 376-85.
- EILERS, M., SCHIRM, S. & BISHOP, J. M. 1991. The MYC protein activates transcription of the alpha-prothymosin gene. *Embo j*, 10, 133-41.
- ELGADI, K. M., MEGUID, R. A., QIAN, M., SOUBA, W. W. & ABCOUWER, S. F. 1999. Cloning and analysis of unique human glutaminase isoforms generated by tissue-specific alternative splicing. *Physiol Genomics*, 1, 51-62.
- ELLISON, D. W. 2010. Childhood medulloblastoma: novel approaches to the classification of a heterogeneous disease. *Acta Neuropathol*, 120, 305-16.
- ELLISON, D. W., ONILUDE, O. E., LINDSEY, J. C., LUSHER, M. E., WESTON, C. L., TAYLOR, R. E., PEARSON, A. D. & CLIFFORD, S. C. 2005. beta-Catenin status predicts a favorable outcome in childhood medulloblastoma: the United Kingdom Children's Cancer Study Group Brain Tumour Committee. *J Clin Oncol*, 23, 7951-7.
- EMWAS, A. H., ROY, R., MCKAY, R. T., TENORI, L., SACCENTI, E., GOWDA, G. A. N., RAFTERY, D., ALAHMARI, F., JAREMKO, L., JAREMKO, M. & WISHART, D. S. 2019. NMR Spectroscopy for Metabolomics Research. *Metabolites*, 9.
- ERAMO, A., RICCI-VITIANI, L., ZEUNER, A., PALLINI, R., LOTTI, F., SETTE, G., PILOZZI, E., LAROCCA, L. M., PESCHLE, C. & DE MARIA, R. 2006. Chemotherapy resistance of glioblastoma stem cells. *Cell Death Differ*, 13, 1238-41.
- ERAN, A., OZTURK, A., AYGUN, N. & IZBUDAK, I. 2010. Medulloblastoma: atypical CT and MRI findings in children. *Pediatr Radiol*, 40, 1254-62.
- ESTELLER, M., GARCIA-FONCILLAS, J., ANDION, E., GOODMAN, S. N., HIDALGO, O. F., VANACLOCHA, V., BAYLIN, S. B. & HERMAN, J. G. 2000. Inactivation of the DNA-repair gene MGMT and the clinical response of gliomas to alkylating agents. *N Engl J Med*, 343, 1350-4.

- FAN, J., YE, J., KAMPHORST, J. J., SHLOMI, T., THOMPSON, C. B. & RABINOWITZ, J. D. 2014. Quantitative flux analysis reveals folate-dependent NADPH production. *Nature*, 510, 298-302.
- FAN, T. W. M., BRUNTZ, R. C., YANG, Y., SONG, H., CHERNYAVSKAYA, Y., DENG, P., ZHANG, Y., SHAH, P. P., BEVERLY, L. J., QI, Z., MAHAN, A. L., HIGASHI, R. M., DANG, C. V. & LANE, A. N. 2019. De novo synthesis of serine and glycine fuels purine nucleotide biosynthesis in human lung cancer tissues. *J Biol Chem*, 294, 13464-13477.
- FARRELL, A. S. & SEARS, R. C. 2014. MYC degradation. *Cold Spring Harb Perspect Med*, 4.
- FIEHN, O. 2002. Metabolomics--the link between genotypes and phenotypes. *Plant Mol Biol*, 48, 155-71.
- FUSS, T. L. & CHENG, L. L. 2016. Evaluation of Cancer Metabolomics Using ex vivo High Resolution Magic Angle Spinning (HRMAS) Magnetic Resonance Spectroscopy (MRS). *Metabolites*, 6.
- GAGE, F. H. & TEMPLE, S. 2013. Neural stem cells: generating and regenerating the brain. *Neuron*, 80, 588-601.
- GAGLIO, D., METALLO, C. M., GAMEIRO, P. A., HILLER, K., DANNA, L. S., BALESTRIERI, C., ALBERGHINA, L., STEPHANOPOULOS, G. & CHIARADONNA, F. 2011. Oncogenic K-Ras decouples glucose and glutamine metabolism to support cancer cell growth. *Mol Syst Biol*, 7, 523.
- GALVAO, R. P., KASINA, A., MCNEILL, R. S., HARBIN, J. E., FOREMAN, O., VERHAAK, R. G., NISHIYAMA, A., MILLER, C. R. & ZONG, H. 2014. Transformation of quiescent adult oligodendrocyte precursor cells into malignant glioma through a multistep reactivation process. *Proc Natl Acad Sci U S A*, 111, E4214-23.
- GANDARILLAS, A. & WATT, F. M. 1997. c-Myc promotes differentiation of human epidermal stem cells. *Genes Dev*, 11, 2869-82.
- GANDOLA, L., MASSIMINO, M., CEFALO, G., SOLERO, C., SPREAFICO, F., PECORI, E., RIVA, D., COLLINI, P., PIGNOLI, E., GIANGASPERO, F., LUKSCH, R., BERRETTA, S., POGGI, G., BIASSONI, V., FERRARI, A., POLLO, B., FAVRE, C., SARDI, I., TEREZIANI, M. & FOSSATI-BELLANI, F. 2009. Hyperfractionated accelerated radiotherapy in the Milan strategy for metastatic medulloblastoma. *J Clin Oncol*, 27, 566-71.
- GAO, P., TCHERNYSHYOV, I., CHANG, T.-C., LEE, Y.-S., KITA, K., OCHI, T., ZELLER, K. I., DE MARZO, A. M., VAN EYK, J. E., MENDELL, J. T. & DANG, C. V. 2009. c-Myc suppression of miR-23a/b enhances mitochondrial glutaminase expression and glutamine metabolism. *Nature*, 458, 762-765.
- GARROW, T. A., BRENNER, A. A., WHITEHEAD, V. M., CHEN, X. N., DUNCAN, R. G., KORENBERG, J. R. & SHANE, B. 1993. Cloning of human cDNAs encoding mitochondrial and cytosolic serine hydroxymethyltransferases and chromosomal localization. *J Biol Chem*, 268, 11910-6.
- GERBER, N. U., MYNAREK, M., VON HOFF, K., FRIEDRICH, C., RESCH, A. & RUTKOWSKI, S. 2014. Recent developments and current concepts in medulloblastoma. *Cancer Treat Rev*, 40, 356-65.
- GHOSH, D., NANDI, S. & BHATTACHARJEE, S. 2018. Combination therapy to checkmate Glioblastoma: clinical challenges and advances. *Clinical and translational medicine*, 7, 33-33.
- GIBSON, P., TONG, Y., ROBINSON, G., THOMPSON, M. C., CURRLE, D. S., EDEN, C., KRANENBURG, T. A., HOGG, T., POPPLETON, H., MARTIN, J., FINKELSTEIN, D., POUNDS, S., WEISS, A., PATAY, Z., SCOGGINS, M., OGG, R., PEI, Y., YANG, Z. J., BRUN, S., LEE, Y., ZINDY, F., LINDSEY, J.

- C., TAKETO, M. M., BOOP, F. A., SANFORD, R. A., GAJJAR, A., CLIFFORD, S. C., ROUSSEL, M. F., MCKINNON, P. J., GUTMANN, D. H., ELLISON, D. W., WECHSLER-REYA, R. & GILBERTSON, R. J. 2010. Subtypes of medulloblastoma have distinct developmental origins. *Nature*, 468, 1095-9.
- GIMPLE, R. C., BHARGAVA, S., DIXIT, D. & RICH, J. N. 2019. Glioblastoma stem cells: lessons from the tumor hierarchy in a lethal cancer. *Genes Dev*, 33, 591-609.
- GINGRAS, A. C., GYGI, S. P., RAUGHT, B., POLAKIEWICZ, R. D., ABRAHAM, R. T., HOEKSTRA, M. F., AEBERSOLD, R. & SONENBERG, N. 1999. Regulation of 4E-BP1 phosphorylation: a novel two-step mechanism. *Genes Dev*, 13, 1422-37.
- GINGRAS, A. C., RAUGHT, B., GYGI, S. P., NIEDZWIECKA, A., MIRON, M., BURLEY, S. K., POLAKIEWICZ, R. D., WYSLOUCH-CIESZYNSKA, A., AEBERSOLD, R. & SONENBERG, N. 2001. Hierarchical phosphorylation of the translation inhibitor 4E-BP1. *Genes Dev*, 15, 2852-64.
- GLUNDE, K., BHUJWALLA, Z. M. & RONEN, S. M. 2011. Choline metabolism in malignant transformation. *Nat Rev Cancer*, 11, 835-48.
- GLUNDE, K., SHAH, T., WINNARD, P. T., JR., RAMAN, V., TAKAGI, T., VESUNA, F., ARTEMOV, D. & BHUJWALLA, Z. M. 2008. Hypoxia regulates choline kinase expression through hypoxia-inducible factor-1 alpha signaling in a human prostate cancer model. *Cancer Res*, 68, 172-80.
- GORRINI, C., HARRIS, I. S. & MAK, T. W. 2013. Modulation of oxidative stress as an anticancer strategy. *Nat Rev Drug Discov*, 12, 931-47.
- GRAY, L. R., TOMPKINS, S. C. & TAYLOR, E. B. 2014. Regulation of pyruvate metabolism and human disease. *Cellular and molecular life sciences : CMLS*, 71, 2577-2604.
- GRILL, J., SAINTE-ROSE, C., JOUVET, A., GENTET, J. C., LEJARS, O., FRAPPAZ, D., DOZ, F., RIALLAND, X., PICHON, F., BERTOZZI, A. I., CHASTAGNER, P., COUANET, D., HABRAND, J. L., RAQUIN, M. A., LE DELEY, M. C. & KALIFA, C. 2005. Treatment of medulloblastoma with postoperative chemotherapy alone: an SFOP prospective trial in young children. *Lancet Oncol*, 6, 573-80.
- GROBNER, S. N., WORST, B. C., WEISCHENFELDT, J., BUCHHALTER, I., KLEINHEINZ, K., RUDNEVA, V. A., JOHANN, P. D., BALASUBRAMANIAN, G. P., SEGURA-WANG, M., BRABETZ, S., BENDER, S., HUTTER, B., STURM, D., PFAFF, E., HUBSCHMANN, D., ZIPPRICH, G., HEINOLD, M., EILS, J., LAWERENZ, C., ERKEK, S., LAMBO, S., WASZAK, S., BLATTMANN, C., BORKHARDT, A., KUHLEN, M., EGGERT, A., FULDA, S., GESSLER, M., WEGERT, J., KAPPLER, R., BAUMHOER, D., BURDACH, S., KIRSCHNER-SCHWABE, R., KONITNY, U., KULOZIK, A. E., LOHMANN, D., HETTMER, S., ECKERT, C., BIELACK, S., NATHRATH, M., NIEMEYER, C., RICHTER, G. H., SCHULTE, J., SIEBERT, R., WESTERMANN, F., MOLENAAR, J. J., VASSAL, G., WITT, H., BURKHARDT, B., KRATZ, C. P., WITT, O., VAN TILBURG, C. M., KRAMM, C. M., FLEISCHHACK, G., DIRKSEN, U., RUTKOWSKI, S., FRUHWALD, M., VON HOFF, K., WOLF, S., KLINGEBIEL, T., KOSCIELNIAK, E., LANDGRAF, P., KOSTER, J., RESNICK, A. C., ZHANG, J., LIU, Y., ZHOU, X., WAANDERS, A. J., ZWIJNENBURG, D. A., RAMAN, P., BRORS, B., WEBER, U. D., NORTHCOTT, P. A., PAJTLER, K. W., KOOL, M., PIRO, R. M., KORBEL, J. O., SCHLESNER, M., EILS, R., JONES, D. T. W., LICHTER, P., CHAVEZ, L., ZAPATKA, M. & PFISTER, S. M. 2018. The landscape of genomic alterations across childhood cancers. *Nature*, 555, 321-327.

- GUCCIONE, E., MARTINATO, F., FINOCCHIARO, G., LUZI, L., TIZZONI, L., DALL'OLIO, V., ZARDO, G., NERVI, C., BERNARD, L. & AMATI, B. 2006. Myc-binding-site recognition in the human genome is determined by chromatin context. *Nat Cell Biol*, 8, 764-70.
- GUO, D., PRINS, R. M., DANG, J., KUGA, D., IWANAMI, A., SOTO, H., LIN, K. Y., HUANG, T. T., AKHAVAN, D., HOCK, M. B., ZHU, S., KOFMAN, A. A., BENSINGER, S. J., YONG, W. H., VINTERS, H. V., HORVATH, S., WATSON, A. D., KUHN, J. G., ROBINS, H. I., MEHTA, M. P., WEN, P. Y., DEANGELIS, L. M., PRADOS, M. D., MELLINGHOFF, I. K., CLOUGHESY, T. F. & MISCHEL, P. S. 2009. EGFR signaling through an Akt-SREBP-1-dependent, rapamycin-resistant pathway sensitizes glioblastomas to antilipogenic therapy. *Sci Signal*, 2, ra82.
- GUO, J., YAO, C., CHEN, H., ZHUANG, D., TANG, W., REN, G., WANG, Y., WU, J., HUANG, F. & ZHOU, L. 2012. The relationship between Cho/NAA and glioma metabolism: implementation for margin delineation of cerebral gliomas. *Acta Neurochir (Wien)*, 154, 1361-70; discussion 1370.
- GUPPY, M., LEEDMAN, P., ZU, X. L. & RUSSELL, V. 2002. Contribution by different fuels and metabolic pathways to the total ATP turnover of proliferating MCF-7 breast cancer cells. *Biochemical Journal*, 364, 309-315.
- HAKUMAKI, J. M. & KAUPPINEN, R. A. 2000. H-1 NMR visible lipids in the life and death of cells. *Trends in Biochemical Sciences*, 25, 357-362.
- HAN, S., WOO, S., KIM, Y. J. & SUH, C. H. 2018. Impact of (68)Ga-PSMA PET on the Management of Patients with Prostate Cancer: A Systematic Review and Meta-analysis. *Eur Urol*, 74, 179-190.
- HANAFORD, A. R., ALT, J., RAIS, R., WANG, S. Z., KAUR, H., THOREK, D. L. J., EBERHART, C. G., SLUSHER, B. S., MARTIN, A. M. & RAABE, E. H. 2019. Orally bioavailable glutamine antagonist prodrug JHU-083 penetrates mouse brain and suppresses the growth of MYC-driven medulloblastoma. *Transl Oncol*, 12, 1314-1322.
- HANAHAH, D. & WEINBERG, R. A. 2000. The hallmarks of cancer. *Cell*, 100, 57-70.
- HANAHAH, D. & WEINBERG, R. A. 2011. Hallmarks of Cancer: The Next Generation. *Cell*, 144, 646-674.
- HASSANEIN, M., QIAN, J., HOEKSEMA, M. D., WANG, J., JACOBOWITZ, M., JI, X., HARRIS, F. T., HARRIS, B. K., BOYD, K. L., CHEN, H., EISENBERG, R. & MASSION, P. P. 2015. Targeting SLC1a5-mediated glutamine dependence in non-small cell lung cancer. *Int J Cancer*, 137, 1587-97.
- HE, T., ZHANG, Y.-J., JIANG, H., LI, X.-H., ZHU, H. & ZHENG, K.-L. 2015. The c-Myc-LDHA axis positively regulates aerobic glycolysis and promotes tumor progression in pancreatic cancer. *Medical oncology (Northwood, London, England)*, 32, 633.
- HE, T. C., SPARKS, A. B., RAGO, C., HERMEKING, H., ZAWEL, L., DA COSTA, L. T., MORIN, P. J., VOGELSTEIN, B. & KINZLER, K. W. 1998. Identification of c-MYC as a target of the APC pathway. *Science*, 281, 1509-12.
- HEGI, M. E., DISERENS, A., GORLIA, T., HAMOU, M., DE TRIBOLET, N., WELLER, M., KROS, J. M., HAINFELLNER, J. A., MASON, W., MARIANI, L., BROMBERG, J. E. C., HAU, P., MIRIMANOFF, R. O., CAIRNCROSS, J. G., JANZER, R. C. & STUPP, R. 2005. MGMT gene silencing and benefit from temozolomide in glioblastoma. *New England Journal of Medicine*, 352, 997-1003.
- HEIDEN, M. G. V., CANTLEY, L. C. & THOMPSON, C. B. 2009. Understanding the Warburg Effect: The Metabolic Requirements of Cell Proliferation. *Science*, 324, 1029-1033.

- HENNERMANN, J. B., BERGER, J. M., GRIEBEN, U., SCHARER, G. & VAN HOVE, J. L. 2012. Prediction of long-term outcome in glycine encephalopathy: a clinical survey. *J Inherit Metab Dis*, 35, 253-61.
- HERRLINGER, U., TZARIDIS, T., MACK, F., STEINBACH, J. P., SCHLEGEL, U., SABEL, M., HAU, P., KORTMANN, R. D., KREX, D., GRAUER, O., GOLDBRUNNER, R., SCHNELL, O., BAHR, O., UHL, M., SEIDEL, C., TABATABAI, G., KOWALSKI, T., RINGEL, F., SCHMIDT-GRAF, F., SUCHORSKA, B., BREHMER, S., WEYERBROCK, A., RENOVANZ, M., BULLINGER, L., GALLDIKS, N., VAJKOCZY, P., MISCH, M., VATTER, H., STUPLICH, M., SCHAFFER, N., KEBIR, S., WELLER, J., SCHAUB, C., STUMMER, W., TONN, J. C., SIMON, M., KEIL, V. C., NELLES, M., URBACH, H., COENEN, M., WICK, W., WELLER, M., FIMMERS, R., SCHMID, M., HATTINGEN, E., PIETSCH, T., COCH, C. & GLAS, M. 2019. Lomustine-temozolomide combination therapy versus standard temozolomide therapy in patients with newly diagnosed glioblastoma with methylated MGMT promoter (CeTeG/NOA-09): a randomised, open-label, phase 3 trial. *Lancet*, 393, 678-688.
- HILL, R. M., KUIJPER, S., LINDSEY, J. C., PETRIE, K., SCHWALBE, E. C., BARKER, K., BOULT, J. K. R., WILLIAMSON, D., AHMAD, Z., HALLSWORTH, A., RYAN, S. L., POON, E., ROBINSON, S. P., RUDDLE, R., RAYNAUD, F. I., HOWELL, L., KWOK, C., JOSHI, A., NICHOLSON, S. L., CROSIER, S., ELLISON, D. W., WHARTON, S. B., ROBSON, K., MICHALSKI, A., HARGRAVE, D., JACQUES, T. S., PIZER, B., BAILEY, S., SWARTLING, F. J., WEISS, W. A., CHESLER, L. & CLIFFORD, S. C. 2015. Combined MYC and P53 defects emerge at medulloblastoma relapse and define rapidly progressive, therapeutically targetable disease. *Cancer cell*, 27, 72-84.
- HOFFMAN, D. W. & RASMUSSEN, C. 2019. Position-Specific Carbon Stable Isotope Ratios by Proton NMR Spectroscopy. *Analytical Chemistry*, 91, 15661-15669.
- HOLZ, M. K. & BLENIS, J. 2005. Identification of S6 kinase 1 as a novel mammalian target of rapamycin (mTOR)-phosphorylating kinase. *J Biol Chem*, 280, 26089-93.
- HOSIOS, A. M., HECHT, V. C., DANAI, L. V., JOHNSON, M. O., RATHMELL, J. C., STEINHAUSER, M. L., MANALIS, S. R. & VANDER HEIDEN, M. G. 2016. Amino Acids Rather than Glucose Account for the Majority of Cell Mass in Proliferating Mammalian Cells. *Dev Cell*, 36, 540-9.
- HOUTEN, S. M. & WANDERS, R. J. A. 2010. A general introduction to the biochemistry of mitochondrial fatty acid beta-oxidation. *Journal of Inherited Metabolic Disease*, 33, 469-477.
- HOVESTADT, V., SMITH, K. S., BIHANNIC, L., FILBIN, M. G., SHAW, M. L., BAUMGARTNER, A., DEWITT, J. C., GROVES, A., MAYR, L., WEISMAN, H. R., RICHMAN, A. R., SHORE, M. E., GOUMNEROVA, L., ROSENCRANCE, C., CARTER, R. A., PHOENIX, T. N., HADLEY, J. L., TONG, Y., HOUSTON, J., ASHMUN, R. A., DECUYPERE, M., SHARMA, T., FLASCH, D., SILKOV, A., LIGON, K. L., POMEROY, S. L., RIVERA, M. N., ROZENBLATT-ROSEN, O., RUSERT, J. M., WECHSLER-REYA, R. J., LI, X. N., PEYRL, A., GOJO, J., KIRCHHOFER, D., LOTSCH, D., CZECH, T., DORFER, C., HABERLER, C., GEYEREGGER, R., HALFMANN, A., GAWAD, C., EASTON, J., PFISTER, S. M., REGEV, A., GAJJAR, A., ORR, B. A., SLAVC, I., ROBINSON, G. W., BERNSTEIN, B. E., SUVA, M. L. & NORTHCOTT, P. A. 2019. Resolving medulloblastoma cellular architecture by single-cell genomics. *Nature*, 572, 74-79.

- HU, B., WANG, Q., WANG, Y. A., HUA, S., SAUVE, C. G., ONG, D., LAN, Z. D., CHANG, Q., HO, Y. W., MONASTERIO, M. M., LU, X., ZHONG, Y., ZHANG, J., DENG, P., TAN, Z., WANG, G., LIAO, W. T., CORLEY, L. J., YAN, H., ZHANG, J., YOU, Y., LIU, N., CAI, L., FINOCCHIARO, G., PHILLIPS, J. J., BERGER, M. S., SPRING, D. J., HU, J., SULMAN, E. P., FULLER, G. N., CHIN, L., VERHAAK, R. G. W. & DEPINHO, R. A. 2016. Epigenetic Activation of WNT5A Drives Glioblastoma Stem Cell Differentiation and Invasive Growth. *Cell*, 167, 1281-1295.e18.
- HU, S. S., LAI, M. M. & VOGT, P. K. 1979. Genome of avian myelocytomatosis virus MC29: analysis by heteroduplex mapping. *Proc Natl Acad Sci U S A*, 76, 1265-8.
- IRTENKAUF, S. M., SOBIECHOWSKI, S., HASSELBACH, L. A., NELSON, K. K., TRANSOU, A. D., CARLTON, E. T., MIKKELSEN, T. & DECARVALHO, A. C. 2017. Optimization of Glioblastoma Mouse Orthotopic Xenograft Models for Translational Research. *Comparative medicine*, 67, 300-314.
- ITKONEN, H. M., MINNER, S., GULDVIK, I. J., SANDMANN, M. J., TSOURLAKIS, M. C., BERGE, V., SVINDLAND, A., SCHLOMM, T. & MILLS, I. G. 2013. O-GlcNAc transferase integrates metabolic pathways to regulate the stability of c-MYC in human prostate cancer cells. *Cancer Res*, 73, 5277-87.
- IVANOV, D. P., COYLE, B., WALKER, D. A. & GRABOWSKA, A. M. 2016. In vitro models of medulloblastoma: Choosing the right tool for the job. *Journal of Biotechnology*, 236, 10-25.
- JACQUES, T. S., SWALES, A., BRZOSOWSKI, M. J., HENRIQUEZ, N. V., LINEHAN, J. M., MIRZADEH, Z., C, O. M., NAUMANN, H., ALVAREZ-BUYLLA, A. & BRANDNER, S. 2010. Combinations of genetic mutations in the adult neural stem cell compartment determine brain tumour phenotypes. *Embo j*, 29, 222-35.
- JAE, H. J., CHUNG, J. W., PARK, H. S., LEE, M. J., LEE, K. C., KIM, H. C., YOON, J. H., CHUNG, H. & PARK, J. H. 2009. The antitumor effect and hepatotoxicity of a hexokinase II inhibitor 3-bromopyruvate: in vivo investigation of intraarterial administration in a rabbit VX2 hepatoma model. *Korean J Radiol*, 10, 596-603.
- JAIN, M., NILSSON, R., SHARMA, S., MADHUSUDHAN, N., KITAMI, T., SOUZA, A. L., KAFRI, R., KIRSCHNER, M. W., CLISH, C. B. & MOOTHA, V. K. 2012. Metabolite profiling identifies a key role for glycine in rapid cancer cell proliferation. *Science*, 336, 1040-4.
- JUCHEM, C. & DE GRAAF, R. A. 2017. B0 magnetic field homogeneity and shimming for in vivo magnetic resonance spectroscopy. *Anal Biochem*, 529, 17-29.
- KASZNICKI, J., SLIWINSKA, A. & DRZEWSKI, J. 2014. Metformin in cancer prevention and therapy. *Ann Transl Med*, 2, 57.
- KATHAGEN, A., SCHULTE, A., BALCKE, G., PHILLIPS, H. S., MARTENS, T., MATSCHKE, J., GUNTHER, H. S., SORIANO, R., MODRUSAN, Z., SANDMANN, T., KUHL, C., TISSIER, A., HOLZ, M., KRAWINKEL, L. A., GLATZEL, M., WESTPHAL, M. & LAMSZUS, K. 2013. Hypoxia and oxygenation induce a metabolic switch between pentose phosphate pathway and glycolysis in glioma stem-like cells. *Acta Neuropathol*, 126, 763-80.
- KAWAUCHI, D., ROBINSON, G., UZIEL, T., GIBSON, P., REHG, J., GAO, C., FINKELSTEIN, D., QU, C., POUNDS, S., ELLISON, D. W., GILBERTSON, R. J. & ROUSSEL, M. F. 2012. A mouse model of the most aggressive subgroup of human medulloblastoma. *Cancer Cell*, 21, 168-80.
- KEITH CHENAULT, H. & WHITESIDES, G. M. 1989. Lactate dehydrogenase-catalyzed regeneration of NAD from NADH for use in enzyme-catalyzed synthesis. *Bioorganic Chemistry*, 17, 400-409.

- KFOURY, A., ARMARO, M., COLLODET, C., SORDET-DESSIMOZ, J., GINER, M. P., CHRISTEN, S., MOCO, S., LELEU, M., DE LEVAL, L., KOCH, U., TRUMPP, A., SAKAMOTO, K., BEERMANN, F. & RADTKE, F. 2018. AMPK promotes survival of c-Myc-positive melanoma cells by suppressing oxidative stress. *Embo j*, 37.
- KIM, D., FISKE, B. P., BIRSOY, K., FREINKMAN, E., KAMI, K., POSSEMATO, R. L., CHUDNOVSKY, Y., PACOLD, M. E., CHEN, W. W., CANTOR, J. R., SHELTON, L. M., GUI, D. Y., KWON, M., RAMKISSOON, S. H., LIGON, K. L., KANG, S. W., SNUDERL, M., VANDER HEIDEN, M. G. & SABATINI, D. M. 2015. SHMT2 drives glioma cell survival in ischaemia but imposes a dependence on glycine clearance. *Nature*, 520, 363-7.
- KIM, J. B., GREBER, B., ARAUZO-BRAVO, M. J., MEYER, J., PARK, K. I., ZAEHRES, H. & SCHOLER, H. R. 2009. Direct reprogramming of human neural stem cells by OCT4. *Nature*, 461, 649-3.
- KING, M. W. 2020. *Lipolysis and the oxidation of fatty acids* [Online]. [Accessed].
- KNIGHT, Z. A. & SHOKAT, K. M. 2007. Chemical Genetics: Where Genetics and Pharmacology Meet. *Cell*, 128, 425-430.
- KOCH, K., HARTMANN, R., SCHROTER, F., SUWALA, A. K., MACIACZYK, D., KRUGER, A. C., WILLBOLD, D., KAHLERT, U. D. & MACIACZYK, J. 2016. Reciprocal regulation of the cholinic phenotype and epithelial-mesenchymal transition in glioblastoma cells. *Oncotarget*, 7, 73414-73431.
- KOHE, S. E., BENNETT, C. D., GILL, S. K., WILSON, M., MCCONVILLE, C. & PEET, A. C. 2018. Metabolic profiling of the three neural derived embryonal pediatric tumors retinoblastoma, neuroblastoma and medulloblastoma, identifies distinct metabolic profiles. *Oncotarget*, 9, 11336-11351.
- KONDOH, H., LLEONART, M. E., GIL, J., WANG, J., DEGAN, P., PETERS, G., MARTINEZ, D., CARNERO, A. & BEACH, D. 2005. Glycolytic enzymes can modulate cellular life span. *Cancer Res*, 65, 177-85.
- KOOL, M., JONES, D. T., JAGER, N., NORTHCOTT, P. A., PUGH, T. J., HOVESTADT, V., PIRO, R. M., ESPARZA, L. A., MARKANT, S. L., REMKE, M., MILDE, T., BOURDEAUT, F., RYZHOVA, M., STURM, D., PFAFF, E., STARK, S., HUTTER, S., SEKER-CIN, H., JOHANN, P., BENDER, S., SCHMIDT, C., RAUSCH, T., SHIH, D., REIMAND, J., SIEBER, L., WITTMANN, A., LINKE, L., WITT, H., WEBER, U. D., ZAPATKA, M., KONIG, R., BEROUKHIM, R., BERGTHOLD, G., VAN SLUIS, P., VOLCKMANN, R., KOSTER, J., VERSTEEG, R., SCHMIDT, S., WOLF, S., LAWRENZ, C., BARTHOLOMAE, C. C., VON KALLE, C., UNTERBERG, A., HEROLD-MENDE, C., HOFER, S., KULOZIK, A. E., VON DEIMLING, A., SCHEURLLEN, W., FELSBERG, J., REIFENBERGER, G., HASSELBLATT, M., CRAWFORD, J. R., GRANT, G. A., JABADO, N., PERRY, A., COWDREY, C., CROUL, S., ZADEH, G., KORBEL, J. O., DOZ, F., DELATTRE, O., BADER, G. D., MCCABE, M. G., COLLINS, V. P., KIERAN, M. W., CHO, Y. J., POMEROY, S. L., WITT, O., BRORS, B., TAYLOR, M. D., SCHULLER, U., KORSHUNOV, A., EILS, R., WECHSLER-REYA, R. J., LICHTER, P. & PFISTER, S. M. 2014a. Genome sequencing of SHH medulloblastoma predicts genotype-related response to smoothed inhibition. *Cancer Cell*, 25, 393-405.
- KOOL, M., JONES, DAVID T. W., JÄGER, N., NORTHCOTT, PAUL A., PUGH, TREVOR J., HOVESTADT, V., PIRO, ROSARIO M., ESPARZA, L. A., MARKANT, SHIRLEY L., REMKE, M., MILDE, T., BOURDEAUT, F., RYZHOVA, M., STURM, D., PFAFF, E., STARK, S., HUTTER, S., SEKER-CIN, H., JOHANN, P., BENDER, S., SCHMIDT, C., RAUSCH, T., SHIH, D.,

- REIMAND, J., SIEBER, L., WITTMANN, A., LINKE, L., WITT, H., WEBER, URSULA D., ZAPATKA, M., KÖNIG, R., BEROUKHIM, R., BERGTHOLD, G., VAN SLUIS, P., VOLCKMANN, R., KOSTER, J., VERSTEEG, R., SCHMIDT, S., WOLF, S., LAWERENZ, C., BARTHOLOMAE, CYNTHIA C., VON KALLE, C., UNTERBERG, A., HEROLD-MENDE, C., HOFER, S., KULOZIK, ANDREAS E., VON DEIMLING, A., SCHEURLLEN, W., FELSBERG, J., REIFENBERGER, G., HASSELBLATT, M., CRAWFORD, JOHN R., GRANT, GERALD A., JABADO, N., PERRY, A., COWDREY, C., CROUL, S., ZADEH, G., KORBEL, JAN O., DOZ, F., DELATTRE, O., BADER, GARY D., MCCABE, MARTIN G., COLLINS, V. P., KIERAN, MARK W., CHO, Y.-J., POMEROY, SCOTT L., WITT, O., BRORS, B., TAYLOR, MICHAEL D., SCHÜLLER, U., KORSHUNOV, A., EILS, R., WECHSLER-REYA, ROBERT J., LICHTER, P. & PFISTER, STEFAN M. 2014b. Genome Sequencing of SHH Medulloblastoma Predicts Genotype-Related Response to Smoothed Inhibition. *Cancer Cell*, 25, 393-405.
- KOOL, M., KORSHUNOV, A., REMKE, M., JONES, D. T., SCHLANSTEIN, M., NORTHCOTT, P. A., CHO, Y. J., KOSTER, J., SCHOUTEN-VAN MEETEREN, A., VAN VUURDEN, D., CLIFFORD, S. C., PIETSCH, T., VON BUEREN, A. O., RUTKOWSKI, S., MCCABE, M., COLLINS, V. P., BACKLUND, M. L., HABERLER, C., BOURDEAUT, F., DELATTRE, O., DOZ, F., ELLISON, D. W., GILBERTSON, R. J., POMEROY, S. L., TAYLOR, M. D., LICHTER, P. & PFISTER, S. M. 2012. Molecular subgroups of medulloblastoma: an international meta-analysis of transcriptome, genetic aberrations, and clinical data of WNT, SHH, Group 3, and Group 4 medulloblastomas. *Acta Neuropathol*, 123, 473-84.
- KOOL, M., KOSTER, J., BUNT, J., HASSELT, N. E., LAKEMAN, A., VAN SLUIS, P., TROOST, D., MEETEREN, N. S., CARON, H. N., CLOOS, J., MRSIC, A., YLSTRA, B., GRAJKOWSKA, W., HARTMANN, W., PIETSCH, T., ELLISON, D., CLIFFORD, S. C. & VERSTEEG, R. 2008. Integrated genomics identifies five medulloblastoma subtypes with distinct genetic profiles, pathway signatures and clinicopathological features. *PLoS One*, 3, e3088.
- KOTTAKIS, F., NICOLAY, B. N., ROUMANE, A., KARNIK, R., GU, H., NAGLE, J. M., BOUKHALI, M., HAYWARD, M. C., LI, Y. Y., CHEN, T., LIESA, M., HAMMERMAN, P. S., WONG, K. K., HAYES, D. N., SHIRIHAI, O. S., DYSON, N. J., HAAS, W., MEISSNER, A. & BARDEESY, N. 2016. LKB1 loss links serine metabolism to DNA methylation and tumorigenesis. *Nature*, 539, 390-395.
- KOUSHI, E., TSOUGOS, I., TSOLAKI, E., FOUNTAS, K. N., THEODOROU, K., FEZOULIDIS, I., KAPSALAKI, E. & KAPPAS, C. 2012. Spectroscopic evaluation of glioma grading at 3T: the combined role of short and long TE. *ScientificWorldJournal*, 2012, 546171.
- KOVANLIKAYA, A., PANIGRAHY, A., KRIEGER, M. D., GONZALEZ-GOMEZ, I., GHUGRE, N., MCCOMB, J. G., GILLES, F. H., NELSON, M. D. & BLUML, S. 2005. Untreated pediatric primitive neuroectodermal tumor in vivo: quantitation of taurine with MR spectroscopy. *Radiology*, 236, 1020-5.
- KREBS, H. A. 1940. The citric acid cycle: A reply to the criticisms of F. L. Breusch and of J. Thomas. *Biochem J*, 34, 460-3.
- KUMAR, V., DWIVEDI, D. K. & JAGANNATHAN, N. R. 2014. High-resolution NMR spectroscopy of human body fluids and tissues in relation to prostate cancer. *NMR Biomed*, 27, 80-9.
- KUNG, C., HIXON, J., CHOE, S., MARKS, K., GROSS, S., MURPHY, E., DELABARRE, B., CIANCHETTA, G., SETHUMADHAVAN, S., WANG, X.,

- YAN, S., GAO, Y., FANG, C., WEI, W., JIANG, F., WANG, S., QIAN, K., SAUNDERS, J., DRIGGERS, E., WOO, H. K., KUNII, K., MURRAY, S., YANG, H., YEN, K., LIU, W., CANTLEY, L. C., VANDER HEIDEN, M. G., SU, S. M., JIN, S., SALITURO, F. G. & DANG, L. 2012. Small molecule activation of PKM2 in cancer cells induces serine auxotrophy. *Chemistry & biology*, 19, 1187-1198.
- KYLE, J. & MICHAEL, D. T. 2019. Medulloblastoma in the age of molecular subgroups: a review. *Journal of Neurosurgery: Pediatrics PED*, 24, 353-363.
- LABUSCHAGNE, C. F., VAN DEN BROEK, N. J., MACKAY, G. M., VOUSDEN, K. H. & MADDOCKS, O. D. 2014. Serine, but not glycine, supports one-carbon metabolism and proliferation of cancer cells. *Cell Rep*, 7, 1248-58.
- LAM, F. C., MORTON, S. W., WYCKOFF, J., VU HAN, T. L., HWANG, M. K., MAFFA, A., BALKANSKA-SINCLAIR, E., YAFFE, M. B., FLOYD, S. R. & HAMMOND, P. T. 2018. Enhanced efficacy of combined temozolomide and bromodomain inhibitor therapy for gliomas using targeted nanoparticles. *Nat Commun*, 9, 1991.
- LANNERING, B., RUTKOWSKI, S., DOZ, F., PIZER, B., GUSTAFSSON, G., NAVAJAS, A., MASSIMINO, M., REDDINGIUS, R., BENESCH, M., CARRIE, C., TAYLOR, R., GANDOLA, L., BJORK-ERIKSSON, T., GIRALT, J., OLDENBURGER, F., PIETSCH, T., FIGARELLA-BRANGER, D., ROBSON, K., FORNI, M., CLIFFORD, S. C., WARMUTH-METZ, M., VON HOFF, K., FALDUM, A., MOSSERI, V. & KORTMANN, R. 2012. Hyperfractionated versus conventional radiotherapy followed by chemotherapy in standard-risk medulloblastoma: results from the randomized multicenter HIT-SIOP PNET 4 trial. *J Clin Oncol*, 30, 3187-93.
- LAW, M., YANG, S., WANG, H., BABB, J. S., JOHNSON, G., CHA, S., KNOPP, E. A. & ZAGZAG, D. 2003. Glioma grading: sensitivity, specificity, and predictive values of perfusion MR imaging and proton MR spectroscopic imaging compared with conventional MR imaging. *AJNR Am J Neuroradiol*, 24, 1989-98.
- LE, A., LANE, A. N., HAMAKER, M., BOSE, S., GOUW, A., BARBI, J., TSUKAMOTO, T., ROJAS, C. J., SLUSHER, B. S., ZHANG, H., ZIMMERMAN, L. J., LIEBLER, D. C., SLEBOS, R. J., LORKIEWICZ, P. K., HIGASHI, R. M., FAN, T. W. & DANG, C. V. 2012. Glucose-independent glutamine metabolism via TCA cycling for proliferation and survival in B cells. *Cell Metab*, 15, 110-21.
- LEE, C.-K., JEONG, S.-H., JANG, C., BAE, H., KIM, Y. H., PARK, I., KIM, S. K. & KOH, G. Y. 2019. Tumor metastasis to lymph nodes requires YAP-dependent metabolic adaptation. *Science*, 363, 644-649.
- LEE, I. H. & FINKEL, T. 2013. Metabolic regulation of the cell cycle. *Curr Opin Cell Biol*, 25, 724-9.
- LEE, J., KOTLIAROVA, S., KOTLIAROV, Y., LI, A., SU, Q., DONIN, N. M., PASTORINO, S., PUROW, B. W., CHRISTOPHER, N., ZHANG, W., PARK, J. K. & FINE, H. A. 2006. Tumor stem cells derived from glioblastomas cultured in bFGF and EGF more closely mirror the phenotype and genotype of primary tumors than do serum-cultured cell lines. *Cancer Cell*, 9, 391-403.
- LEE, J. & WOLFGANG, M. J. 2012. Metabolomic profiling reveals a role for CPT1c in neuronal oxidative metabolism. *Bmc Biochemistry*, 13.
- LEE, J. V., CARRER, A., SHAH, S., SNYDER, N. W., WEI, S., VENNETI, S., WORTH, A. J., YUAN, Z. F., LIM, H. W., LIU, S., JACKSON, E., AIELLO, N. M., HAAS, N. B., REBBECK, T. R., JUDKINS, A., WON, K. J., CHODOSH, L. A., GARCIA, B. A., STANGER, B. Z., FELDMAN, M. D., BLAIR, I. A. &

- WELLEN, K. E. 2014. Akt-dependent metabolic reprogramming regulates tumor cell histone acetylation. *Cell Metab*, 20, 306-319.
- LEE, K. M., GILTNAME, J. M., BALKO, J. M., SCHWARZ, L. J., GUERRERO-ZOTANO, A. L., HUTCHINSON, K. E., NIXON, M. J., ESTRADA, M. V., SANCHEZ, V., SANDERS, M. E., LEE, T., GOMEZ, H., LLUCH, A., PEREZ-FIDALGO, J. A., WOLF, M. M., ANDREJEVA, G., RATHMELL, J. C., FESIK, S. W. & ARTEAGA, C. L. 2017. MYC and MCL1 Cooperatively Promote Chemotherapy-Resistant Breast Cancer Stem Cells via Regulation of Mitochondrial Oxidative Phosphorylation. *Cell Metab*, 26, 633-647.e7.
- LEHUÉDÉ, C., DUPUY, F., RABINOVITCH, R., JONES, R. G. & SIEGEL, P. M. 2016. Metabolic Plasticity as a Determinant of Tumor Growth and Metastasis. *Cancer Research*, 76, 5201-5208.
- LI, F., WANG, Y., ZELLER, K. I., POTTER, J. J., WONSEY, D. R., O'DONNELL, K. A., KIM, J. W., YUSTEIN, J. T., LEE, L. A. & DANG, C. V. 2005. Myc stimulates nuclearly encoded mitochondrial genes and mitochondrial biogenesis. *Mol Cell Biol*, 25, 6225-34.
- LI, H., NING, S., GHANDI, M., KRYUKOV, G. V., GOPAL, S., DEIK, A., SOUZA, A., PIERCE, K., KESKULA, P., HERNANDEZ, D., ANN, J., SHKOZA, D., APFEL, V., ZOU, Y., VAZQUEZ, F., BARRETINA, J., PAGLIARINI, R. A., GALLI, G. G., ROOT, D. E., HAHN, W. C., TSHERNIAK, A., GIANNAKIS, M., SCHREIBER, S. L., CLISH, C. B., GARRAWAY, L. A. & SELLERS, W. R. 2019. The landscape of cancer cell line metabolism. *Nat Med*, 25, 850-860.
- LI, L., LI, Y., QUE, X., GAO, X., GAO, Q., YU, M., MA, K., XI, Y. & WANG, T. 2018. Prognostic significances of overexpression MYC and/or BCL2 in R-CHOP-treated diffuse large B-cell lymphoma: A Systematic review and meta-analysis. *Sci Rep*, 8, 6267.
- LIIMATAINEN, T., LEHTIMAKI, K., ALA-KORPELA, M. & HAKUMAKI, J. 2006. Identification of mobile cholesterol compounds in experimental gliomas by H-1 MRS in vivo: Effects of ganciclovir-induced apoptosis on lipids. *Febs Letters*, 580, 4746-4750.
- LIM, D. A. & ALVAREZ-BUYLLA, A. 2016. The Adult Ventricular-Subventricular Zone (V-SVZ) and Olfactory Bulb (OB) Neurogenesis. *Cold Spring Harb Perspect Biol*, 8.
- LIN, H., PATEL, S., AFFLECK, V., WILSON, I., TURNBULL, D., JOSHI, A., MAXWELL, R. & STOLL, E. 2016. FATTY ACID OXIDATION IS REQUIRED FOR THE RESPIRATION AND PROLIFERATION OF MALIGNANT GLIOMA CELLS. *Neuro-Oncology*, 18, 36-36.
- LIN, R., ELF, S., SHAN, C., KANG, H.-B., JI, Q., ZHOU, L., HITOSUGI, T., ZHANG, L., ZHANG, S., SEO, J. H., XIE, J., TUCKER, M., GU, T.-L., SUDDERTH, J., JIANG, L., MITSCHKE, M., DEBERARDINIS, R. J., WU, S., LI, Y., MAO, H., CHEN, P. R., WANG, D., CHEN, G. Z., HURWITZ, S. J., LONIAL, S., ARELLANO, M. L., KHOURY, H. J., KHURI, F. R., LEE, B. H., LEI, Q., BRAT, D. J., YE, K., BOGGON, T. J., HE, C., KANG, S., FAN, J. & CHEN, J. 2015. 6-Phosphogluconate dehydrogenase links oxidative PPP, lipogenesis and tumour growth by inhibiting LKB1-AMPK signalling. *Nature cell biology*, 17, 1484-1496.
- LIU, L., ULBRICH, J., MULLER, J., WUSTEFELD, T., AEBERHARD, L., KRESS, T. R., MUTHALAGU, N., RYCAK, L., RUDALSKA, R., MOLL, R., KEMPA, S., ZENDER, L., EILERS, M. & MURPHY, D. J. 2012. Deregulated MYC expression induces dependence upon AMPK-related kinase 5. *Nature*, 483, 608-12.

- LIU, Y. Y., ZUCKIER, L. S. & GHESANI, N. V. 2010. Dominant Uptake of Fatty Acid over Glucose by Prostate Cells: A Potential New Diagnostic and Therapeutic Approach. *Anticancer Research*, 30, 369-374.
- LOCASALE, J. W., GRASSIAN, A. R., MELMAN, T., LYSSIOTIS, C. A., MATTAINI, K. R., BASS, A. J., HEFFRON, G., METALLO, C. M., MURANEN, T., SHARFI, H., SASAKI, A. T., ANASTASIOU, D., MULLARKY, E., VOKES, N. I., SASAKI, M., BEROUKHIM, R., STEPHANOPOULOS, G., LIGON, A. H., MEYERSON, M., RICHARDSON, A. L., CHIN, L., WAGNER, G., ASARA, J. M., BRUGGE, J. S., CANTLEY, L. C. & VANDER HEIDEN, M. G. 2011. Phosphoglycerate dehydrogenase diverts glycolytic flux and contributes to oncogenesis. *Nat Genet*, 43, 869-74.
- LODISH H, B. A., ZIPURSKY SL, ET AL. 2000. *Electron Transport and Oxidative Phosphorylation*.
- LOUIS, D. N., OHGAKI, H., WIESTLER, O. D., CAVENEE, W. K., BURGER, P. C., JOUVET, A., SCHEITHAUER, B. W. & KLEIHUES, P. 2007. The 2007 WHO classification of tumours of the central nervous system. *Acta Neuropathologica*, 114, 97-109.
- LOUIS, D. N., PERRY, A., REIFENBERGER, G., VON DEIMLING, A., FIGARELLA-BRANGER, D., CAVENEE, W. K., OHGAKI, H., WIESTLER, O. D., KLEIHUES, P. & ELLISON, D. W. 2016a. The 2016 World Health Organization Classification of Tumors of the Central Nervous System: a summary. *Acta Neuropathologica*, 131, 803-820.
- LOUIS, D. N., PERRY, A., REIFENBERGER, G., VON DEIMLING, A., FIGARELLA-BRANGER, D., CAVENEE, W. K., OHGAKI, H., WIESTLER, O. D., KLEIHUES, P. & ELLISON, D. W. 2016b. The 2016 World Health Organization Classification of Tumors of the Central Nervous System: a summary. *Acta Neuropathol*, 131, 803-20.
- LU, Y., LABAK, C. M., JAIN, N., PURVIS, I. J., GUDA, M. R., BACH, S. E., TSUNG, A. J., ASUTHKAR, S. & VELPULA, K. K. 2017. OTX2 expression contributes to proliferation and progression in Myc-amplified medulloblastoma. *Am J Cancer Res*, 7, 647-656.
- LUAN, W., WANG, Y., CHEN, X., SHI, Y., WANG, J., ZHANG, J., QIAN, J., LI, R., TAO, T., WEI, W., HU, Q., LIU, N. & YOU, Y. 2015. PKM2 promotes glucose metabolism and cell growth in gliomas through a mechanism involving a let-7a/c-Myc/hnRNPA1 feedback loop. *Oncotarget*, 6, 13006-18.
- LUKEY, M. J., KATT, W. P. & CERIONE, R. A. 2017. Targeting amino acid metabolism for cancer therapy. *Drug Discov Today*, 22, 796-804.
- MA, E. H., BANTUG, G., GRISS, T., CONDOTTA, S., JOHNSON, R. M., SAMBORSKA, B., MAINOLFI, N., SURI, V., GUAK, H., BALMER, M. L., VERWAY, M. J., RAISSI, T. C., TSUI, H., BOUKHALED, G., HENRIQUES DA COSTA, S., FREZZA, C., KRAWCZYK, C. M., FRIEDMAN, A., MANFREDI, M., RICHER, M. J., HESS, C. & JONES, R. G. 2017. Serine Is an Essential Metabolite for Effector T Cell Expansion. *Cell Metab*, 25, 345-357.
- MA, X., LI, B., LIU, J., FU, Y. & LUO, Y. 2019. Phosphoglycerate dehydrogenase promotes pancreatic cancer development by interacting with eIF4A1 and eIF4E. *J Exp Clin Cancer Res*, 38, 66.
- MADDOCKS, O. D., BERKERS, C. R., MASON, S. M., ZHENG, L., BLYTH, K., GOTTLIEB, E. & VOUSDEN, K. H. 2013. Serine starvation induces stress and p53-dependent metabolic remodelling in cancer cells. *Nature*, 493, 542-6.
- MADDOCKS, O. D., LABUSCHAGNE, C. F., ADAMS, P. D. & VOUSDEN, K. H. 2016. Serine Metabolism Supports the Methionine Cycle and DNA/RNA

- Methylation through De Novo ATP Synthesis in Cancer Cells. *Mol Cell*, 61, 210-21.
- MADDOCKS, O. D. K., ATHINEOS, D., CHEUNG, E. C., LEE, P., ZHANG, T., VAN DEN BROEK, N. J. F., MACKAY, G. M., LABUSCHAGNE, C. F., GAY, D., KRUISWIJK, F., BLAGIH, J., VINCENT, D. F., CAMPBELL, K. J., CETECI, F., SANSOM, O. J., BLYTH, K. & VOUSDEN, K. H. 2017. Modulating the therapeutic response of tumours to dietary serine and glycine starvation. *Nature*, 544, 372-376.
- MAKWANA, V., RYAN, P., PATEL, B., DUKIE, S. A. & RUDRAWAR, S. 2019. Essential role of O-GlcNAcylation in stabilization of oncogenic factors. *Biochim Biophys Acta Gen Subj*, 1863, 1302-1317.
- MALKIN, D. 2011. Li-fraumeni syndrome. *Genes Cancer*, 2, 475-84.
- MALMER, B., ADATTO, P., ARMSTRONG, G., BARNHOLTZ-SLOAN, J., BERNSTEIN, J. L., CLAUS, E., DAVIS, F., HOULSTON, R., IL'YASOVA, D., JENKINS, R., JOHANSEN, C., LAI, R., LAU, C., MCCARTHY, B., NIELSEN, H., OLSON, S. H., SADETZKI, S., SHETE, S., WIKLUND, F., WRENSCH, M., YANG, P. & BONDY, M. 2007. GLIOGENE - an international consortium to understand familial glioma. *Cancer Epidemiology Biomarkers & Prevention*, 16, 1730-1734.
- MARIN-VALENCIA, I., YANG, C., MASHIMO, T., CHO, S., BAEK, H., YANG, X. L., RAJAGOPALAN, K. N., MADDIE, M., VEMIREDDY, V., ZHAO, Z., CAI, L., GOOD, L., TU, B. P., HATANPAA, K. J., MICKEY, B. E., MATES, J. M., PASCUAL, J. M., MAHER, E. A., MALLOY, C. R., DEBERARDINIS, R. J. & BACHOO, R. M. 2012. Analysis of tumor metabolism reveals mitochondrial glucose oxidation in genetically diverse human glioblastomas in the mouse brain in vivo. *Cell Metab*, 15, 827-37.
- MARSHALL, D. D. & POWERS, R. 2017. Beyond the paradigm: Combining mass spectrometry and nuclear magnetic resonance for metabolomics. *Prog Nucl Magn Reson Spectrosc*, 100, 1-16.
- MARTINDALE, J. L. & HOLBROOK, N. J. 2002. Cellular response to oxidative stress: signaling for suicide and survival. *J Cell Physiol*, 192, 1-15.
- MASHIMO, T., PICHUMANI, K., VEMIREDDY, V., HATANPAA, K. J., SINGH, D. K., SIRASANAGANDLA, S., NANNEPAGA, S., PICCIRILLO, S. G., KOVACS, Z., FOONG, C., HUANG, Z. G., BARNETT, S., MICKEY, B. E., DEBERARDINIS, R. J., TU, B. P., MAHER, E. A. & BACHOO, R. M. 2014. Acetate Is a Bioenergetic Substrate for Human Glioblastoma and Brain Metastases. *Cell*, 159, 1603-1614.
- MATOBA, S., KANG, J. G., PATINO, W. D., WRAGG, A., BOEHM, M., GAVRILOVA, O., HURLEY, P. J., BUNZ, F. & HWANG, P. M. 2006. p53 regulates mitochondrial respiration. *Science*, 312, 1650-3.
- MAXWELL, P. H., WIESENER, M. S., CHANG, G.-W., CLIFFORD, S. C., VAUX, E. C., COCKMAN, M. E., WYKOFF, C. C., PUGH, C. W., MAHER, E. R. & RATCLIFFE, P. J. 1999. The tumour suppressor protein VHL targets hypoxia-inducible factors for oxygen-dependent proteolysis. *Nature*, 399, 271-275.
- MAZUREK, S. 2011. Pyruvate kinase type M2: a key regulator of the metabolic budget system in tumor cells. *Int J Biochem Cell Biol*, 43, 969-80.
- MAZUREK, S., BOSCHEK, C. B., HUGO, F. & EIGENBRODT, E. 2005. Pyruvate kinase type M2 and its role in tumor growth and spreading. *Seminars in Cancer Biology*, 15, 300-308.
- MCGARRY, J. D., LEATHERMAN, G. F. & FOSTER, D. W. 1978. CARNITINE PALMITOYLTRANSFERASE I - SITE OF INHIBITION OF HEPATIC

- FATTY-ACID OXIDATION BY MALONYL-COA. *Journal of Biological Chemistry*, 253, 4128-4136.
- MELIN, B. S., BARNHOLTZ-SLOAN, J. S., WRENSCH, M. R., JOHANSEN, C., IL'YASOVA, D., KINNERSLEY, B., OSTROM, Q. T., LABRECHE, K., CHEN, Y., ARMSTRONG, G., LIU, Y., ECKEL-PASSOW, J. E., DECKER, P. A., LABUSSIÈRE, M., IDBAIH, A., HOANG-XUAN, K., DI STEFANO, A. L., MOKHTARI, K., DELATTRE, J. Y., BRODERICK, P., GALAN, P., GOUSIAS, K., SCHRAMM, J., SCHOEMAKER, M. J., FLEMING, S. J., HERMS, S., HEILMANN, S., NOTHEN, M. M., WICHMANN, H. E., SCHREIBER, S., SWERDLOW, A., LATHROP, M., SIMON, M., SANSON, M., ANDERSSON, U., RAJARAMAN, P., CHANOCK, S., LINET, M., WANG, Z., YEAGER, M., WIENCKE, J. K., HANSEN, H., MCCOY, L., RICE, T., KOSEL, M. L., SICOTTE, H., AMOS, C. I., BERNSTEIN, J. L., DAVIS, F., LACHANCE, D., LAU, C., MERRELL, R. T., SHILDKRAUT, J., ALI-OSMAN, F., SADETZKI, S., SCHEURER, M., SHETE, S., LAI, R. K., CLAUS, E. B., OLSON, S. H., JENKINS, R. B., HOULSTON, R. S. & BONDY, M. L. 2017. Genome-wide association study of glioma subtypes identifies specific differences in genetic susceptibility to glioblastoma and non-glioblastoma tumors. *Nat Genet*, 49, 789-794.
- MENDEZ-LUCAS, A., LI, X., HU, J., CHE, L., SONG, X., JIA, J., WANG, J., XIE, C., DRISCOLL, P. C., TSCHAHARGANEH, D. F., CALVISI, D. F., YUNEVA, M. & CHEN, X. 2017. Glucose Catabolism in Liver Tumors Induced by c-MYC Can Be Sustained by Various PKM1/PKM2 Ratios and Pyruvate Kinase Activities. *Cancer Res*, 77, 4355-4364.
- MENENDEZ, J. A. & LUPU, R. 2007. Fatty acid synthase and the lipogenic phenotype in cancer pathogenesis. *Nature Reviews Cancer*, 7, 763-777.
- MENON, S. & MANNING, B. D. 2008. Common corruption of the mTOR signaling network in human tumors. *Oncogene*, 27 Suppl 2, S43-51.
- MERCHANT, T. E., POLLACK, I. F. & LOEFFLER, J. S. 2010. Brain tumors across the age spectrum: biology, therapy, and late effects. *Semin Radiat Oncol*, 20, 58-66.
- MERIC-BERNSTAM, F., LEE, R. J., CARTHON, B. C., ILIOPOULOS, O., MIER, J. W., PATEL, M. R., TANNIR, N. M., OWONIKOKO, T. K., HAAS, N. B., VOSS, M. H., HARDING, J. J., SRINIVASAN, R., SHAPIRO, G., TELLI, M. L., MUNSTER, P. N., CARVAJAL, R. D., JENKINS, Y., WHITING, S. H., BENDELL, J. C. & BAUER, T. M. 2019. CB-839, a glutaminase inhibitor, in combination with cabozantinib in patients with clear cell and papillary metastatic renal cell cancer (mRCC): Results of a phase I study. *Journal of Clinical Oncology*, 37, 549-549.
- MEYER, N. & PENN, L. Z. 2008. Reflecting on 25 years with MYC. *Nat Rev Cancer*, 8, 976-90.
- MEYERS, S. P., KEMP, S. S. & TARR, R. W. 1992. MR imaging features of medulloblastomas. *AJR Am J Roentgenol*, 158, 859-65.
- MICHELAKIS, E. D., SUTENDRA, G., DROMPARIS, P., WEBSTER, L., HAROMY, A., NIVEN, E., MAGUIRE, C., GAMMER, T. L., MACKEY, J. R., FULTON, D., ABDULKARIM, B., MCMURTRY, M. S. & PETRUK, K. C. 2010. Metabolic Modulation of Glioblastoma with Dichloroacetate. *Science Translational Medicine*, 2.
- MIKHEEV, A. M., RAMAKRISHNA, R., STOLL, E. A., MIKHEEVA, S. A., BEYER, R. P., PLOTNIK, D. A., SCHWARTZ, J. L., ROCKHILL, J. K., SILBER, J. R., BORN, D. E., KOSAI, Y., HORNER, P. J. & ROSTOMILY, R. C. 2012. Increased age of transformed mouse neural progenitor/stem cells recapitulates

- age-dependent clinical features of human glioma malignancy. *Aging Cell*, 11, 1027-1035.
- MIKHEEV, A. M., STOLL, E. A., MIKHEEVA, S. A., MAXWELL, J. P., JANKOWSKI, P. P., RAY, S., UO, T., MORRISON, R. S., HORNER, P. J. & ROSTOMILY, R. C. 2009. A syngeneic glioma model to assess the impact of neural progenitor target cell age on tumor malignancy. *Aging Cell*, 8, 499-501.
- MLYNARIK, V., CUDALBU, C., CLEMENT, V., MARINO, D., RADOVANOVIC, I. & GRUETTER, R. 2012. In vivo metabolic profiling of glioma-initiating cells using proton magnetic resonance spectroscopy at 14.1 Tesla. *NMR Biomed*, 25, 506-13.
- MOOKERJEE, S. A., GERENCSEK, A. A., NICHOLLS, D. G. & BRAND, M. D. 2017. Quantifying intracellular rates of glycolytic and oxidative ATP production and consumption using extracellular flux measurements. *J Biol Chem*, 292, 7189-7207.
- MORANI, F., PHADNGAM, S., FOLLO, C., TITONE, R., AIMARETTI, G., GALETTO, A., ALABISO, O. & ISIDORO, C. 2014. PTEN regulates plasma membrane expression of glucose transporter 1 and glucose uptake in thyroid cancer cells. *J Mol Endocrinol*, 53, 247-58.
- MORENO-SÁNCHEZ, R., MARÍN-HERNÁNDEZ, Á., GALLARDO-PÉREZ, J. C., VÁZQUEZ, C., RODRÍGUEZ-ENRÍQUEZ, S. & SAAVEDRA, E. 2018. Control of the NADPH supply and GSH recycling for oxidative stress management in hepatoma and liver mitochondria. *Biochimica et Biophysica Acta (BBA) - Bioenergetics*, 1859, 1138-1150.
- MORFOUACE, M., SHELAT, A., JACUS, M., FREEMAN, B. B., 3RD, TURNER, D., ROBINSON, S., ZINDY, F., WANG, Y. D., FINKELSTEIN, D., AYRAULT, O., BIHANNIC, L., PUGET, S., LI, X. N., OLSON, J. M., ROBINSON, G. W., GUY, R. K., STEWART, C. F., GAJJAR, A. & ROUSSEL, M. F. 2014. Pemetrexed and gemcitabine as combination therapy for the treatment of Group3 medulloblastoma. *Cancer Cell*, 25, 516-29.
- MORRISH, F., ISERN, N., SADILEK, M., JEFFREY, M. & HOCKENBERY, D. M. 2009. c-Myc activates multiple metabolic networks to generate substrates for cell-cycle entry. *Oncogene*, 28, 2485-91.
- MUKHERJEE, D. & QUINONES-HINOJOSA, A. 2011. Impact of Extent of Resection on Outcomes in Patients with High-Grade Gliomas. *Tumors of the Central Nervous System, Volume 2*.
- MULLARKY, E., LUCKI, N. C., BEHESHTI ZAVAREH, R., ANGLIN, J. L., GOMES, A. P., NICOLAY, B. N., WONG, J. C., CHRISTEN, S., TAKAHASHI, H., SINGH, P. K., BLENIS, J., WARREN, J. D., FENDT, S. M., ASARA, J. M., DENICOLA, G. M., LYSSIOTIS, C. A., LAIRSON, L. L. & CANTLEY, L. C. 2016. Identification of a small molecule inhibitor of 3-phosphoglycerate dehydrogenase to target serine biosynthesis in cancers. *Proc Natl Acad Sci U S A*, 113, 1778-83.
- MURPHY, J. P., GIACOMANTONIO, M. A., PAULO, J. A., EVERLEY, R. A., KENNEDY, B. E., PATHAK, G. P., CLEMENTS, D. R., KIM, Y., DAI, C., SHARIF, T., GYGI, S. P. & GUJAR, S. 2018. The NAD(+) Salvage Pathway Supports PHGDH-Driven Serine Biosynthesis. *Cell Rep*, 24, 2381-2391.e5.
- MURPHY, M. P. 2009. How mitochondria produce reactive oxygen species. *Biochem J*, 417, 1-13.
- NATSUMEDA, M., IGARASHI, H., NOMURA, T., OGURA, R., TSUKAMOTO, Y., KOBAYASHI, T., AOKI, H., OKAMOTO, K., KAKITA, A., TAKAHASHI, H., NAKADA, T. & FUJII, Y. 2014. Accumulation of 2-hydroxyglutarate in gliomas

- correlates with survival: a study by 3.0-tesla magnetic resonance spectroscopy. *Acta Neuropathol Commun*, 2, 158.
- NAWROTH, R., STELLWAGEN, F., SCHULZ, W. A., STOEHR, R., HARTMANN, A., KRAUSE, B. J., GSCHWEND, J. E. & RETZ, M. 2011. S6K1 and 4E-BP1 Are Independent Regulated and Control Cellular Growth in Bladder Cancer. *PLOS ONE*, 6, e27509.
- NELSON, M., DIEBLER, C. & FORBES, W. S. C. 1991. Paediatric medulloblastoma: Atypical CT features at presentation in the SIOP II trial. *Neuroradiology*, 33, 140-142.
- NEWMAN, A. C. & MADDOCKS, O. D. K. 2017. One-carbon metabolism in cancer. *Br J Cancer*, 116, 1499-1504.
- NICHOLAS, D., PROCTOR, E. A., RAVAL, F. M., IP, B. C., HABIB, C., RITOU, E., GRAMMATOPOULOS, T. N., STEENKAMP, D., DOOMS, H., APOVIAN, C. M., LAUFFENBURGER, D. A. & NIKOLAJCZYK, B. S. 2017. Advances in the quantification of mitochondrial function in primary human immune cells through extracellular flux analysis. *PloS one*, 12, e0170975-e0170975.
- NIE, Z., HU, G., WEI, G., CUI, K., YAMANE, A., RESCH, W., WANG, R., GREEN, D. R., TESSAROLLO, L., CASELLAS, R., ZHAO, K. & LEVENS, D. 2012. c-Myc is a universal amplifier of expressed genes in lymphocytes and embryonic stem cells. *Cell*, 151, 68-79.
- NIEMAN, K. M., KENNY, H. A., PENICKA, C. V., LADANYI, A., BUELL-GUTBROD, R., ZILLHARDT, M. R., ROMERO, I. L., CAREY, M. S., MILLS, G. B., HOTAMISLIGIL, G. S., YAMADA, S. D., PETER, M. E., GWIN, K. & LENGYEL, E. 2011. Adipocytes promote ovarian cancer metastasis and provide energy for rapid tumor growth. *Nature Medicine*, 17, 1498-U207.
- NIEMINEN, A. I., ESKELINEN, V. M., HAIKALA, H. M., TERVONEN, T. A., YAN, Y., PARTANEN, J. I. & KLEFSTRÖM, J. 2013. Myc-induced AMPK-phospho p53 pathway activates Bak to sensitize mitochondrial apoptosis. *Proceedings of the National Academy of Sciences*, 110, E1839-E1848.
- NIKIFOROV, M. A., CHANDRIANI, S., O'CONNELL, B., PETRENKO, O., KOTENKO, I., BEAVIS, A., SEDIVY, J. M. & COLE, M. D. 2002. A functional screen for Myc-responsive genes reveals serine hydroxymethyltransferase, a major source of the one-carbon unit for cell metabolism. *Mol Cell Biol*, 22, 5793-800.
- NIKLISON-CHIROU, M. V., ERNGREN, I., ENGSKOG, M., HAGLOF, J., PICARD, D., REMKE, M., MCPOLIN, P. H. R., SELBY, M., WILLIAMSON, D., CLIFFORD, S. C., MICHOD, D., HADJIANDREOU, M., ARVIDSSON, T., PETTERSSON, C., MELINO, G. & MARINO, S. 2017. TAp73 is a marker of glutamine addiction in medulloblastoma. *Genes Dev*, 31, 1738-1753.
- NILSSON, A. & NIELSEN, J. 2017. Genome scale metabolic modeling of cancer. *Metab Eng*, 43, 103-112.
- NILSSON, J. A. & CLEVELAND, J. L. 2003. Myc pathways provoking cell suicide and cancer. *Oncogene*, 22, 9007-9021.
- NILSSON, R., JAIN, M., MADHUSUDHAN, N., SHEPPARD, N. G., STRITTMATTER, L., KAMPF, C., HUANG, J., ASPLUND, A. & MOOTHA, V. K. 2014. Metabolic enzyme expression highlights a key role for MTHFD2 and the mitochondrial folate pathway in cancer. *Nat Commun*, 5, 3128.
- NISHIDA, A., FURUKAWA, A., KOIKE, C., TANO, Y., AIZAWA, S., MATSUO, I. & FURUKAWA, T. 2003. Otx2 homeobox gene controls retinal photoreceptor cell fate and pineal gland development. *Nat Neurosci*, 6, 1255-63.
- NIU, Z., LIU, H., ZHOU, M., WANG, H., LIU, Y., LI, X., XIONG, W., MA, J., LI, X. & LI, G. 2015. Knockdown of c-Myc inhibits cell proliferation by negatively

- regulating the Cdk/Rb/E2F pathway in nasopharyngeal carcinoma cells. *Acta Biochim Biophys Sin (Shanghai)*, 47, 183-91.
- NOBLE, R. A., BELL, N., BLAIR, H., SIKKA, A., THOMAS, H., PHILLIPS, N., NAKJANG, S., MIWA, S., CROSSLAND, R., RAND, V., TELEVANTOU, D., LONG, A., KEUN, H. C., BACON, C. M., BOMKEN, S., CRITCHLOW, S. E. & WEDGE, S. R. 2017. Inhibition of monocarboxyate transporter 1 by AZD3965 as a novel therapeutic approach for diffuse large B-cell lymphoma and Burkitt lymphoma. *Haematologica*, 102, 1247-1257.
- NOH, S., KIM, D. H., JUNG, W. H. & KOO, J. S. 2014. Expression levels of serine/glycine metabolism-related proteins in triple negative breast cancer tissues. *Tumour Biol*, 35, 4457-68.
- NONAKA, H., NAKANISHI, Y., KUNO, S., OTA, T., MOCHIDOME, K., SAITO, Y., SUGIHARA, F., TAKAKUSAGI, Y., AOKI, I., NAGATOISHI, S., TSUMOTO, K. & SANDO, S. 2019. Design strategy for serine hydroxymethyltransferase probes based on retro-aldol-type reaction. *Nat Commun*, 10, 876.
- NORTHCOTT, P. A., BUCHHALTER, I., MORRISSY, A. S., HOVESTADT, V., WEISCHENFELDT, J., EHRENBERGER, T., GROBNER, S., SEGURAWANG, M., ZICHNER, T., RUDNEVA, V. A., WARNATZ, H. J., SIDIROPOULOS, N., PHILLIPS, A. H., SCHUMACHER, S., KLEINHEINZ, K., WASZAK, S. M., ERKEK, S., JONES, D. T. W., WORST, B. C., KOOL, M., ZAPATKA, M., JAGER, N., CHAVEZ, L., HUTTER, B., BIEG, M., PARAMASIVAM, N., HEINOLD, M., GU, Z., ISHAQUE, N., JAGERSCHMIDT, C., IMBUSCH, C. D., JUGOLD, A., HUBSCHMANN, D., RISCH, T., AMSTISLAVSKIY, V., GONZALEZ, F. G. R., WEBER, U. D., WOLF, S., ROBINSON, G. W., ZHOU, X., WU, G., FINKELSTEIN, D., LIU, Y., CAVALLI, F. M. G., LUU, B., RAMASWAMY, V., WU, X., KOSTER, J., RYZHOVA, M., CHO, Y. J., POMEROY, S. L., HEROLD-MENDE, C., SCHUHMANN, M., EBINGER, M., LIAU, L. M., MORA, J., MCLENDON, R. E., JABADO, N., KUMABE, T., CHUAH, E., MA, Y., MOORE, R. A., MUNGALL, A. J., MUNGALL, K. L., THIESSEN, N., TSE, K., WONG, T., JONES, S. J. M., WITT, O., MILDE, T., VON DEIMLING, A., CAPPER, D., KORSHUNOV, A., YASPO, M. L., KRIWACKI, R., GAJJAR, A., ZHANG, J., BEROUKHIM, R., FRAENKEL, E., KORBEL, J. O., BRORS, B., SCHLESNER, M., EILS, R., MARRA, M. A., PFISTER, S. M., TAYLOR, M. D. & LICHTER, P. 2017. The whole-genome landscape of medulloblastoma subtypes. *Nature*, 547, 311-317.
- NORTHCOTT, P. A., KORSHUNOV, A., PFISTER, S. M. & TAYLOR, M. D. 2012a. The clinical implications of medulloblastoma subgroups. *Nat Rev Neurol*, 8, 340-51.
- NORTHCOTT, P. A., KORSHUNOV, A., WITT, H., HIELSCHER, T., EBERHART, C. G., MACK, S., BOUFFET, E., CLIFFORD, S. C., HAWKINS, C. E., FRENCH, P., RUTKA, J. T., PFISTER, S. & TAYLOR, M. D. 2011. Medulloblastoma comprises four distinct molecular variants. *J Clin Oncol*, 29, 1408-14.
- NORTHCOTT, P. A., ROBINSON, G. W., KRATZ, C. P., MABBOTT, D. J., POMEROY, S. L., CLIFFORD, S. C., RUTKOWSKI, S., ELLISON, D. W., MALKIN, D., TAYLOR, M. D., GAJJAR, A. & PFISTER, S. M. 2019. Medulloblastoma. *Nat Rev Dis Primers*, 5, 11.
- NORTHCOTT, P. A., SHIH, D. J., PEACOCK, J., GARZIA, L., MORRISSY, A. S., ZICHNER, T., STUTZ, A. M., KORSHUNOV, A., REIMAND, J., SCHUMACHER, S. E., BEROUKHIM, R., ELLISON, D. W., MARSHALL, C. R., LIONEL, A. C., MACK, S., DUBUC, A., YAO, Y., RAMASWAMY, V.,

- LUU, B., ROLIDER, A., CAVALLI, F. M., WANG, X., REMKE, M., WU, X., CHIU, R. Y., CHU, A., CHUAH, E., CORBETT, R. D., HOAD, G. R., JACKMAN, S. D., LI, Y., LO, A., MUNGALL, K. L., NIP, K. M., QIAN, J. Q., RAYMOND, A. G., THIESSEN, N. T., VARHOL, R. J., BIROL, I., MOORE, R. A., MUNGALL, A. J., HOLT, R., KAWAUCHI, D., ROUSSEL, M. F., KOOL, M., JONES, D. T., WITT, H., FERNANDEZ, L. A., KENNEY, A. M., WECHSLER-REYA, R. J., DIRKS, P., AVIV, T., GRAJKOWSKA, W. A., PEREK-POLNIK, M., HABERLER, C. C., DELATTRE, O., REYNAUD, S. S., DOZ, F. F., PERNET-FATTET, S. S., CHO, B. K., KIM, S. K., WANG, K. C., SCHEURLLEN, W., EBERHART, C. G., FEVRE-MONTANGE, M., JOUVET, A., POLLACK, I. F., FAN, X., MURASZKO, K. M., GILLESPIE, G. Y., DI ROCCO, C., MASSIMI, L., MICHIELS, E. M., KLOOSTERHOF, N. K., FRENCH, P. J., KROS, J. M., OLSON, J. M., ELLENBOGEN, R. G., ZITTERBART, K., KREN, L., THOMPSON, R. C., COOPER, M. K., LACH, B., MCLENDON, R. E., BIGNER, D. D., FONTEBASSO, A., ALBRECHT, S., JABADO, N., LINDSEY, J. C., BAILEY, S., GUPTA, N., WEISS, W. A., BOGNAR, L., KLEKNER, A., VAN METER, T. E., KUMABE, T., TOMINAGA, T., ELBABAA, S. K., LEONARD, J. R., RUBIN, J. B., et al. 2012b. Subgroup-specific structural variation across 1,000 medulloblastoma genomes. *Nature*, 488, 49-56.
- O'BRIEN, J. S. & SAMPSON, E. L. 1965. Lipid composition of the normal human brain: gray matter, white matter, and myelin. *J Lipid Res*, 6, 537-44.
- OLIVIER, M., HOLLSTEIN, M. & HAINAUT, P. 2010. TP53 mutations in human cancers: origins, consequences, and clinical use. *Cold Spring Harb Perspect Biol*, 2, a001008.
- ORTMAYR, K., DUBUIS, S. & ZAMPIERI, M. 2019. Metabolic profiling of cancer cells reveals genome-wide crosstalk between transcriptional regulators and metabolism. *Nat Commun*, 10, 1841.
- OSTROM, Q. T., ADEL FAHMIDEH, M., COTE, D. J., MUSKENS, I. S., SCHRAW, J. M., SCHEURER, M. E. & BONDY, M. L. 2019. Risk factors for childhood and adult primary brain tumors. *Neuro Oncol*, 21, 1357-1375.
- OSTROM, Q. T., GITTLEMAN, H., TRUITT, G., BOSCIA, A., KRUCHKO, C. & BARNHOLTZ-SLOAN, J. S. 2018. CBTRUS Statistical Report: Primary Brain and Other Central Nervous System Tumors Diagnosed in the United States in 2011-2015. *Neuro Oncol*, 20, iv1-iv86.
- OUDARD, S., ARVELO, F., MICCOLI, L., APIOU, F., DUTRILLAUX, A. M., POISSON, M., DUTRILLAUX, B. & POUPON, M. F. 1996. High glycolysis in gliomas despite low hexokinase transcription and activity correlated to chromosome 10 loss. *British Journal of Cancer*, 74, 839-845.
- PACKER, R. J. 2008. Childhood brain tumors: accomplishments and ongoing challenges. *J Child Neurol*, 23, 1122-7.
- PACOLD, M. E., BRIMACOMBE, K. R., CHAN, S. H., ROHDE, J. M., LEWIS, C. A., SWIER, L. J., POSSEMATO, R., CHEN, W. W., SULLIVAN, L. B., FISKE, B. P., CHO, S., FREINKMAN, E., BIRSOY, K., ABU-REMAILEH, M., SHAUL, Y. D., LIU, C. M., ZHOU, M., KOH, M. J., CHUNG, H., DAVIDSON, S. M., LUENGO, A., WANG, A. Q., XU, X., YASGAR, A., LIU, L., RAI, G., WESTOVER, K. D., VANDER HEIDEN, M. G., SHEN, M., GRAY, N. S., BOXER, M. B. & SABATINI, D. M. 2016. A PHGDH inhibitor reveals coordination of serine synthesis and one-carbon unit fate. *Nat Chem Biol*, 12, 452-8.
- PALM, W. & THOMPSON, C. B. 2017. Nutrient acquisition strategies of mammalian cells. *Nature*, 546, 234-242.

- PALOMERO, T., LIM, W. K., ODOM, D. T., SULIS, M. L., REAL, P. J., MARGOLIN, A., BARNES, K. C., O'NEIL, J., NEUBERG, D., WENG, A. P., ASTER, J. C., SIGAUX, F., SOULIER, J., LOOK, A. T., YOUNG, R. A., CALIFANO, A. & FERRANDO, A. A. 2006. NOTCH1 directly regulates c-MYC and activates a feed-forward-loop transcriptional network promoting leukemic cell growth. *Proc Natl Acad Sci U S A*, 103, 18261-6.
- PAN, Z. & RAFTERY, D. 2007. Comparing and combining NMR spectroscopy and mass spectrometry in metabolomics. *Analytical and Bioanalytical Chemistry*, 387, 525-527.
- PANIGRAHY, A., KRIEGER, M. D., GONZALEZ-GOMEZ, I., LIU, X., MCCOMB, J. G., FINLAY, J. L., NELSON, M. D., JR., GILLES, F. H. & BLUML, S. 2006. Quantitative short echo time 1H-MR spectroscopy of untreated pediatric brain tumors: preoperative diagnosis and characterization. *AJNR Am J Neuroradiol*, 27, 560-72.
- PARK, J. H., VITHAYATHIL, S., KUMAR, S., SUNG, P. L., DOBROLECKI, L. E., PUTLURI, V., BHAT, V. B., BHOWMIK, S. K., GUPTA, V., ARORA, K., WU, D. L., TSOUKO, E., ZHANG, Y. Q., MAITY, S., DONTI, T. R., GRAHAM, B. H., FRIGO, D. E., COARFA, C., YOTNDA, P., PUTLURI, N., SREEKUMAR, A., LEWIS, M. T., CREIGHTON, C. J., WONG, L. J. C. & KAIPPARETTU, B. A. 2016. Fatty Acid Oxidation-Driven Src Links Mitochondrial Energy Reprogramming and Oncogenic Properties in Triple-Negative Breast Cancer. *Cell Reports*, 14, 2154-2165.
- PATRA, K. C. & HAY, N. 2014. The pentose phosphate pathway and cancer. *Trends in biochemical sciences*, 39, 347-354.
- PATRA, K. C., WANG, Q., BHASKAR, P. T., MILLER, L., WANG, Z., WHEATON, W., CHANDEL, N., LAAKSO, M., MULLER, W. J., ALLEN, E. L., JHA, A. K., SMOLEN, G. A., CLASQUIN, M. F., ROBEY, B. & HAY, N. 2013. Hexokinase 2 is required for tumor initiation and maintenance and its systemic deletion is therapeutic in mouse models of cancer. *Cancer Cell*, 24, 213-228.
- PERRY, A. & WESSELING, P. 2016. Histologic classification of gliomas. *Handb Clin Neurol*, 134, 71-95.
- PFISTER, S. M., KORSHUNOV, A., KOOL, M., HASSELBLATT, M., EBERHART, C. & TAYLOR, M. D. 2010. Molecular diagnostics of CNS embryonal tumors. *Acta Neuropathol*, 120, 553-66.
- PHILLIPS, H. S., KHARBANDA, S., CHEN, R. H., FORREST, W. F., SORIANO, R. H., WU, T. D., MISRA, A., NIGRO, J. M., COLMAN, H., SOROCEANU, L., WILLIAMS, P. M., MODRUSAN, Z., FEUERSTEIN, B. G. & ALDAPE, K. 2006. Molecular subclasses of high-grade glioma predict prognosis, delineate a pattern of disease progression, and resemble stages in neurogenesis. *Cancer Cell*, 9, 157-173.
- PIKE, L. S., SMIFT, A. L., CROTEAU, N. J., FERRICK, D. A. & WU, M. 2011. Inhibition of fatty acid oxidation by etomoxir impairs NADPH production and increases reactive oxygen species resulting in ATP depletion and cell death in human glioblastoma cells. *Biochimica Et Biophysica Acta-Bioenergetics*, 1807, 726-734.
- PINHEIRO, C., LONGATTO-FILHO, A., AZEVEDO-SILVA, J., CASAL, M., SCHMITT, F. C. & BALTAZAR, F. 2012. Role of monocarboxylate transporters in human cancers: state of the art. *J Bioenerg Biomembr*, 44, 127-39.
- PIZER, B. & CLIFFORD, S. 2008. Medulloblastoma: new insights into biology and treatment. *Arch Dis Child Educ Pract Ed*, 93, 137-44.

- PIZER, B. L. & CLIFFORD, S. C. 2009. The potential impact of tumour biology on improved clinical practice for medulloblastoma: progress towards biologically driven clinical trials. *Br J Neurosurg*, 23, 364-75.
- POLLACK, I. F., FINKELSTEIN, S. D., WOODS, J., BURNHAM, J., HOLMES, E. J., HAMILTON, R. L., YATES, A. J., BOYETT, J. M., FINLAY, J. L. & SPOSTO, R. 2002. Expression of p53 and prognosis in children with malignant gliomas. *N Engl J Med*, 346, 420-7.
- POLLARD, P. J., BRIERE, J. J., ALAM, N. A., BARWELL, J., BARCLAY, E., WORTHAM, N. C., HUNT, T., MITCHELL, M., OLPIN, S., MOAT, S. J., HARGREAVES, I. P., HEALES, S. J., CHUNG, Y. L., GRIFFITHS, J. R., DALGLEISH, A., MCGRATH, J. A., GLEESON, M. J., HODGSON, S. V., POULSOM, R., RUSTIN, P. & TOMLINSON, I. P. 2005. Accumulation of Krebs cycle intermediates and over-expression of HIF1alpha in tumours which result from germline FH and SDH mutations. *Hum Mol Genet*, 14, 2231-9.
- POMEROY, S. L., TAMAYO, P., GAASENBEEK, M., STURLA, L. M., ANGELO, M., MCLAUGHLIN, M. E., KIM, J. Y., GOUMNEROVA, L. C., BLACK, P. M., LAU, C., ALLEN, J. C., ZAGZAG, D., OLSON, J. M., CURRAN, T., WETMORE, C., BIEGEL, J. A., POGGIO, T., MUKHERJEE, S., RIFKIN, R., CALIFANO, A., STOLOVITZKY, G., LOUIS, D. N., MESIROV, J. P., LANDER, E. S. & GOLUB, T. R. 2002. Prediction of central nervous system embryonal tumour outcome based on gene expression. *Nature*, 415, 436-42.
- POMPE, R. S., VON BUEREN, A. O., MYNAREK, M., VON HOFF, K., FRIEDRICH, C., KWIECIEN, R., TREULIEB, W., LINDOW, C., DEINLEIN, F., FLEISCHHACK, G., KUEHL, J. & RUTKOWSKI, S. 2015. Intraventricular methotrexate as part of primary therapy for children with infant and/or metastatic medulloblastoma: Feasibility, acute toxicity and evidence for efficacy. *Eur J Cancer*, 51, 2634-42.
- POSSEMATO, R., MARKS, K. M., SHAUL, Y. D., PACOLD, M. E., KIM, D., BIRSOY, K., SETHUMADHAVAN, S., WOO, H. K., JANG, H. G., JHA, A. K., CHEN, W. W., BARRETT, F. G., STRANSKY, N., TSUN, Z. Y., COWLEY, G. S., BARRETINA, J., KALAANY, N. Y., HSU, P. P., OTTINA, K., CHAN, A. M., YUAN, B., GARRAWAY, L. A., ROOT, D. E., MINO-KENUDSON, M., BRACHTEL, E. F., DRIGGERS, E. M. & SABATINI, D. M. 2011. Functional genomics reveal that the serine synthesis pathway is essential in breast cancer. *Nature*, 476, 346-50.
- QING, G., LI, B., VU, A., SKULI, N., WALTON, Z. E., LIU, X., MAYES, P. A., WISE, D. R., THOMPSON, C. B., MARIS, J. M., HOGARTY, M. D. & SIMON, M. C. 2012. ATF4 regulates MYC-mediated neuroblastoma cell death upon glutamine deprivation. *Cancer cell*, 22, 631-644.
- RAEZ, L. E., PAPADOPOULOS, K., RICART, A. D., CHIOREAN, E. G., DIPAOLO, R. S., STEIN, M. N., ROCHA LIMA, C. M., SCHLESSELMAN, J. J., TOLBA, K., LANGMUIR, V. K., KROLL, S., JUNG, D. T., KURTOGLU, M., ROSENBLATT, J. & LAMPIDIS, T. J. 2013. A phase I dose-escalation trial of 2-deoxy-D-glucose alone or combined with docetaxel in patients with advanced solid tumors. *Cancer Chemother Pharmacol*, 71, 523-30.
- RAJARAMAN, P., MELIN, B. S., WANG, Z., MCKEAN-COWDIN, R., MICHAUD, D. S., WANG, S. S., BONDY, M., HOULSTON, R., JENKINS, R. B., WRENSCH, M., YEAGER, M., AHLBOM, A., ALBANES, D., ANDERSSON, U., FREEMAN, L. E. B., BURING, J. E., BUTLER, M. A., BRAGANZA, M., CARREON, T., FEYCHTING, M., FLEMING, S. J., GAPSTUR, S. M., GAZIANO, J. M., GILES, G. G., HALLMANS, G., HENRIKSSON, R., HOFFMAN-BOLTON, J., INSKIP, P. D., JOHANSEN, C., KITAHARA, C. M.,

- LATHROP, M., LIU, C., LE MARCHAND, L., LINET, M. S., LONN, S., PETERS, U., PURDUE, M. P., ROTHMAN, N., RUDER, A. M., SANSON, M., SESSO, H. D., SEVERI, G., SHU, X.-O., SIMON, M., STAMPFER, M., STEVENS, V. L., VISVANATHAN, K., WHITE, E., WOLK, A., ZELENIUCH-JACQUOTTE, A., ZHENG, W., DECKER, P., ENCISO-MORA, V., FRIDLEY, B., GAO, Y.-T., KOSEL, M., LACHANCE, D. H., LAU, C., RICE, T., SWERDLOW, A., WIEMELS, J. L., WIENCKE, J. K., SHETE, S., XIANG, Y.-B., XIAO, Y., HOOVER, R. N., FRAUMENI, J. F., JR., CHATTERJEE, N., HARTGE, P. & CHANOCK, S. J. 2012. Genome-wide association study of glioma and meta-analysis. *Human genetics*, 131, 1877-1888.
- RAJNEESH, K. F. & BINDER, D. K. 2009. Tumor-associated epilepsy. *Neurosurgical Focus*, 27.
- RAMASWAMY, V., REMKE, M., BOUFFET, E., BAILEY, S., CLIFFORD, S. C., DOZ, F., KOOL, M., DUFOUR, C., VASSAL, G., MILDE, T., WITT, O., VON HOFF, K., PIETSCH, T., NORTHCOTT, P. A., GAJJAR, A., ROBINSON, G. W., PADOVANI, L., ANDRE, N., MASSIMINO, M., PIZER, B., PACKER, R., RUTKOWSKI, S., PFISTER, S. M., TAYLOR, M. D. & POMEROY, S. L. 2016. Risk stratification of childhood medulloblastoma in the molecular era: the current consensus. *Acta Neuropathol*, 131, 821-31.
- RAMBOLD, A. S., COHEN, S. & LIPPINCOTT-SCHWARTZ, J. 2015. Fatty Acid Trafficking in Starved Cells: Regulation by Lipid Droplet Lipolysis, Autophagy, and Mitochondrial Fusion Dynamics. *Developmental Cell*, 32, 678-692.
- RAN, F. A., HSU, P. D., WRIGHT, J., AGARWALA, V., SCOTT, D. A. & ZHANG, F. 2013. Genome engineering using the CRISPR-Cas9 system. *Nat Protoc*, 8, 2281-2308.
- RANDLE, P. J. 1981. CITATION CLASSIC - THE GLUCOSE FATTY-ACID CYCLE - ITS ROLE IN INSULIN SENSITIVITY AND THE METABOLIC DISTURBANCES OF DIABETES-MELLITUS. *Current Contents/Life Sciences*, 24-24.
- RANDLE, P. J. 1998. Regulatory interactions between lipids and carbohydrates: The glucose fatty acid cycle after 35 years. *Diabetes-Metabolism Reviews*, 14, 263-283.
- RANJAN, P., ANATHY, V., BURCH, P. M., WEIRATHER, K., LAMBETH, J. D. & HEINTZ, N. H. 2006. Redox-dependent expression of cyclin D1 and cell proliferation by Nox1 in mouse lung epithelial cells. *Antioxid Redox Signal*, 8, 1447-59.
- RAUSCH, T., JONES, D. T., ZAPATKA, M., STUTZ, A. M., ZICHNER, T., WEISCHENFELDT, J., JAGER, N., REMKE, M., SHIH, D., NORTHCOTT, P. A., PFAFF, E., TICA, J., WANG, Q., MASSIMI, L., WITT, H., BENDER, S., PLEIER, S., CIN, H., HAWKINS, C., BECK, C., VON DEIMLING, A., HANS, V., BRORS, B., EILS, R., SCHEURLIN, W., BLAKE, J., BENES, V., KULOZIK, A. E., WITT, O., MARTIN, D., ZHANG, C., PORAT, R., MERINO, D. M., WASSERMAN, J., JABADO, N., FONTEBASSO, A., BULLINGER, L., RUCKER, F. G., DOHNER, K., DOHNER, H., KOSTER, J., MOLENAAR, J. J., VERSTEEG, R., KOOL, M., TABORI, U., MALKIN, D., KORSHUNOV, A., TAYLOR, M. D., LICHTER, P., PFISTER, S. M. & KORBEL, J. O. 2012. Genome sequencing of pediatric medulloblastoma links catastrophic DNA rearrangements with TP53 mutations. *Cell*, 148, 59-71.
- RAZAK, M. A., BEGUM, P. S., VISWANATH, B. & RAJAGOPAL, S. 2017. Multifarious Beneficial Effect of Nonessential Amino Acid, Glycine: A Review. *Oxid Med Cell Longev*, 2017, 1716701.

- REID, M. A., ALLEN, A. E., LIU, S., LIBERTI, M. V., LIU, P., LIU, X., DAI, Z., GAO, X., WANG, Q., LIU, Y., LAI, L. & LOCASALE, J. W. 2018. Serine synthesis through PHGDH coordinates nucleotide levels by maintaining central carbon metabolism. *Nat Commun*, 9, 5442.
- REILLY, P. T. & MAK, T. W. 2012. Molecular Pathways: Tumor Cells Co-opt the Brain-Specific Metabolism Gene CPT1C to Promote Survival. *Clinical Cancer Research*, 18, 5850-5855.
- REZNIK, E., LUNA, A., AKSOY, B. A., LIU, E. M., LA, K., OSTROVNAYA, I., CREIGHTON, C. J., HAKIMI, A. A. & SANDER, C. 2018. A Landscape of Metabolic Variation across Tumor Types. *Cell Syst*, 6, 301-313.e3.
- RICCIARDI, M. R., MIRABILII, S., ALLEGRETTI, M., LICCHETTA, R., CALARCO, A., TORRISI, M. R., FOA, R., NICOLAI, R., PELUSO, G. & TAFURI, A. 2015. Targeting the leukemia cell metabolism by the CPT1a inhibition: functional preclinical effects in leukemias. *Blood*, 126, 1925-1929.
- RIESS, C., SHOKRAIE, F., CLASSEN, C. F., KREIKEMEYER, B., FIEDLER, T., JUNGHANSS, C. & MALETZKI, C. 2018. Arginine-Depleting Enzymes - An Increasingly Recognized Treatment Strategy for Therapy-Refractory Malignancies. *Cell Physiol Biochem*, 51, 854-870.
- ROBINSON, C. G., PALOMO, J. M., RAHMATHULLA, G., MCGRAW, M., DONZE, J., LIU, L. & VOGELBAUM, M. A. 2010. Effect of alternative temozolomide schedules on glioblastoma O-6-methylguanine-DNA methyltransferase activity and survival. *British Journal of Cancer*, 103, 498-504.
- ROBINSON, G., PARKER, M., KRANENBURG, T. A., LU, C., CHEN, X., DING, L., PHOENIX, T. N., HEDLUND, E., WEI, L., ZHU, X., CHALHOUB, N., BAKER, S. J., HUETHER, R., KRIWACKI, R., CURLEY, N., THIRUVENKATAM, R., WANG, J., WU, G., RUSCH, M., HONG, X., BECKSFORT, J., GUPTA, P., MA, J., EASTON, J., VADODARIA, B., ONAR-THOMAS, A., LIN, T., LI, S., POUNDS, S., PAUGH, S., ZHAO, D., KAWAUCHI, D., ROUSSEL, M. F., FINKELSTEIN, D., ELLISON, D. W., LAU, C. C., BOUFFET, E., HASSALL, T., GURURANGAN, S., COHN, R., FULTON, R. S., FULTON, L. L., DOOLING, D. J., OCHOA, K., GAJJAR, A., MARDIS, E. R., WILSON, R. K., DOWNING, J. R., ZHANG, J. & GILBERTSON, R. J. 2012. Novel mutations target distinct subgroups of medulloblastoma. *Nature*, 488, 43-8.
- ROHRIG, F. & SCHULZE, A. 2016. The multifaceted roles of fatty acid synthesis in cancer. *Nature Reviews Cancer*, 16, 732-749.
- ROLFE, D. F. & BROWN, G. C. 1997. Cellular energy utilization and molecular origin of standard metabolic rate in mammals. *Physiol Rev*, 77, 731-58.
- RON, E., MODAN, B., BOICE, J. D., JR., ALFANDARY, E., STOVALL, M., CHETRIT, A. & KATZ, L. 1988. Tumors of the brain and nervous system after radiotherapy in childhood. *N Engl J Med*, 319, 1033-9.
- ROS, S. & SCHULZE, A. 2013. Balancing glycolytic flux: the role of 6-phosphofructo-2-kinase/fructose 2,6-bisphosphatases in cancer metabolism. *Cancer Metab*, 1, 8.
- ROSSO, S. B. & INESTROSA, N. C. 2013. WNT signaling in neuronal maturation and synaptogenesis. *Front Cell Neurosci*, 7, 103.
- ROUSSEL, M. F. & ROBINSON, G. W. 2013. Role of MYC in Medulloblastoma. *Cold Spring Harb Perspect Med*, 3.
- ROUSSEL, M. F. & STRIPAY, J. L. 2018. Epigenetic Drivers in Pediatric Medulloblastoma. *Cerebellum*, 17, 28-36.
- RUVINSKY, I., SHARON, N., LERER, T., COHEN, H., STOLOVICH-RAIN, M., NIR, T., DOR, Y., ZISMAN, P. & MEYUHAS, O. 2005. Ribosomal protein S6 phosphorylation is a determinant of cell size and glucose homeostasis. *Genes Dev*, 19, 2199-211.

- SAMUDIO, I., HARMANCEY, R., FIEGL, M., KANTARJIAN, H., KONOPLEVA, M., KORCHIN, B., KALUARACHCHI, K., BORNMANN, W., DUVVURI, S., TAEGTMEYER, H. & ANDREEFF, M. 2010. Pharmacologic inhibition of fatty acid oxidation sensitizes human leukemia cells to apoptosis induction. *Journal of Clinical Investigation*, 120, 142-156.
- SAMUELSEN, S. O., BAKKETEIG, L. S., TRETLI, S., JOHANNESSEN, T. B. & MAGNUS, P. 2006. Head circumference at birth and risk of brain cancer in childhood: a population-based study. *Lancet Oncol*, 7, 39-42.
- SARASWATHY, S., CRAWFORD, F. W., LAMBORN, K. R., PIRZKALL, A., CHANG, S., CHA, S. & NELSON, S. J. 2009. Evaluation of MR markers that predict survival in patients with newly diagnosed GBM prior to adjuvant therapy. *Journal of Neuro-Oncology*, 91, 69-81.
- SARKAR, C., PRAMANIK, P., KARAK, A. K., MUKHOPADHYAY, P., SHARMA, M. C., SINGH, V. P. & MEHTA, V. S. 2002. Are childhood and adult medulloblastomas different? A comparative study of clinicopathological features, proliferation index and apoptotic index. *J Neurooncol*, 59, 49-61.
- SATTLER, U. G. A., MEYER, S. S., QUENNET, V., HOERNER, C., KNOERZER, H., FABIAN, C., YAROMINA, A., ZIPS, D., WALENTA, S., BAUMANN, M. & MUELLER-KLIESER, W. 2010. Glycolytic metabolism and tumour response to fractionated irradiation. *Radiotherapy and Oncology*, 94, 102-109.
- SCHAUB, F. X., DHANKANI, V., BERGER, A. C., TRIVEDI, M., RICHARDSON, A. B., SHAW, R., ZHAO, W., ZHANG, X., VENTURA, A., LIU, Y., AYER, D. E., HURLIN, P. J., CHERNIACK, A. D., EISENMAN, R. N., BERNARD, B., GRANDORI, C., CAESAR-JOHNSON, S. J., DEMCHOK, J. A., FELAU, I., KASAPI, M., FERGUSON, M. L., HUTTER, C. M., SOFIA, H. J., TARNUZZER, R., WANG, Z., YANG, L., ZENKLUSEN, J. C., ZHANG, J., CHUDAMANI, S., LIU, J., LOLLA, L., NARESH, R., PIHL, T., SUN, Q., WAN, Y., WU, Y., CHO, J., DEFREITAS, T., FRAZER, S., GEHLENBORG, N., GETZ, G., HEIMAN, D. I., KIM, J., LAWRENCE, M. S., LIN, P., MEIER, S., NOBLE, M. S., SAKSENA, G., VOET, D., ZHANG, H., BERNARD, B., CHAMBWE, N., DHANKANI, V., KNIJNENBURG, T., KRAMER, R., LEINONEN, K., LIU, Y., MILLER, M., REYNOLDS, S., SHMULEVICH, I., THORSSON, V., ZHANG, W., AKBANI, R., BROOM, B. M., HEGDE, A. M., JU, Z., KANCHI, R. S., KORKUT, A., LI, J., LIANG, H., LING, S., LIU, W., LU, Y., MILLS, G. B., NG, K.-S., RAO, A., RYAN, M., WANG, J., WEINSTEIN, J. N., ZHANG, J., ABESHOUSE, A., ARMENIA, J., CHAKRAVARTY, D., CHATILA, W. K., DE BRUIJN, I., GAO, J., GROSS, B. E., HEINS, Z. J., KUNDRU, R., LA, K., LADANYI, M., LUNA, A., NISSAN, M. G., OCHOA, A., PHILLIPS, S. M., REZNIK, E., SANCHEZ-VEGA, F., SANDER, C., SCHULTZ, N., SHERIDAN, R., et al. 2018. Pan-cancer Alterations of the MYC Oncogene and Its Proximal Network across the Cancer Genome Atlas. *Cell Systems*, 6, 282-300.e2.
- SCHLAEPFER, I. R., RIDER, L., RODRIGUES, L. U., GIJON, M. A., PAC, C. T., ROMERO, L., CIMIC, A., SIRINTRAPUN, S. J., GLODE, L. M., ECKEL, R. H. & CRAMER, S. D. 2014. Lipid Catabolism via CPT1 as a Therapeutic Target for Prostate Cancer. *Molecular Cancer Therapeutics*, 13, 2361-2371.
- SCHOLL, M., DAMIAN, A. & ENGLER, H. 2014. Fluorodeoxyglucose PET in Neurology and Psychiatry. *PET Clin*, 9, 371-90, v.
- SCHREIBER-AGUS, N. & DEPINHO, R. A. 1998. Repression by the Mad(Mxi1)-Sin3 complex. *Bioessays*, 20, 808-18.
- SCHWALBE, E. C., LINDSEY, J. C., NAKJANG, S., CROSIER, S., SMITH, A. J., HICKS, D., RAFIEE, G., HILL, R. M., ILIASOVA, A., STONE, T., PIZER, B.,

- MICHALSKI, A., JOSHI, A., WHARTON, S. B., JACQUES, T. S., BAILEY, S., WILLIAMSON, D. & CLIFFORD, S. C. 2017a. Novel molecular subgroups for clinical classification and outcome prediction in childhood medulloblastoma: a cohort study. *Lancet Oncology*, 18, 958-971.
- SCHWALBE, E. C., LINDSEY, J. C., NAKJANG, S., CROSIER, S., SMITH, A. J., HICKS, D., RAFIEE, G., HILL, R. M., ILIASOVA, A., STONE, T., PIZER, B., MICHALSKI, A., JOSHI, A., WHARTON, S. B., JACQUES, T. S., BAILEY, S., WILLIAMSON, D. & CLIFFORD, S. C. 2017b. Novel molecular subgroups for clinical classification and outcome prediction in childhood medulloblastoma: a cohort study. *Lancet Oncol*, 18, 958-971.
- SCHWARZENBOCK, S., SOUVATZOGLOU, M. & KRAUSE, B. J. 2012. Choline PET and PET/CT in Primary Diagnosis and Staging of Prostate Cancer. *Theranostics*, 2, 318-30.
- SCIACOVELLI, M. & FREZZA, C. 2016. Oncometabolites: Unconventional triggers of oncogenic signalling cascades. *Free Radic Biol Med*, 100, 175-181.
- SEARS, R. C. 2004. The life cycle of C-myc: from synthesis to degradation. *Cell Cycle*, 3, 1133-7.
- SELA, M. A., ARMOUR, S. M., MACKENZIE, E. D., BOULAHBEL, H., WATSON, D. G., MANSFIELD, K. D., PAN, Y., SIMON, M. C., THOMPSON, C. B. & GOTTLIEB, E. 2005. Succinate links TCA cycle dysfunction to oncogenesis by inhibiting HIF- α prolyl hydroxylase. *Cancer Cell*, 7, 77-85.
- SHARMA, T., SCHWALBE, E. C., WILLIAMSON, D., SILL, M., HOVESTADT, V., MYNAREK, M., RUTKOWSKI, S., ROBINSON, G. W., GAJJAR, A., CAVALLI, F., RAMASWAMY, V., TAYLOR, M. D., LINDSEY, J. C., HILL, R. M., JAGER, N., KORSHUNOV, A., HICKS, D., BAILEY, S., KOOL, M., CHAVEZ, L., NORTHCOTT, P. A., PFISTER, S. M. & CLIFFORD, S. C. 2019. Second-generation molecular subgrouping of medulloblastoma: an international meta-analysis of Group 3 and Group 4 subtypes. *Acta Neuropathol*, 138, 309-326.
- SHEN, X., VOETS, N. L., LARKIN, S. J., DE PENNINGTON, N., PLAHA, P., STACEY, R., MCCULLAGH, J. S. O., SCHOFIELD, C. J., CLARE, S., JEZZARD, P., CADOUX-HUDSON, T., ANSORGE, O. & EMIR, U. E. 2019. A Noninvasive Comparison Study between Human Gliomas with IDH1 and IDH2 Mutations by MR Spectroscopy. *Metabolites*, 9.
- SHIBAO, S., MINAMI, N., KOIKE, N., FUKUI, N., YOSHIDA, K., SAYA, H. & SAMPETREAN, O. 2018. Metabolic heterogeneity and plasticity of glioma stem cells in a mouse glioblastoma model. *Neuro Oncol*, 20, 343-354.
- SHICHIRI, M., HANSON, K. D. & SEDIVY, J. M. 1993. Effects of c-myc expression on proliferation, quiescence, and the G0 to G1 transition in nontransformed cells. *Cell Growth Differ*, 4, 93-104.
- SHIM, H., CHUN, Y. S., LEWIS, B. C. & DANG, C. V. 1998. A unique glucose-dependent apoptotic pathway induced by c-Myc. *Proceedings of the National Academy of Sciences of the United States of America*, 95, 1511-1516.
- SHIM, H., DOLDE, C., LEWIS, B. C., WU, C. S., DANG, G., JUNGSMANN, R. A., DALLA-FAVERA, R. & DANG, C. V. 1997. c-Myc transactivation of LDH-A: implications for tumor metabolism and growth. *Proc Natl Acad Sci U S A*, 94, 6658-63.
- SILVERA, D., FORMENTI, S. C. & SCHNEIDER, R. J. 2010. Translational control in cancer. *Nat Rev Cancer*, 10, 254-66.
- SIU, I. M., LAL, A., BLANKENSHIP, J. R., ALDOSARI, N. & RIGGINS, G. J. 2003. c-Myc Promoter Activation in Medulloblastoma. *Cancer Research*, 63, 4773.
- SMITH, K. N., SINGH, A. M. & DALTON, S. 2010. Myc represses primitive endoderm differentiation in pluripotent stem cells. *Cell Stem Cell*, 7, 343-54.

- SNELL, K. 1984. Enzymes of serine metabolism in normal, developing and neoplastic rat tissues. *Adv Enzyme Regul*, 22, 325-400.
- SNELL, K., NATSUMEDA, Y. & WEBER, G. 1987. The modulation of serine metabolism in hepatoma 3924A during different phases of cellular proliferation in culture. *Biochem J*, 245, 609-12.
- SNELL, K. & WEBER, G. 1986. Enzymic imbalance in serine metabolism in rat hepatomas. *Biochem J*, 233, 617-20.
- SOM, P., ATKINS, H. L., BANDOYPADHYAY, D., FOWLER, J. S., MACGREGOR, R. R., MATSUI, K., OSTER, Z. H., SACKER, D. F., SHIUE, C. Y., TURNER, H., WAN, C. N., WOLF, A. P. & ZABINSKI, S. V. 1980. A fluorinated glucose analog, 2-fluoro-2-deoxy-D-glucose (F-18): nontoxic tracer for rapid tumor detection. *J Nucl Med*, 21, 670-5.
- SON, J., LYSSIOTIS, C. A., YING, H., WANG, X., HUA, S., LIGORIO, M., PERERA, R. M., FERRONE, C. R., MULLARKY, E., SHYH-CHANG, N., KANG, Y., FLEMING, J. B., BARDEESY, N., ASARA, J. M., HAIGIS, M. C., DEPINHO, R. A., CANTLEY, L. C. & KIMMELMAN, A. C. 2013. Glutamine supports pancreatic cancer growth through a KRAS-regulated metabolic pathway. *Nature*, 496, 101-5.
- SPECTOR, L. G., PANKRATZ, N. & MARCOTTE, E. L. 2015. Genetic and nongenetic risk factors for childhood cancer. *Pediatric clinics of North America*, 62, 11-25.
- STEARNS, D., CHAUDHRY, A., ABEL, T. W., BURGER, P. C., DANG, C. V. & EBERHART, C. G. 2006. c-myc overexpression causes anaplasia in medulloblastoma. *Cancer Res*, 66, 673-81.
- STEIN, M., LIN, H., JEYAMOCHAN, C., DVORZHINSKI, D., GOUNDER, M., BRAY, K., EDDY, S., GOODIN, S., WHITE, E. & DIPAOLA, R. S. 2010. Targeting tumor metabolism with 2-deoxyglucose in patients with castrate-resistant prostate cancer and advanced malignancies. *Prostate*, 70, 1388-94.
- STINE, Z. E., WALTON, Z. E., ALTMAN, B. J., HSIEH, A. L. & DANG, C. V. 2015. MYC, Metabolism, and Cancer. *Cancer Discov*, 5, 1024-39.
- STOLL, E. A., CHEUNG, W., MIKHEEV, A. M., SWEET, I. R., BIELAS, J. H., ZHANG, J., ROSTOMILY, R. C. & HORNER, P. J. 2011. Aging Neural Progenitor Cells Have Decreased Mitochondrial Content and Lower Oxidative Metabolism. *Journal of Biological Chemistry*, 286, 38592-38601.
- STOLL, E. A., MAKIN, R., SWEET, I. R., TREVELYAN, A. J., MIWA, S., HORNER, P. J. & TURNBULL, D. M. 2015. Neural Stem Cells in the Adult Subventricular Zone Oxidize Fatty Acids to Produce Energy and Support Neurogenic Activity. *Stem Cells*, 33, 2306-19.
- STRAUSS, L. G. 1996. Fluorine-18 deoxyglucose and false-positive results: A major problem in the diagnostics of oncological patients. *European Journal of Nuclear Medicine*, 23, 1409-1415.
- STRICKLAND, M. & STOLL, E. A. 2017. Metabolic Reprogramming in Glioma. *Front Cell Dev Biol*, 5, 43.
- STUCKLIN, A. S. G., KUZAN-FISCHER, C. M. & TAYLOR, M. D. 2018. Medulloblastomas. In: DI ROCCO, C., PANG, D. & RUTKA, J. T. (eds.) *Textbook of Pediatric Neurosurgery*. Cham: Springer International Publishing.
- STUMMER, W., PICHLMEIER, U., MEINEL, T., WIESTLER, O. D., ZANELLA, F. & REULEN, H. J. 2006. Fluorescence-guided surgery with 5-aminolevulinic acid for resection of malignant glioma: a randomised controlled multicentre phase III trial. *Lancet Oncol*, 7, 392-401.
- STUPP, R., HEGI, M. E., MASON, W. P., VAN DEN BENT, M. J., TAPHOORN, M. J., JANZER, R. C., LUDWIN, S. K., ALLGEIER, A., FISHER, B., BELANGER, K., HAU, P., BRANDES, A. A., GIJTENBEEK, J., MAROSI, C., VECHT, C. J.,

- MOKHTARI, K., WESSELING, P., VILLA, S., EISENHAUER, E., GORLIA, T., WELLER, M., LACOMBE, D., CAIRNCROSS, J. G. & MIRIMANOFF, R. O. 2009. Effects of radiotherapy with concomitant and adjuvant temozolomide versus radiotherapy alone on survival in glioblastoma in a randomised phase III study: 5-year analysis of the EORTC-NCIC trial. *Lancet Oncol*, 10, 459-66.
- STUPP, R., MASON, W. P., VAN DEN BENT, M. J., WELLER, M., FISHER, B., TAPHOORN, M. J. B., BELANGER, K., BRANDES, A. A., MAROSI, C., BOGDAHN, U., CURSCHMANN, J., JANZER, R. C., LUDWIN, S. K., GORLIA, T., ALLGEIER, A., LACOMBE, D., CAIRNCROSS, J. G., EISENHAUER, E., MIRIMANOFF, R. O., VAN DEN WEYNGAERT, D., KAENDLER, S., KRAUSENECK, P., VINOLAS, N., VILLA, S., WURM, R. E., MAILLOT, M. H. B., SPAGNOLLI, F., KANTOR, G., MALHAIRE, J. P., RENARD, L., DE WITTE, O., SCANDOLARO, L., VECHT, C. J., MAINGON, P., LUTTERBACH, J., KOBIERSKA, A., BOLLA, M., SOUCHON, R., MITINE, C., TZUK-SHINA, T., KUTEN, A., HAFERKAMP, G., DE GREVE, J., PRIOU, F., MENTEN, J., RUTTEN, I., CLAVERE, P., MALMSTROM, A., JANCAR, B., NEWLANDS, E., PIGOTT, K., TWIJNSTR, A., CHINOT, O., RENI, M., BOIARDI, A., FABBRO, M., CAMPONE, M., BOZZINO, J., FRENAY, M., GIJTENBEEK, J., DELATTRE, J. Y., DE PAULA, U., HANZEN, C., PAVANATO, G., SCHRAUB, S., PFEFFER, R., SOFFIETTI, R., KORTMANN, R. D., TAPHOORN, M., TORRECILLA, J. L., GRISOLD, W., HUGET, P., FORSYTH, P., FULTON, D., KIRBY, S., WONG, R., FENTON, D., CAIRNCROSS, G., WHITLOCK, P., BURDETTE-RADOUX, S., GERTLER, S., SAUNDERS, S., LAING, K., SIDDIQUI, J., MARTIN, L. A., GULAVITA, S., PERRY, J., MASON, W., THIESSEN, B., PAI, H., ALAM, Z. Y., EISENSTAT, D., MINGRONE, W., HOFER, S., PESCE, G., DIETRICH, P. Y., THUM, P., BAUMERT, B., RYAN, G. & EUROPEAN ORG RES TREATMENT CANC, B. 2005. Radiotherapy plus concomitant and adjuvant temozolomide for glioblastoma. *New England Journal of Medicine*, 352, 987-996.
- STURM, D., WITT, H., HOVESTADT, V., KHUONG-QUANG, D. A., JONES, D. T., KONERMANN, C., PFAFF, E., TONJES, M., SILL, M., BENDER, S., KOOL, M., ZAPATKA, M., BECKER, N., ZUCKNICK, M., HIELSCHER, T., LIU, X. Y., FONTEBASSO, A. M., RYZHOVA, M., ALBRECHT, S., JACOB, K., WOLTER, M., EBINGER, M., SCHUHMANN, M. U., VAN METER, T., FRUHWALD, M. C., HAUCH, H., PEKRUN, A., RADLWIMMER, B., NIEHUES, T., VON KOMOROWSKI, G., DURKEN, M., KULOZIK, A. E., MADDEN, J., DONSON, A., FOREMAN, N. K., DRISSI, R., FOULADI, M., SCHEURLLEN, W., VON DEIMLING, A., MONORANU, C., ROGGENDORF, W., HEROLD-MENDE, C., UNTERBERG, A., KRAMM, C. M., FELSBERG, J., HARTMANN, C., WIESTLER, B., WICK, W., MILDE, T., WITT, O., LINDROTH, A. M., SCHWARTZENTRUBER, J., FAURY, D., FLEMING, A., ZAKRZEWSKA, M., LIBERSKI, P. P., ZAKRZEWSKI, K., HAUSER, P., GARAMI, M., KLEKNER, A., BOGNAR, L., MORRISSY, S., CAVALLI, F., TAYLOR, M. D., VAN SLUIS, P., KOSTER, J., VERSTEEG, R., VOLCKMANN, R., MIKKELSEN, T., ALDAPE, K., REIFENBERGER, G., COLLINS, V. P., MAJEWSKI, J., KORSHUNOV, A., LICHTER, P., PLASS, C., JABADO, N. & PFISTER, S. M. 2012. Hotspot mutations in H3F3A and IDH1 define distinct epigenetic and biological subgroups of glioblastoma. *Cancer Cell*, 22, 425-37.
- SULLIVAN, M. R., MATTAINI, K. R., DENNSTEDT, E. A., NGUYEN, A. A., SIVANAND, S., REILLY, M. F., MEETH, K., MUIR, A., DARNELL, A. M., BOSENBERG, M. W., LEWIS, C. A. & VANDER HEIDEN, M. G. 2019.

- Increased Serine Synthesis Provides an Advantage for Tumors Arising in Tissues Where Serine Levels Are Limiting. *Cell Metab*, 29, 1410-1421.e4.
- SUN, L., SONG, L., WAN, Q., WU, G., LI, X., WANG, Y., WANG, J., LIU, Z., ZHONG, X., HE, X., SHEN, S., PAN, X., LI, A., WANG, Y., GAO, P., TANG, H. & ZHANG, H. 2015. cMyc-mediated activation of serine biosynthesis pathway is critical for cancer progression under nutrient deprivation conditions. *Cell Res*, 25, 429-44.
- SWARTLING, F. J., GRIMMER, M. R., HACKETT, C. S., NORTHCOTT, P. A., FAN, Q. W., GOLDENBERG, D. D., LAU, J., MASIC, S., NGUYEN, K., YAKOVENKO, S., ZHE, X. N., GILMER, H. C., COLLINS, R., NAGAOKA, M., PHILLIPS, J. J., JENKINS, R. B., TIHAN, T., VANDENBERG, S. R., JAMES, C. D., TANAKA, K., TAYLOR, M. D., WEISS, W. A. & CHESLER, L. 2010. Pleiotropic role for MYCN in medulloblastoma. *Genes Dev*, 24, 1059-72.
- SWARTLING, F. J., SAVOV, V., PERSSON, A. I., CHEN, J., HACKETT, C. S., NORTHCOTT, P. A., GRIMMER, M. R., LAU, J., CHESLER, L., PERRY, A., PHILLIPS, J. J., TAYLOR, M. D. & WEISS, W. A. 2012. Distinct neural stem cell populations give rise to disparate brain tumors in response to N-MYC. *Cancer Cell*, 21, 601-13.
- SWARTZ, S. J. 2018. Investigation of MYC-driven group 3 medulloblastoma using novel regulable cell based models.
- SZELIGA, M., ĆWIKŁA, J., OBARA-MICHLEWSKA, M., CICHOCKI, A. & ALBRECHT, J. 2016. Glutaminases in slowly proliferating gastroenteropancreatic neuroendocrine neoplasms/tumors (GEP-NETs): Selective overexpression of mRNA coding for the KGA isoform. *Experimental and Molecular Pathology*, 100, 74-78.
- TAKAHASHI, K. & YAMANAKA, S. 2006. Induction of pluripotent stem cells from mouse embryonic and adult fibroblast cultures by defined factors. *Cell*, 126, 663-76.
- TAMEIRE, F., VERGINADIS, II, LELI, N. M., POLTE, C., CONN, C. S., OJHA, R., SALAS SALINAS, C., CHINGA, F., MONROY, A. M., FU, W., WANG, P., KOSENKOV, A., YE, J., AMARAVADI, R. K., IGNATOVA, Z., FUCHS, S. Y., DIEHL, J. A., RUGGERO, D. & KOUMENIS, C. 2019. ATF4 couples MYC-dependent translational activity to bioenergetic demands during tumour progression. *Nat Cell Biol*, 21, 889-899.
- TANIMOTO, K., MAKINO, Y., PEREIRA, T. & POELLINGER, L. 2000. Mechanism of regulation of the hypoxia-inducible factor-1 alpha by the von Hippel-Lindau tumor suppressor protein. *Embo j*, 19, 4298-309.
- TANNER, L. B., GOGLIA, A. G., WEI, M. H., SEHGAL, T., PARSONS, L. R., PARK, J. O., WHITE, E., TOETTCHER, J. E. & RABINOWITZ, J. D. 2018. Four Key Steps Control Glycolytic Flux in Mammalian Cells. *Cell Syst*, 7, 49-62.e8.
- TANSEY, W. P. 2014. Mammalian MYC Proteins and Cancer. *New Journal of Science*, 2014, 1-27.
- TAO, B. B., HE, H., SHI, X. H., WANG, C. L., LI, W. Q., LI, B., DONG, Y., HU, G. H., HOU, L. J., LUO, C., CHEN, J. X., CHEN, H. R., YU, Y. H., SUN, Q. F. & LU, Y. C. 2013. Up-regulation of USP2a and FASN in gliomas correlates strongly with glioma grade. *Journal of Clinical Neuroscience*, 20, 717-720.
- TAO, R., MURAD, N., XU, Z., ZHANG, P., OKONECHNIKOV, K., KOOL, M., RIVERO-HINOJOSA, S., LAZARSKI, C., ZHENG, P., LIU, Y., EBERHART, C. G., ROOD, B. R., PACKER, R. & PEI, Y. 2019. MYC Drives Group 3 Medulloblastoma through Transformation of Sox2(+) Astrocyte Progenitor Cells. *Cancer Res*, 79, 1967-1980.

- TATEISHI, K., IAFRATE, A. J., HO, Q., CURRY, W. T., BATCHELOR, T. T., FLAHERTY, K. T., ONOZATO, M. L., LELIC, N., SUNDARAM, S., CAHILL, D. P., CHI, A. S. & WAKIMOTO, H. 2016. Myc-Driven Glycolysis Is a Therapeutic Target in Glioblastoma. *Clin Cancer Res*, 22, 4452-65.
- TAYLOR, M. D., NORTHCOTT, P. A., KORSHUNOV, A., REMKE, M., CHO, Y. J., CLIFFORD, S. C., EBERHART, C. G., PARSONS, D. W., RUTKOWSKI, S., GAJJAR, A., ELLISON, D. W., LICHTER, P., GILBERTSON, R. J., POMEROY, S. L., KOOL, M. & PFISTER, S. M. 2012. Molecular subgroups of medulloblastoma: the current consensus. *Acta Neuropathologica*, 123, 465-472.
- TAYLOR, R. E., BAILEY, C. C., ROBINSON, K. J., WESTON, C. L., ELLISON, D., IRONSIDE, J., LUCRAFT, H., GILBERTSON, R., TAIT, D. M., SARAN, F., WALKER, D. A., PIZER, B. L. & LASHFORD, L. S. 2004. Impact of radiotherapy parameters on outcome in the International Society of Paediatric Oncology/United Kingdom Children's Cancer Study Group PNET-3 study of preradiotherapy chemotherapy for M0-M1 medulloblastoma. *Int J Radiat Oncol Biol Phys*, 58, 1184-93.
- TEDESCHI, P. M., MARKERT, E. K., GOUNDER, M., LIN, H., DVORZHINSKI, D., DOLFI, S. C., CHAN, L. L., QIU, J., DIPOLA, R. S., HIRSHFIELD, K. M., BOROS, L. G., BERTINO, J. R., OLTVAI, Z. N. & VAZQUEZ, A. 2013. Contribution of serine, folate and glycine metabolism to the ATP, NADPH and purine requirements of cancer cells. *Cell Death Dis*, 4, e877.
- TEO, W.-Y., SEKAR, K., SESHACHALAM, P., SHEN, J., CHOW, W.-Y., LAU, C. C., YANG, H., PARK, J., KANG, S.-G., LI, X., NAM, D.-H. & HUI, K. M. 2019. Relevance of a TCGA-derived Glioblastoma Subtype Gene-Classifier among Patient Populations. *Scientific Reports*, 9, 7442.
- TERUNUMA, A., PUTLURI, N., MISHRA, P., MATHE, E. A., DORSEY, T. H., YI, M., WALLACE, T. A., ISSAQ, H. J., ZHOU, M., KILLIAN, J. K., STEVENSON, H. S., KAROLY, E. D., CHAN, K., SAMANTA, S., PRIETO, D., HSU, T. Y., KURLEY, S. J., PUTLURI, V., SONAVANE, R., EDELMAN, D. C., WULFF, J., STARKS, A. M., YANG, Y., KITTLES, R. A., YFANTIS, H. G., LEE, D. H., IOFFE, O. B., SCHIFF, R., STEPHENS, R. M., MELTZER, P. S., VEENSTRA, T. D., WESTBROOK, T. F., SREEKUMAR, A. & AMBS, S. 2014. MYC-driven accumulation of 2-hydroxyglutarate is associated with breast cancer prognosis. *J Clin Invest*, 124, 398-412.
- THOMAS, L. R. & TANSEY, W. P. 2011. Proteolytic control of the oncoprotein transcription factor Myc. *Adv Cancer Res*, 110, 77-106.
- THOMAS, W. D., CHEN, J., GAO, Y. R., CHEUNG, B., KOACH, J., SEKYERE, E., NORRIS, M. D., HABER, M., ELLIS, T., WAINWRIGHT, B. & MARSHALL, G. M. 2009. Patched1 deletion increases N-Myc protein stability as a mechanism of medulloblastoma initiation and progression. *Oncogene*, 28, 1605-15.
- THOMPSON, M. C., FULLER, C., HOGG, T. L., DALTON, J., FINKELSTEIN, D., LAU, C. C., CHINTAGUMPALA, M., ADESINA, A., ASHLEY, D. M., KELLIE, S. J., TAYLOR, M. D., CURRAN, T., GAJJAR, A. & GILBERTSON, R. J. 2006. Genomics identifies medulloblastoma subgroups that are enriched for specific genetic alterations. *J Clin Oncol*, 24, 1924-31.
- ULLAH, M. S., DAVIES, A. J. & HALESTRAP, A. P. 2006. The plasma membrane lactate transporter MCT4, but not MCT1, is up-regulated by hypoxia through a HIF-1alpha-dependent mechanism. *J Biol Chem*, 281, 9030-7.
- VAN DEN HEUVEL, A. P., JING, J., WOOSTER, R. F. & BACHMAN, K. E. 2012. Analysis of glutamine dependency in non-small cell lung cancer: GLS1 splice variant GAC is essential for cancer cell growth. *Cancer Biol Ther*, 13, 1185-94.

- VAN DER CRABBEN, S. N., VERHOEVEN-DUIF, N. M., BRILSTRA, E. H., VAN MALDERGEM, L., COSKUN, T., RUBIO-GOZALBO, E., BERGER, R. & DE KONING, T. J. 2013. An update on serine deficiency disorders. *J Inherit Metab Dis*, 36, 613-9.
- VANDE VOORDE, J., ACKERMANN, T., PFETZER, N., SUMPTON, D., MACKAY, G., KALNA, G., NIXON, C., BLYTH, K., GOTTLIEB, E. & TARDITO, S. 2019. Improving the metabolic fidelity of cancer models with a physiological cell culture medium. *Sci Adv*, 5, eaau7314.
- VARLAKHANOVA, N. V., COTTERMAN, R. F., DEVRIES, W. N., MORGAN, J., DONAHUE, L. R., MURRAY, S., KNOWLES, B. B. & KNOEPFLER, P. S. 2010. myc maintains embryonic stem cell pluripotency and self-renewal. *Differentiation*, 80, 9-19.
- VENNETI, S., DUNPHY, M. P., ZHANG, H., PITTER, K. L., ZANZONICO, P., CAMPOS, C., CARLIN, S. D., LA ROCCA, G., LYASHCHENKO, S., PLOESSL, K., ROHLE, D., OMURO, A. M., CROSS, J. R., BRENNAN, C. W., WEBER, W. A., HOLLAND, E. C., MELLINGHOFF, I. K., KUNG, H. F., LEWIS, J. S. & THOMPSON, C. B. 2015. Glutamine-based PET imaging facilitates enhanced metabolic evaluation of gliomas in vivo. *Sci Transl Med*, 7, 274ra17.
- VERHAAK, R. G. W., HOADLEY, K. A., PURDOM, E., WANG, V., QI, Y., WILKERSON, M. D., MILLER, C. R., DING, L., GOLUB, T., MESIROV, J. P., ALEXE, G., LAWRENCE, M., O'KELLY, M., TAMAYO, P., WEIR, B. A., GABRIEL, S., WINCKLER, W., GUPTA, S., JAKKULA, L., FEILER, H. S., HODGSON, J. G., JAMES, C. D., SARKARIA, J. N., BRENNAN, C., KAHN, A., SPELLMAN, P. T., WILSON, R. K., SPEED, T. P., GRAY, J. W., MEYERSON, M., GETZ, G., PEROU, C. M., HAYES, D. N. & CANC GENOME ATLAS RES, N. 2010. Integrated Genomic Analysis Identifies Clinically Relevant Subtypes of Glioblastoma Characterized by Abnormalities in PDGFRA, IDH1, EGFR, and NF1. *Cancer Cell*, 17, 98-110.
- VERVOORTS, J., LUSCHER-FIRZLAFF, J. M., ROTTMANN, S., LILISCHKIS, R., WALSEMANN, G., DOHMANN, K., AUSTEN, M. & LUSCHER, B. 2003. Stimulation of c-MYC transcriptional activity and acetylation by recruitment of the cofactor CBP. *EMBO Rep*, 4, 484-90.
- VIALE, A., PETTAZZONI, P., LYSSIOTIS, C. A., YING, H., SANCHEZ, N., MARCHESINI, M., CARUGO, A., GREEN, T., SETH, S., GIULIANI, V., KOST-ALIMOVA, M., MULLER, F., COLLA, S., NEZI, L., GENOVESE, G., DEEM, A. K., KAPOOR, A., YAO, W., BRUNETTO, E., KANG, Y., YUAN, M., ASARA, J. M., WANG, Y. A., HEFFERNAN, T. P., KIMMELMAN, A. C., WANG, H., FLEMING, J. B., CANTLEY, L. C., DEPINHO, R. A. & DRAETTA, G. F. 2014. Oncogene ablation-resistant pancreatic cancer cells depend on mitochondrial function. *Nature*, 514, 628-32.
- VICHAI, V. & KIRTIKARA, K. 2006. Sulforhodamine B colorimetric assay for cytotoxicity screening. *Nat Protoc*, 1, 1112-6.
- VITA, M. & HENRIKSSON, M. 2006. The Myc oncoprotein as a therapeutic target for human cancer. *Semin Cancer Biol*, 16, 318-30.
- VIVANCO, I., ROBINS, H. I., ROHLE, D., CAMPOS, C., GROMMES, C., NGHIEMPHU, P. L., KUBEK, S., OLDRINI, B., CHHEDA, M. G., YANNUZZI, N., TAO, H., ZHU, S., IWANAMI, A., KUGA, D., DANG, J., PEDRAZA, A., BRENNAN, C. W., HEGUY, A., LIAU, L. M., LIEBERMAN, F., YUNG, W. K., GILBERT, M. R., REARDON, D. A., DRAPPATZ, J., WEN, P. Y., LAMBORN, K. R., CHANG, S. M., PRADOS, M. D., FINE, H. A., HORVATH, S., WU, N., LASSMAN, A. B., DEANGELIS, L. M., YONG, W.

- H., KUHN, J. G., MISCHEL, P. S., MEHTA, M. P., CLOUGHESY, T. F. & MELLINGHOFF, I. K. 2012. Differential sensitivity of glioma- versus lung cancer-specific EGFR mutations to EGFR kinase inhibitors. *Cancer Discov*, 2, 458-71.
- VLADOIU, M. C., EL-HAMAMY, I., DONOVAN, L. K., FAROOQ, H., HOLGADO, B. L., SUNDARAVADANAM, Y., RAMASWAMY, V., HENDRIKSE, L. D., KUMAR, S., MACK, S. C., LEE, J. J. Y., FONG, V., JURASCHKA, K., PRZELICKI, D., MICHEALRAJ, A., SKOWRON, P., LUU, B., SUZUKI, H., MORRISSY, A. S., CAVALLI, F. M. G., GARZIA, L., DANIELS, C., WU, X., QAZI, M. A., SINGH, S. K., CHAN, J. A., MARRA, M. A., MALKIN, D., DIRKS, P., HEISLER, L., PUGH, T., NG, K., NOTTA, F., THOMPSON, E. M., KLEINMAN, C. L., JOYNER, A. L., JABADO, N., STEIN, L. & TAYLOR, M. D. 2019. Childhood cerebellar tumours mirror conserved fetal transcriptional programs. *Nature*, 572, 67-73.
- VLASHI, E., LAGADEC, C., VERGNES, L., MATSUTANI, T., MASUI, K., POULOU, M., POPESCU, R., DELLA DONNA, L., EVERS, P., DEKMEZIAN, C., REUE, K., CHRISTOFK, H., MISCHEL, P. S. & PAJONK, F. 2011. Metabolic state of glioma stem cells and nontumorigenic cells. *Proceedings of the National Academy of Sciences of the United States of America*, 108, 16062-16067.
- VON BUEREN, A. O., SHALABY, T., OEHLER-JANNE, C., ARNOLD, L., STEARNS, D., EBERHART, C. G., ARCARO, A., PRUSCHY, M. & GROTZER, M. A. 2009. RNA interference-mediated c-MYC inhibition prevents cell growth and decreases sensitivity to radio- and chemotherapy in childhood medulloblastoma cells. *BMC Cancer*, 9, 10.
- VON EYSS, B., JAENICKE, L. A., KORTLEVER, R. M., ROYLA, N., WIESE, K. E., LETSCHERT, S., MCDUFFUS, L. A., SAUER, M., ROSENWALD, A., EVAN, G. I., KEMPA, S. & EILERS, M. 2015. A MYC-Driven Change in Mitochondrial Dynamics Limits YAP/TAZ Function in Mammary Epithelial Cells and Breast Cancer. *Cancer Cell*, 28, 743-757.
- WALSH, K. M., CODD, V., SMIRNOV, I. V., RICE, T., DECKER, P. A., HANSEN, H. M., KOLLMAYER, T., KOSEL, M. L., MOLINARO, A. M., MCCOY, L. S., BRACCI, P. M., CABRIGA, B. S., PEKMEZCI, M., ZHENG, S., WIEMELS, J. L., PICO, A. R., TIHAN, T., BERGER, M. S., CHANG, S. M., PRADOS, M. D., LACHANCE, D. H., O'NEILL, B. P., SICOTTE, H., ECKEL-PASSOW, J. E., VAN DER HARST, P., WIENCKE, J. K., SAMANI, N. J., JENKINS, R. B. & WRENSCH, M. R. 2014. Variants near TERT and TERC influencing telomere length are associated with high-grade glioma risk. *Nat Genet*, 46, 731-5.
- WANG, H., MANNAVA, S., GRACHTCHOUK, V., ZHUANG, D., SOENGAS, M. S., GUDKOV, A. V., PROCHOWNIK, E. V. & NIKIFOROV, M. A. 2008. c-Myc depletion inhibits proliferation of human tumor cells at various stages of the cell cycle. *Oncogene*, 27, 1905-15.
- WANG, Q., LIBERTI, M. V., LIU, P., DENG, X., LIU, Y., LOCASALE, J. W. & LAI, L. 2017. Rational Design of Selective Allosteric Inhibitors of PHGDH and Serine Synthesis with Anti-tumor Activity. *Cell Chem Biol*, 24, 55-65.
- WANG, R., DILLON, C. P., SHI, L. Z., MILASTA, S., CARTER, R., FINKELSTEIN, D., MCCORMICK, L. L., FITZGERALD, P., CHI, H., MUNGER, J. & GREEN, D. R. 2011. The transcription factor Myc controls metabolic reprogramming upon T lymphocyte activation. *Immunity*, 35, 871-82.
- WANG, X., LI, W., PARRA, J. L., BEUGNET, A. & PROUD, C. G. 2003. The C terminus of initiation factor 4E-binding protein 1 contains multiple regulatory features that influence its function and phosphorylation. *Mol Cell Biol*, 23, 1546-57.

- WARBURG, O. 1956. On the origin of cancer cells. *Science*, 123, 309-14.
- WEISS, W. A., TAYLOR, S. S. & SHOKAT, K. M. 2007. Recognizing and exploiting differences between RNAi and small-molecule inhibitors. *Nature chemical biology*, 3, 739-744.
- WELLER, M., WICK, W., ALDAPE, K., BRADA, M., BERGER, M., PFISTER, S. M., NISHIKAWA, R., ROSENTHAL, M., WEN, P. Y., STUPP, R. & REIFENBERGER, G. 2015. Glioma. *Nat Rev Dis Primers*, 1, 15017.
- WELTE, M. A. 2015. Expanding Roles for Lipid Droplets. *Current Biology*, 25, R470-R481.
- WHITE, E. 2013. Exploiting the bad eating habits of Ras-driven cancers. *Genes Dev*, 27, 2065-71.
- WIEMAN, H. L., WOFFORD, J. A. & RATHMELL, J. C. 2007. Cytokine stimulation promotes glucose uptake via phosphatidylinositol-3 kinase/Akt regulation of Glut1 activity and trafficking. *Mol Biol Cell*, 18, 1437-46.
- WIESE, K. E., WALZ, S., VON EYSS, B., WOLF, E., ATHINEOS, D., SANSOM, O. & EILERS, M. 2013. The role of MIZ-1 in MYC-dependent tumorigenesis. *Cold Spring Harb Perspect Med*, 3, a014290.
- WILLETT, M., COWAN, J. L., VLASAK, M., COLDWELL, M. J. & MORLEY, S. J. 2009. Inhibition of mammalian target of rapamycin (mTOR) signalling in C2C12 myoblasts prevents myogenic differentiation without affecting the hyperphosphorylation of 4E-BP1. *Cellular Signalling*, 21, 1504-1512.
- WILLIAM, D., MULLINS, C. S., SCHNEIDER, B., ORTHMANN, A., LAMP, N., KROHN, M., HOFFMANN, A., CLASSEN, C.-F. & LINNEBACHER, M. 2017. Optimized creation of glioblastoma patient derived xenografts for use in preclinical studies. *Journal of Translational Medicine*, 15, 27.
- WILSON, A., MURPHY, M. J., OSKARSSON, T., KALOULIS, K., BETTESS, M. D., OSER, G. M., PASCHE, A. C., KNABENHANS, C., MACDONALD, H. R. & TRUMPP, A. 2004. c-Myc controls the balance between hematopoietic stem cell self-renewal and differentiation. *Genes Dev*, 18, 2747-63.
- WILSON, T. A., KARAJANNIS, M. A. & HARTER, D. H. 2014. Glioblastoma multiforme: State of the art and future therapeutics. *Surg Neurol Int*, 5, 64.
- WISE, D. R., DEBERARDINIS, R. J., MANCUSO, A., SAYED, N., ZHANG, X. Y., PFEIFFER, H. K., NISSIM, I., DAIKHIN, E., YUDKOFF, M., MCMAHON, S. B. & THOMPSON, C. B. 2008. Myc regulates a transcriptional program that stimulates mitochondrial glutaminolysis and leads to glutamine addiction. *Proc Natl Acad Sci U S A*, 105, 18782-7.
- WOLFGANG, M. J., KURAMA, T., DAI, Y., SUWA, A., ASAUMI, M., MATSUMOTO, S., CHA, S. H., SHIMOKAWA, T. & LANE, M. D. 2006. The brain-specific carnitine palmitoyltransferase-1c regulates energy homeostasis. *Proceedings of the National Academy of Sciences of the United States of America*, 103, 7282-7287.
- XIA, Y., YE, B., DING, J., YU, Y., ALPTEKIN, A., THANGARAJU, M., PRASAD, P. D., DING, Z. C., PARK, E. J., CHOI, J. H., GAO, B., FIEHN, O., YAN, C., DONG, Z., ZHA, Y. & DING, H. F. 2019. Metabolic Reprogramming by MYCN Confers Dependence on the Serine-Glycine-One-Carbon Biosynthetic Pathway. *Cancer Res*, 79, 3837-3850.
- XIANG, Y., STINE, Z. E., XIA, J., LU, Y., O'CONNOR, R. S., ALTMAN, B. J., HSIEH, A. L., GOUW, A. M., THOMAS, A. G., GAO, P., SUN, L., SONG, L., YAN, B., SLUSHER, B. S., ZHUO, J., OOI, L. L., LEE, C. G., MANCUSO, A., MCCALLION, A. S., LE, A., MILONE, M. C., RAYPORT, S., FELSHER, D. W. & DANG, C. V. 2015. Targeted inhibition of tumor-specific glutaminase diminishes cell-autonomous tumorigenesis. *J Clin Invest*, 125, 2293-306.

- XIE, J., WU, H., DAI, C., PAN, Q., DING, Z., HU, D., JI, B., LUO, Y. & HU, X. 2014. Beyond Warburg effect--dual metabolic nature of cancer cells. *Sci Rep*, 4, 4927.
- XIE, Z., JONES, A., DEENEY, J. T., HUR, S. K. & BANKAITIS, V. A. 2016. Inborn Errors of Long-Chain Fatty Acid β -Oxidation Link Neural Stem Cell Self-Renewal to Autism. *Cell reports*, 14, 991-999.
- XIONG, J., WANG, L., FEI, X. C., JIANG, X. F., ZHENG, Z., ZHAO, Y., WANG, C. F., LI, B., CHEN, S. J., JANIN, A., GALE, R. P. & ZHAO, W. L. 2017. MYC is a positive regulator of choline metabolism and impedes mitophagy-dependent necroptosis in diffuse large B-cell lymphoma. *Blood Cancer J*, 7, e0.
- YANG, C., KO, B., HENSLEY, C. T., JIANG, L., WASTI, A. T., KIM, J., SUDDERTH, J., CALVARUSO, M. A., LUMATA, L., MITSCHKE, M., RUTTER, J., MERRITT, M. E. & DEBERARDINIS, R. J. 2014. Glutamine oxidation maintains the TCA cycle and cell survival during impaired mitochondrial pyruvate transport. *Mol Cell*, 56, 414-24.
- YANG, L., VENNETI, S. & NAGRATH, D. 2017. Glutaminolysis: A Hallmark of Cancer Metabolism. *Annu Rev Biomed Eng*, 19, 163-194.
- YASUMOTO, Y., MIYAZAKI, H., VAIDYAN, L. K., KAGAWA, Y., EBRAHIMI, M., YAMAMOTO, Y., OGATA, M., KATSUYAMA, Y., SADAHIRO, H., SUZUKI, M. & OWADA, Y. 2016. Inhibition of Fatty Acid Synthase Decreases Expression of Stemness Markers in Glioma Stem Cells. *PLoS One*, 11, e0147717.
- YAU, T., CHENG, P. N., CHAN, P., CHAN, W., CHEN, L., YUEN, J., PANG, R., FAN, S. T. & POON, R. T. 2013. A phase 1 dose-escalating study of pegylated recombinant human arginase 1 (Peg-rhArg1) in patients with advanced hepatocellular carcinoma. *Invest New Drugs*, 31, 99-107.
- YE, J., MANCUSO, A., TONG, X., WARD, P. S., FAN, J., RABINOWITZ, J. D. & THOMPSON, C. B. 2012. Pyruvate kinase M2 promotes de novo serine synthesis to sustain mTORC1 activity and cell proliferation. *Proc Natl Acad Sci U S A*, 109, 6904-9.
- YERLI, H., AGILDERE, A. M., OZEN, O., GEYIK, E., ATALAY, B. & ELHAN, A. H. 2007. Evaluation of cerebral glioma grade by using normal side creatine as an internal reference in multi-voxel 1H-MR spectroscopy. *Diagn Interv Radiol*, 13, 3-9.
- YILDIRIM, Z. & KILIC, N. 2011. Effects of Taurine and Age on Cerebellum Antioxidant Status and Oxidative Stress. *International Journal of Gerontology*, 5, 166-170.
- YING, H., KIMMELMAN, A. C., LYSSIoTIS, C. A., HUA, S., CHU, G. C., FLETCHER-SANANIKONE, E., LOCASALE, J. W., SON, J., ZHANG, H., COLOFF, J. L., YAN, H., WANG, W., CHEN, S., VIALE, A., ZHENG, H., PAIK, J. H., LIM, C., GUIMARAES, A. R., MARTIN, E. S., CHANG, J., HEZEL, A. F., PERRY, S. R., HU, J., GAN, B., XIAO, Y., ASARA, J. M., WEISSLEDER, R., WANG, Y. A., CHIN, L., CANTLEY, L. C. & DEPINHO, R. A. 2012. Oncogenic Kras maintains pancreatic tumors through regulation of anabolic glucose metabolism. *Cell*, 149, 656-70.
- YOSHINO, H., NOHATA, N., MIYAMOTO, K., YONEMORI, M., SAKAGUCHI, T., SUGITA, S., ITESAKO, T., KOFUJI, S., NAKAGAWA, M., DAHIYA, R. & ENOKIDA, H. 2017. PHGDH as a Key Enzyme for Serine Biosynthesis in HIF2 α -Targeting Therapy for Renal Cell Carcinoma. *Cancer Res*, 77, 6321-6329.
- YUAN, T. L. & CANTLEY, L. C. 2008. PI3K pathway alterations in cancer: variations on a theme. *Oncogene*, 27, 5497-510.
- YUE, M., JIANG, J., GAO, P., LIU, H. & QING, G. 2017. Oncogenic MYC Activates a Feedforward Regulatory Loop Promoting Essential Amino Acid Metabolism and Tumorigenesis. *Cell Rep*, 21, 3819-3832.

- YUNEVA, M., ZAMBONI, N., OEFNER, P., SACHIDANANDAM, R. & LAZEBNIK, Y. 2007. Deficiency in glutamine but not glucose induces MYC-dependent apoptosis in human cells. *J Cell Biol*, 178, 93-105.
- YUNEVA, M. O., FAN, T. W., ALLEN, T. D., HIGASHI, R. M., FERRARIS, D. V., TSUKAMOTO, T., MATES, J. M., ALONSO, F. J., WANG, C., SEO, Y., CHEN, X. & BISHOP, J. M. 2012. The metabolic profile of tumors depends on both the responsible genetic lesion and tissue type. *Cell Metab*, 15, 157-70.
- ZAUGG, K., YAO, Y., REILLY, P. T., KANNAN, K., KIARASH, R., MASON, J., HUANG, P., SAWYER, S. K., FUERTH, B., FAUBERT, B., KALLIOMAKI, T., ELIA, A., LUO, X. Y., NADEEM, V., BUNGARD, D., YALAVARTHI, S., GROWNEY, J. D., WAKEHAM, A., MOOLANI, Y., SILVESTER, J., TEN, A. Y., BAKKER, W., TSUCHIHARA, K., BERGER, S. L., HILL, R. P., JONES, R. G., TSAO, M., ROBINSON, M. O., THOMPSON, C. B., PAN, G. H. & MAK, T. W. 2011. Carnitine palmitoyltransferase 1C promotes cell survival and tumor growth under conditions of metabolic stress. *Genes & Development*, 25, 1041-1051.
- ZDRALEVIC, M., BRAND, A., DI IANNI, L., DETTMER, K., REINDERS, J., SINGER, K., PETER, K., SCHNELL, A., BRUSS, C., DECKING, S. M., KOEHL, G., FELIPE-ABRIO, B., DURIVALT, J., BAYER, P., EVANGELISTA, M., O'BRIEN, T., OEFNER, P. J., RENNER, K., POUYSSEGUR, J. & KREUTZ, M. 2018. Double genetic disruption of lactate dehydrogenases A and B is required to ablate the "Warburg effect" restricting tumor growth to oxidative metabolism. *J Biol Chem*, 293, 15947-15961.
- ZHANG, A., SUN, H., XU, H., QIU, S. & WANG, X. 2013. Cell metabolomics. *Omics*, 17, 495-501.
- ZHANG, B., ZHENG, A., HYDBRING, P., AMBROISE, G., OUCHIDA, A. T., GOINY, M., VAKIFAHMETOGLU-NORBERG, H. & NORBERG, E. 2017. PHGDH Defines a Metabolic Subtype in Lung Adenocarcinomas with Poor Prognosis. *Cell Rep*, 19, 2289-2303.
- ZHANG, H., GAO, P., FUKUDA, R., KUMAR, G., KRISHNAMACHARY, B., ZELLER, K. I., DANG, C. V. & SEMENZA, G. L. 2007. HIF-1 inhibits mitochondrial biogenesis and cellular respiration in VHL-deficient renal cell carcinoma by repression of C-MYC activity. *Cancer Cell*, 11, 407-20.
- ZHANG, L., HE, X., LIU, X., ZHANG, F., HUANG, L. F., POTTER, A. S., XU, L., ZHOU, W., ZHENG, T., LUO, Z., BERRY, K. P., PRIBNOW, A., SMITH, S. M., FULLER, C., JONES, B. V., FOULADI, M., DRISSI, R., YANG, Z. J., GUSTAFSON, W. C., REMKE, M., POMEROY, S. L., GIRARD, E. J., OLSON, J. M., MORRISSY, A. S., VLADOIU, M. C., ZHANG, J., TIAN, W., XIN, M., TAYLOR, M. D., POTTER, S. S., ROUSSEL, M. F., WEISS, W. A. & LU, Q. R. 2019. Single-Cell Transcriptomics in Medulloblastoma Reveals Tumor-Initiating Progenitors and Oncogenic Cascades during Tumorigenesis and Relapse. *Cancer Cell*, 36, 302-318.e7.
- ZHAO, X., HENG, J. I., GUARDAVACCARO, D., JIANG, R., PAGANO, M., GUILLEMOT, F., IAVARONE, A. & LASORELLA, A. 2008. The HECT-domain ubiquitin ligase Huwe1 controls neural differentiation and proliferation by destabilizing the N-Myc oncoprotein. *Nat Cell Biol*, 10, 643-53.
- ZHOU, P. T., LI, B., LIU, F. R., ZHANG, M. C., WANG, Q., LI, Y. Y., XU, C., LIU, Y. H., YAO, Y. & LI, D. 2017. Metformin is associated with survival benefit in pancreatic cancer patients with diabetes: a systematic review and meta-analysis. *Oncotarget*, 8, 25242-25250.
- ZHOU, Y. F., ZHOU, Y., SHINGU, T., FENG, L., CHEN, Z., OGASAWARA, M., KEATING, M. J., KONDO, S. & HUANG, P. 2011. Metabolic Alterations in

- Highly Tumorigenic Glioblastoma Cells PREFERENCE FOR HYPOXIA AND HIGH DEPENDENCY ON GLYCOLYSIS. *Journal of Biological Chemistry*, 286, 32843-32853.
- ZHU, H. & BARKER, P. B. 2011. MR spectroscopy and spectroscopic imaging of the brain. *Methods Mol Biol*, 711, 203-26.
- ZHU, J., MA, J., WANG, X., MA, T., ZHANG, S., WANG, W., ZHOU, X. & SHI, J. 2016. High Expression of PHGDH Predicts Poor Prognosis in Non-Small Cell Lung Cancer. *Transl Oncol*, 9, 592-599.
- ZHU, Y., GUIGNARD, F., ZHAO, D., LIU, L., BURNS, D. K., MASON, R. P., MESSING, A. & PARADA, L. F. 2005. Early inactivation of p53 tumor suppressor gene cooperating with NF1 loss induces malignant astrocytoma. *Cancer Cell*, 8, 119-30.
- ZINDY, F., UZIEL, T., AYRAULT, O., CALABRESE, C., VALENTINE, M., REHG, J. E., GILBERTSON, R. J., SHERR, C. J. & ROUSSEL, M. F. 2007. Genetic alterations in mouse medulloblastomas and generation of tumors de novo from primary cerebellar granule neuron precursors. *Cancer Res*, 67, 2676-84.
- ZININ, N., ADAMEYKO, I., WILHELM, M., FRITZ, N., UHLEN, P., ERNFORS, P. & HENRIKSSON, M. A. 2014. MYC proteins promote neuronal differentiation by controlling the mode of progenitor cell division. *EMBO Rep*, 15, 383-91.
- ZOU, D., YI, S., CUI, R., LIU, W., LI, C., ZHONG, S., YU, Z., LI, Z., LV, R., RU, K., WANG, H., AN, G., XU, Y. & QIU, L. 2017. BCL-2 and MYC gain/amplification is correlated with central nervous system involvement in diffuse large B cell lymphoma at leukemic phase. *BMC Med Genet*, 18, 16.
- ZUNDEL, W., SCHINDLER, C., HAAS-KOGAN, D., KOONG, A., KAPER, F., CHEN, E., GOTTSCHALK, A. R., RYAN, H. E., JOHNSON, R. S., JEFFERSON, A. B., STOKOE, D. & GIACCIA, A. J. 2000. Loss of PTEN facilitates HIF-1-mediated gene expression. *Genes Dev*, 14, 391-6.